UNSW SYDNEY

An extension of single phase flow turbulent pipe flow concepts to two-phase flow

Author:
Beattie, David R. H.

Publication Date:
1983

DOI:
https://doi.org/10.26190/unsworks/13886

License:
https://creativecommons.org/licenses/by-nc-nd/3.0/au/
Link to license to see what you are allowed to do with this resource.

Downloaded from http://hdl.handle.net/1959.4/69349 in https://unsworks.unsw.edu.au on 2026-03-03

BEATTIE : Ph.D. thesis.

Errata :-

P 38 : '-0·10' in eq. (3·31) should be '+1·0'

P 39 : Middle figure should be 'sublayer b', and '$m, n = 3, -1$'
" Bottom " " " " c' " " " $= 4, 1$'.

P 75 'j^{n-1}' of eq. (5·7) should be 'j^{k-1}'.

P 192 '$n' - m + 2$' should be '$n' - m + 2$

AN EXTENSION OF SINGLE PHASE FLOW TURBULENT PIPE FLOW CONCEPTS TO TWO-PHASE FLOW

D.R.H. BEATTIE

B.Sc.(Hons), B.E.(Hons), M.Eng.Sc.

A thesis submitted to the School of Nuclear Engineering, the University of New South Wales, for the degree of Doctor of Philosophy

September 1983

I hereby certify that this work has not been submitted for a higher degree to any other university or institution.

D.R.H. Beattie

ABSTRACT

This thesis describes a series of investigations into the hydraulic and thermal characteristics of various turbulent two-phase pipe flows, arising from one particular way of extending to two-phase flow, concepts previously developed for single phase pipe flow, e.g. mixing length, turbulent core, wall boundary or sub-layer, roughness, Reynolds analogy, etc.

This approach predicted a logarithmic core profile of local volumetric flux as a function of wall distance. Accounting for a range of different possible sub-layer fluid structures, it led to a dimensionless profile, and hence directly to a wall friction factor, in terms of dimensionless parameters chosen according to the type of sub-layer.

A 'friction regime' concept was developed, with regimes classified by sub-layer type and two characteristic integers which serve to determine the profile. The relations developed were based on the analysis of world-wide experimental two-phase flow data, and a number of practically useful new friction factor correlations resulted.

For a number of different 'friction regimes', the work was supplemented by additional models and analyses and applied to the prediction of average void fraction, heat transfer coefficient, critical heat flux, pulse propagation velocity and choked flow rate. In many cases, significant agreement was achieved between predictions and published data for which simultaneous measurements of several parameters guaranteed experimental consistency.

ACKNOWLEDGEMENTS

Acknowledgement is due to my employer, the Australian Atomic Energy Commission, for allowing me to undertake this project and for providing appropriate experimental and computational facilities.

I should like to express my appreciation to Professor J.J. Thompson, who served as the supervisor for this study, for the guidance he provided.

CONTENTS

		Page
NOMENCLATURE		v
1.	INTRODUCTION	1
	Chapter 1 references	5
2.	THE OVERALL CONSERVATION EQUATIONS OF TWO-PHASE FLOW	8
	Chapter 2 references	15
3.	TWO-PHASE FLOW STRUCTURE	16
	3.1 Some Considerations on Turbulence in Two-Phase Flow	16
	3.2 Application of Classical Turbulence Techniques: Two-Phase Void Profile Equations	17
	3.3 The Film Region of Annular Flow and a Point of Inflection Criterion	18
	3.4 The Velocity Defect Equation	25
	3.5 Non-dimensional Velocity Profiles	26
	3.6 Some Special Cases	30
	3.7 Non-dimensional Velocity Profile in Terms of Global Dimensionless Groups	34
	3.8 Data Analysis	37
	3.9 Friction Regime Classification Method	41
	3.10 Re-expression in Terms of Generalised Dimensionless Groups	41
	Chapter 3 references	44
4.	FRICTION FACTOR EXPRESSIONS FOR TWO-PHASE FLOW	46
	4.1 Duct Flow Losses	46
	4.2 Re-expression in Terms of Generalised Dimensionless Groups	47
	4.3 Obstruction Loss Coefficient	47
	4.4 Some Considerations on the Effect of Surface Roughness	48
	4.5 Data Analysis	50
	Chapter 4 references	71
5.	AVERAGE VOID FRACTION	73
	5.1 Distributed Flows	74
	5.2 Separated Two-Phase Flows	79
	5.3 Comparison with Data	83

		Page
	Chapter 5 references	91
6.	PROPAGATION PHENOMENA IN GAS/LIQUID SYSTEMS	93
	6.1 The Gas Isentropic Expansion Coefficient	93
	6.2 Liquid-Phase Continuous Flows	95
	6.3 Dry Wall Droplet Flows	105
	6.4 Separated Annular Two-Phase Flows	108
	Chapter 6 references	116
7.	ON THE RELATIONSHIP BETWEEN THE BOILING CRISIS AND WALL SHEAR STRESS	117
	7.1 Introduction	117
	7.2 Experimental Evidence of a Relationship Between the Boiling Crisis and Wall Shear Stress	118
	7.3 The Value of x_o in CHF Equations of the Form $\phi_{cr} = a(x_{cr} - x_o)$	120
	7.4 The Role of Pre-crisis Regime Transitions	125
	Chapter 7 references	136
8.	SOME ASPECTS OF TWO-PHASE HEAT TRANSFER	138
	8.1 Overview of Heat Transfer Behaviour	138
	8.2 Heat Transfer for Convective Boiling Annular Flows	141
	8.3 Post-crisis Heat Transfer	162
	Chapter 8 references	177
9.	CONCLUDING DISCUSSION	179
	9.1 Resume of Present Investigation	179
	9.2 Some Considerations on Data Analysis	181
	9.3 Significant Findings of the Investigation	185
	9.4 Suggestions for Further Research	189
	9.5 Conclusions	191
APPENDICES		192

NOMENCLATURE

a	propagation velocity (ch. 6)
a_o	propagation velocity at low flowrates (ch. 6)
a,b,c,d,e	letters specifying sublayer type (table 3.1)
a,b,c,	equation coefficients
A	flow cross-sectional area
A	volume fraction of annular flow core (ch. 5,6)
A_b	projected area of nucleating bubble onto heated surface (ch.8)
c_1-c_4	'constants' in mixing-length theory (e.g. 3.19 et.seq.)
C_o	phase/velocity distribution parameter (e.g. 5.3, 15, 6.9, 22a)
C_1,C_2	velocity distribution parameters (equs. 6.10, 11)
C_T	temperature/velocity distribution parameter (eq.
C_p	specific heat at constant pressure
C_v	specific heat at constant volume
d	bubble diameter
d_d	departure diameter for wall-nucleating bubble
D	duct equivalent hydraulic diameter
e	specific energy
E	enthalpy flux (eq. 8.33)
f	Fanning friction factor, $\tau_w/(\frac{1}{2}\rho_\delta \langle j\rangle^2)$
F	body force
g	acceleration due to gravity
G	mass flux
h	heat transfer coefficient, $\phi_w/(T_w-T_s)$ (section 8.2); $\phi_w/(T_w-\langle T\rangle)$, (section 8.3)
h	specific enthalpy
H	vertical height
j	local volumetric flux, $u_\ell(1-\alpha) + u_g\alpha$
j^*	shear velocity, $\sqrt{\tau_w/\rho_\delta}$

j^+ dimensionless local velocity, j/j^*

k thermal conductivity

K coefficient of thermal exchange (eq. 6.5)

K wave-length inverse (section 6.4.1)

ℓ flow boundary length

$\dot{M}_\ell$ liquid flowrate to nucleating bubble microlayer

$\dot{M}_{\ell c}$ contribution from core to $\dot{M}_\ell$

$\dot{M}_{\ell r}$ contribution from recirculated flow round nucleating bubble to $\dot{M}_\ell$

m,n integers specifying the core velocity profile form for a given friction regime (see section 3.9)

$\underset{\sim}{n}$ normal vector

N number of layers of bubbles in wall froth region at boiling crisis onset (section 8.2.3)

Nu, Nusselt number $(\phi_w/(T_w-T_s))\ D/k_\ell$ (section 8.2);

$(\phi_w/(T_w-\langle T\rangle))\ D/k_g$ (section 8.3)

P pressure

Q volume flow rate

r radial position

$\underset{\sim}{r}$ radial vector

R radius

Pr Prandtl number, $\mu C_p/k$

Re Reynolds number, $\rho_\delta \langle j\rangle D/\mu_\delta$

s surface (ch. 2)

S film thickness (chs. 3 on)

S^+ dimensionless film thickness, $S\ u^*\ \rho_\delta/\mu_\delta = \frac{S}{D}\ Re\ \sqrt{\frac{f}{2}}$

t time

T temperature

u ensemble averaged axial velocity

u^* single phase shear velocity, $\sqrt{\tau_w/\rho}$

v specific volume (ch. 6)

v local drift velocity (ch. 5)

$\underset{\sim}{V}$ velocity vector

V volume (ch. 2)

$V_{g,\ell}$ void-weighted average drift velocity (ch. 5) for dispersed gas or liquid phases

We Weber number, $\rho_H \langle j \rangle^2 D/\sigma$

$x_{1,2,3}$ orthogonal position vectors (ch. 2)

x flow quality, $G_g/(G_g + G_\ell)$

x_δ static quality (ch. 6), $\rho_g \langle\alpha\rangle/(\rho_g \langle\alpha\rangle + \rho_\ell(1\langle\alpha\rangle))$

y distance from wall

y^+ dimensionless wall distance, $y\, j^* \rho_\delta/\mu_\delta$

z axial co-ordinate

z letter a, b, c, d or e denoting sublayer component of friction regime (table 3.1, section 3.6)

α local void fraction; probability that gas is at a point

α_s fraction of heated surface where heat transfer is affected by nucleating bubbles

β gas volume flow ratio, $Q_g/(Q_g + Q_\ell)$

γ isentropic expansion coefficient

$\delta_{\ell,g}$ binary phase existence variable (ch. 2)

δ viscous sublayer thickness

δ local thermal non-equilibrium parameter (eq. 8.33)

Δ 'disequilibrium', liquid fraction weighted mean non-equilibrium (eq. 8.38)

ε equivalent sand roughness height

ε eddy diffusivity

θ	phase-fraction weighted mean phasic temperature (ch. 8)
θ	azimuthal angle co-ordinate
θ	angle between vertical and flow direction
κ	von Karman coefficient
λ	latent heat
μ	viscosity
ρ	density
σ	surface tension
σ_{ij}	component of stress tensor
$\underset{\approx}{\Sigma}$	stress tensor
τ	shear stress
$\underset{\sim}{\phi}$	heat flux
ϕ_{LO}^2	two-phase friction multiplier, correction factor for friction calculated as if the total mass flow was liquid
ω	wave frequency (section 6.4.1)
Ω	gravitational potential

Subscripts

c	core value (annular flow)
c	centreline value
cond	due to conduction
cr	value at boiling crisis
crit	choked flow condition
d	droplet
e.c.	due to evaporation and condensation
eq	thermal equilibrium value
f	value at film boundary
f	value within film
F	frictional component

g	gas value
h	heat
H	homogeneous value
i,j,k	denotes directions of arbitrary orthogonal co-ordinate system
inf	inflection point location
i.s.	inner sublayer value
ℓ	liquid value
LO	'liquid only', refers to calculation if all flow was all liquid at mixture mass flux
m	momentum
m	maximum value
m	mean value
r	radial component
s	saturation value
TP	two-phase flow
Tr	regime transition value
up	upward flow
w	wall value
z	axial component
δ	value at edge of turbulent core
σ	due to surface tension
τ	due to shear stress
o	denotes suitably-chosen reference value
1,2,3	denotes directions of specific orthogonal co-ordinate system
.	extreme position value

Superscript

*	contribution due to turbulence-induced correlation coefficients
'	fluctuating or perturbed component of variable
'	refers to 'generalised' quantity or dimensionless group (sections 3.10, 4.2)

Operators and special notation

<--->	cross-section averaging operator, $\frac{1}{A}\int_A$--- dA
$\frac{D}{Dt}$	substantial derivative, $\frac{\partial}{\partial t} + u\frac{\partial}{\partial z}$
$\overline{\quad}$	ensemble averaging operator
I_o, J_o, K_o	first-order Bessel functions
(z,m,n)	specifies friction regime, z is letter a-e; m & n are integers. See section 3.9.

CHAPTER 1

INTRODUCTION

The simultaneous flow of water and steam may occur in many water reactors operating under normal or abnormal conditions. Reactor design and assessment must consider low and high quality flow conditions, for a range of mass fluxes, flowing adiabatically or diabatically, in simple channels, or in complex channels such as fuel bundles. The channels may contain local obstructions such as spacers, end plates, or pipe bends.

The need for improved prediction in reactor design and assessment in areas such as two-phase voidage, friction, and heat transfer has been a major stimulus in generating fundamental research into two-phase thermohydraulics.

The importance of two-phase flow models can be gauged from an American Physical Society report on light water reactor safety [1.1]. In this report, eighteen components of loss-of-coolant accident (LOCA) phenomena which are directly influenced by two-phase thermohydraulics were identified. Of these, twelve were considered to have a first-order influence on determining overall LOCA behaviour. LOCA predictive abilities can thus be improved by improved models of the relevant two-phase thermohydraulics phenomena.

Despite the need for accurate prediction of two-phase thermo-hydraulics, and the considerable amount of research generated from this need, our predictive capabilities remain inadequate. This is demonstrated by several surveys on research needs in the two-phase flow field [1.2 - 1.12]. Despite the different origins and dates of these surveys, they show remarkable consensus in indicating that topics such as two-phase friction, void fraction, flow regime predic-

tion, and critical heat flux require further research. This is despite the fact that these topics are among the oldest and most extensively examined in the field of two-phase flow. The extent of the need for two-phase flow research is highlighted by the most recent and thorough of the abovementioned surveys [1.2, 1.3]. This survey is an assessment of basic research needs in all areas of fluid mechanics, and was sponsored by the US Department of Energy. Approximately half the topics are devoted to research in the two-phase flow area. A majority of these are relevant to nuclear engineering. As indicated above, the two-phase topics identified as needing long range fundamental research are consistent with those identified in earlier, less extensive surveys [1.4 - 1.12].

Noticeably lacking in two-phase flow research is any unifying model of the type developed by Prandtl [1.13], whose mixing-length theory of turbulence considerably assisted the development of single phase flow research. Indeed, the foremost recommendation in the US DOE study on fluid mechanics research needs [1.2] is 'Application to and experimental verification of extension of single phase flow theory to multiphase, multicomponent turbulent flows'.

The work reported here is based on the concept that Prandtl's single phase flow mixing-length theory [1.13] could be extended to two-phase flows. Such an extension may assist in the theoretical modelling of several of the aspects of two-phase flow which were (and are) recognised as requiring further research.

The above should not be regarded as implying that single phase flow mixing-length concepts have not previously been incorporated into models of two-phase flow. At the start of this research, the most widely-known such model was that due to Levy [1.14], whose mixing-length theory had partial success in predicting phase and velocity

distributions and pressure gradients. A later version [1.15] considered the entrainment factor in annular flow. Brandt [1.16] considered a mixing-length approach similar to that of Levy, but required experimental void profiles to apply the model. Fritz [1.17] defined a mixing-length model for the core region of annular flow. More recently, an eddy diffusivity model of bubbly flow has been proposed by Sato et al. [1.19]. As with the model of Brandt [1.16], application of the model depends on experimental void profiles. Drew and Lahey [1.20] considered separate mixing-lengths for 'shear induced turbulence' and 'bubble induced turbulence'. The mixing-lengths were found to vary with local voidage.

Von Karman similarity concepts were adapted by Biasi et al. [1.21] in their analysis of annular flow film thickness and velocity distribution.

In addition to these, several models assume that the single phase flow 'universal' velocity profile applies to the film region. A survey of such models is given in section 4.3.4 of [1.22].

Other researchers, e.g. [1.23, 1.24], have used the results of single-phase flow turbulence theory only as a means of suggesting appropriate dimensionless groups for presenting experimental data.

None of the above turbulence models of two-phase turbulent flow have attempted to allow for different flow regimes. However, it is recognised that many overall flow characteristics of interest (wall shear stress, heat transfer coefficient, etc.) depend on flow regime.

The present extension of mixing-length concepts to two-phase flow is therefore performed in such a way to allow for flow regimes. Since flow patterns (annular, bubble, etc.) and their boundaries are studied because of an expected dependence of thermohydraulic correlating equations on flow pattern, flow regimes in this work are based not on

flow patterns but instead on correlating equations required to describe thermohydraulic parameters. This approach avoids the subjectivity that appears in flow pattern studies, and also avoids the assumed one-to-one correspondence between flow patterns and thermohydraulic correlating equations.

The development of concepts in this work parallels that in the development of single-phase mixing-length theory and consequences of this theory. Thus, conservation equations of two-phase flow are considered in order to examine the nature of two-phase Reynolds stresses; mixing-length concepts are applied to these stresses in order to develop non-dimensional velocity profile expressions; these expressions are averaged over the flow section to yield friction factor expressions; and, where appropriate, heat transfer equations are developed from a Reynolds analogue of the hydrodynamic analysis. The analysis also examines consequences of mixing-length theory on phase distribution effects which have no equivalent in single phase flow theory. These distribution effects play a role in two-phase flow void fraction; propagation phenomena; and heat transfer.

The following technical chapters reflect the above approach and consider, in order:

- two-phase flow conservation equations;
- local flow structure;
- wall shear stress;
- average void fraction;
- propagation phenomena;
- the boiling crisis; and
- heat transfer coefficient.

In considering the US DOE recommendation [1.2] 'Application to and experimental verification of single phase flow theory to multiphase,

multi-component turbulent flows', the approach followed from the start of this project was one which considered that sufficient world data already existed to thoroughly test the present extension of mixing-length theory to two-phase flow. Thus, although some experiments were performed by the author, and results were used to test the present theory, these are not reported in the body of the thesis. Rather, the theory is compared with data obtained from the open literature. Related experiments performed by the author are summarised in section 4 of appendix A30; some are described in more detail in appendices A22 and A25.

Chapter 1 References

1.1 H.W. Lewis et al. 'Report to the American Physical Society by the study group on light-water reactor safety, Rev. Mod. Phys. 47, Suppl. No. 1, (1975).

1.2 O.C. Jones Jr. et al. 'Review - Basic research needs in fluid mechanics', J. Fluids Engng. 103, 509 (1981).

1.3 R. Eichhorn et al. 'Basic research in engineering: Fluid dynamics and thermal processes. Report of a workshop held in Lexington, Ky.', FE-2468-53 (1979).

1.4 B.S. Petukhov, 'The problems and the future development of heat-transfer theory', Thermal Engineering 29 (3), 143 (1982).

1.5 A.E. Bergles et al., 'Suggestions for further research and urgent problems on two-phase flows and heat transfer', in 'Two-phase flows and heat transfer; Proceedings of NATO Advanced Study Institute, Istanbul', Vol.III, S. Kakac and T.N. Veziroglu, eds. Hemisphere (1976).

1.6 L. Friedel, concluding remarks of 'Momentum Exchange and Pressure drop in two-phase flow', Ibid, Vol.I.

1.7 D. Gidaspow, 'Workshop report on mathematical modelling' in 'Two-phase transport and reactor safety: Proceedings of the two-phase flow and heat transfer workshop, Fort Lauderdale', Vol.IV, T.N. Veziroglu and S. Kakac, eds. Hemisphere (1976).

1.8 H.K. Fauske, 'Workshop report on nuclear safety', Ibid.

1.9 L.J. Jacobs, 'Workshop report on applications', Ibid.

1.10 E.J. Davis, 'Workshop report on measurement techniques', Ibid.

1.11 A.E. Bergles et al., 'Suggestions for further research on turbulent forced convection in channels and rod bundles' in 'Turbulent forced convection in channels and bundles: Theory and applications to Heat Exchangers and nuclear reactors, Advanced Study Institute Book, S. Kakac and D.B. Spalding, eds. Hemisphere (1978).

1.12 R. Semeria et al. 'Nuclear reactor safety: Panel workshop 6', Proc. 5th Int. Heat Tr. Conf., Tokyo (1976).

1.13 L. Prandtl, 'Über die ausgebildete Turbulenz', Proc. 2nd Intern. Congr. Appl. Mech., Zürich (1926).

1.14 S. Levy, 'Prediction of two-phase pressure drop and density distribution from mixing length theory', J. Ht. Transfer (1963).

1.15 S. Levy, 'Prediction of two-phase annular flow with liquid entrainment', Int. J. Heat and Mass Transfer, 9, 171 (1966).

1.16 F. Brandt, 'Der Reibungsdrick ver lust von Wasser-Dampf-Gemischen und der Voreilgeschwindigkeit des Dampfes gegenüber dem Wasser in senkrechten Kessel rohren'. Dissertation, University of Darmstadt (1958).

1.17 H. Fritz, 'Ein Mischungswegmodell für die vollturbulente adiabatische Nebelströmung mit randschicht', Dissertation, University of Karlsruhe (1969).

1.18 D.A. Sullivan, 'Two-phase annular flow in pipes: Analytic models', Thayer School of Engineering, Dartmouth College, report 27327-10 (1970).

1.19 Y. Sato et al., 'Momentum and heat transfer in two-phase bubble flow', Int. J. Multiphase Flow 7, 167 (1981).

1.20 D.A. Drew and R.T. Lahey, 'A mixing length model for turbulent two-phase flow', Trans ANS, 35, 624 (1980).

1.21 G. Biasi et al. 'Studies on film thickness and velocity distribution of two-phase annular flow', EUR 3765 (1968).

1.22 G.F. Hewitt and N.S. Hall-Taylor, 'Annular two-phase flow', Pergamon (1970).

1.23 E.R. Quandt, 'Measurement of some basic parameters of two-phase flow', A.I.Ch.E.J. 11, 311 (1965).

1.24 P. Alia et al., 'Phase and velocity distribution in two-phase adiabatic annular dispersed flow', CISE-R-109 (1966).

CHAPTER 2

THE OVERALL CONSERVATION EQUATIONS OF TWO-PHASE FLOW

A simplified presentation of the macroscopic ensemble averaged two-phase flow conservation equations is presented here as background to later chapters, which are primarily concerned with providing relations for various terms (shear, voidage, etc.) appearing in the conservation equations. Engineering requirements are for mean values of quantities such as wall shear at the boundary of the flowing two-phase mixture. The mixture conservation equations, averaged over the flow cross-section, incorporate these quantities. This chapter thus considers only a set of conservation equations for the mixture instead of a set for each phase of the mixture. More rigorous and more complete discussions of the two-phase conservation equations are given by Ishii [2.1] and Delhaye [2.2].

The two-phase mixture conservation equations are discussed for the parallel channel flow of a two-phase gas/liquid mixture, as shown in Fig. 2.1, considered as a realisation of a non-stationary random process. The phase at point $\underset{\sim}{r}$ is defined by the two binary variables $\delta_g(\underset{\sim}{r},t)$ and $\delta_\ell(\underset{\sim}{r},t)$ as follows:

State Variable	$\underset{\sim}{r}$ in gas at time t	$\underset{\sim}{r}$ in liquid at time t
$\delta_g(\underset{\sim}{r},t)$	1	0
$\delta_\ell(\underset{\sim}{r},t)$	0	1

Thus, $\delta_\ell(\underset{\sim}{r},t) = 1 - \delta_g(\underset{\sim}{r},t)$.

The voidage $\alpha(\underset{\sim}{r},t)$ is defined as the ensemble average $\overline{\delta_g(r,t)}$. If the flow of Fig. 2.1 is a realisation of a stationary random process,

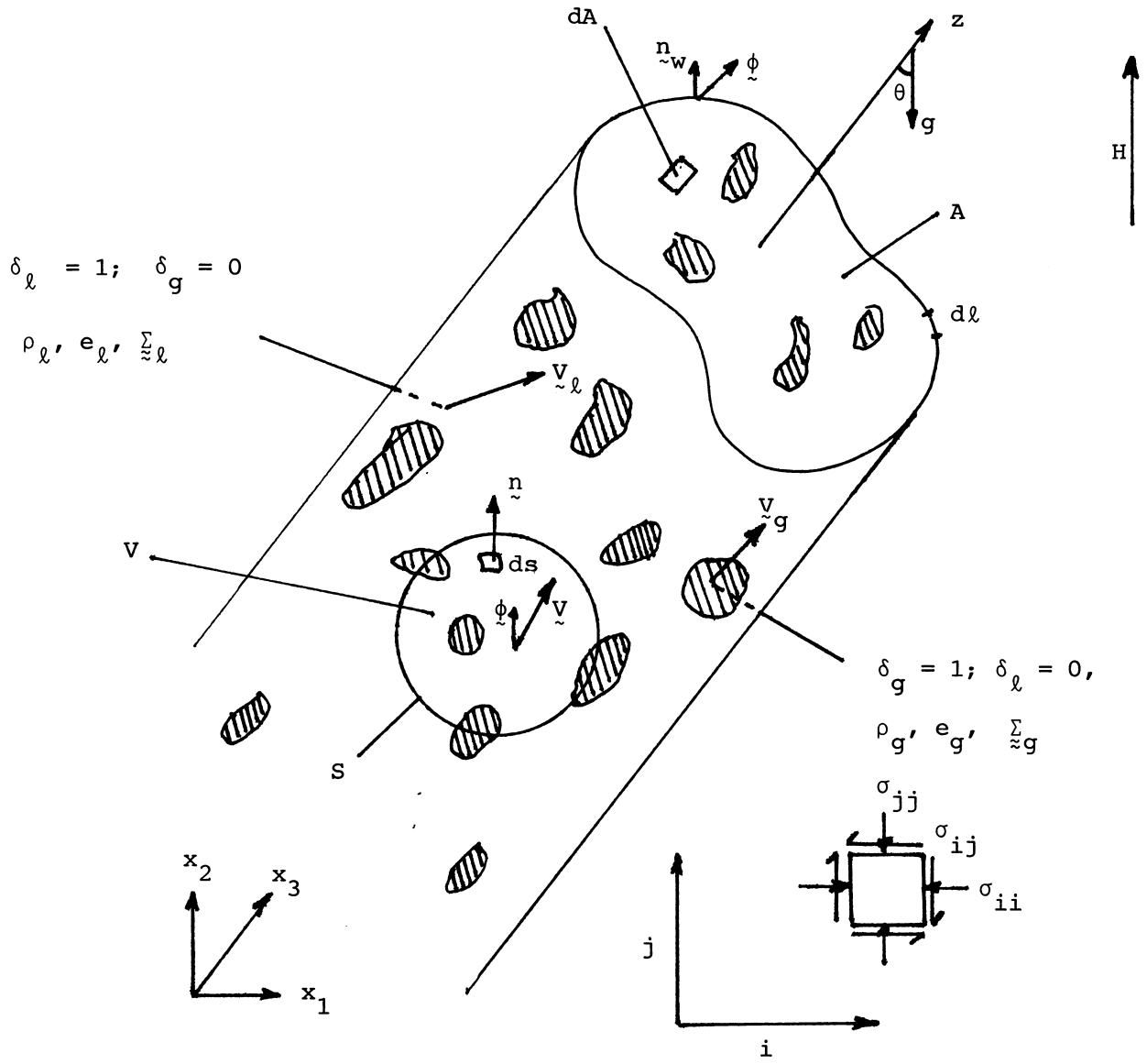

$$V = i_1 V_1 + i_2 V_2 + i_3 V_3$$

Fig. 2.1 Instantaneous local two-phase flow parameters

$$\overline{\delta_g(\underset{\sim}{r},t)} \quad = \quad \alpha(\underset{\sim}{r}).$$

If the stationary process is ergodic,

$$\alpha(\underset{\sim}{r}) \quad = \quad [\delta_g(\underset{\sim}{r},t)]$$

$$= \quad \text{time average of } \delta_g(\underset{\sim}{r},t)$$

i.e. the fraction of time that $\underset{\sim}{r}$ is in the gas phase.

At a point in the gas (liquid) phase, the state is defined by the specific internal energy $e_g(e_\ell)$, density $\rho_g(\rho_\ell)$, velocity vector $\underset{\sim}{V}_g(\underset{\sim}{V}_\ell)$, stress tensor $\underset{\approx}{\Sigma}_g(\underset{\approx}{\Sigma}_\ell)$ with components $(\sigma_g)_{ij}$ $((\sigma_\ell)_{ij})$ and heat flux vector $\underset{\sim}{\phi}$.

It is assumed that no sources or sinks for mass, momentum, or energy, exist, and the only body force for unit mass $\underset{\sim}{F}$ is due to gravity, and is defined in terms of the gravitational potential Ω via

$$\nabla \Omega \quad = \quad -\underset{\sim}{g}.$$

The conservation equations may be written in integral form for an arbitrary finite volume V, with surface s, and outward unit normal vector $\underset{\sim}{n}$ (component n_i). In the following it is assumed that the terms representing the surface tension contributions to the momentum and energy equations can be neglected.

Conservation of mass:

$$\frac{\partial}{\partial t}\int_V (\delta_g\rho_g + \delta_\ell\rho_\ell)\, dV + \int_S (\delta_g\rho_g(V_g)_i + \delta_\ell\rho_\ell(V_\ell)_i)\, n_i\, ds \qquad (2.1)$$

$$= \quad 0$$

Conservation of momentum:

$$\frac{\partial}{\partial t}\int_V (\delta_g\rho_g(V_g)_i + \delta_\ell\rho_\ell(V_\ell)_i)\, dV + \int_V (\delta_g\rho_g + \delta_\ell\rho_\ell)\frac{\partial\Omega}{\partial x_i}\, dV$$

$$+ \int_S (\delta_g(\sigma_g)_{ij} + \delta_\ell(\sigma_\ell)_{ij})\, n_j\, ds + \int_S (\delta_g\rho_g(V_g)_i(V_g)_j$$

$$+ \delta_\ell\rho_\ell(V_\ell)_i(V_\ell)_j)n_j\, ds \qquad = \quad 0 \qquad (2.2)$$

Conservation of energy:

$$\frac{\partial}{\partial t}\int_V \{\delta_g\rho_g(e_g + V_g^2/2 + \Omega) + \delta_\ell\rho_\ell(e_\ell + V_\ell^2/2 + \Omega)\}\, dv$$

$$+\int_S \{\delta_g\rho_g(V_g)_j\,(e_g + V_g^2/2 + \Omega) + \delta_\ell\rho_\ell(V_\ell)_j\,(e_g + V_g^2/2 + \phi)\}\, n_j\, ds$$

$$+\int_S (\delta_g\,(V_g)_i\,(\sigma_g)_{ij} + \delta_\ell(V_\ell)_i\,(\sigma_\ell)_{ij})\, n_j\, ds$$

$$+\int_S [\delta_g\,(\phi_g)_j + \delta_\ell(\phi_\ell)_i\,]\, n_j\, ds$$

$$= \quad 0 \qquad (2.3)$$

These equations may be modified to incorporate the specific enthalpy $h = e + P/\rho$ and the stress tensor decomposition $\sigma_{ij} = P\delta_{ij} + \tau_{ij}$ where τ_{ij} are the deviatoric (shear stress) components. The surface integrals become volume integrals using

$$\int_S X_{ij}\, n_j\, ds \quad = \quad \int_V \frac{\partial X_{ij}}{\partial x_j}\, dV.$$

On taking the ensemble averages, and using the fact that the volume V is arbitrary, the ensemble averaged point conservation equations of two-phase flow are obtained:

Mass:

$$\frac{\partial}{\partial t}\,(\alpha\,\overline{\rho}_g + (1-\alpha)\,\overline{\rho_\ell}) + \frac{\partial}{\partial x_j}\,(\alpha\,\overline{\rho_g(V_g)_j} + (1-\alpha)\,\overline{\rho_\ell\,(V_\ell)_j}) \quad = \quad 0. \qquad (2.4)$$

Momentum:

$$\frac{\partial}{\partial t}\,(\alpha\,\overline{\rho_g(V_g)_i} + (1-\alpha)\,\overline{\rho_\ell(V_\ell)_i}) + (\alpha\,\overline{\rho_g} + (1-\alpha)\,\overline{\rho_\ell})\,\frac{\partial\Omega}{\partial x_i}$$

$$+\frac{\partial}{\partial x_i}\,(\alpha\,\overline{P_g} + (1-\alpha)\,\overline{P_\ell}) + \frac{\partial}{\partial x_j}\,(\alpha\,(\overline{\tau_g})_{ij} + (1-\alpha)\,(\overline{\tau_\ell})_{ij})$$

$$+\frac{\partial}{\partial x_j}\,(\alpha\,\overline{\rho_g(V_g)_i(V_g)_j} + (1-\alpha)\,\overline{\rho_\ell\,(V_\ell)_i(V_\ell)_j})$$

$$= \quad 0. \qquad (2.5)$$

Energy:

$$\frac{\partial}{\partial t}\{\alpha\,\overline{\rho_g(h_g + V_g^2/2 + \Omega)} + (1-\alpha)\,\overline{\rho_\ell(h_\ell + V_\ell'/2 + \Omega)}\}$$

$$-\frac{\partial}{\partial t}(\alpha\,\overline{\rho_g} + (1-\alpha)\,\overline{\rho_\ell})$$

$$+\frac{\partial}{\partial x_j}\{\alpha\,\overline{\rho_g(V_g)_j\,(h_g + V_g^2/2 + \Omega)} + (1-\alpha)\,\overline{\rho_\ell(V_\ell)_j\,(h_\ell + V_g^2/2 + \Omega)}\}$$

$$+\frac{\partial}{\partial x_j}\{\alpha\,\overline{(V_g)_i\,(\tau_g)_{ij}} + (1-\alpha)\,\overline{(V_\ell)_i\,(\tau_\ell)_{ij}}\}$$

$$+\frac{\partial}{\partial x_j}\{\alpha\,\overline{(\phi_g)_j} + (1-\alpha)\,\overline{(\phi_\ell)_j}\}$$

$$= 0. \qquad (2.6)$$

On writing each variable X as $\bar{X} + X'$, the set of conservation equations give rise to a large number of double, triple, and quadruple correlations, most of which must be neglected. Those which must be retained correspond, in stationary random flows, to the time averaged double correlations representing significant turbulent shear stresses and heat fluxes, i.e.

$$\bar{\rho}\,\overline{(V)'_i\,(V)'_j} = (\tau)^*_{ij}$$

$$\text{and} \quad \bar{\rho}\,\overline{(V)'_i\,h'} = (\phi)^*_i\ ,$$

the above being defined for both phases.

For the parallel channel flow of Fig. 2.1, x_3 is identified with the axial co-ordinate z. The outward unit normal at the fixed channel boundary is $\underset{\sim}{n}_w$ and

$$\tau_{i3}\,(n_w)_i = \tau_w = \text{wall shear stress}$$

$$\phi_j\,(n_w)_j = \phi_w = \text{wall heat flux.}$$

Cross-section averaged conservation equations may now be derived from the above point conservation equations, using the definition

$$< X > \quad = \quad \frac{1}{A} \int_A X \, dA$$

The averaged equations given below assume further that τ_{zz} and τ_{zz}^* are negligible, and axial heat flow $\frac{\partial}{\partial z} (\phi_z + \phi_z^*)$ is negligible compared with transverse heat flow and axial heat transport. The equations use the notation u as being equivalent to and instead of the more cumbersome V_z. The bar implying ensemble averaged quantities is omitted for simplicity. The cross-section averaged conservation equations are:

Mass:

$$\frac{\partial}{\partial t} < \rho > + \frac{\partial}{\partial z} \{ < \rho_g \alpha u_g > + < \rho_\ell (1-\alpha) u_\ell > \} \quad = \quad 0 \qquad (2.7)$$

Momentum:

$$\frac{\partial}{\partial t} \{ < \alpha \rho_g u_g > + < \rho_\ell (1-\alpha) u_\ell > \} + g \cos \theta < \rho > + \frac{\partial}{\partial z} < P >$$

$$+ \frac{\partial}{\partial z} \{ < \rho_g \alpha u_g^2 > + < \rho_\ell (1-\alpha) u_\ell^2 > \} + \frac{1}{A} \int \tau_w \, d\ell \quad = \quad 0. \qquad (2.8)$$

Energy:

$$\frac{\partial}{\partial t} \{ < \alpha \rho_g (h_g + u_g^2/2) > + < \rho_\ell (1-\alpha) (h_\ell + u_\ell^2/2) + < \rho \Omega > - < P > \}$$

$$+ \frac{\partial}{\partial z} \{ < \alpha \rho_g u_g (h_g + u_g^2/2 + \Omega) > + < (1-\alpha) \rho_\ell u_\ell (h_\ell + u_\ell^2 + \Omega) > \}$$

$$+ \frac{1}{A} \int q_w \, d\ell \quad = \quad 0. \qquad (2.9)$$

In the above, $< P > \quad = \quad < \alpha P_g + (1-\alpha) P_\ell >$,

$< \rho > \quad = \quad < \alpha \rho_g + (1-\alpha) \rho_\ell >$

and $\Omega \quad = \quad g H.$

The term $\frac{1}{A}\int \tau_w \, d\ell$ of equation (2.8) represents the frictional pressure gradient $\frac{dP}{dz}\Big|_f$. It is often expressed in terms of a friction factor f, as with single phase flow,

$$\frac{dP}{dz}\Big|_f = \frac{4f}{D}\frac{1}{2}\rho u^2 , \qquad (2.10)$$

or in terms of a 'two-phase multiplier' ϕ^2_{LO} which is a factor by which a calculation of $\frac{dP}{dz}\Big|_f$ made by assuming the flow to be all liquid should be multiplied:

$$\phi^2_{LO} = \frac{dP}{dz}\Big|_f \Big/ \frac{dP}{dz}\Big|_{f_{LO}} . \qquad (2.11)$$

As with single phase flows, pressure losses due to local components such as bends, change in area, orifices etc., can be defined in terms of a loss coefficient K

$$\Delta P = K \rho u^2. \qquad (2.12)$$

The two-phase multiplier concept is also often used:

$$\Delta P = \phi^2_{LO} \Delta P_{LO} . \qquad (2.13)$$

The appropriate definition of ρ and u in equations (2.10) and (2.12) are discussed in chapters 3 and 4. In this work, loss coefficients are defined in terms of values of ρ and u upstream of the local component.

For later use, it is convenient to define, for channel flow, a number of additional combinations of local variables:

$$j_g = \alpha u_g; \qquad j_\ell = (1-\alpha) u_\ell$$

$$j = j_g + j_\ell \equiv \text{mixture velocity}$$

$$V_{g,\ell} = u_{g,\ell} - j \equiv \text{drift velocities.}$$

Useful combinations of cross-section average variables are

$$\text{Gas mass flux } G_g = \langle \alpha \rho_g u_g \rangle ;$$

Liquid mass flux $G_\ell = \langle (1-\alpha)\, \rho_\ell\, u_\ell \rangle$;

Total mass flux $G = G_g + G_\ell$;

Quality $x = G_g/G$;

Superficial gas, liquid, and mixture velocities

$\langle j_g \rangle$, $\langle j_\ell \rangle$, $\langle j \rangle$;

Gas volume flow ratio

$\beta = \langle j_g \rangle / \langle j \rangle$; and

Homogeneous density

$\rho_H = \rho_\ell\, (1-\beta) + \rho_g\, \beta$.

These cross-sectional averaged variables are those which can be most readily obtained through the use of simple monitoring equipment on two-phase flow systems.

Chapter 2 references

2.1 M. Ishii, 'Thermo-fluid dynamic theory of two-phase flow', Eyrolles (1975).

2.2 J.M. Delhaye, 'Equations fondamentales des ecoulements diphasiques', parts 1 and 2, CEA-R-3429 (1968).

CHAPTER 3

TWO-PHASE FLOW STRUCTURE

3.1 Some Considerations on Turbulence in Two-Phase Flows

In chapter 2, it was seen that the turbulent stress tensor τ^*_{ij} for two-phase flows is given by

$$\tau^*_{ij} = \alpha \rho_g \overline{(V_g)'_i (V_g)'_j} + (1-\alpha) \rho_\ell \overline{(V_\ell)'_i (V_\ell)'_j}. \qquad (3.1)$$

For developed axisymetric flows of constant physical properties in circular pipes (r,θ,z geometry), the important consequences of turbulence result from the $\tau^*_{r,z}$ component of the turbulent shear stress tensor:

$$\tau^*_{r,z} = \alpha \rho_g \overline{(V_g)'_r (V_g)'_z} + (1-\alpha) \rho_\ell \overline{(V_\ell)'_r (V_\ell)'_z}. \qquad (3.2)$$

In most cases of practical interest, two-phase flows may be regarded as simply connected regions of one phase (bubble, droplet) embedded in multiply connected regions of the other phase. For simplicity these will be defined as 'discontinuous phases' and 'continuous phases' respectively. Some flows (bubble, slug, froth, dry-wall-droplet) have the one phase continuous throughout the flow section. These will be referred to as 'continuous flows'. In others, such as annular flow, the phase comprising the continuous phase is different in different regions of the flow cross-section. Such flows will be referred to as 'separated flows'.

If equation 3.2 is to provide a basis for describing different flow structures in differing flow regimes, it must be able to be developed in different directions. In order to allow this, it is assumed that two-phase flows can be divided into macroscopic spacial regions in which turbulence is restricted to one phase only.

On the basis of this assumption, turbulent regions in two-phase

flow can be regarded as 'gas-phase turbulent', for which equation 3.2 reduces to

$$\tau^*_{r,z} = \alpha \rho_g \overline{(V_g)'_r (V_g)'_z} , \qquad (3.3)$$

or 'liquid-phase turbulent', in which case equation 3.2 becomes

$$\tau^*_{r,z} = (1-\alpha)\rho_\ell \overline{(V_\ell)'_r (V_\ell)'_z} . \qquad (3.4)$$

In order to comply with the assumption described above, contributions to the Reynolds stress from discontinuous elements of a two-phase system, that is, bubbles in bubble flow or droplets in droplet flow, are neglected.

With these assumptions, the applicability of equations (3.3) and (3.4) leads to a classification scheme as follows:

Flow type	Reynolds stresses	Conventional regime examples
Separated	3.3 near wall, 3.4 in core 3.4 near wall, 3.3 in core	Inverse annular Annular
Continuous	3.3 throughout 3.4 throughout	Droplet Bubble

3.2 Application of Classical Turbulence Techniques: Two-Phase Void Profile Equations

In the classical treatment of the single phase version of equation (3.2), i.e.

$$\tau^*_{r,z} = \rho \overline{V'_r V'_z} , \qquad (3.5)$$

assumptions are made which convert that equation to

$$u^* \equiv \sqrt{\tau_w/\rho} = \kappa y \frac{du}{dy} , \qquad (3.6)$$

where κ is the von Karman coefficient [3.1]. Integration of equation (3.6) results in the well-known logarithmic velocity defect equation.

The same classical assumptions applied to equations (3.3) and (3.4) result in

$$u^*_\ell = \sqrt{\tau_w/\rho_\ell} = (1-\alpha)^{\frac{1}{2}} \kappa_\ell y \frac{dj}{dy} \qquad (3.7)$$

(liquid-phase turbulent regions)

and

$$u^*_g = \sqrt{\tau_w/\rho_g} = \alpha^{\frac{1}{2}} \kappa_g y \frac{dj}{dy} \qquad (3.8)$$

(gas-phase turbulent regions)†.

For integration, equations (3.7) and (3.8) require some statement on the radial dependence of voidage. Noting that relationships

$$\frac{dj}{d\alpha} \propto (1-\alpha)^n \quad \text{(liquid phase turbulent regions)}$$

and $$\frac{dj}{d\alpha} \propto \alpha^n \quad \text{(gas phase turbulent regions)}$$

lead to simple integrations of equations (3.7) and (3.8), available data on phase and velocity profiles were examined in order to assess the validity of the above relations. These data indicate that the linear forms

$$\alpha = a_\ell j + b_\ell \quad \text{(liquid phase turbulent regions)} \qquad (3.9)$$

$$= a_g j + b_g \quad \text{(gas phase turbulent regions)}, \qquad (3.10)$$

with a, b being flow dependent but independent of y, describe available data. Typical examples are shown in figures 3.1 and 3.2.*

Although apparently significant in the present treatment, the coefficients a, b do not appear in expressions derived later for quantities such as wall shear stress, average void fraction, etc. This is because, as will be demonstrated in section 3.4, the mean void

† Detailed development of equations (3.7) and (3.8) in terms of mixing length concepts is given in appendix A1.

* The mixture velocity profile was not available for the data of fig. 3.1. The linear trend in fig. 3.1 suggests a similar linear α:j trend.

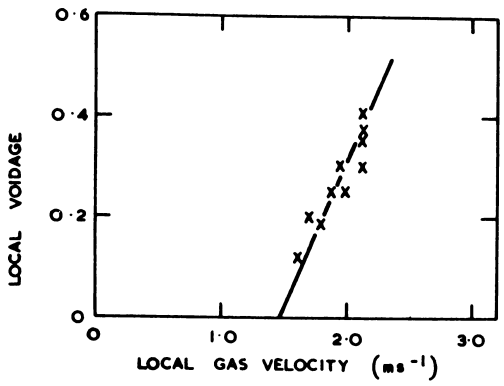

Fig. 3.1 Linear void-velocity relation, adiabatic steam-water liquid-phase turbulent flow, round tube, 80 mm ID, $P = 20.2 \times 10^5$ Pa, $G = 1000$ kg m^{-2}, s^{-1}, $\langle \alpha \rangle = 0.211$, data from [3.2].

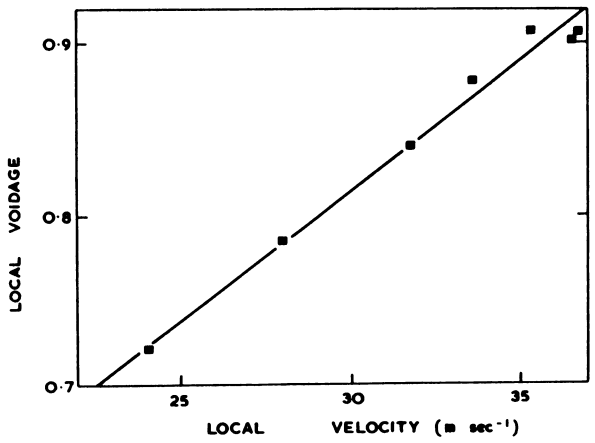

Fig. 3.2 Linear void-velocity relation, adiabatic steam-water gas-phase turbulent flow, round tube, 25.1 mm ID, $P = 5$ MPa, $G = 3799$ kg m^{-2} s^{-1}, $x = 0.155$, data from [3.3].

profile has only a second order influence on the mean velocity profile. For this reason, the actual assumptions introduced to render equations (3.7) and (3.8) integrable - in this case equations (3.9) and (3.10) - can be regarded as not critical in the evaluation of those two-phase flow quantities dependent on the mean velocity profile and this includes most quantities of interest. For the same reason, evaluation of the coefficients a, b has not been pursued in this work.

It is noted that a simpler version of equation (3.9), one of simple proportionality (i.e. $b_\ell = 0$), has proved useful in the drift-flux formulation of mean void fraction [3.4].

From equations (3.7 - 3.10),

$$(1-\alpha)^{3/2} = (1-\alpha_o)^{3/2} - \frac{3a_\ell u_\ell^*}{2\kappa_\ell} \ell n \frac{y}{y_o} \qquad (3.11)$$

(liquid phase turbulent regions)

and

$$\alpha^{3/2} = \alpha_o^{3/2} + \frac{3a_g u_g^*}{2\kappa_g} \ell n \frac{y}{y_o} \qquad (3.12)$$

(gas phase turbulent regions).

These 'void defect equations', named so in analogy with the velocity defect equation of single phase flow, are compared with typical data in figures (3.3) and (3.4). The corresponding void-velocity relations for these data have already been shown in figures (3.1) and (3.2).

It is seen that equations (3.11) and (3.12) are consistent with the data of figures (3.3) and (3.4). Further comparisons of the void defect equations are contained in appendix A1, where it is also demonstrated that the equations are more compatible with data than are the forms $\alpha/\alpha_c = 1 - (r/R)^n$ and $\alpha/\alpha_c = (y/R)^n$, often proposed in the literature.

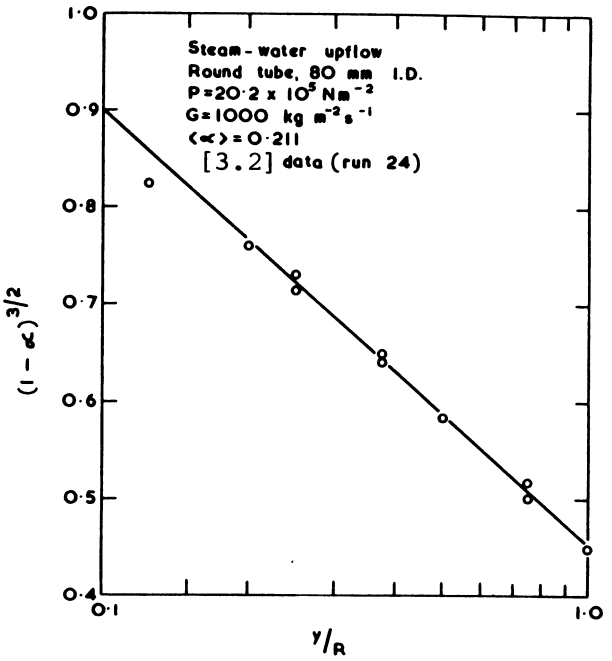

Fig. 3.3 Voidage defect plot, liquid-phase turbulent flow

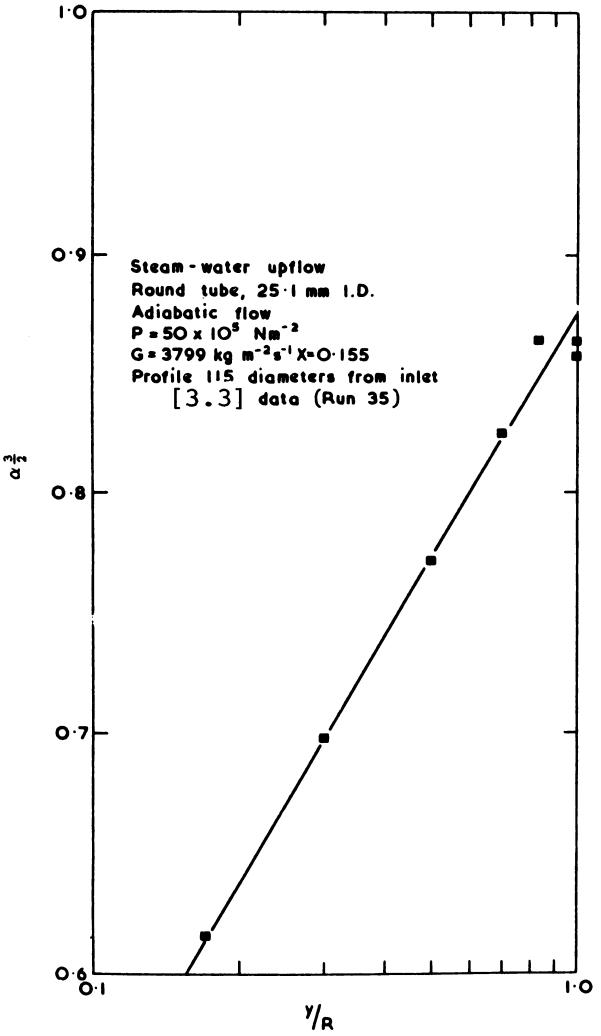

Fig. 3.4 Voidage defect plot, gas-phase turbulent flow

3.3 The Film Region of Annular Flow and a Point of Inflection Criterion

3.3.1 Film thickness definition

Although annular flow film thickness is often regarded as an important parameter [3.5], the actual thickness is not easy to determine experimentally. Wave contributions to the film; droplets in the core; and bubbles in the film give rise to an indistinct transition between the film and core regions. Electrically determined film thicknesses neglect film bubbles or include contributions from outer frothy regions which might more appropriately be considered as part of the core region.

As outlined in section 3.1, annular flow is considered here in terms of a liquid-phase turbulent film and a gas-phase turbulent core. Within this concept, void profile data, which cannot lead to meaningful film thickness data through qualitative examination [3.4], can be quantitatively examined in terms of equations (3.11) and (3.12) to produce simple interpretation of the data. The interpretation is based on the film (core) void profile being compatible with equation (3.11) (equation 3.12), and the interface is given by the intercept of the two equations.

3.3.2 A point of inflection criterion

Interpretation of annular flow void profiles as described above can be supplemented by an inflection point criterion. This criterion arises from equations (3.11) and (3.12) which contain inflection points at

$$y_{inf} = e^{-1/3} y_{\cdot} \quad , \tag{3.13}$$

where $y_{\cdot}$ represents an extreme position on the curves defined by

$$\alpha(y_{\cdot}) = 1 \quad \text{(liquid phase turbulent)}$$

$$\alpha(y_{\cdot}) = 0 \quad \text{(gas phase turbulent)}$$

The inflection point will occur outside the physically meaningful $0 < \alpha < 1$ range for the core region of an annular (or inverse annular) flow, but will occur in the range $0 < \alpha < 1$ for the turbulent region near the wall. Moreover, the inflection point in the equation may occur in the meaningful range $y_{inf} < R$. Equations (3.9) or (3.10) imply a corresponding velocity profile inflection. Velocity profiles containing inflections are unstable [3.7]. The inflection point position given by equation (3.13) may therefore be significant.

Annular flow void profile data [3.4, 3.8-3.12] indicate that the film boundary given by the intercept of equations (3.11) and (3.12) generally coincide with y_{inf} obtained from equation (3.13). An example is given in fig. 3.5.

Defining y_f as the film boundary position given by the intersect of equations (3.11) and (3.12), it is suggested that:

(1) $y_{inf} > R$ is a prerequisite for stable bubble or droplet flow;

(2) $y_{inf} = y_f$ defines a stable annular flow in which there is a balance between droplet entrainment and deposition;

(3) $y_{inf} < y_f$ implies an annular flow with a film that is larger than that required for developed conditions. The flow is unstable, with pressure fluctuations and slugging being associated with the instability. The inflection point suggests an inflection in the profile of some waves*. Waves with such an inflection (the roll waves of [3.5]) are the source of entrained droplets, and the entraining process continues until waves have no inflection points (i.e. are ripple waves) and $y_{inf} \simeq y_f$;

---

* This follows since, with negligible bubbles or droplets, void profiles are equivalent to film thickness probability distributions. Such distributions, e.g. [3.8-3.12] have been interpreted here as void profiles.

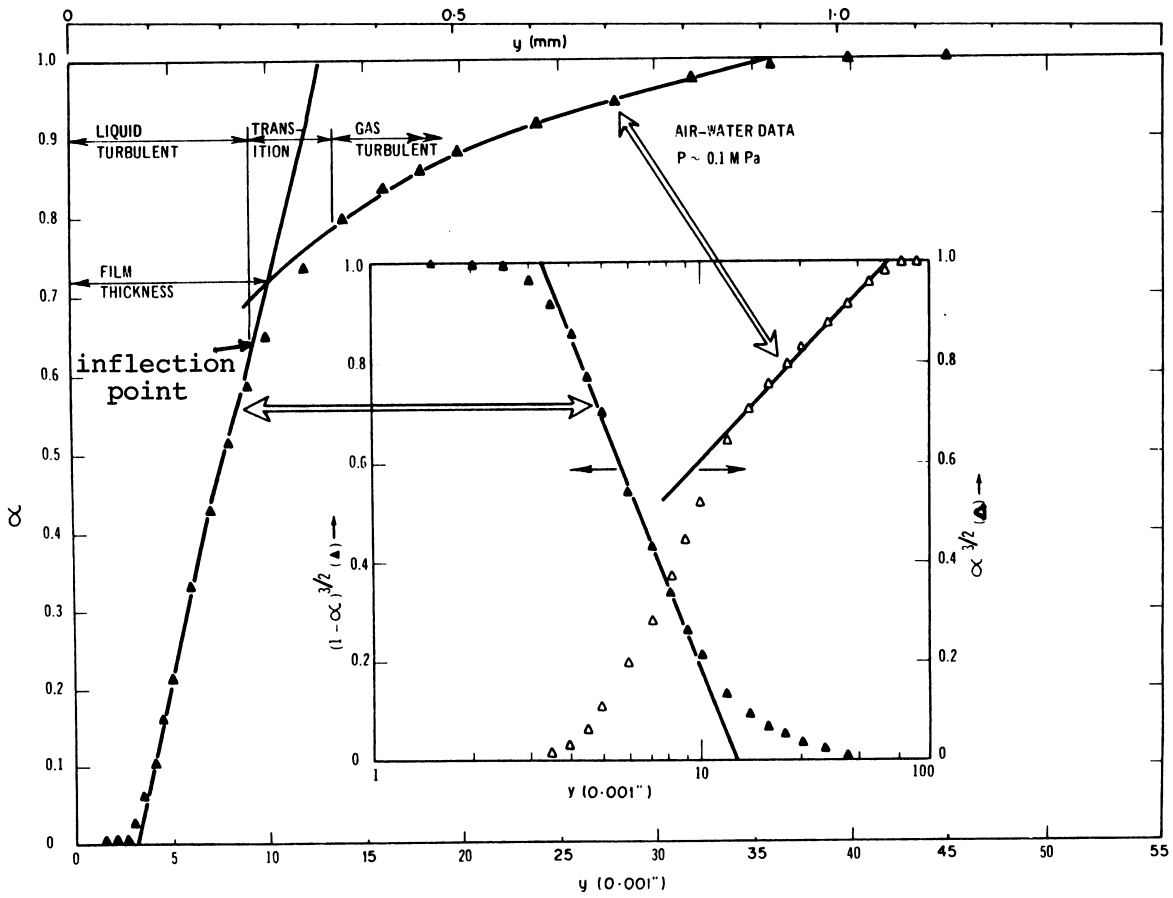

Fig. 3.5 Film region analysis of run 61 data of [3.8]

and

(4) $y_{inf} > y_f$ implies an annular flow with film that is thinner than that required for developed conditions. In this case, excess deposition occurs until the film is such that $y_{inf} \simeq y_f$.

3.4 The Velocity Defect Equation

From equations (3.9-3.12), the void and velocity profiles of two-phase flow depend on the coefficients a, b introduced to render equations (3.7) and (3.8) integrable. It is shown here that a, b only have a second order influence in the velocity profile.

Consider the void defect equation for liquid-turbulent conditions, equation (3.11). Linearising $(1-\alpha)^{3/2}$ about a suitable mean voidage, α_m:

$$(1-\alpha)^{3/2} = (1-\alpha_m)^{3/2} \left(1 - \frac{\alpha-\alpha_m}{1-\alpha_m}\right)^{3/2}$$

$$\cong (1-\alpha_m)^{3/2} - \frac{3}{2}(\alpha-\alpha_m)(1-\alpha_m)^{1/2},$$

and substituting equation (3.9) produces

$$j = j_o + \frac{1}{\kappa_\ell}\sqrt{\frac{\tau_w}{\rho_\ell(1-\alpha_m)}}\,\ell n\,\frac{y}{y_o}. \qquad (3.14)$$

Similar treatment for gas-phase turbulence produces

$$j = j_o + \frac{1}{\kappa_g}\sqrt{\frac{\tau_w}{\rho_g \alpha_m}}\,\ell n\,\frac{y}{y_o}. \qquad (3.15)$$

Annular flow velocity profile data in which data covers both the film and core regions [3.4] indicate that there is no change in velocity profile across the film/core interface. Indirect evidence for the above comes from the annular flow average voidage analyses given in section 5.3, where data support the supposition that the core region velocity profile also applies to the film region. As a result, equations (3.14) and (3.15) can be replaced by a single equation which

covers both separated (i.e. annular) and distributed (bubble, etc.) flow patterns:

$$j = j_o + \frac{j^*}{\kappa} \ln \frac{y}{y_o} \qquad (3.16)$$

where $j^* = \sqrt{\tau_w/\rho}$, with ρ being a suitably chosen mean density.

Equation (3.16) is of the same form as the well-known velocity defect equation of single phase flow. A typical velocity profile is compared with equation (3.16) in figure 3.6. The void defect equation and the void-velocity relation for these data have been shown in figs. 3.2 and 3.4.

3.5 Non-dimensional Velocity Profile

Two-phase flows are modelled here by a near-wall ($y < \delta$) viscous-dominated region together with a turbulent core ($y > \delta$), where δ defines the boundary between the viscous sublayer and turbulent core.

As with classical single phase turbulence theory, equations applicable to the sublayer are used to obtain boundary conditions for the velocity defect equation, equation (3.16), at $y = \delta$.

For this purpose, equation (3.16) is re-expressed as:

$$j = j_\delta + \frac{j^*}{\kappa} \ln \frac{y}{\delta} \qquad (3.17)$$

where $j^* = \sqrt{\tau_w/\rho_\delta}$.

In the more general case where the shear velocity is expressed in terms of a suitably chosen characteristic density ρ instead of ρ_δ, ρ may be chosen to ensure that the von Karman parameter κ takes its single phase value. However, the specific choice $\rho \equiv \rho_\delta$ in equation (3.17) may require values of κ for some flow regimes which differ from the single phase value. It is here supposed that κ as defined by equation (3.17), remains constant for a given flow regime.

The form of boundary conditions for equation (3.17) for different

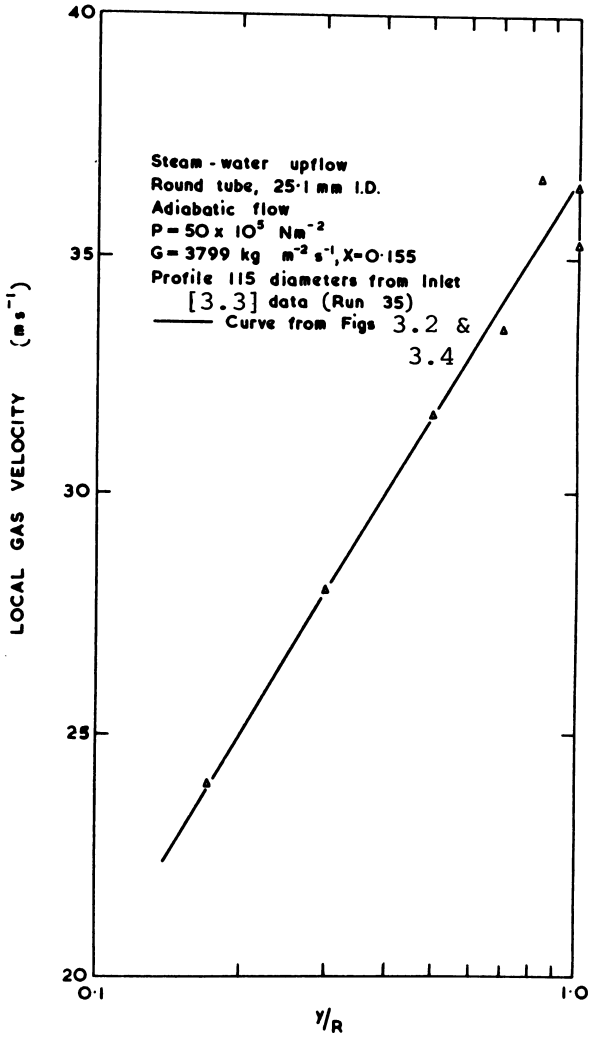

Fig. 3.6 Velocity defect plot, gas-phase turbulent flow

types of two-phase flow are obtained from adaptations of the classical turbulence theory boundary equations for the single phase flow velocity defect equation. The two-phase boundary conditions are described below.

3.5.1 Smooth tube flows

As with single phase flow, the sublayer stress for smooth tube flows is primarily due to viscous forces, and the sublayer velocity profile is obtained by considering the relationship between shear and velocity gradient. The two-phase viscosity is a function of both flow structure and of void fraction, and hence of position. The analysis is simplified by supposing that the sublayer can be modelled by two regions: an inner wall region of constant viscosity μ_w for which

$$\tau \simeq \tau_w = \mu_w \frac{dj}{dy} ,$$

and an outer region of constant viscosity μ_δ, for which

$$\tau \simeq \tau_w = \mu_\delta \frac{dj}{dy} .$$

If the extent of the inner-sublayer region is defined by y_{is}, these two equations can be re-arranged to yield the sublayer velocity profile

$$\left.\begin{aligned} j^+ \equiv j/j^* &= \frac{y\sqrt{\tau_w \rho_\delta}}{\mu_w} , \quad y < y_{is}, \\ &= \frac{\sqrt{\tau_w \rho_\delta}}{\mu_\delta} \left(y - y_{is}\,(1-\mu_\delta/\mu_w)\right), \\ &\qquad y_{is} < y < \delta \end{aligned}\right\} \qquad (3.18)$$

Adapting single phase concepts, it is assumed that the intercept between the sublayer and turbulent core velocity profiles is determined by an equation of the form

$$\frac{j_\delta}{\sqrt{\tau_w/\rho_s}} = c_1$$

where ρ_s is a characteristic sublayer density, suitable choice of which will ensure that c_1 has the same value as in single phase theory, i.e. 11.8. Re-expressing in terms of ρ_δ to suit the objectives of matching sublayer and turbulent core velocity profiles, the boundary condition can be expressed as

$$j_\delta^+ = j_\delta / \sqrt{\tau_w/\rho_\delta} = c_2 \qquad (3.19)$$

where c_2 may differ from the single phase value but is assumed to be constant for a given flow regime.

From equations (3.17), (3.18) and (3.19), the two-phase turbulent core velocity profile for smooth tube flows is of the form

$$j^+ \equiv j / \sqrt{\tau_w/\rho_\delta}$$

$$= (c_2 - \frac{1}{\kappa} \ell n\ c_2) + \frac{1}{\kappa} \ell n \left\{ \frac{\frac{y \sqrt{\tau_w \rho_\delta}}{\mu_\delta}}{1+y_{is}(1-\frac{\mu_\delta}{\mu_w}) \frac{\sqrt{\tau_w \rho_\delta}}{\mu_\delta}} \right\} \qquad (3.20)$$

3.5.2 Rough tube flows

Adopting single phase theory, we assume that if wall roughness elements are of sufficient magnitude for shear to depend on the roughness and not on the fluid viscosity, then the velocity at the characteristic roughness height ε is given by

$$\frac{j\ (y=\varepsilon)}{\sqrt{\tau_w/\rho_s}} = c_3$$

where c_3 is a constant, at least for a given flow regime, and ρ_s is a characteristic sublayer density. For ε as the 'equivalent sand roughness height', suitable choice of ρ_s will ensure that c_3 has the same value as in single phase theory, 8.6. Re-expressing the above in

terms of ρ_δ to suit the objective of matching sublayer and turbulent core velocity profiles, the boundary condition can be expressed as

$$\frac{j\ (y=\varepsilon)}{\sqrt{\tau_w/\rho_\delta}} = c_4 \qquad (3.21)$$

where c_4 may differ from the single phase value but is assumed to be constant for a given flow regime.

From equations (3.17) and (3.21), the two-phase turbulent core velocity profile for rough tube flow of roughness height ε is of the form

$$\frac{j}{\sqrt{\tau_w/\rho_\delta}} = c_4 + \frac{1}{\kappa} \ln \frac{y}{\varepsilon} \qquad (3.22)$$

3.6 Some Special Cases

As well as the unknown parameters c_2, c_4 and κ (assumed constant for a given flow regime), equations (3.20) and (3.25) contain other parameters, such as μ_δ and ρ_δ, for which equations must be given.

In this section, some special cases are considered. These cases do not exhaust all possible options, but have been found, in the present work, to cover most two-phase flows of interest to reactor engineering.

3.6.1 Smooth tube flows which may be characterised by a single sublayer viscosity

The form of equation (3.20) is such that strongly varying sublayer viscosities in smooth tube two-phase flows may be approximated by two-viscosity sublayers. Data analysis has indicated that two-region sublayers are not necessary to describe non-annular flows and annular flow with film thickness larger than the sublayer region: such flow may be characterised by a single sublayer viscosity μ_δ. Under these conditions, equation (3.20) becomes

$$j^+ = (c_2 - \frac{1}{\kappa} \ell n\ c_2) + \frac{1}{\kappa} \ell n \frac{y\sqrt{\tau_w \rho_\delta}}{\mu_\delta} \qquad (3.23)$$

Various options for μ_δ have been found necessary in the present work in order to allow for different sublayer structures:

(a) Bubbly sublayer in which surface movement does not occur:

$$\mu_\delta = \mu_\ell (1 + 2.5\beta) \qquad (3.24)$$

This form is based on Einstein's viscosity expression for solid spheres [3.13]. The local voidage at position δ is unknown and is assumed to be the same as the overall volume flow fraction, β. Although the assumptions behind Einstein's theory are such that it should not apply above about 5% local voidage, direct measurements of bubbly viscosity [3.14] have shown Einstein's equation to be applicable up to 25% voidage. The present work has shown equation (3.24) is valid for the present application of classical turbulence theory up to very high voidages. This appears to be due to an over-estimate of the viscous sublayer void fraction, taken as β, being compensated for by the coefficient 2.5, which data suggest is too low at high void fractions.

The treatment of bubbles as solid spheres is valid for some two-phase bubbly flows because impurities in systems with polar molecules migrate to bubble surfaces and inhibit surface movement.

(b) Bubbly sublayer in which surface movement may occur:

$$\mu_\delta = \mu_\ell \left(1 + \frac{2.5\ \mu_g + \mu_\ell}{\mu_g + \mu_\ell}\ \beta\right) \qquad (3.25)$$

This equation is based on Taylor's [3.15] extension of Einstein's [3.13] theory of viscosity to systems where solid spheres are replaced by bubbles. Taylor's theory allows for viscous dissipation in the gas within bubbles caused by movement of the surface of spherical bubbles.

(c) Sublayer which varies between liquid and gas:

$$\mu_\delta = \mu_\ell (1-\beta) + \mu_g \beta. \qquad (3.26)$$

This equation is proposed for annular flows with a wavy interface which extends to within the viscous sublayer region. It is based on the concept of a local viscosity at the outer edge of the sublayer intermittently changing between μ_ℓ and μ_g, with the intermittency fraction (i.e. local voidage) being assumed to be β.

(d) Dry wall sublayer

$$\mu_\delta = \mu_g.$$

The densities assumed appropriate to the above sublayer models are

$$\rho_\delta = \rho_\ell (1-\beta) + \rho_g \beta$$

for the two-phase sublayers (cases a, b, c), and

$$\rho_\delta = \rho_g$$

for the gas-only sublayer (case d).

3.6.2 Smooth tube flows with a strongly varying sublayer viscosity

The single sublayer viscosities considered above are not suitable for the description of thin film annular flows in which the film is entirely within the viscous sublayer. Such flows have a sublayer viscosity varying between μ_ℓ at the wall and μ_g at the outer region of the sublayer.

In this work, the general two-viscosity sublayer model of section 3.5.1 is used for the description of very thin film annular flows, with μ_ℓ being used for the inner sublayer viscosity up to a distance S corresponding to the film thickness, and μ_g being used for the outer sublayer region.

Adapting the results of section 3.5.1, the velocity profile for annular flows with film entirely within the sublayer is derived to be

$$j^+ = \frac{j}{\sqrt{\tau_w/\rho_g}} = \frac{y\sqrt{\tau_w \rho_g}}{\mu_\ell}, \qquad y < S,$$

$$= \frac{\sqrt{\tau_w \rho_g}}{\mu_g} (y - S(1 - \mu_g/\mu_\ell)),$$

$$S < y < y(j^+ = c_2),$$

$$= (c_2 - \frac{1}{\kappa} \ell n\, c_2) + \frac{1}{\kappa} \ell n \left\{ \frac{\frac{y\sqrt{\tau_w \rho_g}}{\mu_g}}{1 + S(1 - \frac{\mu_g}{\mu_\ell}) \frac{\sqrt{\tau_w \rho_g}}{\mu_g c_2}} \right\}, \qquad (3.27)$$

$$y > y\ (j^+ = c_2).$$

It will be noted that, unlike the case for the single viscosity sub-layer models of section 3.6.1, the core region velocity profiles of thin film annular flows vary with film thickness S. The film thickness S may be obtained from the liquid volume fraction $1-\langle\alpha\rangle$ ($\simeq 4S/D$). A method of calculating $1-\langle\alpha\rangle$ for annular flows is given in chapter 5.

3.6.3 'Rough' wall flows where the roughness is due to attached wall bubbles

Bubbles attached to walls due to heat transfer or flashing may act on the flow in a similar manner to wall roughness elements. The velocity profile equation for rough walls, equation (3.27), should apply if the roughness ε of equation (3.27) is replaced by the size of the largest attached wall bubbles.

Adapting the attached wall bubble force balance analysis of Staub [3.16]*, the dominant forces acting on a bubble of diameter d

---

* The approach of Staub appears invalid near the heat transfer crisis since heat transfer effects prevent bubbles growing to a size where shear forces remove them from the wall. Such bubbles are analysed in chapter 8 from a heat transfer viewpoint.

are the surface tension force F_σ holding the bubble to the wall,

$$F_\sigma \sim d\sigma$$

and an opposing shear force F_τ tending to drag the bubble from the wall

$$F_\tau \sim \tau_w d^2.$$

Other forces (for example, gravity) on attached wall bubbles can be neglected for flow conditions of interest in reactor engineering.

Since wall bubbles will grow until the shear force is sufficient to overcome the surface tension force, the bubble breakaway diameter d_d is then given when $F_\tau = F_\sigma$, i.e. when

$$d_d \sim \sigma/\tau_w.$$

It is now assumed that the above equation is completed by a proportionality constant. Replacing ε of equation (3.22) by d_d, and rearranging leads to

$$\frac{j}{\sqrt{\tau_w/\rho_\delta}} = c_4' + \frac{1}{\kappa} \ell n \frac{y \tau_w}{\sigma} \qquad (3.28)$$

where c_4' incorporates the assumed proportionality constant of the above d_d relation.

As with the two-phase sublayer analysis of section 3.6.1, it is now assumed that, for the purposes of analysing surface-tension dependent velocity profiles in terms of equation 3.32,

$$\rho_\delta = \rho_\ell(1-\beta) + \rho_g\beta.$$

3.7 Non-dimensional Velocity Profile in Terms of Global Dimensionless Groups

The velocity profile expressions of section 3.6 were presented in terms of local non-dimensional velocity $j^+ = \frac{j}{\sqrt{\tau_w/\rho_\delta}}$ as a function of dimensionless wall distance $y^+ = \frac{y\sqrt{\tau_w\rho_\delta}}{\mu_\delta}$ or, in the case of flows with

attached wall bubbles (section 3.6.3), $y^+ = y\,\tau_w/\sigma$. In all cases the core region velocity profile could be expressed in the form

$$j^+ = a\,\ell n\,y^+ + b. \qquad (3.29)$$

In the next chapter, the core region non-dimensional velocity profile is averaged over the flow section to yield expressions for friction factor

$$f = \tau_w/(2\,\rho_\delta < j >^2)$$

in terms of Reynolds number $Re = \rho_\delta\,D/\mu_\delta$ or Weber number $We = \rho_\delta < j >^2 D/\sigma$. It is therefore convenient to express the equations relating the local dimensionless parameters j^+ and y^+ in terms of the overall dimensionless groups f, Re and We through the transformations

$$j^+ = \frac{j}{\sqrt{\tau_w/\rho_\delta}} = \frac{j}{< j >}\sqrt{\frac{2}{f}}$$

and

$$y^+ = \frac{y\sqrt{\tau_w \rho_\delta}}{\mu_\delta} = \frac{y}{R}\,\frac{Re}{2}\sqrt{\frac{f}{2}}$$

or

$$y^+ = \frac{y\,\tau_w}{\sigma} = \frac{y}{R}\,We\,\frac{f}{2}\,.$$

To this group a dimensionless film thickness

$$S^+ = \frac{S\sqrt{\tau_w \rho_\delta}}{\mu_\delta} = \frac{S}{R}\,\frac{Re}{2}\sqrt{\frac{f}{2}}$$

is added to facilitate the analysis for very thin film flows (section 3.6.2).

The special cases considered in section 3.6 are summarised in table 3.1. For convenience, the subscript δ is omitted in the notation for the density and viscosity values at the edge of the turbulent core, i.e. ρ and μ are used instead of ρ_δ and μ_δ.

Table 3.1 Dimensionless group definitions for various two-phase flows

$$\left(j^+ = \frac{j}{\langle j\rangle}\sqrt{\frac{2}{f}},\ f = \frac{D(dP/dz)_f}{2\rho\langle j\rangle^2},\ Re = \frac{\rho D\langle j\rangle}{\mu},\ We = \frac{\rho\langle j\rangle^2 D}{\sigma}\right)$$

Sublayer type	Core region velocity profile
Viscosity dependent flows (a,b,c,d)	$j^+ = a\ \ell n\ y^+ + b,\ y^+ = \frac{y}{R}\frac{Re}{2}\sqrt{\frac{f}{2}}$
Surface-tension dependent flows (e)	$j^+ = a\ \ell n\ y^+ + b,\ y^+ = \frac{y}{R}\,We\,\frac{f}{2}$
Film thickness dependent flows (f)	$j^+ = a\ \ell n\ [y^+(1+S^+(1-\frac{\mu_g}{\mu_\ell}))^{-1}] + b,$ $y^+, S^+ = \frac{y,S}{R}\ \frac{Re}{2}\sqrt{\frac{f}{2}}$

Sublayer notation/ type	Density definition	Viscosity definition
a. Rigid surface bubbles	$\rho = \rho_\ell(1-\beta) + \rho_g\,\beta$	$\mu = \mu_\ell\ (1 + 2.5\ \beta)$
b. Non-rigid surface bubbles	$\rho = \rho_\ell(1-\beta) + \rho_g\,\beta$	$\mu = \mu_\ell\ (1 + \frac{2.5\ \mu_g+\mu_\ell}{\mu_g + \mu_\ell}\ \beta)$
c. Wavy gas/liquid interface	$\rho = \rho_\ell(1-\beta) + \rho_g\,\beta$	$\mu = \mu_\ell\ (1-\beta) + \mu_g\,\beta$
d. Dry wall	$\rho = \rho_g$	$\mu = \mu_g$
e. Attached wall bubbles	$\rho = \rho_\ell(1-\beta) + \rho_g\,\beta$	N.A.
f. Very thin film	$\rho = \rho_g$	$\mu = \mu_g$

3.8 Data Analysis

As indicated in section 3.6, the coefficients a,b in the two-phase non-dimensional velocity profile

$$j^+ = a \ln y^+ + b \qquad (3.30)$$

are expected to have different values for different flow regimes if dimensionless groups are as defined in table 3.1. Analysis of two-phase velocity profile data* obtained from the literature and which also had corresponding shear stress data (in order to obtain valid j^+ and y^+ values) indicated that this was generally so, except for very thin film flows (type (f) in table 3.1); data could be grouped into 'friction regimes', each of which could be characterised by (i) a sublayer type as described in table 3.1 and (ii) specific values of a, b in equation (3.30). Attempts to further interpret data pertaining to very thin film flows were not pursued since flows of this type rarely occur in conditions relevant to reactor engineering.

Examination of the various non-dimensional velocity profiles of the form of equation (3.30), as obtained from the grouping of data into different friction regimes, produced the unexpected result that, within data scatter, various empirical values of the coefficient 'a' of equation (3.30) were found to be elements of a simple geometric progression with factor $\sqrt{2}$, and that, for each value of 'a', various values of 'b' were possible and these were found to be elements of simple arithmetic progressions with differences being proportional to the coefficient 'a'.

---

* The velocity data were analysed subsequent to the analyses of wall shear stress data presented in the next chapter. Generalised equations presented here were inferred from the results of the wall shear data analysis.

Further examination showed that, within experimental data scatter, the various empirically obtained non-dimensional velocity profiles could mostly be generated from generalised equations:

$$j^+ = (\sqrt{2})^{m+5} \{\log y^+ - 0.60\ m - 0.50\ n - 0.10\} , \quad (3.31)$$

for Reynolds number dependent flows apart from very thin film flows (i.e. types a - d of table 3.1), and

$$j^+ = (\sqrt{2})^{m+5} \{\log y^+ - 0.45\ m - 0.15\ n + 1.91\} , \quad (3.32)$$

for Weber number dependent flows (type e of table 3.1), using integer values of m and n. Exceptions to the above were rarely found, and most exceptions conformed to the general pattern if half-integer values were used for m and/or n in equations (3.31) or (3.32).

Some examples of non-dimensional velocity profile are shown in figs. 3.7 and 3.8. Figure 3.7 shows data for 3 friction regimes obtained as part of an experimental examination of hydrodynamics of argon-alcohol flows performed at CISE laboratories [3.17], and fig. 3.8 data were obtained from [3.18, 3.19].

The argon-alcohol data are viscosity dependent, cover a gas density range $10 < \rho_g < 36$ kg m^{-3}, and were obtained with a 25 mm tube. Fig.3.7a covers very high gas velocities ($\langle j_g \rangle > 15$ m s^{-1}); fig. 3.7b is for conditions approximated by $6 < \langle j_g \rangle < 15$ m s^{-1} and $0.3 < \langle j_\ell \rangle < 1$ m s^{-1}; and fig. 3.7c for $\langle j_\ell \rangle > 1$ m s^{-1} and $6 < \langle j_g \rangle < 15$ m s^{-1}.

The dimensionless group definitions for figures 3.7a, 3.7b and 3.7c are given by types d, c and b of table 3.1 respectively. The core region velocity profiles of figure 3.7 a-c are special cases of equation (3.31) with (m,n) values respectively (0,0), (4,1) and (3,-1) respectively. The near wall region data of figure 3.7b is consistent with the viscous sublayer equation $j^+ = y^+$ supposed by the model, and fig. 3.7c has a 'buffer' region, also consistent with equation (3.31)

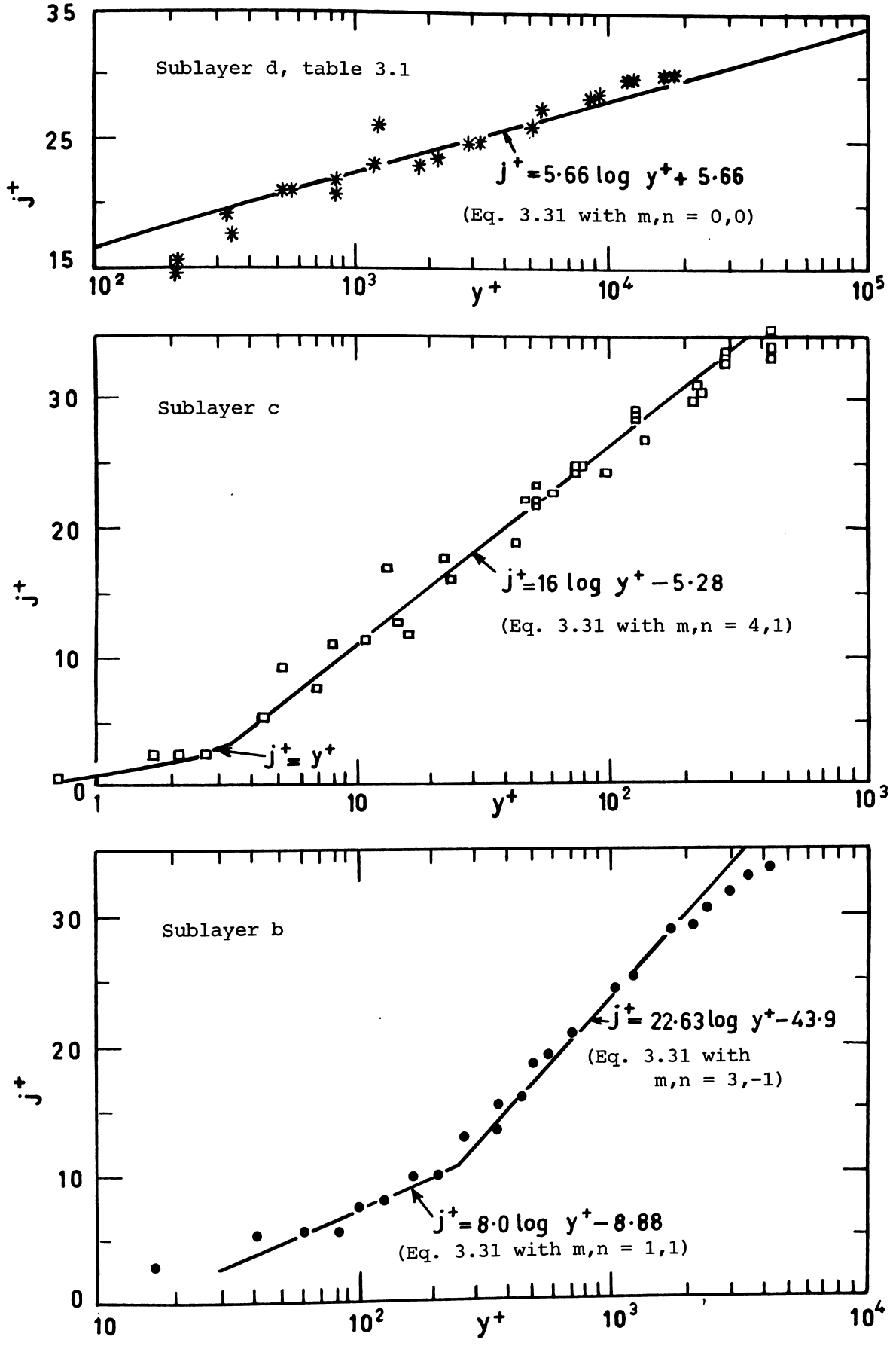

Fig. 3.7. Non-dimensional velocity profiles for argon-alcohol data of [3.17]

but with (m,n) = (1,1).

Figure 3.8 shows some velocity profiles from [3.18, 3.19] for adiabatic steam-water upflow in a 17.1 mm tube at a density ratio $\rho_\ell/\rho_g = 13$. The data are consistent with equation (3.32) with (m,n) = (2,-4).

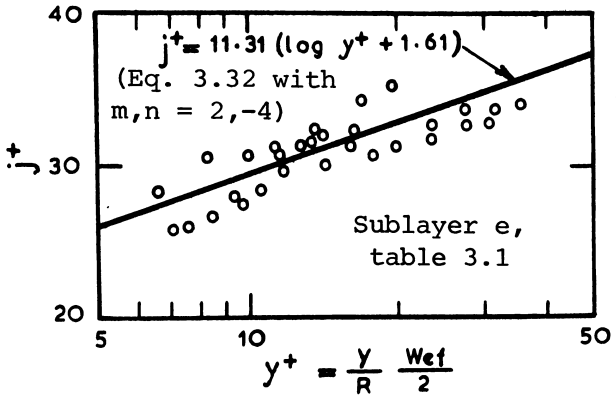

Fig. 3.8 Adiabatic steam-water velocity profiles, $\rho_\ell/\rho_g = 13$. Data from [3.18, 3.19].

The data of figs. (3.7) and (3.10) represent typical viscosity-dependent and surface tension-dependent flows and are presented here because they have associated pressure loss and average void profile data, thus enabling further consequences of the model presented here to be tested against these other data. This will be done in later chapters.

Analyses of other typical viscosity-dependent and surface tension-dependent velocity profiles can be found in appendices A1, A2, A6, A10, A24.

As stated, the form of non-dimensional velocity profile for film thickness dependent flows (type f of table 3.1) has not been satisfactorily resolved in this work. However, film thickness-dependent velocity profile data of [3.20] are consistent with the velocity defect equation, equation (3.16), supposed here to be applicable to these flows.

3.9 Friction Regime Classification Method

The previous section indicates that a viscosity-dependent or surface tension-dependent velocity profile can be obtained from equation (3.31) or (3.32) if m and n are known for the particular regime and if the sublayer type as given in table (3.1) is known.

For the remainder of this work, a notation of the form (z,m,n), in which z is alphabetic and m and n are integers, will respectively indicate the appropriate sublayer type of table 3.1 and relevant m and n values of equation (3.31) or (3.32). The triad (z,m,n) thus specifies a friction regime.

The triad is not sufficient to specify a flow completely. It will be seen in chapter 5, for example, that the triad is necessary but not sufficient to calculate average void fractions.

In terms of this classification, the data of figures 3.7a,b,c and 3.8 are respectively denoted by (d,0,0), (c,4,1), (b,3,-1) and (e,2,-4).

3.10 Re-expression in Terms of Generalised Dimensionless Groups

The coefficients 0.60, 0.50, 0.45 and 0.15 in equations (3.31) and (3.32):

$$j^+ = \sqrt{2}^{\,m+5} \{\log y^+ - 0.60\, m - 0.50\, n + 1.0\} \qquad (3.31)$$

and

$$j^+ = \sqrt{2}^{\,m+5} \{\log y^+ - 0.45\, m - 0.15\, n + 1.91\} \qquad (3.32)$$

are sufficiently close to $\log(\sqrt{2})^4$, $\log \sqrt{10}$, $\log(\sqrt{2})^3$ and $\log \sqrt{2}$ for differences to be insignificant. The equations can thus be re-expressed as

$$\frac{j}{\sqrt{\dfrac{(\tau_w \sqrt{2}^{-3m})}{(\rho \sqrt{2}^{-5m})}}} = \sqrt{2}^{\,5} \left\{ \log \frac{y \sqrt{(\tau_w \sqrt{2}^{-3m})(\rho \sqrt{2}^{-5m})}}{(\mu \sqrt{10}^{\,n})} + 1.0 \right\} \qquad (3.31a)$$

and

$$\frac{j}{\sqrt{\frac{\tau_w \sqrt{2}^{-3m}}{\rho \sqrt{2}^{-5m}}}} = \sqrt{2}^{5} \left\{ \log \frac{2\, y\, (\tau_w \sqrt{2}^{-3m})}{(\sigma \sqrt{2}^{n})} + 1.91 \right\} , \tag{3.32a}$$

or

$$\frac{j}{\sqrt{\frac{\tau_w'}{\rho'}}} = \sqrt{2}^{5} \left\{ \log \frac{y \sqrt{\tau_w' \rho'}}{\mu'} + 1.0 \right\} , \tag{3.33}$$

and

$$\frac{j}{\sqrt{\frac{\tau_w'}{\rho'}}} = \sqrt{2}^{5} \left\{ \log \frac{2\, y\, \tau_w'}{\sigma'} + 1.91 \right\} . \tag{3.34}$$

Thus, equations (3.31) and (3.32), which are generalised equations relating specific j^+ and y^+ parameters

$$j^+ = j/\sqrt{\tau_w/\rho} = \frac{j}{\langle j \rangle} \sqrt{\frac{2}{f}}$$

and $$y^+ = y\sqrt{\tau_w \rho}/\mu = \frac{y}{R} \frac{Re}{2} \sqrt{\frac{f}{2}}$$

or $$y^+ = 2y\, \tau_w/\sigma = \frac{y}{R} We \frac{f}{2} ,$$

where $Re = \frac{\rho \langle j \rangle D}{\mu}$, $f = \frac{2\tau_w}{\rho \langle j \rangle^2}$ and $We = \frac{\rho \langle j \rangle^2 D}{\sigma}$

have been converted to specific equations (equations (3.33) and (3.34)) relating generalised $j^{+'}$ and $y^{+'}$ dimensionless groups

$$j^{+'} = j/\sqrt{\tau_w'/\rho'} = \frac{j}{\langle j \rangle} \sqrt{\frac{2}{f'}}$$

and $$y^{+'} = y\sqrt{\tau_w' \rho'/\mu'} = \frac{y}{R} \frac{Re'}{2} \sqrt{\frac{f'}{2}}$$

or $$y^+ = 2y\, \tau_w'/\sigma = \frac{y}{R} We' \frac{f'}{2} ,$$

where $Re' = \frac{\rho'\langle j\rangle D}{\mu'}$, $f' = \frac{2\tau_w'}{\rho'\langle j\rangle^2}$ and $We^2 = \frac{\rho'\langle j\rangle D}{\sigma'}$.

The generalised parameters ρ', τ_w', μ' and σ' are related to ρ, τ_w, μ and σ by

$$\rho' = \rho \sqrt{2}^{-5m}$$

$$\tau_w' = \tau \sqrt{2}^{-3m}$$

$$\mu' = \mu \sqrt{10}^{n}$$

and $$\sigma' = \sigma \sqrt{2}^{n}.$$

This presentation of the equations appears significant because

- the apparently arbitrary coefficients of equations (3.31) and (3.32) are shown to be simply related;
- equation (3.33) is of the form of the core region component of the universal velocity profile; and
- the factor $\sqrt{2}$ differs by only 1% from the factor $e^{1/3}$ which appeared in the point of inflection criterion (section 3.3) resulting from turbulent velocity profile stability considerations. It is thus plausible that this factor may appear in generalised velocity profile expressions.

Although the formulation in terms of equations (3.33) and (3.34) appears possibly significant, this significance (if any) has not been discovered in the course of the present work.

Chapter 3 References

3.1 H. Schlichting, 'Boundary layer theory', McGraw-Hill, 6th Edn., Chapter XIX.

3.2 D. Malnes, 'Slip ratios and friction factors in the bubble flow regime in vertical tubes', KR-110 (1966).

3.3 N. Adorni et al., 'Large scale experiments on heat transfer and hydraulics with steam-water mixtures: Phase and velocity distribution measurements in a round vertical tube', CISE-R-91 (1964).

3.4 N. Zuber et al., 'Steady state and transient void fraction in two-phase flow systems', GEAP-5416 (1967).

3.5 G.F. Hewitt and N.S. Hall-Taylor, 'Annular two-phase flow', Pergamon (1970).

3.6 P. Alia et al., 'Phase and velocity distribution in two-phase adiabatic annular dispersed flow', CISE-R-109 (1966).

3.7 H. Schlichting, Ibid, p.445.

3.8 D. Webb, 'Studies of the characteristics of downward annular two-phase flow', AERE-R 6426 pt.5 (1970).

3.9 J. Würtz, 'An experimental and theoretical investigation of annular steam-water flow in tubes and annuli at 30-90 bar', RISO-372 (1978).

3.10 P.L. Kirillov et al., 'Measurement of some characteristics of steam-water flow in round tubes at a pressure of 68.6 bar', FEI-421 (1973).

3.11 D. Butterworth, 'Air-water, annular flow in a horizontal tube', AERE-R-6687 (1971).

3.12 G. Valleggi and S. Zanelli, 'On the characteristics of wavy liquid film flowing downwards on a vertical wall', University of Pisa report R74-01 (1974).

3.13 A. Einstein, 'A new determination of molecular dimensions', Ann. Phys. 19, 289 (1906).

3.14 J. Huige and M. Ohki, 'The relationship between the apparent coefficient of viscosity and the void fraction in two-phase flow of mixtures of gas and liquid', Trans. Jap. Soc. Mech. Engng. 37, 97 (1971).

3.15 G.I. Taylor, 'The viscosity of a fluid containing small drops of another fluid', Proc. Roy. Soc. (London) 138, 41 (1932).

3.16 F.W. Staub, 'The void fraction in subcooled boiling - Prediction of the initial point of net vapor generation', Journal of Heat Transfer, 10, 951 (1967).

3.17 P. Alia et al., CISE reports R82, R93, R109.

3.18 P.L. Kirillov et al., 'Calculating the hydraulic losses in an adiabatic high pressure steam-water flow', Thl. Engng. 24, 10, 41 (1977).

3.19 V.I. Subbotin et al., 'Measurement of some characteristics of a steam-water flow in a round tube at pressures of 70 and 100 atm', ASME paper WA-75/HT 21 (1975).

3.20 L.I. Gill et al., 'Sampling probe studies of the gas core in annular two-phase flow: 11 Studies of the effect of phase flowrates on phase and velocity distribution', AERE-R-3955 (1963).

CHAPTER 4

FRICTION FACTOR EXPRESSIONS FOR TWO-PHASE FLOW

4.1 Duct Flow Losses

Round tube friction factor equations are obtained by integrating turbulent core non-dimensional velocity profile equations over the total flow area. As with single phase flow, the two-phase flow results so obtained are assumed to extend to non-circular geometries if the diameter term in dimensionless groups is replaced by the equivalent hydraulic diameter (4 x flow area/sheared perimeter).

The results of this procedure are summarised in table 4.1. The three equations in this table are integrations of velocity profiles given by equations (3.31), (3.32) and (3.28). Equation (4.3) is given only in general form because, as stated in chapter 3, a full analysis of flows dependent on film thickness, which would have resulted in the empirical determination of unknown coefficients in equation (4.3), was not achieved in this work.

Table 4.1 Wall Shear Stresses for a Given Friction Regime (z,m,n)

(Dimensionless groups are defined in section 3.7)

Sublayer type	Friction factor relation	Equation
Viscosity dependent flows (a,b,c,d)	$\frac{1}{\sqrt{f}} = \sqrt{2}^{m+4} \{\log Re\sqrt{f} - 0.60m - 0.50n - 0.10\}$	4.1
Surface tension dependent flows (e)	$\frac{1}{\sqrt{f}} = \sqrt{2}^{m+4} \{\log Wef - 0.45m - 0.15n + 0.96\}$	4.2
Film thickness dependent flows (f)	$\frac{1}{\sqrt{f}} = a - b \log \left(\frac{1}{Re\sqrt{f}} + \frac{1}{c\sqrt{2}} \frac{S}{D} \left(1 - \frac{\mu_g}{\mu_\ell}\right)\right)$	4.3

4.2 Re-expression in Terms of Generalised Dimensionless Groups

Equations (4.1) and (4.2) are generalised equations relating specific dimensionless groups. Through the same transformation procedure described in section 3.10, these general equations may be transformed into specific equations relating the generalised Reynolds number Re' or Weber number We' described in section 3.10. The results are summarised in table 4.2. The same results are obtained by integrating the dimensionless velocity profile equations, equations (3.33) and (3.34), over the flow cross-section of a round tube. It is noted that equation (4.4) is of single phase flow form.

Table 4.2 Wall Shear Stresses for a Given Friction Regime (z,m,n)

(Dimensionless groups are defined in section 3.10)

Sublayer type	Friction factor relation	Equation
Viscosity dependent flows (a,b,c,d)	$\frac{1}{\sqrt{f'}} = 4 \log Re' \sqrt{f'} - 0.4$	4.4
Surface tension dependent flows (e)	$\frac{1}{\sqrt{f'}} = 4 (\log We'f' + 0.96)$	4.5
$f' = 2^m f$, $Re' = \sqrt{2}^{-5m} \sqrt{10}^{-n} Re$, $We' = \sqrt{2}^{-(5m+n)} We$		4.6

4.3 Obstruction Loss Coefficient

As discussed, the single phase friction factor $f = \tau_w / \frac{1}{2}\rho v^2$: Reynolds number $Re = \rho vD/\mu$ relation also applies to two-phase flows if the two-phase friction factor and Reynolds number are appropriately defined. For wet wall flows, this involves defining ρ and v in terms of homogeneous values ρ_H and $\langle j \rangle$; and defining μ according to the nature of the sublayer (table 3.1).

It is assumed that, for local losses (obstructions, contractions, etc.), empirical single phase loss coefficient $K = \Delta P / \frac{1}{2}\rho v^2$: Reynolds

number relations similarly extend to the two-phase situation if physical properties in the two-phase loss coefficient and Reynolds number are defined according to sublayer structure as indicated in table 3.1.

The loss coefficient defined above may be referenced to either upstream or downstream conditions - whichever is used for a given single phase loss coefficient should also be used for the two-phase case. The coefficient does not incorporate the acceleration component of pressure changes with changes in flow area.

4.4 Some Considerations on the Effects of Surface Roughness

It is widely recognised that the effect of surface roughness is less for two-phase pressure losses than for single phase pressure losses. Shires [4.1] has proposed a flow structure 'relaxation' in which, for example, the roughness thickens the film of annular flow, resulting in lower wall velocity gradients and hence also lower shear than for no film alteration.

The previous analysis for smooth tube shear, when considered in terms of possible extension to rough ducts, suggests some alternative mechanisms. These are described below.

4.4.1 Film thickness-dependent flows

Equation (4.3), which relates friction factor f, Reynolds number Re and film thickness S is of the same form as the single phase Colebrook equation relating friction factor f, Reynolds number Re and equivalent sand roughness ε:

$$\frac{1}{\sqrt{f}} = -0.4 - 4 \log \left(\frac{1}{Re\sqrt{f}} + 0.214\, \varepsilon /D\right), \qquad (4.6)$$

but in which the equivalent sand roughness is replaced by a length parameter proportional to the film thickness S. Indeed, the analysis leading to equation (4.3) can be adapted to derive Colebrook's equation

(see appendix A28). If this adaptation is further included in the original derivation of equation (4.3) to allow for surface roughness of height ε, the new derivation leads to equation (4.3) in which the film thickness S is, to a first approximation, replaced by $S + \varepsilon\mu_g/\mu_\ell$.

Since, in most cases, $\mu_g/\mu_\ell \ll 1$ and $\varepsilon < S$,

$$S + \varepsilon\mu_g/\mu_\ell \simeq S,$$

so surface roughness effects can be generally be expected to be smaller in those annular two-phase flows where shear stress depends on film thickness.

4.4.2 Surface tension-dependent flows

As shown in section (3.6.3), surface tension-dependent hydrodynamics result from a model of flows with attached wall bubbles which act as effective duct wall roughness elements. Moreover, the bubbles have been considered to be sufficiently large for the hydrodynamics to be determined only by bubble size and not flow viscosity, i.e. the bubbles render the duct surface 'completely rough'.

Under these circumstances, any natural roughness on the duct surface can be considered to be swamped by the bubble 'roughness'. It follows that the influence of any natural roughness will be smaller than would be the case for single phase flow.

4.4.3 Viscosity-dependent flows

Equation (4.4), which is of the form of the single phase smooth tube Nikuradse equation and which describes pressure losses for viscosity-dependent two-phase flows, was developed from an adaptation of classical single phase smooth tube turbulence theory. The Nikuradse equation of single phase flow is replaced by the semi-empirically based Colebrook equation (equation (4.6)) for flows in ducts with 'natural' roughness. By analogy, it appears plausible that

equation (4.4) should be replaced by a corresponding equation, of the form proposed by Colebrook for two-phase rough wall flows, i.e. by

$$\frac{1}{\sqrt{f'}} = 3.48 - 4 \log (2\varepsilon/D + 9.35/(Re' \sqrt{f'})). \qquad (4.7)$$

The regime-specifying integers m and n (section 3.9), as obtained from data analysis, have been observed in the present work to be generally non-negative. The generalised Reynolds number Re' (table 4.2) will thus usually be considerably smaller than the specific Reynolds number Re since $Re' = \sqrt{2}^{-5m} \sqrt{10}^{-n} Re$. In terms of equation (4.7), a smaller Re' will produce a smaller ε/D effect than would be the case for the corresponding specific Re in Colebrook's equation.

This reasoning suggests that surface roughness effects will be the same as in single phase flow for those viscosity-dependent flows with (m,n) = (0,0) (i.e. $Re' \equiv Re$), but will be less for flow regimes for which $(m,n) \neq (0,0)$.

4.5 Data Analysis

A considerable number of two-phase pressure drop data (~20,000) have been examined in terms of concepts presented in this chapter. Although this thesis is concerned primarily with high pressure steam-water flows, data analysis was not confined to this system because of the general nature of the theory, which thus required data analyses from both one and two component systems and from a variety of geometries for its evaluation. Special attention was given to pressure drop data which contained associated data for other parameters (voidage, flow structure, heat transfer, etc.) since these data could be used to check the inter-relation between various parameters anticipated by the present theory. Pressure drop data of this type analysed include data from refs. [4.2 - 4.5].

Since most data are presented in a form requiring analysis to

extract friction factor data, an extensive data bank was constructed. The high pressure steam-water component of this, being particularly pertinent to this work, is discussed later in section 4.6.5. This was supplemented by analysis of data from a large number of sources (e.g. [4.3]) in which the raw data had already been reduced to, e.g. 'two-phase multiplier' data.

4.5.1 Compatibility of shear and velocity profile data

Figure (4.1) shows various friction factor curves for argon-alcohol viscosity-dependent upflow data [4.4]. Each curve corresponds to a different friction regime. The friction regime map for the data of fig. 4.1 is shown in fig. 4.2. The map also shows the relevant triad (z,m,n) from which the friction factor curves are generated using equation (4.1) or (4.4) or (4.7). As discussed in chapter 3, the same triad specifies the corresponding velocity profiles. Velocity profile data obtained concurrently with the pressure gradient data of fig. 4.1 are consistent with these anticipated profiles. These data have been presented in fig. 3.7.

Figure 4.3 shows typical surface-tension dependent friction factor data. The data correspond to the (e,2,-4) friction regime, and the friction factor curve is that obtained from equation (4.2) or (4.5) using this triad. Velocity profile data obtained simultaneously with the pressure gradient data are also consistent with this triad; these data have been presented in fig. 3.8.

4.5.2 Film thickness dependent data

As stated previously, two-phase flows with characteristics which depend on film thickness have not been extensively analysed in this work. As a result, the form of friction factor equation derived for these flows, equation 4.3, has not been fully tested. However, if flows with large film thicknesses are considered, the equation can be

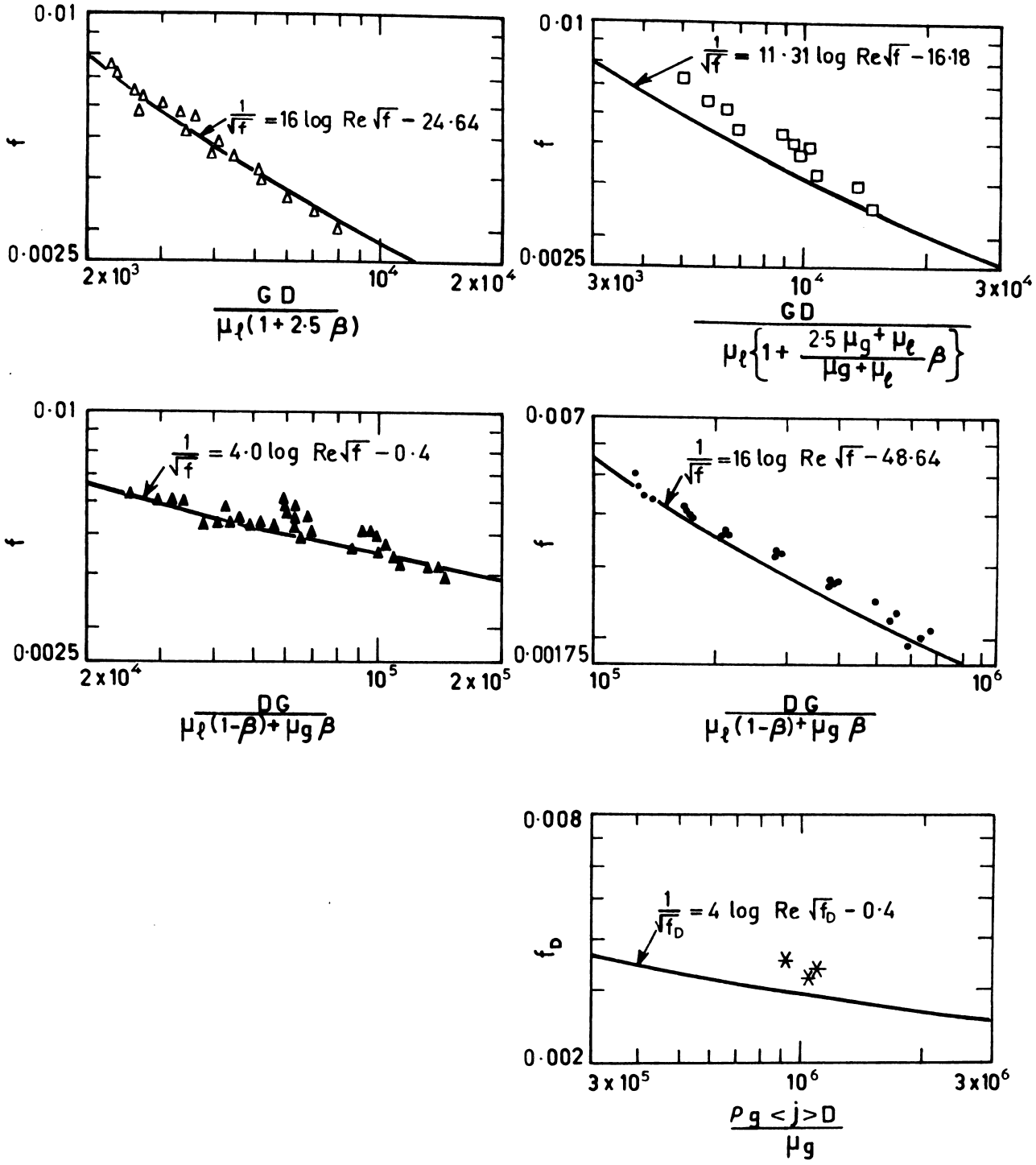

Fig. 4.1 Comparison of predicted and experimental argon-alcohol round tube friction factor data [4.4] for various friction regimes. The notation corresponds to the regime map of fig. 4.2. Corresponding velocity profiles are in fig. 3.7.

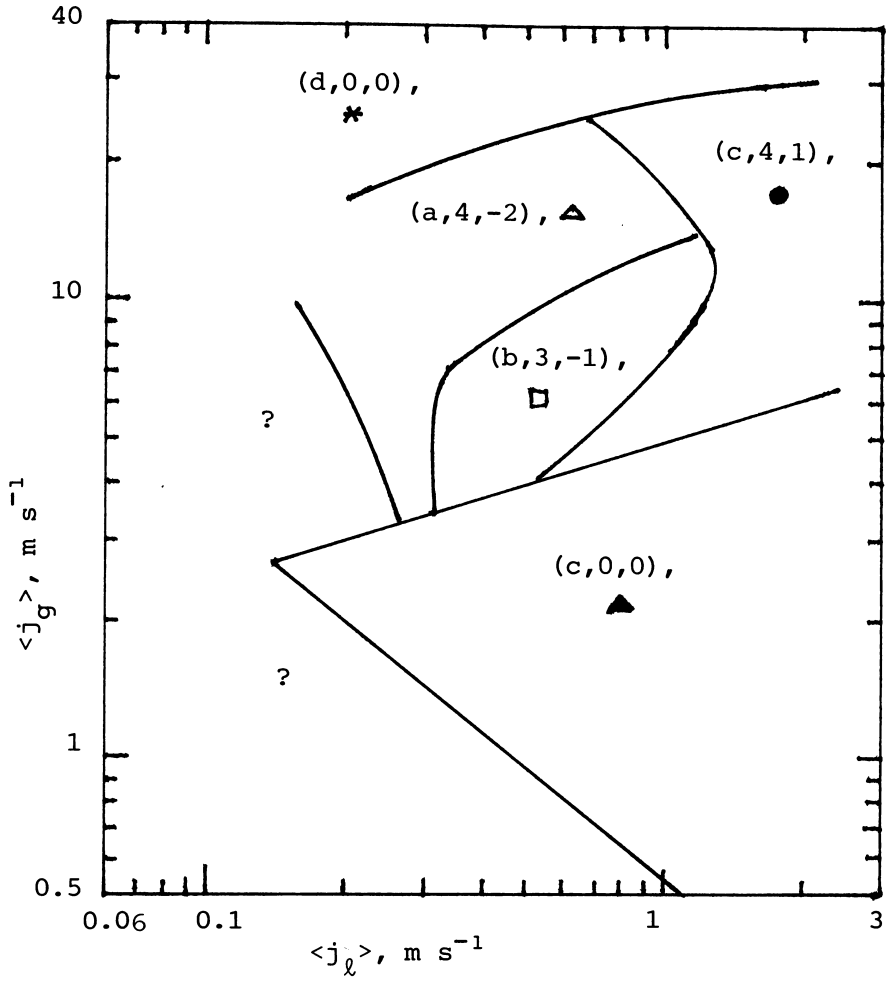

Fig. 4.2 Friction regime map for fig. 4.1 and fig. 3.7

seen to be consistent with at least some trends shown by data. For large thicknesses S, equation 4.3 can be rearranged to the form

$$1/\sqrt{f} = 2.28 + 4 \log a' (D/S)^{b'},$$

where, from the derivation of equation 4.3, $b' = 0.407/\kappa$, with κ being the von Karman coefficient for the two-phase conditions. The relation between film thickness and 'interfacial roughness', which is often used in the analyses of annular flows (e.g. [4.6], section 5.3.2), is based on the value of sand roughness ε required to give an equivalent shear using the single phase equation

$$1/\sqrt{f} = 2.28 + 4 \log D/\varepsilon \quad .$$

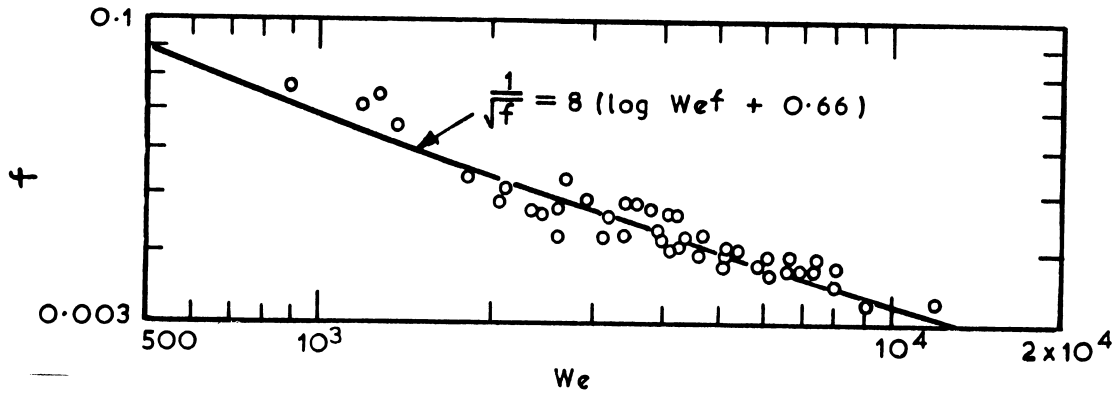

Fig. 4.3 Comparison of experimental and predicted (e,2,-4) friction factors. Adiabatic steam-water upflow in a 17.1 mm tube, ρ_ℓ/ρ_g = 13, data from [4.2]. Corresponding velocity data are in fig. 3.8.

It follows from a comparison of the above two equations that the relation between equivalent sand roughness and film thickness is of the form $\varepsilon \sim (S)^{0.407/\kappa}$.

Experimental κ values for film thickness-dependent flows are not unique (fig. 5.10, [4.6]). Typical values (fig. 5.10, [4.6]) suggest a general approximation to the above relation as $\varepsilon \sim S^{1.3}$. Data presented in figs. 5.11 to 5.13, [4.6] and in [4.7], are broadly consistent with this theoretical expectation.

4.5.3 The effect of surface roughness

The analysis of section 4.4 suggests that surface roughness effects should be the same in two-phase viscosity-dependent flow as in single phase flow for the special case when the parameters (m,n) are (0,0) and should be smaller for other (m,n) values. For all m,n, the single phase curves should apply to the two-phase case when considered in terms of the generalised friction factor and Reynolds numbers of table 4.2. For (m,n) = (0,0), surface roughness effects should be the same as in single phase flow since in this case the generalised friction factor and Reynolds numbers are identical to the actual friction factor and Reynolds numbers.

Figures (4.4) and (4.5) show rough tube (m,n) = (0,0) friction factor data for bubbly (figure 4.4) and dry-wall droplet flow (figure 4.5). The respective friction regimes for these data are (a,0,0) and (d,0,0). Equivalent sand roughness values were obtained from single phase data presented in [4.5, 4.8]. The data are consistent with the analyses of section 4.4.

Rough tube pressure loss data for bubbly sublayer annular flow with (z,m,n) = (b,1,0) and various surface roughnesses [4.9], values obtained from single phase tests, are shown in fig. 4.6 as friction factor f against Reynolds number Re and as generalised friction factor

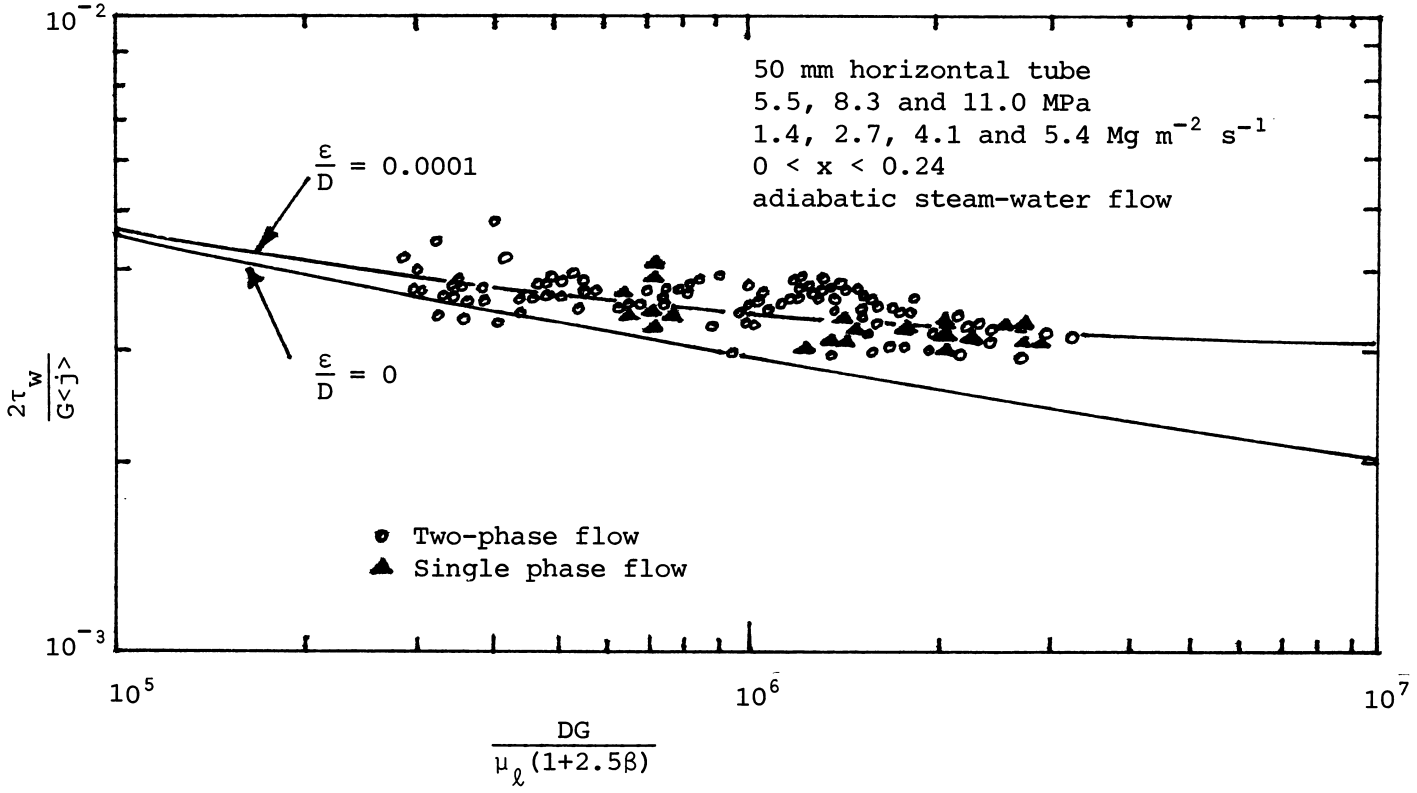

Fig. 4.4 Comparison of predicted and experimental (a,0,0) rough wall bubble flow friction factors. Data from [4.8]

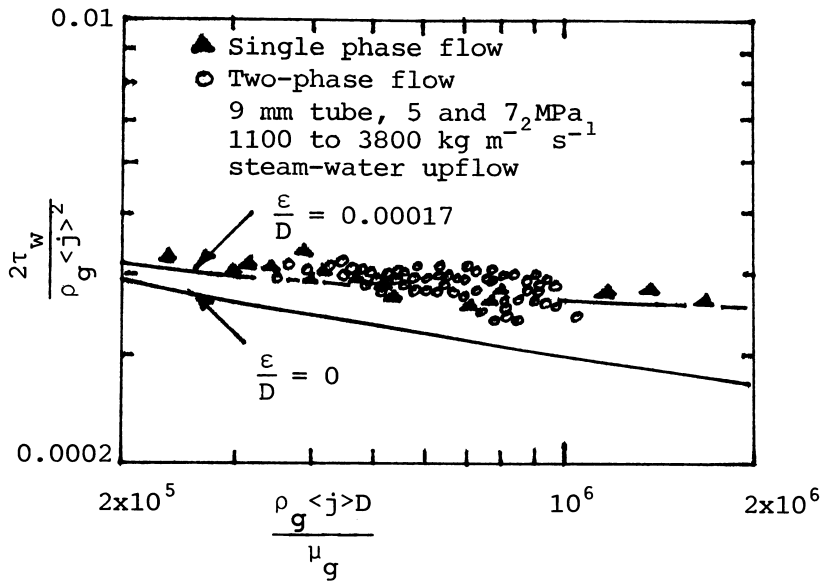

Fig. 4.5 Comparison of predicted and experimental (d,0,0) post-dryout rough wall friction factors. Data from CISE-R-83

f' against generalised Reynolds number Re', and as pressure gradients in fig. 4.7.

Because of the comparative independence on quality, each point on fig. 4.6 actually represents a cluster of points. As expected from section 4.4, the representation of f' versus Re' is consistent with Colebrook's equation. It can be seen that the effect of roughness is less than would be the case for a non-generalised Reynolds number Re at the same flow conditions.

The predicted (b,1,0) pressure gradients for the rough tubes compare favourably with measured values (fig. 4.7). Also shown in this figure are calculated single phase liquid gradients. The influence of roughness is more significant for single phase ccnditions, amounting to 100% in the roughest tube, but this reduces to only a 25% increase in the two-phase case.

It can be seen from the above why surface roughness effects are often not detectable for two-phase flows with more moderate surface

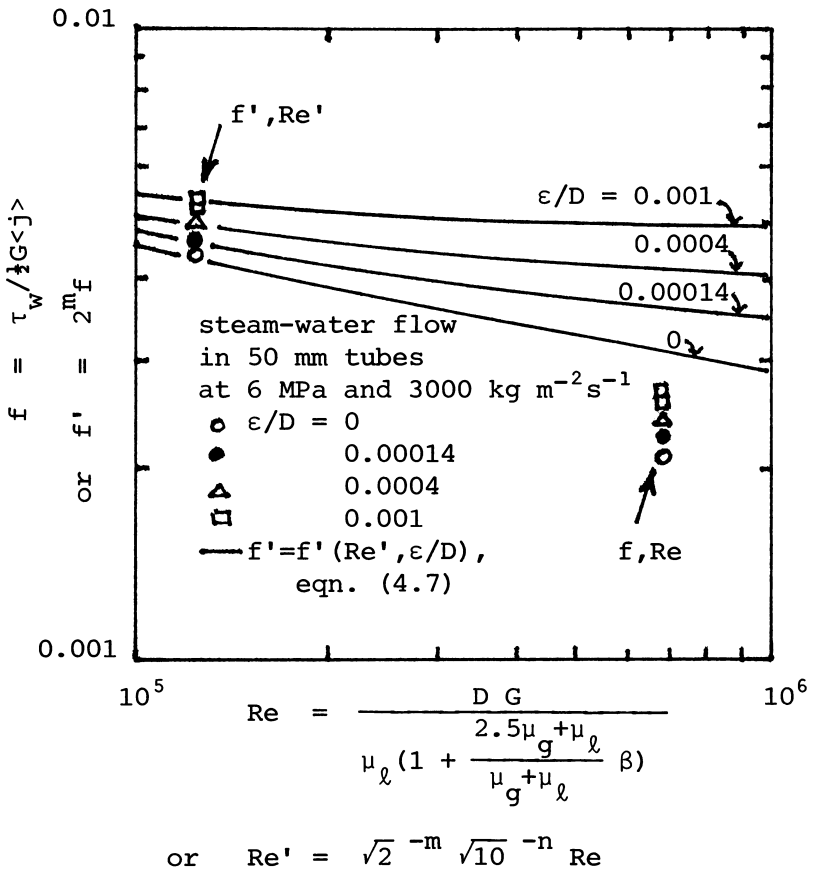

Fig. 4.6 Comparison of experimental (b,1,0) rough wall friction factor data [4.9] with predictions based on equation (4.7). ε/D values are as given in [4.9].

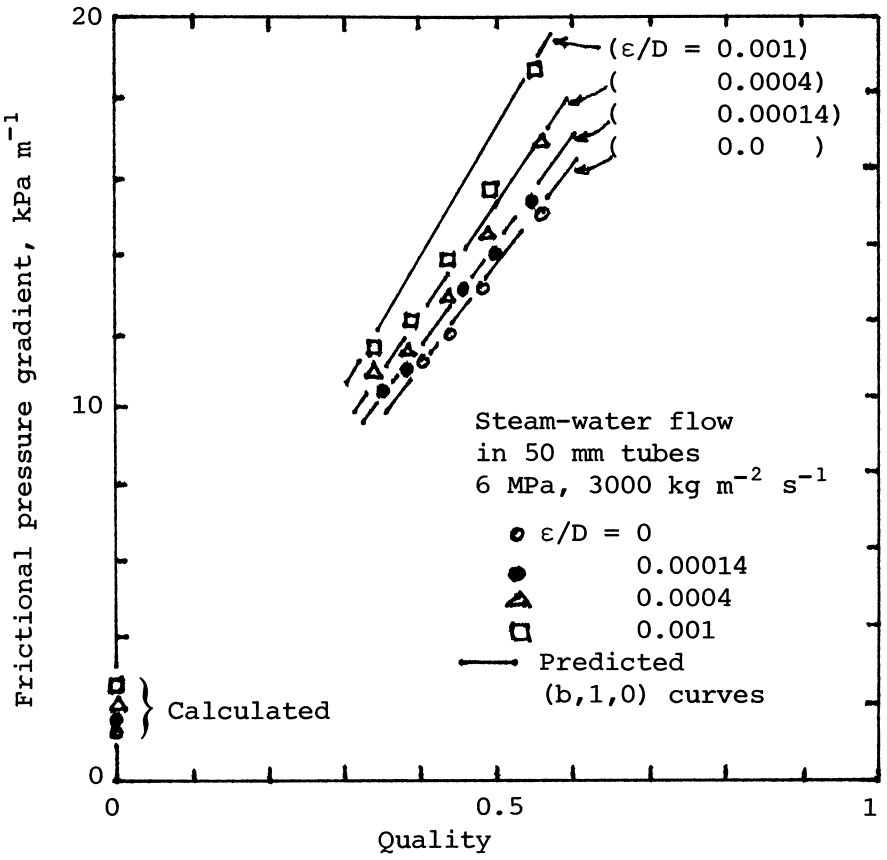

Fig. 4.7 Data of fig. 4.6 presented as pressure gradient vs quality with roughness as parameter

roughnesses than those of [4.9].

4.5.4 Obstruction loss coefficients

A large number of two-phase loss coefficient data covering orifices, spacers and other obstructions were analysed. These include data from [4.8-4.13], which consider obstruction types and flow conditions which are relevant to reactor engineering. The analysis indicates that, in a large fraction of cases, the expectations of section 4.5 are satisfied: empirical relations between single phase loss coefficients and Reynolds number extend to the two-phase case provided physical properties in the dimensionless groups are correctly defined.

The appropriate physical property definitions were found to depend on obstruction type and not on flow conditions. Definitions corresponding to sublayer 'c' (table 3.1), i.e. μ of Re is $\mu_\ell (1-\beta) + \mu_g \beta$, apply to local obstructions, suggesting a tendency of flows to become separated at such obstructions. On the other hand, definitions corresponding to sublayer 'a', i.e. μ of Re is $\mu_\ell (1 + 2.5\beta)$, apply to distributed obstructions, implying a tendency for sublayers to become 'churned' and bubbly for non-local obstructions.

In figs. 4.8 and 4.9, data [4.8, 4.12] for local and distributed losses are compared with predictions based on the above. In order to conform to the presentation of the data of [4.8, 4.12], the comparison is made in terms of two-phase multiplier $\phi^2_{LO} = \Delta P_{TP}/\Delta P_{LO}$, where the LO refers to liquid only with the mixture mass flux, against quality. The predicted curves are readily obtained from the predicted two-phase loss coefficient-Reynolds number relation $K_{TP}\ (Re_{TP})$ from the transformation

$$\phi^2_{LO} = \frac{K_{TP}(Re_{TP}(x))}{K_{LO}\ (Re_{LO})}\ (1 + x\ (\frac{\rho_\ell}{\rho_g} - 1)) \quad .$$

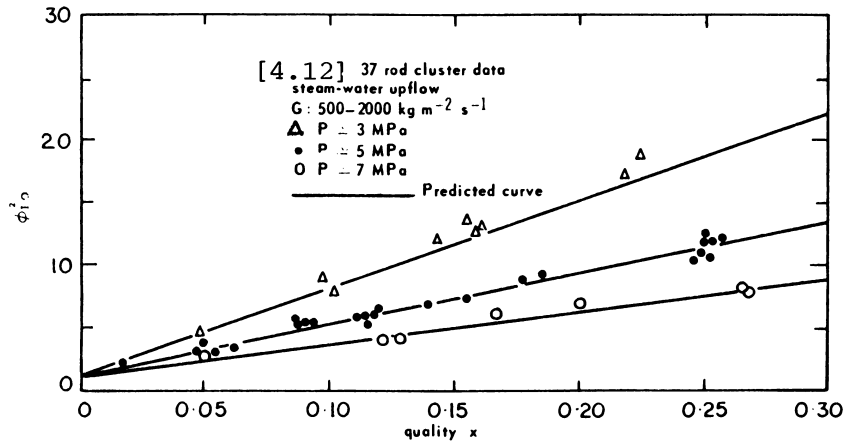

Fig. 4.8 Comparison of predicted and experimental two-phase distributed obstruction multipliers. ϕ^2_{LO} refers to outlet region, including spacer, cables and expansion.

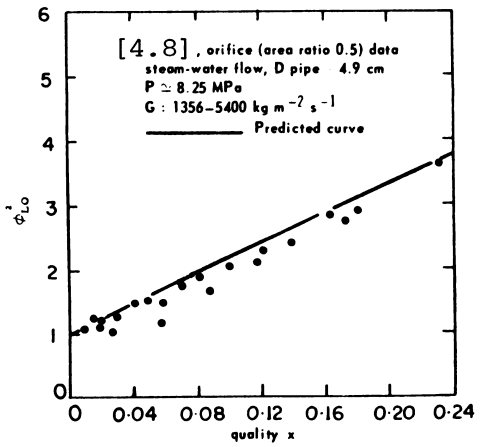

Fig. 4.9 Comparison of predicted and experimental two-phase local obstruction multipliers.

As stated, curves of K_{TP} (Re_{TP}) are assumed to coincide with those of K_{LO} (Re_{LO}). The single phase curves, as obtained empirically for the geometries of figs. 4.8 and 4.9, are presented in [4.8] and [4.12].

4.5.5 High pressure steam-water flows

In view of the importance of high pressure steam-water flows to reactor engineering, a comprehensive analysis of high pressure steam-water pressure loss data, covering some 10^4 data points, was undertaken in an attempt to obtain equations which were sufficiently valid for engineering design purposes.

Unfortunately, the analysis uncovered evidence of entrance effects being rather stronger in two-phase flows than in single phase flow, with the result that data from nominally identical test sections may be incompatible to a strong degree.

Because of the large number of data from CISE laboratories [4.5], the equations given below are biased in favour of these data. An attempt was made by CISE researchers to minimise entrance effects and so the equation below can be considered as being reasonable for 'developed' flows where repeatability of data can more reasonably be expected. Moreover, the CISE data were suitable for the present analysis since a wide range of flow conditions were covered in a systematic way and since other parameters (void fraction, heat transfer coefficient, etc.) were often measured simultaneously, so enabling the theoretical dependence of various characteristics on shear characteristics, as developed in this work, to be tested.

The equations given below can be considered as reasonable for $P > 3$ MPa and $G > 400$ kg m^{-2} s^{-1}.

4.5.5.1 Adiabatic flow in round tubes

Lower quality friction factors are consistent with the (a,0,0)

friction regime (as are nearly all data for bubbly flows); lower intermediate quality data with (c,4,2), which can be considered as applying to semi-annular flows, slugging flows, and annular flows with no entrained bubbles in the film; and higher intermediate quality data with (a,4,0), which is consistent with annular flows with entrained film bubbles. Low mass flux high quality friction factors were not satisfactorily analysed in this work, but data trends are qualitatively consistent with the partially developed 'thin film' friction factor equation, equation (4.3). Higher mass flow (> 2000 kg m^{-2} s^{-1}) high quality friction factors are consistent with the dry wall f(d,0,0) suggesting that under these conditions the gas momentum is sufficient to entrain all the liquid in the form of core droplets.

The boundary between the various friction regimes appears to be such that no shear discontinuity appears at the boundary. The boundary can thus be predicted from the intercept of the shear stress equations relevant to either side of the boundary.

The above can be more neatly expressed by

$$\frac{D(dP/dz)_F}{2G\langle j\rangle^2} = \max\{\min[f(a,0,0);\ f(c,4,2)];\ f(a,4,0);\ \rho_g f(d,0,0)/\rho_H\} \qquad (4.8)$$

which covers the whole quality range. Some qualifying remarks can be found in section 5, appendix A10. The factor ρ_g/ρ_H for the highest quality regime is to allow for different friction factor definitions for wet-wall and dry-wall flows (table 3.1).

A comparison of equation (4.8) with some typical data is shown in fig. 4.10.

For extremely long upstream settling lengths, greater than about 500 diameters, f(a,4,0) of equation (4.8) should be replaced by

f(a,2,0):

$$\frac{D(dP/dz)_F}{2G<j>} = \max \{\min [f(a,0,0);\ f(c,4,2)];\ f(a,2,0);\ \rho_g f(d,0,0)/\rho_H\} \quad (4.9)$$

In fig. (4.11), a comparison of equation (4.9) is made with some data from a test section with a long settling length.

4.5.5.2 Diabatic flow in round tubes

For diabatic pressure drop data obtained from experiments with both pressure taps in the two-phase region, average frictional pressure gradients are assumed here to be equal to the mid-point local frictional pressure gradients. The analysis of appendix 1 of [4.15] shows that this assumption is very reasonable.

Pre boiling-crisis diabatic friction factor data [4.5] are consistent with

$$\frac{D(dP/dz)_F}{2G<j>} = \max \{\min [f(a,0,0);\ f(e,4,0)];\ f(b,4,0)\}; \quad (4.10a)$$

and post crisis data, with

$$\frac{D(dP/dz)_F}{2G<j>} = \rho_g f(d,0,0)/\rho_H \quad (4.10b)$$

This is compared with some typical data in fig. 4.12.

Equation (4.10) is similar to equation (4.8) except, as expected, the shear stress is consistent with attached wall bubbles (sublayer e) for the second regime. The following is noted:

(i) Wall bubbles, which act as roughness elements, have been neglected for the (a,0,0) regime. This leads to a slight under-prediction of shear for this regime, particularly at lower mass fluxes where boiling wall bubbles are expected to be larger. The error is about 20% at 1000 kg m^{-2} s^{-1} but is negligible above 2000 kg m^{-2} s^{-1}. The above indicates that wall bubbles only partially 'roughen' the

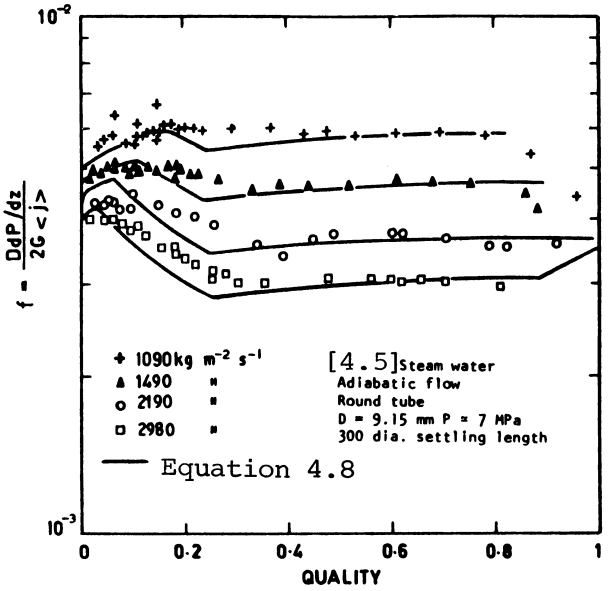

Fig. 4.10 Comparison of predicted and experimental [4.5] round tube adiabatic steam-water friction factors.

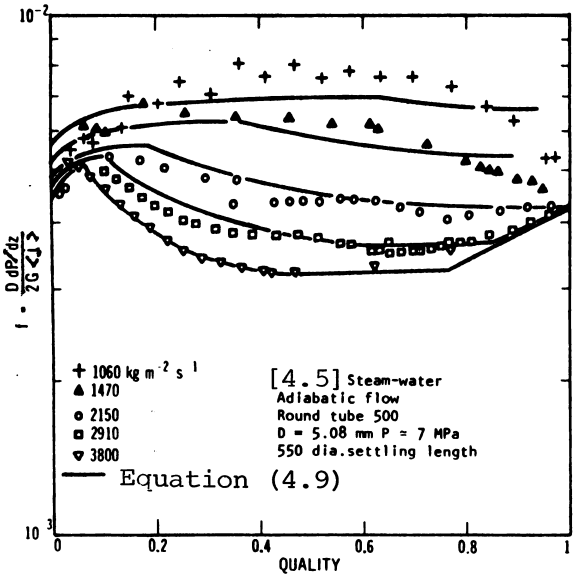

Fig. 4.11 Comparison of predicted and experimental [4.5] adiabatic friction factors for steam-water flow in a round tube with a long upstream flow development length.

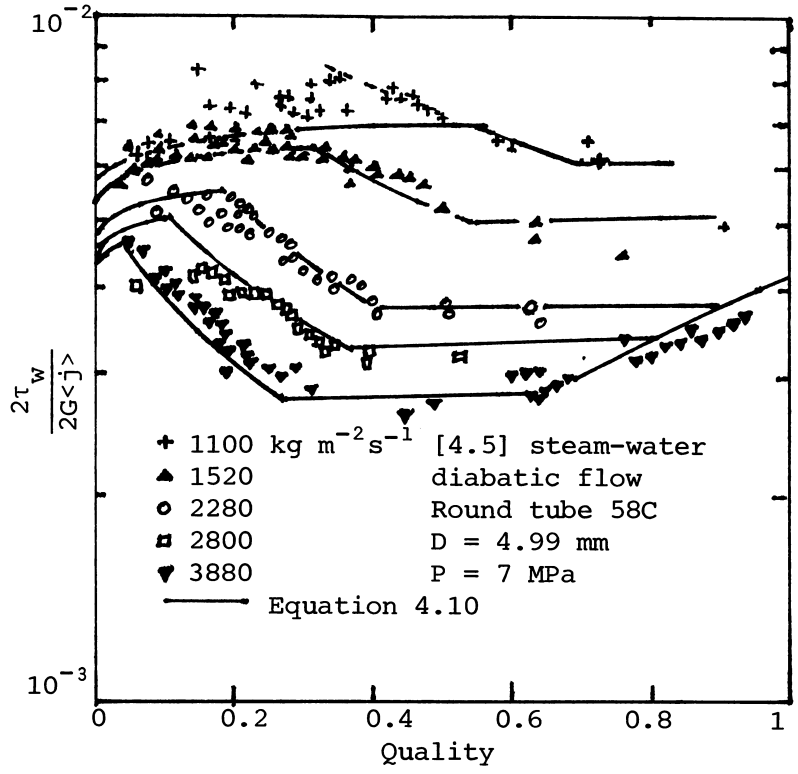

Fig. 4.12 Comparison of predicted and experimental [4.5] round tube diabatic steam-water friction factors.

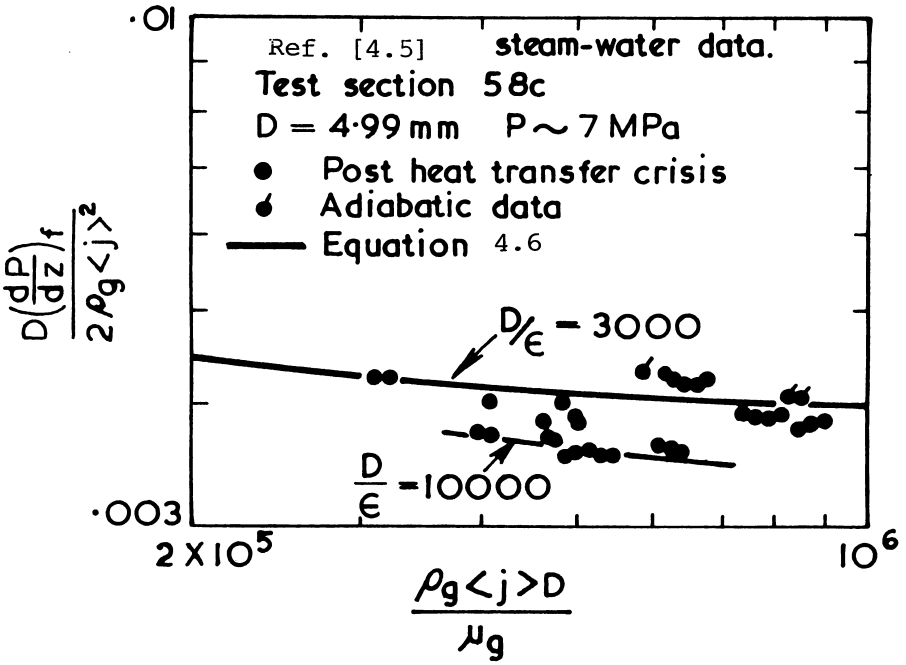

Fig. 4.13 Apparent reduction of roughness with some post-crisis data. Single phase tests [4.5] indicate $D/\varepsilon = 3000$.

surface at lower qualities.

(ii) The 'b' sublayer (see table 3.1) of the higher intermediate quality regime, (b,4,0), suggests an absence of nucleating wall bubbles. This is consistent with current ideas that nucleation is suppressed in annular flows. The Chen heat transfer correlation [4.14], for example, contains a 'boiling suppression factor' which is significant at higher qualities.

(iii) The higher intermediate quality regime, (b,4,0), differs from that for adiabatic flows, (a,4,0), only in the nature of the sublayer bubbles. The 'a' sublayer is due to impurities on bubble surfaces preventing surface movement. This was discussed in section 3.6.1. In the case of diabatic flows, bubbles generated in the heated section may not remain in the heated section for sufficient time for impurities in the fluid to migrate to the bubble surfaces, so surface movement remains possible: 'b' bubbles instead of 'a' bubbles. For low velocity flows in long heated test sections, impurities can migrate to bubble surfaces, and friction data deviate from f(b,4,0) and approach values predicted from f(a,4,0).

(iv) Dry wall Reynolds numbers, $\rho_g <j> D/\mu_g$, are generally of a magnitude that the recommended friction factor, f(d,0,0) depends on the tube surface roughness. This has been demonstrated in fig. 4.5. However, some post boiling-crisis data are consistent with f(d,0,0) only if it is assumed that the surface roughness is considerably less than it actually is. An example is given in fig. 4.13. It is assumed that these data correspond to 'pseudo-dryout' instead of dryout, with superheated liquid remaining in micro-crevices between roughness elements. This would reduce the apparent roughness for the turbulent droplet flow. The concept is consistent with the behaviour of some heat transfer data, discussed in chapter 8, and some critical heat

flux data, discussed in chapter 7.

4.5.5.3 Complex geometries

Rod bundle geometries are of special relevance to nuclear engineering. However, rod spacers, inserted to prevent inter-surface contact, and abrupt changes in flow area at the entrance of rod bundles ensure that flows are not 'developed'. Different rod bundle constructions are such that entrance and spacer effects must differ. Not unexpectedly, although data from individual test rigs can be correlated in terms of the generalised equations in table 4.1, different equations apply to different test sections. Unlike the case for round tubes, no general predictive equations can be given. However, some generalities can be made:

. As with most lower quality data, lower quality friction factors are consistent with the (a,0,0) friction regime;

. Also as with most dry wall data, friction factors for tests in which all surfaces are dry are consistent with the (d,0,0) friction regime;

. Both adiabatic and diabatic friction factors for long test sections with no rod spacers are similar in trends to those for round tubes. Differences in values for the complex geometry data and round tube data occur at intermediate qualities and presumably reflect the rod bundle entrance influence in the bundle data;

. In the case of test sections with localised rod spacers, friction factor behaviour differs from that for round tubes in that the same equations apply for both adiabatic and diabatic conditions. The data tend to be described by

$$\frac{D(dP/dz)_f}{2\rho_H \langle j \rangle^2} = \min [f(a,0,0);\ f(e,m,n)] ,$$

with different m and n values applying to different test sections.

An example is given in fig. 4.14.

The applicability of a sublayer based on a model with attached wall bubbles (sublayer e) for both adiabatic and diabatic data suggests wall bubble generation in adiabatic flows due to low level flashing induced by spacers;

. Boiling appears to be suppressed in test sections with wire-wrapped spacers, with neither diabatic or diabatic data being consistent with sublayer e of table 3.1. Data from [4.16] behave as such; and

. There is some limited evidence that rod bundle geometries with some dry surfaces (i.e post-CHF) behave as equivalent geometries with the dried surface neglected, i.e. the equivalent diameter is defined by (4 x flow area) ÷ (non-dried perimeter). This may be connected with the fact that shear on dry surfaces is generally much smaller than that on wetted surfaces under similar flow conditions, as can be confirmed by comparing the wet wall and dry wall shear stresses using equations presented earlier.

This final point is demonstrated in fig. 4.15. The data in this figure are from an annulus under post-dryout rod conditions and are consistent with the round tube (a,4,0) friction regime when considered in terms of the 'equivalent sheared diameter' described above. The applicability of sublayer 'b' (i.e. of f(b,4,0)) at higher velocity conditions can be explained in terms of the argument concerning bubble surface contamination presented in section 4.5.5.2, point (iii).

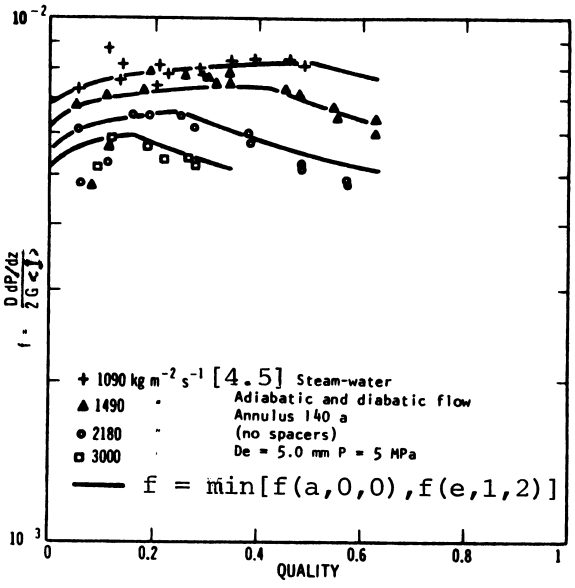

Fig. 4.14 Adiabatic and diabatic friction factors for steam-water flow in an annulus.

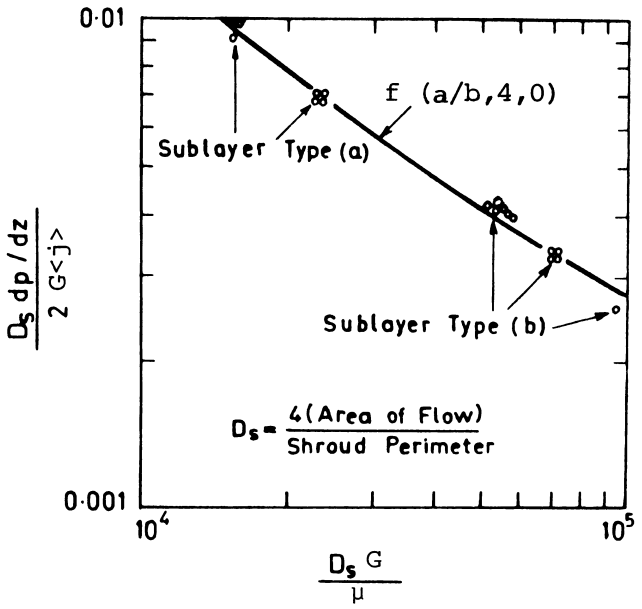

Fig. 4.15 Comparison of predicted and experimental friction factors for an 8.25/5.00 mm annulus [4.5] with an adiabatic shroud and post-crisis rod.

Chapter 4 References

4.1 G.L. Shires, 'A possible mechanism for the attenuation of the effect of wall friction in two-phase flow', AEEW-M1139 (1972).

4.2 P.L. Kirillov et al., 'Measurement of some characteristics of steam-water flow in round tubes at a pressure of 68.6 bar', FEI-421 (1973).

4.3 L. Friedel, 'Model law for friction pressure drop in two-phase flow', V.D.I.-Forschungscheft 572 (1975).

4.4 CISE two-component pressure drop data in CISE-R reports 35, 41, 73, 82, 93, 105, 108, 109.

4.5 CISE steam-water pressure drop data in CISE-R reports 27, 30, 31, 83, 86, 90, 91, 122, 123, 169, 170, 184, 185, 208, 264, 294, 339, 340.

4.6 G.F. Hewitt and N.S. Hall Taylor, 'Annular two-phase flow', Pergamon (1970).

4.7 P.B. Whalley et al., 'Experimental wave and entrainment measurements in vertical annular two-phase flow', AERE-R 7521 (1973).

4.8 D.E. Fitzsimmons, 'Two-phase pressure drop in piping components', H.W.80970 Rev.1 (1964).

4.9 S. Sugawara and T. Kobori, 'Analysis of coolant flow distribution in FUGEN reactor core', Proc. ANS-ASME Int. Topical Meeting on Nuclear Reactor Thermal-Hydraulics, New York (NUREG/CP-0014, p.221) (1980).

4.10 A.E. Janssen and J.A. Kervinen, 'Two-phase pressure drop across contractions and expansions. Water-steam mixture at 600 to 1400 psia', GEAP-4622 (1964).

4.11 T. Kobori et al., spacer, bend and venturi two-phase pressure

drop data contained in PNC reports SN941 74-58 (1974) and PNC SN94178-114 (1975).

4.12 O. Nylund et al., spacer, entrance, and exit two-phase pressure drop data contained in FRIGG reports 1-4 (1968).

4.13 V. Marinelli and P. Grillo, 'Pressure influence on bundle two-phase flow pressure drops', CNEN report RT/ING (73) 12 (1973).

4.14 J.C. Chen, 'Correlation for boiling heat transfer to saturated fluids in convective flow', Ind. Eng. Chem. Proc. Des. Dev. 5 (3) 322 (1966).

4.15 D.R.H. Beattie, 'Two-phase pressure losses: Flow regime effects and associated phenomena', AAEC TM589 (1971).

4.16 P.A. Edwards, 'An experimental study of burnout and pressure drop in 19-rod clusters', AEEW-R 371 (1976).

CHAPTER 5

AVERAGE VOID FRACTION

The relationship between the average void fraction and flow parameters on which it depends is different for different flow patterns. For the purpose of this chapter, it is convenient to consider flow patterns in two broad categories: 'distributed flow patterns', in which one phase is continuous over the flow section, and 'separated flow patterns', in which the flow domain can be divided into a continuous liquid region, perhaps containing elements of the gas phase, and a continuous gas region, perhaps containing elements of liquid. Examples of distributed flows are bubble, slug and droplet flows. Examples of separated flow are annular and stratified flow.

It will be demonstrated in this chapter that, as with other two-phase parameters, the void fraction depends on those factors defining a friction regime, i.e. the sublayer structure and the coefficients of the non-dimensional velocity profile. However, the form of dependence differs for separated and distributed flows. Two further flow pattern effects are important: (i) As discussed below in section (5.1), the void fraction depends in part on the 'drift velocity' which is determined in part by drag on discrete elements of the flow, so the structure of discrete elements also influences the void fraction; and (ii) The regime boundary between separated and distributed flow patterns is important not only for determining which type of voidage prediction equation (separated or distributed) is appropriate, but also because the equation for separated flows developed below in section (5.2) involves this flow pattern boundary.

The analysis in this chapter covers both distributed and separated flows, with stratified flow patterns being neglected as

these are of little interest in reactor engineering. As with other sections of this thesis, the analysis is developed for symmetric flows in round tubes, and results are assumed to apply to other geometries through the use of the equivalent hydraulic diameter.

5.1 Distributed Flows

Low voidage liquid-phase continuous flows (bubble, slug, froth) are considered first (section 5.1.1) using as a basis the'drift-flux equation' developed by Zuber and co-workers [5.1, 5.2] and the results then generalised to high voidage gas-phase continuous droplet flows in section (5.1.2).

A new method is presented for estimating the value of the drift-flux equation's distribution parameter in section 5.1.1.

5.1.1 Liquid phase continuous flows

5.1.1.1 The drift-flux equation

Following Zuber et al. [5.1,5.2], a local drift v is defined by

$$u_g = j + v \; . \tag{5.1}$$

Multiplying by α and averaging over the flow section yields

$$\langle j_g \rangle / \langle \alpha \rangle = C_o \langle j \rangle + V \tag{5.2}$$

where

$$C_o = \langle \alpha j \rangle / (\langle \alpha \rangle \langle j \rangle) \tag{5.3}$$

is the distribution parameter and

$$V = \langle v\alpha \rangle / \langle \alpha \rangle \tag{5.4}$$

is the drift velocity.

The L.H.S. of equation (5.2) is the mean gas velocity. This differs from the mean mixture velocity because (i) the gas tends to concentrate in either the slower moving region ($C_o < 1$) or the faster moving region ($C_o > 1$), usually the latter; and (ii) there is often a buoyancy-induced drift contribution to the gas phase, allowed for

by V in equation (5.2).

If C_o and V are known - see sections 5.1.1.2 and 5.1.1.3 - $\langle\alpha\rangle$ can be obtained from the flow rates using equation (5.2) expressed as

$$\langle\alpha\rangle = \langle j_g\rangle/(C_o \langle j\rangle + V) \tag{5.5}$$

For negligible V this becomes

$$\langle\alpha\rangle = \beta/C_o \tag{5.6}$$

5.1.1.2 The distribution parameter C_o

Consider a generalised version of the distribution parameter as defined by equation (5.3):

$$C_{ok} = \frac{\langle \alpha j^k \rangle}{\langle \alpha j^{n-1} \rangle \langle j \rangle} \quad . \tag{5.7}$$

This reduces to the definition given in equation (5.3) for k = 1, and values of k = 2 and k = 3 are relevant to the prediction of momentum and kinetic energy fluxes, discussed in the next chapter.

Consider the numerator of equation (5.7):

$$\langle \alpha j^k \rangle = \frac{1}{A} \int_A \alpha j^k \, dA \quad .$$

Data analysis indicates that for most data, the local voidage α is negligible except in higher velocity regions where the local velocity is approximately the maximum value j_{max}. Exceptions are low velocity upflow, subcooled boiling, and low velocity non-vertical flows where buoyancy effects may produce partial or total stratification. Such flows have voids concentrating on the lower velocity region, so the present analysis does not apply. The general case is, however, consistent with the void profile given by equation (3.11), which indicates a zero voidage in the near-wall region where the local velocity is expected not to be close to j_{max}. (Data analysis suggests that the present analysis also applies to boiling diabatic flows which

cannot have zero near-wall voidages. The applicability of the analysis to these flows suggests that the near-wall voidages for these flows are not significant.)

Returning now to $\langle \alpha j^k \rangle$: For flows where the voidage can be neglected near the wall,

$$\langle \alpha j^k \rangle \simeq \frac{1}{A} \int_{A-\delta} \alpha j^k \, dA$$

where δ defines the area for which α is negligible

$$\simeq \frac{1}{A} \int_{A-\delta} \alpha j_{max} \, j^{k-1} \, dA$$

since $j \simeq j_{max}$ in the domain $A-\delta$

$$= \frac{j_{max}}{A} \int_{A} \alpha j^{k-1} \, dA$$

$$= j_{max} \langle \alpha j^{k-1} \rangle .$$

As a result, C_{ok} defined by equation (5.7) becomes

$$C_{ok} = j_{max}/\langle j \rangle . \qquad (5.8)$$

For the friction regime (z,m,n), manipulation of equations (3.31) and (3.32) produces

$$C_o(z,m,n) = 1 + 2.6 \, (\sqrt{2})^m \sqrt{f(z,m,n)} \qquad (5.9a)$$

or, in terms of the generalised friction factor given by table (4.2),

$$C_o(z,m,n) = 1 + 2.6 \sqrt{f'(z,m,n)} \qquad (5.9b)$$

In equation (5.9), the 'k' subscript has been omitted from C_o since equation (5.9) indicates that the value is independent of k.

Most bubble flows are for $(z,m,n) \equiv (a,0,0)$, for which equation (5.9) produces $C_o \cong 1.2$ for typical flows. This is consistent with empirically obtained values [5.1,5.2]. The variation of C_o with mass

flow and pressure as predicted from equation (5.9) is also consistent with empirically-observed trends [5.2].

As noted, the analysis leading to equation (5.9) does not apply to some flows described above. A value of $C_o < 1$ can be expected for these flows.

5.1.1.3 The drift velocity V

The drift velocity V for different flow patterns has been considered by others, e.g. [5.1-5.3]. From a reactor engineering viewpoint, the most important drift velocities are for bubble and slug flows. For upflow, (V_{up}) these are given by

$$V_{slug} = 0.35 \sqrt{gD} \tag{5.10}$$

and

$$V_{bubble} = 1.4 [\sigma g (\rho_\ell - \rho_g)/\rho_\ell^2]^{0.25} \tag{5.11}$$

For non-vertical upflows, where θ is the angle between the flow direction and upflow, these can be replaced by

$$V = V_{up} \cos \theta. \tag{5.12}$$

This should result in reasonable estimates of the magnitude of the drift component to equation (5.2), although, as noted in section 10.5 of Wallis' book [5.4], equation (5.12) is not strictly valid for slug flow.

Data analysis performed as part of the present work suggests that two new drift velocities be considered in addition to those normally quoted [5.1-5.3]:

(i) Some distributed flow low voidage flows have shear stresses which correlate with a 'c' definition of viscosity (table 3.1). The distributed nature of the flow coupled with the concept behind the viscosity formulation imply a frothy core rather than a bubbly core. The drift velocity must then be

$$V_{z=c} = 0 \qquad (5.13)$$

irrespective of flow direction; and

(ii) Non-developed bubbly flows empirically have a drift velocity close to

$$V_{N.D.B.F.} = -\langle j_\ell \rangle \qquad (5.14)$$

irrespective of flow direction. A possible explanation is that entrance regions and flow obstructions such as rod bundle spacers collect gas wakes. If the bulk of gas collects at the wakes and is then sheared off the wake into the flow, gas leaving the wakes will momentarily have zero velocity with respect to the duct, and thus a negative velocity, approximately $-\langle j_\ell \rangle$, with respect to the flow. An example is given in fig. 2d(i), Appendix A10.

Similarly, bubbles leaving nucleation sites necessarily have negative drift velocities with respect to the flow. Consequently, average drift velocities for nucleate boiling upflow are expected to be lower than predicted by equation (5.11), for developed flows. In the case of high vapour generation rates, the contribution from recently-generated bubbles may dominate the average drift, resulting in a net negative value. The above is consistent with the diabatic upflow void data of Rouhani [5].

5.1.2 High voidage droplet flows

The analysis contained in section 5.1.1 readily adapts to the case of gas-phase distributed flows:

Defining a gas-phase distributed flow distribution parameter

$$C_{go} = \langle (1-\alpha)\, j^k \rangle \,/\, (\langle (1-\alpha)\, j^{k-1} \rangle \langle j \rangle), \qquad (5.15)$$

then, for droplets confined to the faster-moving central region

$$C_{go} = 1 + 2.6 \sqrt{f(d,0,0)}\,, \qquad (5.16)$$

since the friction regime expected for droplet flows is that described

described in this work as (d,0,0). The friction factor f(d,0,0) can be predicted from equation (4.1).

The drift flux expression now becomes

$$\langle u_\ell(1-\alpha)\rangle / (1-\langle\alpha\rangle) = C_{go}\langle j\rangle + V_d \qquad (5.17)$$

where V_d is the liquid fraction weighted drift between the droplet velocity and the mixture velocity. An expression for V_d is suggested by Zuber and Ishii [5.3]. This expression is, however, the terminal drift velocity, i.e. the value of the drift when a steady drift is achieved. The high velocities of droplet flows means that terminal drift velocities are not often achieved in flow sections of interest. On the other hand, the difficulties in predicting the transient drift velocities are more than compensated for by the fact that they may be neglected when compared with the high mixture velocities encountered with droplet flow. For negligible V_d, equation (5.17) becomes

$$1 - \langle\alpha\rangle = (1-\beta)/C_{go} . \qquad (5.18)$$

5.2 Separated Two-phase Flows

An analysis is presented here for round tube symmetric annular flows with a liquid-phase continuous film and a gas-phase continuous core. Void fraction relations derived can be adapted to inverse annular flows (gas-phase continuous film and liquid-phase continuous core, as expected in the rewetting phase of a LOCA, for example) but no data have been found to validate any such relations.

The relation between annular flow void fraction and volume flows of the gas and liquid is based on the relation between the film thickness and film volume flow obtained by integrating the velocity profile over the film region. Core droplets and film bubbles are allowed for by film and core void parameters α_c, α_f, β_c, β_f

$$\alpha_{c,f} = \frac{1}{a} \int_{c,f} \alpha \, da \tag{5.19}$$

$$\beta_{c,f} = \frac{\int_{c,f} \alpha \, u_g \, da}{\int_{c,f} j \, da} \quad . \tag{5.20}$$

The core area fraction A

$$A = \frac{\int_{c} d\,a}{\int_{c+f} da} = \frac{a_c}{a_c + a_f} \tag{5.21}$$

and core volume flow fraction

$$B = \frac{\int_{c} j \, da}{\int_{c+f} j \, da} \tag{5.22}$$

are then related to the regional void parameters and the overall voidage $\langle\alpha\rangle$ and volume flow ratio β by

$$A = (\alpha_f - \langle\alpha\rangle) \; / \; (\alpha_f - \alpha_c) \tag{5.23}$$

and

$$B = (\beta_f - \beta) \; / \; (\beta_f - \beta_c) \tag{5.24}$$

For a purely liquid film and purely gas core, $A \equiv \langle\alpha\rangle$ and $B \equiv \beta$. The analysis in section 5.2.1 relates A and B. In view of equations (5.23) and (5.24), this can be converted to a relation between $\langle\alpha\rangle$ and β if the regional void parameters α_f, β_f, α_c, β_c are known. Methods of estimating values for these, at least for some flow conditions, are given in section 5.2.2.

5.2.1 The relation between film thickness and film flowrate

The film volume flow Q_f is obtained by integrating the velocity profile derived in chapter 3 over the film region:

$$Q_f = \int_{D/2-S}^{D/2} j\, 2\pi r dr ,$$

where the film thickness S is related to the core area fraction A by

$$S/D = (1 - \sqrt{A})/2$$

The analysis is simplified if it is assumed that the film is thin compared with the diameter, in which case

$$Q_f = \pi D \int_0^S j\, dy \qquad (5.25)$$

The thin film approximation for annular flow was examined as part of the present analysis and was found to be remarkably accurate, even for 'film' thicknesses equal to the duct radius, provided the approximation is used also in the relation between S and A, i.e. $1-A = \pi DS/(\pi D^2/4)$, or $S/D = (1-A)/4$.

Expressing the volume flow expression given by equation (5.25) in terms of the dimensionless quantities of table 3.1,

$$Q_f^+(z,m,n) = \int_{j^+=0}^{S^+(z,m,n)} j^+(z,m,n)\, d\, y^+(z,m,n) \qquad (5.26)$$

where

$$\left.\begin{aligned} Q_f^+ &= \frac{1-B}{4} Re(z,m,n) \\ S^+ &= \frac{1-A}{4} Re(z,m,n) \sqrt{\frac{f(z,m,n)}{2}} \end{aligned}\right\} \begin{array}{l}\text{Viscosity}\\ \text{dependent}\\ \text{flows}\end{array} \qquad (5.27a)$$

$$\left.\begin{aligned} Q_f^+ &= \frac{1-B}{2} We(e,m,n) \sqrt{\frac{f(e,m,n)}{2}} \\ S^+ &= \frac{1-A}{4} We(e,m,n)\, f(e,m,n) \end{aligned}\right\} \begin{array}{l}\text{Surface}\\ \text{tension}\\ \text{dependent}\\ \text{flows}\end{array} \qquad (5.27b)$$

Equations (5.26) and (5.27) may be used in conjunction with velocity profiles given in chapter 3 to relate A and B for a given

friction regime and hence relate $\langle\alpha\rangle$ and β if the regional void parameters α_f, β_f, α_c, β_c are known.

5.2.2 Some considerations on annular flow regional void parameters

Prediction of voidage with equation (5.26) requires knowledge of the regional void parameters α_c, β_c, α_f, β_f. Although a full evaluation of the factors has not been achieved in this work, some trends can be surmised.

This simplest treatment of the parameters is to assume them to be independent of quality for a given mass flow. Although this appears unrealistic, there are two supporting factors for such a treatment:

(i) The available empirical data on high pressure steam-water core liquid flow, such as the data of [5.6], shows the core liquid mass flow generally to be proportional to quality for most of the annular flow regime, with little effect of parameters such as heat flux. Such a proportionality is equivalent to constant β_c. Data supporting the independence of one regional void parameter on quality suggests that the other three parameters might also be independent of quality; and

(ii) Sensitivity studies on equations (5.23),(5.24),(5.26) & (5.27) show liquid in the core region to have little effect on average voidage for lower voidage annular flows and gas in the film region to have little effect at higher voidage annular flows. Errors introduced in average voidage through assumptions of constant regional voidage factors will then be small if α_f and β_f are reasonable for lower voidage annular flows, and α_c and β_c are reasonable for higher voidage annular flows.

The above, together with the assumption of no change in average voidage on undergoing flow pattern transition, indicates that for the purpose of average voidage calculation, α_f and β_f can be identified

with the values of $\langle\alpha\rangle$ and β at the distributed flow/annular flow transition, and α_c and β_c with the values of $\langle\alpha\rangle$ and β at the annular flow/dry wall transition.

Empirical regime maps for high pressure systems [5.7-5.9] indicate that the lower voidage annular flow boundary occurs approximately at a void fraction of 0.55. This indicates that α_f can be assumed to be 0.55 and β_f can be calculated from equation (5.3) as $\beta_f = \langle j_g\rangle/\langle j\rangle\big|_{\langle\alpha\rangle = 0.55}$. Values of α_c and β_c have not been fully established in this work; however, in view of section 4.5.5.1, for adiabatic steam-water flows they may be estimated from the quality at which f(a,4,0) equals ρ_g f(d,0,0)/ρ_H (i.e. the dry wall transition quality) together with equation (5.11). At lower mass fluxes, the calculation indicates that no adiabatic dry wall region exists. Under these conditions, core entrainment can be neglected for the purpose of average voidage prediction.

5.3 Comparison with Data

A consequence of the model proposed in this chapter is that void characteristics depend both on flow pattern and friction regimes. A full test of this is not possible since an extensive data analysis performed as part of this work indicates that a majority of both distributed and separated flow void data were obtained for the f(a,0,0) friction regime. This is because void-measuring techniques are often unsuited for the high void, high velocity conditions expected for other friction regimes.

Although, as stated, most void data apply to the (a,0,0) friction regime, exceptions found covered a number of different friction regime/flow pattern combinations, so a reasonably extensive evaluation of the model was possible. The model was generally compatible with the data. Although an examination of all relevant data is beyond the scope of

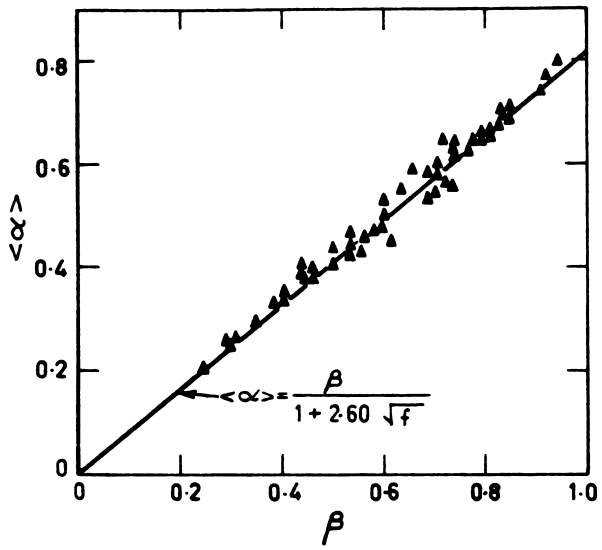

Fig. 5.1a
Liquid-phase-continuous distributed flow.

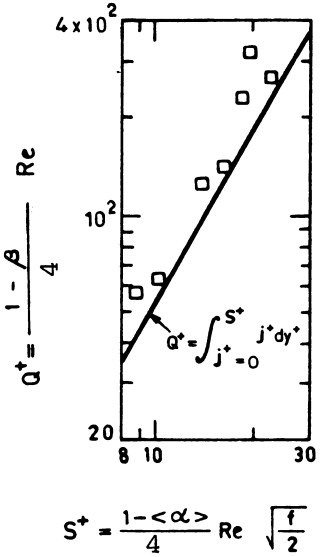

Fig. 5.1b
Separated flow.

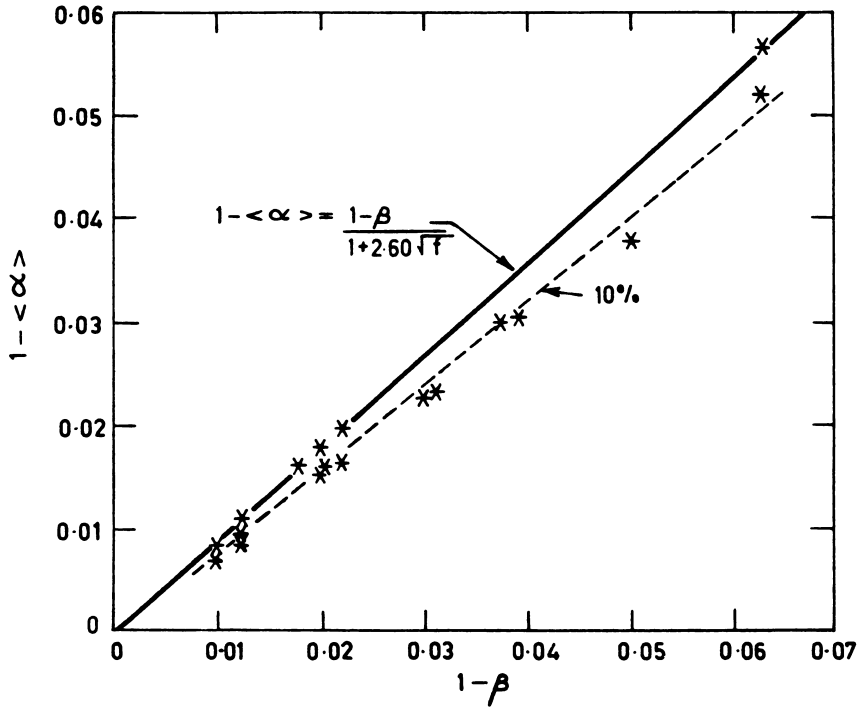

Fig. 5.1c
Gas-phase-continuous distributed flow.

Fig. 5.1 Comparison of argon/alcohol void data [5.10] with theory. Notation as in fig. 4.2. Corresponding pressure gradient and velocity profiles are shown in figs. 4.1 and 3.7.

this work, some typical comparisons of data with equations developed here are presented to demonstrate the applicability of the model.

Figure 5.1 compares equations (5.6), (5.15) and (5.19) and average voidage data argon-alcohol viscosity-dependent upflow [5.10]: figures (5.1a), (5.1b) and (5.1c) being respectively for liquid-flow distributed (c,0,0) flow (for which $V \cong 0$, see section 5.1.1.2), (b,3,-1) annular flow, and dry wall distributed (d,0,0) droplet flow. The flow conditions for these data are as given in the flow regime map of fig. 4.2. Associated pressure drop and velocity profile data, from which the friction regimes were determined, have been presented in figs. (4.1) and (3.7) respectively.

The friction regime for fig. (5.1a), (c,0,0), is not that expected for developed flows, (a,0,0). Moreover, the transition to annular flow does not occur at the voidage value $\langle\alpha\rangle = 0.55$ expected for developed flows (see section 5.2.2). Although the flow conditions thus appear to be for under-developed flows, the data are compatible with the present modelling of the drift-flux equation's distribution parameter and drift velocity.

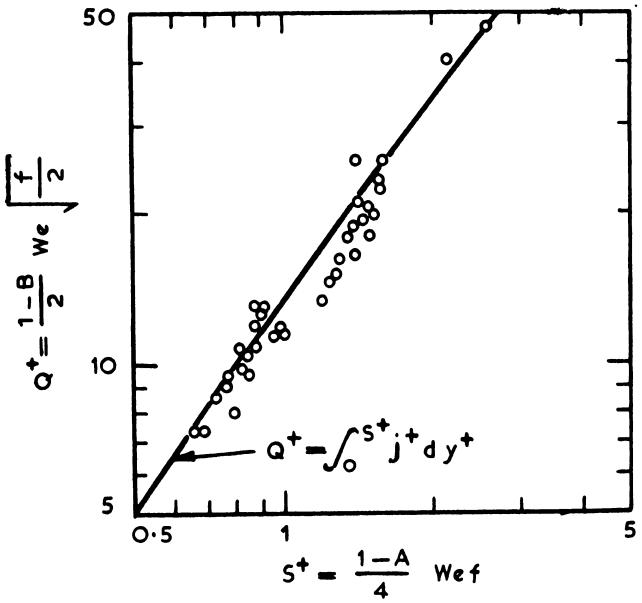

Fig. 5.2 Comparison of (e,2,-4) annular flow data with theory: water adiabatic upflow in a 17.1 mm tube, $\rho_\ell/\rho_g = 13$, data from [5.12]. Corresponding velocity profiles and friction factors are in figs. (3.7) & (4.3).

Some void data for typical annular flow surface tension-dependent (e,2,-4) average voidage data [5.11] are compared with predictions from the present model in fig. 5.2. Associated pressure loss and velocity profile data have been presented in figs. 4.3 and 3.7. Core droplets and film voids have been found to affect average voidage for surface tension-dependent flows to only a small extent except at high voidages (this is demonstrated in fig. 10, appendix A24), and so were neglected in fig. 5.2.

Figure 5.3 considers typical void data for high pressure steam-water flows in various rod bundles. Rod bundle flow geometries are particularly relevant to nuclear engineering. The predictions are for the (a,0,0) friction regime with a bubble drift velocity for distributed flow, and a separated flow/distributed flow transition at $\langle\alpha\rangle = 0.55$, with no core droplets for separated flow. The errors at very low values of $1-\langle\alpha\rangle$ are due to the neglect of core droplets. It is apparent that core droplets have little influence on annular flow voidage at lower average voidages.

Figure 5.3 also contains data obtained immediately downstream of a 37 rod bundle[5.16]. The data disagree with the model and instead agree with the homogeneous prediction $\langle\alpha\rangle = \beta$, suggesting that the flow is homogenised by abrupt changes in flow section.

Figure 5.3 supports the assumed flow pattern transition at $\langle\alpha\rangle \cong 0.55$, although a better prediction of the lowest mass flux data shown would be achieved with a transition voidage of 60%. This feature is common to mass fluxes lower than those encountered under normal reactor operating conditions, and also to pressures lower than encountered under normal reactor conditions. The latter is demonstrated in fig. 5.4, which shows air-water data at atmospheric pressure [5.17] compared with predictions for the (b,0,0) regime. The agree-

Symbol	No. of rods (Test section name)	G kg $m^{-2}s^{-1}$	D mm	P MPa	Ref.
Δ	4	750	21.1	7.1	5.12
o	19 (IT25)	2164	7.5	2.9	5.13
+	1	132	13	3.9	5.14
x	1 (IT45)	3489	9.0	5.0	5.15
∇	1 (IT37)	412	3.0	5.0	5.15
•	Downstream of 37 rods	various	27	5.0	5.16

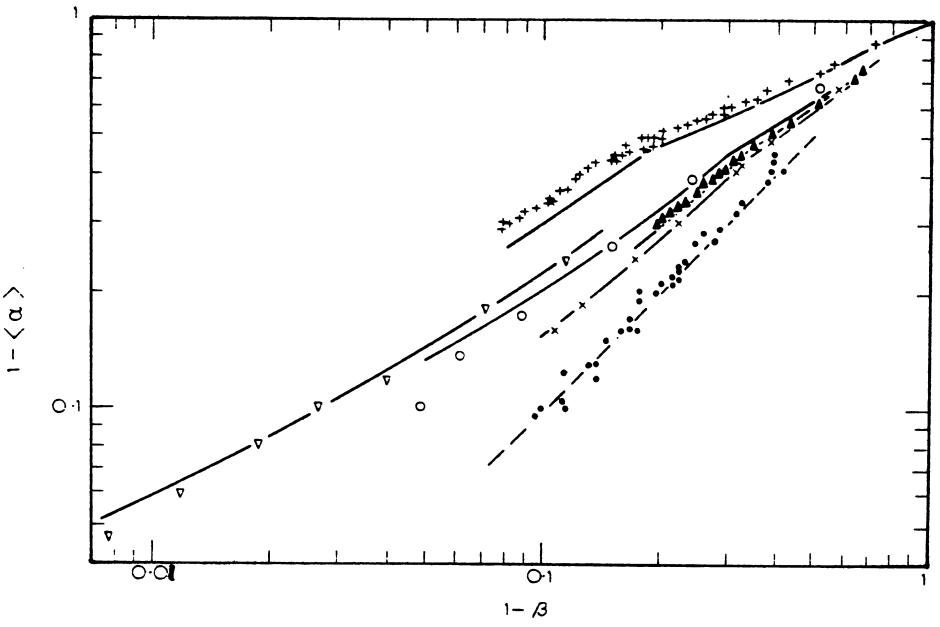

Fig. 5.3 Comparison of typical complex geometry void fraction data with theory

ment in the annular regime has been achieved only through a transition voidage choice of 0.63. The prediction error at very high voidage is again due to the neglect of core entrainment.

The close agreement between the present theory and experimental void data demonstrated in figs. (5.1-5.4) is considered here to be due to correct allowance for friction regime and flow pattern effects, and is not due to special data selection. The data of figs. 5.1, 5.2 and 5.4 were chosen for discussion because of the simultaneous relevance of these data to other chapters of the thesis, and the data of fig. 5.3 were chosen because they representatively covered the experimental range of rod bundle $\langle\alpha\rangle:\beta$ characteristics and covered a wide range of flow parameters (G,D,P).

Although data selection on the basis of good agreement with the present theory has been resisted for the bulk of this thesis, an exception is made in closing this chapter. Void data for air-water upflow at atmospheric pressure in an 11 mm dia. tube [5.18] are considered of interest since the very close agreement between these data and predictions using the present theory cannot be adequately shown via the usual graphical comparison. Moreover, the usual method of assessing predictive methods through error assessment becomes inappropriate since, for these data, the errors are mostly less than experimental errors implied by the number of given significant digits. The data and predictions are compared in table 5.1. It can be seen that the agreement is remarkable: although the bulk of data are given to three significant figures, the discrepancy between experiment and prediction is less than experimental round-off in more than half the cases, and the maximum discrepancy is less than 2%. The close agreement adds confidence to both these data and the predictive method, here being that for the distributed (a,0,0) friction regime (usually

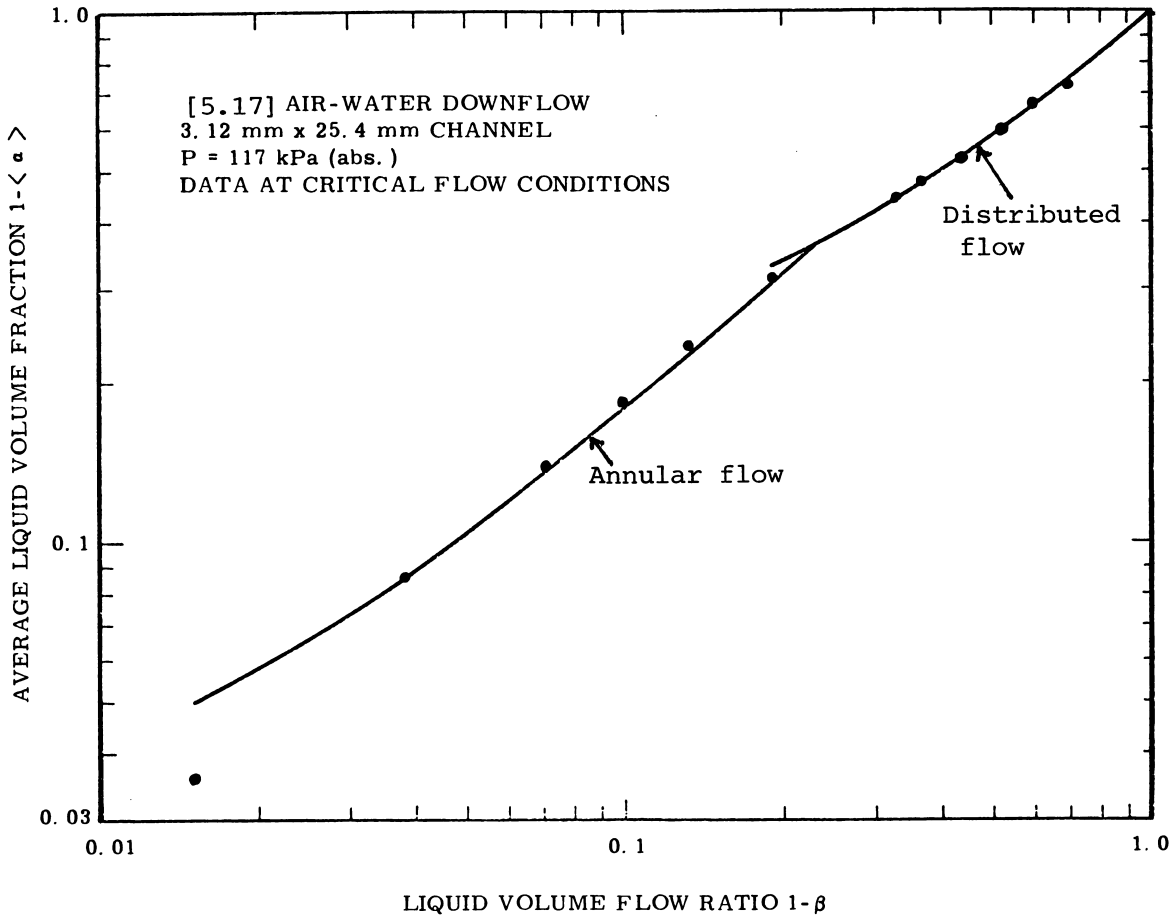

Fig. 5.4 Comparison of theory with low pressure void data

applicable for low void bubble flow data) with a bubble rise velocity of 0.22 m s^{-1} calculated from equation (5.10).

These data are discussed further in Appendix A18.

Table 5.1 Comparison of experimental void fractions [5.18] with those calculated for the (a,0,0) friction regime

$\langle j_\ell \rangle$ m s^{-1}	$\langle j_g \rangle$ m s^{-1}	$\langle \alpha \rangle$, % Expt.	Pred.
2.91	0.11	2.86	2.86
2.91	0.094	2.46	2.46
2.91	0.122	3.16	3.16
2.88	0.22	5.6	5.57
2.87	0.302	7.4	7.48
2.87	0.407	9.8	9.76
2.87	0.42	10	10.0
2.87	0.69	15.2	15.3
2.87	0.755	16.3	16.4
2.78	1.16	23.1	23.2
2.51	1.25	26.1	26.1
2.51	1.84	33.4	33.4
2.51	0.950	21.6	21.5
2.51	0.735	17.7	17.7
2.51	0.54	13.8	13.8
2.51	0.394	10.7	10.6
2.51	0.318	8.8	8.75
2.51	0.228	6.6	6.47
2.51	0.181	5.29	5.22
2.51	0.122	3.64	3.60

Chapter 5 References

5.1 N. Zuber and J.A. Findlay, 'Average volumetric concentration in two-phase flow systems', J. Heat Trans. 87, 453 (1965).

5.2 N. Zuber et al., 'Steady state and transient void fraction in two-phase flow systems', GEAP-5417 (1967).

5.3 M. Ishii et al., 'Drag coefficient and relative velocity in bubbly, droplet or particulate flows', AIChE J. 25, 843 (1979).

5.4 G.B. Wallis, 'One-dimensional two-phase flow', McGraw-Hill (1969).

5.5 S.Z. Rouhani, 'Void measurements in the regions of subcooled and low-quality boiling', AE-238 and AE-239 (1966).

5.6 S.P. Kaznovskii et al., 'Critical heat transfer and distribution of the liquid in disperse annular flow', High Temp. 14, 894 (1977).

5.7 G.G. Bartolomei and R. Georgescu, 'Experimental study of the hydrodynamics of two-phase flow in vertical pipes', IFA (Bucharest) report TR-52, (1966); AERE Trans.1076 (1967).

5.8 A.W. Bennett et al., 'Flow visualisation studies of boiling at high pressure', AERE-R4874 (1965).

5.9 P. Alia et al., 'Liquid volume fraction in adiabatic two-phase vertical upflow-round conduit', CISE-R-105 (1965).

5.10 Argon-alcohol average void data in CISE reports R-82, R-105, R-109 and R-225.

5.11 P.L. Kirillov et al., 'Calculating the hydraulic losses in an adiabatic high pressure steam-water flow', Thermal Engineering 24, (10), 41, (1977).

5.12 V.I. Subbotin et al., 'Measurement of some characteristics of a steam-water flow in a round tube at pressures of 70 and 100

atm', ASME paper WA-75/HT21 (1975).

5.13 E. Schönberg, 'Stability studies for boiling water reactors', EURAEC-2092 (1970).

5.14 G. Agostini et al., 'Density of steam-water mixtures flowing in 19-rod clusters under adiabatic and heated conditions', CISE-R-309 (1971).

5.15 G. Agostini et al., 'Density measurements of steam-water mixtures flowing in adiabatic and heated annular channels', CISE-R-295 (1970).

5.16 O. Nylund et al., 'Hydrodynamic and heat transfer measurements on a full-scale simulated 36-rod Marviken fuel element with uniform heat flux distribution', FRIGG-2 (1968).

5.17 H.K. Fauske, 'Two-phase two- and one-component critical flow', Proc. Symp. on Two-phase Flow, Exeter, Paper G1 (1965).

5.18 V.M. Borishanskiy et al., 'Void fraction and pressure drop in two-phase upflow at atmospheric pressure', Fluid Mechanics Soviet Research 6 (6), 51 (1977).

CHAPTER 6

PROPAGATION PHENOMENA IN GAS/LIQUID SYSTEMS

In this chapter, simplified single phase flow theory for propagation phenomena is adapted for two-phase conditions, with emphasis being placed on a method of allowing for phase and velocity distribution effects. The analysis presented is for the propagation of pulses sufficiently small that equations may be linearised. Compressibility of the liquid phase is neglected, as is flexibility of the containing pipework. Subsequent errors are negligible except at very low voidages, and reference is made to [6.1] where these neglected effects are considered. Mass transfer between the phases is also neglected, i.e. the 'frozen' approach is followed for one-component flows rather than the 'equilibrium' approach. Surveys, e.g. [6.2], indicate that frozen models are more compatible with data, suggesting that the timescale required for phase changes are larger than the transit times of pressure pulses.

6.1 The Gas Isentropic Expansion Coefficient

Later analysis is simplified by an assumption that the passage of pressure pulses occurs isentropically. Since the liquid is considered to be incompressible, the assumption requires an expression for the gas isentropic expansion coefficient. An expression for this is derived as follows:

From the gas equation of state,

$$Pv_g = RT,$$

from which the temperature and specific volume change associated with a pressure pulse ΔP is related by

$$R\Delta T = P\Delta v_g + v_g\Delta P. \qquad (6.1)$$

From basic thermodynamics, the heat added to the gas phase per unit volume ΔQ_g is

$$\rho_g [C_{vg} \Delta T + P \Delta v_g] = Q_g . \quad (6.2)$$

Similarly, for any heat transferred to the liquid, causing a temperature change ΔT_ℓ,

$$\rho_\ell C_\ell \Delta T_\ell = Q_\ell . \quad (6.3)$$

For the overall process to be adiabatic,

$$\alpha Q_g + (1-\alpha) Q_\ell = 0.$$

i.e.

$$x_s Q_g/\rho_g + (1-x_s) Q_\ell/\rho_\ell = 0 \quad (6.4)$$

where x_s is the 'static quality', $\alpha \rho_g/(\alpha \rho_g + (1-\alpha)\rho_\ell)$. In the absence of 'slip', $x_s \equiv x$.

For finely mixed two-phase flow, thermal equilibrium is expected, i.e. $\Delta T_\ell = \Delta T$. For separated flows, where little thermal exchange is expected during a pressure pulse, $\Delta T_\ell = 0$. We introduce a coefficient of thermal exchange, K, defined by

$$\Delta T_\ell = K \Delta T, \quad (6.5)$$

where K lies between 0 and 1.

For little thermal exchange, $K \cong 0$, and for strong thermal exchange, $K \cong 1$. The comparative success of 'frozen' models for one component flows [6.2] suggests the $K \cong 0$ is more appropriate.

Combining equations (6.2) to (6.5),

$$[x_s C_{vg} + K(1-x_s) C_\ell] \Delta T + x_s P \Delta v_g = 0 \quad (6.6)$$

Eliminating ΔT from equations (6.1) and (6.6)

$$\frac{\Delta P}{P} + \frac{K C_\ell (1-x_s) + C_{pg} x}{K C_\ell (1-x_s) + C_{pg} x} \frac{\Delta v_g}{v_g} = 0,$$

where use has been made of

$$R = C_{pg} - C_{vg}.$$

Integration leads to

$$P\, v_g^{\gamma} = \text{constant}, \tag{6.7}$$

where the isentropic expansion coefficient γ is

$$\gamma = \frac{K\, C_\ell\, (1-x_s) + C_{pg}\, x_s}{K\, C_\ell\, (1-x_s) + C_{vg}\, x_x}\,. \tag{6.8}$$

6.2 Liquid-phase Continuous Flows

6.2.1 Necessary distribution parameters

The widely-used method of using slip or voidage correlations to express momentum and kinetic energy fluxes in terms of readily-assessable parameters is not valid since, as discussed in chapter 5, slip or void correlations implicitly quantify a double correlation coefficient, and reduction of averaged momentum and kinetic energy fluxes require the use of higher order correlation coefficients.

In the section 6.2.2, the momentum and kinetic energy fluxes are reduced through the use of the generalised distribution parameter of section 5.1.1.2,

$$C_o = \langle \alpha j^k \rangle / (\langle \alpha j^{k-1} \rangle \langle j \rangle) = 1 + 2.6\, (\sqrt{2})^m \sqrt{f(z,m,n)} \tag{6.9}$$

and velocity distribution parameters

$$C_2 = \langle j^2 \rangle / \langle j \rangle^2 = 1 + 3.77\, (2)^m\, f(z,m,n) \tag{6.10}$$

and

$$C_3 = \langle j^3 \rangle / \langle j \rangle^3 = 1 + 11.3\, (2)^m\, f(z,m,n) - 34.4\, (2)^{3m/s}\, f^{3/2}(z,m,n). \tag{6.11}$$

The RHS of equations (6.10) & (6.11) are obtainable from manipulation of equations (3.31) or (3.32).

As discussed in chapter 4, (z,m,n) for liquid-phase distributed flows is usually (a,0,0). For these flows, equations (6.9) - (6.11) lead to typical C_0, C_2 and C_3 values of 1.2, 1.03 and 1.06 respectively.

The near-unity values of C_2 and C_3 suggest that errors will be small if unity values are assumed. This is so for single phase flows, where the unity assumption is often used. However, the assumption can lead to significant errors at higher voidage distributed two-phase flows, so the expressions developed below incorporate the factors C_2 and C_3.

6.2.2 The wave equation

In the following, local drift between the phases is neglected, i.e. the analysis considers $u_g = u_\ell = j$. Allowance for drift leads to terms which cannot be readily evaluated; in any case, such terms are expected to have only a very small influence on predicted propagation velocities since drift velocities are very small compared with propagation velocities. (The awkward terms resulting from the inclusion of drift velocities can be neglected in the special case of very low flows. An analysis for this, similar to that presented here, is included in appendix A6. The analysis of appendix A6 indicates that, at least for very low flows, the propagation velocities of the present analyses are the same as those when drift is allowed for, provided the gas-content dependent variable is chosen to be void fraction rather than gas volume flow fraction. For non-negligible flow velocities, the analysis of Martin and Padmanabhan [6.3] allows for a constant drift velocity but in effect considers the distribution parameter to be unity.)

Consider now the equations describing conservation of mass and momentum averaged over the flow section, equations (2.7) and (2.8). Using equations (6.9 - 11) together with assumptions stated at the beginning of the chapter, equations (2.7) and (2.8) may be converted to

$$\frac{1}{C_o}\left(\frac{\partial}{\partial t} + C_o \langle j \rangle \frac{\partial}{\partial z}\right) \rho_H + \rho_H \frac{\partial \langle j \rangle}{\partial z} = 0 \qquad (6.12)$$

and

$$\rho_H\left[\frac{\partial}{\partial t} + \left\{C_o + 2(C_2-C_o)\frac{\rho_\ell}{\rho_H}\right\}\langle j\rangle\frac{\partial}{\partial z}\right]\langle j\rangle + \frac{\partial P}{\partial z} + \frac{\partial P}{\partial z}\Big|_F + \frac{\partial P}{\partial z}\Big|_G = 0. \tag{6.13}$$

The convective velocities in the substantial derivatives of equations (6.12) and (6.13) indicate that perturbations in density and momentum convect with velocities which are respectively faster and slower than the mixture velocity $\langle j\rangle$. This is not surprising since variations in density are due to variations in gas content and, in the present model, the gas is confined to the faster moving core region; similarly, variations in momentum are controlled by the slower moving denser region near the wall.

Consider perturbations in density, velocity and pressure ($\delta\rho_H$, $\delta\langle j\rangle$, and δP) to the system. Neglecting gravitational and frictional pressure gradients, as these are small compared with the momentum flux term at the conditions of interest, and noting that if the neglected energy equation, equation (2.9), is replaced by an assumption that the process is isentropic, then $\delta\rho_H = \left(\frac{d\rho_H}{dP}\right)_s \delta P$, then equations (6.12) and (6.13) may be linearised to form

$$\begin{pmatrix} \rho_H\left(\frac{\partial}{\partial t} + \langle j\rangle\left\{C_o+2(C_2-C_o)\frac{\rho_\ell}{\rho_H}\right\}\frac{\partial}{\partial z}\right) & \frac{\partial}{\partial z} \\ \rho_H\frac{\partial}{\partial z} & \frac{1}{C_o}\left(\frac{d\rho_H}{dP}\right)_s\left(\frac{\partial}{\partial t} + C_o\langle j\rangle\frac{\partial}{\partial z}\right) \end{pmatrix}\begin{pmatrix}\delta\langle j\rangle \\ \delta P\end{pmatrix} = 0 \tag{6.14}$$

Characteristic velocities of the system are given by the determinant of the above operating on either $\delta\langle j\rangle$ or δP. The characteristic equation may be rearranged to the form

$$\left(\frac{1}{a^2}\left(\frac{D}{Dt}\right)^2 - \frac{\partial^2}{\partial z^2}\right)(\delta\langle j\rangle \text{ or } \delta P) = 0 \tag{6.15}$$

with

$$\frac{1}{a^2} = \frac{1}{C_o}\left(\frac{d\rho_H}{dP}\right)_s \left(1 + \frac{\langle j\rangle^2}{C_o}\left(\frac{d\rho_H}{dP}\right)_s \left\{(C_2-C_o)\frac{\rho_\ell}{\rho_H}\right\}^2\right)^{-1} \qquad (6.16a)$$

and

$$\frac{D}{Dt} = \frac{\partial}{\partial t} + \langle j\rangle \left(C_o + (C_2-C_o)\frac{\rho_\ell}{\rho_H}\right)\frac{\partial}{\partial z} . \qquad (6.16b)$$

Equation (6.15) is a wave equation which states that for a flow velocity $\langle j\rangle$, perturbations in velocity and pressure (and hence density) propagate with velocity ± a given by equation (6.16a) - note the dependence on $\langle j\rangle$ - with respect not to $\langle j\rangle$ but to $\langle j\rangle\left(C_o + (C_2-C_o)\frac{\rho_\ell}{\rho_H}\right)$. Values of C_o and C_2 are obtained from equations (6.9) and (6.10).

If it is assumed that the quality does not change during the pressure pulse, the low velocity value of a, a_o, may be expressed in terms of voidage as

$$a_o = \frac{\sqrt{\gamma P/\rho_g}}{\left\{\frac{\rho_\ell}{\rho_g}\langle\alpha\rangle - \left(\frac{\rho_\ell}{\rho_g} - 1\right) C_o \langle\alpha\rangle^2\right\}^{\frac{1}{2}}} . \qquad (6.17)$$

As stated, the analysis of appendix A6 indicates that this same result holds if a constant drift velocity V is allowed for. For cases where $\rho_\ell >> \rho_g$, equation (6.17) becomes

$$a_o = \frac{\sqrt{\gamma P/\rho_\ell}}{\left\{\langle\alpha\rangle\left(1 - C_o\langle\alpha\rangle\right)\right\}^{\frac{1}{2}}} \qquad (6.17a)$$

which is similar to the often-quoted equation (e.g. equation (14) of [2] and equation (23) of [4])

$$a = \frac{\sqrt{\gamma P/\rho_\ell}}{\left\{\langle\alpha\rangle\left(1 - \langle\alpha\rangle\right)\right\}^{\frac{1}{2}}} .$$

Returning now to the influence of flow on 'a', equation (6.16a) can be expressed as

$$a = a_o \left(1 + \left\{\frac{\langle j \rangle}{a_o} (C_2 - C_o) \frac{\rho_\ell}{\rho_H}\right\}^2\right)^{\frac{1}{2}}, \qquad (6.18)$$

where a_o is the velocity of sound at negligible flow velocities, given by equation (6.17). This value of 'a' is with respect to $\langle j \rangle$ $(C_o + (C_2 - C_o) \frac{\rho_\ell}{\rho_H})$.

Choked flow occurs if 'a' is zero with respect to the flow boundary, i.e. choked flow occurs when

$$a = \langle j \rangle \left(C_o + (C_2 - C_o) \frac{\rho_\ell}{\rho_H}\right),$$

from which the critical velocity $\langle j \rangle_{crit}$ is obtained as

$$\langle j \rangle_{crit} = \frac{a_o}{\left\{C_o \left[C_o + 2(C_2 - C_o) \frac{\rho_\ell}{\rho_H}\right]\right\}^{\frac{1}{2}}}. \qquad (6.19)$$

It is seen from (6.23) that, since $(C_2 - C_o) < 0$, the critical velocity $\langle j \rangle_{crit}$ is generally larger than the low flow sonic velocity a_o.

In order to conform to the practice of expressing experimental data in terms of critical mass flux G_{crit} or the ratio of this to the homogeneous prediction $G_{crit,H}$ as a function of quality, the above can be re-expressed as

$$G_{crit} = \frac{\{\gamma P \rho_g / x\}^{\frac{1}{2}}}{\left\{1 - (C_o - 1)\left(1 + 2x \left(\frac{\rho_\ell}{\rho_g} - 1\right)\right) + 2 (C_2 - 1)\left(1 + x \left(\frac{\rho_\ell}{\rho_g} - 1\right)\right)\right\}^{\frac{1}{2}}} \qquad (6.20)$$

and

$$\frac{G_{crit}}{G_{crit,H}} = \{1 - (C_o-1)(1 + 2x\,(\frac{\rho_\ell}{\rho_g} - 1)) + 2(C_2-1)(1 + x(\frac{\rho_\ell}{\rho_g} - 1))\}^{-\frac{1}{2}} \tag{6.21}$$

where $$G_{crit,H} \equiv \rho_H \{(\frac{d\rho_H}{dP})_s\}^{-\frac{1}{2}} .$$

The above equations must be solved iteratively since both C_o and C_2 depend on flow. Examination of the equations indicates that the term containing C_2 can be neglected except at higher voidages, when the denominator in the RHS of the equations can become very small. It is expected that a more detailed examination, in which the kinetic energy equation was included, would result in an additional term involving the factor C_3 of equation (6.20).

6.2.3 Comparison with data

To test the present theory, pressure pulse velocity and critical flow data had to satisfy two requirements:

(a) The data needed to be two component rather than one component, thus ensuring no phase change effects; and

(b) The data needed to be for developed, turbulent, straight pipe flow since distribution parameters cannot as yet be predicted for other systems.

As well as these requirements, it is desirable that additional information be present in order that specific aspects of the model may be tested (e.g. void data to give experimental distribution parameter values).

Very few data were found in the literature satisfying these requirements. Most two-component data found were for stationary liquid (pressure pulse propagation velocity) or for nozzle flow (critical flow). Although the analysis does not strictly apply to these data, it has been found that, for distributed flow, suitable choice of distribution parameter (rather than the predicted value) renders the

equations consistent with the data. This is demonstrated in data analysis presented in appendices A6 and A19. It is, however, more appropriate to compare the model with data satisfying the above requirements. Such a comparison is a more rigorous test of the theory since the option of adjusting the distribution parameter is invalidated as this parameter is predictable from the model. The data analysis below is confined to a comparison of the model with data satisfying the requirements stated above.

In considering the fact that the model does not apply to nozzle flow, it should be kept in mind that current reactor design basis accidents involve choked flow from a straight pipe, as discussed here.

Data suitable for testing equations of the model describing (a) the flow pressure pulse velocity, (b) the pressure pulse velocity for intermediate flows, and (c) choked flow, were found in refs. [6.5], [6.6] and [6.7] respectively.

The one unknown for model predictions is the value of the thermal exchange coefficient, K, defined by equation (6.5), which determines the effective isentropic expansion coefficient, equation (6.8). Although specific values of K are unknown, for the present data analyses, the qualities are very small indeed, so for non-negligible K, equation (6.8) indicates $\gamma \cong 1$, a value which is assumed for the data of refs. [6.5], [6.6] and [6.7].

The low flow pressure pulse velocity data of [6.5] are compared with predictions based on the present model and the homogeneous model in fig. 6.1. Both predictions are close to the data, with discrepancies occurring at higher voidages, where both models underpredict, with the present model being closer to the data.

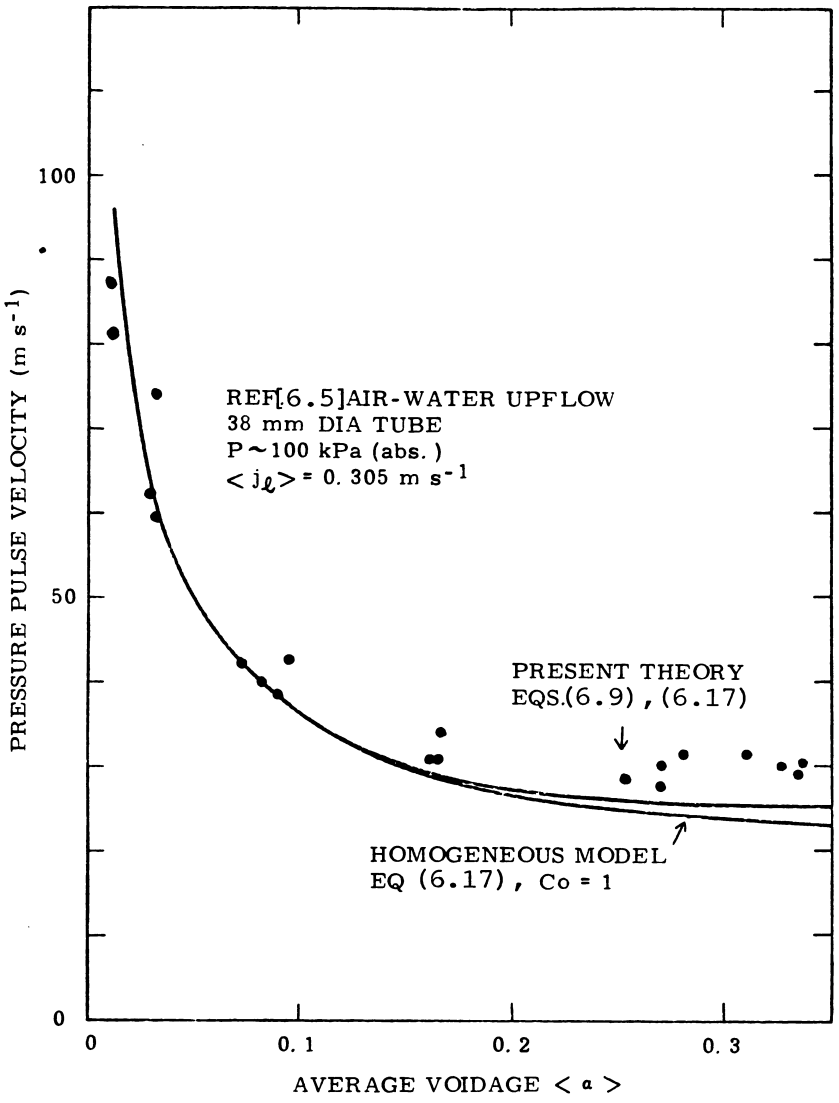

Fig. 6.1 Comparison of theory with pressure pulse propagation velocity data

It is interesting to note that an assumption of $\gamma = \gamma_g$ instead of $\gamma = 1$ would raise the predicted curves of fig. 6.3 by ~18% and so bring agreement between the higher voidage data and the present model. Such a value of γ for this voidage region is plausible since slug flow is plausible for this region. For this flow pattern, little thermal exchange between the phases is expected, i.e. $K \cong 0$ and from equation (6.8), $\gamma \cong \gamma_g$.

The data of fig. 6.1 are for low flows. The analysis of section 6.2.3 indicates that, at higher velocities, the pressure pulse velocity varies with flow velocity in a complex manner. Pressure pulse velocities at intermediate flow velocities [6.6] indicate that the effect of flow on propagation velocities is not simply additive. Predictions from the present model are reasonably close to the data of [6.6].

The choked flow data of [6.7] are compared with predictions based on the present model and the homogeneous model in fig. 6.2. The predictions from the present model are given both for a calculated value of the velocity distribution parameter C_2, and for a unity value of C_2. As discussed in section 6.2.2, it can be seen that correct treatment of this parameter is important at higher voidages.

The homogeneous model predictions are far too low, while the predictions based on the present model are reasonably consistent with the data, with discrepancies becoming pronounced near the distributed flow/annular flow boundary. It is possible that these discrepancies would reduce if the analysis had incorporated the energy equation instead of the assumption of isentropic flow.

The distribution parameter C_o predicted for the data of fig. 6.2 were independently confirmed by analysis of void data obtained simultaneously with the data. This analysis has already been

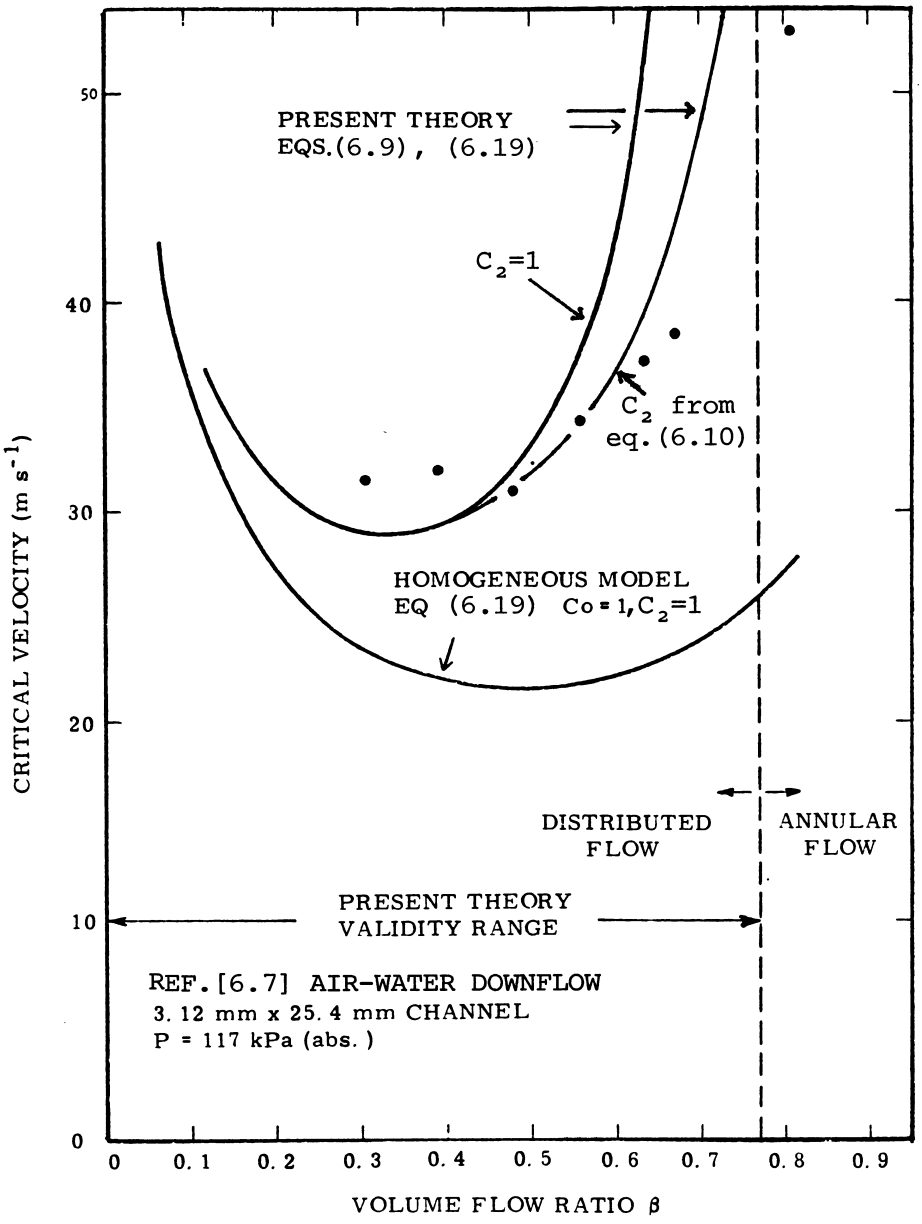

Fig. 6.2 Comparison of theory with choked flow data

summarised in fig. 5.4. The flow pattern transition volume flow ratio of fig. 6.2, $\beta_{Tr} = 0.78$, was obtained from figure 5.4.

6.3 Dry Wall Droplet Flows

Perturbations in droplet flow density, kinetic energy and momentum are associated with perturbations in droplet concentration so, unlike the case for bubble flow, convective velocities for the above perturbed quantities can be expected to be close to the flow velocity. It is therefore anticipated that propagation velocities will be close to those predicted by the homogeneous model, so the factors C_2 and C_3 of equations (6.10) and (6.11) can be assumed to be unity with negligible error being introduced by this assumption.

6.3.1 The wave equation

Droplet flow propagation phenomena can be analysed in a manner analagous to that used in the previous section. Using the same assumptions as in that section (constant area duct, no phase change, constant physical properties, zero drift velocity) and using the droplet distribution parameter of section 5.1.2:

$$C_{go} = \langle(1-\alpha)\ j^k\rangle / (\langle(1-\alpha)\ j^{k-1}\rangle\langle j\rangle) \qquad (6.22a)$$

$$= 1 + 2.6\ \sqrt{f(d,0,0)}\ ,$$

the equations of conservation of mass and momentum, equations (2.7) and (2.8) can be expressed as

$$\frac{1}{C_{go}}\left[\frac{\partial}{\partial t} + C_{go}\langle j\rangle\frac{\partial}{\partial z}\right]\rho_H + \left(1-\frac{1}{C_{go}}\right)\frac{\partial \rho_g}{\partial t} + \rho_H\frac{\partial\langle j\rangle}{\partial z} = 0 \qquad (6.23)$$

and

$$\rho_H\left[\frac{\partial}{\partial t} + \langle j\rangle\left\{C_{go} + 2(1-C_{go})\frac{\rho_g}{\rho_H}\right\}\frac{\partial}{\partial z}\right]\langle j\rangle$$

$$+ (1-C_{go})\langle j\rangle\left[\frac{\partial}{\partial t} + \langle j\rangle\frac{\partial}{\partial z}\right]\rho_g$$

$$+ \frac{\partial P}{\partial z} + \frac{\partial P}{\partial z}\Big|_F + \frac{\partial P}{\partial z}\Big|_G = 0 \qquad (6.24)$$

In obtaining these equations, use has been made of

$$C_{go}\langle\rho\rangle = \rho_H + (C_{go}-1)\,\rho_g, \text{ i.e.}$$

$$\partial\langle\rho\rangle = \frac{1}{C_{go}}\,\partial\rho_H + \left(1 - \frac{1}{C_{go}}\right)\partial\rho_g$$

which follows from the definitions of average and 'homogeneous' densities $\langle\rho\rangle$ and ρ_H, equation (6.22a) for k = 1, and the relation $G = \rho_H\langle j\rangle$.

As expected, the convective velocities as given by the substantial derivatives of equations (6.23) and (6.24) are close to $\langle j\rangle$.

Consider perturbations of density, velocity and pressure ($\delta\rho_H$, $\delta\langle j\rangle$ and δP) to the system. Neglecting gravitational and frictional pressure gradients, as these are small compared with the momentum flux term at the conditions of interest, and noting that $\delta\rho = \frac{d\rho}{dP}\,\delta P$, the conservation equations may be linearised to form

$$\begin{bmatrix} \rho_H\{\frac{\partial}{\partial t} + \langle j\rangle[C_{go} + 2(1-C_{go})\frac{\rho_g}{\rho_H}]\frac{\partial}{\partial z}\} & \frac{\partial}{\partial z} + \frac{d\rho_g}{dP}(1-C_{go})\langle j\rangle(\frac{\partial}{\partial t} + \langle j\rangle\frac{\partial}{\partial z}) \\ \rho_H\frac{\partial}{\partial z} & \frac{1}{C_{go}}\frac{d\rho_H}{dP}(\frac{\partial}{\partial t} + C_{go}\langle j\rangle\frac{\partial}{\partial z}) + (1-\frac{1}{C_{go}})\frac{d\rho_g}{\partial p}\frac{\partial}{\partial t} \end{bmatrix} \begin{bmatrix} \delta\langle j\rangle \\ \delta P \end{bmatrix} = 0,$$

where values of quantities in the operator are initial values prior to the perturbations.

Characteristic velocities of the system are given by the determinant of the above operating on either $\delta\langle j\rangle$ or δP. The characteristic equation may be rearranged into the form

$$\left[\frac{1}{a^2}\left(\frac{D}{Dt}\right)^2 - \frac{\partial^2}{\partial z^2}\right]\ (\delta\langle j\rangle \text{ or } \delta P) = 0 \qquad (6.25a)$$

with

$$a^2 = \frac{1+\langle j\rangle^2\{\frac{1}{C_{go}}\frac{d\rho_H}{dP}(1-C_{go})^2(\frac{\rho_g}{\rho_H})^2 + \frac{d\rho_g}{dP}(1-\frac{1}{C_{go}})[(C_{go}+(1-C_{go})\frac{\rho_g}{\rho_H})^2 - C_o]\}}{\frac{1}{C_{go}}\frac{d\rho_H}{dP} + (1-\frac{1}{C_{go}})\frac{d\rho_g}{dP}} \qquad (6.25b)$$

and

$$\frac{D}{Dt} = \frac{\partial}{\partial t} + \langle j \rangle \left[C_{go} + (1-C_{go}) \frac{\rho_g}{\rho_H}\right] \frac{\partial}{\partial z} . \qquad (6.25c)$$

Equation (6.25a) is a wave equation which states that for a flow velocity <j>, perturbations in velocity and pressure (and hence density) propagate with a velocity ±a given by equation (6.25b) (note the dependence on <j>) with respect not to <j> but to $\langle j \rangle [C_{go} + (1-C_{go}) \rho_g/\rho_H]$. Choked flow occurs when the propagation velocity is zero, which corresponds to

$$a = [C_{go} + (1-C_{go}) \rho_g/\rho_H] \langle j \rangle .$$

Despite the complexity of equations (6.25), the propagation velocities as given by these equations are very close to those of the homogeneous model (equations (6.25) with $C_{go} = 1$), with the homogeneous model tending to underpredict the slow flow pressure pulse velocity and overpredict the choked flow velocity. This is consistent with the expectations outlined at the beginning of this section and is in marked contrast to bubble flow propagation velocities which, as indicated by equations in the previous section, are considerably greater than velocities predicted by the homogeneous model.

6.3.2 Comparison with data

No data were found suitable for testing the present model, as high voidage data found were for wet wall conditions, i.e. for dispersed annular rather than droplet flows. A possible exception is the high voidage steam-water pressure pulse velocity data of [6.9]. These velocity data have been questioned [6.4] since they are an order of magnitude lower than normally obtained at high voidages. (As discussed in section 6.4, pressure pulse velocities for annular flow are close to that for gas flowing alone.) The pressure pulse velocity data of [6.9] are fairly close to but about 45% higher than those for

the homogeneous model, and are within 25% of the predictions of the present equations for gas-phase distributed flow. It is possible that the flow conditions for the data of [6.9] were droplet rather than annular.

6.4 Separated Annular Two-phase Flows

An analysis of annular flow propagation phenomena was not pursued in this work for two reasons:

(i) The kinetic energy and momentum fluxes required for the analyses (or the momentum flux by itself if the simplified method of sections 6.2 and 6.3 is adapted) can, in principle, be expressed as functions of dependent variables by adapting the method used to obtain the film volume flux in the analysis of annular flow voidage (section 5.2). The approach requires the integration of the relevant fluxes over the film region using a velocity profile from chapter 3. As with the analysis of average voidage, film bubbles and core droplets can be allowed for. However, as with the case for volumetric fluxes, kinetic energy and momentum fluxes so obtained would be implicit (rather than explicit) functions of dependent flow parameters such as superficial velocities, etc. Simple explicit functions for the fluxes, such as were achieved in the analysis of distributed flow propagation, cannot be obtained by the method. The analysis of annular flow propagation phenomena in terms of the flow model developed here would thus require the development of a computer program, and this was felt to be beyond the scope of the present work.

(ii) The method followed in the previous parts of this chapter implies that, quite generally, the zero flow pressure pulse propagation velocity is given by $a = \sqrt{\frac{dP}{d\langle\rho\rangle}}$. According to the theory followed so far, this should also apply to low velocity annular flows. However, experimental evidence,e.g.[6.11] indicates that the correct expression

is $a = \sqrt{\frac{dP}{d\rho_c}}$, where subscript c indicates the core value. Usually $\rho_c \cong \rho_g$ for flow conditions for which annular flow pressure pulse velocity data are available. Thus, a pressure pulse travels preferentially through the core, suggesting an electrical parallel resistance analogy, where the path followed is that of least resistance. The fact that this is so indicates that propagation velocity analyses used for distributed flows must be considered more carefully for annular flows.

The remainder of this section will examine reasons why the low flow pressure pulse velocity is close to that for the core region alone.

6.4.1 Low flow pressure pulse propagation

Consider a round tube system, as in fig. 6.3, where film and core void profiles are assumed to be flat. Flow velocities are assumed to be negligible compared with propagation velocities. The behaviour of a pressure pulse can be determined by examining the radial distribution of perturbations in pressure.

For each of the two regions of fig. 6.3, the appropriately simplified mass and momentum equations are

$$\frac{\partial \rho j}{\partial t} = -\nabla P$$

and

$$\frac{\partial \rho}{\partial t} = -\nabla.(\rho j).$$

Eliminating ρj,

$$\frac{1}{a^2}\frac{\partial P}{\partial t^2} = \nabla^2 P$$

where $a_{c,f}$ is as stated in fig. 6.1.

Assume pressure pulse perturbations P' vary with time and axial position as $e^{i\omega t}\, e^{-iKz}$. The radial variation is to be determined. With the above variation, the velocity a of pressure waves of

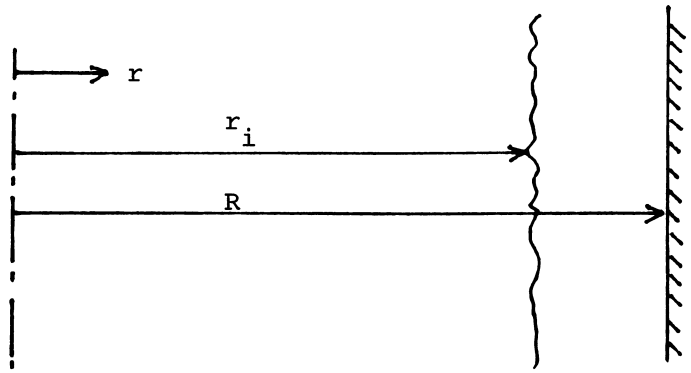

$$j_c = j_{co} + j_c' \qquad j_f = j_{fo} + j_f'$$

$$P = P_o + P' \qquad P = P_o + P'$$

$$a_c^2 = \frac{\partial P}{\partial \rho_c} \qquad a_f^2 = \frac{\partial P}{\partial \rho_f}$$

$$\rho_c = \rho_{co} + \rho_c' \qquad \rho_f = \rho_{fo} + \rho_f'$$

Fig. 6.3 Nomenclature for low velocity annular flow.

Subscripts: c = core, f = film, o = initial value, i = interface value, superscript ' = value of perturbation

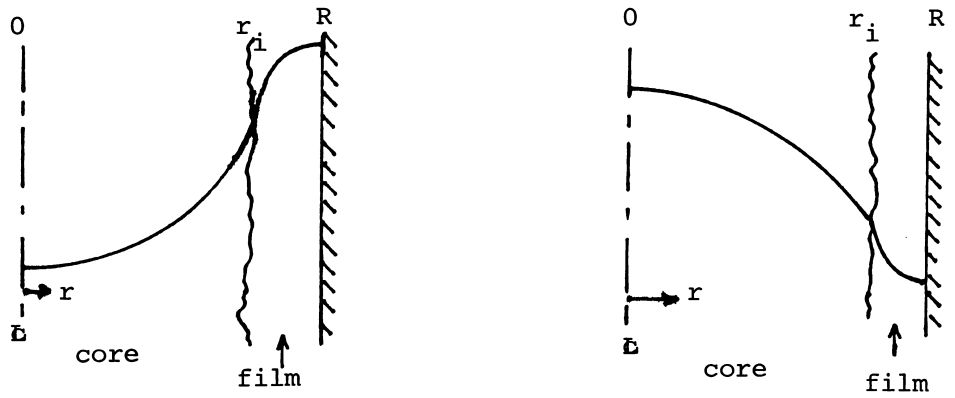

Fig. 6.4 Possible forms of radial distribution of pressure pulses as inferred from boundary conditions

frequency ω is then $a = \omega/K$.

Substitution into the wave equation gives rise to equations describing the radial variations of the perturbations:

Core region:

$$\frac{1}{r}\frac{d}{dr}\left(r\frac{dP'}{dr}\right) + \left(\frac{\omega^2}{a_c^2} - K^2\right) P' = 0 \qquad (6.26)$$

Film region:

$$\frac{1}{r}\frac{d}{dr}\left(r\frac{dP'}{dr}\right) + \left(\frac{\omega^2}{a_f^2} - K^2\right) P' = 0$$

Boundary conditions for the above equations are

(i) P' is symmetric about the centre-line;

(ii) $\frac{\partial P'}{\partial r} = 0$ at $r = R$ and $r = 0$;

(iii) $\frac{1}{\rho_c}\frac{\partial P'}{\partial r}\Big|_{r_i^-} = \frac{1}{\rho_f}\frac{\partial P'}{\partial r}\Big|_{r_i^+}$

and (iv) P' is continuous across the interface at r_i.

From the boundary conditions, the radial distribution of the pressure perturbation must be of a form as shown in fig. 6.4(a) or 6.4(b).

In order to see which general form is appropriate, the values of $\frac{1}{r}\frac{d}{dr}\left(r\frac{dP'}{dr}\right)$ are considered, for each case, in terms of equation (6.26). This leads to:

case a (as in fig. 6.4a):

$$\frac{\omega^2}{a_c^2} - K^2 < 0; \qquad \frac{\omega^2}{a_f^2} - K^2 > 0,$$

implying $a_c > a_f$,

and, case b (as in fig. 6.4b):

$$\frac{\omega^2}{a_c^2} - K^2 > 0; \qquad \frac{\omega^2}{a_f^2} - K^2 < 0,$$

implying $a_f > a_c$.

In reality, the film is approximately all liquid and the core approximately all gas, so $a_f > a_c$. Thus, of the two possibilities, case b is considered realistic. This leads to the solution of equation 6.26 as

$$P' = a_1 J_o \left[\left(\frac{\omega^2}{a_c^2} - K^2\right)^{\frac{1}{2}} r\right], \; r < r_i$$
$$P' = a_2 I_o \left[\left(\frac{\omega^2}{a_f^2} - K^2\right)^{\frac{1}{2}} r\right] + a_3 K_o \left[\left(\frac{\omega^2}{a_f^2} - K^2\right)^{\frac{1}{2}} r\right], \; r > r_i \tag{6.27}$$

where a_1, a_2, a_3 are constants. The small amplitude in the film region implies $a \cong a_c$ which is compatible with data [6.8]. We suppose this to be so and show that the supposition is compatible with equation (6.27).

Consider the film component of equation (6.26). For a thin film, the first term may be approximated by

$$\frac{r_i \left.\frac{dp'}{dr}\right|_{r_i^+} - R \left.\frac{dP'}{dr}\right|_{R^-}}{R\,(R - r_i)}$$

$$= \frac{\left.\frac{dP'}{dr}\right|_{r_i^+}}{(R - r_i)}$$

in view of boundary condition (ii) and since $r_i \cong R$. The film component of equation (6.26) then becomes

$$\frac{1}{P'} \left.\frac{dP'}{dr}\right|_{r_i^+} \cong - \left(\frac{\omega^2}{a_f^2} - K^2\right) (R - r_i) \quad .$$

From the core region component of equation (6.27)

$$\frac{1}{P'} \left.\frac{dP'}{dr}\right|_{r_i^-} \cong - \left(\frac{\omega^2}{a_c^2} - K^2\right)^{\frac{1}{2}} \frac{J_1 \left[\left(\frac{\omega^2}{a^2} - K^2\right)^{\frac{1}{2}} r_i\right]}{J_0 \left[\left(\frac{\omega^2}{a_c^2} - K^2\right)^{\frac{1}{2}} r_i\right]}$$

$$\cong \left(\frac{\omega^2}{a_c^2} - K^2\right) \frac{r_i}{2}$$

since $a = a_c$ implies that $(\frac{\omega^2}{a_c^2} - K^2)^{\frac{1}{2}} r_i$ is small.

In view of the above two equations, boundary condition (iii) becomes

$$\frac{r_i}{2} \left(\frac{\omega^2}{a_c^2} - K^2\right) \cong (R - r_i) \frac{\rho_c}{\rho_f} \left(K^2 - \frac{\omega^2}{a_f^2}\right) .$$

Now $$\frac{2 (R - r_i)}{r_i} \cong \frac{1-A}{A}$$

where A is the area fraction of the core. Thus, the propagation velocity $a = \frac{\omega}{K}$ is approximately

$$a \cong a_c \left[\frac{A + (1-A)\, \rho_c/\rho_f}{A + (1-A)(\rho_c/\rho_f)(a_c/a_f)^2} \right]^{\frac{1}{2}} \qquad (6.28)$$

$$\cong a_c$$

i.e. the propagation velocity is approximately that of the core.

6.4.2 Propagation velocities at moderate flow velocities

For flows with velocities not negligible compared with propagation velocities, the above analysis must be modified. Although the velocity profiles of chapter 3 are used predominantly in this thesis, the present analysis is simplified by assuming flat velocity profiles for the core and film regions, having magnitudes u_f, u_c. The wave equation for each region now becomes

$$\frac{1}{a_{f,c}^2} \left(\frac{\partial}{\partial t} + u_{f,c} \frac{\partial}{\partial z}\right)^2 p' = \nabla^2 p'$$

F or p' varying as $e^{i\omega t} e^{-iKz}$, as before, then

$$\frac{1}{r} \frac{d}{dr} \left(r \frac{dP'}{dr}\right) + \left[\left(\frac{\omega - u_c K}{a_c}\right)^2 - K^2\right] P' = 0 \qquad \text{(core region)}$$

and

$$\frac{1}{r} \frac{d}{dr} \left(r \frac{dP'}{dr}\right) + \left[\left(\frac{\omega - u_f K}{a_f}\right)^2 - K^2\right] P' = 0 \qquad \text{(film region)}$$

which replaces equation (6.26).

The same approximations as were considered in examining the lower velocity case in section 6.4.1 then lead to $a = \omega/K$ being given by

$$\left(\frac{a-u_c}{a_c}\right)^2 + \frac{1-A}{A}\left(\frac{\rho_c}{\rho_f}\right)\left(\frac{a-u_f}{a_f}\right)^2 = 1 + \frac{1-A}{A}\left(\frac{\rho_c}{\rho_f}\right)$$

For most situations, this becomes

$$a \cong u_c + a_c ,$$

i.e. as before, the pressure pulse velocity is approximately that which would occur for the core flow alone.

6.4.3 Comparison with data

The above analysis indicates that the pressure pulse propagation velocity for annular flow should be close to that for the core flowing alone. If the core voidage is known, the pressure velocity can be obtained from the equation for droplet flow, equation (6.25b). Unfortunately, core droplet concentration cannot yet be adequately predicted.

However, all annular flow pressure pulse propagation velocity data found in this project were for low pressure, low flow conditions. For these conditions, droplet concentration is negligible (see e.g. the core void data of [6.10]), so the core propagation velocity should be close to, but, because of the existence of some droplets, slightly less than, the propagation velocity for gas flowing alone, $\sqrt{\gamma P/\rho_g}$.

The data of [6.11], shown in fig. 6.5, are consistent with this.

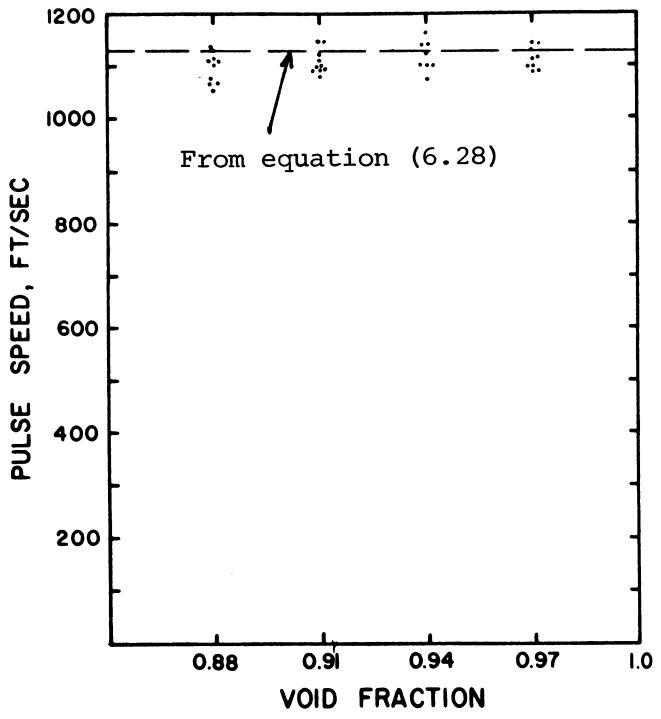

Fig. 6.5 Annular flow pressure pulse speed vs void fraction. Data from [6.11].

Chapter 6 References

6.1 C.S. Martin and M. Padmanabhan, 'Pressure wave propagation in two-phase bubbly air-water mixture', Paper C1, Proc. 2nd Int. Conf. on Pressure Surges, London, BHRA Fluid Engineering (1977).

6.2 H.K. Fauske, 'Propagation of pressure disturbances in two-phase flow', p.639, EUR-4288(E) (1967).

6.3 C.S. Martin and M. Padmanabhan, 'Pressure pulse propagation in two-component slug flow', J. Fluids Engng. 101, 44 (1979).

6.4 S.W. Gouse and R.G. Evans, 'Acoustic velocity in two-phase flow', p.611, EUR-4288(E) (1967).

6.5 L.J. Hamilton et al., 'Propagation of shock wave through two-phase, two-component media', Trans. Am. Nucl. Soc. 10, 660 (1967).

6.6 K. Miyazaki et al., 'Effect of flow on pressure wave propagation on two-component two-phase system', J. Nucl. Sci. Technol. (Tokyo) 10, 127, (1973).

6.7 H.K. Fauske, 'Two-phase two- and one-component critical flow', Proc. Symp. on Two-phase Flow, Exeter, Paper G1 (1965).

6.8 R.E. Collingham and J.C. Firey, 'Velocity of sound in wet steam', I. and E.C., Proc. Des. and Devel. 2, 197, (1963).

6.9 N.I. Seminov and S.I. Kosterin, 'Results of studying the speed of sound in moving gas-liquid systems', Thermal Engng. 11, (6), 59, (1964).

6.10 L.E. Gill et al., 'Sampling probe studies of the gas core in annular two-phase flow', AERE-R 3955 (1963).

6.11 C.W. Garrard and R.S. Wick, 'Pressure pulse propagation in an annular flowing two-phase system', Nucl. Sci. Engng. 36, (3), 427 (1969).

CHAPTER 7

ON THE RELATIONSHIP BETWEEN THE BOILING CRISIS AND WALL SHEAR STRESS

7.1 Introduction

The boiling crisis is defined here as the onset of a sufficiently large dry region on the flow boundary for heat transfer coefficients to be significantly reduced. The term 'boiling crisis' is used here in preference to 'heat transfer crisis' since dry wall conditions may occur with no heat transfer, and since crises connected with the limiting quality phenomenon [7.1] are determined by local quality rather than heat flux.

The dry wall characterising the crisis may be due to the removal of the film region of annular flow by the combined effect of evaporation, entrainment, and deposition (dryout); or to a breakdown in the nucleate boiling heat transfer process (departure from nucleate boiling, or DNB). As discussed in [7.2], other crisis mechanisms exist, but these are generally not relevant for nuclear engineering.

Dryout is necessarily confined to the annular flow regime. DNB is usually considered as being confined to lower quality conditions. However, the hydrodynamic evidence presented in previous chapters of the applicability of the 'e' sublayer of table 3.1, i.e. of annular flow nucleate boiling, suggests that DNB may also occur with high quality annular flows.

Experimentally, the boiling crisis is usually identified by the onset of a temperature transient on the heated surface during the quasi-stationary variation of one flow parameter (usually power) with other parameters (duct dimensions and geometry, heat flux profile, system pressure, mass flux) being kept constant. For the purpose of this thesis, in which emphasis is placed on stationary flows, con-

ditions where crisis temperature transients are initiated are assumed to be identical to those which occur at the crisis location when dry regions reach their equilibrium steady-state temperatures.

7.2 Experimental Evidence of a Relationship between the Boiling Crisis and Wall Shear Stress

Examination of boiling crisis data indicates that, when plotted as power (or heat flux) as a function of quality, with other parameters being kept constant, the plots are better fitted by a series of connected straight lines rather than a smooth curve. For boiling crisis data with associated pressure loss data, the pressure loss data may be converted to friction factor data and interpreted in terms of the friction regime concept of chapter 4. A comparison of boiling crisis and associated friction factor plots indicates that individual lines on the crisis plots may be identified with specific friction regimes.

An example, based on data from [7.3] and [7.4], is shown in fig. 7.1. The predicted friction factor curves, based on equations in chapter 4, is also shown. The applicability range of a particular friction factor curve f(z,m,n) indicates the range of the (z,m,n) regime. It is clear from fig. 7.1 that each straight line of the critical heat flux plot can be identified with a particular range of the friction factor plot, and hence with a particular friction regime. The identified regime is indicated on the CHF plot for regions AB, CD and DE. These regimes are presumed to apply immediately upstream of the crisis location.

The nucleate boiling basis of the 'e' component of the friction regime (e,4,0) suggests that crises within the range AB of the plot may be due to DNB rather than dryout. Similarly, regions CD and DE are interpreted as being dryout.

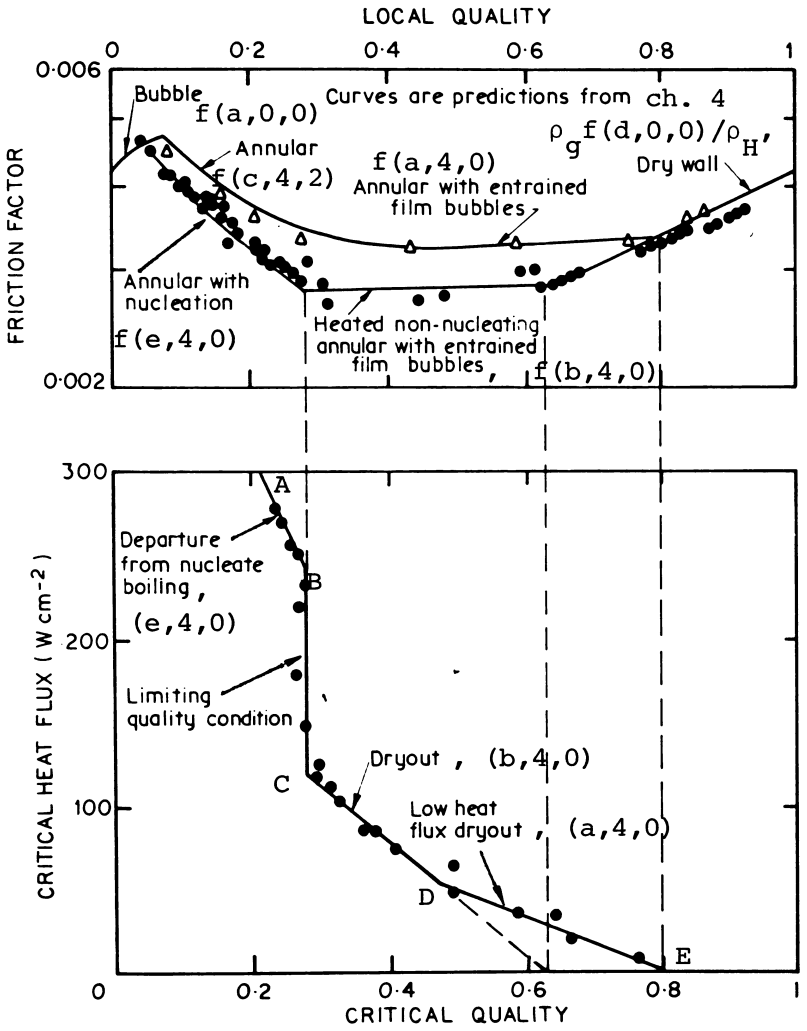

Fig. 7.1 Comparison of predicted and experimental friction factor [7.4] characteristics and the inter-relation with CHF characteristics [7.3] CISE test section 58C, 5 mm dia. tube, 80 cm long, 7 MPg 3800 kg m^{-2} s^{-1}. ● Diabatic, Δ adiabatic.

Also apparent from fig. 7.1 is the inter-connection between intercepts of the various friction factor curves and the qualities at which individual lines on the CHF plot, extrapolated if necessary, intercept the quality axis. This interconnection is discussed in more detail in the following sections.

7.3 The Value of x_o in CHF Equations of the Form $\phi_{cr} = a(x_{cr} - x_o)$

7.3.1 Round tubes

As noted, straight line regions of CHF plots for fixed flow, pressure and geometry, such as regions AB, CD and DE of figure 7.1 can be identified as being specific for a particular pre-crisis friction regime (z,m,n). Each line is of the form

$$\phi_{cr}(z,m,n) = a(z,m,n)\ (x_{cr} - x_o(z,m,n)) \qquad (7.1)$$

where, empirically, $x_o(z,m,n)$ is the quality at which shear stresses are equal for the pre- and post-crisis friction regimes:

$$\tau_w(z,m,n)\ \Big|_{x_o} = \tau_w\ (d,0,0)\ \Big|_{x_o} . \qquad (7.2)$$

An explanation for this can be made in terms of the observation, noted in chapter 4, that for a given flow section, mass flux, and pressure, the variation of adiabatic friction factor with quality contains no discontinuities at regime transition qualities.

The compatibility of some adiabatic friction factors with the dry wall equation f(d,0,0), e.g. the higher quality adiabatic data of fig. 7.1, indicates that some adiabatic flows may be under dry wall conditions even in the absence of heat flux. The shear continuity at a regime boundary implies that the adiabatic dryout transition quality is given when the wet wall shear stress equals that for dry wall conditions. Adiabatic flows introduced at lower qualities will wet the flow boundary; but will not wet the boundary if introduced at higher qualities.

Seen in the context of fig. 7.1, this means that the critical heat flux plot must intercept the critical quality axes (i.e. at zero heat flux) at a quality $x_o(a,4,0)$ given by

$$\tau_w(a,4,0)\,|_{x_o} = \tau_w(d,0,0)\,|_{x_o} .$$

From the friction factor plot, this is about 80% quality. Flows introduced to the test section at this or higher qualities are under dryout conditions with zero heat flux.

Consider now the situation, for the data of fig. 7.1, which would occur if the higher quality pre-crisis diabatic flow friction regime, (b,4,0) existed at zero heat flux as well as under diabatic conditions; i.e. if the transition to (a,4,0) did not occur at lower heat fluxes. The reasoning which indicated that the CHF plot should intercept the quality axis at point E suggests that, in the absence of (a,4,0), it would intercept at x_o defined by

$$\tau_w(b,4,0)\,|_{x_o} = \tau_w(d,0,0)\,|_{x_o} ,$$

i.e. at approximately 65% quality. As indicated in figure 7.1, crises from the (b,4,0) regime lie on a curve CD which extrapolates to the critical quality axis at this quality.

The above can be generalised to indicate that, for critical heat flux curves for a regime (z,m,n) with the form of equation (7.1), $x_o(z,m,n)$ is as given by equation (7.2).

All heat transfer-induced transitions to the dry wall regime occur at qualities less than the adiabatic dry wall regime transition quality. Accordingly, as well as a step rise in wall temperature occurring on transition, there is a step drop in wall shear $\tau_w(z,m,n) - \tau_w(d,0,0)$. Empirically, the step change for shear and temperature both increase with reducing crisis quality. It is possible that the two step changes are related. Any such relation, if found, could assist in the formula-

tion of the coefficient a(z,m,n) required to complete equation (7.1).

7.3.2 Complex geometries

The concepts described above apply equally to complex geometries. However, as discussed in section 4.5.5.3, complex geometry friction factor behaviour differs from that for round tubes, for both pre- and post-crisis conditions. As a consequence of the inter-relation between shear and crisis characteristics described in the preceding section, coefficients in round tube CHF equations will not apply for complex geometries.

Some critical heat flux data for the central rod of an annulus [7.5] are shown in fig. 7.2, together with friction factor data from the same test section [7.5]. The higher quality friction factors, with negligible dependence on quality, correspond to dry rod and wet shroud conditions. The curves are calculated by the method described in section 4.5.5.3. These data are presented in a different form in fig. 4.15. It is noted that the annulus friction factor dependence on quality with the rod dry differs from the dry tube dependence on quality as shown e.g. in fig. 7.1.

The lower quality friction factors of fig. 7.2 correspond to pre-crisis conditions. These friction factors also behave differently to round tube friction factors. The data were not described by any equations discussed in chapter 4, and the friction factor curves shown are empirical curves fitted to the data.

It is seen from fig. 7.2 that, as with round tubes, CHF plots intercept the zero heat flux axis at qualities where the pre- and post-crisis friction factors are equal.

7.3.3 Pseudo-dryout

As reported in section 4.5.5.2, point (iv), some post-crisis friction factor data agree with predicted f(d,0,0) values provided

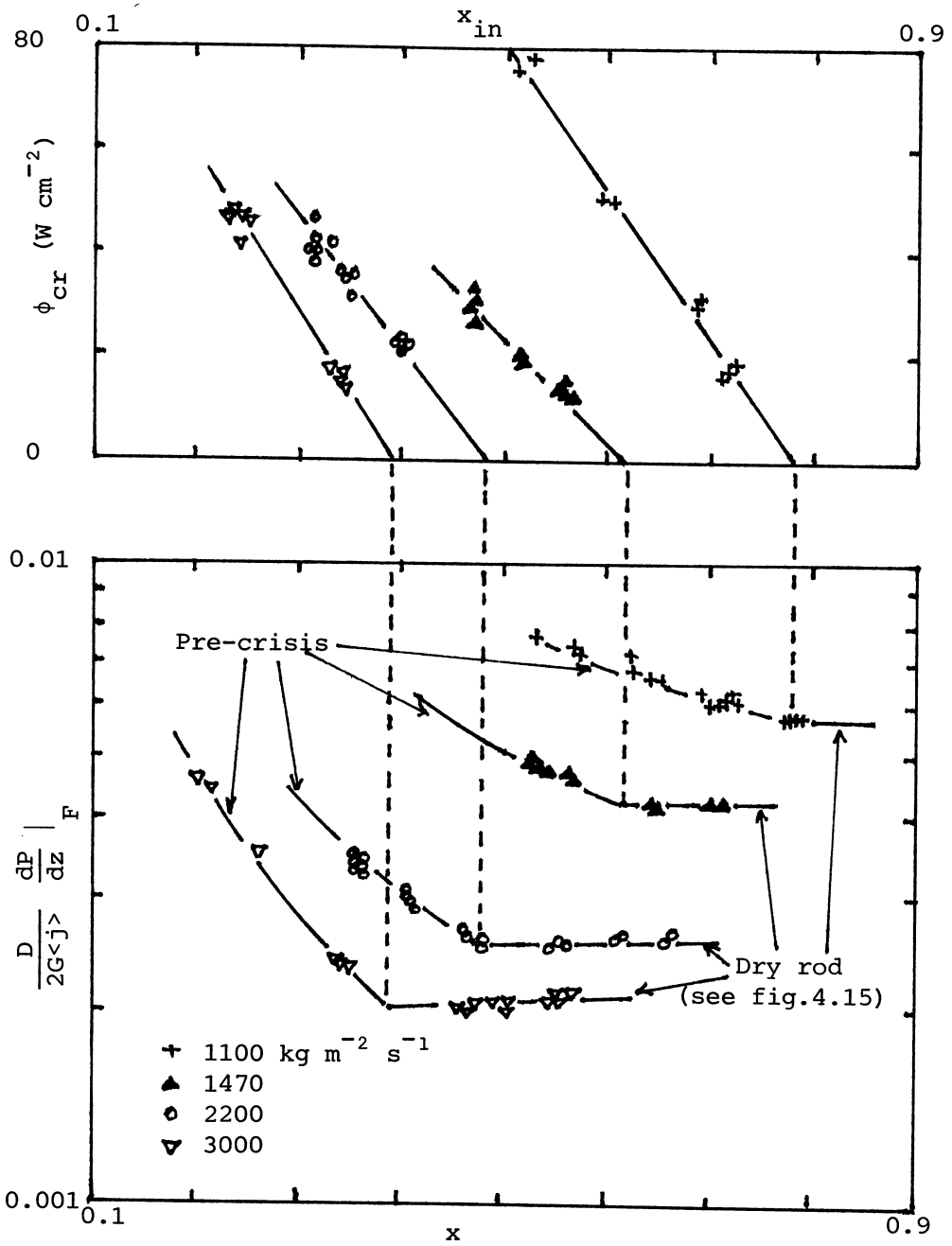

Fig. 7.2 The inter-relation between CHF characteristics for the rod of an annulus [7.5] with friction factor characteristics for the annulus [7.5]. CISE annulus 85, 8.25 mm dia. shroud, 5.02 mm dia. rod, 50 cm long, 7 MPa.

predictions are calculated for a smooth tube instead of for the actual tube roughness. Such friction factors are lower than for calculations based on the actual roughness. In view of the above described dependence of CHF curves on post-crisis friction factors, the CHF curves will depend on whether or not roughness is apparently reduced for post crisis conditions.

Fig. 7.3 shows critical power data at 7 MPa and 2980 kg m^{-2} s^{-1} in 6 mm tubes of various lengths [7.6, 7.7], together with friction factors calculated from equations recommended in Chapter 4. The dry wall friction factors have been calculated for roughness as estimated from information in [7.4], and for assumed zero roughness.

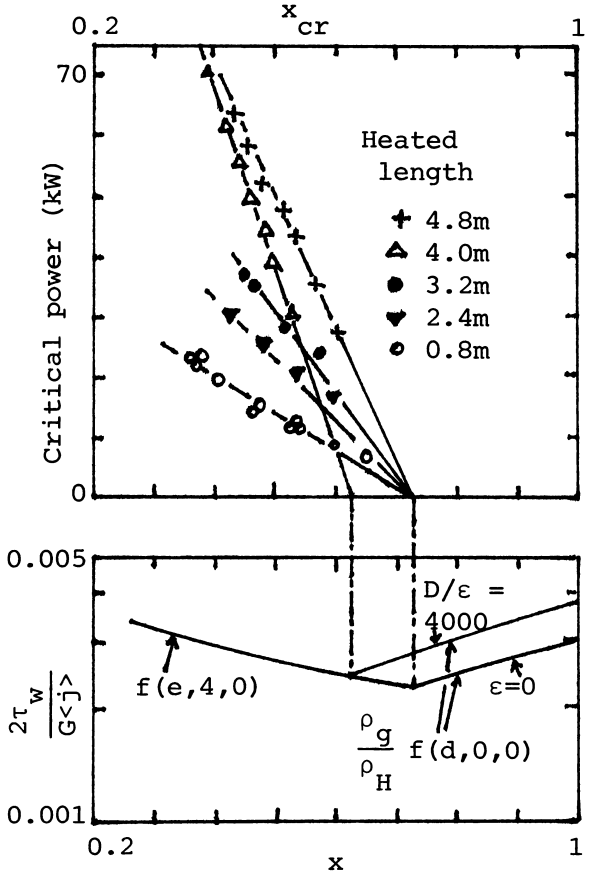

Fig. 7.3 The interrelation between critical power and pressure loss data [7.6,7.7] for 6 mm tubes of various lengths at 2980 kg m^{-2} s^{-1} and 7 MPa

The intercepts of the critical power plots on the zero power axis occur at a quality where f(e,4,0) = f(d,0,0, ε = true ε) for a 4m heated length, and at a quality where f(e,4,0) = f(d,0,0, ε = 0) for the other heated lengths. Since the data for lengths ranging from 2.4 m to 4.8 m were obtained from the same test section with power clamps being shifted, it must be assumed that $\varepsilon \neq 0$ for any of the heated lengths.

An interpretation of the above is that, for some post-crisis conditions, superheated liquid remains in the micro-crevaces between the roughness elements, thus presenting an apparently smoother surface to the turbulent core. Such post-crisis conditions correspond to 'pseudo dryout' rather than dryout. The slow post-crisis temperature rise characterising 'slow burnout' [7.8] is possibly due to the evaporation of residual film liquid during the transition from pseudo-dryout to dryout.

7.4 The Role of Pre-crisis Regime Transitions

7.4.1 The limiting quality phenomenon

Some boiling crises are characterised by a critical or 'limiting' quality which is independent of heat flux. Typical limiting quality crisis data are shown in the region BC of fig. 7.1.

It is postulated here that limiting quality crises are precipitated by a pre-crisis regime change. The appropriate regime change in fig. 7.1 is from an (e,4,0) to a (b,4,0) flow, and the limiting quality occurs when f(e,4,0) = f(b,4,0). This is because pre-crisis friction regime transitions occur with no discontinuity in wall shear (section 4.5.5.2). In concept, each friction regime has an associated CHF curve, and on regime transition, the CHF limit changes discontinuously from one curve to the other.

Consider exit crisis characteristics presented schematically in

fig. 7.4. Curve ABB' is considered as a CHF limit curve for flow regime (z_1,m_1,n_1), and curve C'CD is a corresponding limit for regime (z_2,m_2,n_2). The regime transition quality x_{Tr} satisfies $f(z_1,m_1,n_1)\big|_{x_{Tr}} = f(z_2,m_2,n_2)\big|_{x_{Tr}}$. The regime is defined by $(z_1m_1n_1)$ at lower qualities, so ABB' is the CHF limit for $x_{cr} < x_{Tr}$, i.e. over the range AB. Similarly, C'CD is valid over the region CD. Typical operating characteristics (1), (2) and (3) of the form

$$\phi = \frac{GD\lambda}{4\ell}(x - x_{in}) \tag{7.4}$$

are shown for 3 different inlet qualities. For $x_{in\ 1}$ (curve (1)) the crisis occurs when curve AB is reached since C'C is inapplicable as a limit. For $x_{in\ 2}$ (curve (2)), the crisis occurs at x_{Tr}. This is because at x_{Tr}^-, the operating characteristic is below the limit set by AB, but, at x_{Tr}^+, it is above the limit set by CD, so a crisis is precipitated. For $x_{in\ 3}$ (curve (3)), crisis occurs when limit CD is reached. In the example of fig. 7.4, then, critical heat flux curves in the vicinity of a $(z_1,m_1,n_1):(z_2,m_2,n_2)$ regime boundary comprise the curve ABCD, with AB applying for (z_1,m_1,n_1); CD for (z_2,m_2,n_2) and BC occurring at x_{Tr} satisfying $f(z_1,m_1,n_1) = f(z_2,m_2,n_2)$. (7.4)

Fig. 7.5 compares experimental limiting qualities with those predicted from friction factor data. The friction factor curves are those recommended in Chapter 4. The experimental friction factors agree with the predicted curves, and the limiting qualities agree with the regime transition qualities obtained from the friction factor curves.

Presentation of limiting quality conditions in the Re-We plane

As stated above, the limiting quality condition coincides with boundary between two friction regimes (z_1,m_1,n_1) and (z_2,m_2,n_2), and

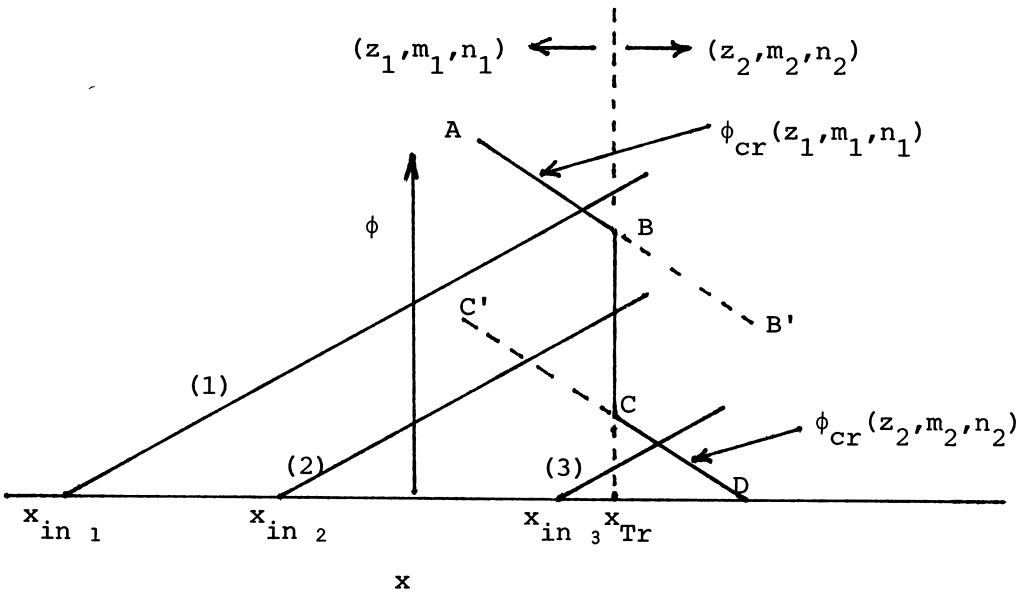

Fig. 7.4 Schematic of CHF plots in the vicinity of $a(z_1,m_1,n_1)$: (z_2,m_2,n_2) regime transition, $\phi_{cr}(z_1,m_1,n_1)\,|_{x_{Tr}} > \phi_{cr}(z_2,m_2,n_2)\,|_{x_{Tr}}$

this boundary is defined by

$$f(z_1,m_1,n_1) = f(z_2,m_2,n_2) \ . \qquad (7.4)$$

The limiting quality data examined in this work were all associated with a regime change from one with nucleate boiling ($z_1 \equiv$ e sublayer of table 3.1) to one with no nucleate boiling ($z_2 \equiv$ a,b and c sublayer of table 3.1). Since these sublayer types define flows which depend on Weber number for the low quality regime and one of the three pre-crisis Reynolds numbers of table 3.1 for the high quality regime, equation (7.4) is equivalent to a relation between Weber number and the relevant Reynolds number, each defined for the limiting quality conditions. Limiting quality data should thus correlate on the Re:We plane.

In the case of CISE data, relevant friction factor equations are

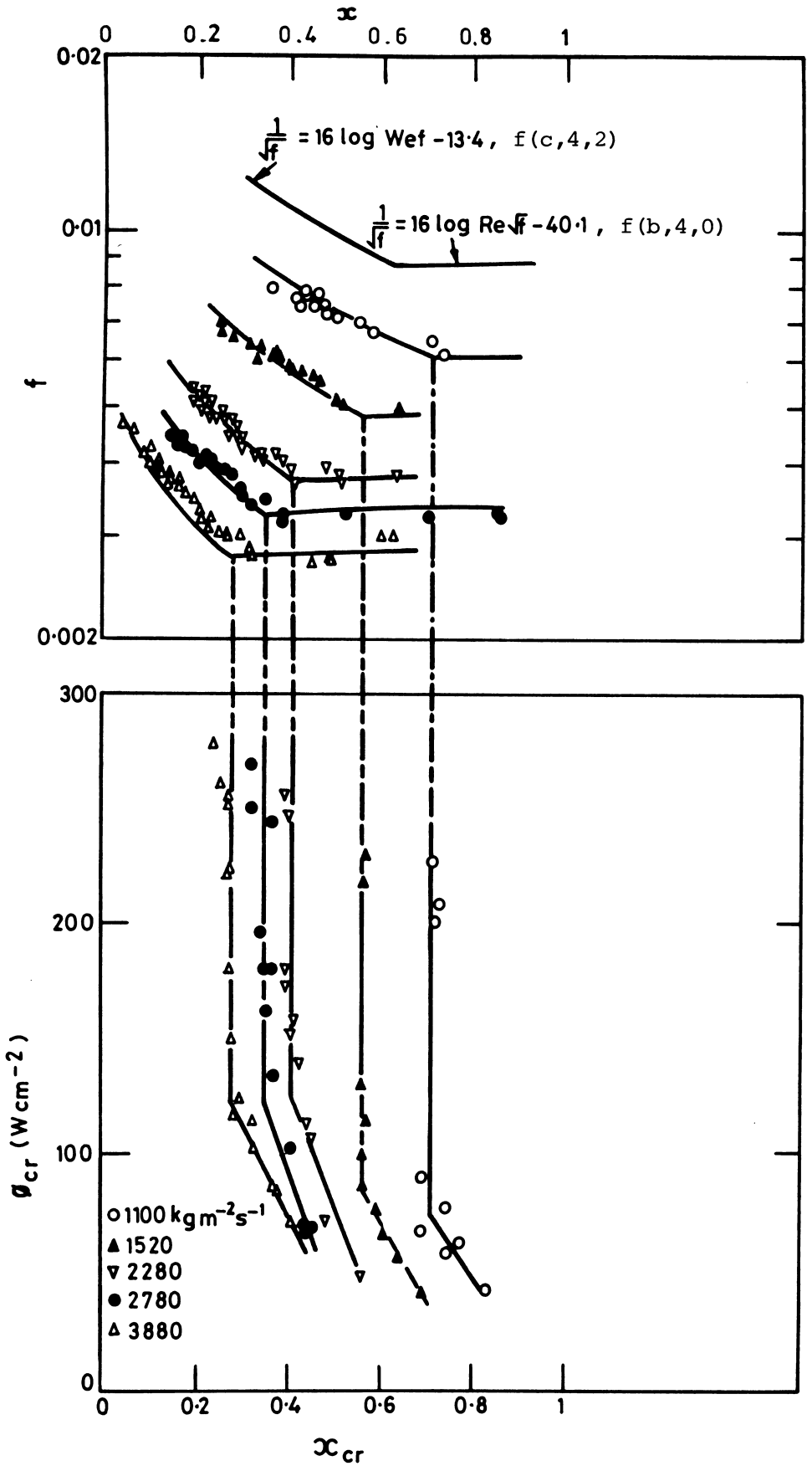

Fig. 7.5 CISE test section 58C critical heat flux [7.3] and pressure loss [7.4] data at 7 MPa

given in Chapter 4 as

$$\frac{1}{\sqrt{f}} = 16 \log Wef - 13.4 \qquad (7.5)$$

(defining f(e,4,0) for the nucleate boiling regime)

and $$\frac{1}{\sqrt{f}} = 16 \log Re_b \sqrt{f} - 40.1 \qquad (7.6)$$

(defining f(b,4,0) for the non-boiling regime).

CISE limiting quality data should thus correlate on the Re:We plane with the correlating equation being obtained by eliminating f from the above equations. Typical CISE limiting quality data, from [7.9], are shown in fig. 7.6 to be consistent with this concept. Each point in fig. 7.6 corresponds to one limiting quality curve of the type shown in fig. 7.5.

CISE limiting quality data are discussed further in appendix A26.

Extensive limiting quality data have been obtained by Doroschuk et al. [7.10], who have provided tables of limiting quality conditions. No pressure loss data are provided to directly confirm the relation between shear stress and limiting quality crises. However, pressure drop data from comparable rigs to that used by Doroschuk (see e.g. the data of fig. 4.3) indicate that, due to the inlet configuration, the pressure loss recommendations of Chapter 4 are likely to be invalid. Limiting quality data from Doroschuk et al. [7.10] will thus disagree with the correlation of CISE data of fig. 7.6. Nevertheless, data should correlate on the We:Re plane.

Figures 7.7 and 7.8 confirm this. The lower pressure data of [7.10] correlate using a Reynolds number type - see table 3.1 - suggesting no film bubbles for the non-boiling regime (fig. 7.7), and the higher quality data (fig. 7.8) correlate using a Reynolds number indicating the presence of film bubbles.

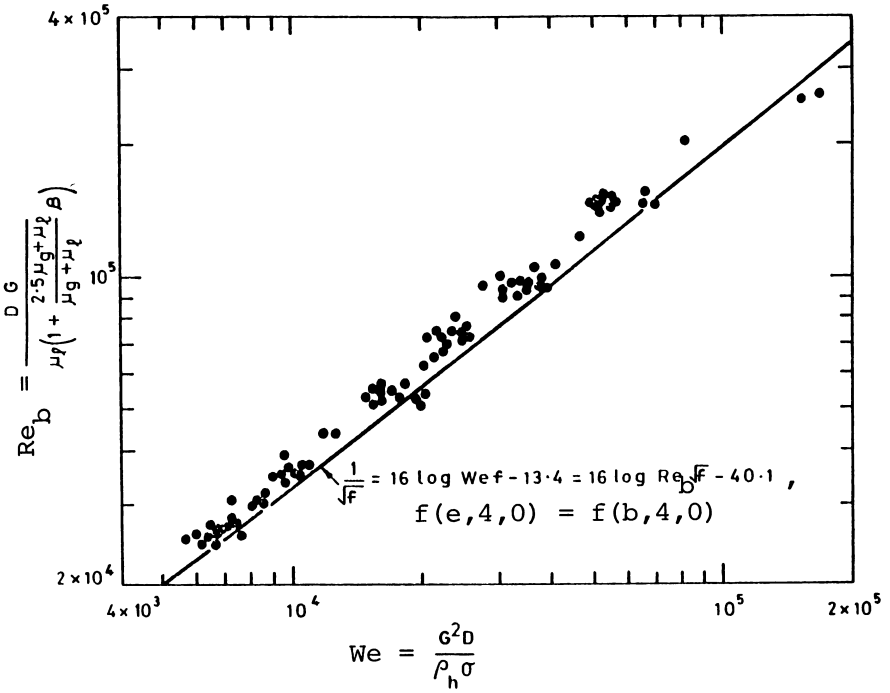

Fig. 7.6 Comparison of CISE limiting quality data [7.9] with predictions based on friction factors equations

7.4.2 Minima in exit crisis characteristics

In conditions of very high mass flow [7.11-7.15], or if test sections contain swirl devices [7.15-7.18], minima may occur in plots of CHF against critical quality. As with the limiting quality phenomenon, these minima may be explained in terms of a friction regime transition which produces a step change in CHF limits. A step reduction with increasing quality produces the limiting quality phenomenon; a step increase produces minima in the total characteristics.

This can be seen by considering the heat transfer characteristic shown schematically in fig. 7.9 for a given mass flow in a given heated test section. ABB' represents a CHF limit curve for a friction regime which exists at qualities less than the regime transition quality x_{Tr}, so is only valid over the region AB. C'CC"D represents a CHF limit curve for a regime which exists for qualities greater than

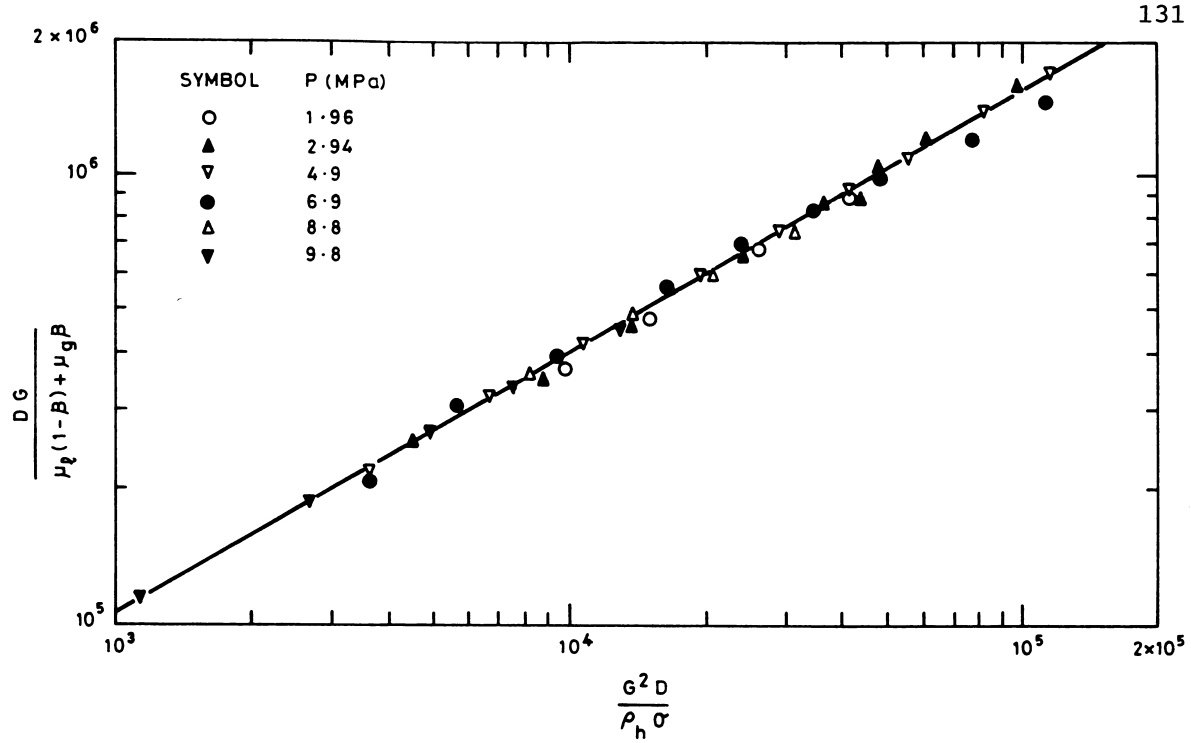

Fig. 7.7 Correlation of VTI lower pressure tabulated limiting quality boiling crisis data for 8 mm tubes [7.10], 300-5000 $kgm^{-2}s^{-1}$

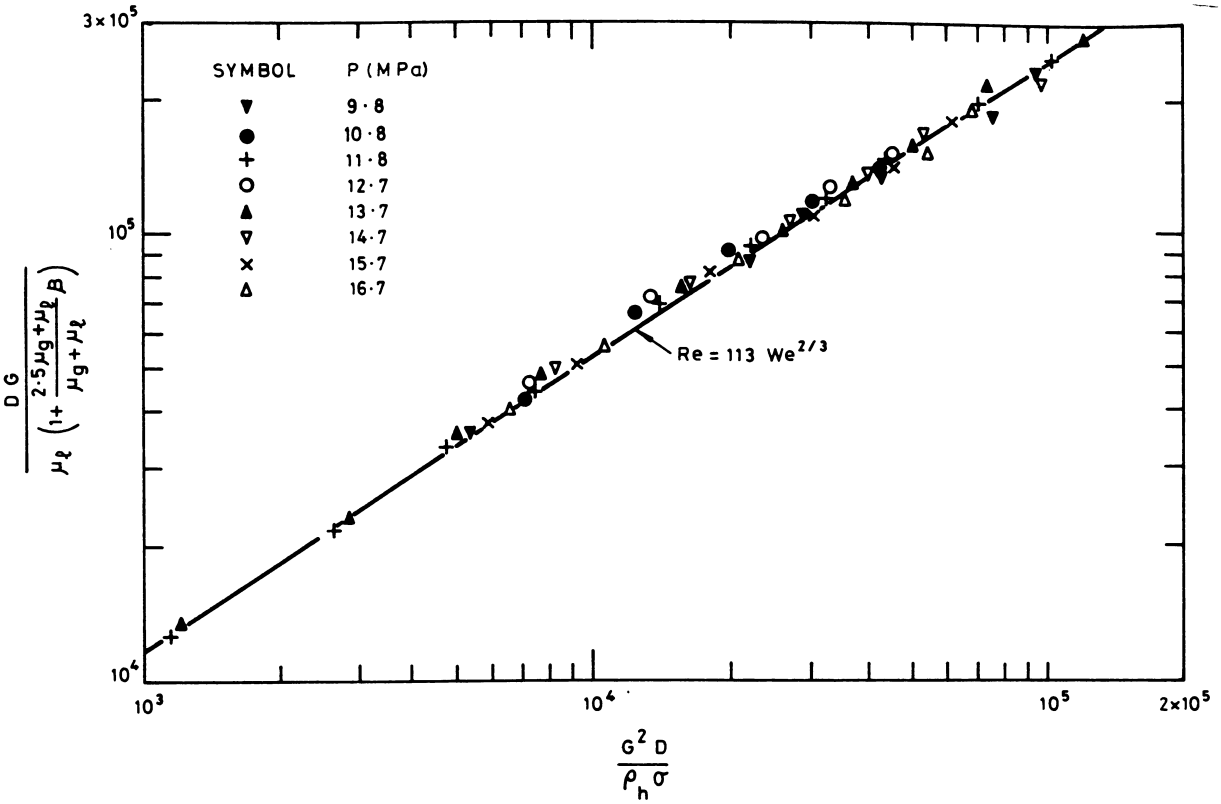

Fig. 7.8 Correlation of VTI higher pressure tabulated limiting quality critical heat flux data for 8 mm tubes [7.10], 300-5000 kg $m^{-2}s^{-1}$

x_{Tr}, so is valid over the region CC"D. Curves (1), (2) and (3) are typical operating characteristics

$$\phi = \frac{GD\lambda}{4\ell} (x - x_{in}) \tag{7.5}$$

for three different inlet qualities x_{in_1}, x_{in_2}, x_{in_3}. A crisis occurs at conditions where the operating characteristic intercepts the appropriate CHF limit. Thus, for x_{in_1} a crisis will occur at a heat flux where curve (1) intercepts AB, i.e. at x_{cr_1}. Similarly for x_{in_3}: the critical quality for x_{in_3} is x_{cr_3}, where CC"D is intercepted by curve (3), not where it intercepts BB' since this is not applicable for $x > x_{Tr}$. For $x_{in_2}-$, curve (2) intercepts AB at $x_{Tr}-$, so crisis conditions are at this point, but at $x_{in_2}+$, curve 3 intercepts ABB' where it no longer applies, and crisis conditions are instead at C" where curve (3) intercepts C'CC"D. Although C'CC"D is valid for $x > x_{Tr}$, region CC" of the valid range can never be achieved. The overall result is a critical heat flux curve ABC"D.

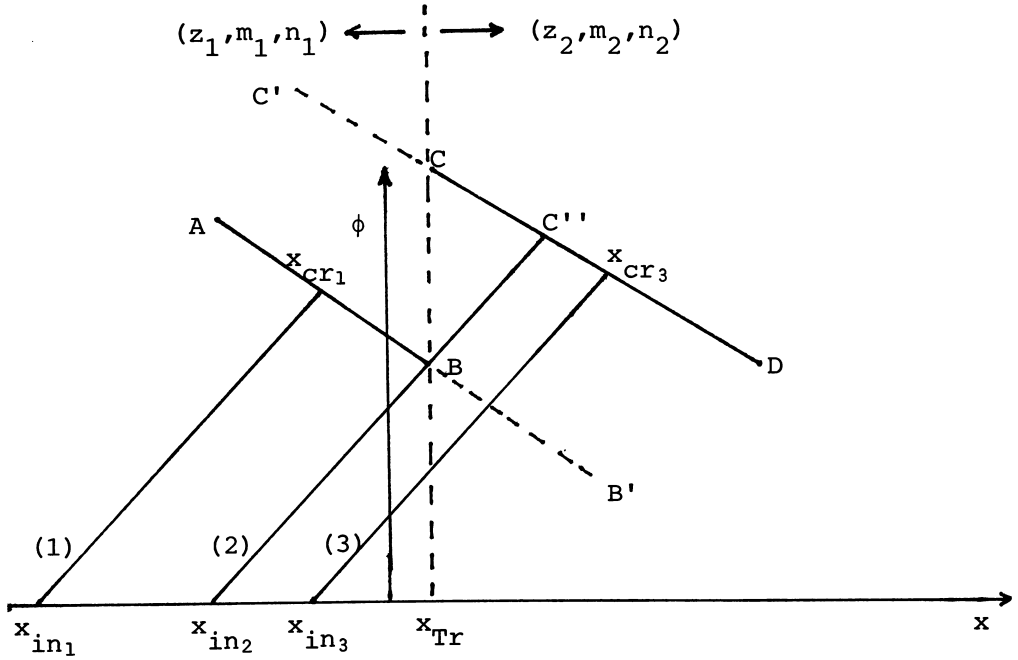

Fig. 7.9 Schematic of CHF plots in the vicinity of a (z_1,m_1,n_1): (z_2,m_2,n_2) regime transition, $\phi_{cr}(z_1,m_1,n_1)\big|_{x_{Tr}} < \phi_{cr}(z_2,m_2,n_2)\big|_{x_{Tr}}$

The above description is idealised, and in reality the step change from B to C" in fig. 7.10 occurs as a smoother transition.

The quality at which the minimum occurs is due to the same regime transition which precipitates limiting quality crises if there is a step reduction (instead of increase) in CHF on regime change, so conditions at which CHF minima occur should also correlate on the Re:We plane.

Reynolds number is plotted against Weber number in fig. 7.10 for conditions where minima occur in exit crisis characteristics for the swirl flow CHF data of [7.18]. In accordance with the above paragraph, the data are correlated by the same equation which correlated the fig. 7.6 limiting quality data from the same laboratory*.

7.4.3 Upstream crises

For uniformly heated tubes, the boiling crisis generally occurs at the highest quality region at the exit. Exceptions occur with sufficiently high mass fluxes, where crisis onset may occur upstream of the exit [7.11-7.15]. For steady crisis conditions, the heated surface at the higher quality region downstream of the crisis may remain wetted.

This phenomena can be explained in terms of concepts of section 7.4.2, describing minima in the exit CHF curves, being generalised to each point in the heated section. The reasoning of section 7.4.2 suggests that for some conditions, a CHF minimum occurs at x_{Tr}, the regime change quality, for each point in the test section. For a heated test section with given flow and inlet quality, and with exit quality larger than x_{Tr}, further heating may produce a crisis at the position where the quality is x_{Tr} before exit crisis conditions are reached.

If this is so, upstream crises should also occur at the transition

---

* The different Reynolds number form reflects swirl-induced mixing - see section 4.5.5.2, point (iii).

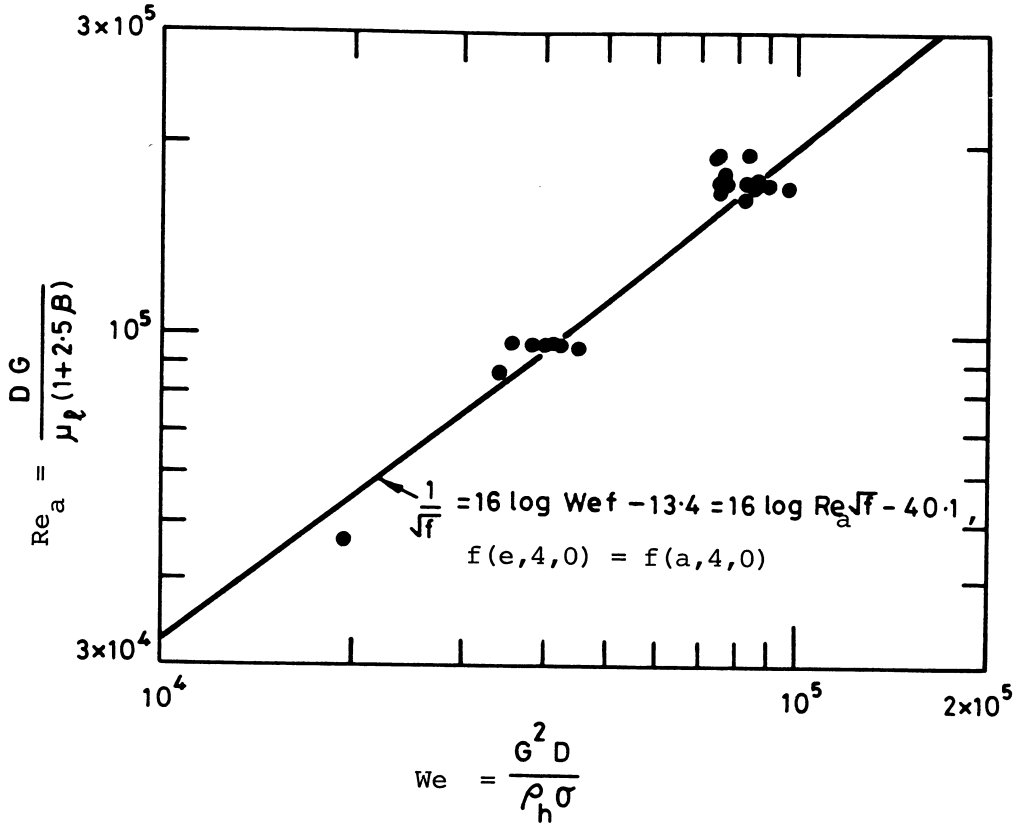

Fig. 7.10 Comparison of conditions where CHF data show minima [7.18] with predictions based on friction factor equations

quality x_{Tr}, and so conditions at upstream crises should also correlate on the We:Re plane. No data source [7.11-7.15] contained sufficient upstream crisis data to test this. (As with the limiting quality data of figs. 7.6 - 7.8, data from different sources may correlate differently on the We:Re plane.)

However, a partial test of the hypothesis can be made. The proposed explanation of upstream crises implies that they should occur at the same quality where a minimum occurs in plots of exit critical heat flux. This follows since both qualities are identified with a regime transition quality x_{Tr}. Figure 7.10, from [7.13], demonstrates that many upstream crises do in fact occur at qualities close to that where a minimum occurs in the exit characteristics. Those data of fig.

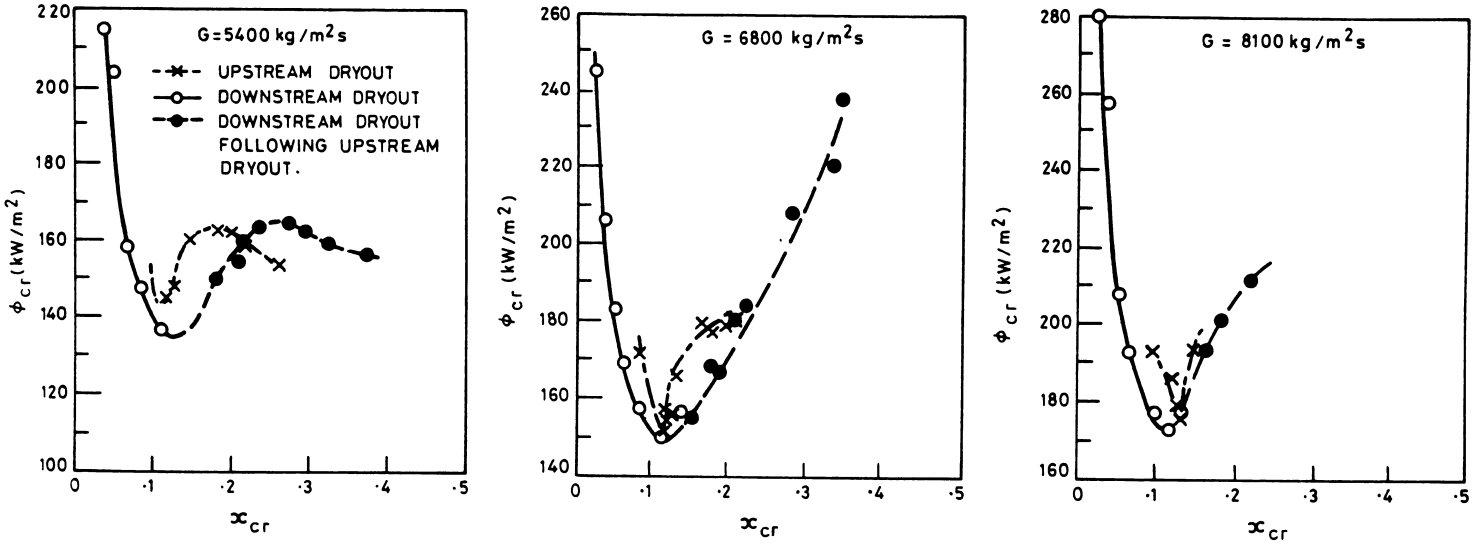

Fig. 7.11 AECL critical heat flux data with minima and upstream heat transfer crises [7.13]

7.10 which do not conform to the pattern - the higher quality upstream crises for 5400 and 6800 kg m^{-2} s^{-1} - were obtained with inlet qualities larger than that where this minimum occurred, thus excluding the possibility of upstream crises occurring at this quality.

References

7.1 J.B. Kitto, 'Critical heat flux and the limiting quality phenomenon', AIChE Symp. Series 76, 199, 57 (1980).

7.2 G.F. Hewitt, 'Critical heat flux in flow boiling', Proc. 6th Int. Heat Transfer Conf., Toronto, Canada, Vol.6, p.143 (1978).

7.3 S. Bertolletti, et al., 'Heat transfer crisis in steam-water mixtures - Experimental data in round tubes and vertical upflow', CISE-R-90 (1964).

7.4 G.P. Gaspari et al., 'Pressure drops in steam-water mixtures', CISE-R-83 (1964).

7.5 N. Adorni et al., 'Pressure drop, heat transfer and burnout measurements in annular tubes with internal and bilateral heating', CISE-R-31 (1961).

7.6 L. Berkowitz et al., 'Pressure drop, heat transfer and burnout measurements with round tubes', CISE-R-27 (1960).

7.7 A. Era et al., 'Heat transfer data in the liquid deficient region for steam-water mixtures at 70 kg/cm² flowing in tubular and annular conduits', CISE-R-184 (1966).

7.8 L.S. Tong, 'Boiling heat transfer and two-phase flow', p.136, John Wiley (1965).

7.9 CISE limiting quality crisis data extracted from CISE reports R90, R122, R169, R27, R83.

7.10 VTI tables of limiting qualities contained in ASME paper 75-WA/HT22 (1975); Thermal Engng 22 (12) 77 (1975); Thermal

Engng 22 (1) 80 (1975); Heat Transfer - Soviet Research 12 (3) 100 (1980); and preprint 3-004 of the Scientific Council of the Academy of Sciences of the USSR (1975).

7.11 M. Merilo, 'Critical heat flux experiments in a vertical and horizontal tube with both freon 12 and water as a cooling', Nucl. Eng. and Des. 44 (1), 1 (1977).

7.12 M. Merilo and S.Y. Ahmad, 'The effect of diameter on vertical and horizontal flow boiling in a tube cooled by freon 12', AECL 6485 (1979).

7.13 D.C. Groeneveld, 'The occurrence of upstream dryout in uniformly heated channels', Paper B6.6, Proc. 5th Int. Heat Transfer Conf. Japan (1974).

7.14 E.D. Waters et al., 'Experimental observations of upstream boiling burnout', Chem. Eng. Prog. Symp. Series 61 (57) 230 (1965).

7.15 B. Matzner et al., 'Critical heat flux in long tubes at 1000 psi with and without swirl promoters', ASME paper 65-WA/HT-30 (1965).

7.16 M.K. Jensen and A.E. Bergles, 'Boiling heat transfer and critical heat flux in helical coils', J. Ht. Transfer 103, 661 (1981).

7.17 F. Mayinger et al., 'Investigations into the critical heat flux in boiling water', EUR 3347 e (1967).

7.18 A. Hassid et al., 'Heat transfer crisis with steam-water mixtures: An experimental study on the increase of critical power with local swirl promoters in round tubes', CISE-R169 (1966).

CHAPTER 8

SOME ASPECTS OF TWO-PHASE HEAT TRANSFER

This chapter considers heat transfer processes for the special cases of (a) nucleate boiling for 'e'-type friction regimes, and (b) dry wall droplet flows. On the basis of the friction factor data analysis of Chapter 4, 'e' friction regimes can be associated with nucleate boiling annular flows, and dry wall droplet flows with post-crisis conditions.

The analysis of this chapter is based mainly on heat transfer data from [8.1]. These data were considered in detail because simultaneously obtained pressure drop data [8.2] could be used to establish the appropriate friction regime. Some of the pressure loss data are presented in figures 4.12 and 7.5. The data of [8.1] are for the inlet and exit of heated tubes of 9 mm and 5 mm diameter with two-phase inlet conditions. The pressure was 7 MPa, the mass flux ranged from 1100 to 3800 kg m^{-2} s^{-1}; the quality range was from zero to near unity; and the heat flux varied from near zero to well beyond the boiling crisis heat flux.

8.1 Overview of Heat Transfer Behaviour

On the basis of the data of [8.1], heat transfer behaviour for nucleate boiling annular flows and for dry wall droplet flows can be subdivided into several sharply delineated and distinct heat transfer regimes. These are shown schematically in figure 8.1, which demonstrates typical exit heat transfer behaviour as heat flux is varied for a given tube with fixed mass flow, inlet quality, and pressure.

Consider the behaviour as heat flux is increased from zero to well beyond the boiling crisis heat flux, and then reduced;

At low heat fluxes, there is a nearly linear variation between heat

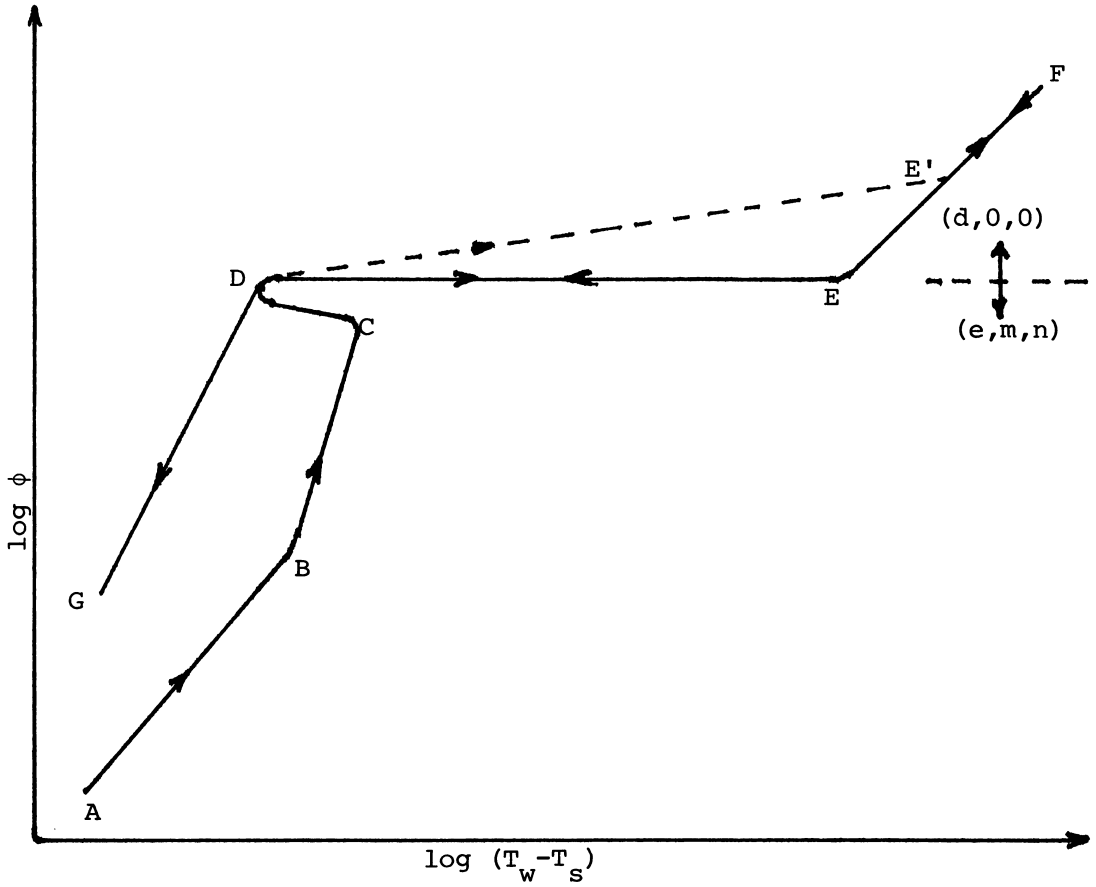

Fig. 8.1 Heat transfer behaviour for (e,m,n) and (d,0,0) flows

flux and wall superheat (region AB of figure 8.1). Heat transfer coefficient varies with heat flux, mass flux, tube diameter, and flow quality. This low heat flux behaviour is considered in more detail in section 8.2.1.

With increasing heat flux, the heat transfer coefficient loses its dependence on mass flux, quality, and tube diameter. Behaviour changes so that the heat flux varies approximately as the cube of the wall superheat (region BC of figure 8.1). This heat transfer behaviour is discussed in section 8.2.2.

When the heat flux is increased to within about 5% of the boiling crisis heat flux, there is often an abrupt improvement of heat transfer, typically by a factor of 2 (CD on figure 8.1). On the basis of data of [8.1] and [8.2], this temperature drop-down occurs if and only if associated pressure loss data indicate attached wall bubble 'roughness'; i.e. if and only if nucleate boiling occurs in the approach to the boiling crisis. Although the pre-crisis temperature dropdown phenomenon has been reported by various authors (e.g. [8.1], [8.3-8.6]), it is not described in current texts on two-phase phenomena. The existence of the phenomenon may not be widely recognised since boiling crises are often detected without recourse to temperature measurements. Moreover, when wall temperatures are measured, temperature scales in boiling crisis experiments are often adjusted to accommodate large changes in wall temperature, so small scale pre-crisis temperature changes may not be noticed.

The heat transfer at the minimum temperature of the pre-crisis wall temperature drop (point D in figure 8.1) is such that the heat flux varies approximately as the square of the wall superheat, with heat transfer being independent of mass flux, diameter, and flow quality. Heat transfer at this condition is discussed in section 8.2.3.

Heat transfer beyond the boiling crisis (EE'F in figure 8.1) is discussed in section 8.3. In the case of 'slow' crises - see section 7.3.3 - post-crisis temperatures may be lower than for 'fast' crises, and characteristics follow DE'F rather than DEE'F (figure 8.1). As discussed in section 8.3, post-crisis conditions for slow crises are believed here to be not true dryout. 'Pseudo-dryout' heat transfer (section DE' of figure 8.1) is discussed briefly in section 8.3.2.

On reducing heat flux, a hysteresis occurs below the critical heat flux, with the return path being DG rather than DCBA. Heat transfer on this return path appears identical to that at the temperature dropdown (point D) and is discussed in section 8.2.3 together with heat transfer at the temperature drop.

8.2 Heat Transfer for Convective Boiling Annular Flows

Several components of nucleate boiling heat transfer have been identified [8.7]. Most are associated with bubble nucleation frequency, and can be neglected for low frequencies. We conclude that nucleation frequencies are low for conditions considered here since the section 3.6.3 model for 'e' sublayer flows, which was shown to be satisfactory in sections 3.8, 4.5.1 and 5.3, is based on the concept of surface tension forces opposing wall bubble departure, whereas Cooper [8.8] has demonstrated that surface tension assists bubble departure for rapidly growing, high nucleation frequency bubbles.

Accordingly, we consider only two components of annular flow nucleate boiling heat transfer: firstly, conductive heat transfer to the single phase region on the wetted bare surface, ϕ_{cond}, and secondly, heat transfer by continuous evaporation (e.) from a liquid microlayer at the root of the bubble, while the bubbles are still attached to the wall, together with corresponding condensation (c.) at the top of the bubble, $\phi_{e.c.}$ The role of these two components is considered

in the following subsections.

8.2.1 Heat transfer at low heat fluxes

Nucleate boiling heat transfer is modelled here by a method outlined in figure 8.2. Wall bubbles are considered as truncated spheres of diameter d, the bases of which consist of evaporating microlayers. The evaporating microlayer of each wall bubble is replenished by liquid mass flow rate $\dot{M}_\ell$. This mass flow is made up of $\dot{M}_{\ell c}$, a contribution from the turbulent core, and a recirculating component due to condensation at the bubble top, $\dot{M}_{\ell r}$. The component $\dot{M}_{\ell c}$ contributes to the growth of the bubble. It is assumed that the fraction of liquid flowing to the bubble microlayer from the turbulent core is constant $1/a_1$, i.e.

$$\dot{M}_\ell / \dot{M}_{\ell c} = a_1. \tag{8.1}$$

The evaporation-condensation component of the heat flux, $\phi_{e.c.}$ is assumed to be uniform over the projected area A_b of the bubble and its recirculating liquid. The sum total of such areas constitutes a fraction α_s of the total heat transfer area. Heat flux due to conduction, ϕ_{cond}, occurs over the fraction $(1-\alpha_s)$ of the surface not directly affected by nucleating wall bubbles. The heat flux is then

$$\phi = \alpha_s \phi_{e.c.} + (1-\alpha_s) \phi_{cond} \tag{8.2}$$

The wall temperature is T_w. Liquid superheat is assumed to be confined to the near-wall viscous-dominated sublayer. From the analysis of appendix A28, this region extends to the outer edge of the bubble layer, i.e. to distance d from the wall.

Consider first the contribution $\phi_{e.c.}$ due to microlayer evaporation and subsequent partial condensation at the top of wall bubbles. The heat transferred by evaporation and condensation is equal to the heat required to raise the liquid flow $\dot{M}_\ell$ from saturation temperature T_s to the wall temperature T_w:

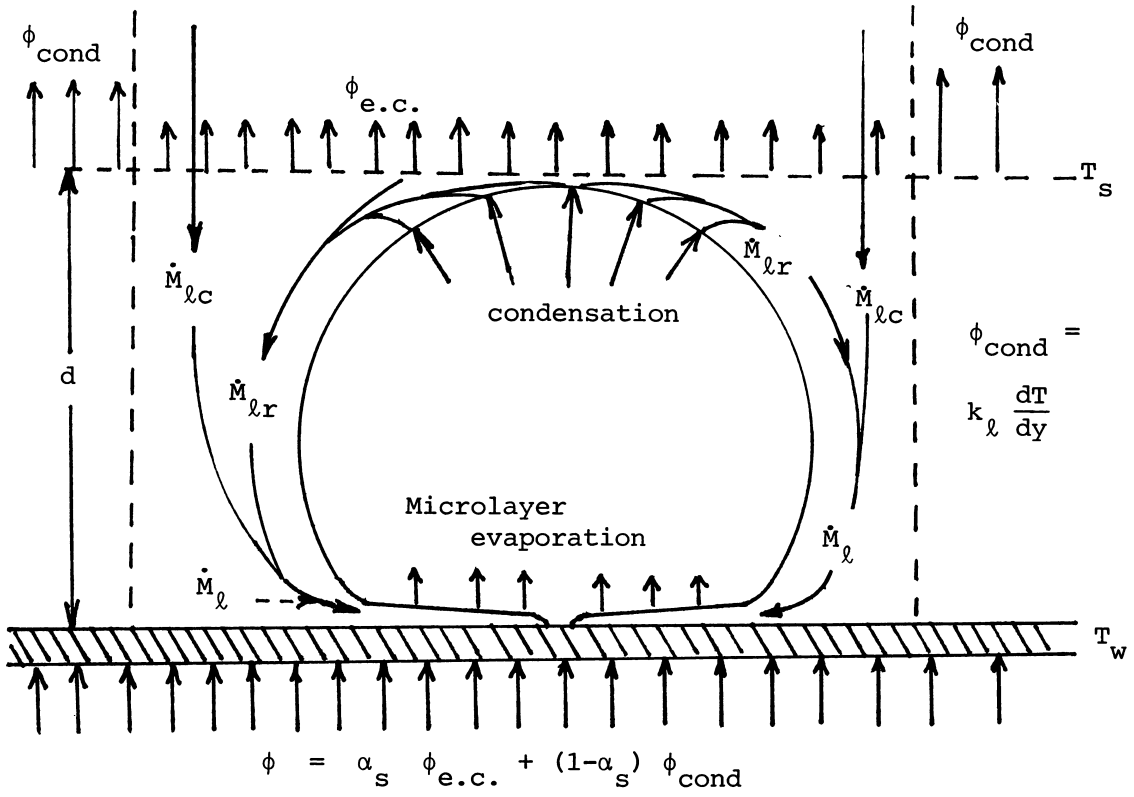

Fig. 8.2 Heat transfer in nucleate boiling

$$\phi_{e.c.} A_b = C_{p\ell} \dot{M}_\ell (T_w - T_s) . \quad (8.3)$$

The net evaporation is due to the liquid flow from the core, $\dot{M}_{\ell c}$. The heat required to vaporise this is that which is applied to that part of the surface which can be associated with the bubble, i.e. to an area A_b/α_s:

$$\dot{M}_{\ell c} \lambda = \phi A_b/\alpha_s \quad (8.4)$$

From equations (8.1), (8.3) and (8.4)

$$\phi_{e.c.} = a_1 C_{p\ell} (T_w - T_s) \phi/(\lambda \alpha_s), \quad (8.5)$$

where a_1 is a constant larger than one.

The contribution due to conduction through the liquid region between bubbles is

$$\begin{aligned} \phi_{cond} &= k_\ell \, dT/dy \\ &\cong k_\ell (T_w - T_s)/d \end{aligned} \quad (8.6)$$

An ensemble average of this contains a mean inverse diameter which is proportional to the bubble breakaway diameter d_d. As described in section 3.6.3, this diameter is given by $d_d \propto \sigma/\tau_w$, or

$$d_d/D \propto (We\ f)^{-1}. \quad (8.7)$$

The mean contribution to conduction is then

$$\overline{\phi}_{cond} = a_2 k_\ell (T_w - T_s) D\ We\ f, \quad (8.8)$$

where a_2 is constant. The bar denoting the ensemble average will henceforth be omitted for simplicity.

From equations (8.2), (8.5) and (8.8) the total heat transfer coefficient $h = \phi/(T_w - T_s)$ is

$$h = a_1 \phi C_{p\ell}/\lambda + (1-\alpha_s) a_2 k_\ell We f/D, \quad (8.9a)$$

or

$$Nu = a_1 Pr_\ell \phi D/(\mu_\ell \lambda) + a_2 (1-\alpha_s) Wef, \quad (8.9b)$$

where $Nu = h D/k_\ell$ is the Nusselt number.

If it is further assumed that α_s is constant, equations (8.9) become

$$h = a_1 \phi C_{p\ell}/\lambda + a_3 k_\ell Wef/D \qquad (8.10a)$$

or

$$Nu = a_1 Pr_\ell \phi D/(\mu_\ell \lambda) + a_3 Wef, \qquad (8.10b)$$

with a_1 and a_3 being constants to be determined empirically. Because the friction factor/Weber number relation depends on friction regime, the Nusselt number variations will also vary with friction regime.

Equations (8.10) predict a linear variation of heat transfer coefficient with heat flux for constant Weber number; and, because friction factor varies with Weber number only for 'e' sublayer flows, a dependence of Nusselt number on only Weber number at sufficiently low heat fluxes. The inlet heat transfer data of [8.1] are suitable for testing this since the experiments described there were performed in groups with constant mass flux and inlet quality, i.e. constant inlet Weber number. The data analysed from [8.1] are confined to those data where associated pressure drop data [8.2] agree with the (e,4,0) friction factor curve.

Typical inlet data of [8.1] are shown in figure (8.3). These data support the predicted linear variation with heat flux. Also shown is the change of characteristic with increasing heat flux to one independent of Weber number, as discussed in section 8.1.

The coefficient a_1 of equation (8.10) is determined from the slope of the lines of figure (8.3) and similar figures. Although assumed to be constant, the data of [8.1] indicates that it is only approximately so, and in fact varies to a small extent with mass flux, tube diameter, and distance from the heated section inlet, in an as yet undetermined manner. However, the data of [8.1] indicate that an assumed constant value of a_1 as 7.7 is reasonable.

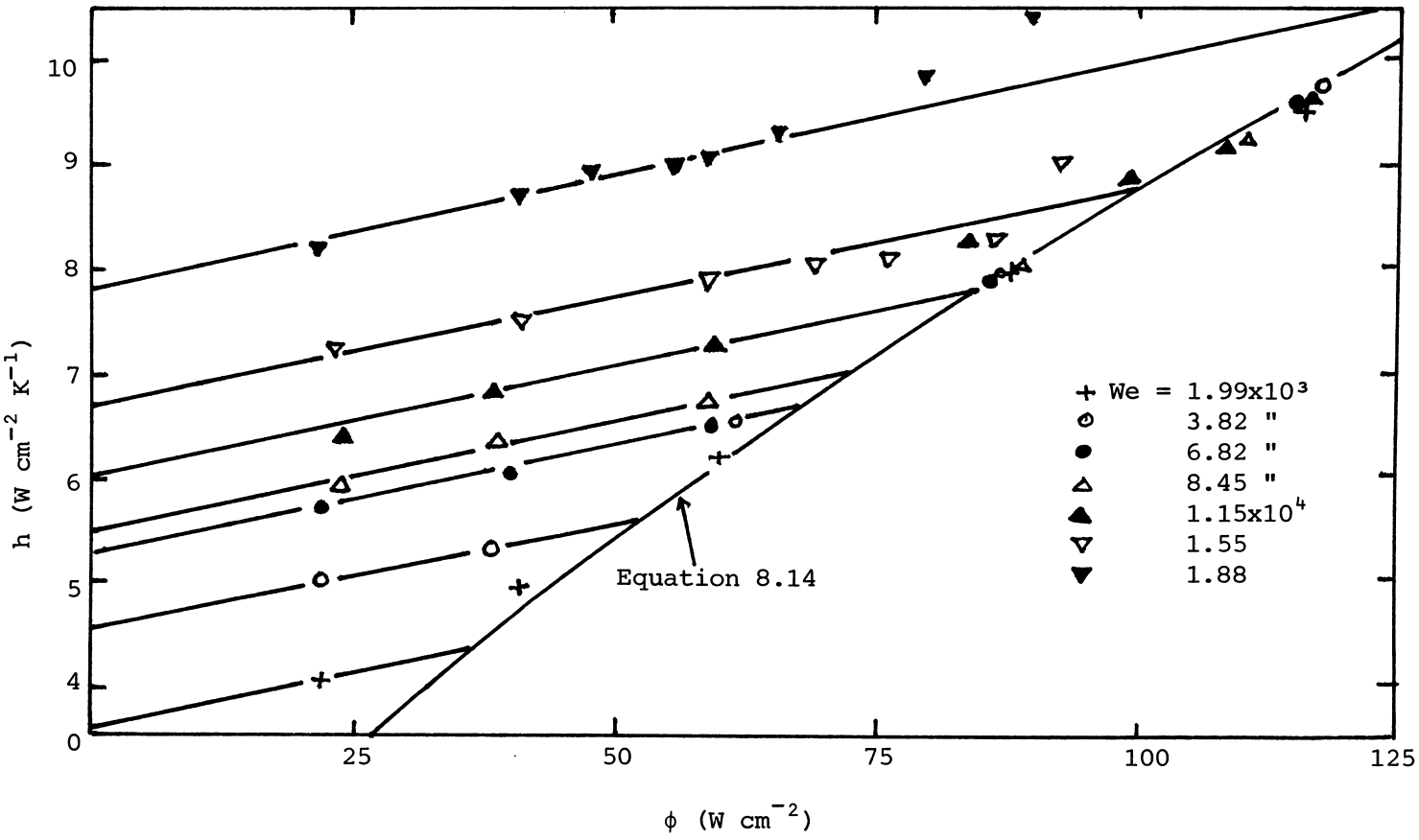

Fig. 8.3 Heat transfer at the inlet of a 5 mm heated tube, P = 7 MPa, G = 2280 kg m^{-2}s^{-1}
Data from [8.1]

The predicted low heat flux dependence on Weber number may be assessed by plotting the figure 8.3 heat transfer coefficient intercepts on the zero heat flux axis as a function of Weber number. Low heat flux Nusselt numbers so determined from figure 8.3 and similar figures are shown in figure 8.4. The predicted dependence is one proportional to the function Wef (e,4,0). Although a slight dependence on tube diameter is apparent, the data are adequately described by the equation

$$Nu\big|_{\phi \to o} = 11.0\ We\ f(e,4,0), \tag{8.11}$$

which is shown as a dotted curve in figure 8.4. A better correlating curve is

$$Nu\big|_{\phi \to o} = 15.7\ We^{0.4}, \tag{8.12}$$

which is shown as a solid line in the figure.

From the above, the inlet (e,4,0) heat transfer data of [8.1] are adequately described by

$$Nu\ (e,4,0) = 15.7\ We^{0.4} + 7.7\ Pr_{\ell}\ \phi D/\mu_{\ell}\lambda. \tag{8.13}$$

This is compared with low heat flux exit (e,4,0) data of [8.1] in figures 8.5 and 8.6. The data are adequately described by the correlation. Errors are largely due to neglect of the variations of the coefficient a_1 of equation (8.10) with mass flux and downstream position.

The above data analysis indicates that the model leading to equations (8.10), although qualitatively correct, is only partially in accord with the data analysed. Nevertheless, the data analysed are sufficiently consistent with the model to indicate that the predicted dependence on friction regime is valid. This indicates that equation (8.13), which is an adaptation of the predicted form in equation (8.10b), should only apply to low heat flux (e,4,0) flows.

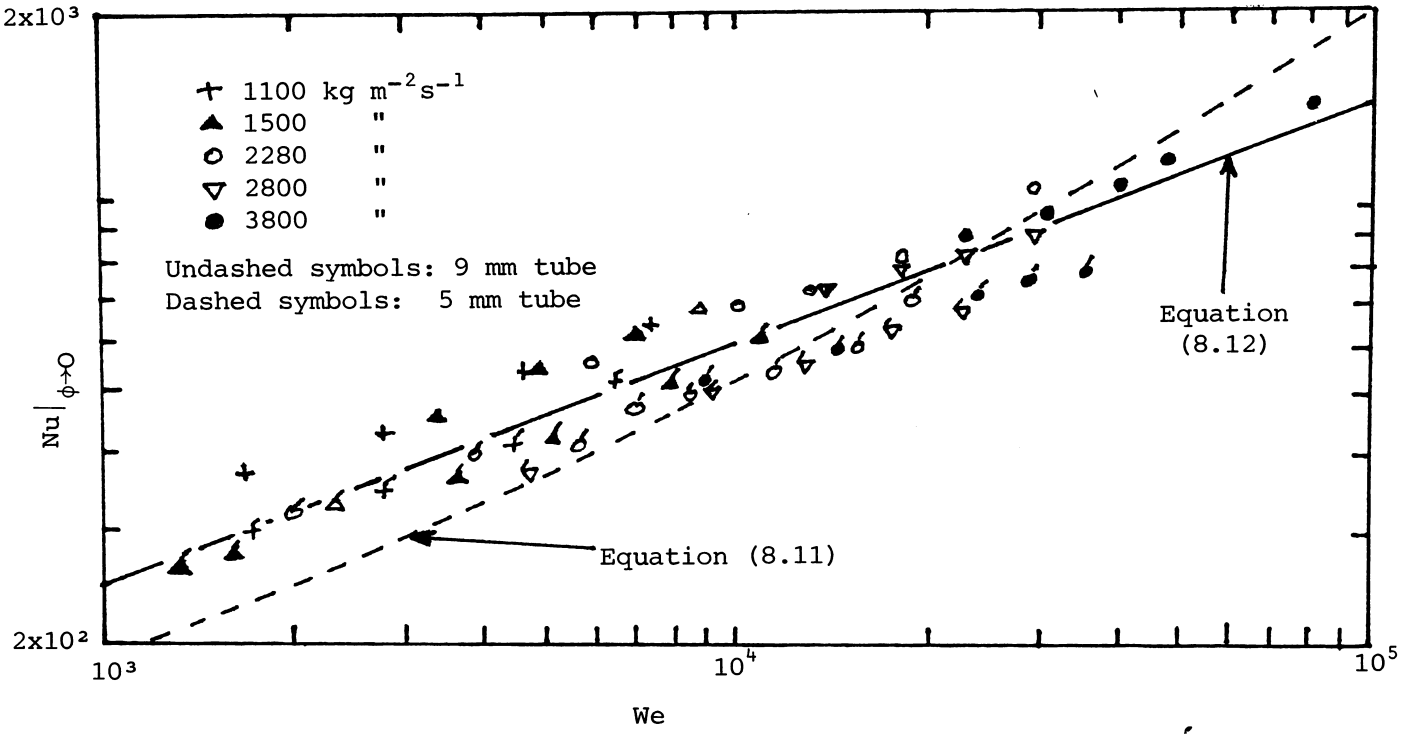

Fig. 8.4 Variation of Nusselt number with Weber number as heat flux approaches zero. Inlet data for 9 mm and 5 mm tubes, P = 7 MPa, 1100 < G < 3800 kg $m^{-2}s^{-1}$. Data from [8.1].

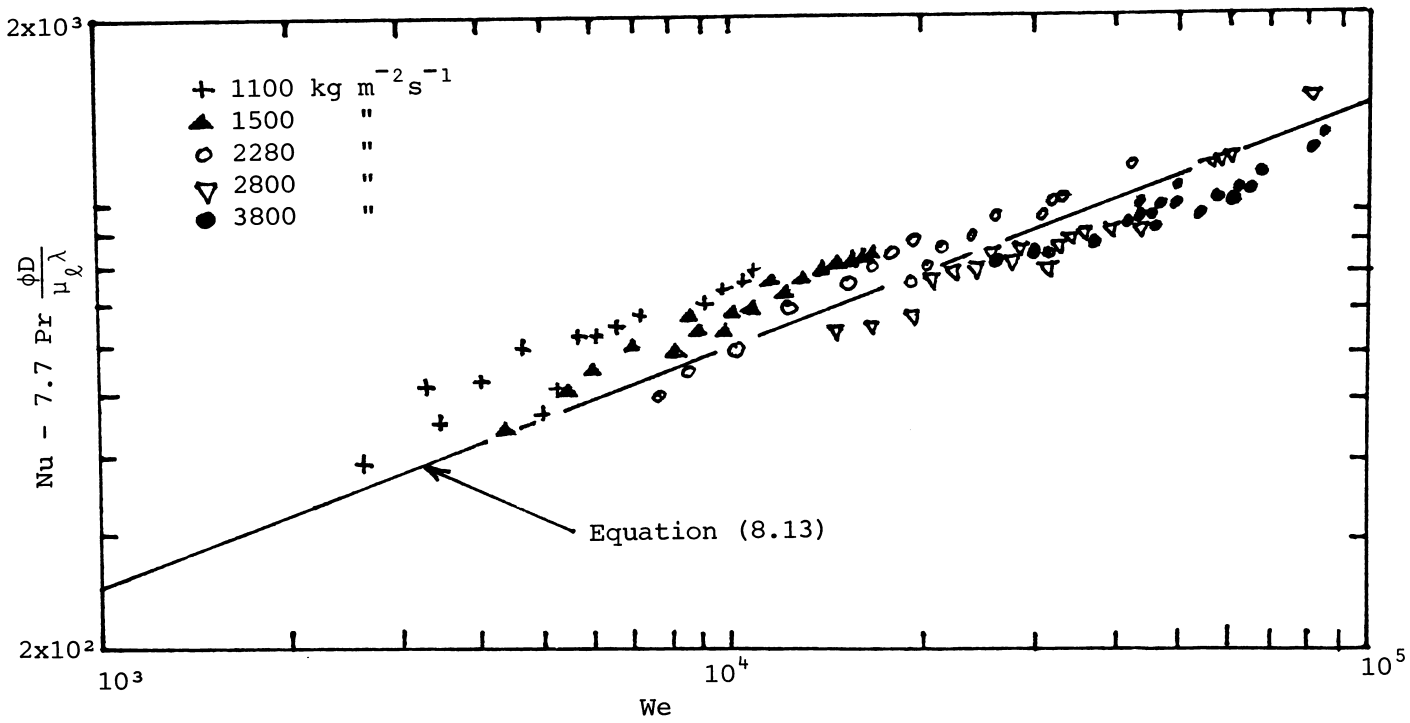

Fig. 8.5 Exit low heat flux heat transfer data for a 9 mm dia., 140 cm long heated tube, 7 MPa, 1100 - 3800 kg $m^{-2}s^{-1}$. Data from [8.1].

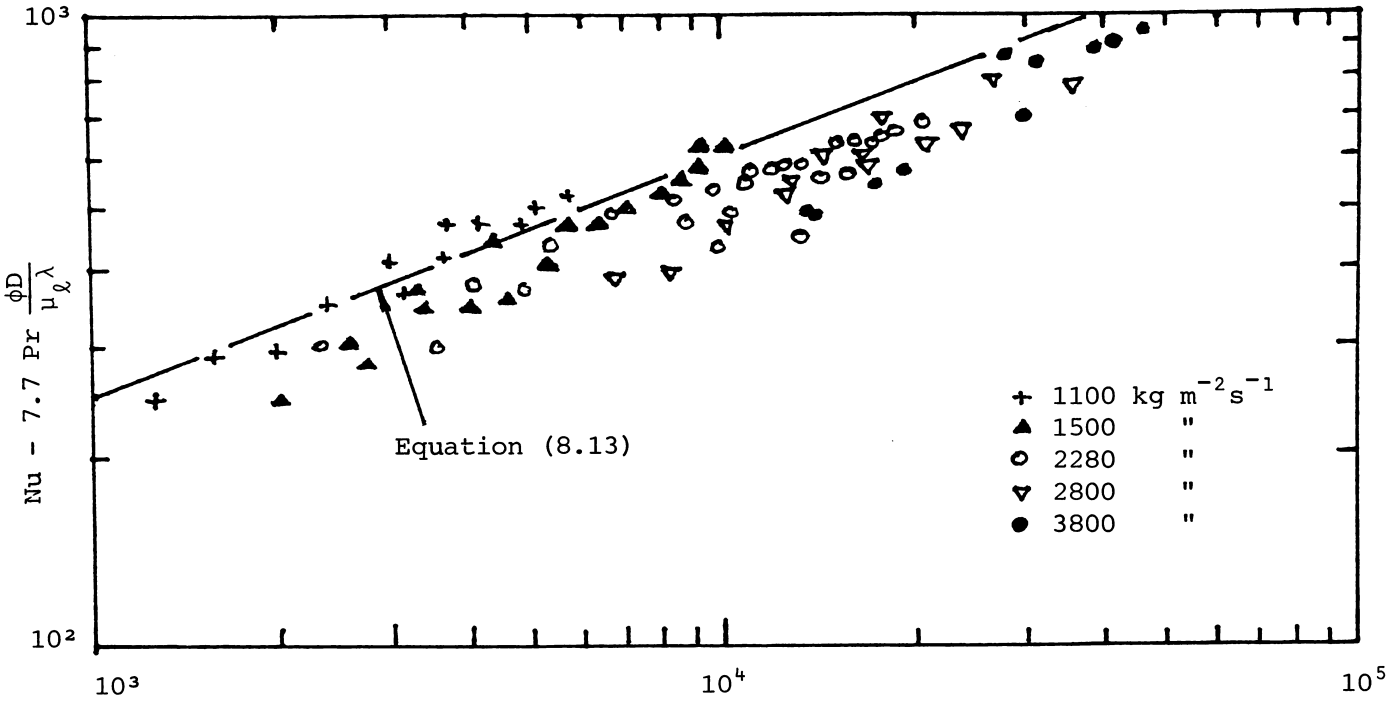

Fig. 8.6 Exit low heat flux heat transfer data for a 5 mm dia., 80 cm long heated tube, 7 MPa, 1100 - 3800 kg $m^{-2}s^{-1}$. Data from [8.1].

8.2.2 Heat transfer at moderate heat fluxes

As discussed in section 8.1, increasing heat flux induces a change of behaviour from one where heat transfer depends on Weber number, as discussed in section 8.2.1, to one with no dependence on Weber number. The change is apparent in the data shown in figure 8.3. Corresponding pressure drop data [8.2] indicate that the change in heat transfer characteristics is not accompanied by a corresponding change in friction factor characteristics. The wall bubbles therefore remain unchanged from a hydrodynamic viewpoint.

The dependence of heat transfer on Weber number, as developed in the model of section 8.2.1, arose from conduction of heat in the liquid between bubbles. The lack of dependence on Weber number at higher heat fluxes suggests that this contribution becomes negligible.

It is hypothesised here that the behaviour results from an increase in nucleation sites with increasing heat flux. This reduces the fraction $(1-\alpha_s)$ of boundary layer liquid not affected by nucleating bubbles. According to the model of section 8.2.1, the contribution due to conduction will disappear when $(1-\alpha_s)$ becomes zero. At this stage, heat transfer will be predominantly due to $\phi_{e.c.}$, i.e. to bubble microlayer evaporation together with condensation at the top of bubbles. However, with sufficient nucleation sites, nucleating bubbles become sufficiently close for the liquid flow $\dot{M}_{\ell}$, which replenishes the evaporating microlayer, to be restricted. This, it is envisaged, causes incomplete replenishment of the microlayer, and heat transfer changes from that described in section 8.2.1 to one for bubbles with depleting microlayers.

The experiments of Judd and Hwang [8.9] indicate that, for pool boiling, microlayer evaporation heat transfer for bubble with depleting microlayers follows a $\phi_{e.c.} \sim (T_w-T_s)^{2.5}$ relation instead of the

$h_{e.c.} \sim \phi$ found in section 8.3.1. A similar power relation can therefore be expected for flow boiling.

Examination of the intermediate heat flux (e,4,0) data of [8.1] shows that the total heat transfer behaviour is similar to the micro-layer evaporation component of pool boiling heat transfer described above. The data are close to

$$\phi = a\,(T_w - T_s)^3$$

with 'a' being independent of diameter, mass flux, quality and distance from the inlet of the heated tube. This is qualitatively consistent with the $\phi_{e.c.}$ model of section 8.2.1, which indicated that the micro-layer evaporation heat transfer coefficient is a function only of heat flux and fluid physical properties.

Some typical data of [8.1] are shown in figure 8.7 in the form of heat transfer coefficient versus heat flux. Also shown is the forced convective nucleate boiling correlation of Alediev et al. [8.10]:

$$\Delta T_s = [\,39.2 - 0.1\,T_s\,]\,(\phi/10^6)^{0.3}, \qquad (8.14)$$

The close agreement is noted. Equation (8.14) is also compared with some intermediate heat transfer data in figure 8.3.

No theoretical dependence on friction regime is predicted, so equation (8.14) is expected to apply to all developed nucleate boiling heat transfer at moderate heat fluxes.

It might be expected that the above explanation for intermediate heat flux heat transfer behaviour implies a change in friction behaviour because of the suggested increase in wall nucleation sites, i.e. in 'roughness' elements. As noted, no change in friction characteristics is apparent for the data of [8.2]. Nevertheless, the hypothesis is compatible with roughened wall shear studies surveyed in [8.4]. In that work, it was shown that friction was independent of

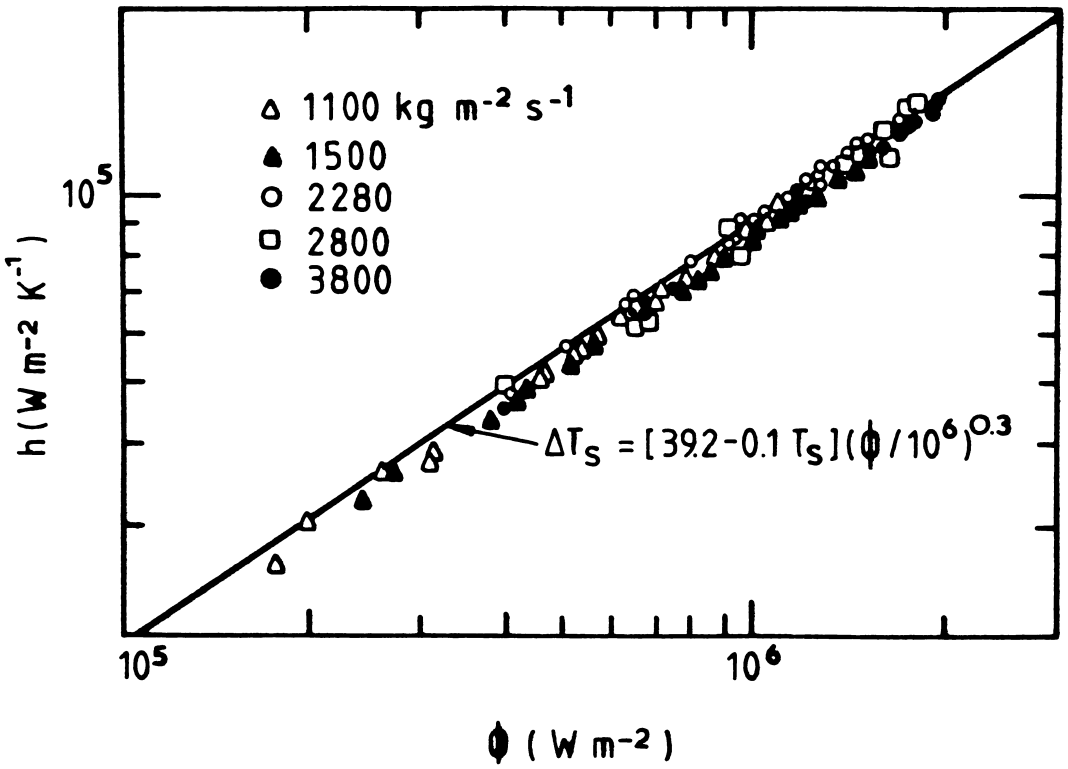

Fig. 8.7 Intermediate heat flux heat transfer behaviour at the exit of a 9 mm dia., 140 cm long heated tube at 7 MPa. Data from [8.1].

roughness density for regular roughness shapes if the fraction of the surface covered by roughness elements was in the range 15% to 60%.

8.2.3 Heat transfer near the boiling crisis: Temperature dropdown and hysteresis

In section 8.2.2, the change of heat transfer behaviour at low heat fluxes to that at moderate heat fluxes was explained as being due to the liquid flow replenishing evaporating bubble microlayers becoming restricted. The heat transfer behaviour in the vicinity of the boiling crisis can be explained by extending this concept. It is postulated that, with increasing heat flux, the liquid flow replenishing microlayer evaporation becomes sufficiently restricted to prevent complete evaporation of the bubble microlayer. The abrupt change in heat transfer near the boiling crisis (point D in figure 8.1) occurs when microlayers disappear. Consequences of this are as follows:

(i) Vapour within attached wall bubbles comes into contact with the heated wall, and consequently reaches higher temperatures than existed before complete microlayer evaporation;

(ii) As described in chapter 2 of [8.7], equilibrium bubble size decreases with vapour superheat. The higher vapour temperature allows bubbles to reach their equilibrium size before they are large enough to be sheared from the heated surface; and

(iii) With no liquid flow replenishing microlayer evaporation, the contribution $\phi_{e.c.}$ of sections 8.2.1 and 8.2.2 becomes zero. Moreover, conduction through the liquid is no longer inhibited so heat transfer reverts to a conduction mechanism through the liquid between bubbles, with a small contribution to conduction through the wall bubbles.

It is noted that wall bubbles so postulated remain static, so further nucleation is prevented.

As noted in section 8.1, a hysteresis occurs in the heat flux

cycle once the temperature dropdown occurs. The present model suggests that this is because, with no liquid flow to replenish bubble microlayers, the microlayers, once removed, cannot reform, and the conduction-only process at the temperature dropdown will persist with reducing heat flux. When the heat flux is sufficiently low for microlayer-free bubbles to become large enough to be sheared from the wall, the heat transfer process will revert to that described in section 8.2.1 or 8.2.2.

Since the temperature dropdown occurs near the boiling crisis, it is assumed that wall bubbles at the dropdown condition are arranged in a close-packed hexagonal array. The heat transfer at the temperature dropdown condition is depicted schematically in figure 8.8.

In considering quantitative consequences of the model outlined above, it is further assumed that, on microlayer evaporation, the wall-bubble vapour reaches thermal equilibrium with the surrounding liquid, i.e. the vapour temperature T_g also varies with distance from the wall.

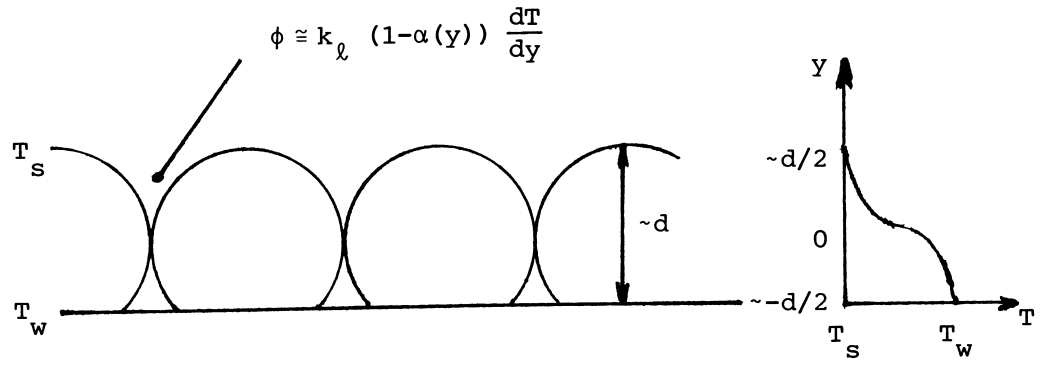

Fig. 8.8 Heat transfer near the boiling crisis

Adapting equation (2.2.6) of [8.7], the principle radii of curvature R_1 and R_2 of wall bubbles will thus also vary with distance from the wall according to

$$\left(\frac{1}{R_1} + \frac{1}{R_2}\right)^{-1} = \frac{\sigma}{\lambda\rho_g} \frac{T_s}{T_g(y) - T_s} .$$

For convenience, a sphere is assumed for the wall bubble shape. The radius is taken to be that which would occur if the vapour temperature was uniform at the mean bubble vapour temperature $T_s + \frac{1}{2}(T_w - T_s)$. From the above equation, the diameter d of the assumed spherical bubbles is then

$$\frac{d}{D} = \frac{8\sigma}{\lambda\rho_g D} \frac{T_s}{T_w - T_s} \quad * . \tag{8.15}$$

Considering thermal conduction through the bubble layer,

$$\phi = [(1-\alpha(y))\, k_\ell + \alpha(y)\, k_g]\, dT/dy, \tag{8.16}$$

where, from simple geometric considerations,

$$\alpha(y) = \frac{\pi}{2\sqrt{3}} \left(1 - \left(\frac{2y}{d}\right)^2\right) . \tag{8.17}$$

In the above, the origin for y is at distance d/2 from the wall.

The temperature profile is obtained by substituting equation (8.17) into (8.16) and integrating from the wall to distance y. The integration is cumbersome, but is simplified if the contribution to heat transfer via conductivity through the vapour is neglected. Since $k_g << k_\ell$ except at high relative pressures, it is assumed that $k_g/k_\ell \cong 0$. Performing the integration with this assumption,

$$\frac{T_w - T(y)}{d} = 6.8834\, (\tan^{-1} 6.2426\, y/d + 1.2607)\, \phi/k_\ell . \tag{8.18}$$

---

* It is interesting that the dimensionless group $\sigma/(\lambda\rho_g D)$, which appears in the present heat transfer analysis only in the approach to the boiling crisis, is a significant dimensionless group in the Green boiling crisis correlation [8.12].

As with the analysis of sections (8.2.1) and (8.2.2) it is assumed that the temperature at the top of the bubble is T_s. From equation (8.18) with y = d/2,

$$\frac{T_w - T_s}{d} = 17.3564\ \phi/k_\ell \ . \qquad (8.19)$$

From equations (8.15), and (8.19),

$$\phi = 0.0288\ k_\ell \frac{\lambda\rho_g}{\sigma T_s} (T_w - T_s)^2 \ , \qquad (8.20)$$

which predicts the heat flux:wall superheat relation at the pre-crisis temperature dropdown and for the subsequent reverse cycle of the hysteresis loop on reducing heat flux.

Observations of the boiling crisis [8.5] reveal the growth of a froth layer at the wall at the crisis onset. If the analysis leading to equation (8.20) is adapted to allow heat transfer through an ordered packed bubble layer N bubbles deep, the relation becomes

$$\phi = \frac{0.0288}{N} k_\ell \frac{\lambda\rho_g}{\sigma T_s} (T_w - T_s)^2 . \qquad (8.21)$$

Although several references were found reporting pre-crisis wall superheat reductions, only three [8.1, 8.3, 8.4] reported heat transfer data at the reductions of wall superheat. One of these [8.1] also reported heat transfer data covering the reverse half-cycle of the hysteresis loop.

Plots of the data show an independence of heat transfer on mass flux, diameter, and quality, but a dependence on coolant type and system pressure.These trends are consistent with equation (8.21). The data follow a $\phi:(T_w - T_s)^2$ trend, also consistent with equation (8.21). Considerable scatter are exhibited in the data. This scatter is consistent with non-unique N for equation 8.21, and suitable low integer number choices of N provides good agreement between the data

and equation (8.21). Within the framework of the model, this indicates a wall bubble layer of arbitrary thickness in the vicinity of the boiling crisis.

The data of [8.1, 8.3, 8.4] at the temperature dropdown and for the reverse half-cycle of the hysteresis loop are compared with equation (8.21) in figures (8.9 - 8.13). It is seen that, although the data cover a range of fluid type and flow conditions, they are compatible with equation (8.21) for non-fixed integer N, representing the thickness of the attached wall bubble layer in units of individual bubble diameters.

Two additional references [8.6, 8.13] were found which reported pre-crisis wall temperature drops and which presented heat transfer coefficient data. It is not clear whether the data reported are for the forward or reverse half-cycles of the hysteresis loop. However, the texts of [8.6, 8.13] indicate that much of the data were obtained after crisis conditions were determined. Thus, much of the data should apply to the reverse half-cycle of the hysteresis loop and so should agree with equation (8.21). Typical of the data, from [8.13], are compared with the equation in figure 8.14. As with the data of figures (8.9 - 8.13), suitable integer choice of N produces reasonable agreement between equation 8.21 and the data.

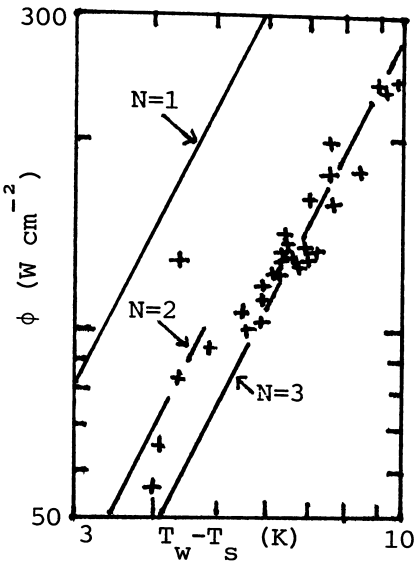

Fig. 8.9 Comparison of the pre-crisis temperature dropdown heat flux with equation (8.21); 5 mm tube, 7 MPa, 1100-3800 kg $m^{-2}s^{-1}$, steam-water data from [8.1]

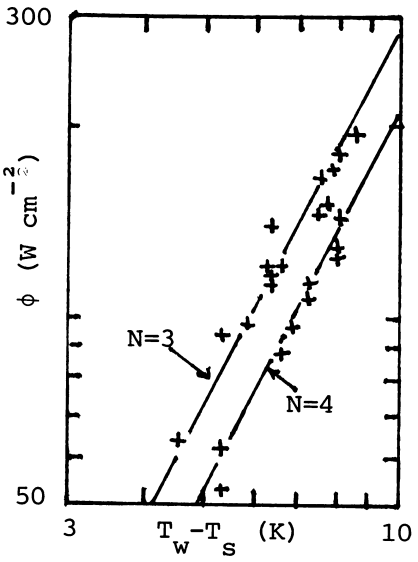

Fig.8.10 Comparison of the pre-crisis temperature dropdown heat flux with equation (8.21); 9 mm tube, 7 MPa, 1100-3800 kg $m^{-2}s^{-1}$, steam-water data from [8.1]

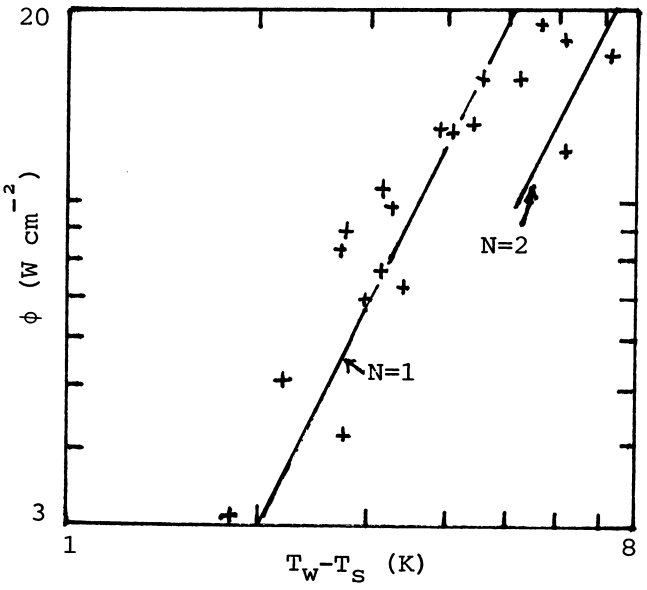

Fig.8.11 Comparison of the pre-crisis temperature dropdown heat flux with equation (8.21); F12 at 1 MPa, data from [8.3]

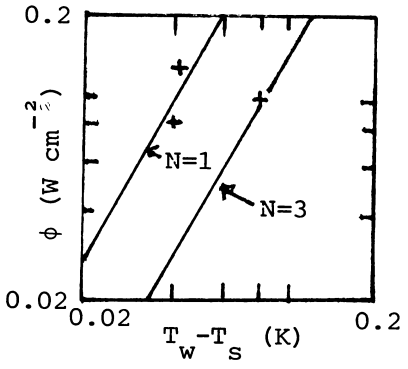

Fig. 8.12 Comparison of the pre-crisis temperature dropdown heat flux with equation (8.21); He data in a 0.47 mm tube, data from [8.4]

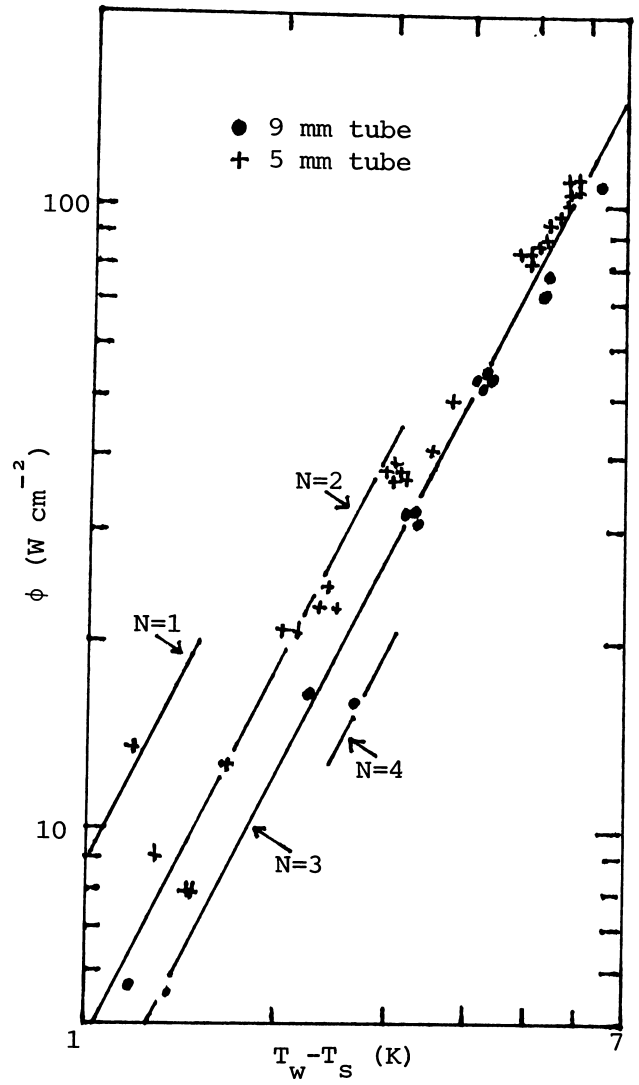

Fig. 8.13 Comparison of heat transfer during the downpath of the hysteresis cycle with equation 8.21. Steam-water at 7 MPa, data from [8.4]

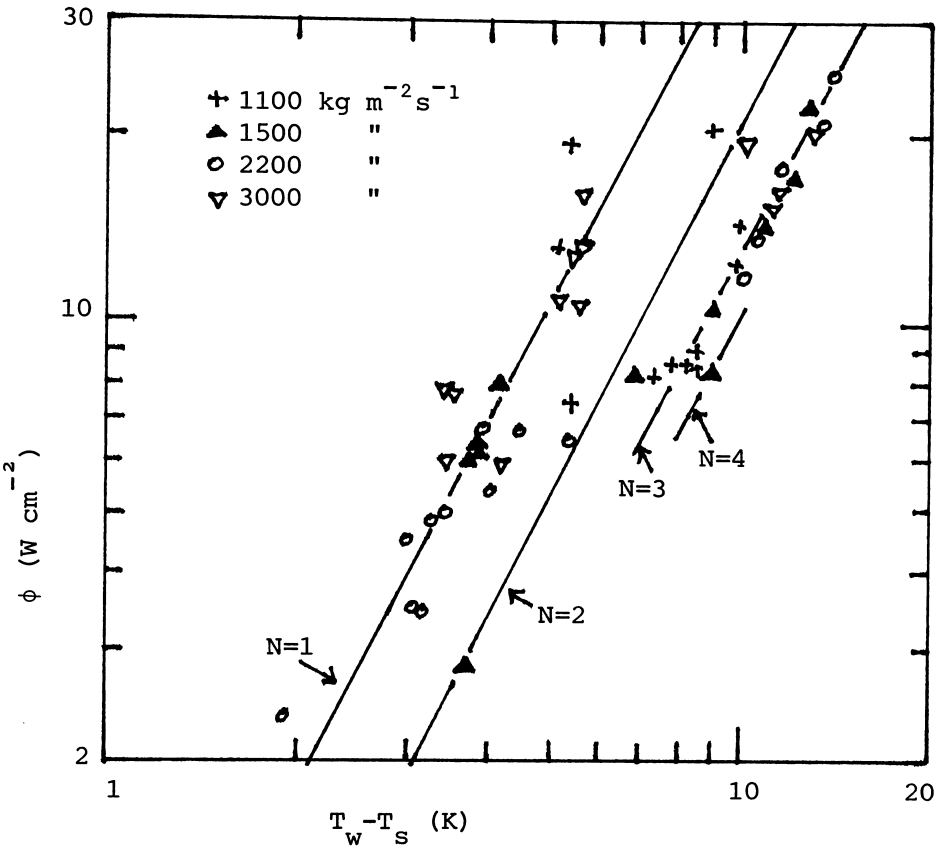

Fig. 8.14 Comparison of [8.13] steam-water heat transfer data with equation (8.21); data for a 0.4 m long 5 mm tube at 4 MPa

8.3 Post-crisis Heat Transfer

8.3.1 Dry wall heat transfer

8.3.1.1 Nusselt number prediction

For post-crisis droplet flows, the assumption that turbulence is confined to the gas phase was found satisfactory in the hydrodynamic analysis of sections 3.6.1 and 4.1. This assumption, together with that of a gas-only sublayer, implies that standard single phase flow heat transfer theory can be extended to yield an expression for droplet flow heat transfer. The Prandtl-Taylor modification of Reynolds analogy - see e.g. section 21.4 of [8.14] - is adapted in this section to yield an expression for post-crisis Nusselt number.

In chapter 3, momentum transport was assumed to be dominated by turbulent processes. In terms of eddy diffusivity of momentum, ε_M, this leads to

$$j(y) - j_\delta = \int_\delta^y \frac{\tau}{\rho_g \varepsilon_M} dy, \qquad (8.22)$$

where δ refers to the edge of the turbulent core and is specified in Prandtl's mixing-length theory by $\delta^+ = 11.8$.

Chapter 3 used a mixing-length approach rather than an eddy diffusivity approach. The equivalence of the eddy diffusivity approach to that described in chapter 3 is demonstrated by assuming, for equation 8.22, $\tau \cong \tau_w$ (as in chapter 3) and $\varepsilon = \kappa y \sqrt{\tau_w/\rho}$. These assumptions reduce equation 8.22 to equation 3.15, derived earlier from mixing-length concepts.

The thermal analogue of equation (8.22) is

$$T(y) - T_\delta = \int_\delta^y \frac{\phi dy}{\rho_g c_{pg} \varepsilon_H}, \qquad (8.23)$$

where ε_H is the eddy diffusivity of heat, and T defines a void-weighted

local temperature: $T = T_g \alpha + T_\ell (1-\alpha)$.

Assuming $\tau \cong \tau_w$, and $\phi \cong \phi_w$, and, applying Reynolds analogy, i.e. also assuming $\varepsilon_H = \varepsilon_M$, equations (8.22) and (8.23) reduce to

$$\frac{\phi_w}{\tau_w C_p} = \frac{(T_w - T(y)) - (T_w - T_\delta)}{j(y) - j_\delta} \tag{8.24a}$$

For later purposes, it is convenient to introduce the cross-section averaged version of equation (8.24a):

$$\frac{\phi_w}{\tau_w C_p} = \frac{(T_w - \langle T \rangle) - (T_w - T_\delta)}{\langle j \rangle - j_\delta} \tag{8.24b}$$

and equation (8.24a) considered for centreline values:

$$\frac{\phi_w}{\tau_w C_p} = \frac{(T_w - T_c) - (T_w - T_\delta)}{j_c - j_\delta} \tag{8.24c}$$

Since the sublayer is assumed to be gas-only,

$$\tau_w = \mu_g \, j_\delta / \delta$$

and

$$\phi_w = k_g \, (T_w - T_\delta)/\delta,$$

so

$$\frac{\phi_w}{\tau_w} = \frac{k_g}{\mu_g} \frac{(T_w - T_\delta)}{j_\delta} . \tag{8.25}$$

Eliminating $(T_w - T_\delta)$ from equations (8.24b) and (8.25),

$$\frac{\phi_w}{\tau_w C_p} = \frac{T_w - \langle T \rangle}{\langle j \rangle} \left(1 + \frac{j_\delta}{\langle j \rangle} \left(\frac{\mu_g C_{pg}}{k_g} - 1\right)\right)^{-1} . \tag{8.26a}$$

Similarly, equations (8.24c) and (8.25) produce

$$\frac{\phi_w}{\tau_w C_p} = \frac{T_w - T_c}{j_c} \left(1 + \frac{j_\delta}{j_c} \left(\frac{\mu_g C_{pg}}{k_g} - 1\right)\right)^{-1} . \tag{8.26b}$$

Since $j_\delta^+ = 11.8$, equation (8.26a) rearranges to

$$Nu = \frac{\frac{f(d)}{2} Re(d) \, Pr_g}{1 + 11.8 \sqrt{\frac{f(d)}{2}} \, (Pr_g - 1)} \tag{8.27}$$

where f(d) and Re(d) are dry wall friction factor and Reynolds number and are as defined in table (3.1):

$$f(d) = \tau_w/(\tfrac{1}{2}\,\rho_g\,\langle j\rangle^2), \tag{8.28}$$

$$Re(d) = \rho_g\,\langle j\rangle\,D/\mu_g \tag{8.29}$$

and

$$Nu = \phi_w D/[k_g\,(T_w-\langle T\rangle), \tag{8.30}$$

$$Pr_g = \mu_g\,C_{pg}/k_g \tag{8.31}$$

Over the range of conditions of interest to reactor engineering, the predictions of equation (8.27) are similar to those of

$$Nu = 0.023\,(Re(d))^{0.8}\,(Pr_g)^{0.4}, \tag{8.32}$$

which is of the form of the single-phase Dittus-Boelter equation. The similarity is demonstrated in fig. 8.15, which compares predictions of the two equations for a pertinent range of Reynolds numbers and for two pressures which represent the upper and lower limits of common reactor operating pressures.

In view of the similarity of predictions of equations (8.27) and (8.32), and the simplicity of equation (8.32), predictions based on equation (8.32) are regarded here as equivalent to those based on equation (8.27) developed from Reynolds analogy.

The predictive method developed here is thus similar to that of Dougall and Rohsenow [8.15], who proposed the extension of the Dittus-Boelter equation to post-crisis flows. However, a significant difference between the Dougall-Rohsenow and the proposed methods exists: although the Dougall-Rohsenow definition of Reynolds and Prandtl numbers for use in equation (8.32) are identical to those proposed here, their Nusselt number is based on T_w-T_s, whereas that which evolved from the above analysis involves $T_w-\langle T\rangle$. Wall temperature predicted using the proposed method will thus be somewhat larger than those predicted by the Dougall-Rohsenow method.

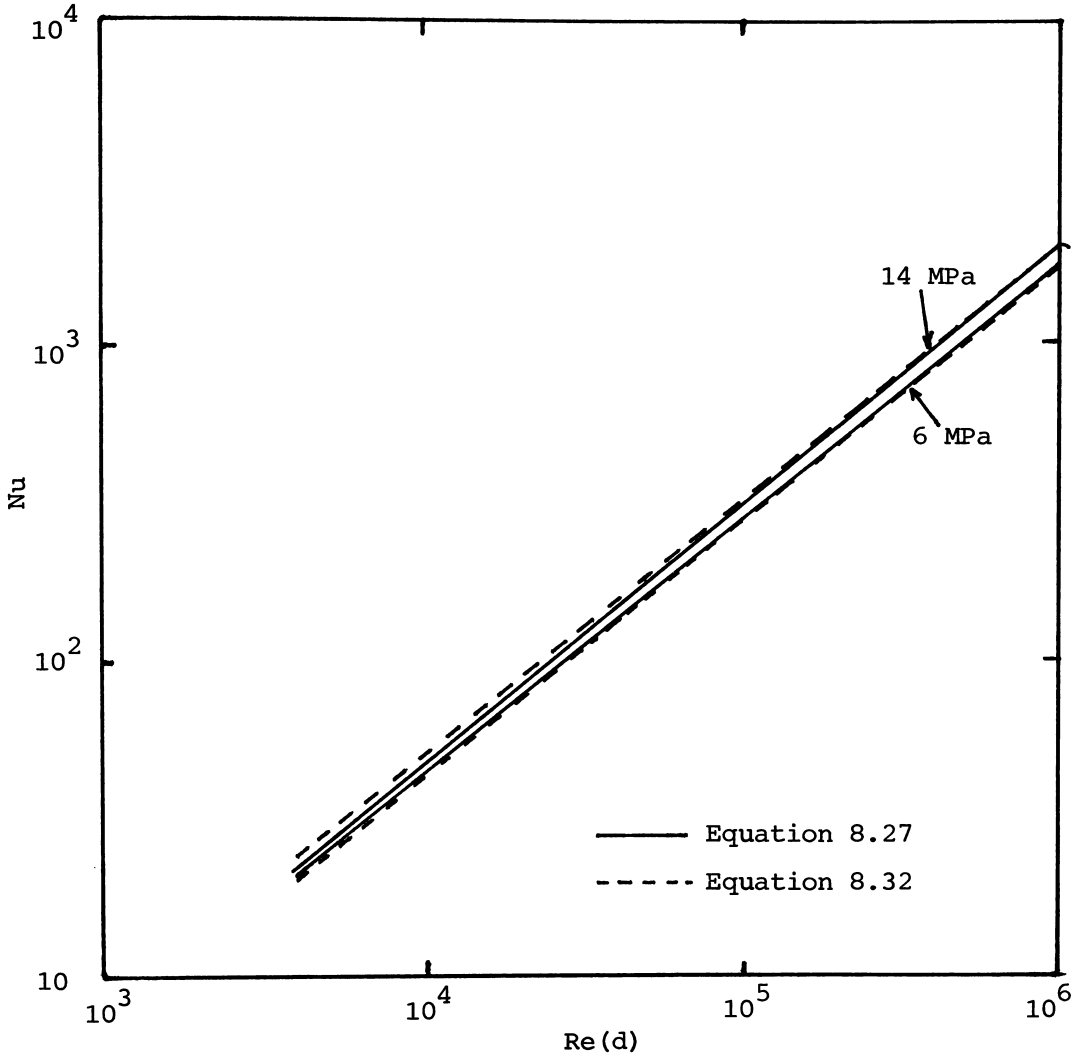

Fig. 8.15 Comparison of equations 8.27 and 8.32 for steam-water at 6 MPa and 14 MPa

<T> is usually unknown and is therefore an unsuitable reference temperature for the wall temperature T_w. A more useful (and usual) reference temperature is the saturation temperature T_s. A method of converting T_w-<T> values, as obtained by the proposed method, to values of T_w-T_s, is given below.

8.3.1.2 The heat transfer analogue of the drift flux equation

A relation between $(T_w - \langle T \rangle)$ and $(T_w - T_s)$ is needed in order that the heat transfer coefficient equations of the previous section may be referenced to the saturation temperature T_s. Such a relation may be obtained from a heat transfer analogue of the hydrodynamic analysis of section 5.1, which led to the drift-flux relations between mean phasic velocities and mean velocity. The analysis below parallels that of section 5.1. Highlights of the analogue between the thermal and hydrodynamic analyses are summarised at the end of the development of the relevant thermal equations.

The relation between <T> and T_s reflects thermal non-equilibrium, i.e. the fact that $T_g \neq T_\ell$. A local non-equilibrium parameter δ is defined by

$$\delta = T - T_\ell , \tag{8.33}$$

where T is the local mixture temperature $T_g\alpha + T_\ell (1-\alpha)$. From equation (8.33),

$$(1-\alpha)\ (T_w - T_\ell) = (1-\alpha)\ (T_w - T) + (1-\alpha)\delta \tag{8.34}$$

applies at each point in the flow.

The mean liquid temperature, weighted according to the liquid distribution, is defined by

$$\theta_\ell = \langle (1-\alpha)\ T_\ell \rangle / \langle 1-\alpha \rangle . \tag{8.35}$$

Averaging equation (8.34) over the flow section produces

$$T_w - \theta_\ell = C_T\ (T_w - \langle T \rangle) + \Delta , \tag{8.36}$$

which is the thermal analogue of the drift-flux equations of section 5.1. In this equation, C_T is the thermal distribution parameter:

$$C_T = \frac{\langle(1-\alpha)\ (T_w-T)\rangle}{\langle 1-\alpha\rangle\ \langle T_w-T\rangle} \tag{8.37}$$

and Δ is the liquid-fraction-weighted non-equilibrium:

$$\Delta = \langle(1-\alpha)\delta\rangle/\langle 1-\alpha\rangle\ . \tag{8.38}$$

The parameter Δ will be referred to as 'dis-equilibrium' to distinguish it between the local 'non-equilibrium' parameter δ.

In order to obtain an equation for the thermal distribution parameter C_T, it is now assumed that droplets are confined to the flatter part of the temperature profile, where the temperature is close to the centreline value T_c. Equation (8.37) then reduces to

$$C_T \cong (T_w-T_c)/(T_w-\langle T\rangle).$$

Using equations (8.26a) and (8.26b) and the fact that $j_\delta^+ = 11.8$, this becomes

$$C_T = \frac{j_c(1 + 11.8\ \sqrt{f(d,0,0)/2}\ (Pr_g-1)(\langle j\rangle/j_c))}{\langle j\rangle\ (1 + 11.8\ \sqrt{f(d,0,0)/2}\ (Pr_g-1))} \tag{8.37a}$$

where $f(d,0,0)$ is the dry-wall friction factor $2\tau_w/(G\langle j\rangle)$ related to the dry-wall Reynolds number $\rho_g\langle j\rangle D/\mu_g$ by Colebrook's equation (see table 3.1, section 3.9, and table 4.1). The ratio $j_m/\langle j\rangle$ is obtained from equation (5.16):

$$j_c/\langle j\rangle = C_{go} = 1 + 2.6\ \sqrt{f(d,0,0} \tag{5.16}$$

Eliminating $j_c/\langle j\rangle$ and $\sqrt{f(d,0,0)}$ from equation (8.37a) and (5.16) produces a relation between C_T and C_{go}:

$$C_T = \frac{C_{go} + 3.21\ (Pr_g-1)(C_{go}-1)}{1 + 3.21\ (Pr_g-1)(C_{go}-1)} \tag{8.37b}$$

For most flows of interest, this leads to $C_T \cong C_{go}$. From equation (5.16), this has a value of approximately 1.15 for typical flows.

As noted, the above analysis parallels exactly that of section 5.1. Table 8.1 summarises the analogous parameters of the hydraulic and thermal analyses. Note that just as differences in bulk phase velocities may exist, even in the absence of local drift (i.e. $v_d = V_d = 0$), because the distributed phase is concentrated in the faster moving region ($C_{go} \neq 1$), so differences in bulk phase temperature may exist, even in the absence of local phase differences ($\delta = \Delta = 0$), because the droplets concentrate in the cooler regions of the flow ($C_T \neq 1$).

Existing thermal analyses allowing for bulk thermal non-equilibrium, as typified by [8.16], do so only through local non-equilibrium effects. In terms of the present analysis, these analyses assume C_T to be unity but disequilibrium Δ is allowed for. An expression for Δ has not been achieved in this work. However, just as the local drift velocity V_d becomes negligible at higher velocities, and hydrodynamic behaviour is dominated by distribution effects, distribution effects may dominate thermal behaviour at high wall superheats, i.e. non-equilibrium effects due to Δ may be negligible. Of necessity, later data analysis (section 8.3.1.3) is performed assuming bulk phase temperature differences to be due to distribution effects only, with no contribution from the local thermal non-equilibrium parameter Δ.

In order to relate $\langle T \rangle$ and T_s, it is further assumed that droplets are at saturation temperature, i.e. $\theta_\ell = T_s$. Equation (8.36) then becomes

$$T_w - T_s = C_T (T_w - \langle T \rangle) + \Delta. \qquad (8.36a)$$

As noted, Nusselt number evaluation provides predictions of $T_w - \langle T \rangle$. This can be converted to prediction of $(T_w - T_s)$ through equation (8.36a) if suitable value of C_T and Δ are incorporated into this equation.

Table 8.1 Analogues between some thermal and hydrodynamic parameters relating phasic differences for dry wall droplet flows

Parameter Type	Hydrodynamic Parameter	Thermal Parameter
1. Local phase difference	Local drift velocity $v_d = u_\ell - j$	Local non-equilibrium $\delta = T - T_\ell$
2. Mean phase difference	Drift flux $V_d = \langle(1-\alpha)\ v_d\rangle/\langle 1-\alpha\rangle$	Dis-equilibrium $\Delta = \langle(1-\alpha)\delta\rangle/\langle 1-\alpha\rangle$
3. Mean liquid value	Mean liquid velocity $= \langle u_\ell(1-\alpha)\rangle/\langle 1-\alpha\rangle$	Mean liquid temperature $\theta_\ell = \langle T_\ell(1-\alpha)\rangle/\langle 1-\alpha\rangle$
4. Parameter for phase and velocity or temperature distribution effects	$C_{go} = \dfrac{\langle(1-\alpha)j\rangle}{\langle 1-\alpha\rangle\langle j\rangle}$ $= 1 + 2.6\sqrt{f(d,0,0)}$	$C_T = \dfrac{\langle(1-\alpha)(T_w-T)\rangle}{\langle 1-\alpha\rangle\ \langle T_w-T\rangle}$ $\cong 1 + 2.6\sqrt{f(d,0,0)}$ (see equation 8.37b)
5. Equation relating bulk parameters	$\dfrac{\langle u_\ell(1-\alpha)\rangle}{\langle 1-\alpha\rangle} = C_{go}\langle j\rangle + V_d$	$\theta_\ell = C_T\ (T_w - \langle T\rangle) + \Delta$

8.3.1.3 Flow quality prediction

The analysis of sections 8.3.1.1 and 8.3.1.2 provide equations relevant to the prediction of post-crisis wall temperatures. However, the dry wall droplet Reynolds number of the analysis, Re(d), depends on the quality:

$$Re(d) = \rho_g <j> D/\mu_g = G[(1-x)\ \rho_g/\rho_\ell + x]\ D/\mu_g$$

For pre-crisis flows, the quality is generally obtained from the energy equation with saturation properties being assumed. The 'equilibrium quality'* x_{eq} so obtained will be inappropriate to the present post-crisis analysis, since, although liquid is assumed to be at saturation conditions, vapour superheat is allowed for.

The enthalpy E

$$E = <\rho_g\ u_g\ h_g \alpha + \rho_\ell\ u_\ell\ h_\ell\ (1-\alpha)> , \qquad (8.38)$$

as obtained from the energy equation (equation 2.9), is readily converted to an expression for equilibrium quality. For $h_\ell = h_{\ell s}$ and $h_g = h_{gs}$, equation (8.38) becomes

$$E = G\ \{(1-x_{eq})\ h_{\ell s} + x_{eq}\ h_{gs}\} . \qquad (8.39)$$

If vapour superheat, as allowed for in this analysis, is included in equation (8.38), the equation provides an expression for true quality x with vapour superheat:

$$E = G\ \{(1-x)\ h_{\ell s} + x h_{gs}\} + <\rho_g\ u_g \alpha\ (h_g - h_{gs})> . \qquad (8.40)$$

Consider the term $<\rho_g\ u_g \alpha\ (h_g - h_{gs})>$. In terms of the vapour specific heat C_{pg}, assumed constant, this becomes

$$< \rho_g\ u_g \alpha\ (h_g - h_{gs}) > \cong \rho_g\ C_{pg} < u_g\ (T - T_s) >,$$

where $T = \alpha T_g + (1-\alpha)\ T_\ell = \alpha\ T_g + (1-\alpha)\ T_s$.

---

* 'Thermal equilibrium' only requires $T_g = T_\ell$. As applied to boiling systems, $T_g = T_\ell = T_s$ is generally implied.

Since the vapour velocity u_g is close to the mixture velocity j for post-crisis flows, $\langle u_g (T-T_s)\rangle = \langle j(T-T_s)\rangle$ is assumed, and, in line with the standard assumption used in resolving the single phase version of equation (8.38), $\langle j(T-T_s)\rangle = \langle j\rangle (\langle T\rangle - T_s)$ is also assumed. From equation (8.36a), the temperature difference $\langle T\rangle - T_s$ may be expressed in terms of the temperature difference $T_w - \langle T\rangle$ of the Nusselt number definition:

$$\langle T\rangle - T_s = (C_T - 1) (T_w - \langle T\rangle) + \Delta .$$

Collecting the above steps,

$$\langle \rho_g u_g \alpha (h_g - h_{gs})\rangle = \rho_g C_{pg} \langle j\rangle [(C_T - 1)(T_w - \langle T\rangle) + \Delta], \quad (8.41)$$

From equations (8.39) - (8.41),

$$x = \frac{x_{eq} - \frac{C_{pg}}{\lambda} \frac{\rho_g}{\rho_\ell} [(C_T - 1)(T_w - \langle T\rangle) + \Delta]}{1 + \frac{C_{pg}}{\lambda} (1 - \frac{\rho_g}{\rho_\ell}) [(C_T - 1)(T_w - \langle T\rangle) + \Delta]} . \quad (8.42)$$

If an expression was available for the disequilibrium term Δ, this could be solved iteratively with equation (8.27) (or equation 8.32) and equation (8.36a) to predict both the true quality and the heated wall temperature T_w.

8.3.1.4 Comparison with data

A full test of the theory of section 8.3 is not possible because of the unresolved disequilibrium function Δ of equation (8.36a). This could be regarded as a floating parameter to be correlated to ensure agreement of the analytic equations with data. However, forcing agreement with data by this method does not allow data to provide a test of other theoretical aspects of section 8.3.1. Consequently, an alternative to correlating data in terms of Δ is followed in this section.

In this section, the effects of Δ are assumed to be negligible,

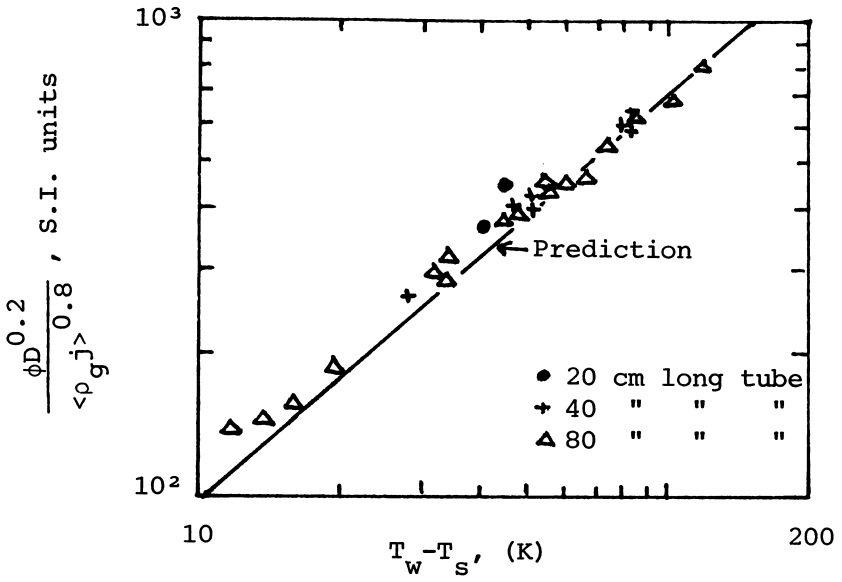

Fig. 8.16. Comparison of predicted and experimental post-crisis heat transfer characteristics for 3900 kg $m^{-2}s^{-1}$ steam-water flow at 7 MPa in 5 mm dia. tubes of various lengths. Data from [8.13].

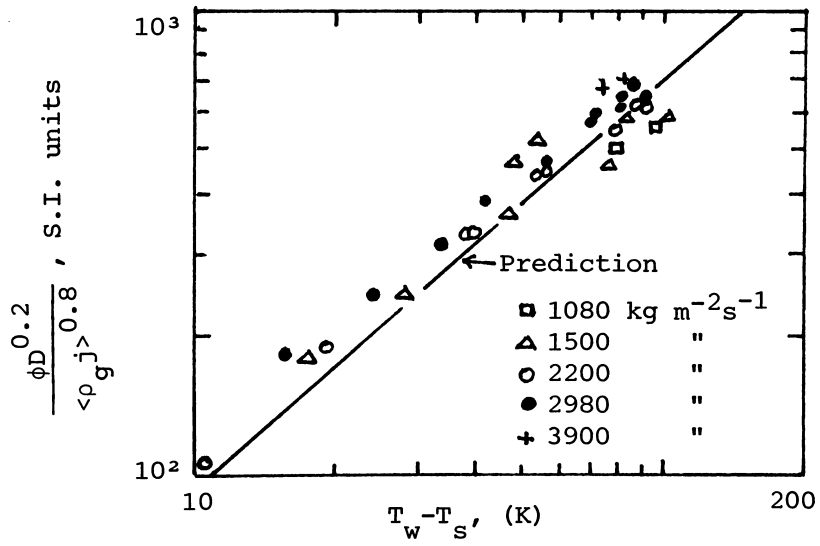

Fig. 8.17. Comparison of predicted and experimental post-crisis heat transfer characteristics for steam-water flow at various mass fluxes in a 140 cm long, 9 mm dia. tube at 7 MPa. Data from [8.1].

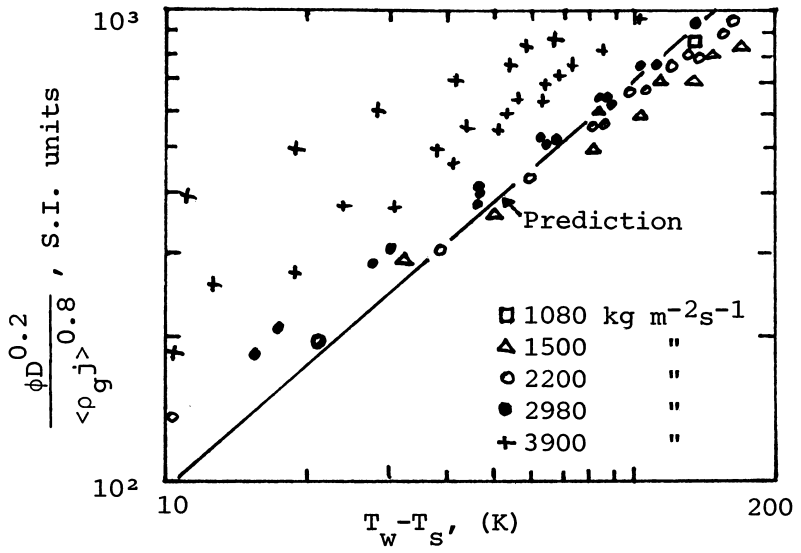

Fig. 8.18. Comparison of predicted and experimental post-crisis heat transfer characteristics for steam-water flow at various mass fluxes in an 80 cm long, 5 mm dia. tube at 7 MPa. Data from [8.1].

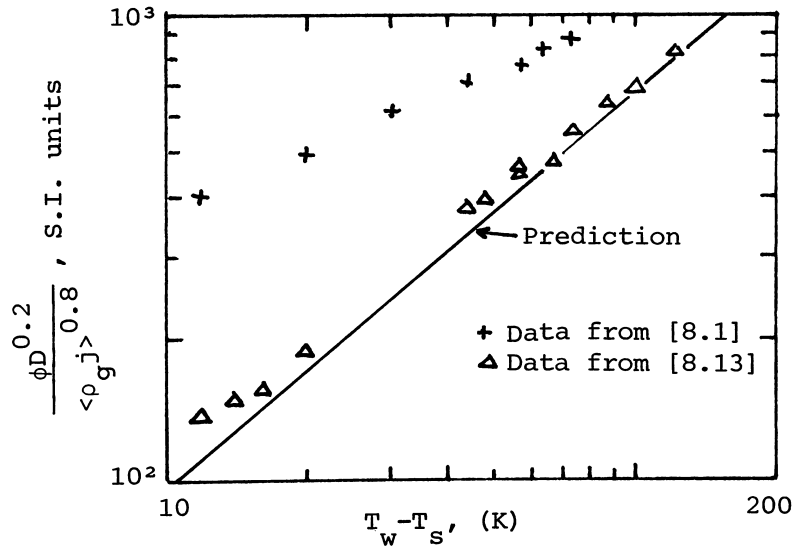

Fig. 8.19. Non-repeatability of post-crisis heat transfer characteristics for steam-water flow at nominally identical conditions: inlet quality ≅ 0.60; pressure ≅ 7 MPa; mass flux ≅ 3800 kg $m^{-2}s^{-1}$; tube diameter ≅ 5 mm; tube length ≅ 80 cm.

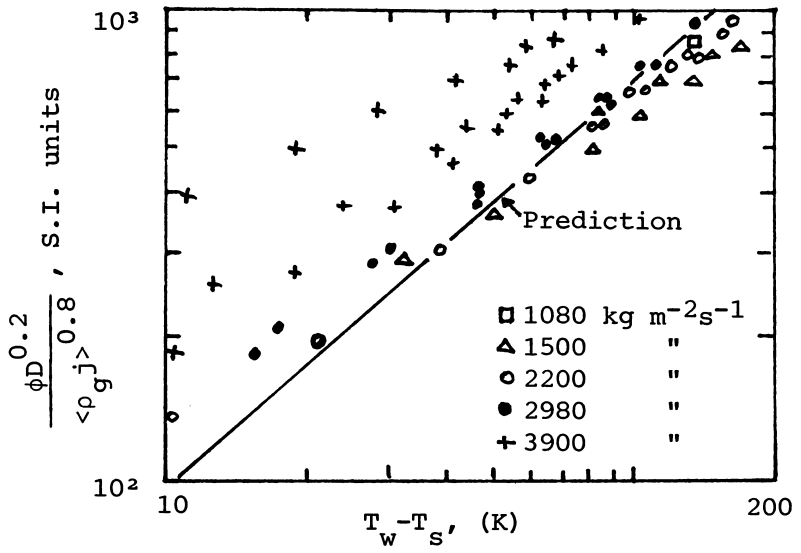

Fig. 8.18. Comparison of predicted and experimental post-crisis heat transfer characteristics for steam-water flow at various mass fluxes in an 80 cm long, 5 mm dia. tube at 7 MPa. Data from [8.1].

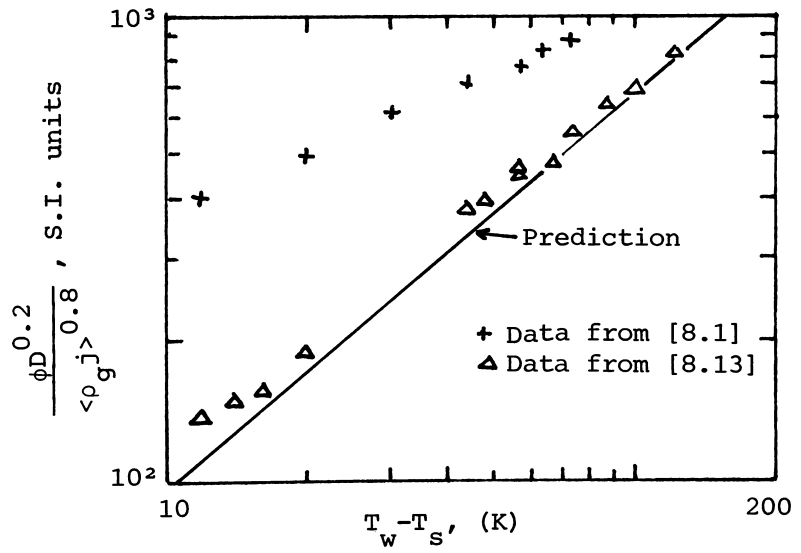

Fig. 8.19. Non-repeatability of post-crisis heat transfer characteristics for steam-water flow at nominally identical conditions: inlet quality ≅ 0.60; pressure ≅ 7 MPa; mass flux ≅ 3800 kg $m^{-2}s^{-1}$; tube diameter ≅ 5 mm; tube length ≅ 80 cm.

data are compared in figure 8.19. It is clear that the present predictive method is adequate for one of the sets of data. The evidence suggests that non-repeatability may occur, and that the present predictive method is reasonable for the maximum wall temperature that may occur but will overpredict wall temperatures for 'irregular' data. A possible explanation of the 'irregularity' of the high mass flux data of figure 8.18 is given in the next section.

The underpredicted wall temperature for the lower mass fluxes of figures 8.17 and 8.18 suggest that the neglected parameter Δ may not be negligible for these conditions. Although the data are not sufficiently extensive to obtain a correlation for Δ, they suggest that Δ is proportional to $(T_w-\langle T\rangle)$ for a given mass flux, with the 'proportionality' constant varying with mass flux. For the data considered, $\Delta/(T_w-\langle T\rangle)$ is about 0.3 for lower mass fluxes considered (1100 and 1500 kg $m^{-2}s^{-1}$), and is negligible (as assumed) for the higher mass fluxes considered (2980 and 3800 kg $m^{-2}s^{-1}$).

The above data analysis indicates that concepts of the present model are reasonable, but evaluation of the neglected parameter Δ is desirable since it is not negligible for some conditions. Some data behave irregularly, with non-repeatability of the data occurring. The predictive method is very conservative for the irregular data.

8.3.2 Pseudo-dryout

In considering the data of figure 8.18 in which wall temperatures are considerably overpredicted by the present method, it was noted that some of these data were obtained under nominally identical conditions to some of the data of figure 8.16, where agreement between prediction and data is closer. The two sets of data are shown in figure 8.19.

Figure 8.19 indicates that post-crisis heat transfer is not unique

for given quality, diameter, heat flux, heated length, mass flux, and pressure. The present prediction method appears to give a plausible estimate of the minimum of a possible range of heat transfer coefficients.

Pressure drop data [8.4] obtained simultaneously with the heat transfer data of figures 8.17 and 8.18 have been presented in figures 4.5 and 4.13. It is seen from the chapter 4 figures that the pressure drop data are consistent with the predicted f(d,0,0) behaviour. However, in the case of some of the 5 mm tube data (figure 4.13), agreement could only be achieved if the roughness was assumed to be lower than the actual tube roughness. A comparison of corresponding pressure loss and heat transfer data from figures 8.17 and 4.5 (9 mm tube), and from figures 8.15 and 4.13 (5 mm tube), indicates that the anomalously high heat transfer data of figure 8.18 can be associated with friction data where roughness is apparently less than the actual roughness.

In point (iv) of section 4.5.5.2, the anomalously low friction factors were explained as being due to 'pseudo dryout', with only the tips of roughness elements being dry and with superheated liquid remaining in the micro-crevaces between roughness elements, thus presenting a smoother flow boundary. Such superheated wall liquid would explain the higher heat transfer coefficients than those predicted for true dry wall conditions.

It is noted that, as discussed in section 7.3.3, boiling crisis data [8.17], obtained simultaneously with those friction factor data and/or heat transfer data which are consistent with the pseudo-dryout hypothesis, are also consistent with this hypothesis.

Chapter 8 References

8.1 S. Bertoletti et al., 'Heat transfer to steam-water mixtures', CISE-R-78 (1964).

8.2 G.P. Gaspari et al., 'Pressure drops in steam-water mixtures. Round tubes - Vertical upflow', CISE-R-83 (1964).

8.3 D.C. Groenveld, 'The thermal behaviour of a heated surface at and beyond dryout', AECL-4309 (1972).

8.4 V.I. Rominov et al., 'Investigating burnouts with helium boiling in a channel', Thermal Engineering, 28, 10, 620 (1981).

8.5 C.B. Parsons and E. Brundrett, 'A combined photographic film thickness and temperature technique for observing dryout', Progress in Heat and Mass Transfer 6, 365 (1972).

8.6 P. Perroud et al., 'Etude experimentale des coefficients d'echanges thermiques, des flux de chaleur critique et des pertes de charge avec des melanges equ-vapeur en ecoulement turbulent dans un tube vertical', CEA-1853 (1960).

8.7 L.S. Tong, 'Boiling heat transfer and two-phase flow', Wiley (1966).

8.8 M.G. Cooper, 'Nucleate boiling', Proc. 6th Int. Heat Transfer Conf. 6, 463 (1978).

8.9 R.L. Judd and K.S. Huang, 'A comprehensive model for nucleate pool boiling heat transfer including microlayer evaporation', J. Heat Transfer 98, 623 (1976).

8.10 I.T. Alediev et al., Teploenergetika 4, 9 (1957) (quoted by G. Guglielmine et al., 'Survey of heat transfer correlations in forced convection boiling', Wärme-und Stoffübertragung 13, 177 (1980)).

8.11 J.M. Robertson et al., 'Turbulent flow in rough pipes', I.E.C. Fundam. 7, 253 (1968).

8.12 W.J. Green and K.R. Lawther, 'Application of a general critical heat flux correlation for coolant flows in uniformly heated tubes to high pressure water and liquid nitrogen', Proc. 7th Int. Heat Transfer Conf., 4, 279 (1982).

8.13 L. Berkowitz et al., 'Results of wet steam cooling experiments: Pressure drop, heat transfer, and burnout measurements with round tubes', CISE-R-27 (1960).

8.14 G.F.C. Rogers and Y.R. Mayhew, 'Engineering thermodynamics', Longmans (1960).

8.15 R.S. Dougall and W.M. Rohsenow, 'Film boiling on the inside of vertical tubes with upward flow of the fluid at low qualities', MIT report TR-9079-26 (1963).

CHAPTER 9

CONCLUDING DISCUSSION

9.1 Résumé of Present Investigation

Mixing-length theory was used to formulate voidage and velocity defect equations for the turbulent core of two-phase flow. The voidage equations reflect an assumption that, locally, turbulence is confined to the continuous phase of the mixture, and so are able to allow for flow pattern effects. The turbulent velocity profile, which is of the familiar semi-logarithmic form, is, to a first order approximation, independent of the shape of the void profile and hence of the flow pattern*. Six different sublayer structures (bubbly with rigid-surfaced bubbles; bubbly with bubbles having freely-moving surfaces; wavy gas-liquid interface; gas-only; attached wall bubbles; and very thin liquid films) were considered for boundary conditions to the turbulent core. They led to non-dimensional velocity profiles with dimensionless group definitions which depend on the sublayer structure. Coefficients in the logarithmic profile may differ from those of the single phase equation, but remain constant for a given 'friction regime'. Empirically-observed values of these coefficients form parts of well-defined simple series rather than continuous spectra.

A triad (z,m,n), in which z is a letter specifying the sublayer structure, and m and n are integers from which the coefficients in the logarithmic profile may be obtained, specifies a friction regime (section 3.9).

Friction factor expressions were obtained by averaging the non-dimensional velocity profile. The Reynolds analogue of the dry wall

---

* Except insofar as the sublayer structure, which influences velocity profile, is determined by flow pattern.

friction factor expression provided a heat transfer coefficient for post-boiling crisis flows. Nucleate boiling heat transfer was modelled in terms of the nature of bubbles being generated on the heated surface.

Average voidage for annular flow was derived from the relation between film thickness and film flow rate obtained by integrating the velocity profile over the film region, with allowance being made for core droplets and film bubbles. Average voidage for distributed flow was derived using the Zuber 'drift-flux' equation, with distribution parameter values being determined from friction factor values. When coupled with the post-crisis heat transfer coefficient equation, the Reynolds analogue of the drift flux equation enabled thermal non-equilibrium to be evaluated.

A general form of the two-phase distribution parameter in terms of higher order correlation coefficients was utilised to deduce momentum and kinetic energy fluxes. These enabled the prediction of propagation phenomena such as sonic velocity and choked flow.

Although developed for flow through round tubes, the various theoretical expressions were also applied to the prediction of flows through ducts of complex cross-section. Values of mixing-length coefficients may be different under these conditions.

It was found that specification of friction regime in terms of sublayer type and non-dimensional velocity profile coefficients is necessary for prediction of the various parameters mentioned above. On the basis of approximately 10,000 world pressure drop data, recommendations were given for high pressure steam-water flows. With some qualifications, the regime boundaries are consistent with a requirement for continuity of wall shear stress at the boundaries. This continuity does not extend to some other characteristics, and

the discontinuity in critical heat flux at a friction regime boundary provided an explanation of the heat-flux-independent 'limiting quality' boiling crisis, and also upstream dryout. Similarly, the adiabatic dry wall friction regime boundary provided a zero heat flux limit of the boiling crisis quality.

9.2 Some Considerations on Data Analysis

Throughout this thesis, theoretical developments have been supported by favourable comparison with data obtained from the open literature. Supplementary data analysis of several thousand similar data was performed, and a vast majority of these also support the concepts of the thesis. Because of the large number of topics considered in the thesis, predictions developed for each topic were evaluated by comparison with representative data only.

It may appear that

(a) the extraordinarily large number of friction regimes apparently possible, each with unique coefficients in the various thermohydraulic equations of the thesis, is such that coefficients may be chosen to ensure agreement between a given data set and the appropriate equation of the thesis; and

(b) with such a large number of data having been analysed, 'representative' data chosen to demonstrate particular aspects may in fact have been unintentionally chosen from those data which demonstrated more favourable agreement with the proposed model.

In this respect, the following points should be noted:

(a) Although the thesis has noted that different friction regimes apparently may pertain to nominally identical data from different sources, presumably reflecting differences in entrance conditions, etc., it has also noted that, for conditions relevant to nuclear engineering, virtually all low quality data have been found to be consistent with a

particular friction regime [(a,0,0), using the notation of section 3.9]; similarly, virtually all relevant dry wall data have been found to be for the (d,0,0) regime. Coefficients in equations covering these conditions are thus set and so cannot be adjusted to force agreement of equations with relevant data;

(b) Although various friction regimes are possible for intermediate qualities, and equations for different regimes have different coefficients and different dimensionless groups, constraints on the possible coefficients and dimensionless groups are in fact rather severe. In the case of friction factors, for example, demonstration of consistency of a particular data set with one of the proposed friction regimes required that (i) the data be correlated by one of six possible pairs of dimensionless groups definitions; and (ii) in the case of friction factor/Reynolds number correlations, a shift of the correlating curve on both axes brings agreement of the correlating curve and the single phase friction factor/Reynolds number curve for the channel, with the restriction that the friction factor shift be by a factor 2^{m} with integer m, and the Reynolds number shift be by a factor $\sqrt{2}^{-5m}\ \sqrt{10}^{-n}$, with the same integer m and with integer n. Similar constraints occur if the friction factor depends on Weber number; and

(c) In order to demonstrate the claimed interrelation between various thermohydraulic parameters, data selected for discussion in this thesis were, where possible*, confined to data in which several thermohydraulic parameters were simultaneously measured. This

---

* Very few data were found for assessing some predictions, such as the magnitude of the effect of wall roughness at intermediate qualities (section 4.3.3). Relevant data selection was restricted to those data available, and the luxury of choosing data with other measured parameters was not possible.

(i) severely restricted the choice of data for discussion in the thesis, and (ii) ensured that, once the friction regime was determined on the basis of e.g. friction factor data, friction-regime dependent coefficients in equations for other thermohydraulic parameters were then determined and could no longer be adjusted to force agreement of the model with other measured parameters. Table 9.1 indicates those friction regimes where predictions for different parameters are compared, in the thesis, with individual data sets covering simultaneously-obtained measurements of the relevant parameters. Appropriate figures of the text which compare the theory and experimental data are also given. Similar comparisons of theory with data covering simultaneously-obtained measurements of friction, average voidage, and velocity profile can be found in appendix A10 for the (c,1,4), (a,2,0), and (b,3,0) regimes, and in appendix A24 for the (e,0,-1), (e,1,-3), (e,1,-1), (e,1,0), (e,1,1), (e,2,2) and (e,2,-2) regimes.

Although a large number of data have been considered, no error analysis has been performed in relation to comparisons between data and equations developed in this work. This is because emphasis in this work has been given to data interpretation in order to understand fundamental phenomena, rather than development of predictive equations. Although understanding of mechanisms is seen as a step in the development of improved predictive techniques, the investigation did not reach a stage where the relevant friction regime can be predicted for all given conditions, and a proper comparison between theory and data would require that a data bank be subdivided into different friction regimes. It is noted, however, that a simplified version of the thesis' wall shear stress model, in which regime effects are partially accounted for implicitly, is recommended in appendix A29 for initial

Topic / Friction regime	Velocity profile	Wall shear stress	Average void fraction	Propagation velocities	Boiling crisis	Heat transfer coefficient
a,0,0		4.12 7.1			7.1	
b,0,0			5.4	6.2		
c,0,0		4.1	5.1			
d,0,0		4.12 7.1 4.13				8.18
d,0,0		4.5				8.17
d,0,0	3.7	4.1	5.1			
e,2,-4	3.8	4.3	5.2			
b,3,-1	3.7	4.1	5.1			
a,4,0		4.15			7.2	
b,4,0		4.15			7.2	
b,4,0		7.1 4.12			7.1	
e,4,0		4.12 7.5			7.5	8.3,4,6, 9,13
c,4,1	3.7	4.1				

Table 9.1 Table of figures which present data for a given friction regime and for which the different parameters were obtained simultaneously in the same set of experiments.

estimates of frictional pressure gradients. As discussed in appendix A29, an error analysis resulting from comparison with an extensive data bank showed that this simple predictive method agreed with the data as well as the best of alternative predictive methods.

9.3 Significant Findings of the Investigation

(i) Friction regimes, which are determined by the nature of appropriate dimensionless group definitions and by the coefficients which appear in the non-dimensional velocity profile, play a larger role in determining two-phase thermohydraulic characteristics than do flow patterns. Unlike flow patterns, whose definitions tend to be qualitative rather than quantitative, and whose boundary determination is often subjective, friction regimes are defined in a quantitative manner, and friction regime boundaries are objectively determined by considering changes in observed quantifiable characteristics (from those consistent with one friction regime to those consistent with another).

(ii) Empirically-observed values of the two coefficients of the non-dimensional velocity profile which partially specify a friction regime indicates that 'permitted' values form parts of simple series. (This enabled friction regimes to be quantified partly in terms of m and n, a pair of integer numbers.) This suggests the existence of eigenvalues in some facets of turbulence, and may assist in the further understanding of the turbulent flow field.

(iii) Specification of a friction regime determines coefficient values for equations describing velocity profile, friction factor, average void fraction, propagation phenomena, heat transfer coefficient (for some conditions), and critical heat flux, and also determines the nature of dimensionless groups appearing in relations for these quantities. Viewed alternatively, an interrelation exists between the

abovementioned thermohydraulic parameters, and the nature of the interrelation is determined by the friction regime.

(iv) Partially-developed or fully-developed predictive techniques have been obtained for non-dimensional velocity profile (for symmetric flows in round ducts), friction factor, average voidage, propagation phenomena, heat transfer coefficient, and critical heat flux. For practical purposes, the predictive techniques can be considered complete for bubbly flow velocity profile, friction factor, average voidage, and (if no phase change occurs) propagation velocities; and for post-crisis droplet flow velocity profile, friction factor, average voidage, propagation velocities (if no phase change occurs), and heat transfer coefficient. In order to extend the predictive abilities where full development of the model was not achieved, some tentative recommendations were given for friction regime prediction, and also for annular flow film bubble concentration for voidage prediction. These tentative recommendations are based on analyses of data from CISE laboratories and are limited to steam-water flowing at conditions encountered in nuclear reactors.

(v) When the friction regime concept is incorporated into dimensionless group definitions - yielding 'generalised dimensionless groups', see sections 3.10 and 4.2 - instead of coefficients in expressions relating specific dimensionless groups, the non-dimensionless velocity profile and friction factor expressions were transformed into the familiar single-phase form for all viscosity-based friction regimes. The generalised dimensionless group definition incorporated very simple functions of the regime-specifying integers m and n.

(vi) The thin-film sublayer model (section 3.6.2) led to a friction factor equation (equation 4.3) similar to the Colebrook

friction factor equation for single phase flows in ducts with partially-roughened walls, but with dimensionless roughness being replaced by dimensionless film thickness. The model is thus an alternative to those annular flow friction models based on a gas flow in a rough duct, with roughness due to interfacial waves, which lead to a friction dependence on film thickness. The limited applicability of the thin-film model found in this work suggests that care should be taken in generalising interfacial roughness models based on thin film air-water data to high pressure annular flows. The thin film model also led to a simple derivation (appendix A28) of the Colebrook equation by simulating single phase rough wall flow by two-phase flow in a smooth duct. To the author's knowledge, a derivation of Colebrook's equation has not been achieved previously.

(vii) Boiling crisis characteristics depend not only on friction regimes but also on friction regime boundaries as determined from assessment of hydrodynamic characteristics.

(viii) In view of point (vii), the different friction regimes that occur for simple and complex geometries - see section 4.5.5.3 - provide an explanation for the reason why boiling crisis correlations for simple geometries do not extend to complex geometries. Complex geometry friction regime differ from those for simple geometries because of the lack of development ensured by rod bundle spacers and because the complex geometry flow boundary is only partially dry in post-crisis conditions.

(ix) The analysis of boiling crisis (ch.8), heat transfer in the approach to boiling crisis (ch.7), and shear stress in diabatic pre-crisis flows (ch.4), all point to the existence of nucleate boiling at the crisis onset for most annular flow crises of practical interest. This suggests that departure-from-nucleate-boiling

mechanisms may play a larger role in annular flow crises than is generally accepted.

(x) A 'pseudo-dryout' condition has been identified and associated with 'slow' boiling crises. Wall temperature and friction factors with 'pseudo-dryout' are lower than for true dryout, and associated boiling crisis qualities are higher than for true dryout. Pseuod-dryout friction factors, and associated boiling crisis qualities are quantitatively consistent with a 'dryout' condition in which super-heated liquid remains in the surface roughness micro-crevaces of the heated surface, and pseudo-dryout heat transfer coefficients are qualitatively consistent with this concept.

(xi) In the case of distributed flows in which the dispersed phase is concentrated in the faster regions of the flow, the analysis has provided a method of predicting values of the Zuber distribution parameter C_o, and has generalised this distribution parameter to (i) higher order correlation coefficients relevant to the resolution of momentum and kinetic energy fluxes, enabling propagation phenomena to be examined, and (ii) to a thermal distribution parameter useful in modelling post-crisis heat transfer.

(xii) Pressure propagation velocities for two-phase flow are referenced to a velocity which is <u>not</u> the mixture velocity, and also depend significantly on flow velocity. A consequence is that low velocity sonic velocity may differ significantly from critical flow velocity for a given mass quality. The difference is less for post-crisis droplet flows, for which the homogeneous model provides a reasonable estimate for both velocities.

(xiii) Care should be taken in generalising empirically-based equations to post crisis conditions since such equations are often based only on pre-boiling crisis data. The present analysis indicates

that pre-crisis wall shear stress, 'slip', and propagation velocities are respectively close to; above; and well above those predicted by the homogeneous model, whereas post-crisis values of the same quantities are respectively well below; below; and close to values predicted by the homogeneous model.

(xiv) Explanations were provided (section 4.4) for the reduced influence of surface roughness for two-phase flows as compared to roughness influence for single phase flow.

9.4 Suggestions for Further Research

The nature of the present research, in which several topics have been considered in an attempt to find a unifying concept relating them, is such that it has proved impractical to consider individual topics in great detail. Some topics, such as thin film annular flows, were considered only superficially since they do not play a significant role in nuclear reactor flows. Moreover, considerable simplification has been used in the analysis of some topics. This is evident in, for example, the chapter on propagation phenomena, which allowed for phase and velocity distribution effects in the development of a simplified analysis of propagation velocities, but which neglected phase change, dissipation, and dispersion. Consequently, the investigation has provided many topics which require further examination in order to improve the applicability of the concepts presented. The investigation also suggested several topics which may be amenable to investigation in terms of the present concepts.

These topics include:

(i) The prediction of appropriate friction regimes for given flow, inlet, and other boundary conditions.

(ii) The correspondence between friction regimes (and their boundaries) and flow patterns (and their boundaries). This is

relevant for those topics such as average voidage which depend on friction regime and also on flow pattern.

(iii) The prediction of bubble concentration in annular films and droplet concentration in annular cores. The analysis indicates that values of these concentrations are required for the prediction of annular flow average voidage and propagation velocities. Their values are also relevant in the prediction of the dryout phenomenon.

(iv) The extension of the mixing-length concepts to highly assymetric flows, such as stratified flows and flows in complex geometries with different sublayer structures on different surfaces. (The latter was partially incorporated into present analysis only for flows in multi-surface channels in which some surfaces are dry (post-crisis) and in which the remaining surfaces all have the same sublayer structure - see sections 4.5.5.3 and 7.3.2.)

(v) Further development of the thin film annular flow model of sections 3.6.2, 4.1 and 4.4.1.

(vi) Extension of the analysis of section 6.4 to provide a fuller account of phase and velocity distribution effects in annular flow propagation velocities.

(vii) Extension of the analysis of chapter 6 to allow for phase change, dispersion, and dissipation in propagation phenomena.

(viii) Extension of the analysis of chapter 7 to provide a complete model of boiling crisis in terms of the friction regime concept.

(ix) Development of an expression for the void-weighted average local dis-equilibrium parameter Δ of section 8.3.1.2

to complete the dry-wall thermohydraulic analysis of section 8.3.

(x) Sub-cooled boiling thermohydraulics.

(xi) Extension of the analysis of chapter 8 to incorporate heat transfer for non-nucleating annular flows; nucleate boiling heat transfer for low quality bubbly flows; and to non-nucleating two-component flows.

(xii) Allowance of attached wall bubble 'roughness' for low quality flows. (A full analysis was provided for higher quality flows - see section 3.6.3, and 4.1, 4.4.2 and 4.5.3, but as noted in section 4.5.5.2, wall bubbles only 'partially roughen' low quality flows, and this roughness effect was neglected.)

9.5 Conclusions

Single-phase turbulent flow mixing-length theory has been extended to two-phase systems in a manner that allows for different flow regimes. Results of the mixing-length concept were applied to the topics of flow structure, friction factor, average voidage, propagation velocities, heat transfer coefficient, and boiling crisis heat flux, and indicated that interrelations exist between these parameters. Equations developed from the model are compatible with relevant data.

APPENDICES

Appendices A1-A31 consist of publications arising from the present research program. The publications are listed in table A1.

As noted in chapter 9, the structure of the thesis has placed limitations on the extent to which individual topics of the thesis can be discussed in detail, and also on the quantity of data which can reasonably be presented in support of theoretical concepts of the thesis. More detailed discussions of topics and more extensive supporting data analyses can be found in these appendices. Table A2 indicates which topics of the thesis are discussed in each publication. The six topics of table A2 are the topics of chapters 3-9 respectively.

Appendices A23, A27 and A30 contain material outside the scope of the thesis. Of these publications, sections 3, 3 and 4 respectively are related to the thesis. Appendices A22 and A25 discuss experiments performed by the author as part of the evaluation program for some of the thesis topics. Appendix A28 discusses a single-phase flow topic - roughened wall thermohydraulics - and so appears to be outside the scope of the thesis. Its inclusion here is justified on the basis that flow in roughened ducts has been modelled in A28 by a two-phase annular flow with the physical properties of the two phases differing only in their viscosities.

The friction regime notation (z,m,n) of the thesis is presented as (m,n',z) in the appendices, with

$$n = n' - m + z$$

for viscosity-dependent flow (z = a, b, c or d), and

$$n = n'$$

for surface tension-dependent flows (z = e). The transformation of n' of the appendices to that of the thesis was performed to facilitate the

development of the partially unified interpretation of individual friction regimes, as presented at the end of chapter 3.

TABLE A1. Publications arising from research program

Appendix	Title	Names of co-authors	Where published or presented
A1	Two-phase flow structure and mixing-length theory		N.E.D., 21 (1), 46 (1971)
A2	A note on the calculation of two-phase pressure losses		N.E.D., 25 (3), 395 (1973)
A3	Drag reduction phenomena in gas-liquid systems		Proc. BHRA Internat. Conf. on Drag Reduction, St. Johns College, Cambridge, Sept. 4-6 (1974)
A4	Friction factors and regime transitions in high pressure steam-water flows		ASME paper 75 WA/HT4 (1975)
A5	Letter to editor on bubbly two-phase flow		AIChEj 22, 959, (1976)
A6	Pressure pulse and critical flow behaviour in distributed gas/liquid systems		Proc. BHRA 2nd. Internat. Conf. on Pressure Surges, London, Sept. 22-24 (1976)
A7	The effect of flow velocity on two-phase propagation phenomena	J.J. Thompson	As above
A8	Two-phase fluid mechanics and heat transfer in the dry wall region		Proc. 2nd Australasian Conf. on Heat and Mass Transfer, Sydney, Feb. (1977)
A9	Discussion on downflow slug flow		J. Fluids. Engng. 99, 263 (1977)
A10	Some aspects of two-phase flow drag reduction		Proc. BHRA 2nd Int. Conf. on Drag Reduction, Cambridge UK, Aug. (1977)

Appendix	Title	Names of co-authors	Where published or presented
A11	Letter to editor on bubble swarm characteristics		Can. J. Chem. Eng. 55, 663, (1977)
A12	Relationship between wall shear stress and the heat transfer crises phenomenon with vapour/liquid flows	K.R. Lawther	Paper FB23, 6th Int. Tr. Conf. Toronto, Aug. 1978
A13	Discussion on flow boiling critical heat flux	K.R. Lawther	Discussion volume, Proc. 6th Int. Ht. Tr. Conf, Toronto (1978)
A14	Discussion on high pressure steam-water flow characteristics		As above
A15	Discussion on two-phase helium flow pressure drop		As above
A16	Letter to editor on forced convection boiling heat transfer	K.R. Lawther	AIChEJ, 25, 384, (1979)
A17	Two-phase pressure loss and void fraction characteristics in rod bundle geometries		Proc. 18th IAHR Congress, Cagliari, Sardinia, Sept. 1979
A18	Letter to editor on void fraction and pressure drop in two-phase flow		Fluid Mechanics - Soviet Research 8, 2, 169 (1979)
A19	Choked foam flows in a convergent-divergent nozzle		Int. J.Multiphase Flow 6, 273 (1980)
A20	A point of inflection criterion for annular two-phase flow		European Two-phase Flow Group Meeting, Strathclyde Uni., June 1980
A21	Discussion of slug flow pressure pulse propagation		J. Fluid Engng. 102 249, 1980

Appendix	Title	Names of co-authors	Where published or presented
A22	Experiments on air-water flows in an eccentric-annular channel	K.R. Lawther	Proc. 7th Austsn. Hydraulics & Fluid Mechanics Conf., Brisbane, Aug. (1980)
A23	The accurate measurement of flow rates in gas and gas-liquid systems using a radio-tracer technique	G.L. Hanna	Proc. 8th Nat. Chem. Eng. Conf. Melbourne, Aug.1980
A24	An evaluation of two bubble detachment models for two-phase flow		Proc. ANS-ASME Int. Meeting on Nuclear Reactor Thermal Hydraulics, New York, Oct. (1980) (NUREG/CP-6014, p1343)
A25	Two-phase hydrodynamic experiments with axial flow through seven-rod clusters	K.R. Lawther	Int. J. Multiphase Flow 7, 423 (1981)
A26	Hydrodynamic regime change effects on critical heat flux charasteristics		European Two-phase Flow Group Meeting, Eindhoven, June 1981
A27	Contribution to 1981 ETPFG Meeting Calculation Exercise on Post-crisis Heat Transfer	B.J. Azzopardi	As above
A28	A smooth tube analogue of roughened wall thermo-hydraulics		AERE report R10194 (1981). Also HTFS paper RS377, Proc. 1981 HTFS Research Symposium
A29	A simple two-phase frictional pressure drop calculation method	P.B. Whalley	Int. J. Multiphase Flow, 8, 83 (1982)

Appendix	Title	Names of co-authors	Where published or presented
A30	Thermohydraulics aspects of nuclear safety research in Australia	A.G. Chapman G.W.K. Ford W.J. Green K.R. Lawther J. Marshall W.J. Turner	Proc. Inst. Mech. Eng. Conf. on Heat and Fluid Flow in Nuclear and Process Plant Safety, London, May 1983, Paper C102/83

Table A2

Topics of Individual Publications

Appendix	Void and/or velocity distribution	Friction factor	Average void fraction	Propagation phenomena	Boiling crisis	Heat transfer coefficient
A1	✓					
A2		✓				
A3	✓	✓				
A4		✓				
A5		✓				
A6	✓	✓	✓	✓		
A7				✓		
A8	✓	✓	✓	✓		✓
A9			✓			
A10	✓	✓	✓			
A11			✓			
A12		✓			✓	
A13		✓			✓	
A14	✓	✓	✓			
A15		✓				
A16	✓	✓	✓			
A17		✓	✓			
A18		✓	✓			
A19				✓		
A20	✓					
A21				✓		
A22	✓	✓				
A23	✓					
A24	✓	✓	✓			
A25	✓	✓	✓			
A26		✓				
A27						✓
A28	✓	✓				
A29		✓				
A30	✓	✓	✓	✓	✓	✓

NUCLEAR ENGINEERING AND DESIGN 21 (1972) 46–64. NORTH-HOLLAND PUBLISHING COMPANY

TWO-PHASE FLOW STRUCTURE AND MIXING LENGTH THEORY

D.R.H. BEATTIE
A.A.E.C. Research Establishment, Lucas Heights, Australia

Received 16 July 1971

A statistical approach to two-phase inertia forces leads to a mixing length theory in which different flow structures correspond to different flow regimes.

The theory is used in conjunction with void and velocity profile data to examine developing and developed flow profiles for bubble and dispersed annular flows. One- and two-component flows are considered for various channel geometries. Asymmetric profiles such as those that result from asymmetric heating or horizontal flows are also described by the theory.

In the case of annular flows liquid film thickness measurements are consistent with the theory. Shear stress data suggest a Prandtl mixing length constant slightly less than that for single phase flow theory. The core profiles at the boiling crisis condition are consistent with a local reduction of the liquid film to zero thickness.

1. Introduction

If the development of single phase flow theory is taken as a guide, any real understanding of the nature of two-phase flow structure is not likely to be gained until more is known about the nature of turbulence within two-phase flow.

Expressions so far developed for two-phase flow from fundamental turbulence theory have largely been based on adapting single phase flow theory to the two-phase flow situation. While these attempts have generally been partially successful, the approach is somewhat oversimplified; fundamental differences between differing flow regimes, for example, have not been accounted for.

This paper attempts to take these differences into account. While the theory presented adapts Prandtl's theory of turbulent single phase flow, empirical concepts extended to the two-phase case are restricted to the interpretation of eddy diffusivity. Expressions for the two-phase turbulent stress tensor components are based on an examination of the basic flow equations rather than an extrapolation of expressions for the single phase case.

This, together with certain assumptions, has permitted the separate development of differing flow structure equations for bubble and droplet (or mist) flow. The expressions obtained are tested by comparing them with flow structure data.

2. The concept of local voidage

Two-phase flows with constituents of constant physical properties may be described as a special case of compressible single phase flow in which parameters may undergo step changes of value with the restriction that if one parameter changes, so does every other. Point values in the fluid are either gas values or liquid values. The instantaneous description of this flow may be simplified by introducing a binary variable, δ, having the value one (or zero) if the point considered is in the gas (or liquid) region.

The ensemble average of this quantity δ at a point in the flow, or the probability that gas is at the point, is the local voidage α;

$\bar{\delta} = \alpha^*$.

3. Two-phase Reynolds shear stresses

Since two-phase flow is regarded here as a special case of single phase flow, the concept of two-phase Reynolds shear stresses is developed from consideration of the steady-state inertial force per unit volume for the x-direction I_x.

In the steady state †

$$I_x = \nabla \cdot (\rho U \mathbf{U}) .$$

The y-component in this expression, ρUV, can be described in terms of the previously introduced δ;

$$\rho UV = \rho_g U_g V_g \delta + \rho_l U_l V_l (1-\delta) ,$$

i.e.

$$\rho UV = \rho_g U_g V_g ,$$

if the point considered is in a gas region ($\delta=1$), or

$$\rho UV = \rho_l U_l V_l ,$$

if the point considered is in a liquid region ($\delta=0$).

* The cross sectional average of the local voidage, $\langle\alpha\rangle$, differs from a widely used definition of voidage as the fraction of cross section occupied by the gas phase. In present notation, the latter definition is in fact $\langle\delta\rangle$. Note that the ensemble average of this coincides with $\langle\alpha\rangle$ since $\overline{\langle\delta\rangle} = \langle\bar{\delta}\rangle = \langle\alpha\rangle$.

† The lagrangian expression $I_x = \rho\, \partial U/\partial t + \rho \mathbf{U} \cdot \nabla U$ is misleading and only valid for mass-conservative systems. Unless 'closed system' is regarded as being synonymous with 'constant mass system', Newton's second law for a closed system is

$$I_x = \frac{D}{Dt} \rho U = \rho \frac{DU}{Dt} + U \frac{D\rho}{Dt} .$$

The first term is the lagrangian expression, which combines with the second (expressed, from mass balance considerations, as $D\rho/Dt = (\partial\rho/\partial t) + \nabla \cdot \rho \mathbf{U}$) to form

$$I_x = \frac{\partial}{\partial t} \rho U + \nabla \cdot (\rho U \mathbf{U}) .$$

Extension of the lagrangian expression to two-phase systems, e.g. [1], leads to incorrect expressions for flows involving mass transfer and slip; an impulse occurring on phase change is not accounted for. The problem may be overcome by treating the impulse as an applied force.

The ensemble average of this is

$$\overline{\rho UV} = \overline{\rho_l U_l V_l (1-\delta)} + \overline{\rho_g U_g V_g \delta}$$

$$= \overline{\rho_l U_l V_l}(\overline{1-\delta}) + \overline{\rho_g U_g V_g}\,\bar{\delta} ,$$

since δ can take values of 1 or 0 only. Since ρ_l and ρ_g are assumed constant

$$\overline{\rho UV} = \rho_l (1-\alpha) \overline{U_l V_l} + \rho \alpha \overline{U_g V_g} .$$

U and V are here, as in single phase theory, treated as their average values, u, v, with superimposed fluctuating quantities U', V'. Under these conditions

$$\overline{\rho UV} = \rho_l (1-\alpha) u_l v_l + \rho_g \alpha u_g v_g$$

$$+ \rho_l (1-\alpha) \overline{U_l' V_l'} + \rho_g \alpha \overline{U_g' V_g'} .$$

The last two terms are two-phase Reynolds shear stress terms.

4. Application of mixing length theory

Two-phase flows generally consist of continuous and discontinuous phases. To a first approximation there is no velocity variation within an element of the discontinuous phase (a bubble in bubble flow or a droplet in mist flow). There is, however, likely to be considerable velocity variation within a comparably sized element of the continuous phase. It is therefore reasonable to treat turbulence as existing predominantly in the continuous phase.

The Reynolds shear stress expression developed in section 3 now becomes:
for bubble flow

$$\tau = \rho_l (1-\alpha) \overline{U_l' V_l'} , \tag{1a}$$

for droplet flow

$$\tau = \rho_g \alpha \overline{U_g' V_g'} . \tag{1b}$$

Since viscous effects can be neglected except in the wall region these expressions can be taken as the total shear stresses within the flow.

Eqs. (1a) and (1b) may be analysed by Prandtl

mixing length theory provided there is information on the voidage profile. A linear relation between the local continuous phase velocity and the local voidage is assumed, i.e.
for bubble flow

$$\alpha = au_l + b \,, \tag{2a}$$

for droplet flow

$$\alpha = cu_g + d \,. \tag{2b}$$

A less general assumption of direct proportionality between voidage and velocity has been shown by Zuber et al. [2] to be reasonable for macroscopic 'slip' behaviour.

Application of Prandtl mixing length theory to eqs. (1) and (2) (see appendix for details) then gives, for round tubes:
for bubble flow

$$(1-\alpha)^{3/2} = (1-\alpha_c)^{3/2} - \frac{u_l^* a}{\frac{2}{3}k} \ln \frac{y}{R} \,, \tag{3a}$$

for droplet flow

$$\alpha^{3/2} = \alpha_c^{3/2} + \frac{u_g^* c}{\frac{2}{3}k} \ln \frac{y}{R} \,, \tag{3b}$$

where
$u_l^* = \sqrt{(\tau_w/\rho_l)}$,
$u_g^* = \sqrt{(\tau_w/\rho_g)}$,
α = local voidage at position y,
y = distance from duct wall,
k = mixing length constant (= 0.4 for single phase flow),
R = duct radius,
subscript c refers to value at duct centre and subscript w refers to value at duct wall.

For non-circular ducts, R in eqs. (3a) and (3b) should be replaced by the relevant distance from the wall to the position of maximum (or minimum, see section 5.2) voidage. In cluster geometries void profiles may be 'smeared out' and treated as smoother profiles in simple geometries.

Eqs. (3a) and (3b) will be referred to as the voidage deficiency equations as they are analogous to the single phase velocity deficiency equation. As is the case with single phase flow, the voidage deficiency equations cannot be used for prediction until they are at least coupled to a theory describing the laminar sublayer. Such a theory is outside the scope of this paper. The remainder of this paper will therefore be concerned with the ability of eqs. (2a), (2b), (3a) and (3b), with suitable coefficients, to describe experimental data.

Data from both one-component (water, freons 11, 12 and 22) and two-component (air-water, nitrogen-water, argon-water, argon-ethyl-alcohol, nitrogen-sodium/potassium alloy, and nitrogen-mercury) systems in varying degrees of development have been used to test the theory. Geometries considered include round tubes, rectangular sections, annuli, and clusters of varying dimensions. Only specific examples can be discussed here, but these are representative of all data examined.

5. The voidage deficiency equation for bubble flow

5.1. *Comparison of the bubble flow voidage deficiency equation with empirical formulations*

Zuber et al. in their theoretical treatment of slip [2] concluded that empirical curves of the form

$$\alpha/\alpha_c = 1 + \sum_1^m C_n (r/R)^n$$

do not adequately describe radial void profiles because of prominent inflection points in the curves. They found that data were better described by the smoother form

$$\alpha/\alpha_c = 1 - (r/R)^n \,. \tag{4a}$$

To demonstrate this, Zuber et al. compared eq. (4a) with data from Petrick [3]. Their curves are reproduced in fig. 1 together with a comparison of the same data with the voidage deficiency equation. Although eq. (4a) is suitable for evaluating the macroscopic effect of phase distribution (as has been done in [2]), the data are more closely described by the voidage deficiency equation.

Similarly, the voidage deficiency equation appears to describe data as well as, or better than, another widely used from (e.g. [4])

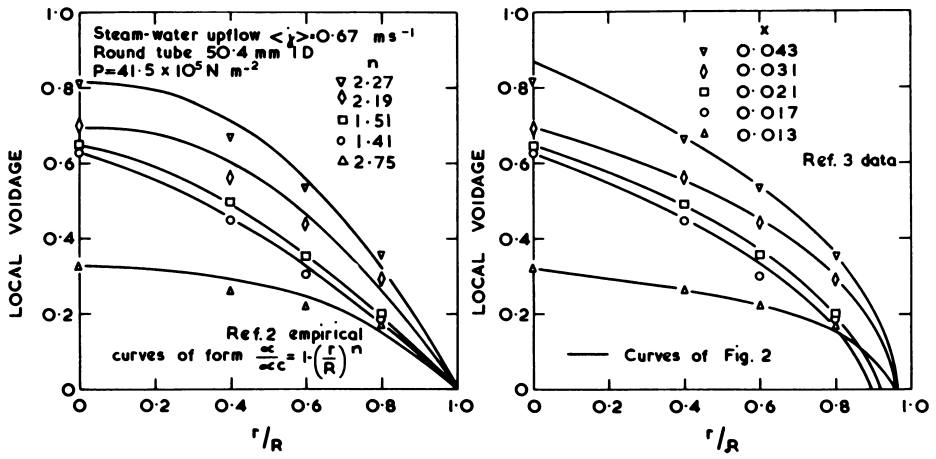

Fig. 1. Comparison of bubble flow data, voidage deficiency equation, and empirical curves.

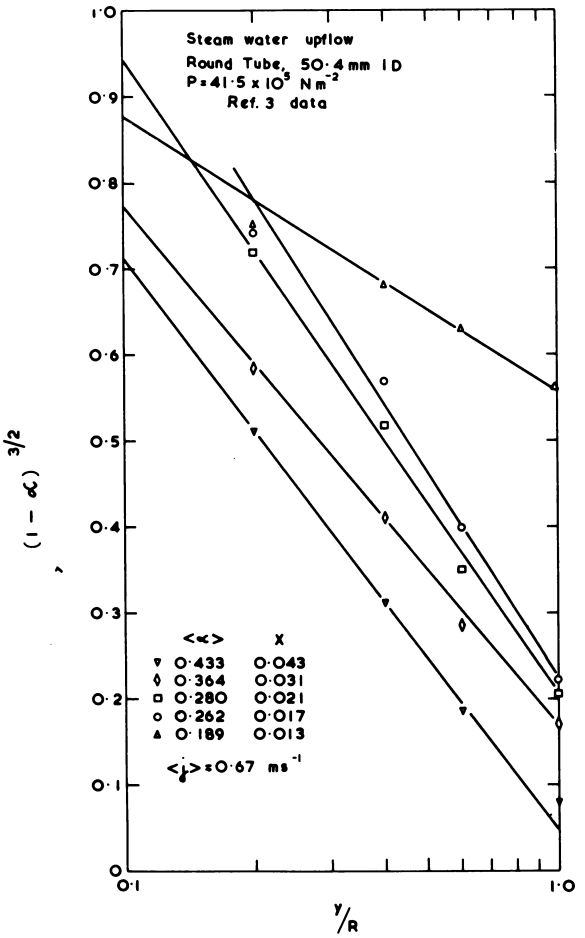

Fig. 2. Voidage deficiency plot of bubble flow data.

$$\frac{\alpha}{\alpha_c} = \left(1 - \frac{r}{R}\right)^n .$$

A comparison of this form and eq. (3a) is made with data from Neal [4] in fig. 3. For the particular case discussed, Neal found n to be 0.0863.

5.2. *Comparison of the bubble flow voidage deficiency equation with developing flow data*

In this paper, 'developed' flows are taken to mean flows for a given regime in which the normalised profile does not change farther downstream. Under this definition accelerating flows may be developed, and non-development (due to a regime change or subcooled boiling) need not be associated with a geometric entrance region.

Profiles of the same flow but at differing distances from the entrance, taken from [4], are shown in figs. 3 and 4. Referring to fig. 4, the voidage deficiency plot of the data near the inlet is similar to the plots of the more developed downstream data except that the slope has changed sign.

Experimental data indicate that, as in the above example, there is a strong tendency for a voidage minimum to occur at or near the duct centre for non-developed flows. This is expected for subcooled boiling profiles, e.g. [2], and for two-component flows where the gas is introduced in the wall region, e.g. [5],

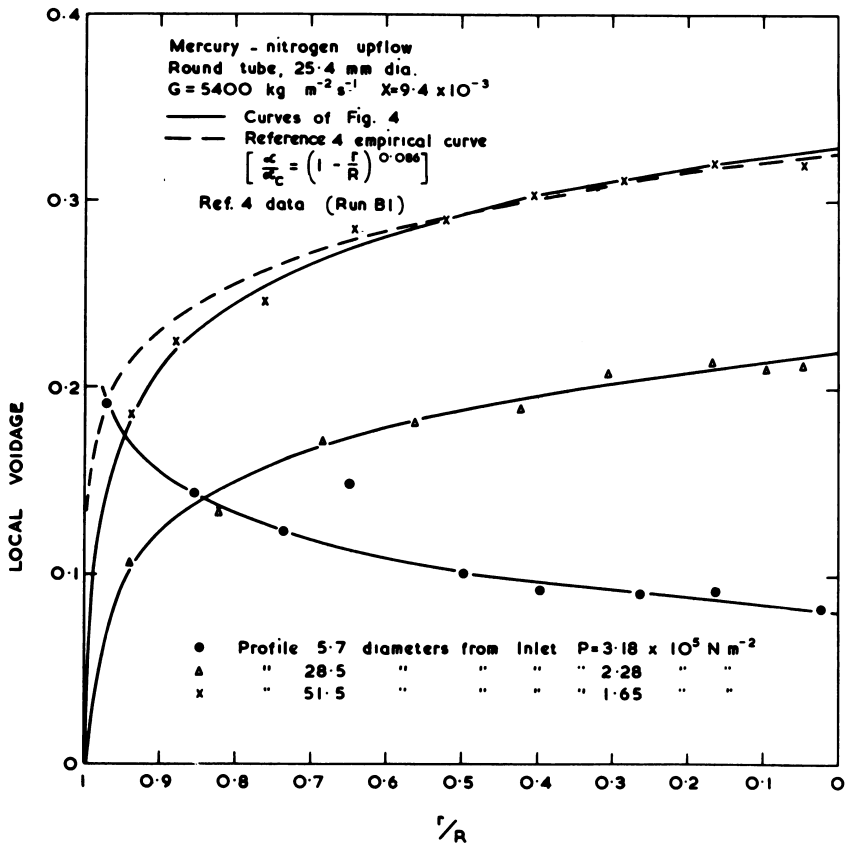

Fig. 3. Void profiles from developing bubble flow.

and not unexpected in cases of flow area changes, e.g. [6], but *is* unexpected in systems where the liquid is introduced into the wall region, e.g. [4], or where the gas is introduced in a central region, e.g. [7]. An example from [4] has been discussed; an example from [7] is given in fig. 5.

Existing data show a fundamental difference between subcooled boiling behaviour and the behaviour of two-component flows with the gas introduced through a porous wall. In the former, flow development starts from the wall region and moves inwards, e.g. [8, 9] as is the case in single phase flow; in two-component flows, flow development begins in the central region, [4, 5]. Bubbling through a porous wall does not, therefore, completely simulate the boiling process, as is often assumed, although the different behaviour quoted is possibly due to thermal non-equilibrium effects, and the analogy may be invalid only for the subcooled boiling region.

5.3. *Comparison of the bubble voidage equation with asymmetric profiles*

Asymmetry due to horizontal flow, e.g. [10], asymmetrically heated one component flow, e.g. [11] and non-completed flow development (most references) are described by eq. (3a) provided that the distance y extends from the wall to the voidage maximum (or minimum).

An example is shown in figs. 5 and 5a, where an asymmetric profile from a highly non-developed flow [7] is examined.

In many cases, if R is replaced by the relevant wall to maximum (or minimum) voidage distance, a voidage deficiency plot results in one line describing the profile, instead of one for each side of the asymmetric profile. Data from [12] shown in figs. 6 and 6a

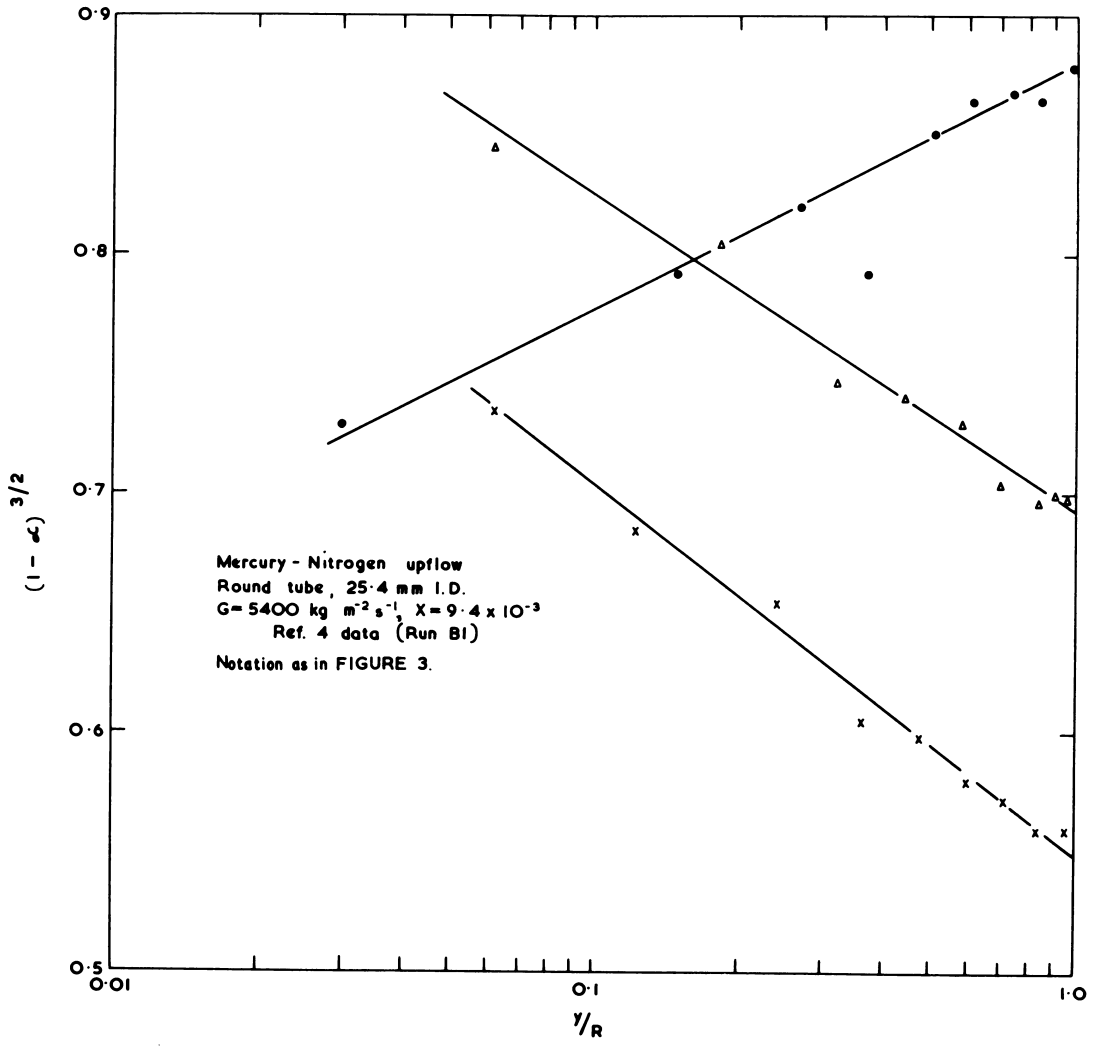

Fig. 4. Voidage deficiency plot of developing bubble flow.

demonstrate this feature.

5.4. *Velocity profiles in bubble flow*

Eq. (3a) has been shown to describe void profiles in bubble flow. The assumed similarity of the liquid velocity profile [eq. (2a)] is harder to test because of a lack of reliable data. Local liquid velocities are generally obtained by techniques in which considerable disturbance of the flow is expected. Neal [4], for example, obtained local liquid velocities from a combination of impact probe readings (the theory behind this is in itself debatable, see [11]) and independently determined void profiles. The velocity behaviour is not consistent with eq. (2a), whereas figs. 3 and 4 have shown that the void behaviour (determined by conductivity methods) is well described by eq. (3a), the validity of which depends on eq. (2a). The most likely explanation of this is that the velocity data are questionable.

In fact, similar comments apply to all liquid velocity data for bubble flow that this author has encountered. Reliable *gas* velocity profiles have however been obtained from steam–water bubble flow [5]. If Zuber's treatment of bubble flow slip is

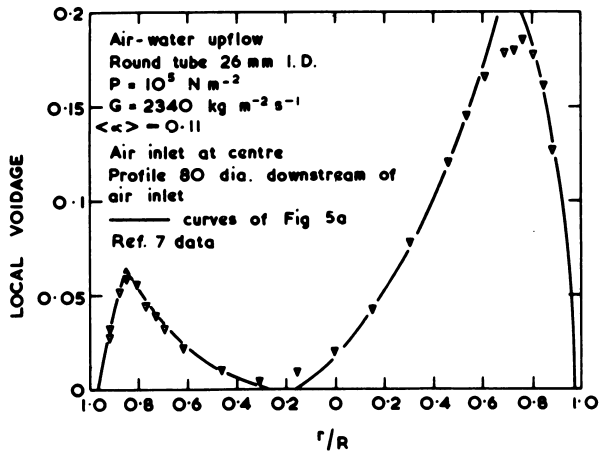

Fig. 5. Void profile for asymmetric bubble flow.

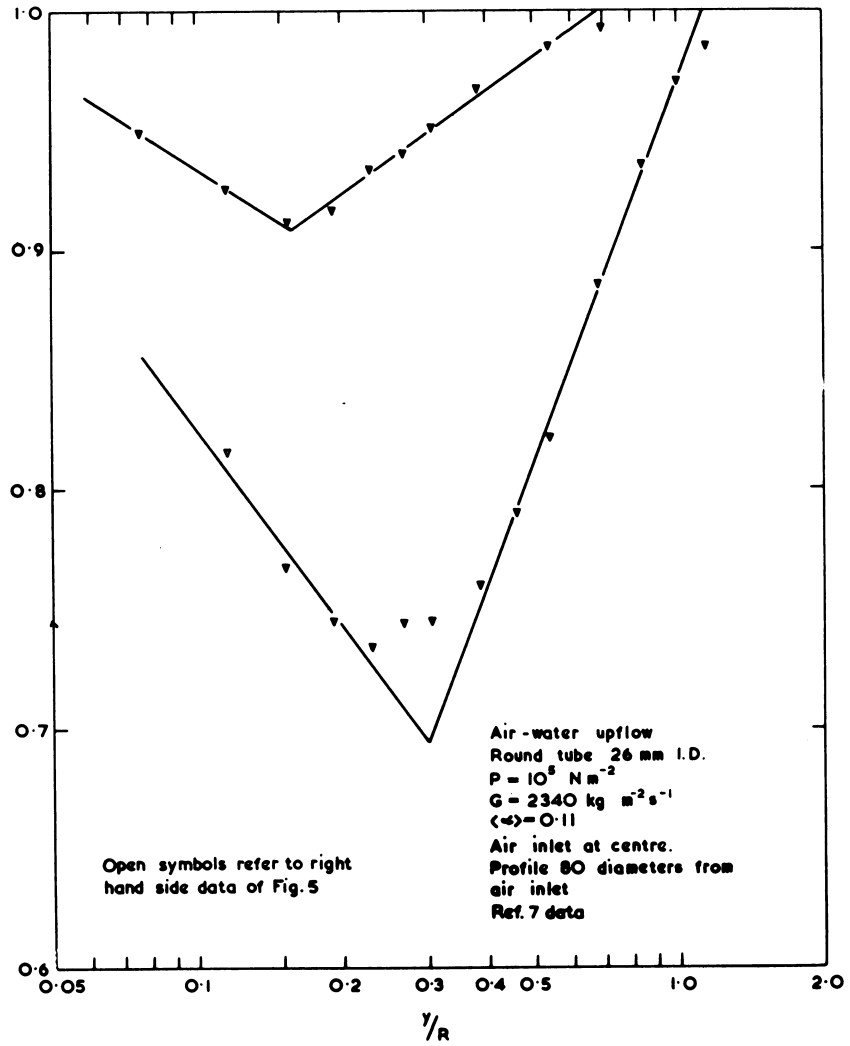

Fig. 5a. Voidage deficiency plot of asymmetric non-developed bubble flow data.

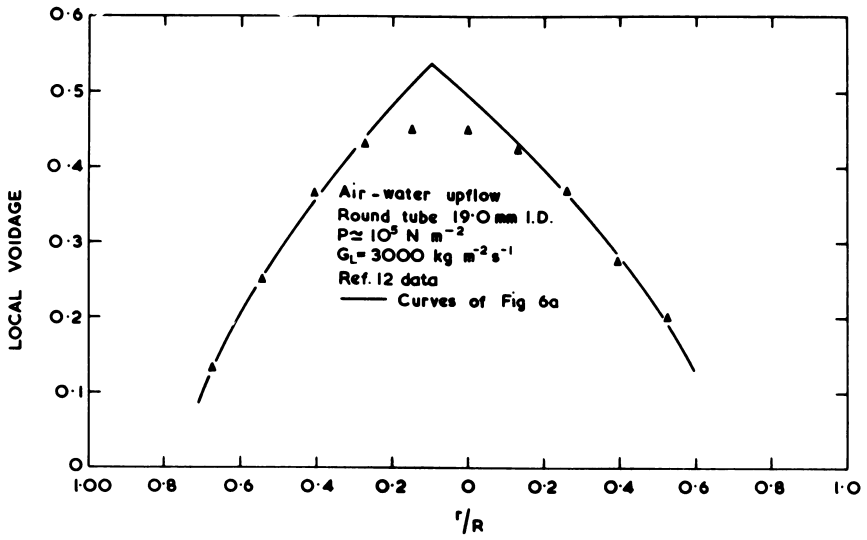

Fig. 6. Void profile for asymmetric bubble flow.

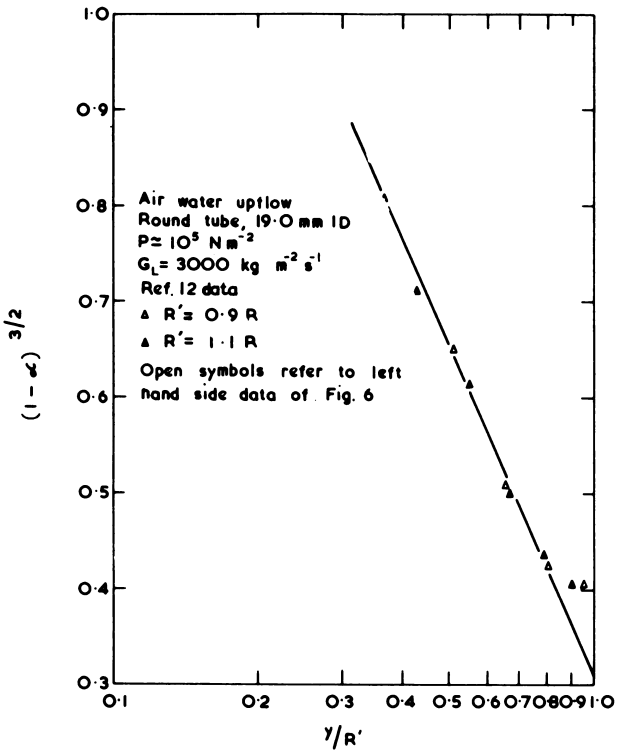

Fig. 6a. Voidage deficiency plot of asymmetric bubble flow data.

correct [2], the local gas and liquid velocity difference is reasonably constant over a cross-section. An equation of the form of (2b) should then approximate the data.

This in fact is the case. A typical example [5] is analysed in figs. 7, 8 and 9. The curves in fig. 7 satisfactorily describe both the void and velocity profiles.

Generally speaking, then, eq. (3a) describes void data well, but an analysis of velocity data to test the validity of eq. (2a) [upon which eq. (3a) is partially based] has proved inconclusive. However there are indications that eq. (2a) may be valid.

6. The voidage deficiency equation for the core region of dispersed annular flow

6.1. *Comparison of the droplet flow voidage deficiency equation with empirical formulations*

Steam–water profiles from Adorni et al. [13] have been curve-fitted by Zuber et al. [2] with equations of the form

$$\alpha/\alpha_c = 1 - (r/R)^n , \tag{4a}$$

$$u/u_c = 1 - (r/R)^m . \tag{4b}$$

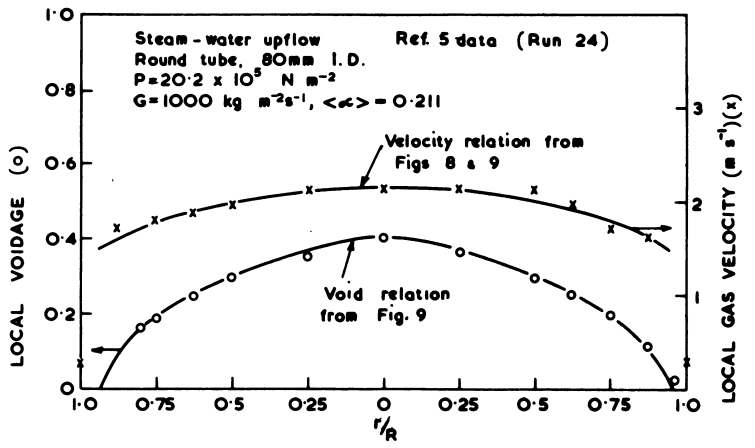

Fig. 7. Void and velocity profiles for bubble flow.

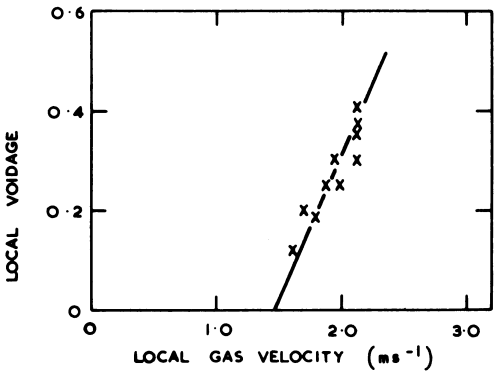

Fig. 8. Voidage velocity relation for data of fig. 7..

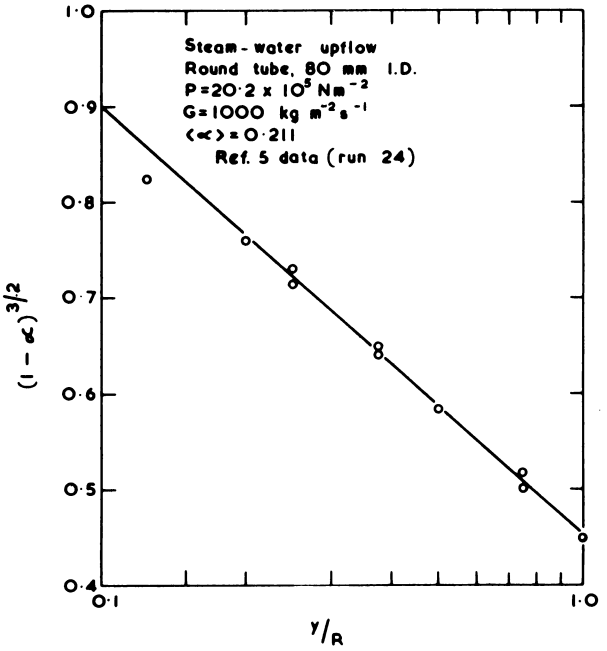

Fig. 9. Voidage deficiency plot of bubble flow data.

Fig. 10 compares the curves of [2] and those of eqs. (2b) and (3b), using suitably chosen coefficients, for one example of data from [13]. Again, although eqs. (4a) and (4b) are suitable for determining macroscopic 'slip' behaviour (as demonstrated in [2]) eqs. (2b) and (3b) give closer agreement with the data.

A different form of empirical curve, based on an extension of the single phase velocity deficiency equation, has been used by the Harwell [14, 15] and the C.I.S.E. [16] groups to fit their velocity profiles. An equation of the form

$$u_g - u_{gc} = \frac{\sqrt{\tau_w/\rho_g}}{k'} \ln \frac{y}{R} \qquad (5)$$

is assumed, with k' being a constant (for a given profile), in analogy with single phase flow behaviour.

This equation does describe data quite well. The velocity data of fig. 10 are plotted on a velocity deficiency plot in fig. 13 with the curve obtained from eqs. (2b) and (3b). The curve is very close to the

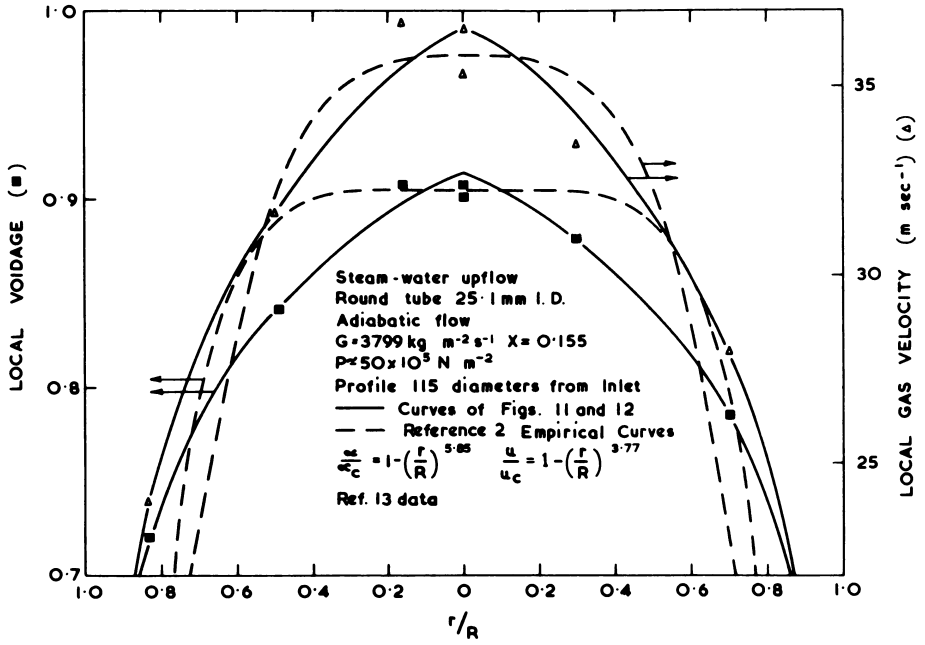

Fig. 10. Comparison of dispersed flow data, voidage deficiency equation and empirical curves.

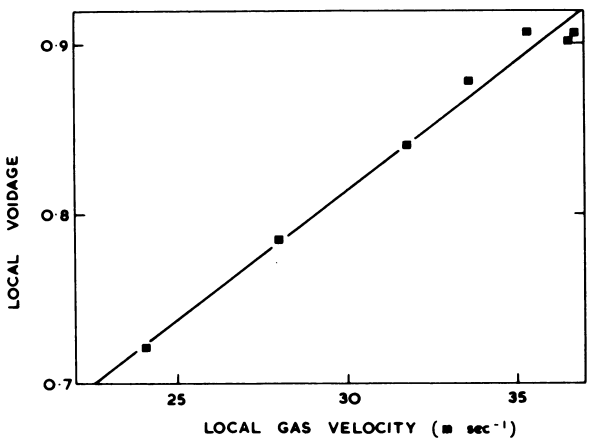

Fig. 11. Voidage-velocity relation for data of fig. 10.

form of eq. (5). The agreement is not surprising, since eqs. (2b) and (3b) combine to form

$$\left(u_g + \frac{d}{c}\right)\left(\frac{\alpha}{\alpha_c}\right)^{1/2} - \left(u_{gc} + \frac{d}{c}\right) = \frac{\sqrt{\tau_w/\rho_g}}{\frac{2}{3}k\sqrt{\alpha_c}} \ln\frac{y}{R},$$

which, for data with flat core profiles, $[(\alpha/\alpha_c)^{1/2} \sim 1]$, approximates the form of eq. (5), with $k' = \frac{2}{3}k\sqrt{\alpha_c} \simeq 0.27$ for high core voidage (assuming the single phase value of k, 0.4). In addition, k' should decrease with decreasing α_c, i.e. increasing entrainment. Empirically determined values of k' [14, 15 and 16] are in agreement with these expectations.

6.2. *Behaviour at the heat transfer crisis*

Figs. 14 and 15 show the influence of heat transfer on a set of void profile data from [13]. From adiabatic flow up to an applied power of 65 kW there is, apart from an increase in voidage, no change in the curves, whereas at 67 kW there is a flattening of the profile and an increase of scatter in the data.

An interpretation of this consistent with the voidage deficiency plot of the data is that the liquid film thickness has remained approximately constant up to the crisis condition, where it has, at least locally, decreased. The shear stress, and hence the slopes of the lines of fig. 15, are determined by the film thickness, i.e. the slopes are constant until the crisis, when the slope becomes flatter. The increased scatter may be associated with a non-uniform film around the periphery.

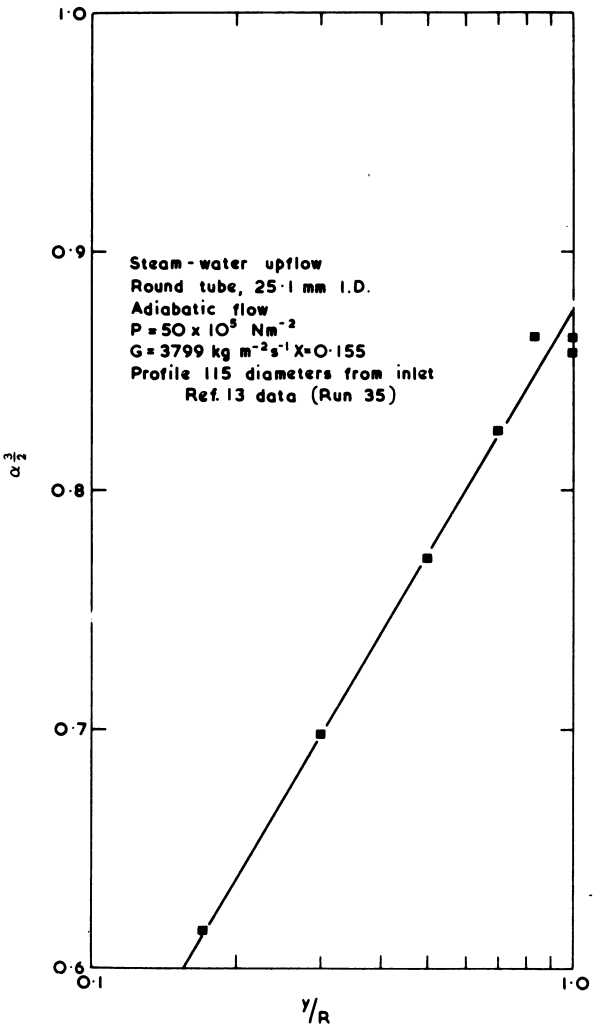

Fig. 12. Voidage deficiency plot of dispersed annular flow data.

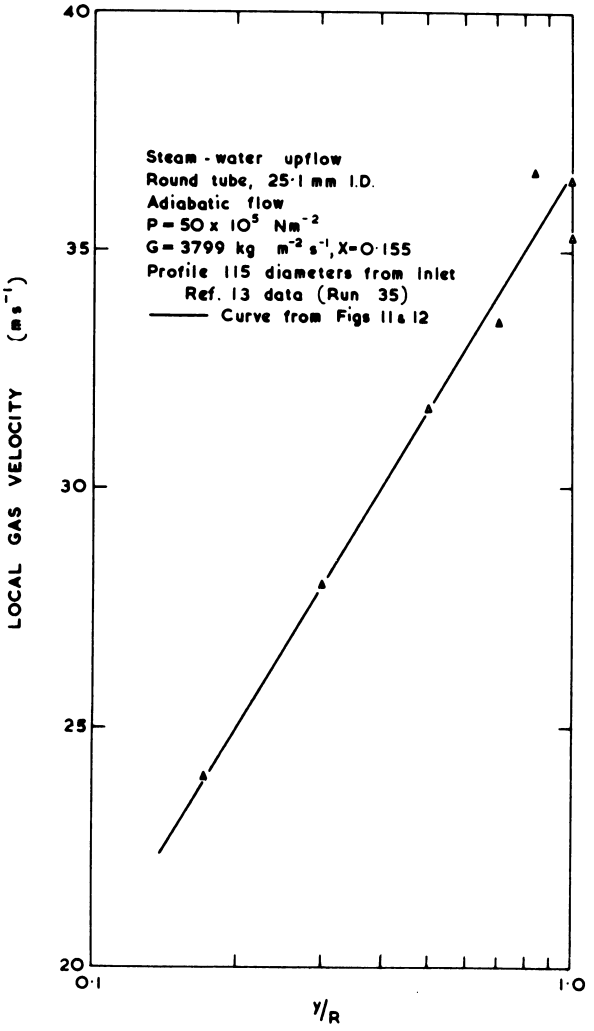

Fig. 13. Velocity deficiency plot of dispersed annular flow data.

Associated pressure drop data for the four profiles do not, however, show a decrease of the pressure gradient at the crisis onset as might be expected from the above argument, (although such behaviour is quite common, see [17]). This is probably because the gradient given is the average over a large distance, and will not be affected by a local exit reduction in the gradient. This is substantiated by a consideration of the mixing length constant determined from the pressure drop data, the slopes of the lines of fig. 15, and the gradient of the associated local voidage – local gas velocity plots. The value of k for the three pre-crisis is 0.28, but this jumps to 0.52 for the crisis profile. The latter value might be explained by the use of the average pressure gradient over the section rather than an exit gradient of lower value.

6.3. *Developing core profiles*

Developing two-component dispersed annular flow profiles from [18] are analysed in figs. 16 and 17 *.

* See footnote on page 58.

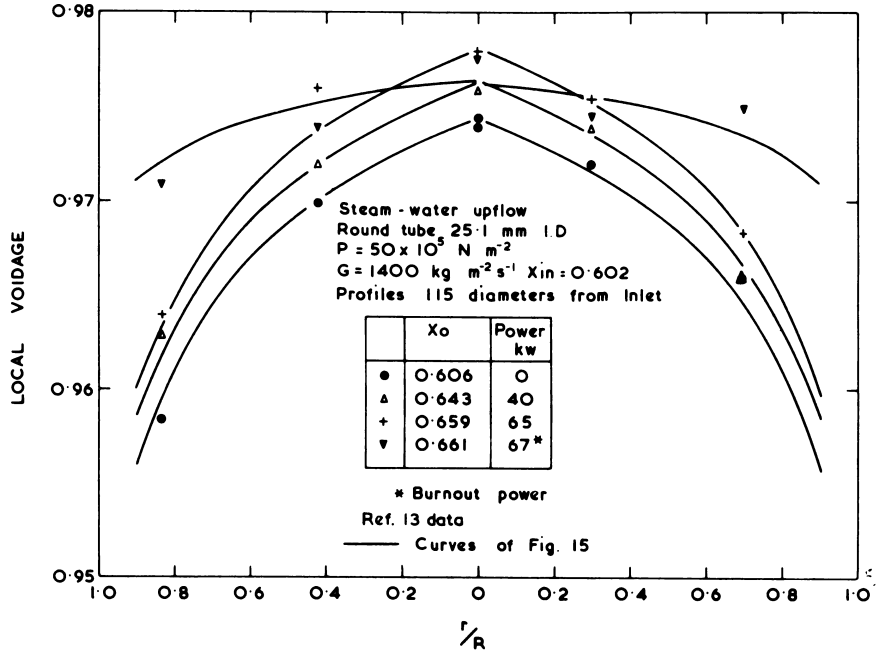

Fig. 14. Effect of heat transfer on dispersed annular flow.

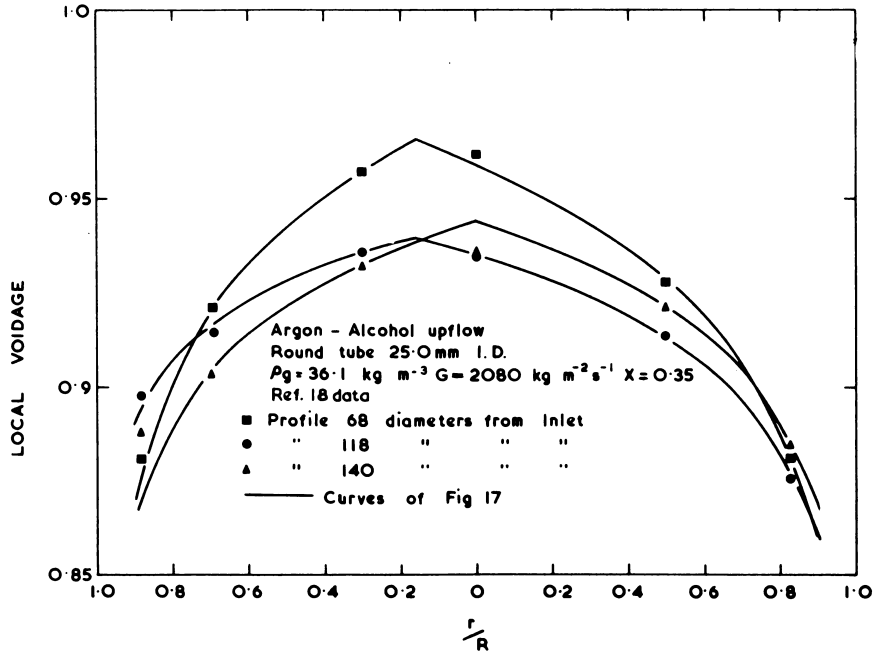

Fig. 16. Developing dispersed annular flow profiles.

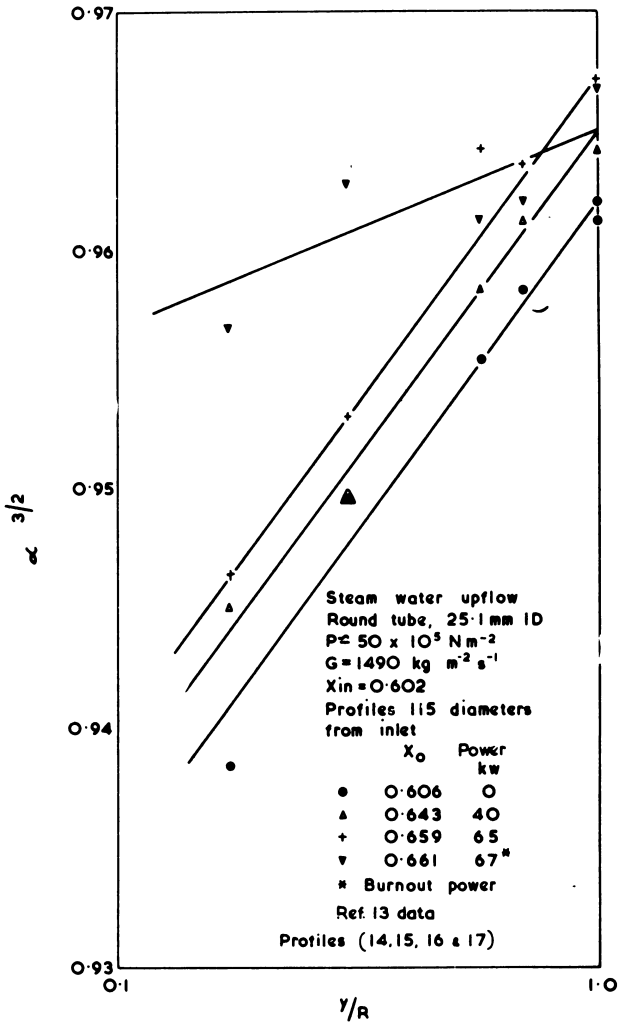

Fig. 15. Voidage deficiency plot of diabatic steam–water dispersed annular flow.

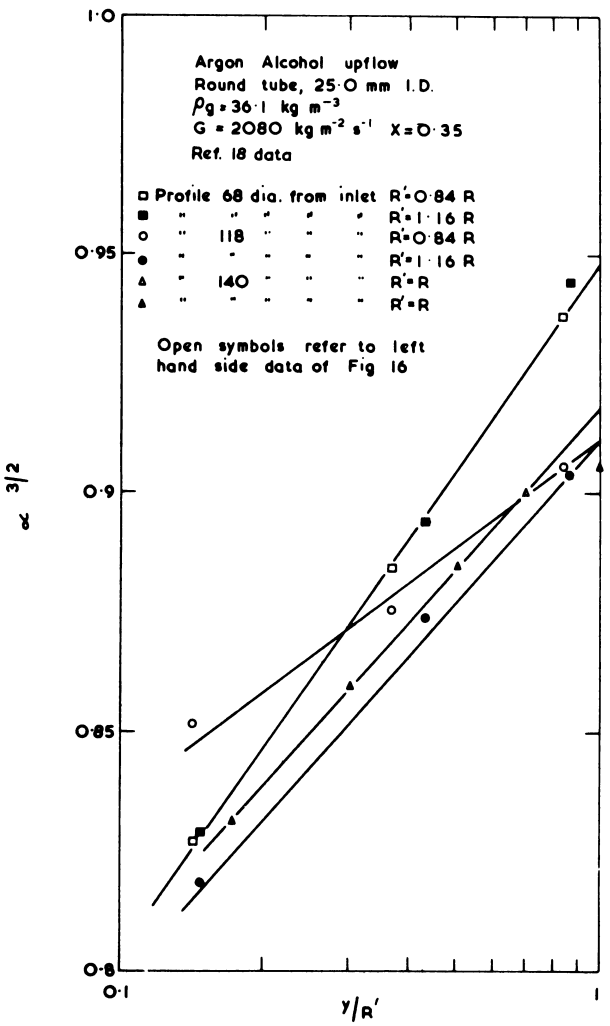

Fig. 17. Voidage deficiency plot of developing dispersed annular flow.

The development can be traced as follows:

The profile at 68 diameters from the mixer is asymmetric. The separate half-profiles, however, are similar; identical voidages occur for each half-profile at corresponding proportional distances from the wall. The wall to maximum voidage distance has replaced the duct radius in the voidage deficiency plot (fig. 17) with the result that both sides of the profile are described by the one line.

At a further 50 diameters downstream the profile remains asymmetric and the half-profiles have lost any semblance of similarity. Separate lines are necessary in the voidage deficiency plot to describe

* The fig. 16 data at r/R = 0.88 are shown on the other side of the duct centre in [18]. This is contrary to the usual C.I.S.E. approach of incrementing radial measurement positions on alternating sides of the centre, and produces unrealistic 'kinks' in the figures in [18]. It is therefore assumed that the positioning should be as shown in fig. 16. The plots of fig. 17 indicate that a surprising degree of coincidence would have to be admitted if this assumption is incorrect.

each side of the profile. The right half-profile appears more fully developed than the left; in fig. 17, the slope of the line through the points corresponding to the right half-profile is the same as the slope for a profile further downstream again.

This last profile (at 140 diameters from the mixer) is completely symmetric. The lower gradient of the voidage deficiency plot of this profile compared with the slope for the profile at 68 diameters from the inlet indicates (theoretically) a lower wall shear stress. This is consistent with shear stress data given in [18], where the variation of shear stress with downstream position was also examined. Association of the lower stress with a thinner wall film and hence higher entrainment would explain the core voidage reduction with increasing distance from the inlet, apparent in fig. 17.

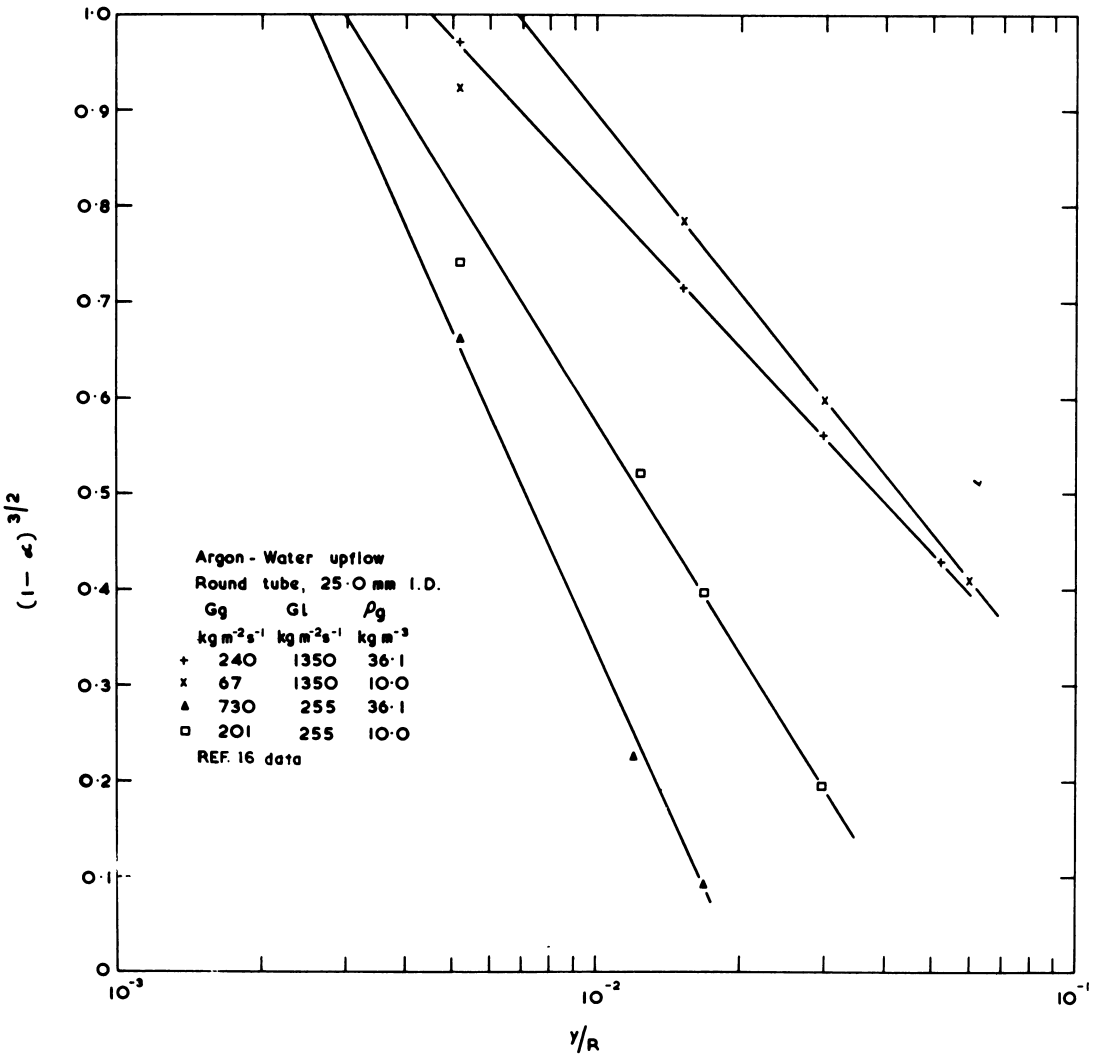

Fig. 18. Voidage deficiency plot covering film region of dispersed annular flow.

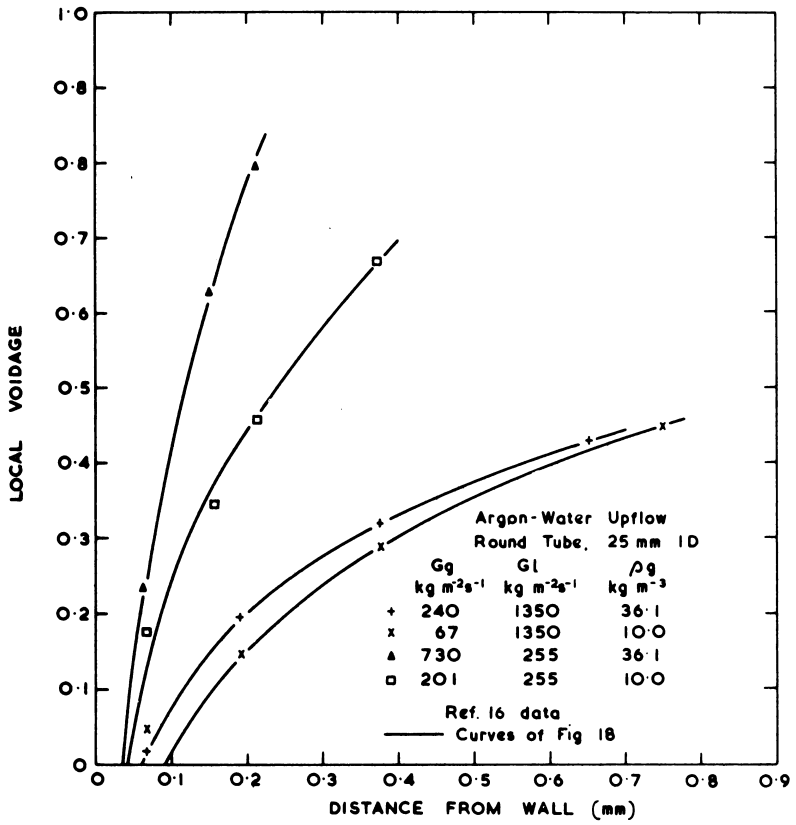

Fig. 19. Void profiles for film region of dispersed annular flow.

7. The voidage deficiency equation for the film region of dispersed annular flow

7.1. *Bubble flow in the film region*

Alia et al. [16], describe the film region of dispersed annular flow as a continuous liquid region with a discontinuous gas region. If this is correct, the film void profile should conform to the voidage deficiency equation for bubble flow. This is the case; data from [16] are shown in fig. 18 as bubble voidage deficiency plots and in fig. 19 as more conventional voidage profiles.

7.2. *Film thickness evaluation*

Film voidage is described by an equation of the form of eq. (3a), and core voidage by eq. (3b). The position where the two equations intercept is taken as the core-film interface. Fig. 20 shows data plotted as $\alpha^{3/2}$ against $\ln(y/R)$. Straight lines describe the core data well, but not the film data. The curves describing the film data in fig. 20 have been transposed from fig. 18. Fig. 20 incidentally demonstrates a fundamental difference, also apparent with other data, that for given components, the core void profiles are determined only by the overall liquid volume flow fraction, but this is not so for the film profile.

Except for a transition region, the core-film interface position can be readily determined from plots such as those in fig. 20. For the data of figs. 18 to 20, film thicknesses f are given in table 1. Also shown are the values of film thicknesses S, determined from electrical conductivity measurements (that is, the film thickness if no gas is present), and, for comparative purposes, the net liquid thickness calculated by multiplying f by the average film liquid volume fraction (obtained from integrating the voidage deficiency equations over the film region. The last

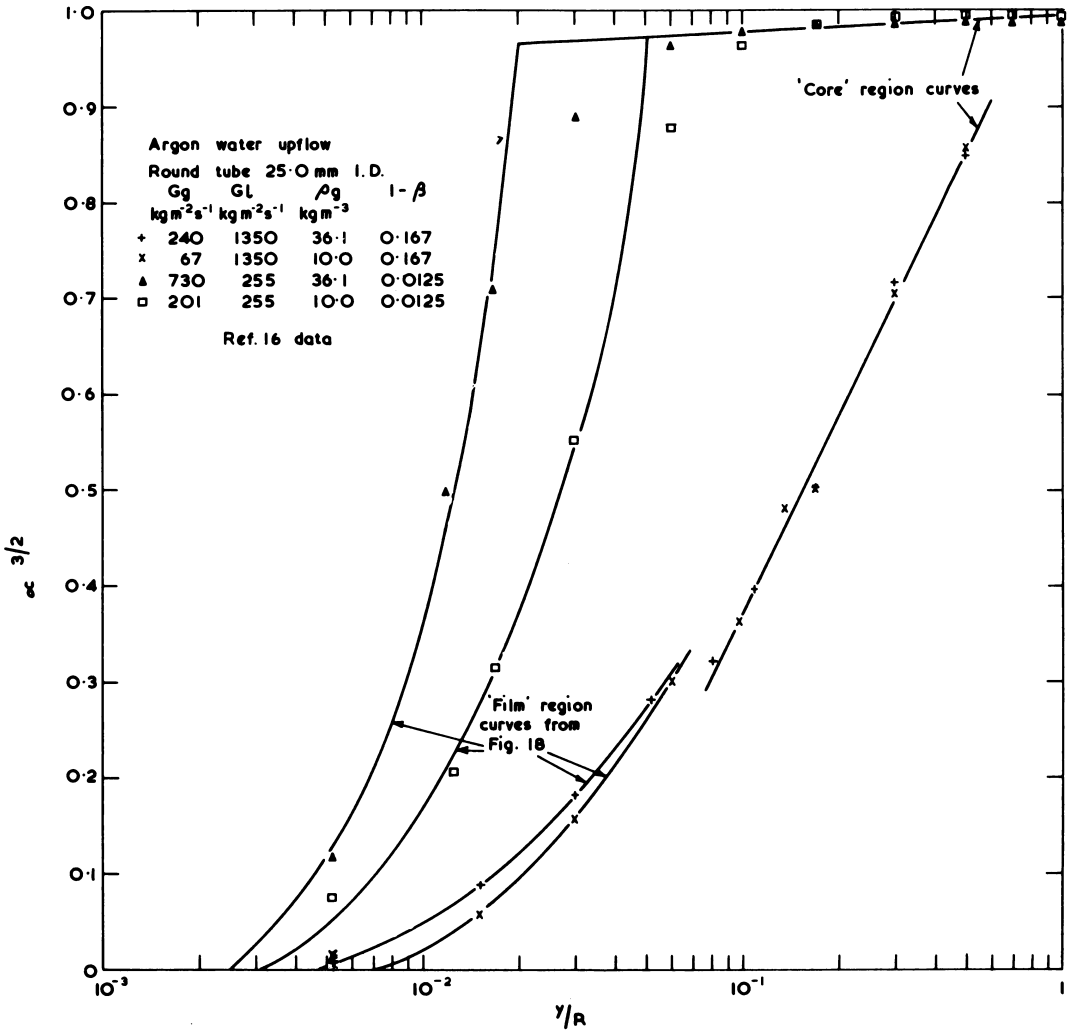

Fig. 20. Influence of volumetric flow fraction in the core and film regions. Determination of film thickness.

Table 1
Comparison of measured film thickness and film thickness determined from void profiles, ref. [16] data.

Gas flow [kg m^{-2} s^{-1}]	Liquid flow [kg m^{-2} s^{-1}]	Gas density [kg m^{-2}]	Film thickness f [mm]	Electrically measured film S [mm]	Calculated liquid thickness $f\langle 1-\alpha\rangle_f$ [mm]	$\frac{S - f\langle 1-\alpha\rangle_f}{S}$ [%]
240	1350	36.1	0.83	0.470	0.57	−21
67	1350	10	0.83	1.40	0.57	60
730	255	36.1	0.25	0.175	0.14	20
201	255	10	0.635	0.24	0.28	−17

column gives the percentage difference between the calculated and measured liquid thicknesses.

The numbers in table 1 are only rough estimates; the values of S were scaled from figures in [16] and are therefore likely to be in error, and the value of f clearly is subject to errors from (at least) neglect of the transition region obvious from data in fig. 20. Nevertheless, the table indicates satisfactory agreement between measured and calculated liquid thickness, in three of the four cases considered, the other case showing a marked and inexplicable discrepancy.

The most conservative conclusion that can be drawn is that although the void profile for dispersed annular flow can be described by separate equations, one for the core and one for the wall region, the interpretation given above concerning the film thickness is generally reasonable but may be grossly incorrect. This, of course, is not the only possibility; for instance, the factor of 3 difference between the measured 'electric' film thickness S for data denoted by X and + in fig. 20 can (perhaps) be questioned considering the obvious closeness of the void profiles shown in fig. 20

8. Conclusions

By assuming that turbulence is associated only with the continuous component of a two-phase mixture, two-phase Reynolds shear stress expressions can be derived from first principles.

Flow structure equations obtained using the Prandtl mixing length concept satisfactorily describe the flow structure of bubble flow and of droplet flow. These equations are helpful in interpreting flow development behaviour, heat transfer effects, and film structure in annular flow.

Acknowledgements

The author wishes to acknowledge the support and encouragement of Dr. K.R. Lawther (Head of Heat Transfer Section) under whose supervision the work has been carried out, and also valuable discussions with Professor J.J. Thompson (Nuclear Engineering School, University of N.S.W.) in relation to the statistical nature of two-phase flow.

Notation

a, b, c = coefficients,
c', c'' = constants of integration,
C_n, d = coefficients,
f = film thickness,
G = mass velocity,
I = inertial force per unit volume,
j = $u_g\alpha + u_l(1-\alpha)$,
k = mixing length constant,
m = exponent,
n = exponent,
P = pressure,
Q = volume flow rate,
$\mathbf{r}$ = position vector,
r = radial position,
S = electric film thickness,
R = radius of round tube,
R' = wall-voidage maximum (or minimum) distance,
$\mathbf{U}$ = velocity vector,
U, V, W = components of $\mathbf{U}$,
u^* = $\sqrt{\tau_w/\rho}$,
u, v, w = statistical averages of U, V and W,
W = power,
X = mass quality $G_g/(G_l + G_g) = G_g/G$,
y = distance from wall,
α = voidage, = $\overline{\delta}$,
β = volumetric flow ratio, $Q_g/(Q_g + Q_l)$,
δ { = 1 at point in gas region, = 0 at point in liquid region,
ρ = density,
τ = shear stress

Subscripts
c = value at duct centre,
f = film region,
g = value for gas phase,
in = inlet value,
l = value for liquid phase,
out = outlet value,
w = value at duct wall,
x, y, z = components values in rectilinear co-ordinates (z-co-ordinate = axial direction).

Superscripts
$'$ = fluctuating component of quantity about mean.

Operators

∇ = 'nabla' = $i\frac{\partial}{\partial x} + j\frac{\partial}{\partial y} + k\frac{\partial}{\partial z}$,

$\frac{\partial}{\partial t}$ = partial derivative with respect to time,

$\frac{D}{Dt}$ = substantial derivative, = $\frac{\partial}{\partial t} + \mathbf{U}\cdot\nabla$,

$\langle\ \rangle$ = average over cross-section,

$-$ = ensemble average.

Appendix

Derivation of voidage deficiency equations

a. Bubble flow

From eq. (1a)

$$\tau = \rho_l(1-\alpha)\,\overline{U_l'V_l'}\,.$$

Following single phase Prandtl mixing length theory assumptions

$$\tau \simeq \tau_w\,,$$

$$\overline{U_l'V_l'} = \left(ky\frac{du_l}{dy}\right)^2\,,$$

$$\therefore u_l^* = \sqrt{\tau_w/\rho_g} = (1-\alpha)^{1/2}ky\frac{du_l}{dy}\,.$$

But, from eq. (2a), $du_l = -a^{-1}\,d(1-\alpha)$, so

$$\frac{au_l^*}{k}\frac{dy}{y} = -(1-\alpha)^{1/2}\,d(1-\alpha)\,.$$

Integrating

$$(au_l^*/\tfrac{2}{3}k)\ln y = -(1-\alpha)^{3/2} + c'\,.$$

The constant of integration may be removed by noting that $y = R$, $\alpha = \alpha_c$, so that

$$(1-\alpha)^{3/2} = (1-\alpha_c)^{3/2} - \left(\frac{au_l^*}{\frac{2}{3}k}\right)\ln(y/R)\,.$$

b. Droplet flow

From eq. (1b)

$$\tau = \rho_g\alpha\,\overline{U_g'V_g'}\,.$$

Assume

$$\tau = \tau_w\,,$$

$$\overline{U_g'V_g'} = \left(ky\frac{du_g}{dy}\right)^2\,,$$

$$\therefore u_g^* = \sqrt{\tau_w/\rho_g} = \alpha^{1/2}ky\frac{du_g}{dy}\,.$$

But, from (2b), $du_g = c^{-1}\,d\alpha$, so that

$$cu_g^*/k = \alpha^{1/2}\,d\alpha\,.$$

Integrating

$$cu_g^*/\tfrac{2}{3}k = \alpha^{3/2} + c''\,.$$

But $\alpha = \alpha_c$ at $y = R$, so

$$\alpha^{3/2} = \alpha_c^{3/2} + \left(\frac{cu_g^*}{\frac{2}{3}k}\right)\ln(y/R)\,.$$

Strictly speaking the assumptions on which the Prandtl mixing length approach are based (shear stress independent of radius and mixing length proportional to the distance from the wall) limit the theory to the region near the wall. However, inaccuracies in the two assumptions tend to cancel each other out, and the resulting deficiency equations apply over most of the core. In fact, as well as being simpler and mathematically more amenable, Prandtl's theory tends to agree with single phase data better than more sophisticated theories involving fewer assumptions.

The assumptions behind Prandtl mixing length theory are most critical at the duct centre. The assumption of a constant shear stress over the duct clearly breaks down at the centre (it should be zero here) with the result that profiles predicted by the theory, as opposed to experimental profiles, do not have a zero gradient at the centre. This is apparent in the figures of this report.

References

[1] A.E. Dukler, M. Wicks and R.G. Cleveland, Frictional pressure drop in two-phase flow: B. An approach through similarity analysis. A.I.Ch. E. 10, 1 (1964) 44.
[2] N. Zuber, F.W. Staub, G. Bijwaard and P.G. Kroeger, Steady State and transient void fraction in two-phase flow systems, GEAP-5417 (Jan. 1967).
[3] M. Petrick, A study of vapour carry under and associated problems, ANL-6581 (July 1962).
[4] L.G. Neal, Local parameters co-current mercury–nitrogen flow, ANL-6625 (Jan. 1963).
[5] D. Malnes, Slip ratios and friction factors in the bubble flow regime in vertical tubes, KR-110 (May 1966).
[6] M. Petrick, Two-phase air–water flow phenomena, ANL-5787 (Mar. 1958).
[7] H. Olsen, Theoretical and experimental investigation of impedance void meters, KR-118 (Aug. 1967).
[8] J.L.L. Baker, Flow regime transitions at elevated pressures in vertical two-phase flow, ANL-7093 (Sept. 1965).
[9] R. Martin, Mesure du taux de vide á haute pression dans un canal chauffant, CEA-R-3781 (Sept. 1969).
[10] B.L. Richardson, Some problems in horizontal two-phase flow, ANL-5949 (Dec, 1959).
[11] F.W. Staub, G. Walmet, Heat transfer and hydraulics; The effect of subcooled voids; Final report, NYO-3679-8 (May 1969).
[12] N. Miller and R.E. Mitchie, Measurement of local voidage in liquid–gas two-phase flow systems using a universal probe, J. Brit. Nucl. Eng. Soc. 9, 2 (April 1970).
[13] N. Adorni, G. Peterlongo, R. Ravetta and F.A. Tacconi, Large scale experiments on heat transfer and hydrodynamics with steam–water mixtures: Phase and velocity distribution measurements in a round vertical tube, CISE-R-91 (Oct. 1964).
[14] L.E. Gill, G.F. Hewitt and J.W. Hitchon, Sampling probe studies of the gas core in annular two-phase flow; Part 1 – The effect of length on phase and velocity distribution; AERE-R-3954 (November 1962).
[15] L.E. Gill, G.F. Hewitt and P.M.C. Lacey, Samping probe studies of the gas core in annular two-phase flow; Part II – Studies of the effect of phase flow rates on phase and velocity distribution, AERE-R-3955 (June 1963),
[16] P. Alia, L. Cravarolo, A. Hassid and E. Pedrocchi, Phase and velocity distribution in two-phase adiabatic annular dispersed flow, CISE-R-109 (December 1966).
[17] S. Bertoletti, J. Lesage, C. Lombardi, G. Peterlongo, M. Silvestri, G. Soldaine and F. Weckermann, Heat transfer and pressure drop with steam–water spray; a critical survey of experiments performed at CISE from November 1, 1959 – January 31, 1961. CISE-R-36 (April 1961).
[18] L. Cravarolo, A. Hassid and E. Pedrocchi, Further investigation on two-phase adiabatic annular dispersed flow: effect of length and of some inlet conditions on flow parameters, CISE-R-93 (September 1964).

NUCLEAR ENGINEERING AND DESIGN 25 (1973) 395–402. © NORTH-HOLLAND PUBLISHING COMPANY

A NOTE ON THE CALCULATION OF TWO-PHASE PRESSURE LOSSES

D.R.H. BEATTIE
AAEC Research Establishment, Private Mail Bag, Sutherland 2232, Australia

Received 26 March 1973

The calculation of axial differences in static pressure for two-phase flow along a pipe is discussed in relation to the evaluation of two-phase friction. Two-phase friction equations derived from mixing length theory are summarised. The equations compare favourably with data covering the following fluid conditions at the wall: bubble flow, wavy gas–liquid interface, flow with very small bubbles, attached wall bubbles, and dry wall.

1. Introduction

Static pressure differences for flow along a pipe usually have three components: friction (discussed here), gravitation, and acceleration. Calculation of the gravitational contribution

$$\int(\rho_\ell(1-\langle\alpha\rangle)+\rho_g\langle\alpha\rangle)\,g\,dh,$$

depends on a voidage correlation. For those flow patterns where gravity contributes significantly to the total pressure difference, satisfactory voidage correlations can be found in ref. [1]. For other cases (annular flows) less satisfactory correlations exist; fortunately gravity plays only a small part here and a calculation using the homogeneous model will suffice.

An exact treatment of the acceleration component has not yet been achieved. The widely accepted application of a void correlation, which involves the never stated assumption that

$$\langle\rho_\ell u_\ell^2(1-\alpha)+\rho_g u_g^2\,\alpha\rangle=\rho_\ell\frac{\langle u_\ell(1-\alpha)\rangle^2}{\langle 1-\alpha\rangle}+\rho_g\frac{\langle u_g\alpha\rangle^2}{\langle\alpha\rangle},$$

is certainly incorrect. On the other hand, there is growing evidence that a homogeneous treatment, as follows:

$$\langle\rho_\ell u_\ell^2(1-\alpha)+\rho_g u_g^2\,\alpha\rangle=\frac{G^2}{\rho_\ell}\left[1+X\left(\frac{\rho_\ell}{\rho_g}-1\right)\right],$$

is fairly reasonable. Thus the difference between the values of this quantity at two points in a pipe is regarded as the acceleration component of the pressure difference between the two points.

In many cases, particularly for high flow rates, the frictional losses are the dominating component. Single-phase frictional pressure gradients can be calculated using a friction factor

$$f=\rho D\,(\mathrm{d}P/\mathrm{d}z)/2G^2,$$

the value of which depends on the surface roughness ratio ϵ/D and a second dimensionless group $R=DG/\mu$, the Reynolds number, as given by Colebrook's equation:

$$1/\sqrt{f}=3.48-4\log\left[2\epsilon/D+9.35/R\sqrt{f}\,\right]. \qquad (1)$$

Analysis has shown that eq. (1) also holds for the two-phase flow situation provided f and R are appropriately defined for the particular type of two-phase flow. The analysis was initiated as a result of a fairly extensive study of two-phase pressure drop data [2, 3]. In this work, a particular method of plotting two-phase friction data resolved these results rather precisely into groups with similar characteristics, suggesting fairly distinct flow regime effects. As a first step towards explaining this, Prandtl's mixing length theory was adapted to the turbulent core of two-phase flow [4]. Separate phase and velocity distribution expressions were obtained for bubble and droplet flow. Comparison with flow structure data showed them to be not unreasonable.

The two-phase mixing length theory has since been extended by applying boundary conditions as set by the flow in the vicinity of the duct wall. It now appears that the different characteristics found in refs. [2, 3] were not due to differences in the flow structure of the turbulent core, but rather to those in the flow close to the wall. Although this work is still in progress, certain useful results have emerged. These results are presented here. A more complete description of this work, including derivations, more extensive comparisons with data, discussions of ranges of applicability, etc. will be published later.

2. Two-phase flow friction losses

2.1. Pipes

Five separate models describing flow near the wall have been considered: (1) bubbly flow; (2) wavy gas–liquid interface; (3) flow with very small bubbles; (4) attached wall bubbles; and (5) dry wall *. For these models, friction factor f, surface roughness ratio ϵ/D, and a dimensionless group R are related by eq. (1) provided f and R are defined as in table 1.

It will be noticed that except for the last case the dimensionless group R is a form of Reynolds number. The group R in the attached wall bubble model is actually $2.4\sqrt{We}$, where We is a two-phase Weber number. (The Weber number is a measure of the relative magnitude of inertia and surface tension forces.) The value 2.4 is an as yet unoptimised empirical coefficient. Also, the development of this model is such that, irrespective of its true value, ϵ must be placed equal to zero for pressure loss calculations for this type of flow.

Since it is a widely used parameter, table 1 also contains expressions for the two-phase multiplier

$$\Phi_{LO}^2 = \frac{dP}{dz} \Big/ \frac{dP}{dz}\Big|_{LO},$$

where the subscript LO indicates a calculation as if the flow was all liquid with the mixture mass velocity. This applies to those flows in which eq. (1) can be approximated by a Blasius type approximation $f \propto R^{-0.2}$. This cannot be done as readily for the attached wall bubble model since here the dimensionless group R lies in a range where the exponent of the Blasius type approximation to eq. (1) is different from that for the 'liquid only' part of the two-phase multiplier expression.

The demarcation of the various flow regimes is an as yet unsolved problem, and, judging from the difficulty in accurately separating the single phase laminar and turbulent regimes, is likely to remain so for some time. As a first estimate of ranges of applicability, each model can be considered to apply to the type of flow in the example column of table 1.

To obtain the frictional component of the pressure difference in cases where the quantities vary axially, the local frictional pressure gradient should be integrated between the points of interest.

2.2. Complex geometries

Following single phase experience, it would appear reasonable to extend the pipe equations to complex geometries through the use of the equivalent hydraulic diameter (4 × flow area ÷ total perimeter) provided flow patterns near separate surfaces are the same. Of special interest to reactor engineers are rod clusters with heated rods in an unheated shroud, where different types of wall flows may be expected. Data analysis to date has, nevertheless, shown that the attached wall void model equations are applicable here if the hydraulic diameter concept is used.

2.3. Piping components

Just as the single phase friction-factor–Reynolds number relation can be extended to the two-phase situation, the single phase loss coefficient (K) – Reynolds number (R) relation applicable to a given component (expansion, contraction, etc.) holds for the two-phase situation if K and R are defined as in table 2. Also shown is the two-phase multiplier ($\Delta P/\Delta P_{LO}$) for conditions where the Reynolds number dependence is an inverse one-fifth relation. Bend losses do not conform to either of the cases summarised in table 2.

* Other flow types include those which are an inversion of those considered, e.g. a dry wall with attached wall droplets can be considered as an inversion of the attached wall bubble model. These flows are regarded as being uncommon, and in any case interchanging gas and liquid quantities in tables 1 and 2 results in appropriate definitions for these flows.

3. Comparison with data

For demonstration only, figs. 1–7 show comparisons between predictions from the recommended equations and one example of data taken from the literature for each of the flow types in tables 1 and 2. The values of ϵ used in figs. 3 and 4 where obtained from single phase data given in ref. [12].

The steam–water data presented in figs. 3–5 were based on analysis of the raw data of refs. [7–9] with the homogeneous model being used for the acceleration component and, in the absence of flow regime information, the Jones void correlation [13] being used for the gravity component calculation. Due to the small contribution of this component, errors involved do not strongly affect the frictional component evaluation. Fluid properties used are those corresponding to saturation conditions at the test section midpoint.

In the case of the diabatic data in figs. 4 and 5, the calculated average frictional pressure gradient between the inlet and outlet is taken to be the local point gradient midway between the two points. It has been shown [2, 3] that such an assumption is reasonable if the variation of the frictional gradient with quality is approximately linear and/or the quality difference between the two points is small.

The data presented in figs. 1, 2 and 7 were based on data already reduced to the frictional pressure gradient (or its equivalent) in refs. [5, 6, 11]. As recommended here, the homogeneous model was used for the acceleration component in ref. [5]; the acceleration component was small and neglected in ref. [6], and the authors of ref. [11] did not state their method of allowing for this component.

4. Discussion and conclusions

Although the agreement between data and the recommended curves is encouraging, the possibility of various errors compensating for each other must be considered. There is, however, some evidence (not necessarily based on data presented here) that the various techniques used are reasonable:

(1) The gravitational component is small or correctly accounted for since flow orientation does not affect the final friction factor plot.

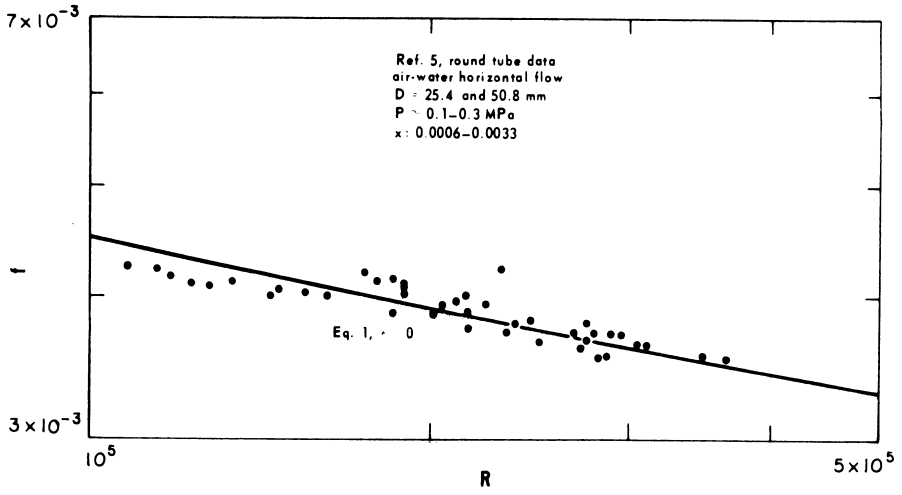

Fig. 1. Comparison of equation for bubble flow near wall with data

$$\left[f = \frac{\rho_\ell D \, dP/dz}{2G^2 \left\{ 1 + X \left(\frac{\rho_\ell}{\rho_g} - 1 \right) \right\}} \, , R = \frac{DG}{\mu_\ell} \, \frac{1 + X \left(\frac{\rho_\ell}{\rho_g} - 1 \right)}{1 + X \left(\frac{(3.5\mu_g + 2\mu_\ell)\rho_\ell}{(\mu_g + \mu_\ell)\rho_g} - 1 \right)} \right].$$

Table 1.
Definitions for two-phase friction calculations for ducts and channels.

Sublayer structure	Example	f	R	Φ^2_{LO}
Bubble	Bubble flow	$\dfrac{\rho_\ell D\, dP/dz}{2G^2\left\{1+X\left(\dfrac{\rho_\ell}{\rho_g}-1\right)\right\}}$	$\dfrac{DG}{\mu_\ell}\dfrac{1+X\left(\dfrac{\rho_\ell}{\rho_g}-1\right)}{1+X\left(\dfrac{(3.5\mu_g+2\mu_\ell)\rho_\ell}{(\mu_g+\mu_\ell)\rho_g}-1\right)}$	$\left\{1+X\left(\dfrac{\rho_\ell}{\rho_g}-1\right)\right\}^{0.8}\left\{1+X\left(\dfrac{(3.5\mu_g+2\mu_\ell)\rho_\ell}{(\mu_g+\mu_\ell)\rho_g}-1\right)\right\}^{0.2}$
Wavy gas/liquid interface	Annular flow with no entrainment	as above	$\dfrac{DG}{\mu_\ell}\dfrac{1+X\left(\dfrac{\rho_\ell}{\rho_g}-1\right)}{1+X\left(\dfrac{\rho_\ell\mu_g}{\rho_g\mu_\ell}-1\right)}$	$\left\{1+X\left(\dfrac{\rho_\ell}{\rho_g}-1\right)\right\}^{0.8}\left\{1+X\left(\dfrac{\rho_\ell\mu_g}{\rho_g\mu_\ell}-1\right)\right\}^{0.2}$
Very small bubbles	Flow following obstruction (bubble or annular flow)	as above	$\dfrac{DG}{\mu_\ell}\dfrac{1+X\left(\dfrac{\rho_\ell}{\rho_g}-1\right)}{1+X\left(3.5\dfrac{\rho_\ell}{\rho_g}-1\right)}$	$\left\{1+X\left(\dfrac{\rho_\ell}{\rho_g}-1\right)\right\}^{0.8}\left\{1+X\left(\dfrac{3.5\rho_\ell}{\rho_g}-1\right)\right\}^{0.2}$
Dry wall	Post 'burnout' flow	$\dfrac{\rho_\ell^2 D\, dP/dz}{2\rho_g G^2\left\{1+X\left(\dfrac{\rho_\ell}{\rho_g}-1\right)\right\}^2}$	$\dfrac{DG\rho_g}{\mu_g\rho_\ell}\left\{1+X\left(\dfrac{\rho_\ell}{\rho_g}-1\right)\right\}$	$\left(\dfrac{\mu_g}{\mu_\ell}\right)^{0.2}\left(\dfrac{\rho_g}{\rho_\ell}\right)^{0.8}\left\{1+X\left(\dfrac{\rho_\ell}{\rho_g}-1\right)\right\}^{1.8}$
Flow with attached wall bubbles	Boiling flow	$\dfrac{2\rho_\ell D\, dP/dz}{G^2\left\{1+X\left(\dfrac{\rho_\ell}{\rho_g}-1\right)\right\}}$	$2.4\left[\dfrac{G^2D\left\{1+X\left(\dfrac{\rho_\ell}{\rho_g}-1\right)\right\}}{\rho_\ell\sigma}\right]^{\frac{1}{2}}$	complex

Table 2.
Definitions for two-phase loss calculations for obstruction.

Influence of obstruction on flow	Example	K	R	Φ^2_{LO}
Flow is separated at obstruction	Orifice	$\dfrac{\rho_\ell \Delta P}{G^2\left\{1 + X\left(\dfrac{\rho_\ell}{\rho_g} - 1\right)\right\}}$	$\dfrac{DG}{\mu_\ell}\dfrac{1 + X\left(\dfrac{\rho_\ell}{\rho_g} - 1\right)}{1 + X\left(\dfrac{\rho_\ell \mu_g}{\rho_g \mu_\ell} - 1\right)}$	$\left\{1 + X\left(\dfrac{\rho_\ell}{\rho_g} - 1\right)\right\}^{0.8}\left\{1 + X\left(\dfrac{\rho_\ell \mu_g}{\rho_g \mu_\ell} - 1\right)\right\}^{0.2}$
Flow is churn-turbulent at obstruction	Rod spacers, expansion, etc.	As above	$\dfrac{DG}{\mu_\ell}\dfrac{1 + X\left(\dfrac{\rho_\ell}{\rho_g} - 1\right)}{1 + X\left(3.5\dfrac{\rho_\ell}{\rho_g} - 1\right)}$	$\left\{1 + \left(X\dfrac{\rho_\ell}{\rho_g} - 1\right)\right\}^{0.8}\left\{1 + X\left(\dfrac{3.5\rho_\ell}{\rho_g} - 1\right)\right\}^{0.2}$

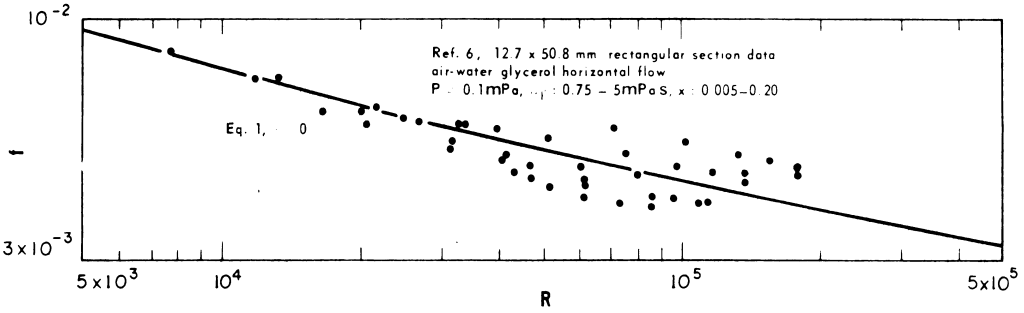

Fig. 2. Comparison of equation for wavy interface near wall with data

$$\left(f = \frac{\rho_\ell D\, dP/dz}{2G^2\left\{1 + X\left(\frac{\rho_\ell}{\rho_g} - 1\right)\right\}},\ R = \frac{DG}{\mu_\ell}\ \frac{1 + X\left(\frac{\rho_\ell}{\rho_g} - 1\right)}{1 + X\left(\frac{\rho_\ell \mu_g}{\rho_g \mu_\ell} - 1\right)}\right).$$

(2) Adiabatic data exist which, along with diabatic data such as those presented in figs. 4 and 5, are consistent with the dry wall and attached wall void models. The homogeneous evaluation of the acceleration component is thus reasonable when the acceleration is due to a change of phase.

(3) Loss coefficient data for sudden expansions (where the acceleration component must be added to the measured pressure difference to give the loss component) and for sudden contractions (where the acceleration component is subtracted) are consistent both with each other and the model. The homogeneous evaluation of the acceleration component is thus reasonable when the acceleration is due to a sudden change of flow area.

On the other hand, it must be stated that, despite the number of alternative friction models presented here, there are many data in the literature which are inconsistent with all of them.

It is recommended that static pressure differences

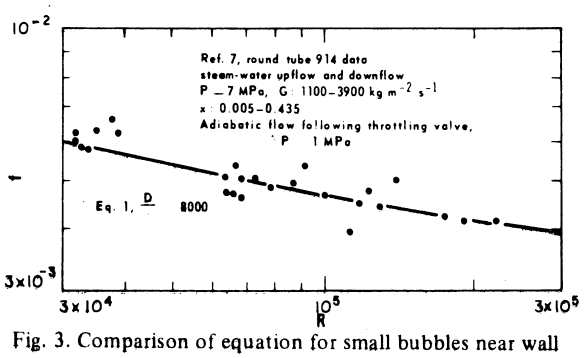

Fig. 3. Comparison of equation for small bubbles near wall with data

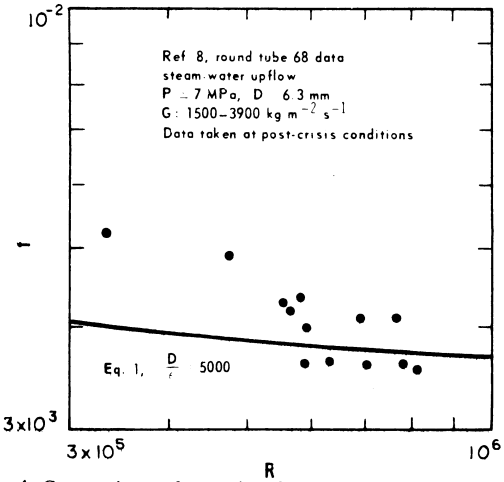

Fig. 4. Comparison of equation for dry wall with data

$$\left(f = \frac{\rho_\ell D\, dP/d_z}{2G^2\left\{1 + X\left(\frac{\rho_\ell}{\rho_g} - 1\right)\right\}},\ R = \frac{DG}{\mu_\ell}\ \frac{1 + X\left(\frac{\rho_\ell}{\rho_g} - 1\right)}{1 + X\left(3.5\frac{\rho_\ell}{\rho_g} - 1\right)}\right).$$

$$\left(f = \frac{\rho_\ell^2\, D\, dP/dz}{2\rho_g G^2\left\{1 + X\left(\frac{\rho_\ell}{\rho_g} - 1\right)\right\}},\ R = \frac{DG\,\rho_\ell}{\mu_g\,\rho_g}\left\{1 + X\left(\frac{\rho_\ell}{\rho_g} - 1\right)\right\}\right)$$

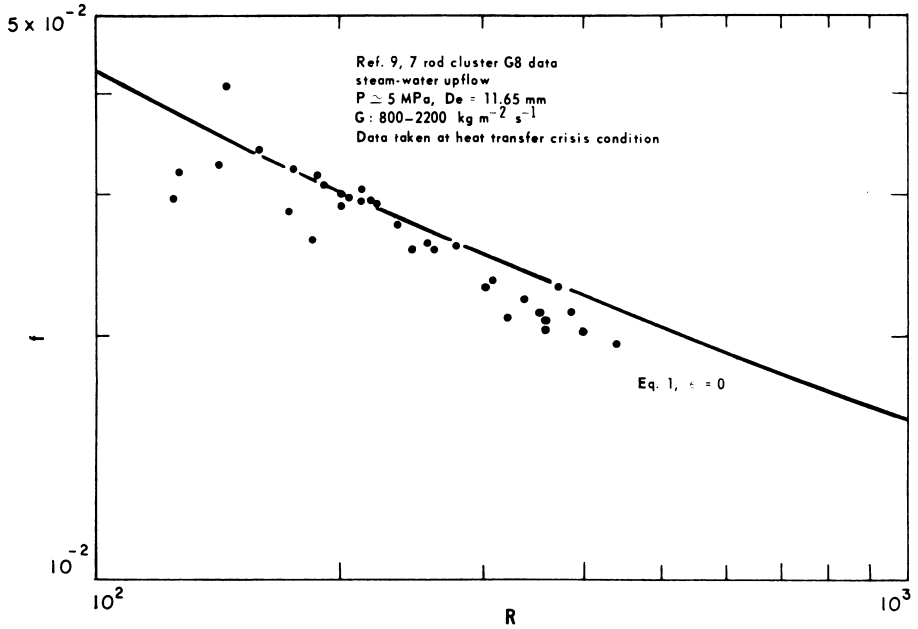

Fig. 5. Comparison of equation for attached wall voids with data

$$\left(f = \frac{2\,\rho_{\ell} D\,\mathrm{d}P/\mathrm{d}z}{G^2\left\{1 + X\left(\frac{\rho_{\ell}}{\rho_g} - 1\right)\right\}}\right.$$

$$\left. R = 2.4\left[\frac{G^2 D\left\{1 + X\left(\frac{\rho_{\ell}}{\rho_g} - 1\right)\right\}}{\rho_{\ell}\sigma}\right]^{\frac{1}{2}}\right)$$

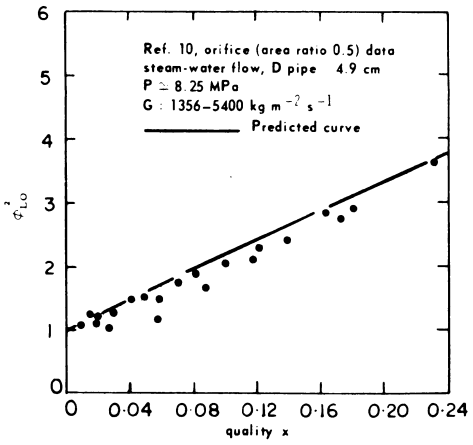

Fig. 6. Comparison of equation for separated flow past an obstruction with data.

for two-phase flow be evaluated by adding the separate components (friction, acceleration and gravitation) as calculated by methods given in this paper.

Acknowledgements

The author would like to thank Dr. K.R. Lawther (Head, Heat Transfer Section), Mr. G.W.K. Ford (Chief, Engineering Research Division) and Professor J.J. Thompson (Head, School of Nuclear Engineering, University of New South Wales) for helpful discussions and encouragement concerning this work.

Nomenclature

D	= hydraulic diameter
f	= friction factor
G	= mass flux
h	= height
K	= loss coefficient
R	= dimensionless group (tables 1 and 2)
u	= local velocity
We	= Weber number
X	= mass quality $Gg/(Gg + Ge)$
α	= local voidage

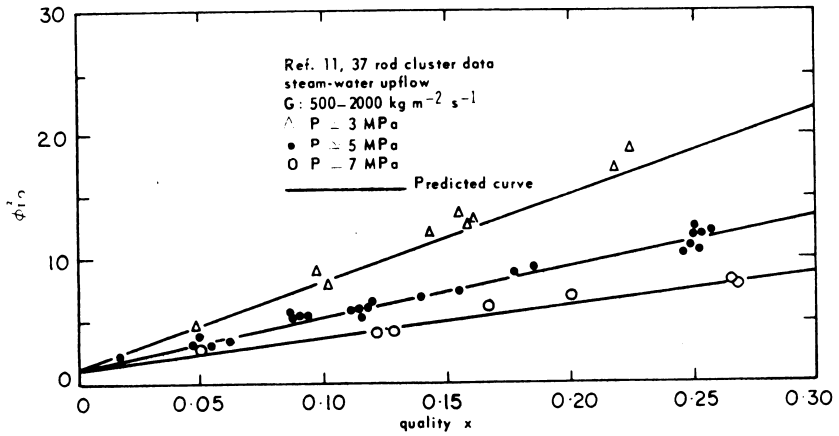

Fig. 7. Comparison of equation for churn-turbulent flow past an obstruction with data. Φ^2_{LO} refers to outlet region, including spacer, cables, and expansion.

ϵ = surface roughness
μ = viscosity
ρ = density
σ = surface tension
$\Phi^2_{LO} = \dfrac{dP/dz}{dP/dz|_{LO}}$; $\Delta P/\Delta P_{LO}$ two-phase multiplier
dP/dz = frictional pressure gradient
ΔP = pressure loss at piping component
$\langle \cdots \rangle$ = quantity is averaged over flow cross section

Subscripts
ℓ = liquid
g = gas
LO = calculated as if flow was all liquid with mixture mass flux.

References

[1] N. Zuber et al., Steady state and transient void fraction in two-phase flow systems, GEAP 5417, Jan. (1967).
[2] D.R.H. Beattie, Two-phase pressure losses – flow regime effects and associated phenomena, Australian Atomic Energy Commission Report, AAEC/TM589, May (1971).
[3] D.R.H. Beattie, A study of two-phase flow pressure drop correlations, M.Eng.Sc. Thesis, School of Nuclear Engineering, University of New South Wales, 1971.
[4] D.R.H. Beattie, Two-phase flow structure and mixing length theory, Nucl. Eng. Des. 21, 1, 46 (1972).
[5] E.M. Kopalinsky, A study of bubbly two-phase flow, Ph. D. Thesis, School of Mechanical Engineering, University of New South Wales, 1971.
[6] J.F. Fohrman, The effect of the liquid viscosity in two-phase, two component flow, Argonne National Laboratory Report, ANL-6256, Nov. (1960).
[7] G.P. Era et al., Heat transfer crisis and pressure drop for steam–water mixture at 70 kg/cm^2 flowing upwards and downwards in circular conduits, CISE-R-185, Jan. (1967).
[8] CISE, A research program in two-phase flow, Jan. (1963).
[9] N. Adorni et al., Heat transfer crises with steam–water mixtures in complex geometries: Experimental data in annuli and clusters CISE-R-123, Dec. (1964).
[10] D.E. Fitzsimmons, Two-phase pressure drop in piping components, HW-80970 rev. 1, Mar. (1964).
[11] O. Nylund et al., Hydrodynamic and heat transfer measurements on a fullscale simulated 36-rod Marviken fuel element with non-uniform radial heat flux distribution, FRIGG 3 (1969).
[12] G.P. Gaspari et al., Pressure drops in steam–water mixtures, CISE-R-83, Jan. (1964).
[13] A.B. Jones et al., Hydrodynamic stability of a boiling channel, KAPL-2208 (1962).

International Conference on
Drag Reduction
4th-6th September, 1974

PAPER D3

DRAG REDUCTION PHENOMENA IN GAS-LIQUID SYSTEMS

D.R.H. Beattie (B.Sc., B.E., M.Eng.Sc.),
Australian Atomic Energy Commission, Australia.

Summary

An extensive survey of two-phase adiabatic gas-liquid pressure drop data has revealed some anomalously low pressure drop results. As in single phase flow, the lower drag is associated with departure of the velocity distribution from the 'universal' velocity profile. In many cases, velocity profile and/or pressure loss data are consistent with Karman's buffer region velocity equation extrapolated to cover the whole core. A friction factor expression derived from this equation is in good agreement with data except in entrance regions where data are up to 15% above the prediction. A discussion is given of (a) the connection between two-phase reduction and hydrodynamic dryout, and (b) the effect of drag reduction on the average void fraction. Evidence is given of drag reduction associated with boiling and with two-phase flows over obstructions.

A separate two-phase drag reduction phenomenon which does not occur in single phase flow is caused by changes in sublayer structure. Such changes necessitate redefinition of fluid physical property terms in the Reynolds number and friction factor. It is shown that single phase relations then apply for the various two-phase flow conditions.

Held at Churchill College, Cambridge, England

Organised and sponsored by BHRA Fluid Engineering, Cranfield, Bedford, England.

Copyright BHRA Fluid Engineering.

NOMENCLATURE

Co	Zuber's distribution parameter
D	diameter
f	friction factor
G	mass flux
j	local mixture velocity
j^+	non-dimensional local mixture velocity
K	loss coefficient
P	pressure
Q	volume flowrate
R	dimensionless flow parameter defined in text
We	Weber number
X	quality
y	wall distance
y^+	non-dimensional wall distance
z	axial distance
α	local void fraction
β	average volume flow ratio $Q_g/(Q_g + Q_\ell)$
ε	surface roughness height
μ	viscosity
ρ	density
δ	surface tension

Subscripts

a	associated with a rigid surfaced bubble sublayer
b	associated with a flexible bubble sublayer
c	associated with a sublayer containing a wavy gas-liquid interface
d	associated with flows with attached wall voids
e	associated with dry wall flows
g	gas quantity
ℓ	liquid quantity

Operator

<--->	quantity is averaged over the flow cross section

1. INTRODUCTION

The frictional loss in flowing liquid systems may be reduced by introducing of a small amount of a suitable additive to the liquid. The effect is achieved either by lowering the viscosity in the laminar sublayer, or by changing the distribution of the Reynold's stresses in the turbulent region of the flow.

Similar effects occur in flowing gas-liquid systems without the aid of additives. Under certain conditions the structure of the flow is altered, resulting in changes to the effective sublayer viscosity and/or the turbulent eddy diffusivity. Furthermore, because of the additional variables in two-phase flows, two-phase drag reduction has a more pronounced effect on cross sectional averaged quantities (such as momentum flux) than in single phase flows.

Since two-phase drag reduction occurs without additives and the consequences are more far-reaching than for single phase flows, it is important that suitable design equations should be available. This paper concentrates on those types of adiabatic two-phase drag reduction of interest to the reactor engineer. Some equations describing the hydrodynamics of such flows are presented, together with a method of establishing one set of boundary conditions for such flows. Conditions under which two-phase drag reduction occurs have not been fully established, nor have equations describing diabatic two-phase drag reduction, or two-phase drag reduction under low pressure conditions. For simplicity, discussion will be limited mainly to round tube geometries.

2. TWO-PHASE PRESSURE LOSSES

2.1 Flows with Single-Phase Like Turbulence

Recently it has been shown (Ref. 1) that much of the available two-phase pressure loss data can be correlated to within a few per cent by modified single phase equations. The method uses Colebrook's friction-factor equation

$$1/\sqrt{f} = 3.48 - 4 \log \left(2\varepsilon/D + 9.35/(R\sqrt{f})\right) \qquad (1)$$

where f and R are the two-phase friction factor and a non-dimensional flow parameter, generally a form of Reynold's number. These are defined according to the nature of the sublayer:

(a) for dry wall two-phase flows

$$f_a = D \frac{dp/dz}{2\rho_g \langle j \rangle^2} \quad , \quad R_a = \frac{D\rho_g \langle j \rangle}{\mu_g}$$

(b) for flows with rigid-surfaced bubbles in the sublayer

$$f_b = D \frac{dp/dz}{2\rho \langle j \rangle^2} \quad , \quad R_b = \frac{D\rho \langle j \rangle}{\mu_\ell (1 + 2.5\,\beta)}$$

(c) for flows with flexible bubbles in the sublayer

$$f_c = D\,\frac{dp/dz}{2\rho\,\langle j\rangle^2}\ , \quad R_c = \frac{D\rho\,\langle j\rangle}{\mu_\ell\left\{1 + \dfrac{2.5\,\mu_g + \mu_\ell}{\mu_g + \mu_\ell}\,\beta\right\}}\ ;$$

(d) for flows with a wavy gas-liquid interface within the sublayer

$$f_d = D\,\frac{dp/dz}{2\rho\,\langle j\rangle^2},\quad R_d = \frac{D\rho\,\langle j\rangle}{\mu_\ell\,(1-\beta) + \mu_g\beta}\ ;\ \text{and}$$

(e) for flows with attached wall voids

$$f_e = D\,\frac{2dp/dz}{\rho\,\langle j\rangle^2}\ , \quad R_e = 2.4\left\{\frac{\rho\,\langle j\rangle^2 D}{\sigma}\right\}^{\frac{1}{2}}$$

For this type of flow, Eq. (1) is applicable if ε is put equal to zero regardless of the true roughness. Note that R here is basically a two-phase Weber number.

In the above definitions, $\rho = \rho_\ell\,(1-\beta) + \rho_g\beta$.
As is the case with single phase flows, Eq. (1) arises from non-dimensional velocity profile of the form

$$j^+ = 5.5 + 2.5\,\ell n\ y^+ \quad \text{(smooth tube)} \tag{2}$$

and $$j^+ = 8.5 + 2.5\,\ell n\ y/\varepsilon \quad \text{(rough tube)} \tag{3}$$

where $$j^+ = \frac{j}{\langle j\rangle}\sqrt{\frac{2}{f}}$$

and $$y^+ = \frac{y}{D}\,R\sqrt{\frac{f}{2}}$$

In addition to the implicit validity of Eqs. (2) and (3) due to the agreement of Eq. (1) with data, Eq. (2) has been confirmed by several two-phase velocity profile measurements. As in single phase flow, Eq. (2) holds only above $y^+ = 30$; below this point the curve can be described by

$$j^+ = y^+ \qquad (\text{for } y^+ \le 5) \tag{4}$$

and $$j^+ = -3.05 + 5.0\,\ell n\ y^+ \quad (\text{for } 5 \le y^+ < 30) \tag{5}$$

2.2 Other Two-Phase Flows

It was noted that although Eq. (1) generally applied, often data could be classified on the basis of groupings of f and R which yielded correlations differing from Eq. (1). These correlations tended to have reduced values of f with respect to Eq. (1) at high R values, and increased f value at lower R values. Data with lower friction values with respect to Eq. (1) were more common.

The different correlations suggested that the sublayer models associated with f and R still applied, but Eqs. (2) and (3), upon which Eq. (1) is based, were not valid for some two-phase flows. This idea was reinforced by several smooth tube velocity profile results found in the literature which disagreed with Eq. (2).

An examination of these anomalous pressure drop and velocity profile data showed that a large fraction of them were consistent with the 'universal' velocity profile being replaced by a profile in which the buffer region curve, Eq. (5), extends over the whole turbulent core. The associated friction factor equation, obtained by averaging Eq. (5) over the flow area, is

$$\frac{1}{\sqrt{f}} = 8.15 \log (R\sqrt{f}) - 11.11 \qquad (6)$$

Systems where Eq. (6) applies form a special class of their own and will be referred to in this paper as 'buffer layer dominated' systems.

3. CLASSIFICATION OF TWO-PHASE DRAG REDUCTION MECHANISMS

The preceding section indicates that two-phase systems may be classified according to the nature of both the sublayer and the non-dimensional velocity profile. In addition, the treatment of other two-phase quantities (specifically, those that depend on the nature of the void profile) necessitates further classification into distributed or separated systems.

The frequently encountered non-repeatability of two-phase pressure loss data provides examples of drag reduction (of the lower friction data with respect to the higher friction data). The reduction is due to changes in the sublayer and/or turbulent core, and may be classified according to which change causes the reduction.

The different drag reduction mechanisms are illustrated in Fig. 1*. This figure shows data obtained from a given test section for two different mass fluxes. The open symbol data (Ref. 2) were obtained with a long 'settling length' upstream of the test section. The pressure drop values are below the closed symbol data (Ref. 3) which were obtained from the same test section under nominally identical conditions except that a throttling valve was placed just upstream of the test section.

There is a noticeable reduction in friction with the longer settling length. Curve fitting the data with the appropriate equations from Section 2 shows that the reduction is due either to a change of sublayer from a rigid surfaced bubble system to a system having free-surfaced bubbles or a wavy gas-liquid interface; or to a change in the core to a buffer layer dominated structure.

---

* Values of D/ε used for the graphs of Figs. 1 and 4 were obtained from single phase data (Ref. 2).

4. EXTENDED BUFFER REGION VELOCITY DATA

As stated, many velocity data are consistent with Eq. (5) extending over the whole core. Six data sets, covering a wide range of conditions and each from a separate reference, are shown in Fig. 2. A rigid surfaced bubble sublayer was assumed for all the data of Fig. 2 except those from (Refs. 4 and 7) where the assumption of a sublayer with flexible bubbles gave slightly better agreement with Eq. (5). These exceptions are consistent with the idea that the rigid surface associated with some bubbles is due to impurities in the liquid concentrating on bubble surfaces. The effect is expected to be less for liquids with non-polar molecules (Ref. 4 data) and also for lower velocity data with resulting larger bubbles (Ref. 7 data).

Plots such as those of Fig. 2 require assumptions about both the sublayer structure and also the friction factor relation.* An incorrect assumption of either shifts the plot without changing the slope. Consistency of the final plot with the assumptions (for example the data of Fig. 2, where Eq. (6) was assumed to hold, imply the validity of Eq. (6)) is sufficient to justify the approach.

Where friction data are available with the velocity profiles, these tend to confirm the assumptions. One noticeable exception, (from Ref. 8) is in Fig. 2. These velocity data imply a buffer layer dominated core, whereas the pressure drop associated with this profile, along with other pressure drop data (Ref. 8) indicates that Eq. (1) rather than Eq. (6) (the buffer layer dominated friction equation) describes the friction characteristics. A tentative explanation is that the velocity data, which were measured downstream of the pressure taps, were obtained in a region where the flow structure changed because of increased distance from the entrance (see Section 5.1) or because of the influence of the velocity measuring probe.

5. BUFFER LAYER DOMINATED FRICTION FACTORS

5.1 Entrance Effects

As might be expected from single phase experience, entrance region friction factors for buffer layer dominated flows are slightly above those predicted from Eq. (6). The effect is more pronounced than for single phase flows. Typical data from (Ref. 10) measured 36 diameters from a gas-liquid mixer, are shown in Fig. 3a. The data approach Eq. (6) with increasing R, as might also be expected from single phase experience. The data of Fig. 3a cover a reasonably wide range of conditions, as can be seen from Fig. 3b. (Most of the other data from (Ref. 10) are slightly above the prediction of Eq. (1) using the attached wall void grouping for f and R, f_e and R_e. These data approach Eq. (1) with increasing values of R_e).

With increasing distance from the entrance, the drag reduced data approach Eq. (6) (Fig. 3c). An additional effect of distance is to change the regime boundary conditions. The highest R data of Fig. 3c were obtained at $G_g = 820$ kg $m^{-2}s^{-1}$ and $G_\ell = 2060$ kg $m^{-2}s^{-1}$. This is outside the range

---

* Only a small fraction of two-phase flow structure data in the literature have associated pressure loss data. This is surprising considering the connection between turbulence and wall shear.

of applicability of Eq. (6) at 36 diameters from the entrance (see Fig. 3b), but Eq. (6) is evidently valid further downstream (> 116 diameters). Similar changes of the buffer layer dominated regime boundary can be inferred from the steam-water data of (Ref. 12).

5.2 The Relation Between Two-Phase Drag Reduction and Hydrodynamic Dryout

For adiabatic gas-liquid flows with sufficiently high values of mass flux and quality, liquid may be stripped from the wall and be completely contained as liquid droplets within the turbulent core. Friction losses for such flows are described by Colebrook's equation (Eq. (1)), using the dry wall groupings of f and R, f_a and R_a.

For convenience, these flows may be considered as occupying a certain region of the mass flux-quality plane. Substitution of the various sublayer dimensionless groups into Eq. (1) shows that a large step reduction in frictional pressure drop would have to occur at the boundary of the dry wall region for Eq. (1) to be valid for wet wall flows near the boundary.

Extensive analysis of high pressure steam-water data shows that such a step change does not occur, and friction data for conditions near hydrodynamic dryout are described by Eq. (6) using the rigid surfaced bubble sublayer groupings of f and R. Flows near the dryout condition are thus buffer layer dominated, and appear to act as a partial transition between the lower quality wet wall high friction flows and the high quality dry wall low friction flows, both of which are given by Eq. (1). In fact, the boundary between the dry wall regime and the buffer layer dominated regime appears to occur when the pressure losses associated with each type of flow are equal, i.e. when

$$\frac{4f_a}{D}\ \frac{1}{2}\rho_g \langle j\rangle^2 = \frac{4f_b}{D}\ \frac{1}{2}\left\{\rho_l\ (1-\beta) + \rho_g\beta\right\}\langle j\rangle^2$$

where $f_a = f_a\left(\frac{\rho_g D \langle j\rangle}{\mu_g}\right)$ and is given by Eq. (1)

and $f_b = f_b\left(\frac{\left\{\rho_l\ (1-8\beta) + \rho_g\beta\right\}\langle j\rangle D}{\mu_l\ (1+2.5\beta}\right)$ and is given by Eq. (6)

$$\text{i.e. } f_a/f_b = \beta + \rho_l\ (1-\beta)/\rho_g \qquad (7)$$

Fig. 4a shows an empirical sublayer regime map, using the mass flux-quality plane, based on data of (Ref. 2). As can been seen, Eq. (7) appears to give a reasonable approximation to the boundary of the dry wall regime. Fig. 4b indicates that the assumed sublayer and core structure assigned to each point of Fig. 4a are reasonable. Each point in Fig. 4b corresponds to one of Fig. 4a, with corresponding points having the same symbol.

5.3 Effect of Drag Reduction on Voidage

As stated, the effects of the drag reduction phenomenon are more far reaching for two-phase systems than for single phase systems. Quantities

significantly influenced by drag reduction in two-phase systems but not (where applicable) in single phase systems include the cross-sectional averaged value of voidage, momentum and kinetic energy fluxes, pressure pulse propagation velocity, and the onset of choking. As an example, the case of voidage in distributed two-phase systems is discussed.

As shown by Zuber et al (Ref. 13), the averaged voidage of a horizontal distributed two-phase flow system may be given by

$$\langle\alpha\rangle = \beta/Co \tag{8}$$

where Co is a 'distribution parameter'. Typical empirically determined values for Co are 1.2 (round tubes) and 1.4 (rectangular channels).

It will be shown elsewhere that the ratio (maximum velocity)/(average velocity) represents a reasonable estimate of Co. Manipulation of Eqs. (2) and (5) then shows that

$$Co = 1 + 2.65\sqrt{f} \tag{9}$$

for flows where f is given by Eq. (1),

and $$Co = 1 + 5.3\sqrt{f} \tag{10}$$

for flows where f is given by Eq. (6).

For typical values of R, Eqs. (9) and (10) predict respective Co values of 1.2 and 1.4. This suggests that the rectangular section data analysed in (Ref. 13) contained buffer layer dominated flows.

Data from (Ref. 14) can be used to test the validity of Eq. (10) for atypical conditions. Void profile and pressure loss data showed that the flows were distributed, buffer layer dominated, with a wavy gas-liquid interface within the sublayer (a classification which implies visual classification as slug, semi-annular, or froth). The data included very low values of R_d, with the result that drag was increased with respect to Eq. (1) rather than reduced, as expected from Eq. (6).

Average void data were converted to values of Co using Eq. (8) and plotted as a function of R_d (Fig. 5). Although Co values are much larger than those normally encountered (Ref. 13), data are in reasonable agreement with Eq. (10) except at very low values of R_d. The discrepancy here is at least partly due to the neglect of the laminar sublayer (which is no longer negligible at these conditions) in the development of Eq. (10).

Data and Eq.(10) both approach the Zuber et al (Ref. 13) recommendation, Co = 1.4, for normally encountered values of R_d.

6. OTHER TYPES OF TWO-PHASE DRAG REDUCTION

6.1 Drag Reduction at Obstructions

In (Ref. 1) it was suggested that plots of the two-phase loss coefficient $K = \Delta P \left\{\left[\rho_l (1 - \alpha) + \rho_g \alpha\right] \langle j\rangle^2\right\}^{-1}$ against the appropriate Reynold's number R should coincide with the single phase loss coefficient - Reynold's number plot.

Air-water experiments on a 6-pin spacer for a 12.7 mm rod in a 25.4 mm tube showed this to be only partially true. The choice of the wavy gas-liquid sublayer grouping of R, R_d, was necessary to correlate the data, but the plot fell fairly distinctly onto two lines (Fig. 6). One line agrees with the single phase data, but the other has drag reduction characteristics at the higher values of R_d.

Furthermore, although friction data downstream of the spacer were generally correlated by Colebrook's equation (Eq. (1))using the rigid-surfaced bubble sublayer groupings for f and R, R_b and f_b, some of the friction data obtained simultaneously with reduced loss coefficients were correlated by Eq. (6) using the wavy gas-liquid interface sublayer grouping of R, R_d, suggesting that two-phase drag reduction may be induced by upstream disturbances.

6.2 Flows with Attached Wall Voids

The recommended use of Eq. (1) for attached wall voids summarised in Section 2.1, has been found to apply to two-component flows in complex and simple geometries, and to diabatic steam-water flows in complex geometries but not for diabatic steam-water flows in round tubes. For the latter conditions, data correlations of friction factor with the Weber number grouping of R, R_e, indicate an attached wall void sublayer, but the plot shows drag reduction characteristics.

An example, based on diabatic steam-water data from (Ref. 2) is shown in Fig. 7. This figure also shows two-component data from (Ref. 15) to demonstrate the validity of the (Ref. 1) attached wall void equations for some round tube geometries.

6.3 Low Pressure Data

Velocity profile and/or pressure loss data for low pressure separated gas-liquid flows tend to show drag reduction characteristics. The velocity data are steeper and friction data are lower than for buffer layer dominated flows. Examples can be found in the low pressure data of (Ref. 2) and (Ref. 4).

7. CONCLUSIONS

Drag reduction may occur in gas-liquid systems without additives. The reduction is associated with changes in the sublayer and/or changes in the turbulence structure.

A large fraction of data where reduction is due to changes in the turbulence structure are consistent with the buffer region of the universal velocity profile extending over the whole core. A friction factor: Reynold's number relationship for such data is given by Eq. (6). The boundary conditions for such flows depend on the entrance length except for an upper limit which is determined by Eq. (7).

8. ACKNOWLEDGEMENTS

Helpful discussions with Dr. K.R. Lawther (Head, Heat Transfer Section, AAEC) and Professor J.J. Thompson (Head, School of Nuclear Engineering, UNSW) are gratefully acknowledged.

The data of Figure 6 were based on experiments performed by Mr. C. Evans.

9. REFERENCES

1. Beattie, D.R.H. - A note on the calculation of two-phase pressure losses. Nuclear Engineering and Design 25, 4, pp 395-402 (August 1973).

2. Gaspari, G.P., Lombardi, C. and Peterlongo, G. - Pressure drops in steam-water mixtures. C.I.S.E. report R-83 (January 1964).

3. Era, A., Gaspari, G.P., Hassid, A. and Zavattarelli, R. - Heat transfer crisis and pressure drop for steam-water mixtures at 70 kg/cm^2 flowing upwards and downwards in circular conduits. C.I.S.E. report R-185 (January 1967).

4. Jepsen, J.C. and Ralph, J.H. - Hydrodynamic studies of two-phase upflow in pipelines. Proc. Institute of Mechanical Engineers 184, pt 3C, Paper 20 (September 24-25 1969).

5. Schraub, F.A., Simpson, R.L. and Janssen, E. - Air-water flow structure data for a round tube, concentric and eccentric annulus, and nine-rod bundle, General Electric report G.E.A.P. 5739 (January 1969).

6. Alia, P., Cravarolo, L., Hassid, A. and Pedrocchi, E. - Phase and velocity distribution in two phase adiabatic annular dispersed flow. C.I.S.E. report R-109 (December 1966).

7. Malnes, D. - Slip ratios and friction factors in the bubble flow regime in verticle tubes. K.R. report 110 (May 1966).

8. Adorni, N., Peterlongo, G., Ravetta, R. and Tacconi, F.A. - Phase and velocity distribution measurements in a round vertical tube. C.I.S.E. report R 91 (October 1964).

9. Vella, S. and Zavattorelli, R. - Final results of steam-water mixing and separation experiments: Phases distribution and separation efficiency. Ansaldo report LAB-STU1469 (October 1961).

10. Adorni, N., Casagrande, I., Cravarolo, L., Hassid, A. and Silvestri, M. - Experimental data on two-phase adiabatic flow: Liquid film thickness, phase and velocity distribution, pressure drops in vertical gas-liquid flow. C.I.S.E. report R 35 (March 1961).

11. Cravarolo, L., Hassid, A. and Pedrocchi, E. - Further investigation on two-phase adiabatic annular-dispersed flow: effect of length and of some inlet conditions on flow parameters. C.I.S.E. report R-93 (September 1964).

12. Alessandrini, A., Peterlongo, G. and Ravetta, R. - Critical heat flux and pressure drop measurements in round vertical tubes at the pressure of 51 kg/cm^2 abs. C.I.S.E. report R 86 (December 1963).

13. Zuber, N., Staub, F.W., Bijwaard, G. and Kroeger, P.G. - Steady state and transient void fraction in two-phase flow systems. General Electric report GEAP 5417 (January 1967).

14. Fohrman, M.J. - The effect of the liquid viscosity in two-phase, two-component flow. Argonne National Laboratory report 6256 (November 1960).

15. Casagrande, I., Cravarolo, L., Hassid, A. and Pedrocchi, E. - Adiabatic dispersed two-phase flow: further results on the influence of physical properties on pressure drop and film thickness. C.I.S.E. report R 73 (May 1963).

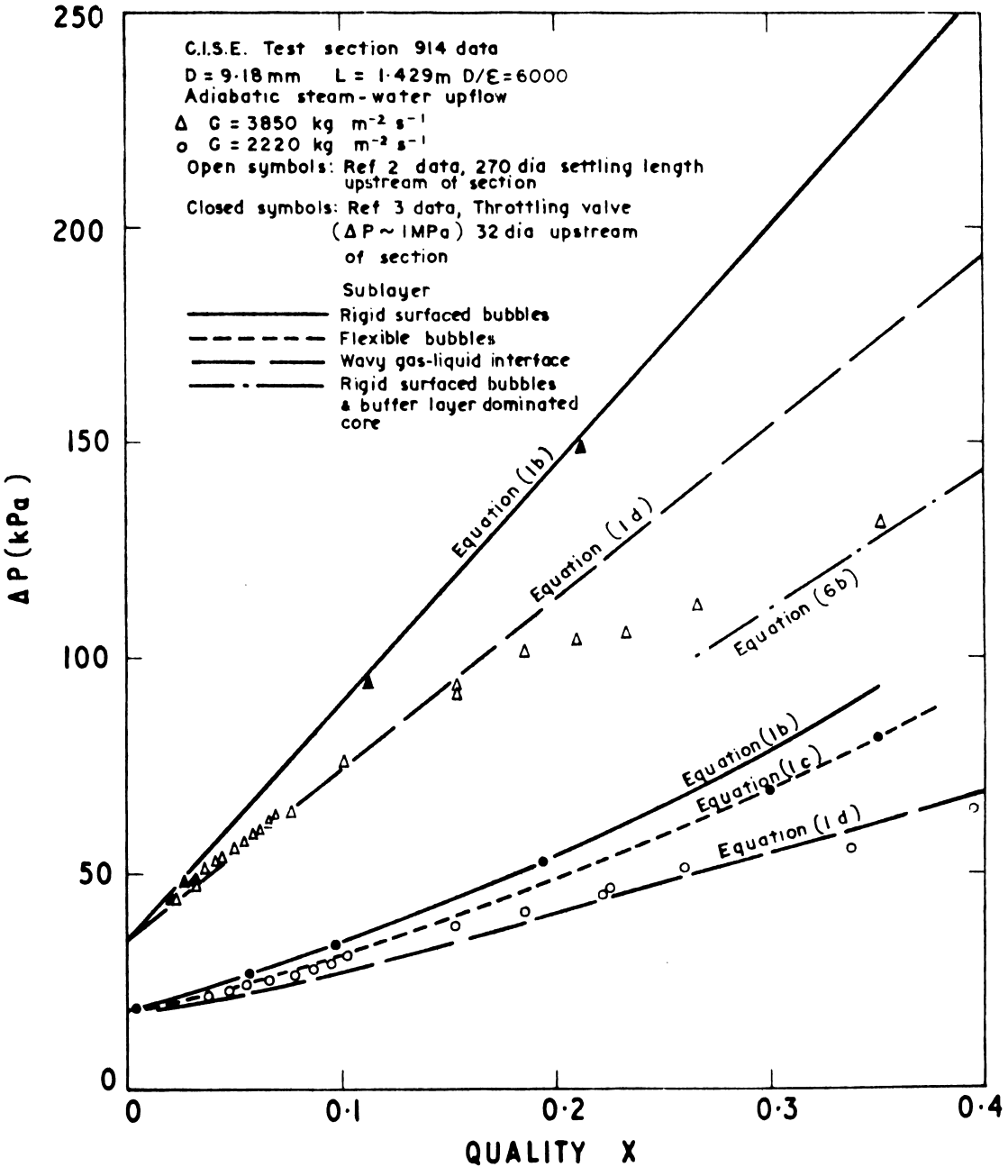

Fig.1 Examples of two-phase drag reduction

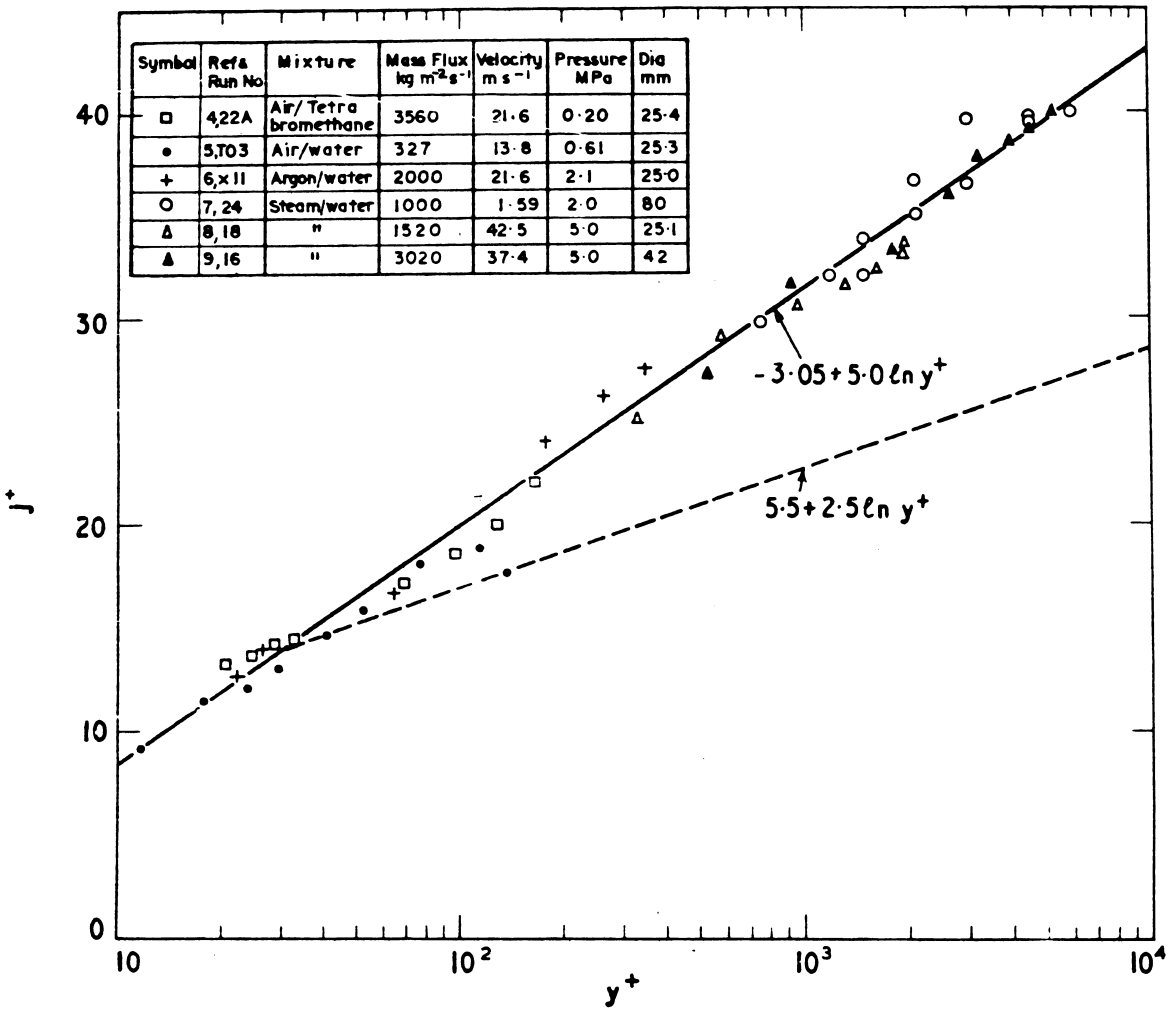

Fig. 2 Extended buffer region velocity profile data

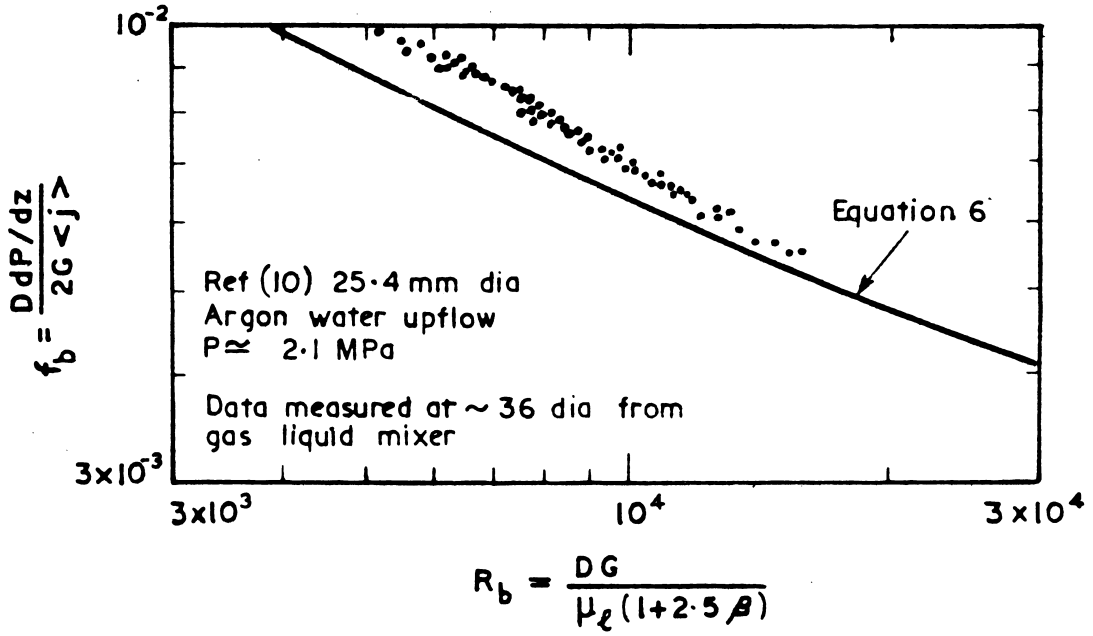

Fig. 3a Undrprediction of friction factor in entrance regions

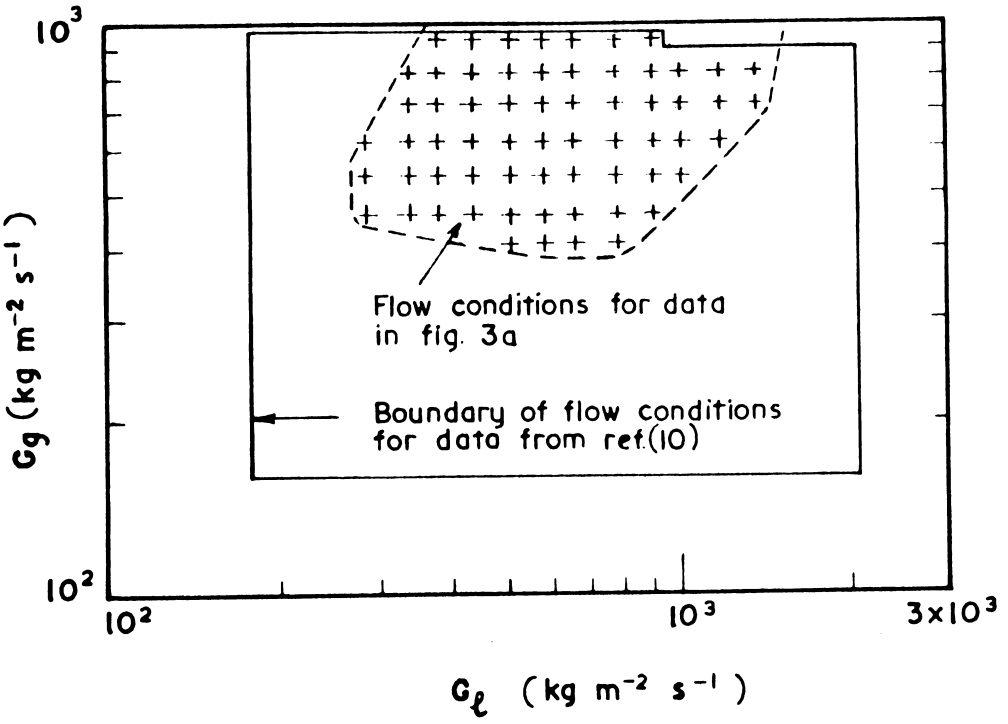

Fig. 3b Flow conditions for data of Fig. 3a

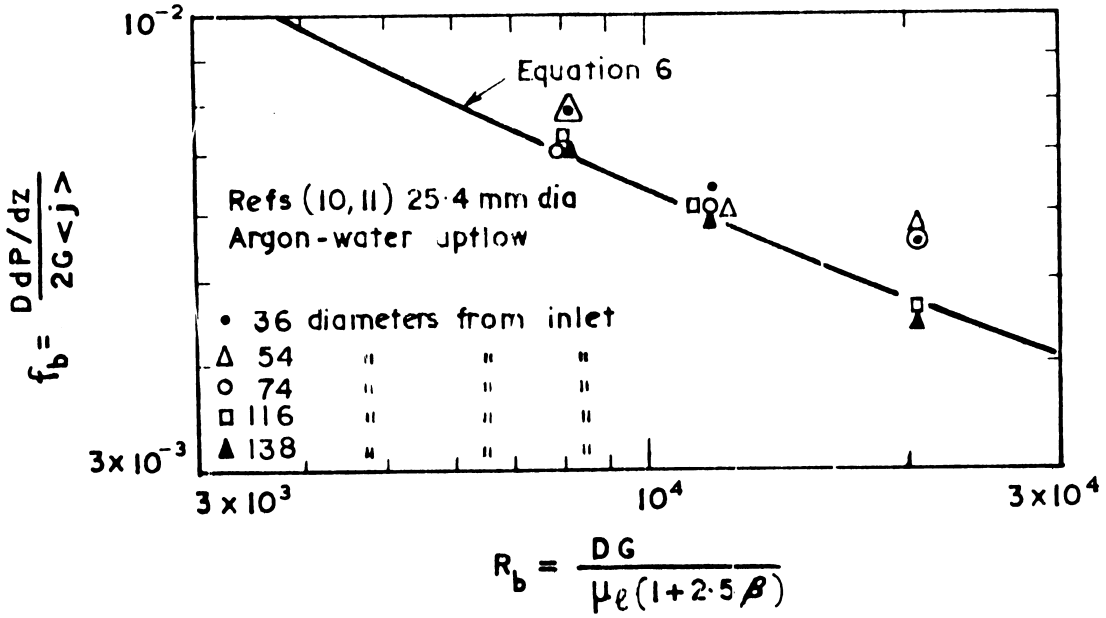

Fig. 3c Effect of length on friction factor

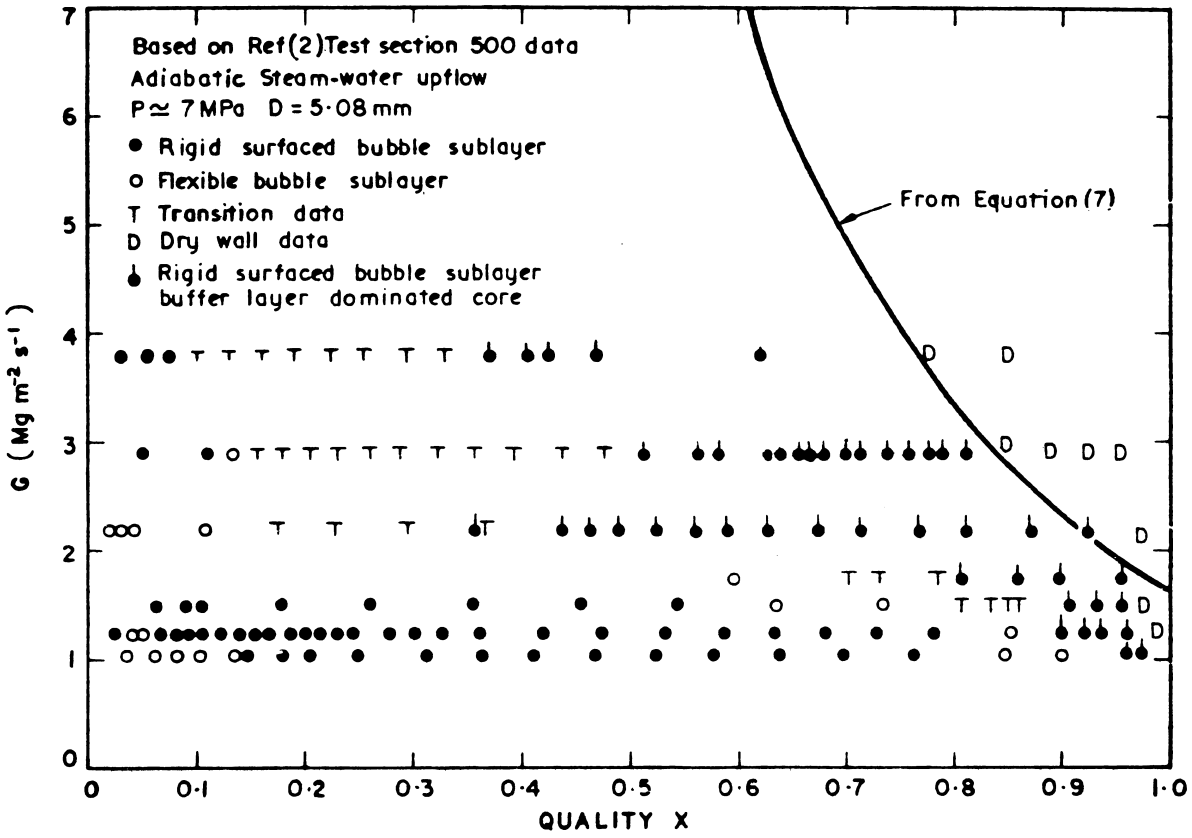

Fig.4a Empirical sublayer regime map and comparison of theoretical boundary of hydrodynamic dryout region with data

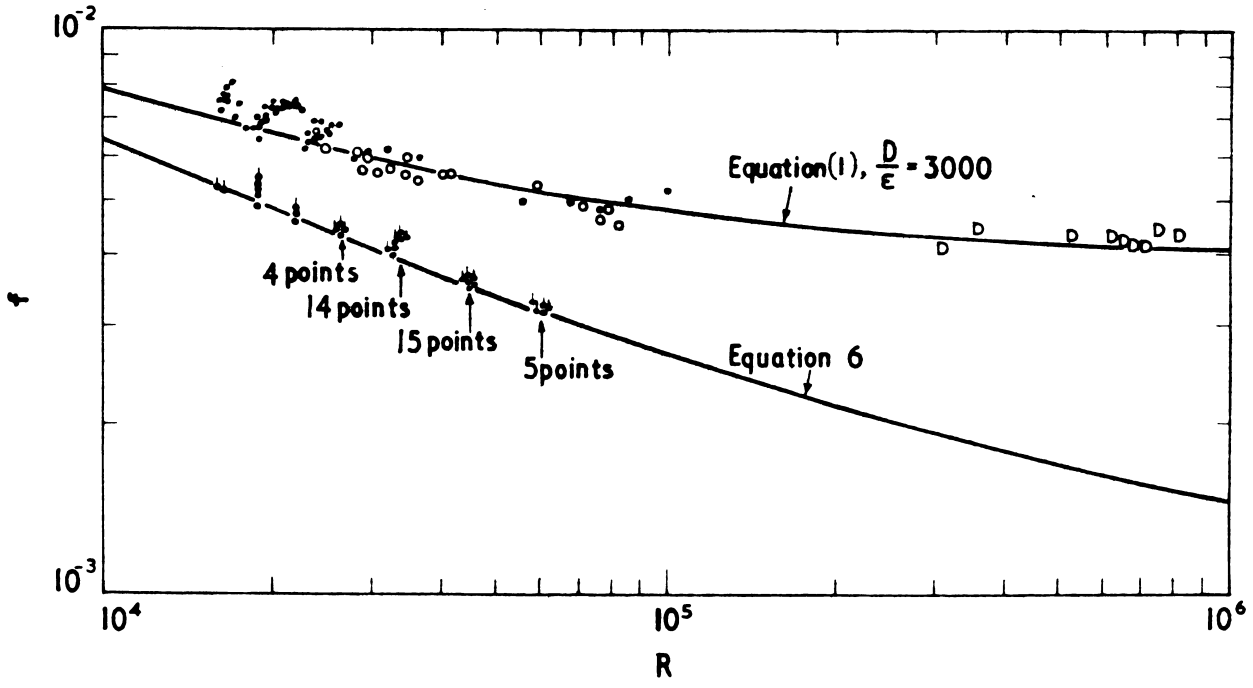

Fig.4b Friction factors for data of fig.4a notation as in fig.4a

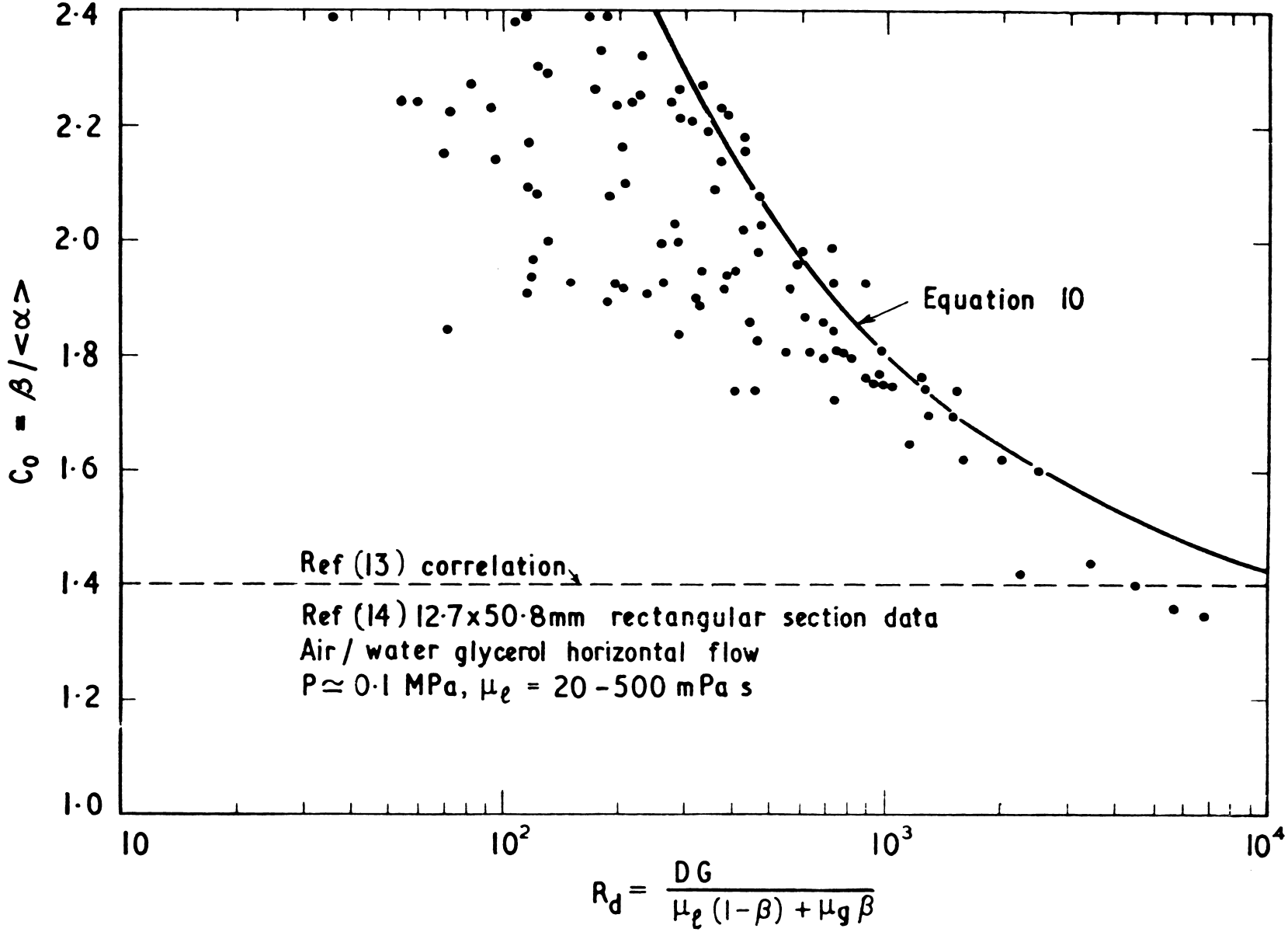

Fig. 5 Comparison of theory, voidage data, and empirical correlation for buffer-layer dominated flows

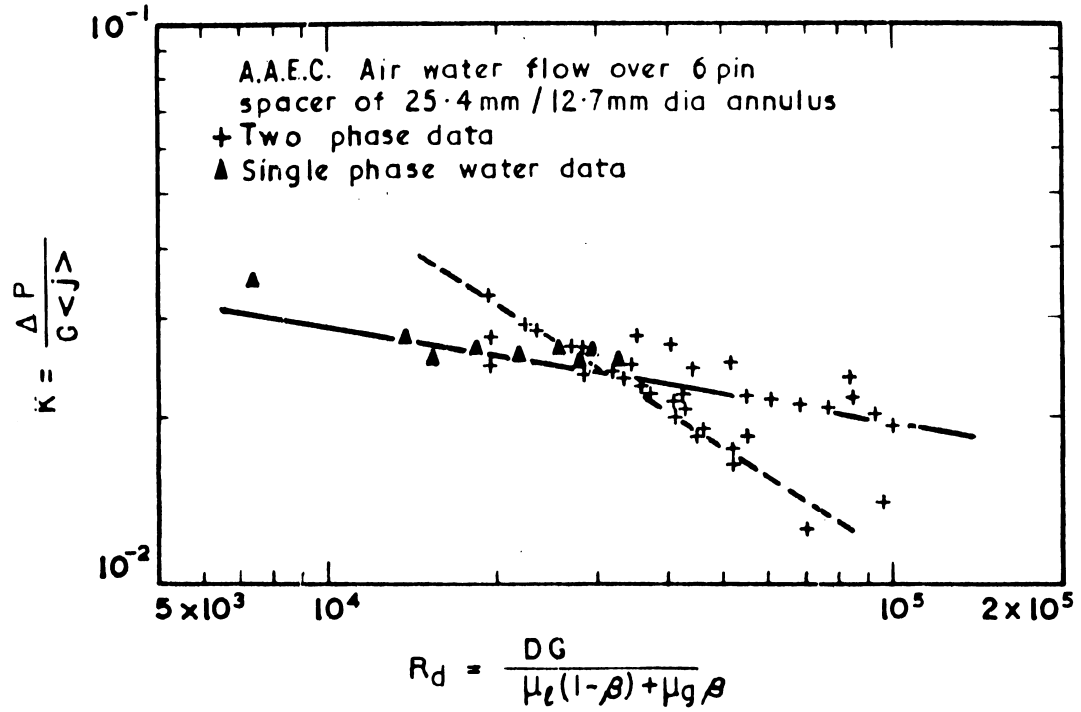

Fig. 6 Non-repeatable two-phase loss coefficient data with drag reduction characteristics

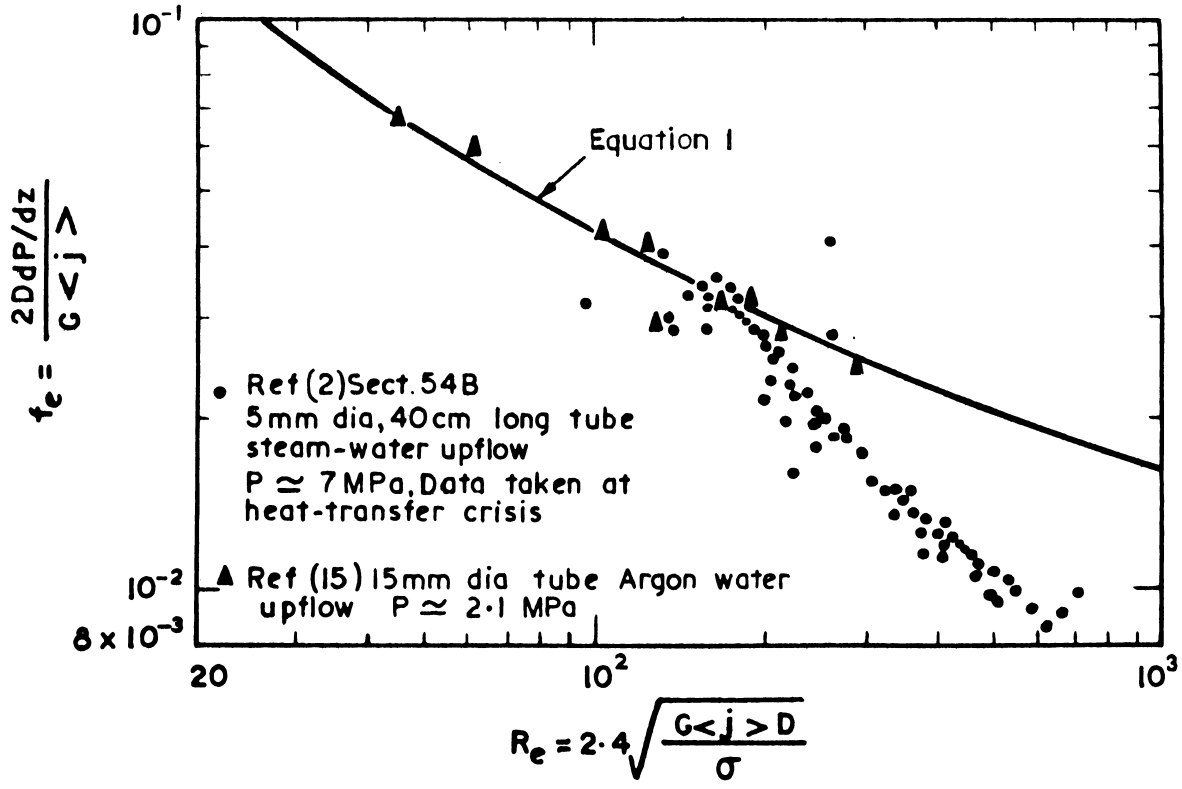

Fig. 7 Anomalous diabatic steam water data with drag reduction characteristics

in USA

an ASME publication

The Society shall not be responsible for statements or opinions advanced in papers or in discussion at meetings of the Society or of its Divisions or Sections, or printed in its publications. *Discussion is printed only if the paper is published in an ASME journal or Proceedings.*
Released for general publication upon presentation.
Full credit should be given to ASME, the Technical Division, and the author(s).

$3.00 PER COPY
$1.50 TO ASME MEMBERS

Friction Factors and Regime Transitions in High Pressure Steam-Water Flows

D. R. H. BEATTIE

A.A.E.C. Research Establishment,
Sutherland, N.S.W. Australia

Frictional characteristics are used to define flow regimes and a multiple regime classification, based largely on frictional effects, is discussed. Regime types and boundaries are determined for typical adiabatic and diabatic flow in round tubes, annuli, and rod clusters, with and without flow disturbing influences, by curve fitting data with selected friction factor expressions based on mixing length theory. Resulting equations and their ranges of applicability are tentatively recommended for design purposes. All regime boundaries are qualitatively consistent with the concept of continuity of entropy production rate across a regime boundary. This concept should prove useful in improving methods for predicting the heat transfer crisis.

Contributed by the Heat Transfer Division of The American Society of Mechanical Engineers for presentation at the Winter Annual Meeting, Houston, Texas, November 30-December 4, 1975. Manuscript received at ASME Headquarters July 25, 1975.

Copies will be available until August 1, 1976.

Discussion on this paper will be received at ASME Headquarters until January 5, 1976.

Friction Factors and Regime Transitions in High Pressure Steam-Water Flows

D. R. H. BEATTIE

ABSTRACT

Frictional characteristics are used to define flow regimes and a multiple regime classification, based largely on frictional effects, is discussed.

Regime types and boundaries are determined for typical adiabatic and diabatic flow in round tubes, annuli, and rod clusters, with and without flow disturbing influences, by curve fitting data with selected friction factor expressions based on mixing length theory. Resulting equations and their ranges of applicability are tentatively recommended for design purposes.

All regime boundaries are qualitatively consistent with the concept of continuity of entropy production rate across a regime boundary. This concept should prove useful in improving methods for predicting the heat transfer crisis.

NOMENCLATURE

A	= entropy production rate due to viscous dissipation, kg $m^{-1}s^{-3}K^{-1}$
B	= entropy production rate due to heat transfer, kg $m^{-1}s^{-3}K^{-1}$
C	= entropy production rate due to flow redistribution kg $m^{-1}s^{-3}K^{-1}$
D	= equivalent diameter, m
f	= friction factor
g	= total entropy production rate, kg $m^{-1}s^{-3}K^{-1}$
G	= mass flux, kg $m^{-2}s^{-1}$
j_+	= volumetric flux, m s^{-1}
j^*	= $(j/\langle j\rangle)/\sqrt{f/2}$
P	= pressure, Pa
dP/dz	= frictional pressure gradient, Pa m^{-1}
$\underset{\sim}{q}$	= heat flux, W m^{-2}
Re	= Reynolds number
T	= absolute temperature, K
We	= Weber number
y_+	= wall distance, m
y^*	= $(y/D)\,Re\sqrt{f/2}$
β	= gas volume flow ratio, $\langle j_g\rangle/(\langle j_g\rangle + \langle j_\ell\rangle)$
ε	= wall roughness height, m
$\underset{\sim}{\Lambda}$	= driving force for flow redistribution, m s^{-2}
μ	= viscosity, Pa s
ρ	= density, kg m^{-3}
σ	= surface tension, N m^{-1}
$\underset{\sim}{\tau}$	= stress tensor, Pa

Subscripts

g	= gas
ℓ	= liquid
w	= wall
<--->	= quantity is averaged over flow section

INTRODUCTION

It has long been recognized from observations of two-phase flows that a number of distinct flow regimes are possible. Also, it has been recognized that, from a design viewpoint, knowledge of regime boundaries is as likely to be as important in two-phase flow, as knowledge of the laminar-turbulent flow regime boundary is in single phase flow.

Owing to the limited understanding of two-phase fluid mechanics, regime change effects have been considered of secondary importance, with emphasis being placed on attempts to obtain design equations which are reasonably valid for all regimes. The need for increased accuracy has resulted in such equations being replaced by a series of equations, each relating to a different regime. For example, although the homogeneous model was once regarded as being sufficient for estimating void fraction, momentum flux, pressure loss, etc., recent works concentrate on different models for each regime [1][1], and newer empirical or semi-empirical equations for voidage [2] and pressure loss [3] incorporate regime change effects.

Visual interpretation can be highly subjective, and it is not surprising that different visually-based recommendations for regime boundary estimation can be highly contradictory [3]. Since knowledge of flow regimes is important as an aid in choosing design equations, the subjectivity associated with visual classifications can best be removed by associating regime boundaries with changes in those quantitative fluid mechanical characteristics of interest to the designer.

Because of the availability of pressure drop data, frictional characteristics are used here to define various regimes and a multiple regime classification, based largely on frictional effects is discussed. It is believed that such regimes may be significant for the interpretation of other phenomena, e.g. heat transfer.

Regime types and regime boundary behaviour discussed here have been based largely on an analysis of data from high pressure steam-water systems of interest to the reactor engineer.

2. CLASSIFICATION OF TWO-PHASE FLOW REGIMES

As stated, we specify flow regimes partly by the nature of the frictional characteristics of each regime. According to an as yet unpublished extension

[1] Numbers in brackets designate reference at end of paper

of a two-phase mixing length theory [4], the frictional behaviour may be classified by a system involving the definition of several parameters:

(i) The nature of the sublayer. This determines the form of the non-dimensional group relevant to friction calculations. The important sublayer types and the corresponding dimensionless groups are

(a) Dry wall sublayers:

$$Re = D\rho_g \langle j \rangle / \mu_g \qquad (a)$$

(b) Sublayer containing rigid surfaced bubbles:

$$Re = D\rho \langle j \rangle / \{\mu_\ell (1 + 2.5\beta)\} \qquad (b)$$

(c) Sublayer containing bubbles with a non-rigid surface:

$$Re = D\rho\langle j\rangle \Big/ \left\{ \mu_\ell \left(1 + \frac{2.5\mu_g + \mu_\ell}{\mu_g + \mu_\ell} \beta \right) \right\} \qquad (c)$$

(d) A wavy gas-liquid interface extends to within the laminar sublayer:

$$Re = D\rho\langle j\rangle / \{\mu_\ell (1 - \beta) + \mu_g \beta\} \qquad (d)$$

(e) Sublayer containing attached wall voids:

$$We = D\rho\langle j\rangle^2 / \sigma \qquad (e)$$

In the above, $\rho = \rho_\ell (1 - \beta) + \rho_g \beta$.

Viscosities used in the Reynolds numbers are respectively based on the gas only value, Einstein's model for rigid spheres [5], Taylor's model for bubbles [6], and a void-weighted average. The gas density is used for the dry wall case; ρ as defined above is assumed to be applicable to other sublayers. The Weber number is a consequence of an assumed effective roughness given by a bubble breakaway diameter obtained from a balance between surface tension and shear forces.

The friction factor for the above dimensionless groups is

$$f = \frac{DdP/dz}{2\rho\langle j\rangle^2}$$

except for the dry wall case,

where $$f = \frac{DdP/dz}{2\rho_g\langle j\rangle^2} \ .$$

(ii) The nature of the non-dimensional velocity profile. This determines the relation between the friction factor and the relevant dimensionless groups. Friction factor relations relevant to this paper are:

$$1/\sqrt{f} = 3.48 - 4 \log (2\varepsilon/D + 9.35/Re\sqrt{f})$$

(or the appropriate single phase equation for geometries where the above is invalid) (1)

$$1/\sqrt{f} = 8.15 \log Re\sqrt{f} - 11.1 \qquad (2)$$

$$1/\sqrt{f} = 16 \log Re\sqrt{f} - 43 \qquad (3)$$

$$1/\sqrt{f} = 16 \log Re\sqrt{f} - 56.7 \qquad (4)$$

$$1/\sqrt{f} = 16 \log Re\sqrt{f} - 72.4 \qquad (5)$$

$$1/\sqrt{f} = 5.66 \log We\ f + 1.7 \qquad (6)$$

$$1/\sqrt{f} = 14 \log We\ f - 10.4 \qquad (7)$$

The different coefficients are a consequence of the fact that, empirically, coefficients appearing in the two-phase non-dimensional velocity profile do not have unique values. The set of equations is not exhaustive. The applicability of equations (1) and (2) to some two-phase flows has already been demonstrated in [7] and [8].

Thus, friction calculations imply a double classification of two-phase flows, involving the sublayer structure (which defines the relevant group) and the non-dimensional velocity profile form (which defines the relation between dimensionless groups). The second classification may be subclassified according to the value of the coefficient of the log term in equations (1) to (7) - generally part of the series $4(2)^{n/2}$ - and the value of the constant in the right hand side of equations (1) to (7).

In addition to the classification of regimes according to the nature of frictional characteristics, the treatment of two-phase quantities which depend on the nature of the void profile necessitates further classification into distributed or separated systems. The high voidage separated flow friction data from [9] demonstrate the need for this. Contrary to the separated flow friction data from [10] which are described by equation (1d)[1] Fig.1 demonstrates that the data from [9] are described by equation (1c) which has been shown to be valid for some bubble flows [7]. Thus, although the data were from flows having an annular appearance, the flows, contrary to one's intuition, can be associated with the same frictional regime as some bubble flows. On the other hand, the behaviour of associated void data from [9] for the same separated flows differ markedly from distributed flow void behaviour. Frictional information is thus insufficient to specify all flow characteristics.

3. DATA ANALYSIS

Analysis of several thousand high pressure steam-water friction data has indicated that low quality (presumably visually bubbly) flows and high

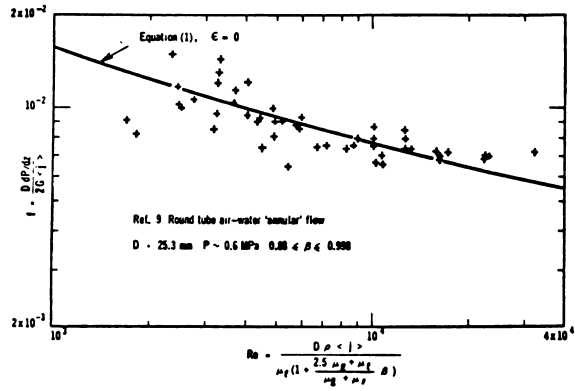

Fig.1. Bubble-flow like friction for separated flow data

[1] Equation (1d) means equation (1) is used with Reynolds number defined by equation (d).

quality dry wall flows are each described by equations (1b) and (1a) respectively, with almost complete generality. However, equation types and hence flow regimes applicable to intermediate qualities are strongly dependent on other factors (geometry type, entrance effects, etc.) and it has become necessary to develop several sets of equations, each applicable to a given set of circumstances.

Representative high pressure steam-water friction data are discussed below to demonstrate the method of determining flow regimes and boundaries. Each example given is typical of other data of its type. Data reduction, and the reduction of integrated diabatic values to local values, is discussed in [11]. Where applicable, surface roughness values used in equation (1) were obtained from single phase data given with the data analysed.

3.1 Adiabatic Flow in Round Tubes with Long Upstream Settling Length

For round tube adiabatic flows with long settling lengths (≥500 diameters) upstream of the test section, data are described by equations (1b), (4d), (2b), and (1a) for increasing levels of steam quality respectively. The boundaries between separate quality ranges, i.e. regime boundaries, are accurately given by the intersects of the equations.

In Fig. 2, it can be seen that the data are described as above except for low mass flux, high quality data. In this region, the recommended equations must break down since, in the quality range, equation (2b) no longer gives a friction factor less than the unity quality value, and equations (2b) and (1a) can no longer intersect. The low mass flux high quality approach to the unity quality friction factor is via a different undetermined mechanism. Nevertheless, the data of Fig.2 are adequately described by the above equations, even for low mass flux high quality flows.

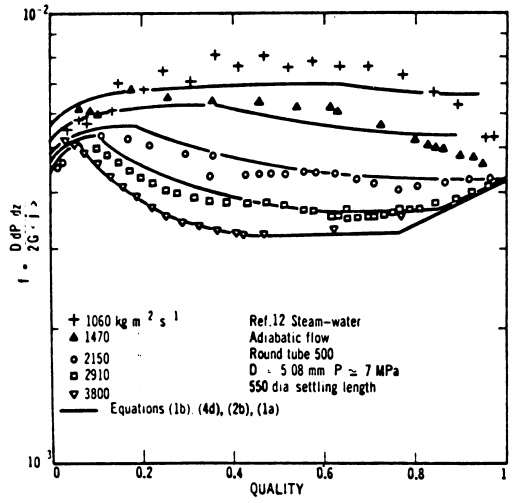

Fig.2. Adiabatic friction factors for a round tube with a long upstream settling length

3.2 Adiabatic Flow in Round Tubes with Shorter Settling Lengths

Most data in this class are curve-fitted as in section (3.1) except equation (2b) is replaced by equation (3c). An example is shown in Fig.3. Discrepancies again exist between the data and the equations for low mass flux high quality conditions.

Other data of this type are described by equations (1b), (4d), (2b) and (1a), as in section (3.1), except that regime changes occur anomalously at qualities differing from those given by the intersects of the various equations, resulting in discontinuities in the friction factor curves. Two examples are shown in Fig.4. One of these examples demonstrates a further effect of shorter settling lengths, namely a tendency towards non-reproducibility, due presumably to a transition from shorter settling length characteristics to longer settling length characteristics at a non-unique position in the test section.

As stated, intermediate to high quality data from systems without long upstream settling lengths are generally described by equation (3c). Sometimes equation (3b) describes this regime better. The difference between the two equations is in the nature of the bubble sublayer. In explanation, it is supposed that owing to the polar nature of water molecules, impurities in the fluid concentrate on gas-liquid interfaces. This tends to cause bubbles sufficiently small to act as rigid sphere. Thus, in the data discussed so far in this paper it might be assumed that sublayer bubbles are extremely small except when equation (3c) is applied (Fig.3). In the latter case, the flexibility of the larger sublayer bubbles has not been destroyed by the small amount of impurities present. For laboratories where water control is not expected to be stringently monitored, these bubbles may still behave as rigid spheres. Thus, for example, the intermediate to high quality data from the University of Minnesota [14] is described by equation (3b) and not by equation (3c).

3.3 Adiabatic Flow in Large Diameter Tubes

Most data indicate that the first two regimes for round tube adiabatic flows are described by equations (1b) and (4d). The data are, however, from small diameter tubes, and equations (1b) and (4d) become meaningless when applied to the riser region

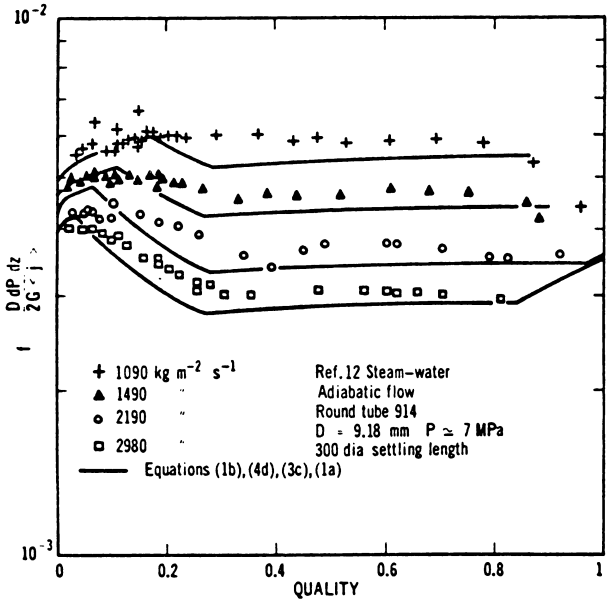

Fig.3. Adiabatic friction factors for a round tube with a short settling length

of a reactor: the intersect of equations (1b) and (4d) no longer occurs in the positive quality range.

Large diameter (7.62 cm) high mass flux (up to 2667 kg $m^{-2}s^{-1}$) data [15] indicate that equation (4d) is replaced by equation (5d). The changed coefficient in the friction factor expression is sufficient to cause the intersect of the two equations to occur at positive qualities.

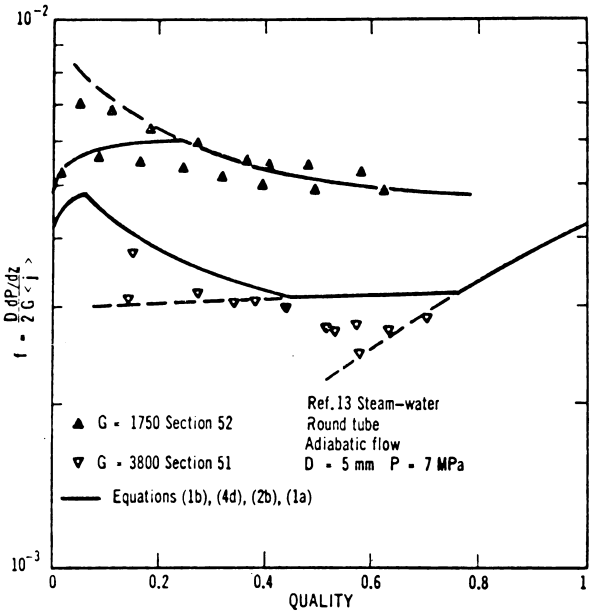

Fig.4. Discontinuities in and non-reproducibility of adiabatic friction factor curves for round tubes with short settling length

3.4 Unobstructed Diabatic Flow in Round Tubes

Data are described for low, intermediate and high qualities by equations (1b), (7e) and (1a) respectively. Regime boundaries are approximately given by the intersect of the different curves, except where dryout occurs in the region where the pre-dryout data is described by equation (7e). The friction factor then drops discontinuously towards the dry wall value given by equation (1a).

Typical round tube diabatic flow data are shown in Fig.5. Lower quality post-dryout data approach the dry wall equation rather than agree with it because the pressure taps were such that only some of the test section was in the dryout condition.

3.5 Diabatic Flow in Round Tubes with an Upstream Obstruction

Fig.6 shows upflow and downflow data from [16] obtained at heat transfer crisis conditions with (closed symbols) and without (open symbols) a throttling value of ($\Delta P \sim 1$ MPa) 32 diameters upstream of the test section. The test section is the same as that from which the data of Fig.4 were obtained.

The data without the upstream disturbance are adequately described by the diabatic flow recommendations given in section (3.4), as are the low mass flux data with the upstream disturbance.

The higher mass flux data are, however, noticeably changed by the upstream disturbance, and are better described by equation (3b) involving a bubble sublayer, rather than by equation (7e) involving attached wall voids. In view of the similarity to the intermediate quality adiabatic data from the

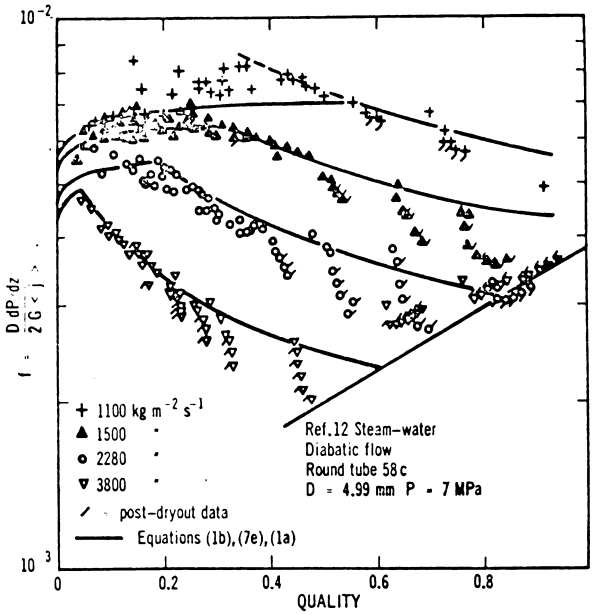

Fig.5. Diabatic friction factors for a round tube

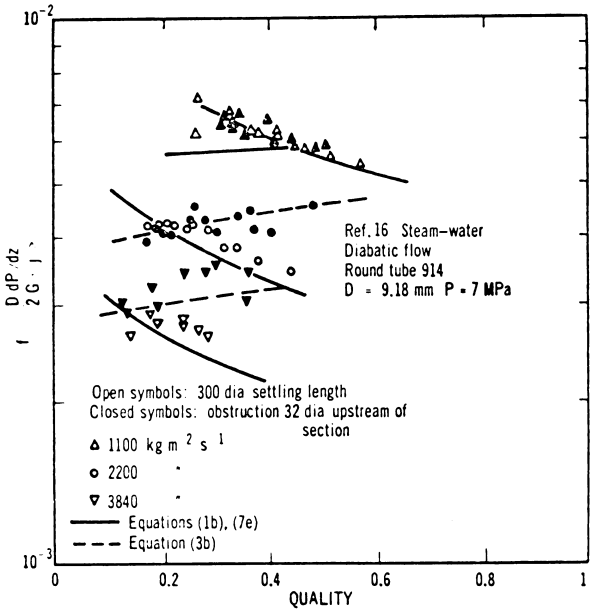

Fig.6. Diabatic friction factors for a round tube with (closed symbols) and without (open symbol a throttling valve ($\Delta P \sim 1$ MPa) upstream disturbance

same test section (Fig.3) described by equation (3c) and of the earlier discussion of bubble types (section (3.2)), it is reasonable to conclude that in this case the effect of the obstruction has been to reduce bubble size and to suppress the boiling mechanism at high mass fluxes.

Similar trends can be found in some of the non-developed inlet flow data from [12].

3.6 Flow in Annuli and Rod Clusters Where Spacer Effects are Small

Adiabatic and diabatic annulus and rod cluster

data (for lower and intermediate qualities) tend to be described by equation (1b) and (6e) respectively, provided spacers are separated by at least forty equivalent diameters. The regime change occurs at the intersect of the two equations. An example having both adiabatic and heat transfer crisis data, from [17], is shown in Fig.7.

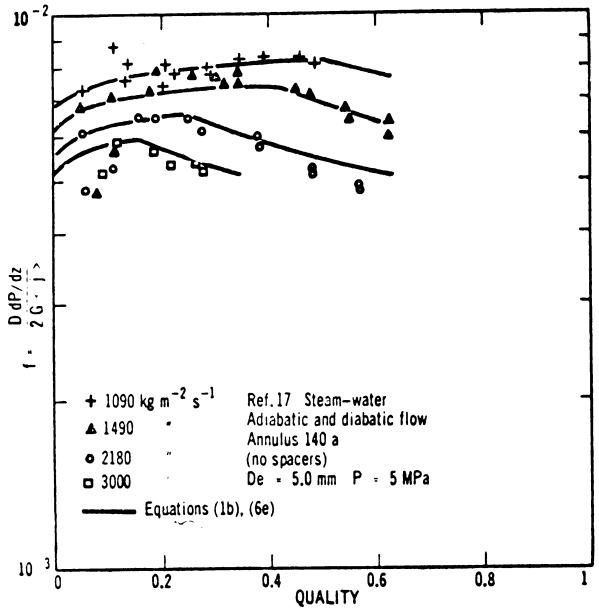

Fig.7. Adiabatic and diabatic friction factors for a cluster geometry with small spacer effects

As in round tube flows, adiabatic high mass flux, high quality data from [18], for example, indicate a hydrodynamically-induced dry wall regime where friction is given by equation (1a) occurs for qualities above that given by the intersect of equations (6e) and (1a). Furthermore, limited evidence from [19] suggests that heat transfer induced dryout on only some surfaces results in a step drop in friction factor to a value which may be estimated from the pre-dryout equations with the equivalent hydraulic diameter being replaced by (4 × area)/(non-dried perimeter). It is supposed that equation (1a) applies if all surfaces are dry.

3.7 Flow in Annuli and Rod Clusters with strong Spacer Influence

Spacers in complex geometries cause effects similar to those of development-destroying influences in round tube flows: different equations are necessary to describe the data; regime boundaries do not coincide with the intersects of the friction equations describing the separate regimes; and data scatter is more pronounced. Unlike flows discussed so far, there is no set of equations which appears to be generally applicable to flows of this type.

Thus, the 37-rod cluster data in Fig.8, from a test section with a spacer every twenty equivalent diameters [20], behaves differently to the complex geometry data of Fig.7. Equation (6e) no longer holds (in this particular case it is replaced by the round tube diabatic flow equation (7e)). The attached wall void regime extends to anomalously low qualities to the extent that the nearly zero quality 1000 kg $m^{-2}s^{-1}$ data point in Fig.8 has a friction factor more than twice that expected from equation (1b) which describes nearly all low quality data for all flow geometries.

Other data, from [21], for example, indicate that wire wrap spacers may have similar effects.

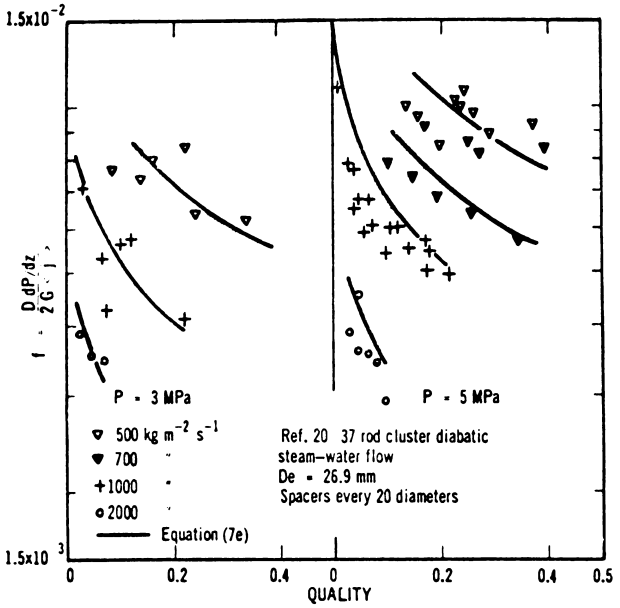

Fig.8. Diabatic friction factor data for a cluster geometry with strong spacer influence

4. DISCUSSION

Different equations have been shown to compare favourably with data from steam-water flowing under various conditions. Although data analysis has not been sufficiently extensive to permit definite recommendations for friction factor calculations, the examples in section 3 may be used as a guide in estimating steam-water pressure losses. Tentative recommendations based on these and other examples are summarized in Table 1. Furthermore, analysis of Freon 12 data from [22] indicates that the equations also apply to Freon systems used to model high pressure steam-water systems.

As demonstrated, regime types and boundaries between regimes are determined by geometry, heat flux, flow conditions (mass flux and quality) and flow development. The boundaries may be estimated from the intersect of the different friction factor expressions. From section 3, this estimate appears to be exact for flows where outside effects are minimal but it is only approximate where there is flow disturbance, heat transfer, etc. These influences cause changes in both regime boundaries (resulting in step changes in friction factors at the boundaries) and in regime types (changing the validity of a given friction factor equation). The deviations of regime boundaries from those estimated by the intersects of the various friction factor curves are of interest because of the special case of the onset of dry wall flows; this is of particular interest to the reactor engineer. A suggested method of estimating this shift is discussed below.

4.1 Influences Affecting Regime Types

Estimation of the regime types expected for a given situation must be based on a data analysis such as that given in section 3. The findings are, on the whole, consistent with out expectations. For example, the equations applicable to increasing quality levels

TABLE 1 FRICTION BEHAVIOUR IN HIGH PRESSURE STEAM-WATER SYSTEMS

Flow System			Equations[1]
Round Tubes	Adiabatic Flow	Settling length > 500D	1b, 4d[2], 2b, 1a
		Settling length $\lesssim$ 500D, D<6mm	As above[3]
		Settling length $\lesssim$ 500D, D>6mm	1b, 4d[2], 3c[4], 1a
	Diabatic Flow	Unobstructed	1b, 7e, 1a[5]
		Upstream obstruction, G<1500 kg $m^{-2}s^{-1}$	As above
		Upstream obstruction, G>1500 kg $m^{-2}s^{-1}$	1b, 4d[2], 3b, 1a[5]
Annuli & Clusters		Spacer Separation >40D	1b, 6e, 1a[5,6]
		Spacer Separation <40D	Behaviour unresolved

Notes:

1. Regime boundaries ≡ equation validity limits are given by equation intersects unless otherwise specified.
2. Replace 4d with 5d if 1b:4d intersect occurs at x<0 (D<20mm) or x<0.1 (D>20mm).
3. Reduce regime boundary qualities by ~0.1.
4. Replace 3c with 3b for non-distilled water or settling length <60D.
5. Regime boundary given by appropriate critical heat flux correlation in diabatic flow case.
6. Use predryout equations with D=4 Area/non-dried perimeter if only some surfaces are dry.

in round tube adiabatic flows are consistent with visual classifications of bubble flow, annular flow, annular flow with entrained bubbles in the film, and (for high mass flux flows where film stripping might be expected) dry wall flows. It should be noted that consistency of data with a given equation does not necessarily imply that the flow structure is that originally envisaged in the equation development. Thus, the 'plug', 'slug', 'sluggish annular', 'annular', 'stratified froth', and 'froth' flow data from [10] are all consistent with equation (1d), which was originally developed for 'annular' flows only.

Changes in regime type caused by heat transfer effects are not unexpected but similar changes caused by entrance region and obstruction effects are less so. In the case of adiabatic flow, a possible explanation can be found by examining the non-dimensional velocity profiles inferred from the friction factor equations associated with the different regimes. Thus, for example, equation (4), which is valid for intermediate quality adiabatic flows in round tubes with short settling lengths (section 3.2), implies that a non-dimensional profile of the form

$$j^+ = 10 \ln y^+ - 37$$

describes the velocity profile except near the tube wall. This equation does not intersect the sublayer equation $j^+ = y^+$. Since there is evidence that both equations apply to different y^+ ranges, a point of inflection in the velocity profile is implied. From single phase theory [23], such velocity profiles are expected to be unstable. It is thus not surprising that for longer upstream settling lengths (section 3.1), equation (4) is replaced by equation (2), implying a core velocity profile given by

$$j^+ = 5 \ln y^+ - 3.05 .$$

This profile is identical to that found in the 'buffer' region of single phase flows and is tangential to the sublayer equation at $y^+ = 5$, implying a stable velocity profile. Thus, the entrance region involves an evolution of flow regime as well as the expected velocity profile development in each regime.

4.2 Entropy Production Rate and Regime Boundaries

A hypothesis which may prove useful in estimating regime boundaries is that the cross-sectional averaged entropy production rate is continuous at the regime boundary. As discussed in [24] and [25], where there are no chemical changes, entropy production rate per unit volume is given by

$$g = A + B + C$$

where $A = (\underset{\sim}{\tau} : \nabla \underset{\sim}{j})/T$

= contribution from viscous dissipation,

$B = (\underset{\sim}{q} \cdot \nabla \ln T)/T$

= contribution from heat transfer

$C = (\rho_\ell \underset{\sim}{j}_\ell \cdot \underset{\sim}{\Lambda}_\ell + \rho_g \underset{\sim}{j}_g \cdot \underset{\sim}{\Lambda}_g)/T$

= contribution from flow redistribution

At our present stage of understanding, these quantities cannot be averaged over a flow cross section. However, in order to obtain an estimate of parameters involved, it is reasonable to suppose that

$$\langle A \rangle \sim \tau_w \langle j \rangle / (T_w D)$$

and $$\langle B \rangle \sim q \ln T / (T_w D)$$

Thus, continuity of <g> for adiabatic flows (<B> = 0) with no obstruction or entrance effects (<C> = 0) implies continuity of wall shear and hence of friction factor at a regime boundary.

Since wall temperatures in pre-dryout diabatic flows are close to the saturation temperature, <B> is approximately continuous across pre-dryout diabatic regime changes and, for these conditions together with <C> = 0, regime changes again occur making friction factor plots continuous.

The hypothesis implies that, for <C> = 0, heat transfer induced dryout occurs when

$$[\tau_w \langle j \rangle / T_w]^{\text{dryout}}_{\text{pre-dryout}} \sim -[q \ln T_w / T_w]^{\text{dryout}}_{\text{pre-dryout}}$$

Since $T_w \simeq T_{sat}$ for pre-dryout flows, this implies that dryout depends on the post-dryout heat transfer coefficient and on the post-dryout and pre-dryout friction factors. The above equation is consistent with the observed effects of surface roughness influences on the onset of dryout [26] and of larger temperature rises occurring with lower quality and lower mass flux dryouts where there are larger step changes in friction factor. Furthermore, differences in empirical dryout correlations for round tubes and rod clusters can, under the present hypothesis, be associated with different friction factor behaviour for these two geometries.

Similarly, the fact that lower mass flux and low quality friction factors (generally given by equation (1b)) differ in behavour to higher mass flux and higher quality friction factors is consistent with the tendency for empirical dryout correlations to be split into high and low mass flux or quality ranges or to apply only to a limited range.

Introduction of the flow redistribution contribution to entropy production rate, <C>, qualitatively explains the observed effects of spacers and other flow disturbing influences on regime boundaries in both adiabatic and diabatic flows. It is worth noting that spacer distribution effects have been observed to have strong influence on dryout [27], [28].

Since there is considerable qualitative agreement between observed behaviour and the implications of a supposition of a requirement of continuity of entropy production rate across a regime boundary, it is suggested that even though terms in the entropy production rate expression cannot be evaluated exactly the concept may be useful in suggesting parameters which should appear in dryout correlations. It may also be used to suggest methods of incorporating spacer and other effects into calculation techniques. Adaptation to semi-local conditions in subchannel analyses may also prove useful.

5. CONCLUSIONS

Association of flow regimes with physical effects rather than appearance allows regime types and boundaries to be determined quantitatively rather than qualitatively.

Empirical analysis of regime types and regime boundaries as defined by frictional characteristics, and of the effects of various influences on these regime types and boundaries, appears to be consistent with the hypothesis that regime changes occur such that there is no step change in the entropy production rate. This hypothesis may prove useful in predicting regime transitions (including that associated with the heat transfer crises) for any flow condition. Techniques have been presented for estimating friction factors for a wide variety of steam-water flow situations.

6. ACKNOWLEDGEMENT

Helpful discussions with Professor J.J. Thompson, Head, School of Nuclear Engineering, U.N.S.W., are gratefully acknowledged.

7. REFERENCES

1. Wallis, G.B. 'One-Dimensional Two-Phase Flow' McGraw Hill, New York, 1969.
2. Zuber, N., Staub, F.W., Bijwaard, G., and Kroeger, P.G. 'Steady State and Transient Void Fraction in Two Phase Flow Systems' GEAP 5417, Jan. 1967, General Electric Co., San Jose, Calif.
3. Choe, W.G., and Weisman, J. 'Flow Patterns and Pressure Drop in Cocurrent Vapour-Liquid Flow' Department of Chemical and Nuclear Engineering, University of Cincinnati, Ohio, 1974.
4. Beattie, D.R.H., 'Two-phase Flow Structure and Mixing Length Theory' Nuclear Engineering and Design, Vol 21, 1972 pp 46-64.
5. Einstein, A., 'A New Determination of Molecular Dimensions' Annalen der Physik, Vol 19, 1906, pp 289-306.
6. Taylor, G.I., 'The Viscosity of a Fluid Containing Small Drops of Another Fluid' Proceedings of the Royal Society, Vol 138, 1932, pp 41-48.
7. Beattie, D.R.H., 'A Note on the Calculation of Two-Phase Pressure Losses', Nuclear Engineering and Design, Vol 25, 1973, pp 395-402.
8. Beattie, D.R.H., 'Drag Reduction Phenomena in Gas-Liquid Systems' Proceedings of the International Conference on Drag Reduction, B.R.H.A., Sept 1974.
9. Schraub, F.A., Simpson, R.L., and Janssen, E. 'Air-Water Flow Structure Data for a Round Tube, Concentric and Eccentric Annulus, and Nine-rod cluster' GEAP 5739, Jan. 1969, General Electric Co., San Jose, Calif.
10. Richardson, B.L., 'Some Problems in Horizontal Two-Phase Two-Component Flow' ANL-5949, Dec. 1958, Argonne National Laboratory, Lemont, Ill.
11. Beattie, D.R.H., 'Two-phase Pressure Losses:- Flow Regime Effects and Associated Phenomena', AAEC/TN589, May 1971, Australian Atomic Energy, Commission, Lucas Heights, Australia.
12. Gaspari, G.P., Lombardi, C., and Peterlongo, G. 'Pressure Drops in Steam-Water Mixtures' CISE R 83, Jan. 1964, Centro Informazioni Studi Esperienze Milano, Italy.
13. Berkowitz, L., et al. 'Results of Wet Steam Cooling Experiments: Pressure Drop, Heat Transfer and Burnout Measurements with Round Tubes' CISE-R-27, Oct. 1960, Centro Informazioni Studi Esperienze, Milano, Italy.
14. Moen, R.H. 'An Investigation of the Steam-Water System at High Pressure and High Temperatures' Ph.D Thesis, University of Minnesota, 1956.
15. Fukuda, K., Kawada, A., and Kobori, T. 'Two-Phase Flow characteristics in a Horizontal Tube and its Application to Quality Meter' SN941-74-57, Sept. 1974, Power Reactor and Nuclear Fuel Development Corporation, Ibaraki, Japan.
16. Era, A., et al. 'Heat Transfer Crisis and Pressure Drop for Steam-Water Mixtures at 70 kg/cm^2 Flowing Upwards and Downwards in Circular Conduits' CISE-R-185, Jan. 1967, Centro Informazioni Studi Esperienze, Milano, Italy.
17. Adorni, N., et al. 'Heat Transfer Crises with Steam-Water Mixture in Complex Geometries: Experimental Data in Annuli and Clusters' CISE-R-123, 1966, Centro Informazioni Studi Esperienze, Milano, Italy.
18. Tarasova, N.V., et al. 'Pressure Drop of Boiling Subcooled Water and Steam-Water Mixture Flowing in Heated Channels' Proc. 3rd International Heat Transfer Conference, 1966.
19. Moeck, E.O. 'Annular-Dispersed Two-Phase and Critical Heat Flux' AECL 3656, May 1970, Atomic Energy of Canada Limited, Chalk River, Canada.
20. Nylund, O. et al. 'Hydrodynamic and Heat Transfer Measurements on a Full-Scale Simulated 36-Rod BHWR Fuel Element with Non-Uniform Axial and Radial Heat Flux Distribution' FRIGG-4, ASEA-ATOM, Vasteras, Sweden.
21. Matzner, B., and Neill, J.S. 'Forced-Flow Boiling in Rod Bundles at High Pressure' DP 857, Sept. 1963, E.I. du Pont de Nemours and Co., Wilmington, Delaware.
22. Fredal, L., and Mayinger, F. 'Scaling of Two-Phase Friction Pressure Drop' European Two-Phase Flow Group Meeting, Harwell, June 1974.

23. Schlichting, H. P445, 'Boundary Layer Theory', 6th ed. McGraw Hill, New York, 1968.
24. Bird, R.B., Stewart, W.E., and Lightfoot, E.N. 'Transport Phenomena' Wiley, New York, 1960.
25. Bird, R.B., Curtiss, C.F., and Hirschfelder, J.O. 'Fluid Mechanics and the Transport Phenomena' , Chemical Engineering Progress Symposium Series, No. 16, Vol.51, 1955, pp 69-85.
26. Burck, E., Hufschmidt, W. and De Clercq, E. 'The Influence of Artificial Roughness on the Increase in Critical Heat Flux for Water under Forced convection in Annuli' EUR 404d, 1968.
27. Ilic, V. and Lawther, K.R. 'The Effect of Spacers on Burnout in an Annulus with a Uniformly Heated Central Rod Cooled by Freon-12' First Australasian Conference on Heat and Mass Transfer, Monash University, May, 1973.
28. Ilic, V. 'An Examination of the Influence of Spacers on Burnout in an Annulus cooled by Freon-12' AAEC/E349, April, 1975, Australian Atomic Energy Commission, Lucas Heights, Australia.

LETTERS TO THE EDITOR

To the Editor:

Kopalinsky and Bryant in "Friction Coefficients for Bubbly Two-Phase Flow in Horizontal Pipes," *AIChE J.*, **22**, 82, (1976), have presented an interesting analysis of pressure drop data for bubbly two-phase flow. The data were analysed in the framework of a homogeneous model in which the calculated acceleration component, which was significant near the test section exit in some cases, was subtracted to leave the frictional component. Data for this component were curve-fitted, resulting in a stated friction factor dependence on Reynolds number, flow quality, axial position, and tube diameter. Expressions for the friction factor in conjunction with the calculated acceleration component agreed well with the data, and it was suggested that these could be applied more generally for this class of flow.

The general applicability of the expressions must, however, be questioned on at least two points: (1) the authors imply that the stated dependence of friction on distance is more likely to be a compensation for incorrect assessment of the acceleration component than a true comment on friction, thus raising doubts about the calculational procedures for pressure drop for conditions when the relative magnitudes of the frictional and acceleration components differ from those studied by the authors; and (2) at the lower limit of bubbly flow (zero quality), the recommended friction equations are inconsistent with standard single phase equations.

The data analysed by the authors (Kopalinsky, 1971) have been previously shown (Beattie, 1973) to be consistent with a two-phase version of the single phase Colebrook equation (notation as in Kopalinsky and Bryant, 1976):

$$1/\sqrt{C_f} = 3.48 - 4\log[2\epsilon/D + 9.35/Re\sqrt{C_f}] \quad (1)$$

in which ϵ is an effective surface roughness dimension; and C_f and Re are appropriately defined for the particular two-phase regime. For the bubbly regime

$$C_f = \frac{D(dP/dz)_{\text{friction}}}{2Gu}$$

and

$$Re = \frac{DG}{\mu_l(1 + 2.5\alpha)}.$$

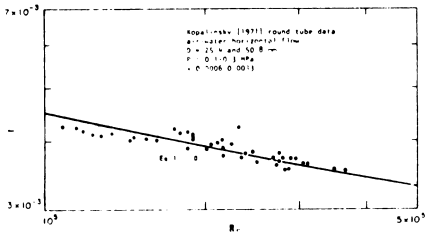

Fig. 1. Friction factor-Reynolds number relation for two-phase bubble flow.

Figure 1 shows that representative data of Kopalinsky (1971) measured between pressure taps 1 and 5 (these data were chosen because of the small contribution from the acceleration component) as analysed by Beattie (1973) agree with equation (1) at least as well as with the recommended equations of Kopalinsky and Bryant (1976).

In view of the above and because equation (1) has been shown to be valid for a wide range of bubble flows (see e.g. Beattie, 1975), allows for surface roughness effects, and can be justified from basic theoretical considerations, this equation is clearly preferable for prediction of the frictional component of bubbly flows.

D. Beattie,
AAEC Research Establishment,
Lucas Heights, N.S.W.,
Australia.

LITERATURE CITED

Beattie, D. R. H., "A Note on the Calculation of Two-Phase Pressure Losses," *Nuc. Eng. and Des.*, **25**, 395 (1973).

———, "Friction Factors and Regime Transitions in High Pressure Steam-Water Flows," ASME paper 75-WA/HT4 (1975).

Kopalinsky, E. M., "A Study of Bubbly Two-Phase Flow," Ph.D. thesis, School of Mechanical & Industrial Engineering, The University of New South Wales, Sydney, Australia (1971).

———, and R. A. A. Bryant, "Friction Coefficients for Bubbly Two-Phase Flow in Horizontal Pipes," *AIChE J.*, **22**, 82 (1976).

Reply

Quite clearly Mr. Beattie has misunderstood the paper. We have not implied "dependence of friction on distance is more likely to be a compensation for incorrect assessment of the acceleration component etc." What we say is that the average friction coefficient depends on compressibility and not on the pipe length alone and that the coefficients are accurate in the range specified. Error in assessment of the acceleration component occurs only in a narrow region near the pipe exit when the Mach number there is close to unity. The lower limit of bubbly flow (zero quality) suggested by Mr. Beattie highlights the danger of drawing conclusions from theoretical studies which are not paralleled by experimental work. In practice, a stable bubbly flow regime can be sustained only over a relatively restricted range of flow parameters. It is not possible to achieve a continuous transition from a mixture quality of zero to a mixture quality of unity. Thus correlations for the bubbly flow regime cannot be expected to converge to those for single phase flows. Indeed it is somewhat remarkable that friction coefficients for water flows could be estimated from the equations we propose with a maximum error of only 14% and average errors substantially less.

We note that our data for low Mach number flows is predicted by Mr. Beattie's equation (1).

R. A. A. Bryant
The University of New South Wales
Kensington, N.S.W. Australia
E. M. Kopalinsky
University of Birmingham
Birmingham, England

PAPER D3

SECOND
INTERNATIONAL CONFERENCE ON
PRESSURE SURGES

22nd-24th September 1976

PRESSURE PULSE AND CRITICAL FLOW BEHAVIOUR IN DISTRIBUTED GAS-LIQUID SYSTEMS

D.R.H. Beattie B.Sc., B.E., M.Eng.Sc.

Australian Atomic Energy Commission

Summary

Two-phase propagation phenomena are relevant to water-cooled nuclear reactor safety analysis. The concept of a semi-empirical 'distribution parameter', originally developed for predicting average voidages in distributed two-phase flow systems, is considered. Two-phase mixing length theory provides a basis for the first-principle evaluation of the distribution parameter, which allows for two-phase flow regime effects, and also enables extension of the concept to the prediction of average kinetic energy, momentum, and other fluxes. Parameters so obtained are used to obtain expressions for distributed two-phase flow pressure pulse and critical flow velocities. In contrast to single-phase flow behaviour, these velocities are not equal in two-phase flows.

Theoretical expressions for voidage, pressure pulse velocity, and critical flow velocity compare satisfactorily with relevant data. Two-component data are used for these velocity comparisons to avoid the problem of thermal non-equilibrium.

Held at The City University, London, England.
Organised and sponsored by BHRA Fluid Engineering, Cranfield, Bedford, England in conjunction with The City University, London.
Copyright BHRA Fluid Engineering 1976.

NOMENCLATURE

a	pressure pulse propogation velocity
A	flow area
C_ℓ	specific heat of liquid
C_p	specific heat of gas at constant pressure
C_v	specific heat of gas at constant volume
C_o	distribution parameter
C_1-C_4	constants appearing in flow structure theory
D	diameter
f	friction factor, $2\ \tau_w/(\bar{\rho}\ \langle j\rangle^2)$
G	mass flux
j	mixture velocity, $u_\ell(1-\alpha) + u_g\ \alpha$
j^*	shear velocity, $\sqrt{\tau_w/\bar{\rho}}$
j^+	non-dimensional velocity, j/j^*
k	mixing length coefficient
K	kinetic energy flux averaged over cross section
M	momentum flux averaged over cross section
P	pressure
Q	volume flow
Re	Reynolds number, $D\ G/\mu_\delta$
u	local phase velocity
V	drift velocity of gas
x	quality
y	wall distance
y^+	non-dimensional wall distance, $y\ j^*\ \rho/\mu_\delta$
z	axial dimension
α	local voidage
β	volume flow ratio, $Q_g/(Q_g + Q_\ell)$
γ	mixture polytropic index
δ	sublayer thickness
ε	surface roughness height

μ	dynamic viscosity
ρ	density
$\bar{\rho}$	$\rho_\ell(1-\beta) + \rho_g\beta$
τ	shear stress

Subscripts

f	frictional component
G	gravitational component
g	gas value
ℓ	liquid value
δ	value at position δ
ε	value at position ε
w	value at wall

Operator

<--->	quantity is averaged over the flow cross section

1. INTRODUCTION

Pressure surges and their effects give rise to engineering problems in a number of industrial fields. In situations where there is only partial understanding of mechanisms involved, as in the flow of boiling water in light water reactors, the designer incorporates adequate safety factors to compensate for any margin of ignorance.

In the case of the above example, however, considerations which include public concern for safety aspects related to reactor depressurisation during a hypothetical loss-of-coolant accident, have led to a situation where greater understanding of some two-phase flow processes is desirable.

In this paper, an outline is given of a two-phase flow structure theory developed from Prandtl mixing length concepts. The flow structure theory is used to develop expressions for choked flow and pressure pulse propagation velocities, both being relevant to reactor safety, for the special case of two-phase low quality distributed flow, (i.e. those flows where the liquid phase is continuous throughout the flow section). Emphasis is placed on adequate allowance for phase and velocity distribution effects rather than a rigorous derivation of propagation phenomena.

The theory assumes no mass transfer between phases which will be considered elsewhere; comparative data analysis was confined to two-component systems to ensure that this assumption was valid.

The theory is developed for round ducts. Where appropriate, the concept of equivalent diameter is assumed to apply. The extension of the theory to gas-phase continuous, distributed two-phase flows (also relevant to reactor safety studies) is straight-forward but has not been presented here owing to a lack of relevant data to test its validity.

Consequences of intermediate steps in the theory which relate to velocity profiles, friction factors, voidage, etc., have been* (e.g. Refs. 1,2) or will be (e.g. Ref. 3) examined in more detail elsewhere.

2. THEORY

2.1 Two-phase Flow Structure

2.1.1 Bubble flow velocity defect equation

The present theory is based on the phase and velocity distribution expressions given in Ref. 4. By assuming that turbulence is confined to one phase only of a two-phase flow, it was shown that the phase and velocity distributions for bubble flow are given by

$$(1-\alpha)^{3/2} = (1-\alpha(y_o))^{3/2} - \frac{3C_1\sqrt{\tau_w/\rho_\ell}}{2k} \ln\frac{y}{y_o} , \quad (1)$$

and

$$\alpha = C_1 u_\ell + C_2 , \quad (2)$$

where C_1 and C_2 are unknown coefficients, and y_o is a suitably chosen reference wall distance.

The equation may be simplified by linearising $(1-\alpha)^{3/2}$ about a suitably chosen mean value α_m:

---

*The theoretical basis of phenomena discussed has not however been presented in Refs.1,2

$$(1-\alpha)^{3/2} = (1-\alpha_m)^{3/2}(1-(\alpha-\alpha_m)/(1-\alpha_m))^{3/2} \simeq (1-\alpha_m)^{3/2} - \frac{3}{2}(\alpha-\alpha_m)(1-\alpha_m)^{\frac{1}{2}} .$$

Substituting this and equation (2) into equation (1), and choosing α_m such that

$$\rho_\ell (1-\alpha_m) = \rho_\ell (1-\beta) + \rho_g \beta = \bar{\rho} \text{ leads to}$$

$$u_\ell = u_\ell(y_o) + \frac{j^*}{k} \ell n \frac{y}{y_o}$$

where $j^* = \sqrt{\tau_w/\bar{\rho}}$. The velocity equation is of the form of a velocity defect equation. It is convenient to express this in terms of the mixture velocity $j = u_\ell(1-\alpha) + u_g \alpha$ instead of the liquid velocity u_ℓ. Assuming $u_\ell - u_\ell(y_o) \simeq j - j(y_o)$, then

$$j = j(y_o) + \frac{j^*}{k} \ell n \frac{y}{y_o} . \tag{3}$$

2.1.2 Sublayer boundary conditions

For smooth wall ducts, the two-phase laminar shear is treated as $\tau = d(\mu j)/dy$ to allow for variation in two-phase viscosity. The sublayer volumetric flux profile meets that of the turbulent core at a distance δ from the duct wall. The wall shear is then

$$\tau_w = \frac{d}{dy}(\mu j) = \frac{\mu_\delta j_\delta}{\delta} .$$

Rearranging, and assuming (as in single-phase flow) that the resulting dimensionless group is constant, gives

$$j_\delta/j^* = \bar{\rho}\, j^*\, \delta/\mu_\delta = C_3. \tag{4a}$$

Sublayer viscosity depends on the local topology. Using the theoretical expressions of Einstein (Ref. 5) and Taylor (Ref. 6), and assuming $\alpha_\delta = \beta$, then, for a sublayer containing rigid surfaced bubbles (as might be expected for impurities in a liquid of polar molecules),

$$\mu_\delta = \mu_\ell (1 + 2.5\beta), \tag{5a}$$

and for sublayer bubbles where surface movement can occur,

$$\mu_\delta = \mu_\ell \left(1 + \frac{2.5\,\mu_g + \mu_\ell}{\mu_g + \mu_\ell}\,\beta\right). \tag{5b}$$

The above adaptation of single-phase, smooth tube sublayer theory may equally apply to a rough tube, in which case, for roughness height ε,

$$j_\varepsilon/j^* = C_4, \tag{4b}$$

where C_4 is a constant.

2.1.3 Non-dimensional bubble flow turbulent core velocity profile

Substitution of equations (4) into equation (3), assuming single-phase values for the various constants lead to,

$$j^+ = 5.5 + 2.5 \ell n\, y^+ \text{ (smooth tubes)}, \tag{6a}$$

and

$$j^+ = 8.5 + 2.5 \ell n\, (y/\varepsilon) \text{ (rough tubes)}, \tag{6b}$$

as in single-phase flow, where

$$y^+ = \bar{\rho}\, j^*\, y/\mu_\delta = \frac{y}{D}\, Re \sqrt{\frac{f}{2}} ,$$

and

$$j^+ = j/j^* = \frac{j}{\langle j \rangle} \sqrt{\frac{2}{f}} ,$$

where f is the friction factor and Re is the Reynolds number,

$$f = \frac{2\tau_w}{\rho \langle j \rangle^2} , \quad Re = D\, G/\mu_\delta$$

with μ being given by equations (5).

2.1.4 Friction-factor equation

As in single-phase flow, averaging equations (6) leads to friction factor expressions which may be generalised as Colebrook's equation:

$$1/\sqrt{f} = 3.48 - 4 \log (2\varepsilon/D + 9.35/Re\sqrt{f}) . \qquad (7)$$

2.2 The Distribution Parameter

2.2.1 Relevance to average voidage behaviour

The distribution parameter was introduced by Zuber and his co-workers in their generalisation and extension of earlier work on two-phase average voidage behaviour (e.g. Ref. 7). The parameter is a correlation coefficient accounting for the fact that the average gas velocity is greater than that of the mixture partly because the gas concentrates in faster moving regions.

Following Zuber et al. (Ref. 7), the local gas velocity u_g is faster than the local mixture velocity j by a drift velocity V assumed constant over the cross section

$$u_g = j + V. \qquad (8)$$

Therefore $\langle \alpha u_g \rangle = \langle \alpha j \rangle + \langle \alpha \rangle V$

where <---> indicates the average value over the cross-section. $\langle \alpha u_g \rangle$ and $\langle j \rangle$, being the superficial gas and mixture velocities, are usually known, but $\langle \alpha j \rangle$ is not. Introducing the distribution parameter

$$C_o = \frac{\langle \alpha j \rangle}{\langle \alpha \rangle \langle j \rangle} , \qquad (9a)$$

then the mean gas velocity $\langle \alpha u_g \rangle / \langle \alpha \rangle$ is

$$\langle \alpha u_g \rangle / \langle \alpha \rangle = C_o \langle j \rangle + V. \qquad (10)$$

Empirical values of C_o and semi-empirical values of V, both of which are approximately constant for a given flow regime, are given in Ref. 7. Equation (10) can thus be used for predicting $\langle \alpha \rangle$, although its form, which gives $\langle \alpha u_g \rangle / \langle \alpha \rangle$ instead of $\langle \alpha \rangle$, is physically more realistic since raw void data may be analysed by plotting $\langle \alpha u_g \rangle / \langle \alpha \rangle$ against $\langle j \rangle$, the resulting straight line giving values of C_o and V directly for the flow examined.

2.2.2 Analytic prediction of distribution parameter values

Although Zuber et al. (Ref. 7) present a sound theoretical basis for C_o, they give empirical values for it. The present theory allows C_o to be predicted from first principles for most turbulent distributed flows. Exceptions are subcooled boiling flows and some entrance region flows.

Considering $\langle \alpha j \rangle = \frac{1}{A} \int_A \alpha\, j\, dA,$

equation (1) indicates that the voidage extrapolates to zero not at the wall but at a given distance from it. Defining δA as the area where the voidage is zero, then

$$\langle \alpha j \rangle = \frac{1}{A} \int_{A-\delta A} \alpha j dA.$$

Analysis of data where both void and velocity profiles are given indicates that for most flows, $j \tilde{=} j_{max}$ in $A-\delta A$. Therefore

$$\langle \alpha j \rangle = \frac{j_{max}}{A} \int_{A-\delta A} \alpha dA = \frac{j_{max}}{A} \int_{A} \alpha dA,$$

$$= j_{max} \langle \alpha \rangle.$$

From the definition of C_o in equation (9a)

$$C_o = j_{max}/\langle j \rangle. \tag{11}$$

Manipulating equations (6) results in

$$C_o = 1 + 2.65 \sqrt{f}\ , \tag{12}$$

where f is given by equation (7).

2.2.3 Extension to the evaluation of momentum and kinetic energy fluxes

Considering the importance of momentum and kinetic energy fluxes in the evaluation of flow propagation phenomena, for example, it is unfortunate that two-phase treatments of these are nearly always incorrect. These treatments use a voidage correlation in one form or another to treat velocities appearing in the momentum and kinetic energy fluxes. A more rigorous treatment than these shows that this is invalid: a voidage correlation gives information on the double correlation $\langle \alpha j \rangle$ which cannot be used to give information on higher order correlations $\langle \alpha j^2 \rangle$ and $\langle \alpha j^3 \rangle$, for these need to be reduced to evaluate average momentum and kinetic energy fluxes. The mistake arises from a loose one-dimensionalisation of point equations by replacing ∇ with $\frac{d}{dz}$, thus overlooking the fact that rigorous averaging of the point equations implies that $\frac{d}{dz}$ operates on cross sectional averaged quantities.

The higher order correlations can be treated with the present model. As defined by equation (9a), C_o could be converted to equation (11) for most flows because the local voidage is usually zero in the region where the velocity profile is varying rapidly. If this is true for the α profile, it is also true for an αj^n profile, and equation (9a) can be generalised to

$$C_o = \frac{\langle \alpha j^n \rangle}{\langle \alpha j^{n-1} \rangle \langle j \rangle} \tag{9}$$

which, in conjunction with equation (12), can be used to evaluate distributed flow momentum and kinetic energy fluxes.

Consider the cross section averaged momentum flux

$$M = \langle \rho_\ell u_\ell^2 (1-\alpha) + \rho_g u_g^2 \alpha \rangle.$$

Assuming ρ_ℓ and ρ_g are constant over a cross section, applying equations (8) and (9) and, as in single phase flow, assuming $\langle j^2 \rangle = \langle j \rangle^2$,

$$M = \rho_\ell \langle j \rangle^2 + (\rho_\ell - \rho_g) \langle \alpha u_g \rangle (C_o \langle j \rangle + V) + \rho_\ell V^2 \left\langle \frac{\alpha}{1-\alpha} \right\rangle .$$

Unfortunately $\left\langle \frac{\alpha}{1-\alpha} \right\rangle$ cannot at present be readily evaluated. Since $V \ll \langle j \rangle$ in regions where accurate assessment of M is required, it is reasonable to neglect terms with V. So doing and then converting to the more widely used parameters, mass flux G and quality x,

$$M = \frac{G^2}{\rho_\ell}\left\{1 + x\left(\frac{\rho_\ell}{\rho_g} - 1\right)\right\}\left\{1 - (C_o-1)\, x\left(\frac{\rho_\ell}{\rho_g} - 1\right)\right\} . \qquad (13)$$

The term $1-(C_o-1)\, x\left(\frac{\rho_\ell}{\rho_g} - 1\right)$ represents a correction to the homogeneous model.

Similarly, for turbulent two-phase distributed flow, the average kinetic energy flux K becomes

$$2K = \langle \rho_\ell u_\ell^3 (1-\alpha) + \rho_g u_g^3 \alpha \rangle$$

$$= \frac{G^3}{\rho_\ell^2}\left\{1 + x\left(\frac{\rho_\ell}{\rho_g} - 1\right)\right\}^2\left\{1 - (C_o^2-1)\, x\left(\frac{\rho_\ell}{\rho_g} - 1\right)\right\} . \qquad (14)$$

In general

$$\langle (\rho_\ell(1-\alpha) + \rho_g\alpha) j^n \rangle = \frac{G^n}{\rho_\ell^{n-1}}\left\{1 + x\left(\frac{\rho_\ell}{\rho_g} - 1\right)\right\}^{n-1}\left\{1 - (C_o^{n-1}-1)\, x\left(\frac{\rho_\ell}{\rho_g} - 1\right)\right\} .$$

2.3 Propagation Phenomena

The theory presented in this section is not completely rigorous but was developed to examine phase and velocity distribution effects using the theory of Section 2.2. To test adequately the theoretical consequences of phase and velocity distribution effects, theory and later data analysis do not take mass transfer into consideration. Compressibility of the liquid is neglected, and phase densities are assumed constant over a flow cross section.

Equations solved are those for mass and momentum, which are made one-dimensional by averaging point equations over a flow cross section (this being done since propagation velocities of interest are axial propagation velocities averaged over the flow cross section):

$$\frac{\partial}{\partial z}\{\rho_\ell \langle u_\ell(1-\alpha)\rangle + \rho_g \langle u_g \alpha \rangle\} + \frac{\partial}{\partial t}\{\rho_\ell (1-\langle\alpha\rangle) + \rho_g \langle\alpha\rangle\} = 0 , \qquad (15)$$

and

$$\frac{\partial F}{\partial z} + \frac{\partial M}{\partial z} + \frac{\partial P}{\partial z}\Big|_f + \frac{\partial P}{\partial z}\Big|_G + \frac{\partial}{\partial t}\{\rho_\ell \langle u_\ell (1-\alpha)\rangle + \rho_g \langle u_g\alpha \rangle\} = 0 . \qquad (16)$$

Instead of an energy equation, an assumption is made that density changes isentropically. From Ref. 8 this can be expressed as

$$P\,\rho_g^{-\gamma} = \text{const.} \qquad (17)$$

where

$$\gamma = \frac{x\,C_p + (1-x)\,C_\ell}{x\,C_v + (1-x)\,C_\ell} . \qquad (18)$$

Note that for the case of no mass transfer, conservation of mass can be given for each phase:

$$\frac{\partial}{\partial z}\rho_\ell \langle u_\ell (1-\alpha)\rangle + \frac{\partial}{\partial t}\rho_\ell \langle 1-\alpha \rangle = 0 , \qquad (15a)$$

and

$$\frac{\partial}{\partial z}\rho_g \langle u_g\alpha \rangle + \frac{\partial}{\partial t}\rho_g \langle\alpha\rangle = 0 . \qquad (15b)$$

2.3.1 Critical flow

Critical flow is considered for the steady state situation. Equations (15a and b) for the conservation of mass become

$$\frac{d < u_\ell (1-\alpha) >}{dz} = 0 ,$$

and $$\frac{d}{dz} < u_g \alpha > = - \frac{< \alpha u_g >}{\rho_g} \frac{d\rho_g}{dP} \cdot \frac{dP}{dz} ,$$

Adding, $$\frac{d<j>}{dz} = - \frac{< \alpha u_g >}{\rho_g} \frac{d\rho_g}{dP} \cdot \frac{dP}{dz} .$$

Consider $\frac{dM}{dz}$ appearing in the steady state momentum equation. In terms of G and <j>

$$\frac{dM}{dz} = \frac{d}{dz} \{ C_o G <j> + (1-C_o) \rho_\ell <j>^2 \}$$

$$= \{ C_o G + 2(1-C_o) \rho_\ell <j> \} \frac{d<j>}{dz}$$

$$= -\{ C_o G + 2(1-C_o) \rho_\ell <j> \} \frac{< \alpha u_g >}{\rho_g} \frac{d\rho_g}{dP} \frac{dP}{dz} .$$

Equation (16) then becomes

$$\frac{dP}{dz} = \frac{\frac{dP}{dz}\Big|_G + \frac{dP}{dz}\Big|_f}{\{ C_o G + 2(1-C_o) \rho_\ell <j> \} \frac{< \alpha u_g >}{\rho_g} \frac{d\rho_g}{dP} - 1} .$$

The critical condition occurs when $\frac{dP}{dz}$ becomes infinite, i.e. when

$$\{ C_o G + 2(1-C_o) \rho_\ell <j> \} \frac{< \alpha u_g >}{\rho_g} \frac{d\rho_g}{dP} = 1 .$$

Rearranging and using equation (17), the critical mass flux is given by

$$G_{crit} = \frac{\{ \gamma P \rho_g / x \}^{\frac{1}{2}}}{\{1 - (C_o - 1)(1 + 2x \left(\frac{\rho_\ell}{\rho_g} - 1 \right))\}^{\frac{1}{2}}} . \qquad (19)$$

The numerator is the homogeneous model prediction, and the denominator represents a correction to the homogeneous model. Since, from equation (12), C_o is slightly dependent on G, equation (19) must be solved iteratively.

2.3.2 Pressure pulse propagation velocity

During the passage of a pressure pulse, a fluid element undergoes a rapid change in which friction, gravity, and the axial variation in momentum are assumed to be negligible. Under these circumstances, equation (16) becomes

$$\frac{\partial P}{\partial z} + \frac{\partial}{\partial t} \{ \rho_\ell < u_\ell (1-\alpha) > + \rho_g < u_g \alpha > \} = 0 . \qquad (20)$$

The neglected terms are those causing pressure pulse dissipation and slight changes to propagation velocity. Operating on equations (15) and (20) by $\frac{\partial}{\partial t}$ and $\frac{\partial}{\partial z}$ respectively, subtracting and assuming a linear variation of density with pressure,

$$< \rho_\ell (1-\alpha) + \rho_g \alpha > = < \rho_\ell (1-\alpha) + \rho_g \alpha >_o + (P-P_o) \frac{d}{dP} < \rho_\ell (1-\alpha) + \rho_g \alpha >$$

leads to

$$\frac{\partial^2 P}{\partial z^2} - \frac{1}{a^2} \frac{\partial^2 P}{\partial t^2} = 0, \qquad (21)$$

with

$$\frac{1}{a^2} = \frac{d}{dP} < \rho_\ell (1-\alpha) + \rho_g \alpha > . \qquad (22)$$

Equation (21) is a statement that a pressure pulse will travel with velocity 'a' given by equation (22). Substituting equation (10) into equation (22) and expressing in terms of quality (this remains constant for no mass transfer):

$$\frac{1}{a^2} = \frac{d}{dP} \left\{ \rho_\ell + \frac{\rho_\ell \left(1 - \frac{\rho_\ell}{\rho_g}\right) x}{C_o \left\{1+x\left(\frac{\rho_\ell}{\rho_g} - 1\right)\right\} + \frac{\rho_\ell V}{G}} \right\} .$$

The bubble drift velocity V is a terminal velocity which will not change during a rapid transient, i.e. $\frac{dV}{dp} \sim 0$. By differentiating, re-expressing in terms of voidage, and then making use of equation (17),

$$a = \frac{\sqrt{\gamma P/\rho_g}}{\left\{ \frac{\rho_\ell}{\rho_g} <\alpha> - \left(\frac{\rho_\ell}{\rho_g} - 1\right) C_o <\alpha>^2 \right\}^{\frac{1}{2}}} .$$

Note that $\sqrt{\gamma P/\rho_g}$ is the gas only pressure pulse propagation velocity. Since $\rho_\ell/\rho_g >> 1$ in most cases

$$a = \frac{\sqrt{\gamma P/\rho_\ell}}{\left\{ <\alpha> (1-C_o <\alpha>) \right\}^{\frac{1}{2}}} . \qquad (23)$$

3. COMPARISON WITH DATA

To test the present theory, pressure pulse velocity and critical flow data had to satisfy the following requirements:

(a) the data needed to be two-component rather than one-component, thus ensuring no phase change effects;

(b) the liquid phase needed to be continuous throughout the flow cross-section; and

(c) the data needed to be for straight pipe turbulent flow (C_o cannot as yet be predicted for other systems).

As well as these requirements, ideally some additional information should be present in order that specific aspects of the theory may be tested (e.g. void data to give experimental C_o values, friction data to test equation (7) etc.).

Very few data were found in the literature satisfying these requirements. Only a few two-component distributed flow data were found and these were mainly for stationary liquid (pressure pulse propagation velocity) or for nozzle flow (critical flow).

It is straightforward enough to choose C_o values to make the theory fit these data, but it is more satisfying if data can be predicted with no empiricism involved in the choice of C_o. It must be remembered that presently defined maximum credible reactor accidents involve choked flow from a straight pipe, as discussed in the present theory.

It is not the intention of this paper to demonstrate the validity of the theories of sections (2.1) and (2.2) by direct comparison with data. Various aspects have been (e.g. Refs. 1,2) or will be (e.g. Ref. 3) examined in more detail elsewhere*.

Nevertheless, a set of void data, from Ref. 9, is compared with values predicted from equations (7), (10) and (12) in Fig. 1. The data are shown because they were obtained at the choked flow conditions discussed in the next paragraph. The experimental rather than the predicted choked flow, and the viscosity as defined by equation (5b) (this gave slightly better agreement with data than equation (5a), which is usually valid for air-water flows), were used in the Reynolds number. The data confirm the theory for the prediction of lower quality voidage. The curve corresponding to the higher void data is a theoretical curve for annular flow (Ref. 3). An empirical aspect of the annular flow theory is the voidage at the boundary between distributed flow and annular flow. For the data of Fig. 1, the theory indicates that this boundary occurs at a volume flow ratio of 76%. This is, therefore, the upper limit for which equation (19) can be expected to be valid.

Choked flow data (Ref. 9) corresponding to the void data of Fig. 1 are shown in Fig. 2, together with the present prediction (equations (5b), (7), (12), (18) and (19)) and the homogeneous model (equations (18) and (19) with $C_o = 1$). The present theory is acceptably close to the data except near the upper limit of the distributed flow regime.

Only one other set of choked flow data was found suitable for testing the present theory (Ref. 10). The data are shown in Fig. 3, together with the present and homogeneous theories. In the absence of any guide to viscosity, equation (5a) was used for the viscosity expression; the alternative causes little change in the final prediction. Data were in the pressure range 15-50 kPa at the choking plane and, for suitable comparison, velocities were normalised to the average pressure by multiplying by the square root of the average to individual pressure ratio for each data point. The present theory is closer to the data than the homogeneous model, although the theory considerably underpredicts some of the data.

Suitable pressure pulse velocity data for testing the theory were also hard to find. Data from Ref. 11 are shown in Fig. 4, together with predictions from the present theory (equations (5a), (7), (12), (18) and (23)), and the homogeneous model (equations (18) and (23) with $C_o = 1$). The predictions from the present theory are again acceptable and closer to the data than the homogeneous model. Phase and velocity distribution effects are clearly less than in the case of choked flow even though C_o values are comparable for Figs. 2, 3 and 4.

Most two-phase pressure pulse data involve stationary liquid through which gas is bubbled. Although C_o values cannot be predicted for these systems, there are several indications that values may be considerably higher than for flow systems. Data should then be further from the homogeneous model. Stationary liquid data from Refs. 12 and 13 are shown in Figs. 5 and 6. Although the data are further from the homogeneous model than in the case of a flowing liquid, equation (23) fits the data with suitable choices of C_o values which, although large compared with turbulent flow values, are reasonable for the systems examined.

---

*Note that present experimental methods for measuring two-phase momentum flux involve reaction determining techniques which homogenise the flow. Associated data are consequently closer to the homogeneous model than to the theory of Section 2.2.3, but this does not disprove the present theory as applied to pipe flow. The validity of the consequences of equation (13) as presented here is indirect confirmation of equation (13).

The present theory also indicates that, quite apart from phase and velocity distribution effects, pressure pulse velocities should be higher for stationary liquids. This arises from the effect of γ on pressure pulse velocity (equation 23). For stationary liquid, the mass flow is 100% gas, and equation (18) indicates $\gamma = C_p/C_v$ (the actual polytropic values - 1.4 for air and 1.3 for steam - were used instead of this), whereas for the flow systems considered, most of the mass is carried in the liquid phase, and, from equation (18), $\gamma \to 1$.

4. DISCUSSION

The present model involves no empiricism - at least for turbulent flow in straight pipes - and subsections of the model, such as those concerning voidage, etc., are consistent with reality. Furthermore, expected variations of C_o with geometry explain the observed dependence of choked flow on geometry, a fact which is ignored in most models. As such the model is superior to most comparable models. Nevertheless, its usefulness is limited because of the limited conditions for which the theory was developed and, in the case of choked flow, because the critical pressure must be presumed.

The basic flow structure theory on which the model is based, and immediate consequences of the flow structure theory, have been adequately confirmed (Refs. 1, 2, 3, 4). Unfortunately, the comparison of data and theory in section 3 indicates that the theory as applied to propagation phenomena is not as accurate as might be expected considering the apparent validity of the basic flow structure theory. Nevertheless, errors are acceptable when compared with those of other theories. For example, the root mean square errors for the data of Fig. 3 when compared with the present theory, the homogeneous model with $\gamma = 1.4$ (the value for air), the homogeneous model with $\gamma = 1$, and the theories of Ref. 9 and Ref. 14 are 19%, 29%, 34%, 82% and 445%, respectively.

One source of error in the case of pressure pulse velocity is the assumption of developed flow. Flow experiments necessarily involve pipework bends in the vicinity where propagation velocity is measured. Actual C_o values will consequently be larger than those predicted from equation (12) for developed flow. Consequently, pressure pulse velocity based on the assumption of developed flow will underpredict data (Fig.4).

While on the topic of pressure pulse propagation velocity, it is interesting to note that the present theory suggests a regime boundary criterion for distributed and separated (e.g. annular) flows. Equation (23) indicates that the pressure pulse velocity becomes very large as $\langle\alpha\rangle$ approaches $1/C_o$. Other work, Ref. 15 for example, indicates that separated flow pressure pulse velocity is approximately equal to that for gas only flowing. It is suggested that the regime change occurs such that there is no discontinuity in pressure pulse propagation velocity, i.e. at the intersect of equation (23) and the corresponding separated flow equation. This is consistent with the findings of Smith et al. (Ref. 16). That the transition should occur in the vicinity of $\langle\alpha\rangle \simeq 1/C_o$ is physically consistent with equation (10): according to that equation, increasing gas flow for a given liquid flow causes $\langle\alpha\rangle$ to approach $1/C_o$ and, for sufficient gas flow, separated flow must occur.

The theory of section (2.1), although apparently valid, is incomplete. In particular, the assumption that single phase flow structure coefficients apply to two-phase flows is not always true. In other cases, the theory holds but with different coefficients. Resulting friction factor equations corresponding to equation (7) are of the same form but with different coefficients (e.g. Ref. 1 and Ref. 2). For these flows, the basic principles of the theory still apply, but, for different friction regimes, the distribution parameter expression, equation (12), is replaced by $C_o = 1 + 0.66\ n\ \sqrt{f}$ where n is the coefficient of the log $Re\sqrt{f}$ term in the equation used to give f. Such distributed two-phase flows do occur (e.g. Ref. 1, section 5.3), although rarely. Normally, a change in friction regime induces a change of distributed flow to separated flow to avoid the step change in void behaviour implied by the step change in the value of C_o. The velocity profile for such distributed two-phase flows is steeper than normally encountered. The assumption of a flat core profile leading up to the distribution parameter expression (section 2.2.2) is thus more gross for these

flows. Errors may be significant in applying the theory to the kinetic energy flux, for example, where C_o^2 terms occur.

Finally, it is worth noting that the present theory indicates that, unlike the single phase flow case, distributed two-phase flow pressure pulse and choked flow velocities are different, with the choked flow velocity always being larger than the pressure pulse propagation velocity.

5. CONCLUSIONS

Techniques presented in this paper for incorporating phase and velocity distribution effects into two-phase distributed flow pressure pulse velocity and choked flow theories are adequate. No empirically determined coefficients are necessary when applying the method to turbulent straight duct flows.

6. ACKNOWLEDGMENTS

Helpful discussions with Dr. K.R. Lawther (Leader, Heat Transfer Section, AAEC), Professor J.J. Thompson (Head, School of Nuclear Engineering, UNSW), and with Mr. V. Ilic (AAEC) are gratefully acknowledged.

7. REFERENCES

1. Beattie, D.R.H.: 'Drag reduction phenomena in gas-liquid systems', Proc. International Conference on Drag Reduction. Paper D.3. Organised by Brit. Hydromech. Res. Assoc., Cranfield (Sept. 4th - 6th, 1974).

2. Beattie, D.R.H.: 'Friction factors and regime transitions in high pressure steam-water flows', ASME Winter Annual Meeting, paper 75-WA/HT4. Organised by Heat Transfer Division, ASME (Nov. 30th - Dec. 4th, 1975).

3. Beattie, D.R.H.: 'Void fraction and regime transitions in two-phase flow', Paper in preparation.

4. Beattie, D.R.H.: 'Two-phase flow structure and mixing length theory'. Nucl. Eng. and Des., 21 pp. 46-64 (1972).

5. Einstein, A.: 'A new determination of molecular dimensions', Ann.Phys.(Leipzig), 19, 4, pp.289-306, (1906).

6. Taylor, G.I.: 'The viscosity of a fluid containing small drops of another fluid', Proc. R. Sec. (London), 138, pp.41-48 (1932).

7. Zuber, N., Staub, F.W., Bijwaard, G. and Kroeger, P.G.: 'Steady state and transient void fraction in two-phase flow systems', General Electric Co. Report GEAP 5417 (Jan. 1967).

8. Miyazaki, K., Fujii-e, Y. and Suita, T.: 'Propagation of pressure wave in air-water two-phase system (II)', J.Nucl.Sci.Technol. (Tokyo), 8, 12, pp.673-681, (Dec. 1971).

9. Fauske, H.K.: 'Two-phase, two-and one-component critical flow', Proc.Symp. on Two-Phase Flow, University of Exeter, England. Paper G1. Organised by Dept. of Chem.Eng., University of Exeter (1965).

10. Ilic, V. and Bryant, R.A.A.: 'An experimental study of choked flow in short pipes with low air/water mass fractions', Submitted to J.Fluids Eng. (tabulated data obtained from personal communication with V. Ilic).

11. Hamilton, L.J., Nyer, R. and Schrock, V.E.: 'Propagation of shock wave through two-phase, two-component media', Trans.Am.Nucl.Soc., 10, p.660 (1967).

12. Miyazaki, K., Fujii-e, Y. and Suita, T.: 'Propagation of pressure wave in air-water two-phase system, (1)', J.Nucl.Sci.Technol.(Tokyo), 8- 11 pp.606-613, (Nov. 1971).

13. Dejong, V.J. and Firey, J.C.: 'Effect of slip and phase change on sound velocity in steam-water mixtures and the relation to critical flow', Ind.Eng.Chem., Process Des.Dev., 7, 3, pp.454-463 (July 1975).

14. Fauske, H.K.: 'Contribution to the theory of two-phase, one component critical flow', Argonne National Laboratories Report ANL-6633 (1963).

15. Henry, R.E., Grolmes, M.A. and Fauske, H.K.: 'Propagation velocity of pressure waves in gas-liquid mixtures', Paper 1, 'Co-current gas-liquid flow', Plenum Press, 1969 (Proceedings of an International Symposium organised by the University of Waterloo, Canada).

16. Smith, R.V., Martindale, W.R. and Linsted, R.D.: 'Two-phase sonic velocity measurements for separated flow', ASME Winter Annual Meeting, paper 75 - WA/HT-34, organised by Heat Transfer Division, ASME (Nov. 30th - Dec. 4th, 1975).

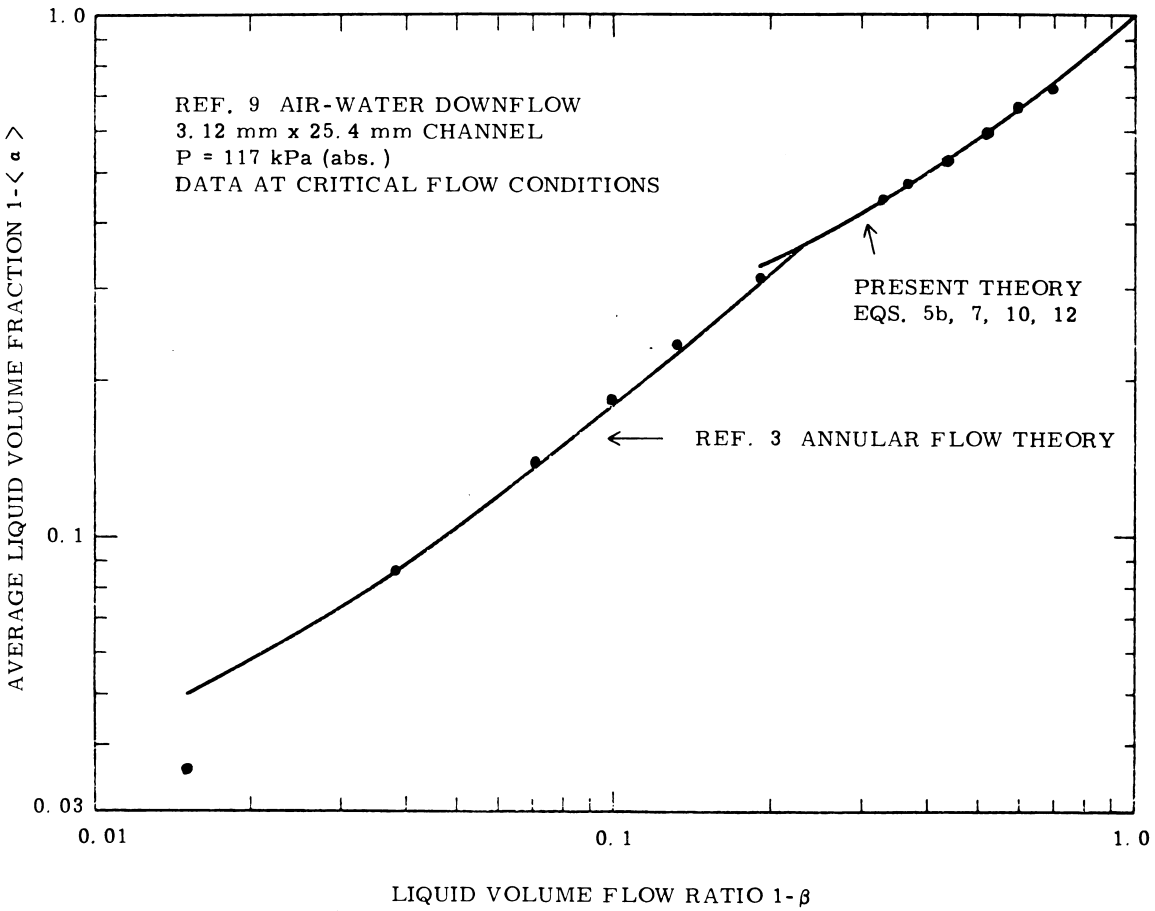

Fig. 1. Comparison of theory with void data for the choked flow data of Fig. 2.

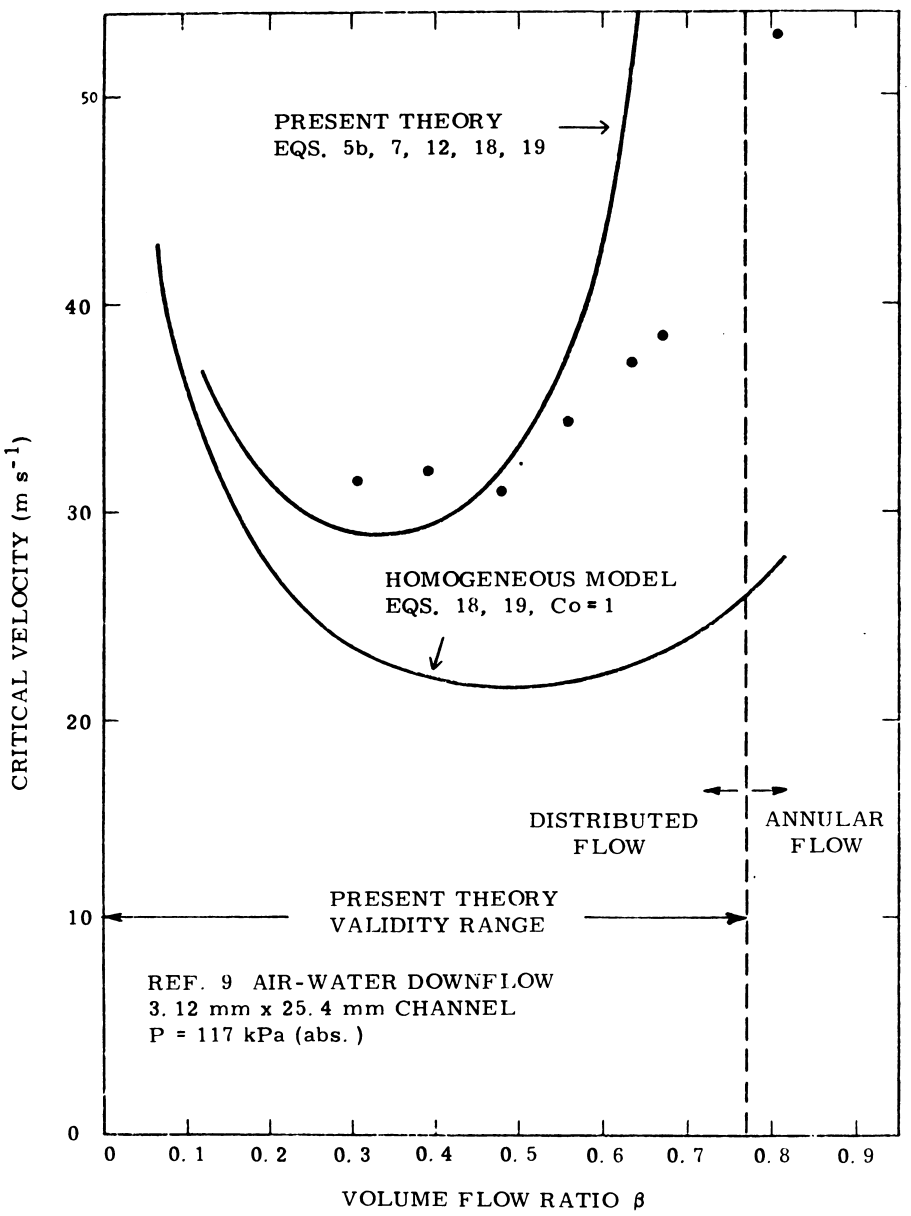

Fig. 2. Comparison of theory with choked flow data

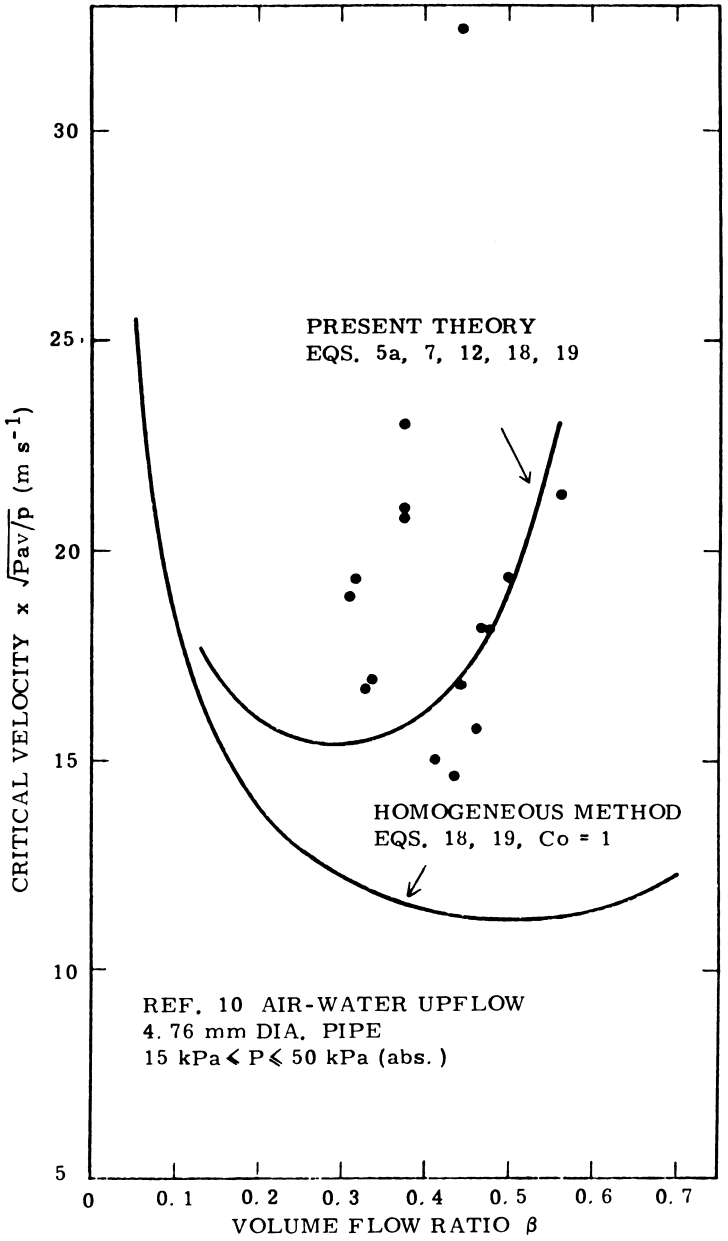

Fig. 3. Comparison of theory with choked flow data

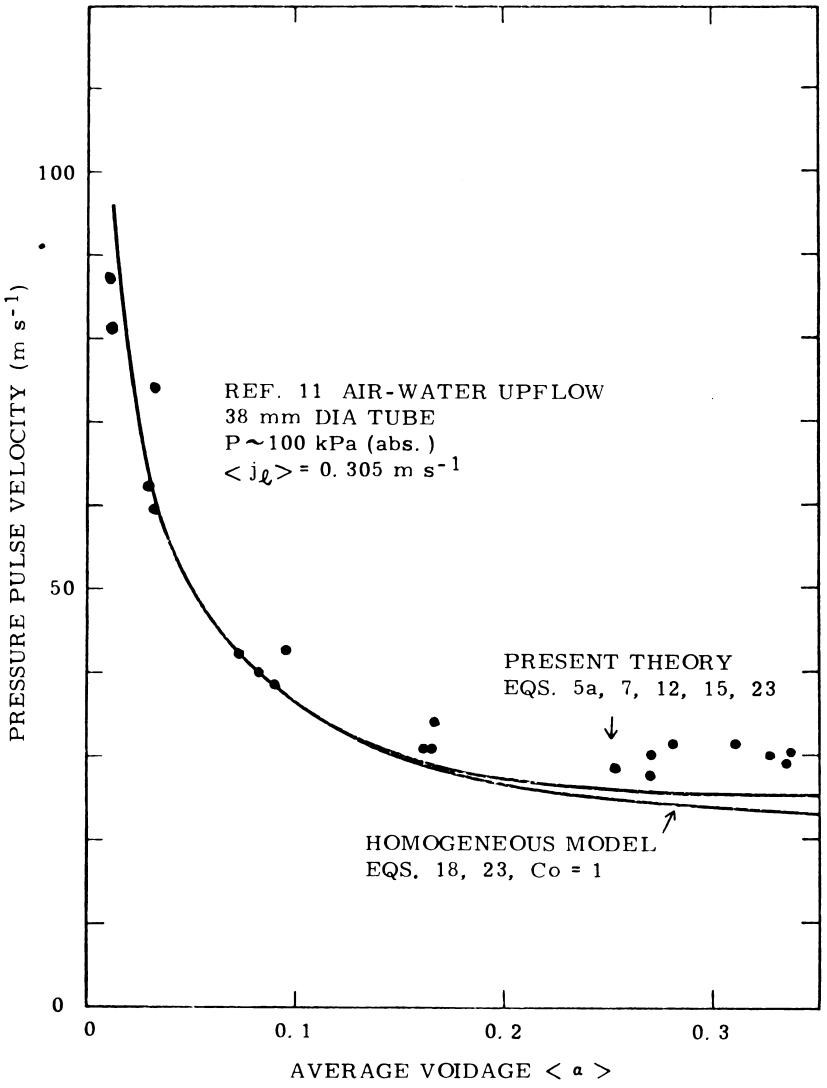

Fig. 4. Comparison of theory with pressure pulse propagation velocity data

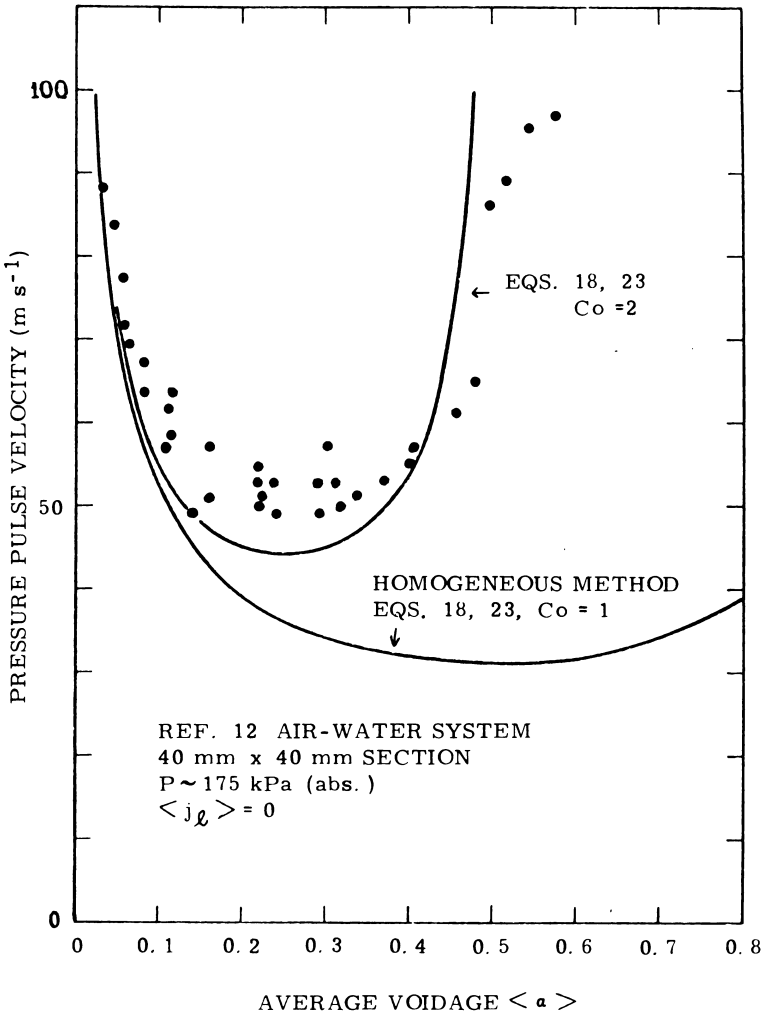

Fig. 5. Consistency of theory with pressure pulse propagation velocity data in non-turbulent flow

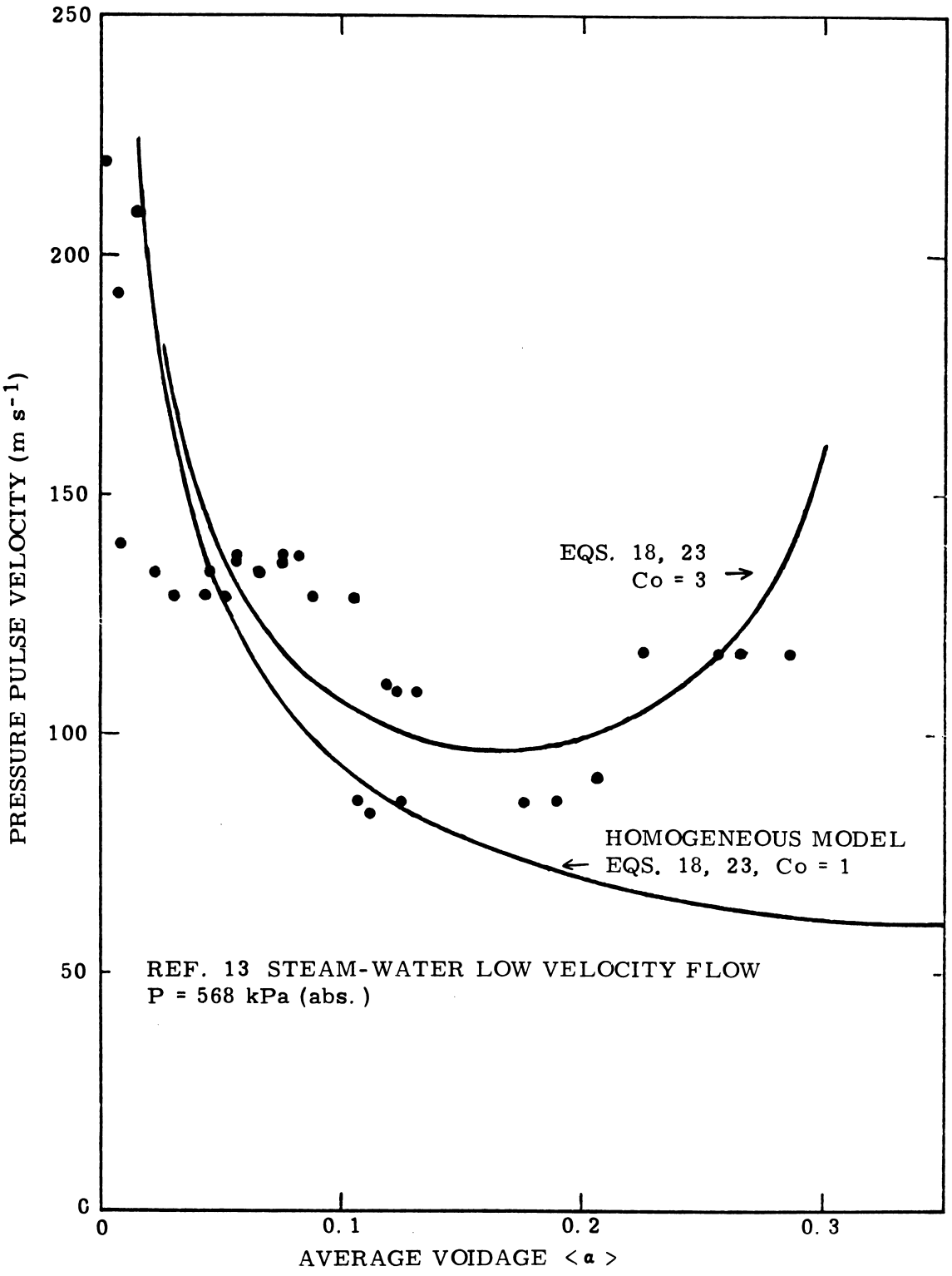
250
200
150
100
50
0
PRESSURE PULSE VELOCITY (m s^{-1})
EQS. 18, 23
Co = 3
HOMOGENEOUS MODEL
EQS. 18, 23, Co = 1
REF. 13 STEAM-WATER LOW VELOCITY FLOW
P = 568 kPa (abs.)
0
0.1
0.2
0.3
AVERAGE VOIDAGE <α>
Fig. 6. Consistency of theory with pressure pulse propagation velocity data in non-turbulent flow

SUPPLEMENTARY MATERIAL

THE EFFECT OF FLOW VELOCITY ON TWO-PHASE PROPAGATION PHENOMENA

D. R. H. Beattie
Australian Atomic Energy Commission
J. J. Thompson
University of New South Wales, Australia

The two-phase critical flow and pressure pulse propagation theory of section 2.3 of ref. (1) considers only two flow conditions (zero and critical velocity) and is thus not general. Furthermore, the zero velocity condition contradicts the turbulent flow requirement of the theory.

The effect of flow velocity is expected to be different to that in single phase flow since cross-sectional averaged perturbations in density and momentum, being controlled respectively by phenomena in the faster moving core region and the slower denser region near the wall, convect with velocities which differ from that of the mixture as a whole. Unlike the case in single phase flow, a dependence of the effective propagation velocity on flow velocity is thus expected. The flow velocity required to render propagation stationary (choked flow) should differ from the propagation velocity in a non-flow system, as already quantitatively demonstrated in ref. (1). A more general two component two-phase pipe flow theory, giving the complete dependence on flow velocity, is given below, using the notation of ref. (1).

Noting that $G = \bar{\rho}\langle j\rangle$ and that $\delta\bar{\rho} = C_o\,\delta\langle\rho\rangle$ for zero drift and C_o treated as a constant, equations (15) and (16) of ref. (1) can be expressed as

$$\frac{1}{C_o}\left(\frac{\partial}{\partial t} + C_o\langle j\rangle\frac{\partial}{\partial z}\right)\bar{\rho} + \bar{\rho}\,\frac{\partial\langle j\rangle}{\partial z} = 0 \quad . \qquad \ldots(1)$$

and

$$\bar{\rho}\left[\frac{\partial}{\partial t} + \langle j\rangle\left\{C_o + 2(1-C_o)\frac{\rho_\ell}{\bar{\rho}}\right\}\frac{\partial}{\partial z}\right]\langle j\rangle + \frac{\partial P}{\partial z} + \left.\frac{\partial P}{\partial z}\right|_f + \left.\frac{\partial P}{\partial z}\right|_G = 0 \qquad \ldots(2)$$

We note that the convective velocities as given by the form of the substantial derivatives behave as expected.

Consider perturbations of density, velocity and pressure ($\delta\bar{\rho}$, $\delta\langle j\rangle$, and δP) to the system. Neglecting gravitational and frictional pressure gradients as these are small compared with the momentum flux term at the conditions of interest, and noting that $\delta\bar{\rho} = \left(\frac{d\bar{\rho}}{dP}\right)_s \delta P$, equations (1) and (2) may be linearised to form

$$\begin{pmatrix} \bar{\rho}\left(\frac{\partial}{\partial t} + \langle j\rangle\left\{C_o + 2(1-C_o)\frac{\rho_\ell}{\bar{\rho}}\right\}\frac{\partial}{\partial z}\right) & \frac{\partial}{\partial z} \\ \bar{\rho}\,\frac{\partial}{\partial z} & \frac{1}{C_o}\left(\frac{d\bar{\rho}}{dP}\right)_s\left(\frac{\partial}{\partial t} + C_o\langle j\rangle\frac{\partial}{\partial z}\right) \end{pmatrix}\begin{pmatrix} \delta\langle j\rangle \\ \delta P \end{pmatrix} = 0 \qquad \ldots(3)$$

where values of quantities in the operator are initial values prior to the perturbations.

Characteristic velocities of the system are given by the determinant of the above operating on either $\delta\langle j\rangle$ or δP. The characteristic equation may be rearranged into the form

$$\left(\frac{1}{a^2}\left(\frac{D}{Dt}\right)^2 - \frac{\partial^2}{\partial z^2}\right) \quad (\delta\langle j\rangle \text{ or } \delta P) = 0 \qquad \ldots(4)$$

with

$$\frac{1}{a^2} = \frac{1}{C_o}\left(\frac{d\bar{\rho}}{dP}\right)_s \left(1 + \frac{\langle j\rangle^2}{C_o}\frac{d\bar{\rho}}{dP}\left\{(1-C_o)\frac{\rho_\ell}{\bar{\rho}}\right\}^2\right)^{-1} \qquad \ldots(4a)$$

and

$$\frac{D}{Dt} = \frac{\partial}{\partial t} + \langle j\rangle \quad \left(C_o + (1-C_o)\frac{\rho_\ell}{\bar{\rho}}\right)\frac{\partial}{\partial z} \qquad \ldots(4b)$$

Equation (4) is a wave equation which states that for a flow velocity $\langle j\rangle$, perturbations in velocity and pressure (and hence density) propagate with velocity $\pm a$ given by equation (4a) with respect to $\langle j\rangle\left(C_o+(1-C_o)\,\rho_\ell/\bar{\rho}\right)$. C_o can be obtained by methods given in ref. (1).

The zero mixture velocity value of a given by equation (4a) agrees with the value in ref. (1), where drift velocity effects were included, provided $\left(\frac{d\bar{\rho}}{dP}\right)_s$ is expressed in terms of $\langle\alpha\rangle$ instead of β.

Choked flow in the present model occurs when the propagation velocity is zero, i.e., is the solution of $a = \left(C_o+(1-C_o)\,\rho_\ell/\bar{\rho}\right)\langle j\rangle$. The lowest mass flux solution would normally occur at the outlet plane, but entrance condition influences on C_o may be such that the lowest mass flux solution occurs at the inlet, as has been observed in some two-phase choked flow experiments. The choked flow velocity as given by the present method is identical to that given by equation (19) of ref. (1).

The ref. (1) comparison of theory with low flow and critical velocity data clearly extends to the present theory. Propagation velocity data for intermediate flow velocities are given in ref. (2) and indicate that the effect of flow on propagation velocities is not simply additive. The present theory is reasonably close to the data of ref. (2).

REFERENCES

(1) Beattie, D.R.H. - 'Pressure Pulse and Critical Flow Behaviour in Distributed Gas-Liquid Systems': Paper D3, this Conference.

(2) Miyazaki, K., Nakayami, I., Fujii, Y., and Suita, T. - 'Effect of Flow on Pressure Wave Propagation on Two-Component Two-Phase System'. J. Nucl. Sci. Technol. (Tokyo) 10, 2, pp 127-129 (Feb. 1973).

Second Australasian Conference on Heat and Mass Transfer
The University of Sydney, February 1977, pp 329-337

TWO-PHASE FLUID MECHANICS AND HEAT TRANSFER IN THE DRY WALL REGION

D.R.H. BEATTIE
Australian Atomic Energy Commission, Research Establishment, Lucas Heights, NSW, 2232.

SUMMARY

Two-phase dry wall flows are induced by hydrodynamic and/or heat transfer effects.

Velocity profile and friction factor expressions are developed by applying single-phase sublayer boundary conditions to a previously developed two-phase turbulent flow structure theory. Loss coefficient predictive methods are extended to obstructions and partially-dry geometries. The velocity profile form leads to predictive methods for cross-section averaged mass, momentum, and kinetic energy fluxes, and hence for average voidage, pressure pulse propagation velocity, and choked flow velocity. Methods for predicting dry wall regime boundaries are discussed.

Application of Reynolds' analogy leads to predictive methods for the degree of thermal non-equilibrium and heat transfer coefficient. An extended transition to dryout is identified.

The various theoretical expressions, which involve no empirically determined coefficients, are in agreement with available experimental data.

1. INTRODUCTION

Recent developments in nuclear, aerospace, and other engineering fields, have led to a situation where greater understanding is desirable of dry wall two-phase flows consisting of a continuous gas phase with entrained solid or liquid particles. Dry walls in gas-liquid flows are caused by hydrodynamic stripping by the flow of the film of annular flow, and/or heat transfer effects, and in gas-solid flows by an entraining action of the flow on particulate matter at sufficient flow rates. Some fluid mechanical and heat transfer aspects of such flows are developed with emphasis being placed on gas-liquid flows for phenomena where gas-liquid and gas-solid flows behave differently. Theory is based on a round tube geometry and, where appropriate, is assumed to apply to other geometries via the equivalent diameter concept.

2. APPLICABILITY OF THE UNIVERSAL VELOCITY PROFILE

The nature of flows considered here allows single phase gas boundary conditions to be applied to two-phase turbulent flow structure equations [Beattie, 1972]. On the assumption that turbulence is confined to the continuous phase of two-phase flows the theory led to the following core void and velocity profile expressions for gas phase continuous flows:

$$\alpha = a\, u_g + b \qquad (1)$$

$$\text{and } \alpha^{3/2} = \alpha_\delta^{3/2} + \frac{3u^* a}{2\kappa}\, \ell n \frac{y}{\delta} \qquad (2)$$

with a,b unknown coefficients. Available data were consistent with the equations.

Equation (2) extrapolates to unity voidage not at the wall but at a given distance from it. The position δ where the laminar sublayer and turbulent core velocity profiles intersect is assumed to be in the single phase region.

The above may be simplified by the approximation valid for $\alpha \gtrsim 0.6$, (certainly valid for expected voidages, $\gtrsim 0.95$); $\alpha^{3/2} = (1 + (\alpha-1))^{3/2} \simeq 1 + 3/2\,(\alpha-1)$.

Substitution of this and equation (1) into equation (2) yields

$$u_g = u_{g\delta} + \frac{u^*}{\kappa}\, \ell n \frac{y}{\delta} \quad . \qquad (3)$$

Since a and b no longer appear, the gas velocity profile is largely independent of the void profile. This is confirmed by droplet data [Cravarolo et al. 1964] where axially varying radial profiles of local liquid volume fractions occur with no variation in gas velocity profile.

In terms of the more convenient mixture velocity $j = u_g \alpha + u_\ell (1-\alpha)$,

$$j - j_\delta = u_g - u_{g\delta} + [(1-\alpha)(u_\ell - u_g) - (1-\alpha_\delta)(u_{\ell\delta} - u_{g\delta})] \simeq u_g - u_{g\delta} \ ,$$

since $\alpha \simeq 1$ and, except for some gas solid flows, $u_\ell \simeq u_g$ [Cravarolo et al. 1964; Adorni et al. 1964; Alia et al. 1966; Rao & Dukler 1971]. Thus

$$j = j_\delta + \frac{u_g^*}{\kappa} \ln \frac{y}{\delta} \quad .$$

As discussed, $j \equiv u_g$ for $y \lesssim \delta$ and, from single phase considerations

$$j_\delta / u_g^* = \rho_g \delta u_g^* / \mu_g = 11.6 \quad . \tag{4}$$

If it is further assumed that $\kappa = 0.4$ as in single phase flow,

$$j^+ = 5.5 + 2.5 \ln y^+ \tag{5a}$$

with $$j^+ = j/u_g^* \quad \text{and} \quad y^+ = \rho_g u_g^* y/\mu_g \quad . \tag{6a}$$

Similarly it can be shown that for rough walls of roughness height ε

$$j^+ = 8.5 + 2.5 \ln(y/\varepsilon) \quad . \tag{5b}$$

Three round tube gas-liquid flow velocity profiles are compared with equation (5a) in fig.1. The data of Adorni et al. [1964] were obtained under post heat-transfer crisis conditions (i.e. a heat transfer induced dry wall, confirmed by thermocouple response), and the data of Alia et al. [1966] were from argon-alcohol experiments where void profile data indicated dry wall conditions. Dry wall gas-solid flow structure data [Rao & Dukler 1971; Soo et al. 1964; Reddy & Pei 1969] also confirm equation (5a).

3. FRICTION LOSSES IN DRY WALL TWO-PHASE FLOWS

3.1 Round Tubes

Averaging equations (5) over the flow section and expressing in terms of the friction factor and Reynolds number defined by

$$f = \frac{D\,(dP/dz)_f}{2\rho_g \langle j \rangle^2} \quad \text{and} \quad Re = \frac{\rho_g \langle j \rangle D}{\mu_g} \tag{6b}$$

leads to equations which, as in single-phase flow, can be generalised as Colebrook's equation:

$$1/\sqrt{f} = 3.48 - 4 \log (2\varepsilon/D + 9.35/(Re\sqrt{f})) \quad . \tag{7}$$

Typical adiabatic and post heat-transfer-crisis data [Gaspari et al. 1964] are compared with equation (7) in fig.2. Associated single phase data in the same reference indicate that $D/\varepsilon = 3000$ is appropriate for the test section under consideration. Equation 7, with this value of D/ε, is highly consistent with the adiabatic steam-water data, and with some of the diabatic data, but some diabatic data behave as if the surface roughness has been reduced. This point will be discussed later.

3.2 Other Geometries

Following single phase experience, it would appear reasonable to extend equation (7) (or its equivalent for those geometries where equation 7 is invalid for single phase flow) to other geometries through the use of the equivalent hydraulic diameter $D_e = 4\,A/p$ if all flow surfaces are dry. Dry wall pressure losses from several annuli [Tarasova et al. 1966; Klyushnev & Tarasova 1966; Przhiyalkovskii et al. 1965] confirm this. Some of these data are shown in fig.3.

Extending the concept, the single-phase loss coefficient/Reynolds number curve for an obstruction should be valid for two-phase dry wall systems if flow properties are appropriately defined. Empirical observations of air-coal dust flow through an orifice [Carlson et al. 1948] are consistent with this supposition.

More interesting for nuclear reactor applications are systems such as rod clusters with only some dry surfaces. Data analysis and semi-theoretical expressions [Beattie 1975] both indicate that wet wall shear stresses are considerably greater than dry wall shears except in the vicinity of hydrodynamically induced dryout. Pre-dryout expressions [Beattie 1975] might then apply through the use of an equivalent sheared diameter $D_s = 4\,A/p_s$ involving the non-dried out rather than total perimeter.

Theoretical considerations applied to an annulus of wetted shroud radius r_2, and dry rod radius r_1, are consistent with the above. Evaluation of the friction factor involves averaging a non-dimensional velocity profile between the shroud and the assumed zero shear location at the rod surface. The relevant step in the calculation is

$$\langle \ln y \rangle = 3/2 + \ln (r_2 - r_1) + r_1/(r_1 + r_2) \quad .$$

Since f is usually only weakly dependent on Re, it is reasonable to replace the term $r_1/(r_1+r_2)$ by an approximation $\ln (1 + r_1/r_2)$. This then leads to the usual relations with D being replaced by D_s.

Figure 4 compares data from annuli with heat-transfer induced dry central rods [Moeck 1970; Era et al. 1966] and a low quality two-phase friction expression, equation 7 with appropriately

defined friction factor and Reynolds number [Beattie 1975]. The wet wall expression with D_e being replaced by D_s results in reasonable agreement with the data except for a slight under-prediction presumably due to neglecting the non-zero shear at the central rod surface.

4. BOUNDARY CONDITIONS FOR DRY WALL TWO-PHASE FLOWS

Data analysis indicates that at the dry wall regime boundary for gas-liquid flows the frictional pressure gradient is continuous for developed adiabatic flows - some examples are given in fig.3* -but discontinuities occur in the frictional gradient at the boundary in the presence of flow disturbances (e.g. spacers or grids in complex geometries), or heat transfer. In the case of heat transfer, there is an associated discontinuity in the heated wall temperature. This tends to be large when the regime change is not near that for developed adiabatic flows (i.e. when the step change in frictional pressure gradient is large) and the regime change then constitutes the heat transfer crisis which must be avoided in many industrial situations.

All regime change data are qualitatively consistent with the concept that the entropy production rate (which has contributions from viscous dissipation, heat transfer, and flow redistribution) remains constant across a regime boundary. The components to the entropy production rate cannot be evaluated at present, but from an analysis by Bird [1955] would be expected to vary as $\tau_w <j>/(T_w D)$ (viscous dissipation), $\phi \ell n\, T_w/(T_w D)$ (heat transfer), and $G\Lambda/T_w$ (flow redistribution). If the concept is correct, the dry wall regime boundary for no flow disturbance should be consistent with

$$[\tau_w <j>/T_w]^{dry}_{wet} \sim - [\phi \ell n\, T_w/T_w]^{dry}_{wet} .$$

Knowledge of the wall shear behaviour on both sides of the boundary should then be sufficient for predicting the regime boundary for developed adiabatic flows, as in fig.3. The dry wall shear may be obtained by methods discussed in this paper; some wet wall shear stress equations are given by Beattie [1975].

If the concept is correct, prediction of heat-transfer-induced dryout would require knowledge of wall temperatures. The wet wall temperature is very close to the saturation temperature; the dry wall temperature may be estimated by methods given in section 6.

The supposition of continuity of entropy production rate across a regime boundary, although tentative, is qualitatively consistent with many observed phenomena (e.g. the magnitude of the wall temperature at the heat transfer crisis, and, via the effect of friction factor, the dependence of the heat transfer crisis on geometry, flow regime, spacer geometry, etc.). In view of the importance of the as yet inadequately explained crisis, this supposition should be investigated further.

5. PHASE AND VELOCITY DISTRIBUTION EFFECTS

5.1 Average Liquid Volume Fraction

Important parameters such as density are often predicted using empirical or semi-empirical equations to predict the average voidage $<\alpha>$. This is unacceptable for high voidage flows of the type discussed in this paper since, via the dominance of the denser dispersed phase, the value of $1-<\alpha>$ rather than $<\alpha>$ determines the mixture density, and small errors in estimates of $<\alpha>$ may be magnified into unacceptable errors in $(1-<\alpha>)$ as $<\alpha>$ approaches unity.

The development of the pre-dryout void correlation of Zuber & Findlay [1965] may be adapted to give the following relation for the average liquid velocity for dry wall flows:

$$<u_\ell(1-\alpha)>/<1-\alpha> = C_o <j> + V \qquad (8)$$

Where $C_o = <j(1-\alpha)>/(<j>(1-<\alpha>)$ is a dry wall distribution parameter, and $V = u_\ell - j$ is a drift velocity, assumed constant over the flow section. Dry wall drift velocity expressions are not as established as those for wet wall flows. Fortunately, empirical observations for droplet flow [Cravarolo et al. 1964; Adorni et al. 1964; Alia et al. 1966; Rao & Dukler 1971] indicate V is small compared with $<j>$ and may be neglected. This is not always true for gas-solid flows. For negligible V, equation (8) becomes

$$<1-\alpha> = (1-\beta)/C_o . \qquad (9)$$

An estimate of C_o may be obtained by assuming that the velocity profile varies mainly in the gas-only region near the wall. This is not true of some gas-particle systems, where electrostatic charge effects encourage a migration of particles to the wall. If a drift is allowed for the average liquid velocity is then approximately $j_c + V$. Comparison with equation (8) leads to

$$C_o = j_c/<j> \qquad (10)$$

---

* Because of its greater relevance, the wet wall friction factor is used instead of the definition given by equation (6b) as the ordinate axis on fig.3, which contains both wet and dry wall friction data.

which, from equation (5), can be evaluated from

$$C_o = 1 + 2.65\sqrt{f} \qquad (11)$$

where f is given by equation (7).

The only gas-liquid void data which could test the above theory were for adiabatic argon-alcohol flows in a 15 mm tube [Colombo et al. 1967]. Dry wall conditions were assumed for data where $(1-\langle\alpha\rangle) < (1-\beta)$, as expected from the above, whereas $(1-\langle\alpha\rangle) > (1-\beta)$ for wet wall data. Although no direct verification of this assumption was available, phase and velocity distribution data of argon-alcohol flows [Alia et al. 1966 discussed in section 2] indicate that dry walls are expected in a 25 mm tube for similar flow conditions. In any case, the data are consistent with equations (9) and (11) (fig.5).

Gas-particulate void data with non-negligible drift [Richardson & McLeman 1960] are consistent with equation (8) with $C_o = 1.10$, being slightly less than values expected from equation (11) (~ 1.2).

5.2 Momentum and Kinetic Energy Fluxes

The widely used application of voidage correlations for the evaluation of the cross section average momentum and kinetic energy fluxes, i.e.

$$M = \langle\rho_\ell u_\ell^2 (1-\alpha) + \rho_g u_g^2 \alpha\rangle \text{ and } 2K = \langle\rho_\ell u_\ell^3 (1-\alpha) + \rho_g u_g^3 \alpha\rangle$$

is incorrect. The evaluation of M and K requires knowledge of $\langle\alpha j^2\rangle$ and $\langle\alpha j^3\rangle$ respectively, whereas voidage equations implicitly or explicitly contain information on $\langle\alpha j\rangle$ only.

The present model allows the distribution parameter to be extended beyond its original application. C_o, as defined by $\langle(1-\alpha)j\rangle/(\langle 1-\alpha\rangle\langle j\rangle)$ could be expressed as $j_c/\langle j\rangle$ because the value of $(1-\alpha)$ was zero in the region where the j profile varied most rapidly. If this is true for the value of $(1-\alpha)$, it is also true for the value of $(1-\alpha)\, j^{n-1}$ and the distribution parameter may be generalised as

$$C_o = \langle(1-\alpha)\, j^n\rangle / \left(\langle(1-\alpha)\, j^{n-1}\rangle \langle j\rangle\right) = j_c/\langle j\rangle \quad . \qquad (12)$$

For zero drift velocity*, $u_\ell = u_g = j$. Applying equation (12) and the assumptions $\langle j^2\rangle = \langle j\rangle^2$ and $\langle j^3\rangle = \langle j\rangle^3$ (as in single phase flow) and expressing in terms of the more readily determinable variables G and $\langle j\rangle$, give

$$M = C_o G \langle j\rangle + (1-C_o)\, \rho_g \langle j^2\rangle \qquad (13)$$

and

$$2K = C_o^2 G \langle j\rangle^2 + (1-C_o^2)\, \rho_g \langle j\rangle^3 \quad . \qquad (14)$$

5.3 Propagation Phenomena in Dry Wall Two-Phase Flow Systems

The theory of this section is confined to constant area ducts, and phase change is neglected. The theory thus strictly applies only to two-component constant area duct systems. As applied to one-component systems it becomes one of the 'frozen model' theories where phase changes are quite reasonably neglected.

Assumptions are that physical properties are constant over a cross section, liquid is incompressible, the drift velocity is zero, and the distribution parameter is essentially constant. From equation (9) it can be shown that

$$\partial\langle\rho\rangle = \frac{1}{C_o}\partial\bar{\rho} + \left(1-\frac{1}{C_o}\right)\partial\rho_g$$

using this, equation (13), and the fact that $G = \bar{\rho}\langle j\rangle$, allows the equations for conservation of mass and momentum to be expressed as

$$\frac{1}{C_o}\left[\frac{\partial}{\partial t} + C_o\langle j\rangle\frac{\partial}{\partial z}\right]\bar{\rho} + \left(1-\frac{1}{C_o}\right)\frac{\partial\rho_g}{\partial t} + \bar{\rho}\frac{\partial\langle j\rangle}{\partial z} = 0$$

and

$$\bar{\rho}\left[\frac{\partial}{\partial t} + \langle j\rangle\left\{C_o + 2(1-C_o)\frac{\rho_g}{\bar{\rho}}\right\}\frac{\partial}{\partial z}\right]\langle j\rangle + (1-C_o)\langle j\rangle\left[\frac{\partial}{\partial z} + \langle j\rangle\frac{\partial}{\partial z}\right]\rho_g + \frac{\partial P}{\partial z} + \frac{\partial P}{\partial z}\Big|_f + \frac{\partial P}{\partial z}\Big|_{grav.} = 0$$

Consider perturbations of density, velocity and pressure ($\delta\bar{\rho}$, $\delta\langle j\rangle$ and δP) to the system. Neglecting gravitational and frictional pressure gradients, as these are small compared with

* Retention of V leads to terms such as $V\langle\alpha^{-1}\rangle$ which cannot at present be evaluated. Retention of V and suitable assumptions on such terms show that the effect of V is very small indeed.

the momentum flux term at the conditions of interest, and noting that $\delta\rho = \frac{d\rho}{dP}\delta P$, the conservation equations may be linearised to form

$$\begin{bmatrix} \bar{\rho}\left\{\frac{\partial}{\partial t} + \langle j\rangle\left[C_o + 2(1-C_o)\frac{\rho_g}{\bar{\rho}}\right]\frac{\partial}{\partial z}\right\} & \frac{\partial}{\partial z} + \frac{d\rho_g}{dP}(1-C_o)\langle j\rangle\left(\frac{\partial}{\partial t} + \langle j\rangle\frac{\partial}{\partial z}\right) \\ \bar{\rho}\frac{\partial}{\partial z} & \frac{1}{C_o}\frac{d\bar{\rho}}{dP}\left(\frac{\partial}{\partial t} + C_o\langle j\rangle\frac{\partial}{\partial z}\right) + \left(1 - \frac{1}{C_o}\right)\frac{d\rho_g}{dP}\frac{\partial}{\partial t} \end{bmatrix} \begin{bmatrix} \delta\langle j\rangle \\ \delta P \end{bmatrix} = 0$$

where values of quantities in the operator are initial values prior to the perturbations.

Characteristic velocities of the system are given by the determinant of the above operating on either $\delta\langle j\rangle$ or δP. The characteristic equation may be rearranged into the form

$$\left[\frac{1}{a^2}\left(\frac{D}{Dt}\right)^2 - \frac{\partial^2}{\partial z^2}\right](\delta\langle j\rangle \text{ or } \delta P) = 0 \qquad (15)$$

with

$$a^2 = \frac{1 + \langle j\rangle^2\left\{\frac{1}{C_o}\frac{d\bar{\rho}}{dP}(1-C_o)^2\left(\frac{\rho_g}{\bar{\rho}}\right)^2 + \frac{d\rho_g}{dP}\left(1-\frac{1}{C_o}\right)\left[\left(C_o + (1-C_o)\frac{\rho_g}{\bar{\rho}}\right)^2 - C_o\right]\right\}}{\frac{1}{C_o}\frac{d\bar{\rho}}{dP} + \left(1-\frac{1}{C_o}\right)\frac{d\rho_g}{dP}} \qquad (15a)$$

and

$$\frac{D}{Dt} = \frac{\partial}{\partial t} + \langle j\rangle\left[C_o + (1-C_o)\frac{\rho_g}{\bar{\rho}}\right]\frac{\partial}{\partial z} \qquad (15b)$$

Equation (15) is a wave equation which states that for a flow velocity $\langle j\rangle$, perturbations in velocity and pressure (and hence density) propagate with velocity $\pm a$ given by equation (15a) (note the dependence on $\langle j\rangle$) with respect not to $\langle j\rangle$, but to $\langle j\rangle\,[C_o + (1-C_o)\rho_g/\bar{\rho}]$. Choked flow occurs when the propagation velocity is zero, which corresponds to $a = [C_o + (1-C_o)\rho_g/\bar{\rho}]\langle j\rangle$.

Despite the complexity of equations (15), the propagation velocities as given by equations (15) are very close to those of the homogeneous model (equations (15) with $C_o = 1$), with the homogeneous model tending to underpredict the slow flow pressure pulse velocity and overpredict the choked flow velocity.

Data for testing the above are rare since virtually all high-void propagation velocity data are for wet wall flows. However, the high void steam-water pressure pulse velocity data of Seminov & Kosterin [1964] have been questioned [Gouse & Evans 1967] since the data are an order of magnitude lower than normally found for high voids (the annular flow pressure pulse velocity is very close to that of the gas phase flowing by itself). These data are fairly close to, but about 45% higher than, those for the homogeneous model and are within 25% of the present model using C_o calculated by equation (11). Similarly, low frequency aerosol data* [Temkin & Dobbins 1966] appear to be consistent with the theory.

6. HEAT TRANSFER EFFECTS

Steady state diabatic flows for one-component dry wall two-phase droplet systems are considered in this section. Analysis of such flows is complicated because the heat-flux induced temperature profile implies that the usual assumption of saturation physical properties may be invalid. Although neither this effect (loosely termed thermal non-equilibrium) nor the heat transfer mechanism is adequately understood, situations arise where prediction of both the heated surface temperature and the degree of non-equilibrium are important.

Application of Reynolds' analogy to the flow model previously discussed leads to predictive methods for these quantities. As stated, the relevant features of the model are that turbulence (and hence eddy diffusion of heat as well as momentum) is confined to the gas phase, and that liquid droplets are confined to the region where profiles are flat and magnitudes may be approximated by centreline values. Droplets are thus not expected to contribute to the radial transport of heat, as confirmed by observed droplet trajectories [Cumo et al. 1970a], but evaporate via heat transferred from the gas. Droplets are then expected to be at saturation temperature, and gas in the two-phase core at a higher temperature. The temperature difference, designated $\Delta T_{g\ell}$ below, is analogous to the drift velocity of section 5.1 and, for reasons given, is independent of radial position.

The heat transfer coefficient may be obtained by using the above concepts in a two-phase adaptation of the Prandtl-Taylor modification of Reynolds' analogy, as presented for example by Rogers & Mayhew [1972]. Application of the analogy to the gas phase of the flow leads to

* High frequency components of pressure pulses rapidly attenuate in two-phase systems.

$$\frac{\phi\ D}{k_g\ (T_w - \langle T_g \rangle)} = \frac{\tau_w}{\rho_g \langle j \rangle^2} \frac{\rho_g \langle j \rangle D}{\mu_g} \frac{\mu_g C_{pg}}{k_g} \left[1 + \left(\frac{\mu_g C_{pg}}{k_g} - 1 \right) \frac{j_\delta}{\langle j \rangle} \right]^{-1}$$

This result suggests the use of the Dittus-Boelter equation with two-phase definitions of dimensionless groups being as given in the above equation:

$$\frac{\phi\ D}{k_g\ (T_w - \langle T_g \rangle)} = 0.023 \left(\frac{\rho_g \langle j \rangle D}{\mu_g} \right)^{0.8} \left(\frac{C_{pg}\ \mu_g}{k_g} \right)^{0.4} \qquad (16)$$

The physical basis for the Prandtl-Taylor analogy suggests that C_{pg} be evaluated at the core gas temperature ($T_s + \Delta T_{g\ell}$), and μ_g and k_g, at $\frac{1}{2}(T_w + T_s + \Delta T_{g\ell})$.

The average gas temperature $\langle T_g \rangle$ must be expressed in terms of the saturation temperature T_s before equation (16) can be used to predict wall temperatures (T_w). From the definition of $\Delta T_{g\ell}$,

$$T_w - T_s = T_w - T_{gc} + \Delta T_{g\ell} \quad .$$

Direct application of Reynolds' analogy gives

$$\frac{T_w - T_{gc}}{T_w - \langle T_g \rangle} = \frac{j_c}{\langle j \rangle} = C_o \quad . \qquad (12a)$$

Hence $$T_w - T_s = C_o\ (T_w - \langle T_g \rangle) + \Delta T_{g\ell} \qquad (17)$$

which may be used in conjunction with equation (16) to predict T_w. A remaining problem in applying this and the previously discussed theory, is that, as stated, quantities calculated assuming thermal equilibrium are not correct under diabatic conditions. Since all relevant parameters can be expressed in terms of quality, non-equilibrium can be allowed for if quality can be expressed in terms of equilibrium quality. Consider the relevant term in the energy equation: $Gh \equiv \langle \rho_\ell\ h_\ell\ u_\ell\ (1-\alpha) + \rho_g\ h_g\ u_g\ \alpha \rangle$. From the model, $h_\ell = h_{\ell s}$, and $h_g = h_{gc}$ for $\alpha < 1$. Neglecting density variations and, following single phase analysis, assuming

$$\langle h_g\ u_g \rangle \simeq \langle h_g \rangle \langle j \rangle \quad ,$$

then $$h = (h_{\ell s} + (\langle h_g \rangle - h_{gc})\ \rho_g/\rho_\ell)(1-x) + \langle h_g \rangle\ x \quad .$$

Expressing this in terms of $x_{eq} = (h - h_{\ell s})/(h_{gs} - h_{\ell s})$, and (via the definition of specific heat) of temperature, ultimately leads to

$$x = \frac{x_{eq}\ (h_{gs} - h_{\ell s}) - C_{pg}(\rho_g/\rho_\ell)(C_o - 1)\ (T_w - \langle T_g \rangle)}{(h_{gs} - h_{\ell s}) + C_{pg}\ (1 - \rho_g/\rho_\ell)\ (C_o - 1)\ (T_w - \langle T_g \rangle) + C_{pg}\ \Delta T_{g\ell}} \qquad (18)$$

This must be solved simultaneously with equation (16).

Except for the unknown quantity $\Delta T_{g\ell}$, equations (16, 17, 18) are sufficient for predictive purposes. Prediction of $\Delta T_{g\ell}$ requires further work; preliminary estimates may however be obtained from empirical observations of Cumo et al. (1970b).

As in the earlier sections, adequate confirmation of the theory of this section is difficult because, apart from heat transfer coefficient data, there are few relevant data available. However, the expected temperature profile in the continuous phase, with the dispersed phase at saturation temperature, has been experimentally confirmed for bubble flows [Stefanovic et al. 1970]. Heat transfer data [Berkowitz et al. 1960; Bertolletti et al. 1964] have been compared with the theory, with the assumption $\Delta T_{g\ell} = 0$. Calculated thermal non-equilibrium was small. Measured differences between wall and saturation temperatures are compared with theoretical expectations in fig.6 which shows that non-reproducibility may occur, and that the theory gives an approximate estimate of the maximum temperature difference likely to be encountered.

It is of interest that the friction data of fig.2 were obtained simultaneously with the heat transfer data of Bertolletti et al. [1964]. Lower than expected temperature differences appear to be associated with lower than expected friction factors. Therefore the transition between the onset of dryout and the complete dry wall region of a heated channel, involving both wet and dry sections of the wall, may extend further than usually supposed, with superheated liquid being contained in microcrevices between heated wall roughness elements in the latter part of the transition region. This would explain the apparent reduction in surface roughness

(fig.2) and reduction in wall temperatures (fig.6) of some 'dry wall' data when compared with other data for nominally identical conditions.

7. DISCUSSION AND CONCLUSIONS

The present theory for a two-phase flow system is based on a model which restricts turbulent transport to the continuous phase, the dispersed phase being confined to regions with flat velocity and temperature profiles. Various consequences of this model have been considered and, despite the lack of relevant two-phase wall data, its predictive ability has been confirmed by data comparison in a number of areas. Furthermore, application of the principles of the model to bubble flows [Beattie 1976], leads to different expected behaviour for the various phenomena considered. In the bubble flow case, more data are available for confirming the model in areas such as choked flow behaviour.

It is interesting to compare differences between bubble and dry wall flow behaviour. Bubble flow pressure losses, liquid volume fraction, and propagation velocities are all considerably greater than the widely-used homogeneous model predictions; whereas for dry wall flows, pressure losses are considerably less than, liquid volume fractions less than, and propagation velocities about equal to, the homogeneous model predictions. An unfortunate consequence of this is that current models used in, for example, reactor safety codes may be grossly incorrect for dry wall flows, since the models tend to be based on wet wall data.

Differences between wet and dry wall behaviour can be attributed to the nature of the dispersed phase. Consider, for example, perturbations in the concentration of dispersed phase. Resulting perturbations in density convect with the dispersed phase velocity in both cases, but differences occur for momentum and kinetic energy flux perturbations. Since the dense phase contributes most to these, perturbations convect at about the dispersed phase velocity in dry wall flows, but not with bubble flows. The closeness of the dry wall propagation velocities to the homogeneous predictions (section 5.3) is associated with the closeness of the velocities in the substantial derivatives inherent in section 5.3 to the velocity of the dispersed phase. This is clearly not the case for bubble flows.

The present model uses no empiricism in comparing theory with data, despite the wide range of application. Comparable published models tend to involve empiricism even for limited applications. Thus, the theory of Chisholm & Sutherland [1970], for example, invokes an empirical function which has different values depending on whether their theory is being applied to pressure loss or voidage prediction.

An unexpected feature of the present model, indicated by the disappearance of a and b from equations after equation (2), is that all gross phenomena (even average voidage) are independent of the nature of the void profile. This is particularly surprising in the case of the distribution parameter since this parameter as introduced by Zuber & Findlay [1965] inherently depended on the void profile form.

It is concluded that the present dry wall flow model and consequent predictive models are reasonable, and that empirically based wet wall models are grossly incorrect for dry wall flows.

8. ACKNOWLEDGEMENTS

Helpful discussions with Dr. K.R. Lawther (Leader, Heat Transfer Section, AAEC) and Professor J.J. Thompson (Head, School of Nuclear Engineering, UNSW) are gratefully acknowledged.

REFERENCES

Adorni, N. et al. Centro Informazioni Studi Experienze report, CISE-R-91 [1964].
Alia, P. et al. CISE-R-109 [1966].
Beattie, D.R.H. Nucl. Eng. Des., 21, 46 [1972].
Beattie, D.R.H. American Society of Mechanical Engineers paper 75-WA/HT-4 [1975].
Beattie, D.R.H. Paper D3, 'Second International Conference on Pressure Surges' BHRA Fluid Engineering, London [1976].
Berkowitz, L. et al. CISE-R-27 [1960].
Bertolletti, S. et al. CISE-R-78 [1964].
Bird, R.B. et al. CEP Symp. Ser. No.16, 51, p.69 [1955].
Carlson, H.M. et al. Trans. ASME 70 p.65 [1948].
Chisholm, D. & Sutherland, L.A. Paper 4, Proc. Inst. Mech. Eng. 1969-70, 184, Pt.3C, 24 [1970].
Colombo, A. et al. CISE-R-225 [1967].
Cravarolo, L. et al. CISE-R-93 [1964].
Cumo, M. et al. Paper presented at European Two-Phase Flow Group Meeting, Milan, [1970a].
Cumo, M. et al. Paper B. 3.5, 4th Int. Heat Trans. Conf. [1970b].
Era, A. et al. CISE-R-184 [1966].
Gaspari, G.P. et al. CISE-R-83 [1964].
Gouse, S.W. & Evans, R.G. Paper 5.1, Symp. on Two-Phase Flow Dynamics, EUR.4288e [1967].

Klyushnev, V.E. & Tarasova, V.E. Therm. Eng. 13, (11), 87 [1966].
Moeck, O.E. Atomic Energy of Canada Ltd., Report AECL 3656 [1970].
Przhiyalkovskii, M.M. et al. Therm. Eng. 12, (11), 65 [1965].
Rao, C.S. & Dukler, A.E. Ind. Eng. Chem. Fundam. 10, (3), 520 [1971].
Reddy, K.V.S. & Pei, D.C.T. Ind. Eng. Chem. Fundam. 8, (3), 490 [1969].
Richardson, J.F. & McLeman, M. Trans. Inst. Chem. Engrs., 35, 257 [1960].
Rogers, G.F.C. and Mayhew, Y.R. 'Engineering Thermodynamics Work and Heat Transfer', Longman [1972].
Seminov, N.I. & Kosterin, S.I. Therm. Eng., 11, (6), 59 [1964].
Soo, S.L. et al. Ind. Eng. Chem. Fundam. 3, (2), 98 [1964].
Stefanovic, M. et al. Paper B 4.12, 4th Int. Heat Trans. Conf. [1970].
Tarasova, N.V. et al. Paper 133, 3rd Int. Heat Trans. Conf. [1966].
Temkin, S. & Dobbins, R.A. Brown University Div. of Engineering report AD 632911 [1966].
Zuber, N. & Findlay, J.A. J. Heat Trans. 87, 453 [1965].

NOTATION

A	flow area
C	specific heat
C_o	distribution parameter
D	diameter
f	friction factor
g	acceleration due to gravity
G	mass flux
h	specific enthalpy
j	$u_\ell(1-\alpha) + u_g\alpha$
j^+	j/u_g^*
k	thermal conductivity
K	kinetic energy flux
M	momentum flux
p	perimeter
P	pressure
Q	volume flow rate
r	radius
Re	$\rho_g \langle j \rangle D/\mu_g$
t	time
$\Delta T_{g\ell}$	local gas-liquid temperature difference
u	velocity
u^*	$\sqrt{\tau_w/\rho}$
V	$u_\ell - j$
x	quality
y	distance from wall
y^+	$\rho_g u_g^* y/\mu_g$

<---> quantity is average over flow section

α	voidage
β	$Q_g/(Q_g+Q_\ell)$
δ	intersect distance from the wall of 'sublayer' and turbulent core velocity profiles
ε	wall roughness
κ	mixing length coefficient
Λ	driving force for flow redistribution
μ	dynamic viscosity
ρ	density, $\rho_\ell(1-\alpha) + \rho_g\alpha$
$\bar{\rho}$	$\rho_\ell(1-\beta) + \rho_g\beta$
τ	shear stress
ϕ	heat flux

Subscripts

c	centreline value
e	equivalent value
eq	equilibrium value
f	frictional component
g	gas value
grav	gravitational component
ℓ	liquid value
s	saturation value (thermodynamic properties)
s	relevant to non-dried perimeter
w	value at wall
δ	value at position δ

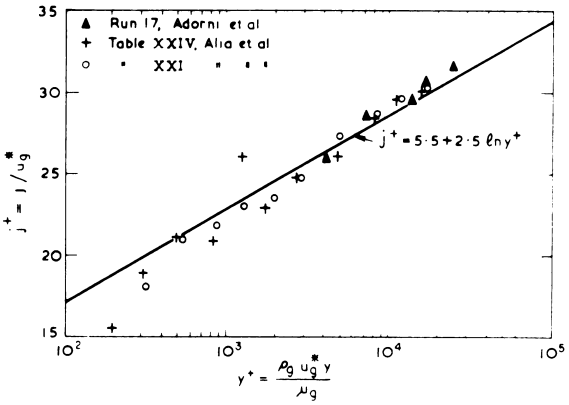

Fig.1 Dry wall two-phase velocity profiles

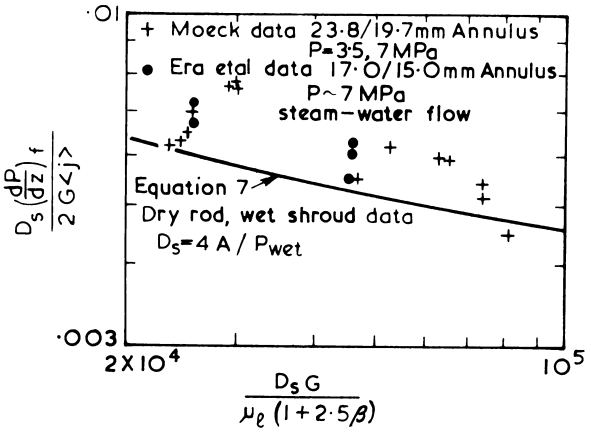

Fig.4 Partially dry wall friction data, annular geometry

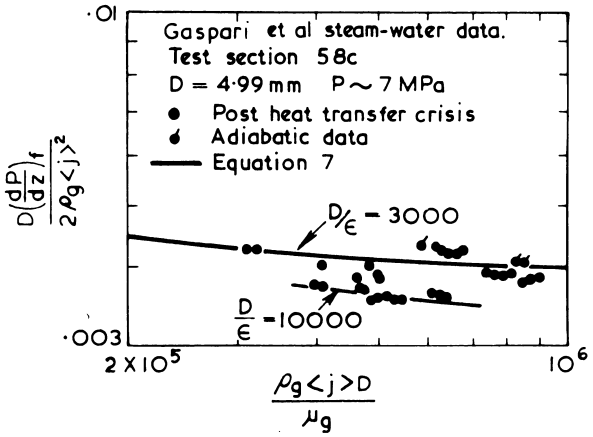

Fig.2 Dry wall friction data, round tube geometry

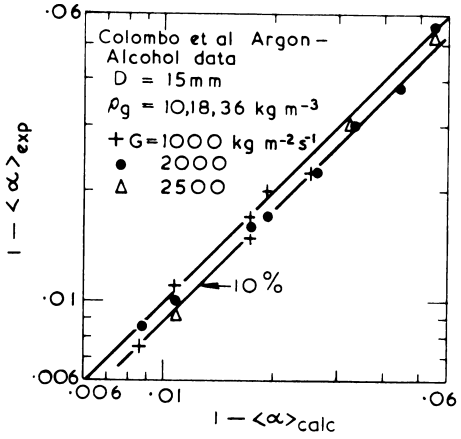

Fig.5 Dry wall liquid volume fraction

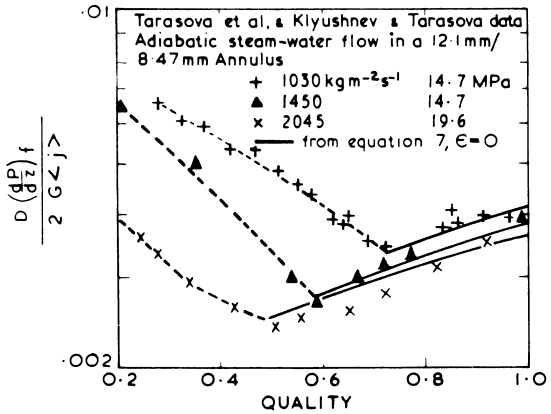

Fig.3 Regime boundary determination from wet wall (low quality) and dry wall (high quality) friction data, annular geometry

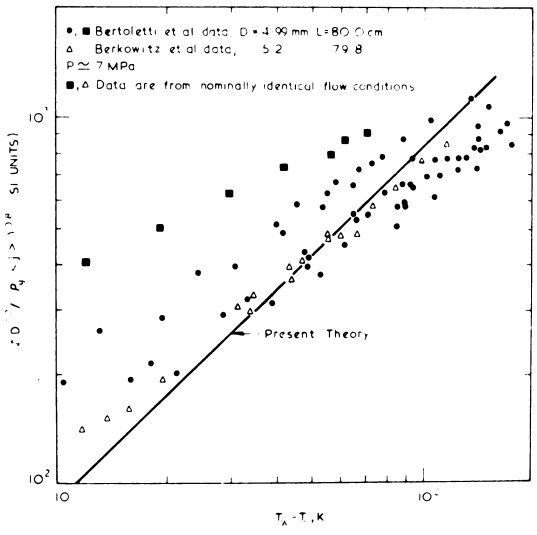

Fig.6 Post dryout heat transfer data

partial explanation of the unorthodox drift velocity values.

As noted by Martin, developed flow distribution parameter values have been associated with the maximum/average velocity ratio. As long as voids are confined to the flatter region of the velocity profile, this association is necessary. Furthermore, under such circumstances, the distribution parameter can be generalised and used for the prediction of other two-phase quantities (momentum flux, choked flow, etc.) [22][3]. The situation becomes less predictable if, as is the case with the downflow experiments described, voids concentrate in the steeper region of the velocity profile.

The lower degree of development observed with downflow slug behaviour may not be confined to slug flow. Difficulty was reported in maintaining slug flow with certain conditions. Similar non-development of downward bubble flow near the bubble/slug flow boundary might be expected. It is significant that recently reported air-water downward bubble flow data [23] were correlated by a distribution parameter which, like the present values (but unlike other downflow bubble data), was significantly less than the developed flow value. Furthermore, the bubble data of [23] are very close to the slug flow equation obtained by interpolating between parameter values reported by Martin to allow for diameter effects.

Similarly, a comparison of the reference [24] steam-water void data for slug and non-slug up and down flow indicates that, as observed by Martin, significant changes occur in the drift velocity behaviour with changed orientation.

Since equations of the form of Martin's equation (1) are used for predictive purposes, it is appropriate to note that the experimental technique employed is such that V_b does not have the widely used interpretation $\langle j_g \rangle / \langle \alpha \rangle$. The two interpretations would be significantly different only where nonslug bubbles contribute significantly to the voidage, as shown in Martin's Fig. 7. (The zero V_b of Table 1 corresponding to Fig. 7(d) clearly does not imply a zero $\langle j_g \rangle / \langle \alpha \rangle$). Also, an error has occurred in the discussion of the zero net flow data. $\langle j \rangle = \langle j_l \rangle + \langle j_g \rangle = 0$ does not imply $\langle j_l \rangle = \langle j_g \rangle = 0$, as stated. The nonzero value of V_b in Table 2, corresponding to Fig. 10(f), for instance, implies a nonzero local $\langle j_g \rangle$, and so the zero $\langle j \rangle$ implies $\langle j_l \rangle = -\langle j_g \rangle$ in the region of interest, even though both velocities are zero away from the bubble.

Nevertheless, his data do provide a useful basis from which downward slug flow behaviour can be reasonably estimated, even though he has not generalized his results into recommended equations. He has helped to remove present gaps in knowledge of two-phase slug flow.

APPENDIX A9

Vertically Downward Two-Phase Slug Flow[1]

D. BEATTIE.[2] Professor Martin's paper is a useful reminder that, even with fields as thoroughly researched as two-phase slug flow, care must be taken in applying supposedly general equations to unorthodox situations. Experimental values of both the distribution parameter and the drift velocity differ significantly from those generally recommended for slug flow. The unexpected distribution parameter values have been logically explained in terms of observed eccentricities in the slug paths. Observed distribution parameter values furthermore provided a

[1]By C. Samuel Martin, published in the December, 1976 issue of the JOURNAL OF FLUIDS ENGINEERS, TRANS ASME, Series I, Vol. 98, pp. 715–722.

[2]Research Scientist, AAEC Research Establishment, Lucas Heights, Australia.

Additional References

22 Beattie, D. R. H., "Pressure Pulse and Critical Flow Behaviour in Distributed Gas-Liquid Systems," *Proc. 2nd International Conference on Pressure Surges*, Paper D.3, organized by Brit. Hydromech. Res. Assoc., Cranfield (Sept. 22–24, 1976).

23 Arosio, S., Bartolini, R., Lorenzi, A., and Sotgia, G., "Two-Phase Downward Flow in Large Diameter Ducts - Preliminary Results," *Energia Nucleare*, Vol. 23, No. 4, Apr. 1976, p. 224.

24 Janssen, E., and Kervinen, J. A., "Two-phase Pressure Drop in Straight Pipes and Channels: Water-Steam Mixtures at 600 to 1400 psia," GEAP-4616, May 1964.

[3]Numbers in brackets designate Additional References at end of discussion.

Second International Conference on

Drag Reduction

August 31st - September 2nd, 1977

PAPER D1

SOME ASPECTS OF TWO-PHASE FLOW DRAG REDUCTION

D.R.H. Beattie, B.Sc., B.E., M.Eng.Sc.,

Australian Atomic Energy Commission, Australia

Summary

Drag reduction is characterised by coefficients in the non-dimensional velocity profile $j^+ = a \log y^+ + b$ which differ from those normally encountered. In the case of drag reduction in gas-liquid flows with no drag reducing additives, empirically obtained values of a and b suggest that only certain well-defined values exist, and that these values appear to form parts of some simple series. Similarly, only well-defined types of sub-layers exist. Flows are therefore classified by the triad (m, n, z) where m and n are integers from which the non-dimensional velocity profile coefficients can be calculated, and z specified the sub-layer structure.

Typical data are subdivided into groups each having a particular (m, n, z) set. For each group, a demonstration is given of the compatability of data for velocity profile, friction factor, and average void fraction with the theoretical expressions for those parameters determined by the appropriate (m, n, z) set.

The (m, n, z) sets for high pressure steam-water flows are tabulated. Compatibility with typical steam-water data is demonstrated.

Held at St. John's College, Cambridge, England.

Organised and sponsored by BHRA Fluid Engineering, Cranfield, Bedford, MK43 0AJ.

© BHRA Fluid Engineering.

NOMENCLATURE

a_1-a_5	mixing length theory coefficients
a,b,c,d,e	sublayer types (Table 1)
f	friction factor (Table 1)
j	local mixture velocity, $u_\ell(1-\alpha)+u_g\alpha$
j^+	non-dimensional velocity (Table 1)
m,n	integers in generalised equations (13)-(16)
u	local phase velocity
y	wall distance
y^+	non-dimensional wall distance (Table 1)
z	flow direction
A	area fraction of core for separated flow
B	volume flow fraction of core for separated flow
C_o	distribution parameter
D	equivalent diameter
G	mass flux
P	pressure
Q^+	non-dimensional film flowrate in separated flow
Re	Reynolds number
S^+	non-dimensional film thickness in separated flow
V	drift velocity, u-j
We	Weber number
α	local voidage
β	volume flow ratio, $\langle j_g \rangle / \langle j \rangle$
μ	dynamic viscosity
σ	surface tension
ρ	density

Subscripts

c	value for core of separated flow
f	value for film of separated flow
F	frictional component
g	gas value
ℓ	liquid value

Operator

<--->	quantity is averaged over the flow section

1. INTRODUCTION

Pressure losses for low quality (i.e. with low gas content) gas-liquid bubble flows and for high quality gas-liquid dry-wall flows are consistent with the single-phase Colebrook friction factor equation if the relevant dimensionless groups are appropriately defined (Ref. 1). An examination of the variation of friction factor with quality for these two flow types shows that for the intermediate quality region, pressure losses are not consistent with the Colebrook equation.

Flows encountered in the intermediate region are characterised by velocity profiles which deviate from the 'universal' profile and, as such, are similar to single phase drag-reduced flows generated by small amounts of suitable additives, although additives are not necessary to stimulate two-phase drag reduction.

This paper examines various aspects of two-phase drag reduction of the type encountered without drag-reducing additives. Some preliminary aspects have been reported in Ref. 2. Since then several papers have appeared on the topic (e.g. Ref.3) but all are concerned with the effect of additives on two-phase pressure losses.

A feature which distinguishes two-phase drag reduction without additives from additive-induced drag reduction (for both single and two-phase flows) appears to be the strong suggestion in the former of eigen-value characteristics of the type often encountered in the solution of bounded field problems. This behaviour may be significant in the further interpretation of the turbulent flow field.

2. BACKGROUND TWO-PHASE FLOW EQUATIONS

Two-phase flow equations relevant to the examination of gas-liquid flow drag reduction are summarised below. Their derivation, which is outside the scope of this paper, will be given in Ref. 4. Relevant aspects of the theory are in Refs. (5-8). Where appropriate, use of the equivalent diameter renders the equations applicable to non-circular ducts.

2.1 Definition of Dimensionless Groups

As in single phase flow, the nature of the sub-layer flow near the wall determines the form of the dimensionless-group definitions. The various possible structures of the two-phase sub-layer lead to different definitions of the same basic dimensionless groups, each definition being valid for the particular sub-layer structure. Five sub-layer types are considered here. Others can be postulated, but these are either unrealistic or lead to dimensionless group definitions which are either identical, or very close, to those for the five sub-layer types considered. The sub-layer types are:

(a) A liquid sub-layer containing rigid surface bubbles. Bubble flows, some bubble/slug flows, and annular flows with entrained bubbles in the liquid film have sub-layers of this type if the sub-layer bubble surfaces are rigid. Surfactant impurities have this effect on small bubbles in liquids with polar molecules;

(b) A liquid sub-layer containing non-rigid-surface bubbles. Typical flows with this sub-layer are similar to those above, except that bubble surface movement can occur, allowing viscous dissipation within the bubble;

(c) A sub-layer in which local instantaneous shear stress alternates between values expected from calculations based on a treatment of the local flow as gas only or liquid only. 'Annular' flows consisting of a wavy liquid film with no entrained bubbles and a gas, droplet, or froth core; and some 'slug' flows, have sub-layers of this type;

(d) A gas-only sub-layer, ('dry-wall' flows) as expected with, for example, post heat-transfer crisis flows; and,

(e) A liquid sub-layer with attached wall bubbles protruding within the turbulent flow, as expected e.g. for some diabatic flows.

Dimensionless-group definitions for the five sub-layer types are summarised in Table 1.

TABLE 1. DIMENSIONLESS-GROUP DEFINITIONS FOR VARIOUS TWO-PHASE FLOW SUB-LAYER TYPES

Sub-layer Type	Pressure Loss Characteristics	Local Structure
Viscosity dependent flows (a,b,c,d)	$f = \frac{D(dP/dz)_F}{2\rho\langle j\rangle^2} = f(Re = \frac{\rho\langle j\rangle D}{\mu})$	$j^+ = \frac{j}{\langle j\rangle}\sqrt{\frac{2}{f}} = j^+(y^+ = \frac{y}{R}\frac{Re}{2}\sqrt{\frac{f}{2}})$
Surface-tension dependent flows (e)	$f = \frac{D(dP/dz)_F}{2\rho\langle j\rangle^2} = f(We = \frac{\rho\langle j\rangle^2 D}{\sigma})$	$j^+ = \frac{j}{\langle j\rangle}\sqrt{\frac{2}{f}} = j^+(y^+ = \frac{y}{R} We \frac{f}{2})$

Sub-layer Notation/ Type	Density Definition	Viscosity Definition
a. Rigid surface bubbles	$\rho = \rho_\ell(1-\beta) + \rho_g\beta$	$\mu = \mu_\ell(1+2.5\ \beta)$
b. Non-rigid surface bubbles	$\rho = \rho_\ell(1-\beta) + \rho_g\beta$	$\mu = \mu_\ell(1 + \frac{2.5\ \mu_g + \mu_\ell}{\mu_g + \mu_\ell}\beta)$
c. Wavy-gas/liquid interface	$\rho = \rho_\ell(1-\beta) + \rho_g\beta$	$\mu = \mu_\ell(1-\beta) + \mu_g\beta$
d. Dry wall	$\rho = \rho_g$	$\mu = \mu_g$
e. Attached wall bubbles	$\rho = \rho_\ell(1-\beta) + \rho_g\beta$	N.A.

2.2 Non-dimensional Velocity Profiles

Two-phase non-dimensional velocity profiles have much in common with single phase behaviour. Round tube non-dimensional velocities and wall distances as defined in Table 1 are related by

$$j^+ = a_1 + a_2 \ln y^+ \qquad (1)$$

in the turbulent region. A number of such equations may be necessary for a complete description of the turbulent velocity profile (cf. the 'buffer' and 'turbulent' regions of single phase flow) and, as in single phase flow, the region adjacent to a smooth wall is assumed to be described by

$$j^+ = y^+ \quad . \qquad (2)$$

2.3 Friction Factor Relations

Averaging equation 1 over the flow section leads to equations of the form

$$1/\sqrt{f} = a_3 + a_4 \log Re\sqrt{f} \qquad (3)$$

for viscosity dependent flows, and

$$1/\sqrt{f} = a_5 + a_4 \log We\ f \qquad (4)$$

for surface tension dependent flows.

2.4 Average Void Fraction

The behaviour of the average void fraction $\langle\alpha\rangle$, and also of some other quantities, depends on whether the flow is distributed (one phase is continuous throughout the flow section) or separated (the flow section can be divided into liquid-phase continuous and gas-phase continuous regions). Note that the discussion of sub-layer types in section 2.1 indicates that, while a particular flow type implies a particular sub-layer type in some cases, evidence of a particular sub-layer is not sufficient to indicate whether a flow is distributed or separated.

2.4.1 Distributed two-phase flows

Liquid-phase continuous distributed flow void fractions are described by

$$\langle j_g\rangle/\langle\alpha\rangle = C_o \langle j\rangle + V_g \qquad (5)$$

and gas-phase continuous void fractions, by

$$\langle j_\ell\rangle/\langle 1-\alpha\rangle = C_o \langle j\rangle + V_\ell \quad . \qquad (6)$$

In the above, C_o is a 'distribution parameter' given by

$$C_o = 1 + 0.66\, a_4 \sqrt{f} \qquad (7)$$

where a_4 is the logarithmic term coefficient in equation 3 or 4 used to obtain f. The V_g and V_ℓ are dispersed phase 'drift velocities' which account for the fact that the local dispersed phase velocities differ from the local mixture velocities ($V_{g,\ell} = u_{g,\ell} - j$). Values of V_g can be found in Ref. 9 for some flows. Values for V_ℓ are at present unknown but, fortunately, can be considered to be negligible at the high velocities encountered in gas-phase continuous distributed two-phase flows.

For negligible drift velocities, equations 5 and 6 are equivalent to the simpler expressions

$$\langle\alpha\rangle = \beta/C_o \qquad (5a)$$

and

$$1-\langle\alpha\rangle = (1-\beta)/C_o \qquad (6a)$$

where β is the fraction of gas flowing by volume.

Note that one of the sub-layers a,b,c,e of section 2.1 would apply in the friction factor calculation for equations 5 and 5a; and sub-layer d, for equations 6 and 6a.

2.4.2 Separated two-phase flows

The following equations apply to annular flows with a liquid-phase continuous film and a gas-phase continuous core. The equations presumably can be adapted to inverse annular flows (gas-phase continuous film and liquid-phase continuous core) but not data have been found to confirm this.

Entrainment is allowed for by introducing core and film voidages, α_c, α_f, and gas volume flow ratios β_c, β_f, all treated as having flat profiles over the appropriate regions of the flow cross section. The area fraction of the core, A, and the volume flow fraction of the core, B, (i.e. the volume flowrate) are then given by

$$A = (\alpha_f - \langle\alpha\rangle)/(\alpha_f - \alpha_c) \qquad (8)$$

and $$B = (\beta_f - \langle\beta\rangle)/(\beta_f - \beta_c) \quad . \tag{9}$$

For no entrainment, $A \equiv \langle\alpha\rangle$ and $B \equiv \beta$. Film entrainment effects are significant only at lower voidage annular flows ($\langle\alpha\rangle \sim 0.5$) and core entrainment effects, only at higher void annular flows ($\langle\alpha\rangle \gtrsim 0.9$). Entrainment will be discussed more fully elsewhere (Ref. 8). In the present paper, entrainment is neglected since the flow conditions discussed are such that the effects of entrainment on average void values are mostly quite small.

Defining non-dimensional film volume flowrate Q^+ and film thickness S^+ by

$$Q^+ = \frac{1-B}{2(1+\sqrt{A})}\,Re \tag{10a}$$

$$S^+ = \frac{1-\sqrt{A}}{2}\,Re\sqrt{\frac{f}{2}} \tag{11a}$$

(Viscosity dependent flows)

$$Q^+ = \frac{1-B}{1+\sqrt{A}}\,We\sqrt{\frac{f}{2}} \tag{10b}$$

and $$S^+ = (1-\sqrt{A})\,We\,\frac{f}{2} \tag{11b}$$

(Surface tension dependent flows)

then $$Q^+ = \int_{j^+=o}^{S^+} j^+ \, dy^+ \tag{12}$$

For known entrainment conditions, equation 12 may be used to calculate voidages for separated flows. Instead of $\langle\alpha\rangle$, the method, in fact, predicts $1-\langle\alpha\rangle$ which is more significant than $\langle\alpha\rangle$ at the low $1-\langle\alpha\rangle$ values normally encountered in annular flow, since apparently small errors in $\langle\alpha\rangle$ become unacceptable errors in $1-\langle\alpha\rangle$. Moreover, percentage errors in density calculations are approximately equal to percentage errors in $1-\langle\alpha\rangle$.

3. GENERALISED TWO-PHASE FLOW DRAG REDUCTION EQUATIONS

Drag reduction is characterised by mixing length coefficients which are different from those usually encountered in flow structure or pressure loss equations. Coefficient values for additive-induced drag reduction appear to form part of a continuous spectrum of values; in two-phase flows with no additives, they appear to form part of a spectrum of discrete values. An analysis of values obtained for empirical coefficients a_1 to a_4 in equations 1 and 3 indicates that nearly all velocity profile and friction factor equations for viscosity dependent two-phase flows with no additives can be generated from

$$j^+ = (\sqrt{2})^{m+5}\,\{\log y^+ - (0.11\,m + 0.50\,n)\} \quad , \tag{13}$$

and from the integrated form of equation (13)

$$1/\sqrt{f} = (\sqrt{2})^{m+4}\,\{\log Re\sqrt{f} - (0.11\,m + 0.50\,n + 1.1)\} \quad , \tag{14}$$

by appropriate integer choices for m and n.

Similarly, with the exception of a particular class of flow which is discussed later, friction factor equations for surface-tension dependent flows can all be generated from

$$1/\sqrt{f} = (\sqrt{2})^{m+4} \{\log We\ f - (0.2\ m + 0.3\ n - 1.1)\} \quad (15)$$

with the implied velocity profile expression

$$j^+ = (\sqrt{2})^{m+5} \{\log y^+ - (0.2\ m + 0.3\ n - 2.05)\} \quad , \quad (16)$$

again with integer choices for m and n. Equations 15 and 16 are more tentative than equations 13 and 14, largely because of a relative scarcity of surface-tension dependent flow data.

As well as being relevant in friction factor and velocity profile relations, the values of m and n are relevant for specifying the average voidage characteristics of the flow, as is indicated by the theoretical expressions of section 2.4. For example, the distribution parameter, as given by equation 7, becomes

$$C_o = 1 + 2.60\ (\sqrt{2})^m \sqrt{f} \quad . \quad (17)$$

The significance of n for distributed flow voidage is less evident, its influence on the distribution parameter being via f (equation 14). Similarly, for given m and n, the sub-layer type affects f, and hence C_o, owing to the dependence of dimensionless parameter definitions on sub-layer type (Table 1).

Reference to section 2.4.2 indicates that m,n and sub-layer type have a similar effect on separated flow void characteristics. They also have similar effects on other two-phase flow phenomena (momentum flux, choked flow, etc.).

Considering equations 13 and 14 it is worth noting that the usual smooth tube single-phase equations are generated by (m,n) = (0,-2). For some situations, the Nikuradse equation is inadequate in single phase flows. For those situations, the correct single phase equation should be used in the two-phase case for flows in which (m,n) = (0,-2). For example, equation 14, with (m,n) = (0,-2) and sub-layer d, describes smooth tube dry wall two-phase flows. The equation should be replaced by Colebrook's equation if the tube wall is rough.

It is also worth noting that equation 13 with (m,n) = (2,0) generates an equation very close to that used to describe the buffer region in single-phase flow.

3.1 Friction Regime Classification Method

At this stage it is appropriate to introduce the concept of 'friction regimes'. A friction regime is characterised by the sub-layer type as described in section 2.1 and the coefficients 'a' in equation 3 or 4.

In this paper, a notation of the form (m,n,z), in which m and n are integers and z is a letter, will respectively indicate the relevant m and n values of equations 13 to 16 and the appropriate sub-layer type described in section 2.1. The triad (m,n,z) thus specifies a friction regime.

The above convention is not sufficient to specify a flow completely. Other relevant information is required (e.g. separated or distributed flow).

4. COMPARISON WITH DATA

Many of the features encountered in the analysis of two-phase drag reduced data are of special relevance to two-phase fluid mechanics research only. In keeping with the conference theme, this section considers only drag reduction aspects of the data analysed. The detailed analysis will be reported elsewhere (Ref. 10).

4.1 Examples of Friction Factor Data Characterised by m=4

Although data with various m and n values will be discussed later, it is

interesting to see the trend in a family of friction factor curves with constant m and varying n. Typical two-phase data covering the range (4,0 to 8,c) are shown in Fig. 1.

Two points about Fig. 1 are worth noting. Firstly, the wide range of Reynolds numbers (several cycles) involved in such data sets has allowed the n coefficient, 0.50, in equations 13 and 14, to be determined with some accuracy. Similarly, the range of m values encountered in the analysis of data has led to reasonably accurate assessments of other empirical parameters. Secondly, the data of Fig. 1 correspond to genuine reductions in drag losses even though much of the friction data are above values expected from the Nikuradse equation. This is a result of changes in sub-layer structure occurring in friction regimes. Consider, for example, the data corresponding to (4,4,c). The same data are shown in a different form in the second region of the data in Fig. 5a. There they are lower than would be expected from the trend shown by the lowest quality data as characterised by (0,-2,a) in which the m and n values correspond to the Nikuradse equation. In this context, drag reduction is quite evident.

In the remainder of this section pressure loss data are discussed in which there is associated flow structure and average voidage data.

4.2 Argon-water Upflow in Round Tubes

Round tube argon-water upflow data, as reported in Refs. 11 to 18, have been analysed in terms of the non-dimensioned parameters of section 2. Data cover the gas density range $10 \leqslant \rho_g \leqslant 36.1$ kg m^{-3}. Most data are for a 25 mm tube, some for a 15 mm tube.

Data were sorted into groups having the same set of (m,n,z) values. The regime map so obtained is shown in Fig. 2a. Experimental friction factors, velocity profiles and average voidages are compared with the theoretical equations, using the appropriate (m,n,z) values, in Figs. 2b, 2c and 2d. Because of the vast number of data involved, each symbol on Fig. 2a corresponds to representative data only for $\rho_g = 36.1$ kg m^{-3}, although the regime map applies for other gas densities. Other data in Figs. 2 cover all the values of gas density in the data examined. Theoretical rather than experimental values of friction factors were used for Figs. 2c and 2d.

The regime map of Fig. 2a is only approximate. Data for different axial positions indicated a dependence of regime boundaries on flow development, as expected from theoretical considerations (Ref. 19). Regime boundaries are such that shear stresses are approximately continuous across a boundary.

The velocity measuring probes apparently influenced the flow causing the regime boundaries for the velocity data to be shifted. This shift explains the existence of an additional regime type in the velocity data. A similar probe effect on steam-water data was noted in Ref. 2. It will be noted that, as is the case of the 'universal' velocity profile, when the turbulent core must be subdivided according to velocity profile behaviour, each portion of the profile is consistent with equation 13 with appropriate integer choices for m and n.

The boundary of the (2,1,e) data of Fig. 2a, marked ▼, coincides with the visually-based bubble regime boundary Ref. 14. Such coincidences of visually-based boundaries with those obtained by the present method are rare. Nevertheless, on that basis the void data for this regime were treated as being for distributed flow, (Fig. 2d(i)). The negative, rather than the normal positive, drift velocity (V) indicated by Fig. 2d(i), is flowrate dependent and therefore is consistent with the attached bubble sub-layer for these data. The distribution parameter (C_o) values of Fig. 2d(i) are consistent with the empirical value of m=2 for the data.

Although shear stress data for conditions marked ? in Fig. 2a could not be correlated by the present model, the lower void data for these conditions are consistent with a zero drift velocity, and m=0 together with the experimental value of friction factor being used in equation 17 (Fig. 2d(ii)).

Separated flow void data for each of the regimes of Fig. 2a are shown in

Fig. 2d(iii), together with the theoretical curves (equation 12) for the appropriate m and n values. Since $\frac{1-\sqrt{\alpha}}{2}$ $Re\sqrt{f/2}$ is approximately proportional to the liquid volume fraction, errors in the abscissa represent errors in calculated liquid volume fractions. Errors are larger for smaller liquid volume fractions where neglected entrainment effects are expected to be more significant.

Fig. 2 shows that friction factors, velocity profiles and average voidage values for the argon-water flows considered are compatible with the theoretical equations of section 2 when analysed in terms of the generalised equations of section 3.

4.3 Argon-Alcohol Upflow in Round Tubes

Argon-ethyl alcohol data reported in Refs. 15 to 18 which also covered the range $10 \leqslant \rho_g \leqslant 36.1$ kg m^{-3} were analysed similarly to the argon-water data (section 4.2). The results are shown in Fig. 3.

Void data for conditions marked Δ and • in Fig. 3a were omitted from the analysis since core entrainment, which is not included in the present analysis, cannot be reasonably neglected for these regimes, which border the dry wall regime (marked *).

The visually-based 'bubble flow' regime boundary for the data (Ref. 14) approximately coincides with the ▲ boundary of Fig. 3a, hence void data for the friction regime (0,-2,c) were treated as being for distributed flows (Fig. 3d(i)). Despite the visual interpretation of the flow, the sub-layer type suggests that bubble flow is unlikely and that on the contrary the flow has a froth core. Since drift velocities can be expected to be zero for froth flows, the data were analysed in terms of equation 5a, instead of equation 5, together with equation 17.

For dry wall flows the drift velocities, which are expected to be small compared with the large flow velocities encountered under these flow conditions, were neglected in the analysis of the dry wall void data (Fig. 3d(iii)).

As was the case for the argon-water data, the argon-alcohol data are compatible with the equations of sections 2 and 3, although different friction regimes were encountered for the differing flow constituents.

4.4 Separated Surface Tension Dependent Flow Data

Data analysis results reported in sections 4.2 and 4.3 confirm the consistency of average voidage data, shear stress data, and velocity profile data with the theoretical equations in sections 2 and 3 for distributed and separated viscosity dependent flows, and, except for the absence of associated velocity profile data, also for distributed surface tension dependent flows, but not for separated surface tension dependent flows.

Some separated surface tension dependent flow data for the friction regime (1,2,e) have been analysed to evaluate the compatibility of such velocity profile, void fraction, and friction factor data with theory. The data are for argon-water upflow in a seven-rod cluster, covering the gas density range $10 \leqslant \rho_g \leqslant 36.1$ kg m^{-3} (Ref. 20), and for steam-water upflow in a 17 mm tube at 7 MPa (Ref. 21). The data involved are the higher quality data from Ref. 20 and the lower quality adiabatic data from Ref. 21.

The data, resolved into appropriate non-dimensional terms, are compared with the theoretical curves in Fig. 4. The data are in reasonable agreement with the theoretical equations expected for the (1,2,e) friction regime. The discrepancy of the lower y^+ velocity data (Fig. 4b) is not significant since it is the core profile that determines the flow characteristics. In any case, the void data are consistent with a treatment in which the core profile is assumed to extrapolate to j=0 (Fig. 4c), suggesting that the lower y^+ velocity data of Fig. 4b may be in error.

The results of section 4.2 and this section indicate that, in addition to the previously noted dependence of friction regimes on flow constituents, the friction regimes are also flow geometry dependent.

5. EQUATIONS FOR HIGH PRESSURE STEAM-WATER FLOWS

An earlier paper (Ref. 19) presented recommended equations for calculating friction losses in high pressure steam-water flows. The equations were based on an analysis of approximately 10^4 sets of data, and allowed for entrance, heat transfer and geometry effects. They applied for $P \gtrsim 2$ MPa and $G \gtrsim 200$ kg $m^{-2}s^{-1}$. A U.K. comparison with a wide range of experimental friction data for adiabatic two-phase flows in round tubes (Ref. 22) showed that the Ref. 19 equations for such flows were superior to alternative equations for the mass flux and pressure conditions for which the Ref. 19 equations were developed, but were inferior to alternatives at lower pressures and when applied to non-steam-water systems. In view of the data analysis results of section 4, the latter result is not surprising. The equations of Ref. 19 incorporated the friction regime concept of the present work, but were developed before the existence of the generalised equations of section 3 was recognised.

With one exception, all the Ref. 19 equations could be made to conform to the present generalised equations with only minor alterations to their empirical coefficients. The new equations are specified by the parameters given in Table 2. A comparison with various data is shown in Fig. 5.

TABLE 2. FRICTION REGIMES FOR HIGH PRESSURE STEAM WATER SYSTEMS ($P \gtrsim 2$ MPa, $G \gtrsim 200$ kg $m^{-2}s^{-1}$)

Use in conjunction with equations of sections 2 and 3

Flow System			Friction regimes, in order of increasing quality[1]
Round Tubes	Adiabatic Flow	Settling length > 500D	(0,-2,a); (4,4,c)[2,3]; (2,0,a); (0,-2,d)
		Settling length $\lesssim$ 500D, D < 6 mm	As above[4]
		Settling length $\lesssim$ 500D, D > 6 mm	(0,-2,a); (4,4,c)[2,3]; (4,2,a); (0,-2,d)
	Diabatic Flow	Unobstructed	(0,-2,a); (3.61, 3.74, e); (0,-2,d)[5]
		Upstream obstruction, G < 1500 kg $m^{-2}s^{-1}$	As above
		Upstream obstruction G > 1500 kg $m^{-2}s^{-1}$	(0,-2,a); (4,4,c)[2,3]; (4,2,a); (0,-2,d)[5]
Annuli and rod Clusters		Spacer separation > 40D	(0,-2,a); (1,2,e); (0,-2,d)[5,6]
		Spacer separation < 40D	Variable behaviour

Notes:

1. Friction regime boundaries (≡ friction factor equation validity limits) are given by intersects of friction factor equations unless otherwise specified.
2. Replace (4,4,c) with (4,6,c) if (0,-2,a):(4,4,c) intersect occurs at $x < 0$ (D < 20 mm) or $x < 0.1$ (D > 20 mm). When (0,-2,a):(4,6,c) intersect occurs at $x < 0$, replace (4,6,c) with (4,8,c).
3. Omit the second regime when the friction equations for the first and third regimes intersect at a lower quality than the intersect for the first and second regimes.
4. Reduce regime boundary qualities by ~ 0.1.
5. Regime boundary given by appropriate critical heat flux correlation in diabatic flow case.
6. Use pre-dryout equations with D=4. Flow area/(non-dried perimeter) if only some surfaces are dry (Ref. 7).

Not all high pressure steam-water data conform with the equations to the same extent as the Fig. 5 data. Where disagreement occurs, it is usually because the friction regime differs from expectations. The data then conform to the equations for that regime. Examples are the (4,1,a) set of data in Fig. 1 and the steam-water data of section 4.4.

Confirmatory void and velocity profile data have not been presented here. Using Table 2 as a guide, virtually all existing high pressure steam water void data are for the (0,-2,a) regime. These agree with the theoretical equations for this regime provided entrainment is taken into account in separated flow voidage calculations. The little void data that could be found for other friction regimes (Ref. 3) also agree with the theory.

6. DISCUSSION

Apart from the coefficients in the generalised equations of section 3, and the evaluation of appropriate friction regimes, the present model uses no empiricism, despite the wide range of applications. Comparable published models tend to involve empiricism even for limited applications. For example, the method of Ref. 23, invokes an empirical function which has different values depending on whether it is being applied to pressure loss or voidage prediction.

It has been seen that the triad (m,n,z) characterises two-phase void values, velocity profiles, and pressure losses, all in a coherent fashion. The generalised equations of section 3, as applied to the theory of Refs. 6 and 7 also indicate that other phenomena (such as those for choked flow and heat transfer coefficient) are similarly characterised.

The generalised equations for viscosity dependent flows (equations 13 and 14) differ in some respects from those for surface-tension dependent flows (equations 15 and 16). The logarithmic term coefficients remain the same for the two flow types, but the other terms behave differently. This is not surprising; mixing length theory indicates that the logarithmic term coefficients are determined solely by the turbulent transport in the core of the flow. Such transport is expected to be identical for the two flow types. The other terms are determined by boundary conditions which apply to the turbulent core, and these are different for the two flow types. In a similar way, and for the same reasons, the logarithmic term coefficients in single phase equations are the same for smooth and roughened walls, whereas the other coefficients in the single phase equations are altered by the changed boundary conditions.

The spectrum of discrete values for friction regime parameters does not occur with all two-phase friction regimes. Exceptions tend to be encountered for low mass flowrates at extremely high voidages, of the type analysed so extensively by the Harwell group (e.g. Ref. 24), where, for example, changes in mixing length coefficients are smooth rather than discontinuous. It is postulated that the mechanism by which drag is reduced for these flows is different from that of the present work. Flow conditions are such that the liquid film at the wall is expected to be so thin as to fall within the laminar sub-layer. Such a film may act as a compliant coating.

Apart from the above exception, all two-phase friction regimes with drag reduction characteristics involve a two-region flow, with the interface between the regions lying in the vicinity of the sub-layer. Given present views that turbulence is generated in the sub-layer region, it is possible that the drag reduction is due to the interface inhibiting the turbulence transport. This appears particularly likely in the present model, whose basis (Ref. 5) suggests that, locally, turbulence is confined to one phase only, and that the turbulence-carrying phase for two-region flows is different on different sides of the interface separating the regions. The inhibition of turbulence transport, as opposed to the inhibition of turbulence generation in single-phase drag reduction (Ref. 25), is a possible cause of differences between single- and two-phase drag reduction characteristics.

Although single-phase drag reduction behaviour tends not to have the spectrum of discrete values of the type noted here, analysis of single-phase drag reduction data

indicates that particular f:Re curves are preferred. Single-phase drag reduction data were not considered in the development of the generalised equations of section 3, but the preferred f:Re curves tend to agree with equation 14 with appropriate integers chosen for m and n. Examples of such single phase data are: much of the data of Ref. 26 ((m,n) = (5,1)), and of Ref. 27 ((4,0)). If half-integers are considered, Virk's initial (Ref. 28), (4.5,0) and revised (Ref. 29) (5,0.5) 'maximum drag reduction asymptotes' also conform to the generalised equation 14.

Finally, the present work provides suitable equations for three types of two-phase flow system (steam-water, argon-water and argon-alcohol). They should not be generalised to other systems, and in any case, should be treated with caution. Thus, the (2,1,e) regime of Fig. 2, marked ▼, appears to apply only for conditions when a particular wall device, used for shear stress measurements (Ref. 14) was used. Void data obtained for similar flow conditions in the absence of the wall-shear device (Ref. 18) are shown in Fig. 6. A comparison of Fig. 6 and Fig. 2d(i) suggests that the friction regime is different for the two cases.

7. CONCLUSIONS

In the application of mixing length theory to two-phase flow, the generalised dimensionless velocity profile may be characterised by two parameters, m and n. Theoretical velocity profiles, pressure drops and average voidages agree with experimental data when m and n are restricted to discrete integer values associated with a particular type of sub-layer (z), so that the triad (m,n,z) may be chosen as the basis for two-phase flow classification and prediction.

Further work is necessary to interpret low mass flux, very high voidage flows which are not compatible with the proposed classification scheme, and provide a basis from which terms in the triad (m,n,z) may be estimated for any given flow.

8. ACKNOWLEDGEMENTS

Helpful discussions with Dr. K.R. Lawther (Head, Heat Transfer Section, AAEC) and Professor J.J. Thompson (Head, School of Nuclear Engineering, UNSW) are gratefully acknowledged.

9. REFERENCES

1. Beattie, D.R.H.: Nucl. Eng. Des. 25, 395 (1973).
2. Beattie, D.R.H.: Paper D3, Int. Conf. on Drag Reduction, BHRA Fluids Engng, Cranfield, U.K. (Sept. 1974).
3. Thwaites, G.R., et al.: Chem. Eng. Sci. 31, 481 (1976).
4. Beattie, D.R.H.: Ph.D Thesis, School of Nucl. Eng., UNSW (in preparation).
5. Beattie, D.R.H.: Nucl. Eng. Des. 21, 46 (1972).
6. Beattie, D.R.H.: Paper D3, 2nd Int. Conf. on Pressure Surges, BHRA Fluids Engng, Cranfield, U.K. (Sept. 1976).
7. Beattie, D.R.H.: p.329, Proc. 2nd Australasian Conf. on Heat and Mass Transfer, University of Sydney (Feb. 1977).
8. Beattie, D.R.H.: 'Void fraction and regime transitions in two-phase flow' paper in preparation.
9. Zuber, N. and Findlay, J.A.: J. Heat Transfer, 87, 453 (1965).
10. Beattie, D.R.H.: Australian Atomic Energy Commission - report in preparation.
11. Adorni, N., et al.: CISE-R-35 (1961).
12. Adorni, N., et al.: CISE-R-41 (1961).
13. Casagrande, I., et al.: CISE-R-73 (1963).
14. Cravarolo, L., et al.: CISE-R-82 (1964).
15. Cravarolo, L., et al.: CISE-R-93 (1964).
16. Alia, P., et al.: CISE-R-105 (1965).
17. Alia, P., et al.: CISE-R-109 (1966).
18. Colombo, A., et al.: CISE-R-225 (1967).
19. Beattie, D.R.H.: ASME paper 75-WA/HT-4 (1975).
20. Alia, P., et al.: CISE-R-108 (1968).
21. Subbotin, P.L., et al.: FEI-421 (1973).
22. Clarke, C.J.T.: Engineering Sciences Data Unit - U.K. - private communication. See also ESDU Data Item 76018 (1976).

23. Chisholm, D. and Sutherland, L.A.: Paper 4, Proc. Inst. Mech. Eng. (1969-70), 184, pt 3c, 24 (1970).
24. Hewitt, G.F. and Hall Taylor, N.S.: 'Annular Two-Phase Flow', Pergamon Press (1970).
25. Achia, B.U. and Thompson, D.W.: Paper A2, Int. Conf. on Drag Reduction, BHRA Fluid Engng. Cranfield, U.K. (Sept. 1974).
26. McMillan, M.L.: C.E.P. Symposium Series, No. 111, 67, 27 (1971).
27. White, A.: Nature, 214, 585 (1967).
28. Virk, P.S., et al.: J. Fluid Mech. 30, 305 (1967).
29. Virk, P.S., et al.: J. Appl. Mech. 37, 488 (1970).
30. Gaspari, G.P., et al.: CISE-R-83 (1964).
31. Fukuda, K., et al.: SN941 74-57 (1974).
32. Harrison, R.F.: ME Thesis, School of Engineering, University of Auckland (1975).
33. Adorni, N., et al.: CISE-R-31 (1961).

CISE reports are available from Centro Informazioni Studi Esperienze Documentation Service, Casella Postale 3986-20100 Milan, Italy; FEI reports from Physical Energetics Institute, Obninsk, USSR; ESDU reports from Engineering Sciences Data Unit, 251-259 Regent St., London, WIR 7AD, UK; SN reports from O-arai Engineering Centre, Power Reactor and Nuclear Fuel Development Corporation, Ibaraki, Japan.

Symbol	Friction regime (See section 3.1)	Refs	Note: All data (except that marked ▽) are upflow
Δ	(4,0,a)	14 (Table 9)	Argon-alcohol, see Δ data of Fig. 3
0	(4,1,a)	33	Steam-water high quality adiabatic flow at 7 MPa in 8.25 mm/5.02 mm annulus
x	(4,2,a)	30	Steam-water intermediate quality, adiabatic flow at 5 and 7 MPa in a 9.18 mm tube. See Fig. 5b
•	(4,3,c)	14 (Table 9)	Argon-alcohol, see • data of Fig. 3
+	(4,4,c)	30	Steam-water lower intermediate quality, high mass flux adiabatic flow at 7 MPa in a 5 mm tube. See Fig 5a
▽	(4,6,c)	31	Steam-water lower intermediate quality adiabatic horizontal flow at 7 MPa in a 76.2 mm tube
▲	(4,8,c)	32	Steam-water flow at 2 MPa in a 200 mm tube

Fig. 1. Notation

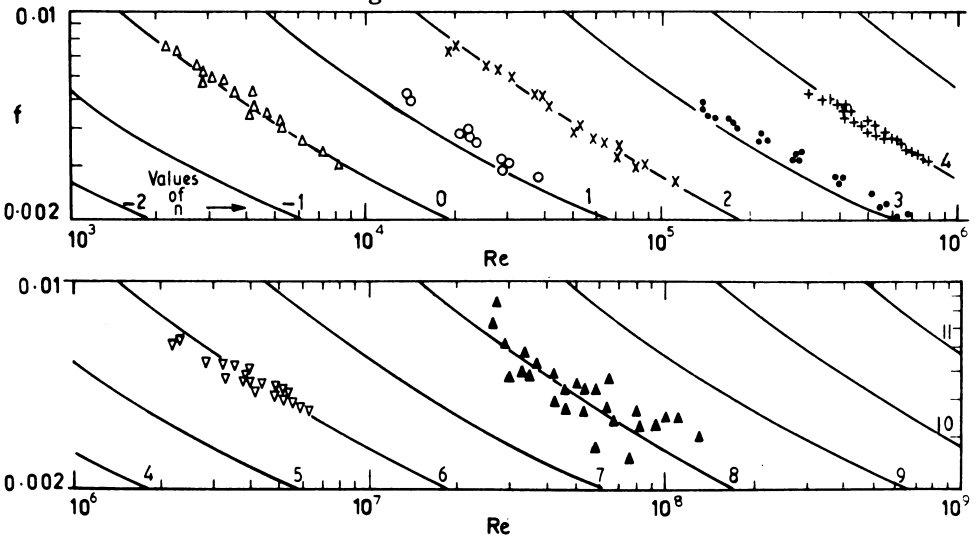

Fig. 1. Friction factors for m = 4

Symbol	Friction regime (See section 3.1)	Core region velocity profile and friction factor expression	Velocity profile between core region and wall
Δ	(1,3,c)	$j^+ = 8 \log y^+ - 12.88$ $1/\sqrt{f} = 5.66 \log Re\sqrt{f} - 15.33$	a) ? ($m \leq -4$) b) $j^+ = y^+$
x	(2,0,a)	$j^+ = 11.31 \log y^+ - 2.49$ $1/\sqrt{f} = 8.0 \log Re\sqrt{f} - 10.56$	$j^+ = y^+$
0	(3,1,b)	$j^+ = 16 \log y^+ - 13.28$ $1/\sqrt{f} = 11.31 \log Re\sqrt{f} - 21.84$	a) $j^+ = 2.83 \log y^+ + 2.04$ [(m,n) = (-2,-1)] b) $j^+ = y^+$
+	(4,1,a)	$j^+ = 22.63 \log y^+ - 21.27$ $1/\sqrt{f} = 16 \log Re\sqrt{f} - 32.64$	a) $j^+ = 5.66 \log y^+ + 2.83$ [(m,n) = (0,-1)] b) $j^+ = y^+$
∇ and ▼ (Fig. 2d(i))	(2,1,e)	$j^+ = 11.31 \log y^+ + 15.27$ $1/\sqrt{f} = 8 \log Wef + 3.20$	?
? and • (Fig. 2d(ii))	(0,?,?)	Friction data uncorrelatable with present model. The experimental void:friction-factor relation is consistent with m=0 (Fig.2d(ii))	

Fig. 2. Notation

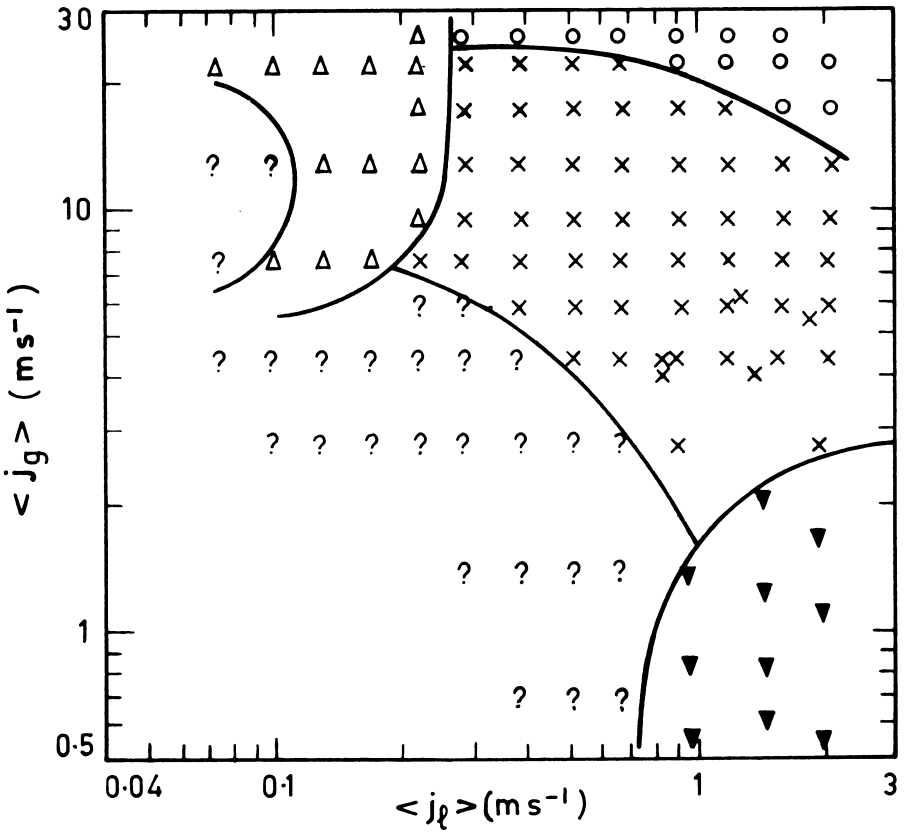

Fig. 2a. Friction regime map

Fig.2 Flow characteristics for argon-water upflow in round tubes. Data from refs. 11 to 18

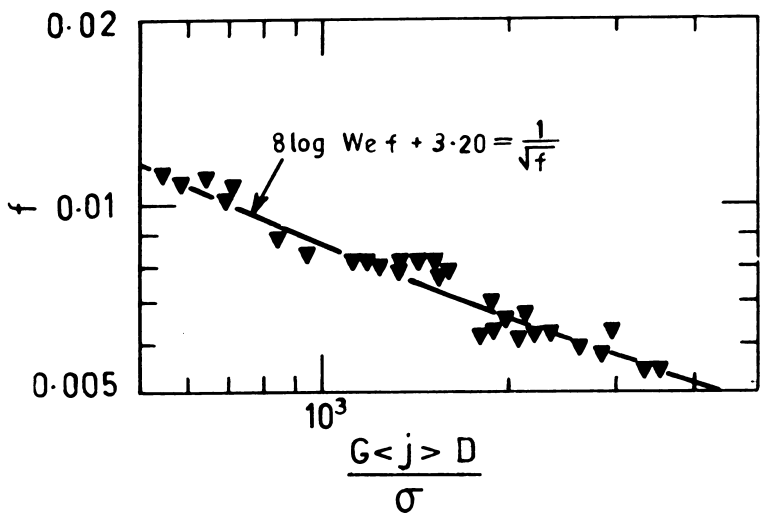

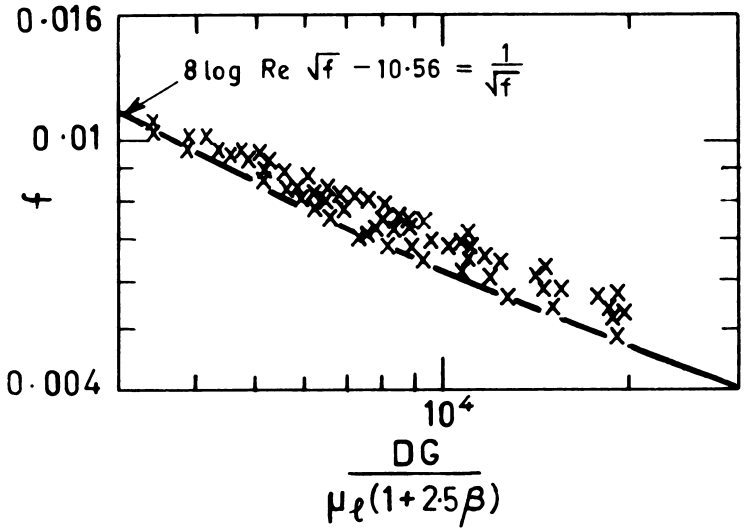

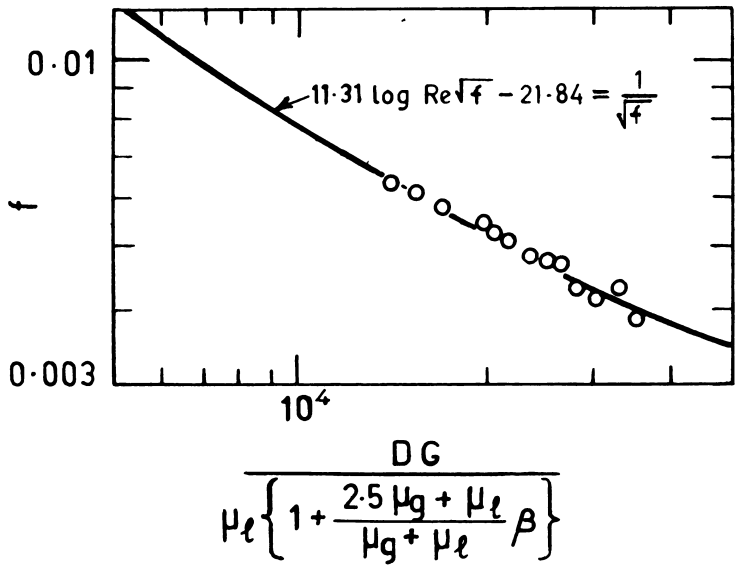

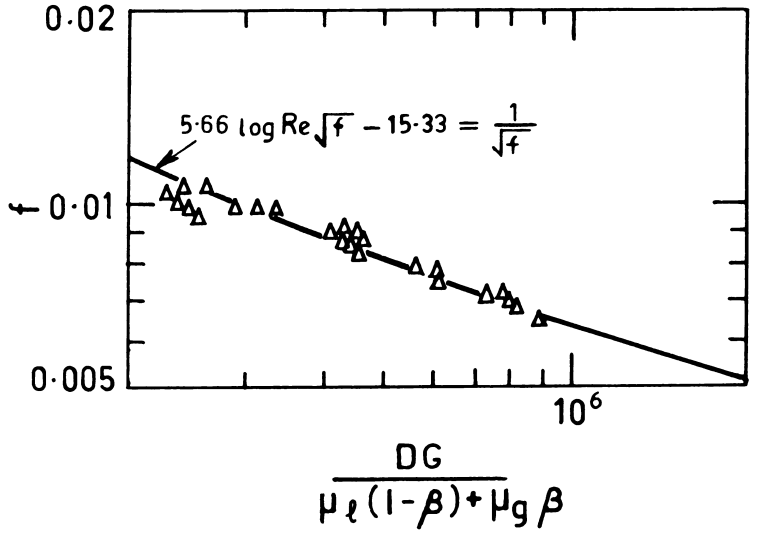

Fig. 2b. Friction factor data. Notation as in Fig. 2a.

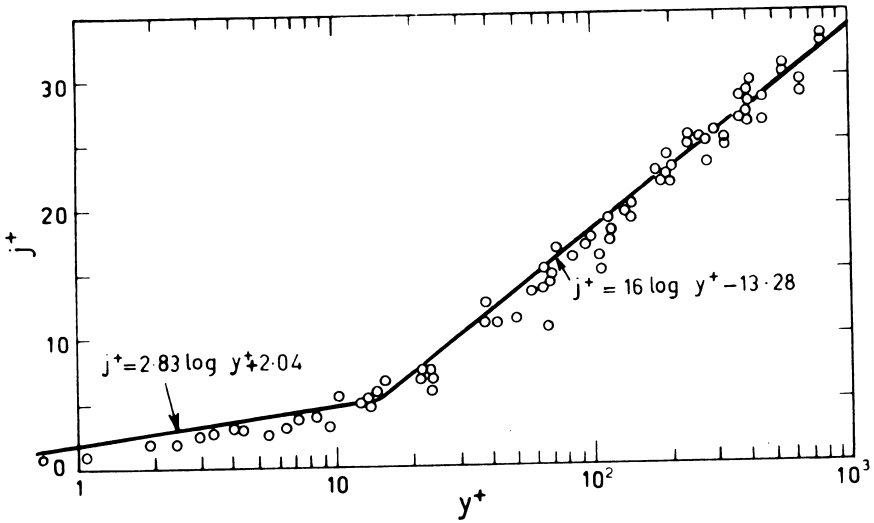

Fig. 2c I

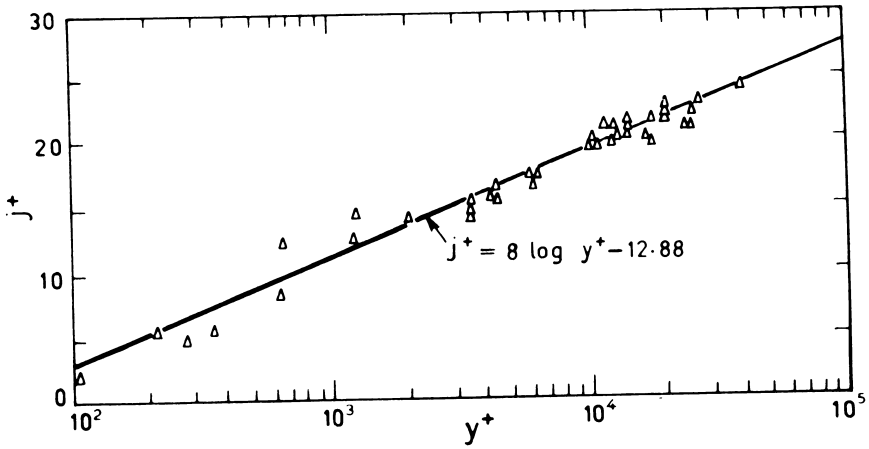

Fig. 2c II

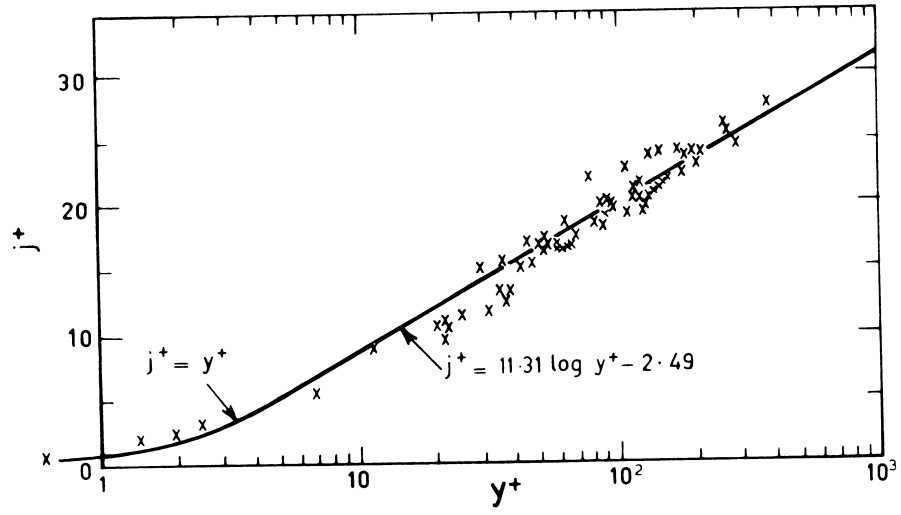

Fig. 2c III

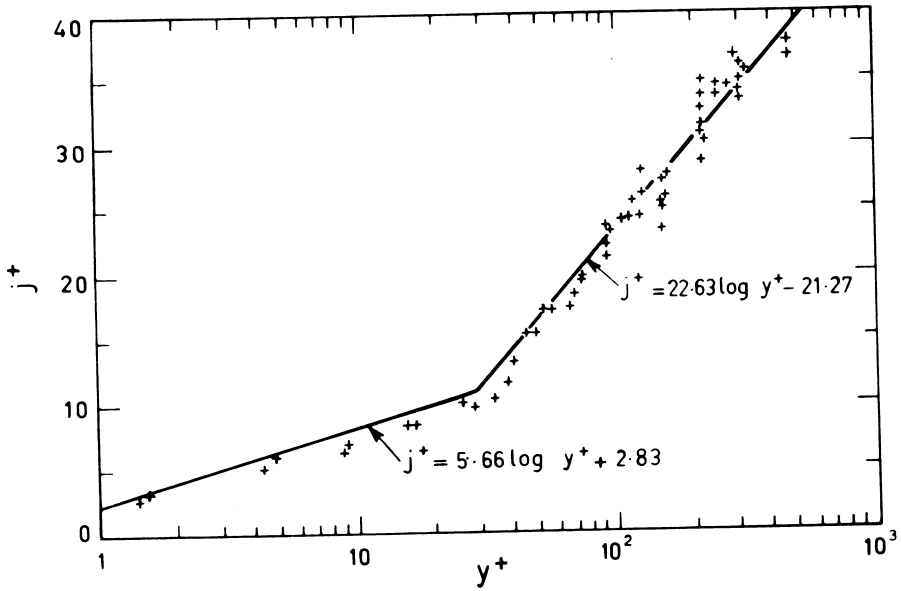

Fig. 2c IV

Fig. 2c. Non-dimensional velocity profiles. Notation as in Fig. 2a.

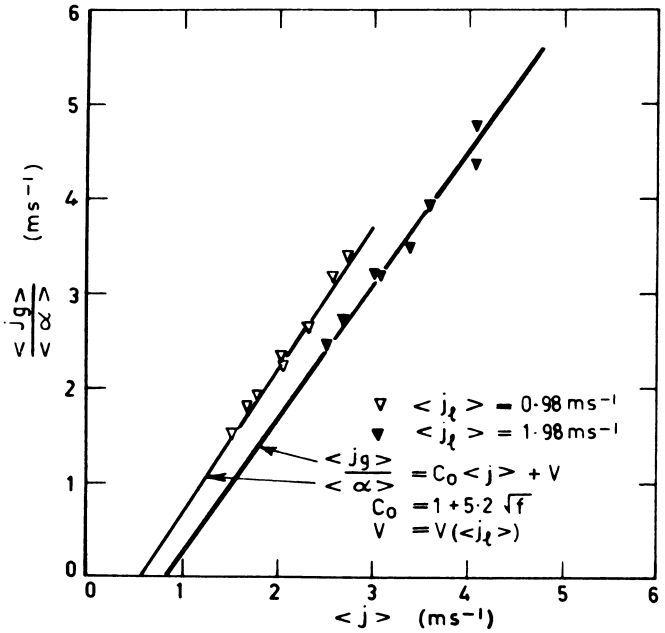

Fig. 2d I
High mass flux distributed flow (Ref. 18 data excluded)

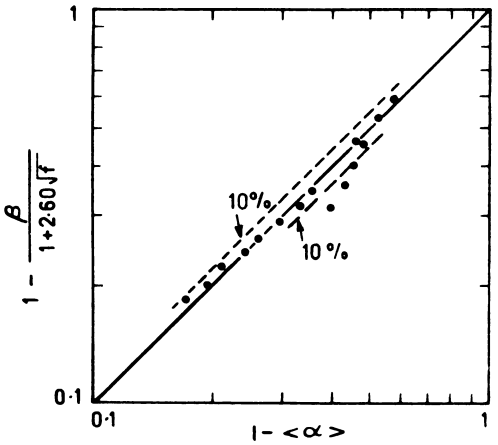

Fig. 2d II
Low mass flux distributed flow.

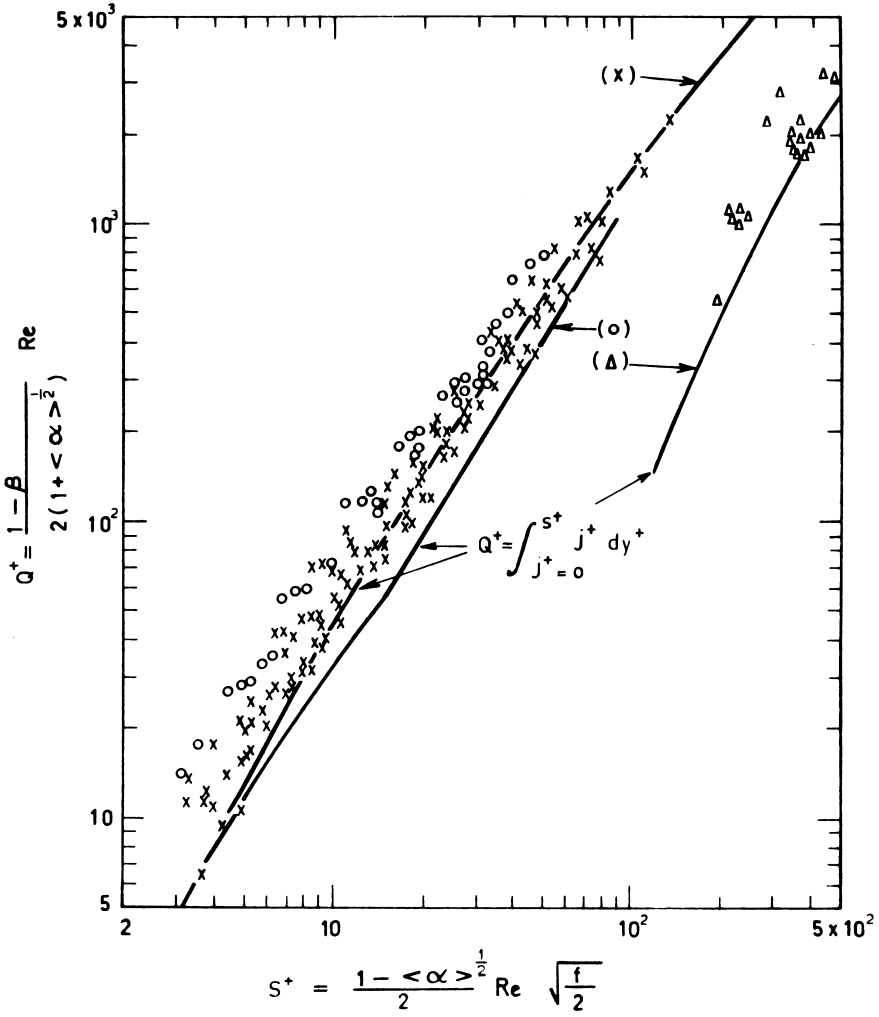

Fig. 2d III
Separated flow.

Fig. 2d. Average voidage behaviour. Notation as in Fig. 2a.

Symbol	Friction regime (See section 3.1)	Core region velocity profile and friction factor expression	Velocity profile between core region and wall
*	(0,-2,d)	$j^+ = 5.66 \log y^+ + 5.66$ $1/\sqrt{f} = 4.0 \log Re\sqrt{f} - 0.4$	a) $j^+ = 11.31 \log y^+ - 2.49$ [(m,n) = (2,0)] b) $j^+ = y^+$
•	(4,3,c)	$j^+ = 22.63 \log y^+ - 43.9$ $1/\sqrt{f} = 16.00 \log Re\sqrt{f} - 48.6$	a) $j^+ = 8 \log y^+ - 8.88$ [(m,n) = (1,2)] b) ? c) $j^+ = y^+$
□	(3,0,b)	$j^+ = 16 \log y^+ - 5.28$ $1/\sqrt{f} = 11.31 \log Re\sqrt{f} - 16.2$	$j^+ = y^+$
Δ	(4,0,a)	$j^+ = 22.63 \log y^+ - 9.96$ $1/\sqrt{f} = 16.0 \log Re\sqrt{f} - 24.64$	$j^+ = y^+$
▲	(0,-2,c)	$j^+ = 5.66 \log y^+ - 5.66$ $1/\sqrt{f} = 4.0 \log Re\sqrt{f} - 0.4$	a) $j^+ = 11.31 \log y^+ - 2.49$ [(m,n) = (2,0)] b) $j^+ = y^+$
?	?	Friction data uncorrelatable with present model	

Fig. 3 Notation.

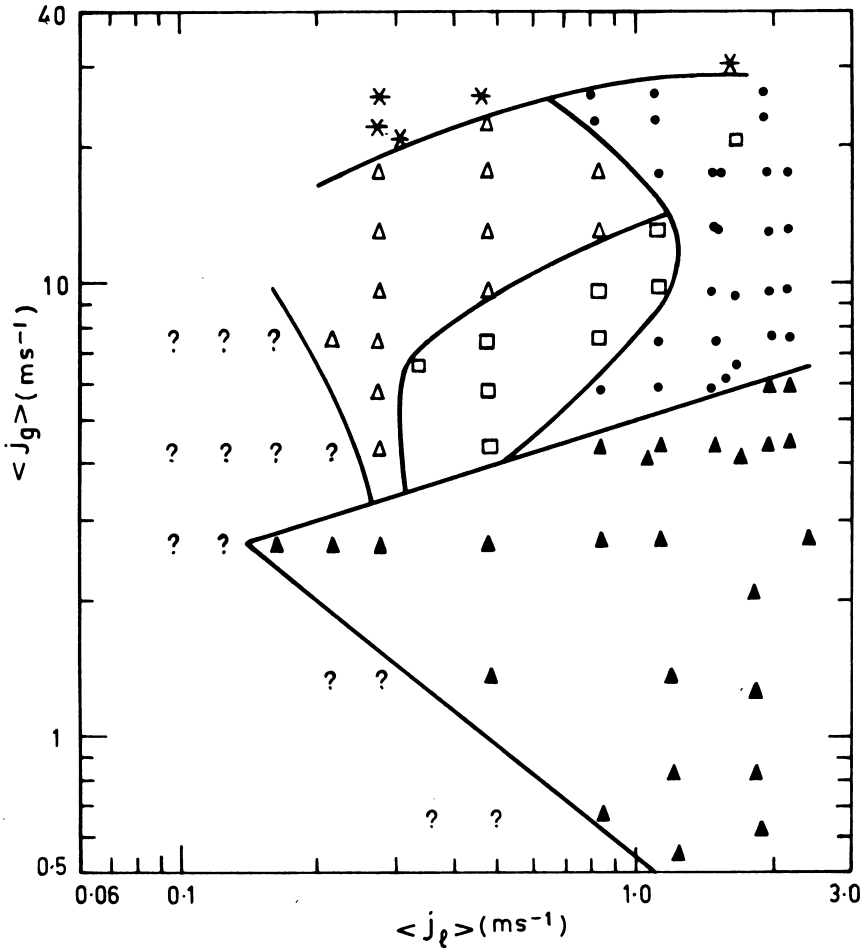

Fig. 3a. Friction regime map.

Fig. 3 Flow characteristics for argon-alcohol upflow data in round tubes. Data from Refs. 15 to 18.

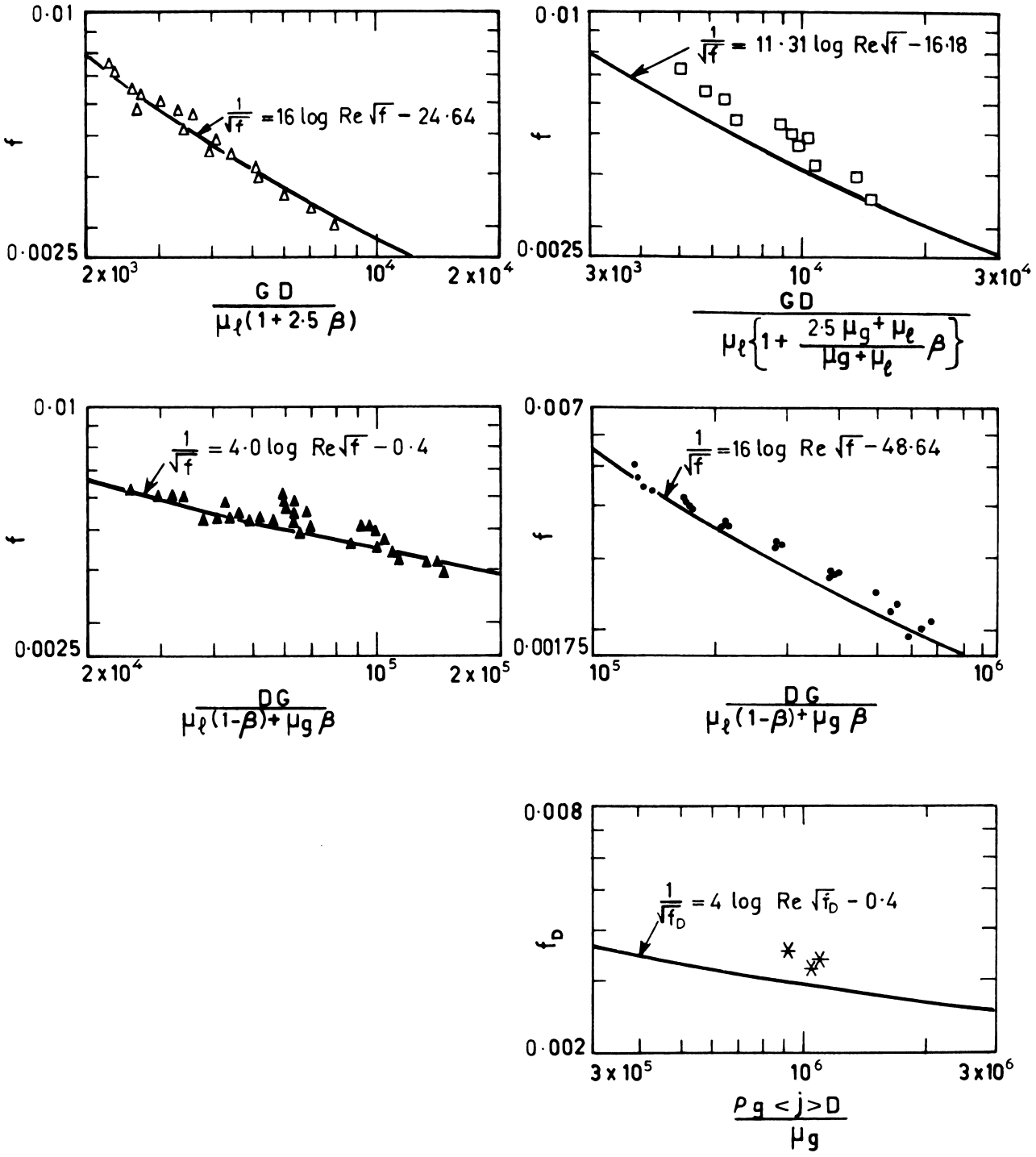

Fig. 3b. Friction factor data. Notation as in Fig. 3a.

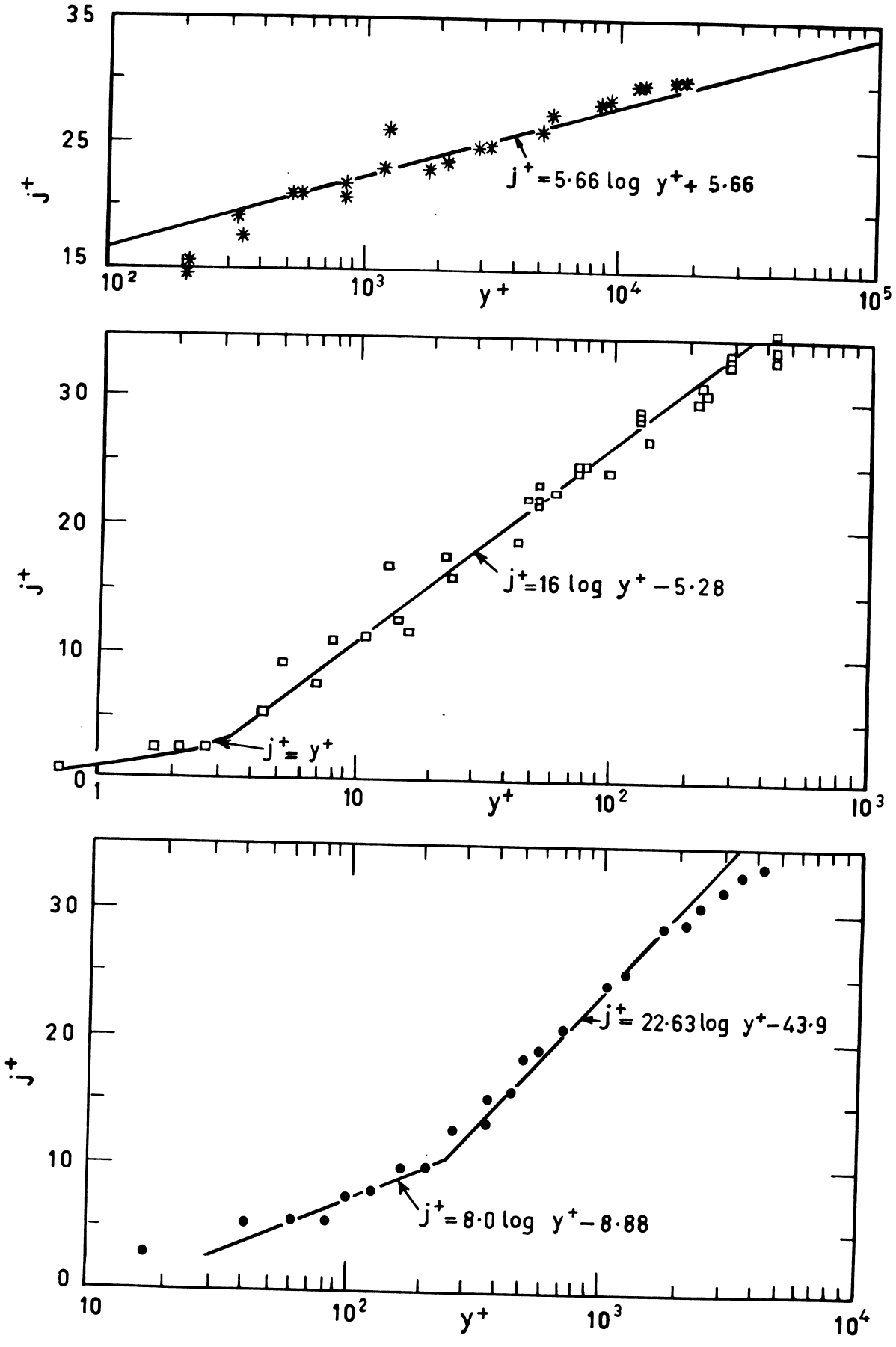

Fig. 3c. Non-dimensional velocity profiles. Notation as in Fig. 3a.

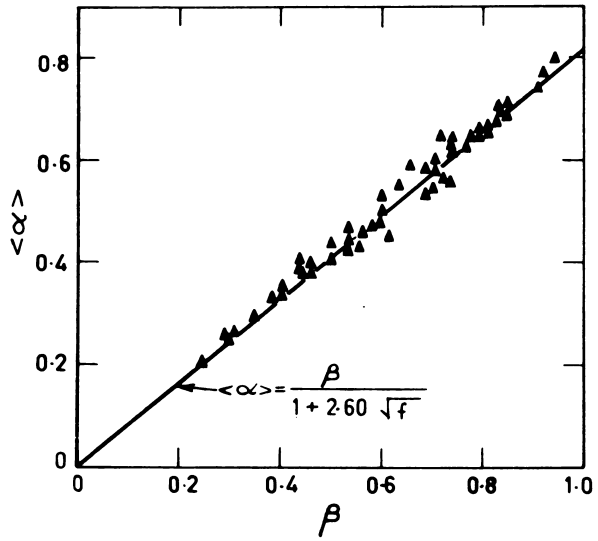

Fig. 3d I.
Liquid-phase-continuous
distributed flow.

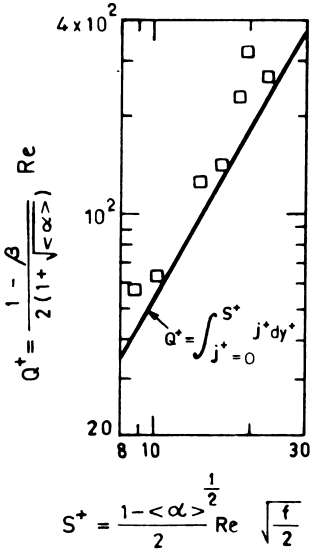

Fig. 3d II.
Separated flow.

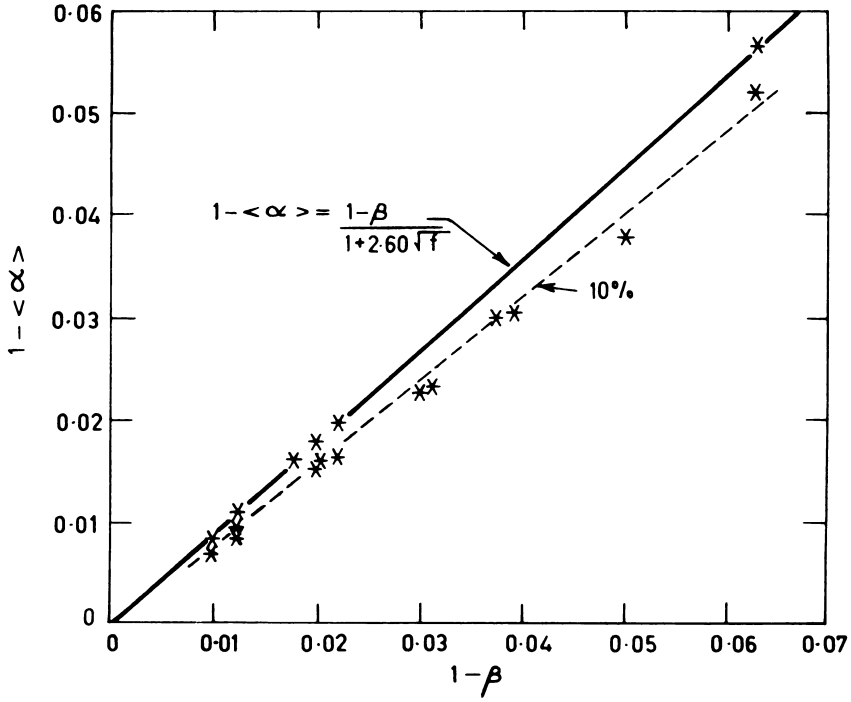

Fig. 3d III.
Gas-phase-continuous
distributed flow.

Fig. 3d. Average voidage behaviour. Notation as in Fig. 3a.

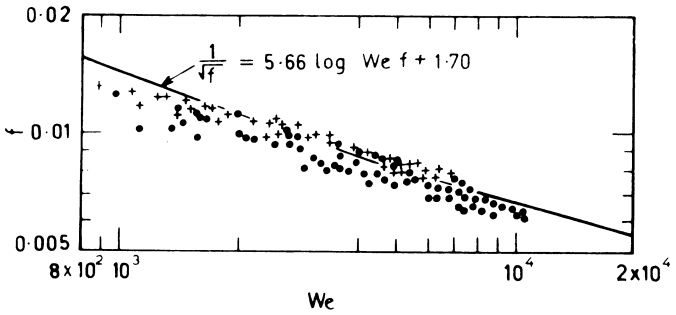

Fig. 4a. Friction factor data.

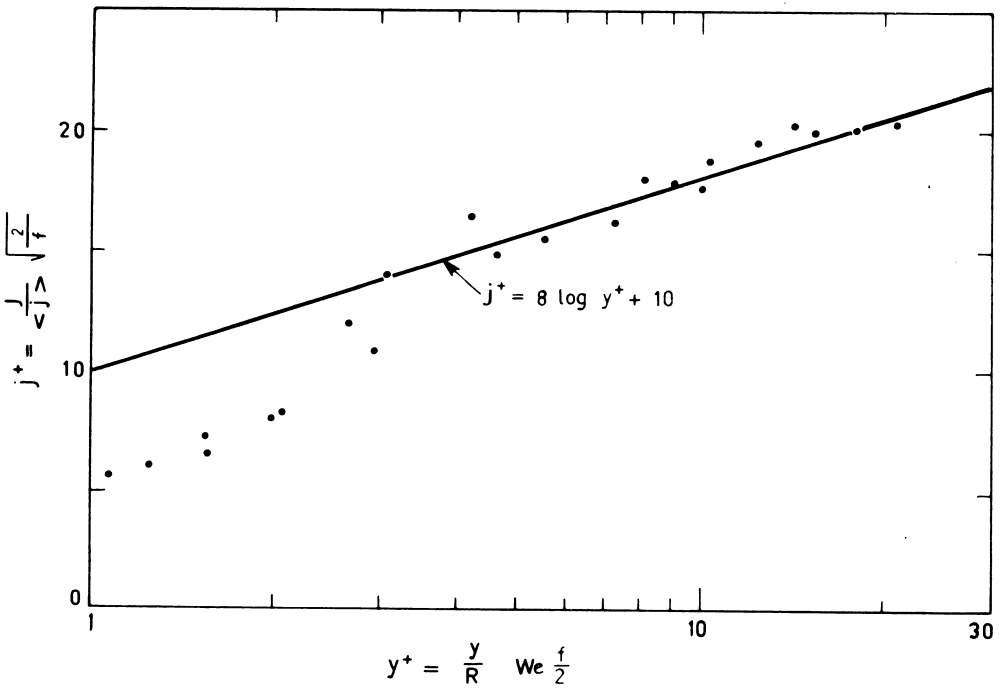

Fig. 4b. Non-dimensional velocity profiles.

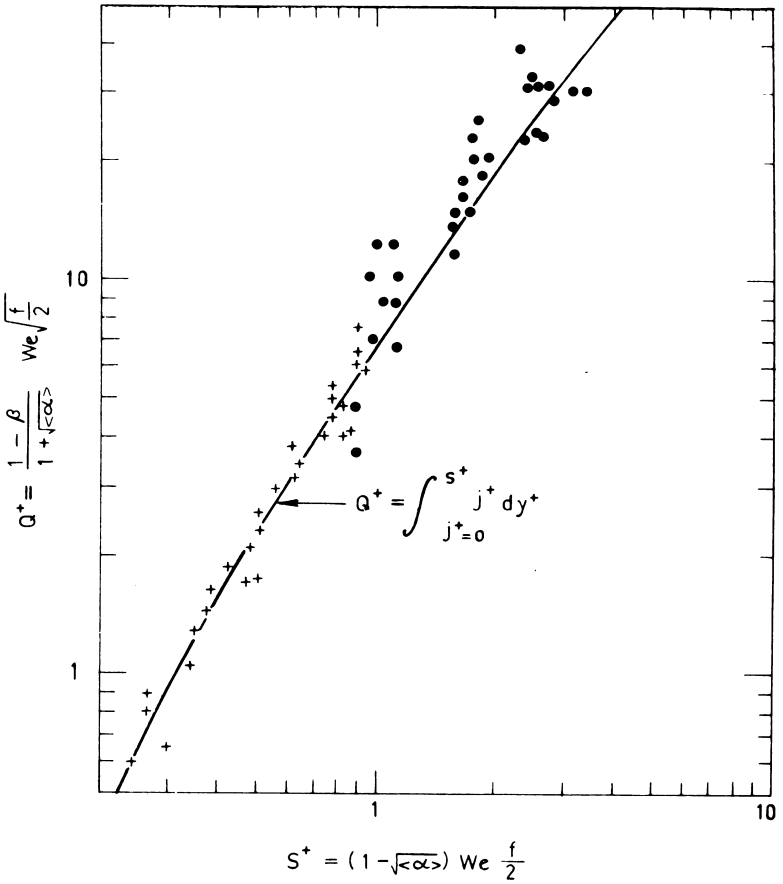

Fig. 4c. Average void fraction behaviour.

Fig. 4. Flow characteristics for separated (1, 2, e) flow data. Data from Ref. 20(+) and Ref. 21 (.).

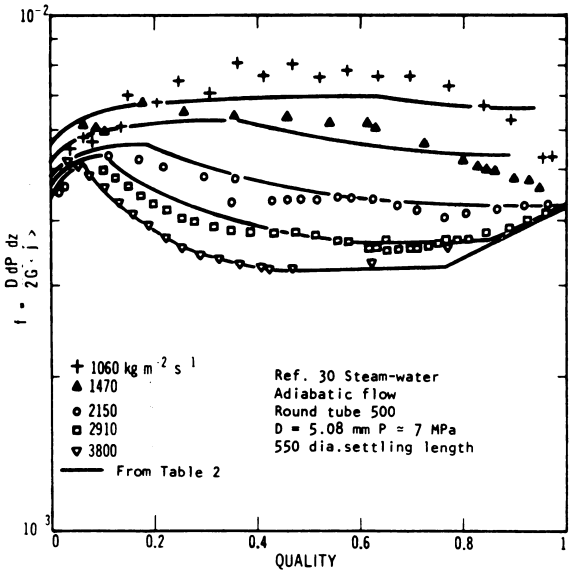

Fig. 5a. Round tube adiabatic flow with long settling length.

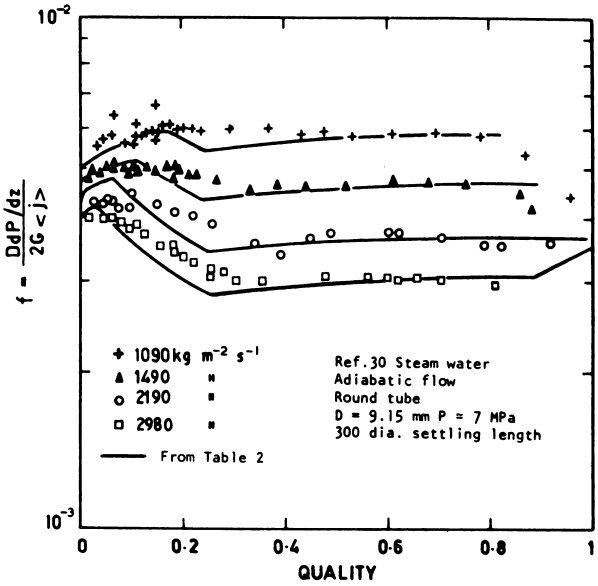

Fig. 5b. Round tube adiabatic flow with short settling length.

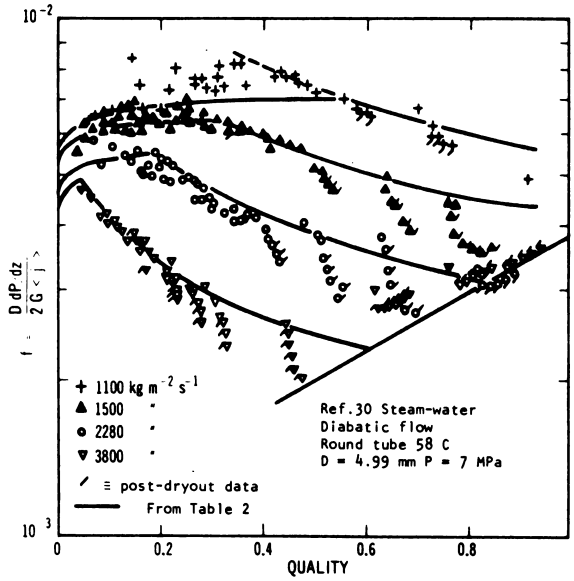

Fig. 5c. Round tube diabatic flow.

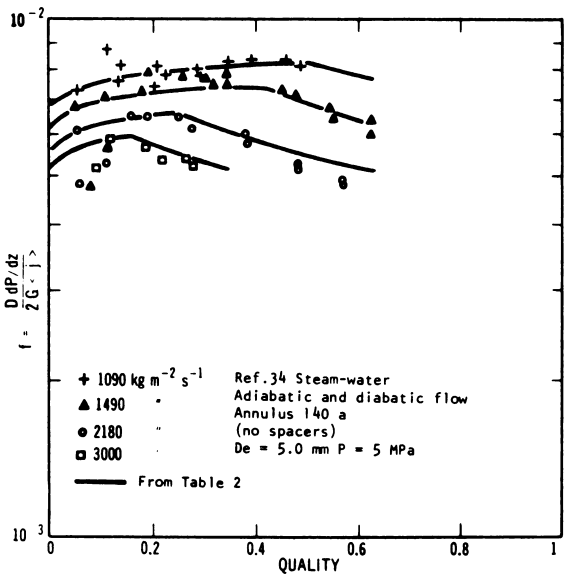

Fig. 5d. Flow in an annulus with no spacers.

Fig. 5. Friction factors for high pressure steam-water flows.

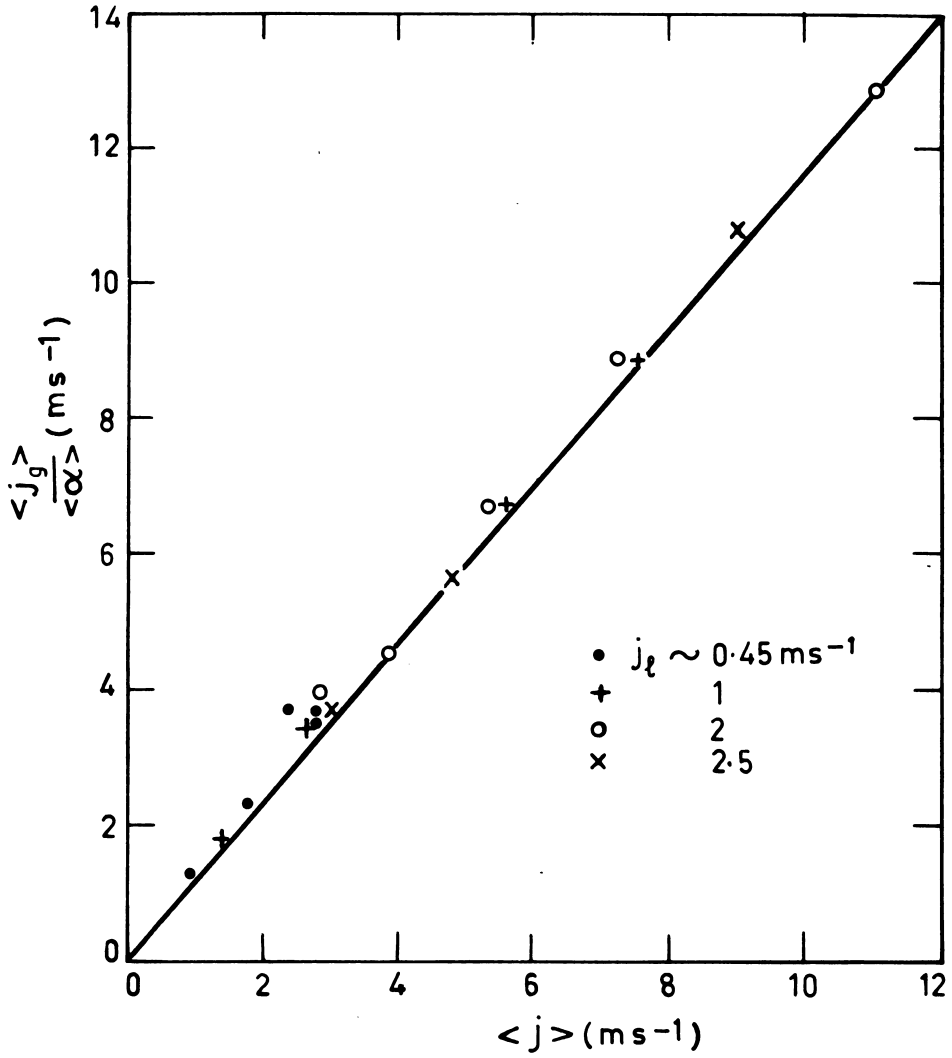

Fig. 6. Average voidage behaviour for high mass flux distributed argon-water flow in a round tube. Data from Ref. 18. Compare with Fig. 2d I.

APPENDIX A11

Bubble Swarm Characteristics in Bubble Columns

Can. C. Chem. Eng. 54, 503 (1976)

Editor, Can. J. Chem. Eng.:

Following an analysis of their own and other data, Kumar et al[1] have proposed new correlations for various bubble column characteristics. Of these, their correlations for gas holdup

$$x = 0.728\,u_g^* - 0.485\,(u_g^*)^2 + 0.0975\,(u_g^*)^3 \quad \ldots\ldots (1)$$

(their notation) and bubble swarm characteristic velocity

$$\overline{u^*}_o = 1.37 + 1.90\,u_g^* + 1.42\,(u_g^*)^2 - 0.16\,(u_g^*)^3 \quad \ldots\ldots (2)$$

deserve some comment.

An examination of the holdup data shown by Kumar et al[1] in their Figure 2 indicates that the gas holdup data can be suitably described by an equation of the form

$$x = (1.37/u_g^* + 1.25)^{-1} \quad \ldots\ldots (3)$$

Rearranging Equation (3),

$$u_g/x = 1.25\,u_g + 1.37\,(\gamma g \Delta\rho/\rho_l^2)^{1/4} \quad \ldots\ldots (4)$$

which can be seen to be a special case, for zero liquid flow, of the Zuber and Findlay[2] equation

$$u_g/x = C_o\,(u_g + u_l) + V \quad \ldots\ldots (5)$$

where C_o is a distribution parameter resulting from phase and velocity distribution effects, and V is a 'drift velocity' associated with buoyancy influences on the dispersed phase.

A direct transposition of Equation (1) into the u_g^*/x: u_g^* plane does not yield a straight line, but a curve consistent with non-constant coefficients in Equation (4). Data scatter is, however, such that appropriately chosen constant coefficients give a suitable description of the data over the whole voidage range examined.

In relation to Equation (5) as applied to bubble flow, Zuber et al[3] suggest $C_o = 1.2$ (this value does not always hold for zero u_l[4] or for down flow[5]) and, $V = 1.41\,(\gamma g \Delta\rho/\rho_l^2)^{1/4}$, the coefficient 1.41 lying between the values 1.53 proposed by Harmathy[6] and 1.18 proposed by Peebles and Garber[7]. Equation (4) is thus reasonably consistent with the recommendations of Zuber et al [3].

Since the data of Kumar et al[1] seem to be consistent with an equation of the form of Equation (5), a curve fit of their data with this form is preferable to that chosen by Kumar et al[1], as Equation (5) applies also to non-zero liquid flows. Valuable information concerning void and velocity profile behaviour (via the distribution parameter value), and individual bubble rise velocity with respect to the mixture velocity (via the drift velocity value), could also have been obtained for their system. Furthermore, recent work[8,9] generalising the work of Zuber and Findlay[2], has indicated that knowledge of the distribution parameter can be useful for evaluating quantities other than gas holdup values.

Unfortunately, as indicated by their discussion of their Equations (9) and (10), Kumar et al[1] were aware of the work of Zuber et al[2,3] but chose not to analyse their data in the u_g/x: u_g plane, which would have yielded appropriate distribution parameter and drift velocity values for their system. Instead, they compared their data with Equation (5) using an arbitrary and non-recommended distribution parameter value, and for their low flow data, an invalid drift velocity value.

At this stage, it is appropriate to note that Equation (4) can be re-expressed in terms of dimensionless quantities used by the authors[1] to yield

$$\overline{u_o^*} = 1.37 + 1.25\,u_g^* \quad \ldots\ldots (6)$$

Except for the fact that Equations (1), (2) and (6) all approach $\overline{u_o}^* = 1.37$ $(= 1/0.728)$ at low u_g values, I have been unable to reconcile Equation (6) with Equation (2). It appears that Equations (1) and (2), as proposed by the authors, are incompatible, even though these equations should be different versions of the same information on their data behaviour. This discrepancy may arise from experimental techniques used. Although directly measured holdup values (x) can be converted to characteristic velocity values $\overline{u_o} = u_g/x$, this second parameter may have been determined independently. Unfortunately, details have not been given of experimental techniques used for the determination of x and $\overline{u_o}$, which may have explained the apparent inconsistency between Equations (1) and (2).

D. Beattie,
AAEC Research Establishment,
Private Mail Bag,
Sutherland, 2232, Australia.

References

(1) Kumar, A., Degalseesan, T. E. Laddha, G. S. and Hoelscher, H. E., Can. J. Chem. Eng. 54, 503 (1976).
(2) Zuber, N., and Findlay, J. A., J. Heat Transfer 87, 453 (1965).
(3) Zuber, N. Staub, F. W., Bijwaard, G. and Kroger, P. G., General Electric report GEAP 5417 (1967).
(4) Towell, G. D., Strnad, B. S., and Acherman, G. H., AIChE-I. Chem. E. Symp. Ser. No. 10, 97, (1965). (Data as quoted by Kumar et al[1]).
(5) Lorenzi, A. and Sotgia, G., Energia Nucleare 23, 396 (1976).
(6) Harmathy, T. Z., AIChE J. 6, 281 (1960).
(7) Pebbles, F. N. and Garber, H. J., Chem. Eng. Progr. 49, 88 1953.
(8) Beattie, D. R. H., Paper D3, Second Int. Conf. on Pressure Surges, City Univ., London (BHRA Fluid Engineering, Cranfield), England (1976).
(9) Beattie, D. R. H., Paper in Second Australasian Conference on Heat & Mass Transfer, Sydney, Feb. 16-18, 1977.

★ ★ ★

RELATIONSHIP BETWEEN WALL SHEAR STRESS AND THE HEAT TRANSFER CRISIS PHENOMENON WITH VAPOUR/LIQUID FLOWS

D.R.H. Beattie
K.R. Lawther

AAEC Research Establishment, Lucas Heights, NSW, Australia

ABSTRACT

Critical heat flux characteristics for vapour/liquid flows are examined in terms of the relation between the heat transfer crisis and wall shear stresses. A comparison of dryout data with corresponding pressure drop data shows that critical heat flux is related to the relevant pre-dryout and post-dryout friction regimes. From a consideration of experimental data for relatively low heat fluxes, a pseudo-dryout condition is identified corresponding to a 'slow burnout' condition. Observed differences in critical heat flux characteristics for flows in tube and complex channel geometries are shown to be related to differences in shear stress characteristics.

NOMENCLATURE

D	= channel diameter
D_s	= shear equivalent diameter {= 4 x (flow area)/(non-dried perimeter)}
dp/dz	= frictional pressure gradient
$\dot{m}$	= coolant mass flux
p	= pressure
$\dot{Q}$	= heating power input
$\dot{q}$	= critical heat flux (CHF)
v	= flow velocity
x	= flow quality
x^*	= characteristic hydrodynamic dryout quality
Re	= Reynolds number
We	= Weber number
ε	= characteristic surface roughness dimension
η	= dynamic viscosity
ξ	= friction factor
ρ	= density
σ	= surface tension
ψ	= vapour volumetric flow fraction

Subscripts

g = vapour	out = outlet condition
ℓ = liquid	r = rod
in = inlet condition	sh = shroud

INTRODUCTION

The temperature of a surface transferring heat to a boiling flow is usually within a few degrees of the saturation temperature of the coolant. This situation occurs for all heat fluxes up to a particular 'critical heat flux' (CHF), above which 'vapour blanketing' of the heated surface occurs and, for a heat-flux-controlled surface, excessive surface temperatures may result.

Although the mechanism of the heat transfer crisis is qualitatively understood (for example, in annular flow it is usually associated with reduction of the thickness of liquid film on the heating surface to zero (1)), a detailed understanding is lacking, and present heat transfer crisis equations are essentially empirical. This is unsatisfactory since important applications of such equations, particularly those concerned with nuclear reactor engineering, involve extrapolation to conditions which differ considerably from the experimental conditions on which they were based.

In this paper, a method of reducing empiricism in dryout correlations is examined. The method is based on an examination of the heat transfer crisis in terms of its effect on pressure loss characteristics and, in effect, quantitatively allows for the hydromechanical contribution to removing liquid from the heating surface during heat transfer crisis. This contribution, in which liquid is dragged from the film at the wall to form droplets in the turbulent core, can be substantial enough at sufficiently high values of coolant mass flux and quality to strip all the liquid from the surface even under adiabatic conditions (2,3), resulting in a hydrodynamically-induced dryout.

RELATION BETWEEN DRYOUT AND TWO-PHASE FRICTION

In an analysis of two-phase friction data (3), it was noted that there was no discontinuity of shear stress at the boundary between hydrodynamically-induced dryout and wet-wall adiabatic flow conditions. Thus, for a given flow section and mass flux, the flow quality at which the friction factor equations for the wet-wall and dry-wall regimes intersect must be the dryout quality corresponding to the zero heat flux limit of a diabatic dryout curve. An analysis of dryout data in terms of dryout heat flux, $\dot{q}$, versus coolant quality, x, with mass flux as a parameter, indicates that plots can be subdivided into a series of straight lines of the form

$$\dot{q} = a(x - x^*). \qquad (1)$$

As anticipated, the lines corresponding to low heat flux values intersect the zero heat flux axis at qualities given by the intersects of the adiabatic wet-wall and dry-wall friction factor

equations, even when this intersect does not occur in the sensible quality range (i.e. $x > 1$).

A recent extension of the two-phase flow analysis (4) provided equations for both adiabatic and diabatic two-phase friction. Boundaries between different friction regimes (a 'friction regime' corresponds to flow conditions in which a particular friction factor relation applies) were examined in terms of entropy production rates. In the special case of the dry-wall regime boundary, which corresponds to the heat transfer crisis in diabatic flow, it was supposed that the increase of wall temperature occurring at the crisis (which increases the rate of entropy production due to heat transfer) and the accompanying reduction of shear stress at the heating surface (which reduces the rate of entropy production due to viscous dissipation) occur such that there is no net change in entropy production rate.

On this basis, it can be surmised that the dryout curve corresponding to a given friction regime should extrapolate to a zero heat flux quality given by the intersect of the dry-wall and the appropriate wet-wall friction factor equations, even if the friction regime does not border the dry-wall regime, since, according to the entropy production hypothesis, if the two regimes were next to each other, the zero heat flux dryout would occur such that there would be no discontinuity in wall shear stress.

Data analysis in which CHF data form a series of straight lines of the form of equation (1) shows that, in fact, each straight line portion can be associated with a particular friction regime, and that the value of x^* for that regime is the quality at which the friction factor equations for that regime and the dry-wall regime intersect.

This paper considers the relationship between pre- and post-dryout shear stress characteristics and the zero CHF limit for different regions on CHF: quality plots. Because of uncertainties associated with the prediction of shear stresses, data analysis is confined to dryout data for which there is associated pressure drop data. Since dryout is a local phenomenon, and pressure drop data correspond to average pressure gradients between pressure tapping locations, data analysis is further confined to those data where quality does not change substantially between pressure tappings. Under these conditions it is likely that only one friction regime would apply for the flow being considered.

TWO-PHASE PRESSURE LOSS EQUATIONS

Relationships between two-phase friction factor and Reynolds or Weber numbers are presented in references (4) and (5). Equations relevant to data discussed in this paper are

$$1/\sqrt{\xi} = 3.48 - 4 \log (2\varepsilon/D + 9.35/(Re\sqrt{\xi})), \quad (2)$$

$$1/\sqrt{\xi} = 16 \log Re\sqrt{\xi} - 40.6, \quad (3)$$

$$\text{and } 1/\sqrt{\xi} = 14 \log We\ \xi - 10.4. \quad (4)$$

Dimensionless group definitions for the above equations depend on the nature of the sublayer structure. For wet-wall flows,

$$\xi = D(dp/dz)/(2\ \dot{m}\ v) \quad (a,b,c)$$

$$\text{and} \quad Re = D\ \dot{m}/\eta \quad (a,b)$$

$$\text{with} \quad \eta = \{1 + 2.5\psi\}\eta_\ell \quad (a)$$

$$\text{or} \quad \eta = [1 + \{(2.5\eta_g + \eta_\ell)/(\eta_g + \eta_\ell)\}\ \psi]\eta_\ell \quad (b)$$

depending on the nature of sublayer bubbles. Relations (a) apply for entrained bubbles which have rigid surfaces, (b) for other bubbles, except for flows with attached wall bubbles where relations (c) apply, as expected for diabatic flows, in which the friction factor depends not on the Reynolds number but on the Weber number

$$We = D\ \dot{m}\ v/\sigma \quad (c)$$

For dry-wall flows,

$$\xi = D(dp/dz)/(2\ \rho_g v^2) \text{ and } Re = D\ v\ \rho_g/\eta_g \quad (d)$$

In this paper, a letter (a,b,c or d) is used to specify the sublayer type. Thus, equation (2d) refers to equation (2) with a sublayer such that dimensionless groups (d) apply (i.e. dry-wall flows). It will be noted that equation (2) is the Colebrook equation developed for single-phase flow.

The following friction equations recommended for steam/water flows (4,5) will be used later in the data analysis:

(i) equation (2d) for dry-wall flows;
(ii) equation (3a) for high quality adiabatic wet-wall flows in round tubes; and
(iii) equation (4c) for high quality pre-dryout diabatic flows in round tubes.

Wet-wall pressure losses for flows in complex channel geometries behave differently. Relevant equations are not given here because, as will be seen, suitable complex geometry data for testing the present concepts necessarily have pressure losses which are inconsistent with the earlier recommendations (4,5). We note, however, that a dryout situation can occur in complex geometries in which not all flow boundaries are subject to dryout. Theoretical considerations and limited experimental evidence (6) suggest that for such cases, pre-dryout pressure loss equations apply provided equivalent diameter, D_s, is used.

DRYOUT AND PSEUDO-DRYOUT

Almost all two-phase dry-wall shear stress data are consistent with equation (2d). The appropriate value of surface roughness for equation (2) however depends on the relevant surface condition.

Dryout is the normal surface condition for post heat-transfer-crisis conditions. No liquid exists on the surface; post-dryout pressure losses are consistent with equation (2d) with the single phase value of ε/D also applying to the two-phase case; equilibrium conditions for dryout are achieved rapidly; where instrumentation is suitable for detecting such events, the crisis is often (but not always) reported to be preceded by a decrease in wall temperature with increasing heat flux at heat fluxes very close to the critical heat flux; and post-dryout heat transfer data are consistent with Reynolds' analogy being applied to dry-wall two-phase flows (6).

However, there is circumstantial evidence that some reported 'dryout' conditions are not really dryouts at all (6). The evidence suggests that

superheated liquid remains in the micro-crevices of the surface roughness elements at the wall, with only the peaks of the surface roughness elements actually being dry. The net effect is that, although measured wall temperatures are greater than for wet-wall flows, temperatures are less than expected for true dryout. More importantly, from the point of view of the current analysis, the roughness of the surface is apparently reduced as far as the droplet-laden steam flow is concerned, so it is similar to that for a smooth duct. To differentiate this type of 'dryout' condition from the normal dryout it is called a 'pseudo-dryout' in this paper. These pseudo-dryouts usually occur at low heat fluxes, are generally not preceded by a wall temperature decrease, and the wall temperature rise following a pseudo-dryout is slow (probably reflecting a slow rate of removal of the residual superheated liquid from the wall micro-crevices).

Since dry-wall two-phase flows are usually at Reynolds numbers where surface roughness effects are significant, the quality at which wet-wall and dry-wall friction factors are equal will depend on whether it is a true dryout or a pseudo-dryout.

DATA ANALYSIS

The concepts presented in this paper are suitably illustrated by considering published dryout data from 6 mm tubes of various lengths, a 5 mm tube, and a narrow annulus.

The interpretation of the value of x^* in equation (1) as the quality at which the wet-wall and dry-wall shear stresses become equal, indicates that it should be independent of heated length. Thus, even though the dependence of dryout heat flux on heated length may be complex, straight line plots of the form of equation (1) should extrapolate to the same zero heat flux quality (x^*) for a given mass flux and heated channel geometry, irrespective of the heated length, provided the dryout data correspond to the same friction regime.

6 mm Tube Data

Dryout data for water in 6 mm tubes (7,8) are shown in fig.1 together with friction factor data obtained from average pressure gradients measured over the heated length with dryout conditions at the exit.

It can be seen that none of the friction data is consistent with the recommended relation for diabatic flow (4,5), i.e. no data fall on the curve corresponding to eqn (4c). Instead, data either fall on a lower friction curve, or agree with the recommended curve for adiabatic flow, eqn (3a). These data were chosen because the measured pressure gradients are useful for interpreting the CHF data. However, much published data, in which values of x^* (obtained from the intersect of eqns (4c) and (2d)) are consistent with extrapolation of the CHF data to zero heat flux, have average frictional pressure gradients which agree with eqn (4c).

The tendency for some low heat flux diabatic pressure gradients to agree with recommendations for adiabatic instead of diabatic flows is regarded as evidence that heat transfer under low heat flux forced convective evaporation conditions does not stimulate bubble nucleation.

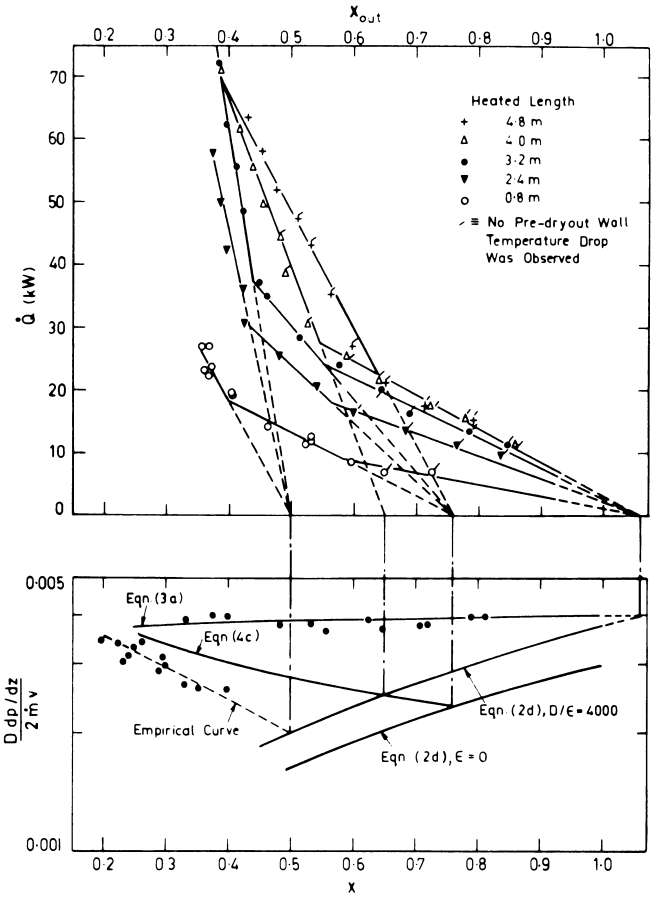

Fig.1 Critical Power and Pressure Loss Data (7,8) for 6 mm Tubes of Various Lengths at $\dot{m}$ = 2980 kg m^{-2} s^{-1} and p = 7 MPa

It will be seen that the wet-wall friction curves intersect the dry-wall and pseudo-dry-wall equations at qualities equal to the x^* values of eqn (1); as anticipated, these values are independent of heated length. We note that although average pressure losses are not consistent with eqn (4c), the intersects of the curve for this equation with the dry-wall equations give values of x^* which are consistent with much of the dryout data, suggesting that the friction regime corresponding to eqn (4c) was, in fact, appropriate in the vicinity of the dryout, even though the equation is apparently invalid for most of the distance between the pressure tappings used in measuring the pressure gradient. There are two additional features of the data which support this view:

(1) Most of the CHF data for which eqn (4c) is assumed to apply are associated with the x^* value corresponding to pseudo-dryout. A check on post-'dryout' heat transfer coefficients (7) corresponding to the data of fig.1 shows that wall temperatures were lower than for true dryout.

(2) It has been shown (11) that heat transfer coefficients for boiling flow in a thin liquid film improve when the film thickness is reduced to a size comparable to the size of bubbles detaching from the heated surface. This is due to bubbles bursting through the film surface before detach-

ment, allowing more rapid bubble release and rewetting of the bubble nucleation site. Since annular flow dryout is associated with the disappearance of a liquid film, a marked improvement in pre-dryout heat transfer coefficient might be expected in the vicinity of dryout if bubble nucleation exists within the film. In agreement with this, fig.1 indicates that pre-dryout wall temperature decreases were generally observed for those dryouts where the friction data are consistent with a boiling sublayer, but not for those lower heat flux dryout data where a non-boiling sublayer is consistent with the friction data.

Obviously there are pitfalls in assuming that average pressure gradients, as measured over a distance, allow local gradients to be deduced in the vicinity of dryout. We next consider data for which eqn (4c) is consistent with the average frictional pressure gradient data obtained at CHF conditions but, in this case, the equation appears to be invalid in the vicinity of dryout.

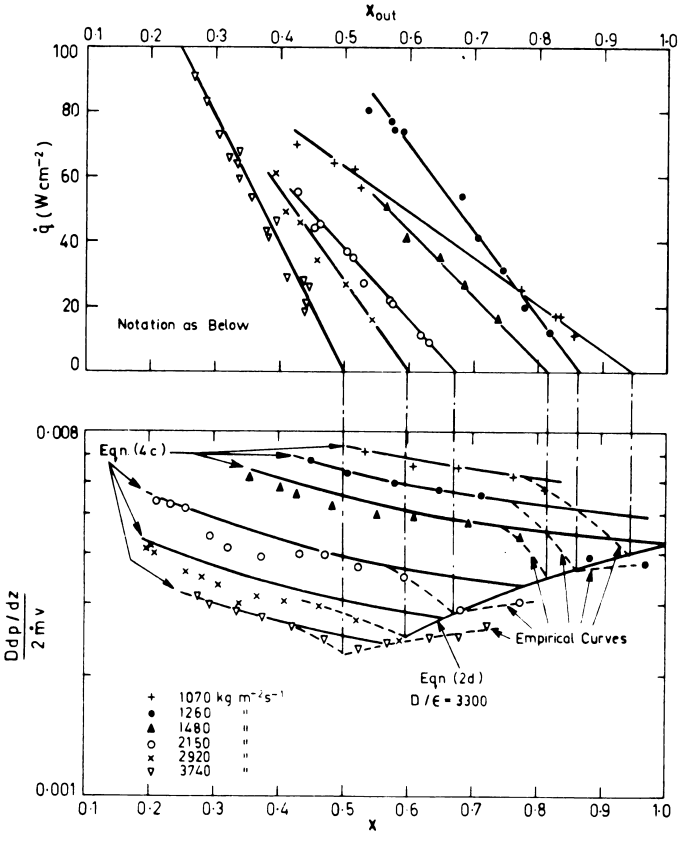

Fig.2 Critical Heat Flux and Pressure Loss Data (12,9) for 1.5 m Heated Length 5 mm Tube at Various Mass Fluxes and p = 7 MPa

5 mm Tube Data

CHF data (12) for a 5 mm tube test section are shown in fig.2 together with corresponding friction data (9). Equation (4c) is acceptably close to the friction data except in the vicinity of the intersect with the dry-wall equation (2d). (Some data fall below the true dry-wall relation for which the surface roughness was obtained from single-phase friction data (7), indicating that the dryouts for these data are actually pseudo-dryouts. To simplify the plot, CHF data corresponding to these pseudo-dryouts have been omitted from fig.2.)

The interpretation of fig.2 is that eqn (4c) is valid except near dryout. At low heat fluxes the quality increment over the test section is less, so the measured pressure gradients correspond more closely to those near the dryout location. Friction data near eqn (2d) are for low heat fluxes. The pre-dryout friction factors, which are lower than eqn (4c) values near the dry-wall equation are thus more representative of pre-dryout friction factors than is eqn (4c). As can be seen from fig.2, values of x^* corresponding to eqn (1) are given by the intersect of eqn (2d) with the empirical curves drawn through the friction data points near eqn (2d), instead of by the intersect of eqns (4c) and (2d).

Annulus Data

Two-phase friction characteristics for axial flow through annulus and rod cluster geometries are different from those for round tubes (4,5). An examination of CHF and friction data indicates that normally encountered complex geometry pressure loss data are not representative of gradients in the vicinity of the heat transfer crisis.

Adequate testing of the present concepts on complex geometry data thus requires data in which the friction factors differ from those normally encountered. Suitable data for a particular annulus test section are given in references (13) and (14) The data are particularly interesting because some of these correspond to a dry rod with a wet shroud As expected from (6), these data are consistent with adiabatic round tube friction characteristics provided the equivalent diameter is appropriately defined (fig.3).

The present interpretation of heat transfer crisis provides two explanations for the fact that criti-

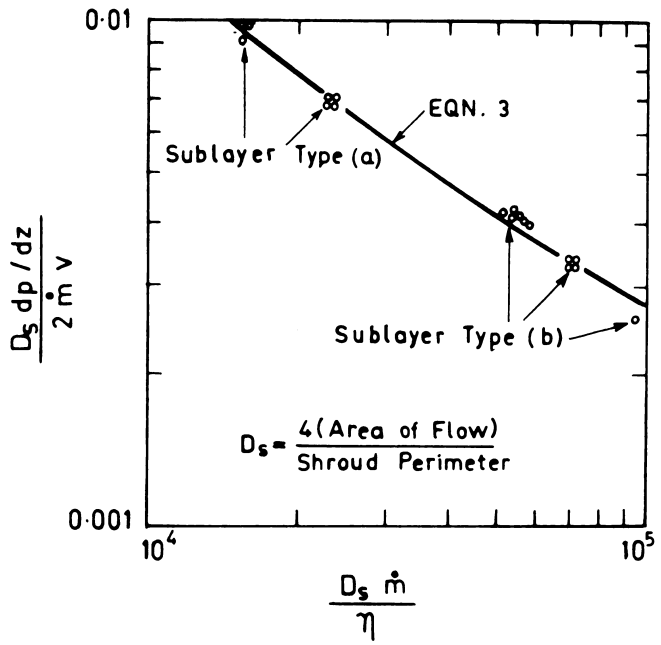

Fig.3 Compatibility of Friction Factor Data, for 8.25/5.0 mm Annulus (13,14) having Dry Rod, with Adiabatic Round Tube Equation

cal heat flux characteristics for annuli differ from those for round tubes. Both are evident in the data under consideration. The first is that, as stated, pre-dryout two-phase pressure loss characteristics for annuli are different from those for round tubes (4,5). The value of x^* applicable to eqn (1) and determined from the intersect of the wet-wall and dry-wall friction curves will, therefore, be different for the two systems. The second reason is that additional 'dry-wall' equations, corresponding to not all boundary surfaces being subjected to dryout conditions (as in the case of fig.3) may be necessary for complex geometries. The values of x^* obtained from these equations will necessarily be lower than those using eqn (2d).

The annulus data selected (13,14) are particularly suitable for analysis because dryout heat fluxes are presented for both rod and shroud with various heat fluxes on the other surface. An interesting feature of the data is that, for a given friction regime, CHF data fall on a single line, irrespective of the heat flux on the other surface, provided data are plotted as a function of inlet (instead of exit, i.e. dryout) quality. This indicated that the usual local conditions hypothesis does not apply and that the 'drying out' of a film from a heated surface depends on the power applied to that surface only and not the power applied to the channel as a whole. (A consequence of this is that the boiling length used in boiling crisis models should be replaced by an 'annular flow length'. For such critical heat flux situations, the two lengths would in general be similar.) The same zero heat flux intercept of the plots (i.e. x^*) necessarily occurs for both methods of plotting the data.

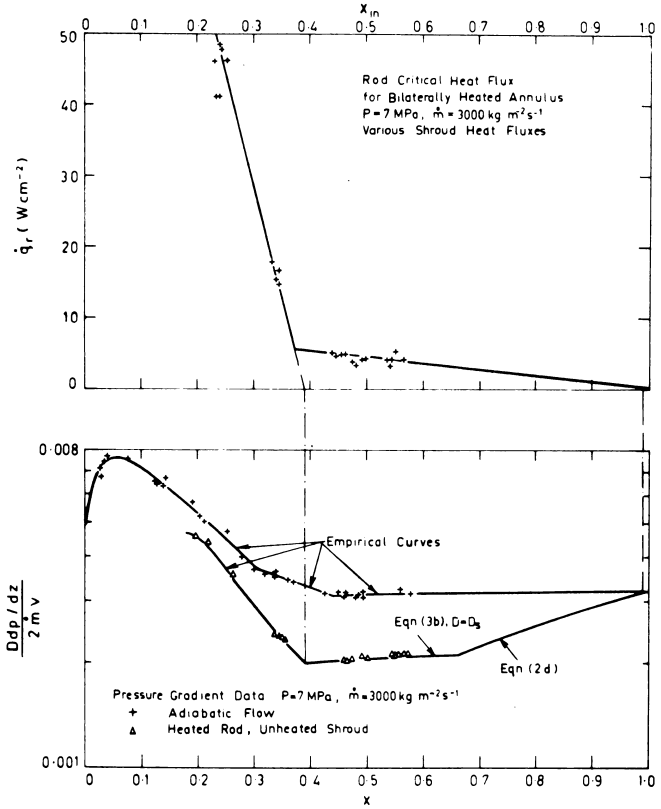

Fig.4 Rod Critical Heat Flux and Pressure Loss Data (13,14) for 0.5 m Heated Length 8.25 mm/5.0 mm Annulus

Critical heat flux and friction data (13,14) are given in figs. 4, 5 and 6 as representative of all data for that particular annulus.

Figure 4 presents CHF data for the central rod (with various heat fluxes on the shroud) together with relevant friction data. The empirical friction curve for the heated rod data is interpreted as being for wet-wall flows. For reasons already given, the data agreeing with eqn (3b) are expected to correspond to a dry rod. (This is confirmed by the fact that the pressure gradients for this region (13,14) were obtained at post-dryout heat flux conditions on the rod.) The value of x^* for the friction regime corresponding to the empirical friction curve for the heated rod should then be given by the intersect of this curve, not with eqn (2d) (as was the case with round tube flows), but with eqn (3b). The rod CHF data are consistent with this as shown. At sufficiently low rod heat fluxes, an adiabatic type of behaviour occurs. The CHF curve then approaches a zero heat flux quality ($x \sim 1$) given by the intersect of the adiabatic friction curve with eqn (2d).

The quality at which eqns (3b) and (2d) intersect is not relevant to the rod CHF data. Consistency with eqn (2d) implies that both surfaces are dry, so it is relevant to heat transfer crisis on the shroud, since it indicates that the shroud will be dried out by hydrodynamic effects at this quality.

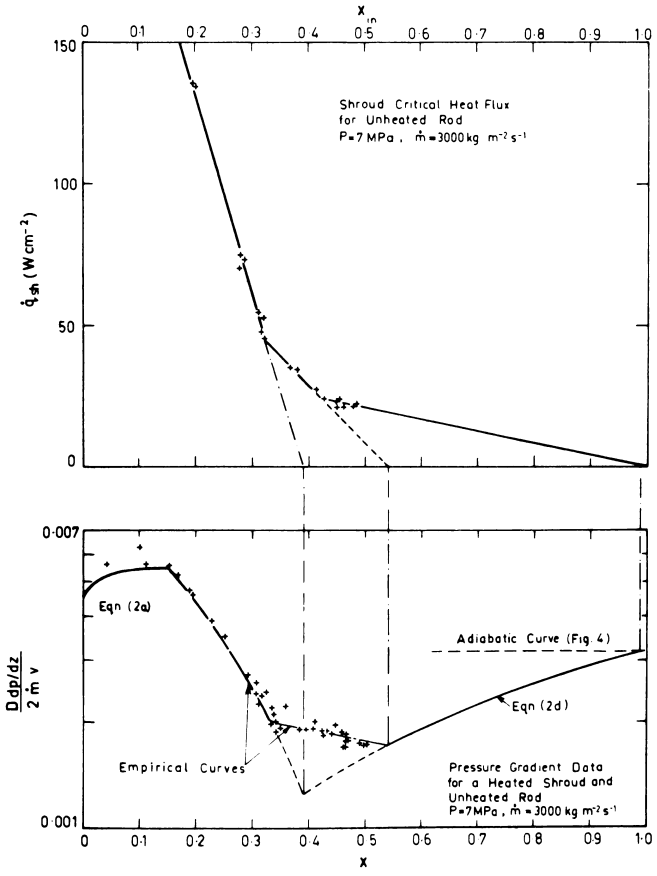

Fig.5 Shroud Critical Heat Flux and Pressure Loss Data (13,14) for 0.5 m Heated Length 8.25 mm/5.0 mm Annulus

Figure 5 shows shroud CHF data for unheated rod, together with corresponding friction data. The intersects of the two empirical friction curves with the dry-wall equation (2d), occur at qualities corresponding to x^* values consistent with the CHF data. At low enough shroud heat fluxes, the flow behaves hydrodynamically as adiabatic flow and, like the low CHF data for the rod, the final x^* value would be given by the intersect of eqn (2d) with the adiabatic friction curve (at $x \sim 1$).

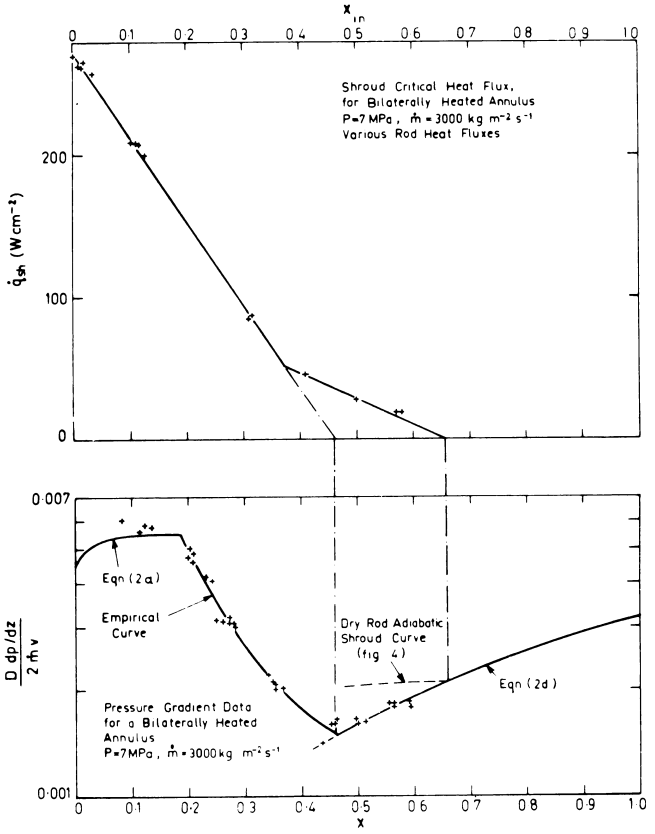

Fig.6 Shroud Critical Heat Flux and Pressure Loss Data (13,14) for 0.5 m Heated Length 8.25 mm/5.0 mm Annulus

Figure 6 shows shroud CHF data for heated rod conditions, together with the relevant friction data. The lower value of x^* for the CHF data corresponds to the intersect of the empirical friction curve with eqn (2d). At low shroud heat fluxes, the flow behaves as if the shroud was unheated. Because of the effects of the heated rod, the appropriate x^* value is given by the intersect of eqn (2d), not with the adiabatic friction curve, but with the friction curve corresponding to adiabatic shroud and heated rod. The CHF data are consistent with this.

CONCLUSIONS

Heat transfer crisis data for vapour/liquid flows can be subdivided into a series of straight line plots of critical heat flux: quality. Each straight line portion can be associated with a different friction regime, and extrapolates to a characteristic hydrodynamic dryout quality, which is given by the intersect of friction factor equations for the appropriate pre-dryout and post-dryout friction regimes. Some reported 'dryout' data correspond to a pseudo-dryout condition in which a small amount of liquid remains on the heated surface but characteristics similar to dry-out are observed. Heat transfer crisis characteristics for flows in tube and annular channels differ because of differences in pre-dryout friction characteristics, and because annular channel dryout usually corresponds to dry-wall conditions at only part of the flow boundary.

ACKNOWLEDGEMENTS

The authors would like to thank Professor J.J. Thompson (School of Nuclear Engineering,University of NSW) for helpful discussions and Miss June Woolley for assistance with typing and layout of the paper.

REFERENCES

1. Hewitt G.F. and Hall Taylor N.S., Annular Two-Phase Flow. Pergamon Press, 1970
2. Przhiyalkovskii M.M. et al., Thermal Engineering, Vol.12, p.65-70, 1965
3. Beattie D.R.H., Drag Reduction Phenomena in Gas-Liquid Systems. Proceedings of International Conference on Drag Reduction, BHRA Fluid Engineering, UK, paper D3, September 4-6, 1974
4. Beattie D.R.H., Friction Factors and Regime Transitions in High Pressure Steam-Water Flows. ASME Winter Annual Meeting, paper 75-WA/HT-4, November 30-December 4, 1975
5. Beattie D.R.H., Some Aspects of Two-Phase Flow Drag Reduction. Paper in Second International Conference on Drag Reduction, BHRA Fluid Engineering, UK, August 30-September 2, 1977
6. Beattie D.R.H., Two-Phase Fluid Mechanics and Heat Transfer in the Dry-Wall Region. Proceedings of Second Australasian Conference on Heat and Mass Transfer, p.329, February 16-18, 1977
7. Era A. et al., Heat Transfer Data in the Liquid Deficient Region for Steam-Water Mixtures at 70 kg/cm^2 Flowing in Tubular and Annular Conduits. Centro Informazioni Studi Esperienze Report CISE-R-184, 1966
8. Berkowitz L. et al., Pressure Drop, Heat Transfer, and Burnout Measurements with Round Tubes. CISE Report R-27, 1960
9. Gaspari G.P. et al., Pressure Drops in Steam-Water Mixtures. CISE Report R-83, 1964
10. Brevi R. and Cumo M., Int.J. Heat Mass Transfer, Vol.14, p.483-489, 1971
11. Mesler R., AIChE Journal, Vol.22, No.2, p.246-252, 1976
12. Bertoletti S. et al., Heat Transfer Crisis in Steam-Water Mixtures - Experimental Data in Round Tubes and Vertical Upflow. CISE Report R-90, 1964
13. Adorni N. et al., Pressure Drop, Heat Transfer and Burnout Measurements in Annular Tubes with External Heating. CISE Report R-30, 1960
14. Adorni N. et al., Pressure Drop, Heat Transfer and Burnout Measurements in Annular Tubes with Internal and Bilateral Heating. CISE Report R-31, 1961

Session No. KS-13

Author: G.F. Hewitt

Title: Critical Heat Flux in Flow Boiling

Discusser: D.R.H. Beattie and K.R. Lawther
Australian Atomic Energy Commission
Lucas Heights, NSW, Australia

The section on Inter-relation between CHF and Frictional Pressure Gradients, P159, raises a number of matters concerning paper FB-23 (ref.79) (1) and contains a number of misconceptions. These are considered in turn.

(a) The flow velocity, v, in paper FB-23 is the total volumetric flow rate per unit flow area.
(b) In fig.33, 'hydrodynamically induced dryout' is dryout under adiabatic conditions; x_1 does not correspond to such a condition. If EF corresponds to adiabatic conditions, and $x_3<1$, then x_3 corresponds to a hydrodynamic dryout condition.
(c) All the data discussed in paper FB-23 are consistent with the hypothesis, within expected experimental errors.
(d) Adiabatic dryout cannot occur if the friction factor remains above the value corresponding to unit quality, a situation which exists for low pressure air-water flows. Hydrodynamic induced dryout is expected to occur at high vapour mass fluxes, and the quality at the onset of hydrodynamic dryout is a function of Reynolds number. For a given mass flux the velocity becomes high at low pressures, hence the critical flow limitation observed in the Harwell air-water experiments. For typical pipe sizes (~1 cm dia.) steam-water adiabatic dryout occurs at mass fluxes above ~2000 kg $m^{-2}s^{-1}$. The film extraction data of ref. 73, particularly if considered in conjunction with ref.1 of that paper, are consistent with this. Refs.3 and 5 of paper FB-23 discuss high pressure, fully developed (for practical purposes) adiabatic two-component data in which each of (i) voidage profiles, (ii) average voidage values, (iii) friction factors, and (iv) velocity profile data, independently indicates dry wall conditions.
(e) The location of pressure tappings is discussed in paper FB-23 and in the references from which the data were obtained.
(f) The influence of previous history of the flow was taken into account; CHF data with associated pressure drop data were chosen so that such influences, if any, would be reflected in both CHF and pressure drop characteristics. In fact, rather than concentrate on developed flow data - such data are consistent with the model of paper FB-23 - non-developed data were specifically considered to demonstrate the generality of the concepts. It is relevant that the AAEC pressure loss equations, as given in refs.4 and 5 of paper FB-23, are the only ones, to our knowledge, which allow for entrance and heat transfer effects.
(g) The suggested smooth liquid film explanation of apparently very low pressure gradients is (i) inconsistent with the AAEC model, (in which pressure gradient depends on sublayer viscosity

Session No. KS-13

Author: G F Hewitt

Title: Critical Heat Flux in Flow Boiling

and not film thickness characteristics); (ii) inconsistent with the Harwell hydrodynamics model (in which the effective wall roughness is considerably larger than the film thickness); and (iii) inappropriate to dryout wall temperatures, while the 'pseudo-dryout' hypothesis of paper FB-23 is consistent with both the lower than expected wall temperature and shear stress values for dryout conditions. It is relevant that the pressure loss data of fig.1 of paper FB-23, corresponding to low CHF values, agree with adiabatic trends despite the expected thinner films under diabatic conditions.
(h) The boiling boundary influence on wall shear is not a 'potential' one. It is well established. Several publications have considered the influence with subcooled boiling (e.g. J. Heat Trans. p.151, 1968). The hydrodynamics of boiling flows were examined in detail in ref.5 of paper FB-23. As discussed in paper FB-23 pre-dryout temperature characteristics add further support to the AAEC view of boiling pressure gradients.
(i) In spite of the author's claim to the contrary, the Harwell model predictions for pressure losses are known to be poor at high mass flux, high quality conditions, a fact explicitly stated in ref. 83 . This is demonstrated by comparing the predictions in fig.34 with available data (see Fig.1)

References

1. D.R.H. Beattie and K.R. Lawther, Paper FB-23, this conference.
2. Z.L. Miropolski et al. Thermal Engineering, 12 (5) 80, May 1965.

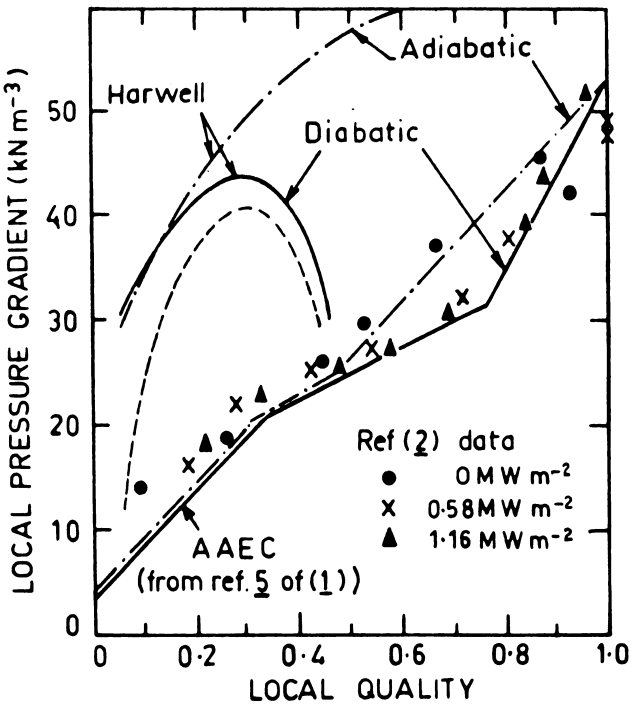

Fig.1 Steam-water Pressure Losses
(8 mm tube, 9.8 MPa, 1500 kg $m^{-2}s^{-1}$)

APPENDIX A14

Session No. PS-3

FB-8

Author: P.L. Kirillov et al.

Title: Investigation of Steam-Water Flow Characteristics at High Pressures

Discusser: D.R.H. Beattie
Australian Atomic Energy Commission
Lucas Heights, NSW, Australia

A simpler interpretation of the authors' data can be postulated, and such an interpretation of their diabatic flow data at 7 MPa (1) has already been published (2). The relevant data are consistent with attached wall bubbles, the size of which is determined by a balance of shear and surface tension forces, acting as surface roughness elements. The resultant velocity profile (which depends on the Weber number), this profile integrated over the film region, and the profile integrated over the whole tube, are in agreement with the authors' velocity profile data, void fraction data, and friction factor data, respectively.

Using the notation of (2), the authors' data (•) are shown in figures 1-3 together with some argon-water data (3) from a seven-rod cluster (+). The low y^+ velocity profile discrepancy is compatible with the authors' neglect of slip in the film region for their sampling probe data.

The trends of the authors' data differ from trends shown by other high pressure steam-water data. Did the authors add an electrolyte to their system to facilitate film thickness measurements?

References

1. P.L. Kirillov et al. Report FEI-421, 1973.
2. D.R.H. Beattie, Paper D1, Proc. 2nd Int. Conf. Drag Reduction, BHRA Fluid Engineering, Cranfield UK, 1977.
3. P. Alia et al. CISE report R108 (1968).

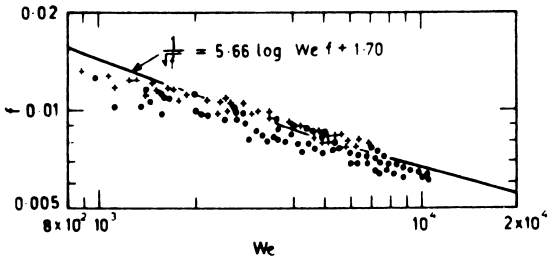

Fig.1 Friction factor data

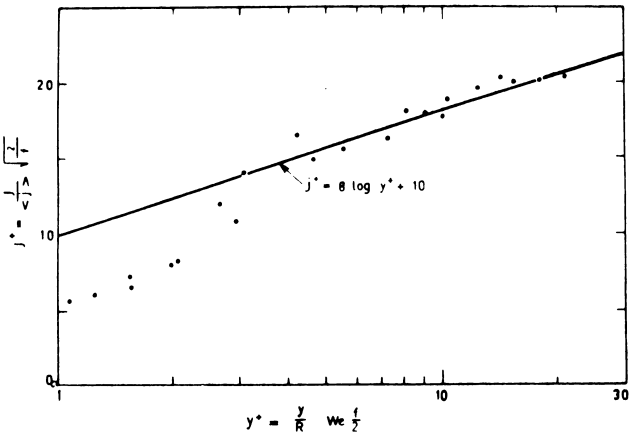

Fig.2 Non-dimensional velocity profiles

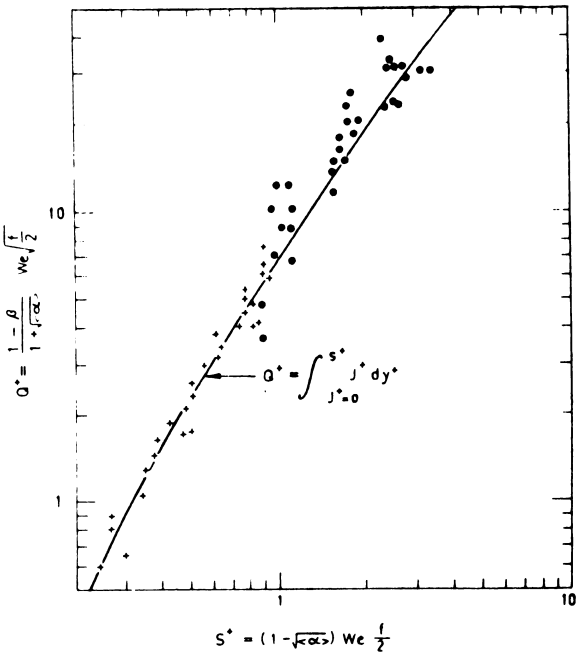

Fig.3 Average void fraction data

Session No. PS-3
FB-7

APPENDIX A15

Author: V.I. Deev et al.

Title: Pressure Drop in a Two-phase Flow of Helium under Adiabatic Conditions and with Heat Supply

Discusser: D.R.H. Beattie
Australian Atomic Energy Commission
Lucas Heights, NSW, Australia

It is interesting that the authors' lower quality and higher quality helium data are compatible with equations developed for high pressure steam-water flows (1). Using the same notation as in paper FB-7, the relevant equations (1) can be approximated by

$$\Delta P^{+} = (3.5\ \eta_0/\eta_1)^n\ x$$

for bubbly flows, annular flow with bubbly film, etc; and

$$\Delta P^{+} = x^{2-n}$$

for dry wall flows, where n is the exponent in the single phase equation

$$\xi = a\ Re^{-n} \quad .$$

However, in considering the ΔP^{+} vs $\bar{x}$ relation, the authors' intermediate quality data differ substantially from the corresponding intermediate quality steam-water data, even though the latter are qualitatively similar to the helium data of Keilin et al. (the authors' fig.5).

In terms of the above equations, the authors' assumption that $\xi_1/\xi_0 = 1$ (i.e. n = 0), for data in their fig.5, appears valid for the data of de la Harpe et al., but not for the Keilin et al. data, where n = 0.2 appears to be more appropriate. However, the original data presentation of Keilin et al. is such that the transposition onto the authors' fig.5 is not affected by the value of ξ_1/ξ_0.

Reference

D.R.H. Beattie, Paper D1, Proc. 2nd Int. Conf. Drag Reduction, BHRA Fluid Engineering, Cranfield, UK, 1977.

LETTERS TO THE EDITOR

To the Editor:

Mesler's views on boiling in thin films (*AIChE J.*, **22**, 246, 1976), as applied to forced convection two-phase annular flow (*AIChE J.*, **23**, 448, 1977), are at variance with currently accepted views on annular flow, which consider the bubble nucleation mechanism to be suppressed and the film region to be devoid of entrained bubbles at high void fraction. Recent AAEC research results are consistent with the views of Mesler (1977).

An examination of fluid mechanical aspects of two-phase flow (Beattie 1977) has indicated that the film region of adiabatic or diabatic forced convection annular flow sometimes contains bubbles, some of which may be attached to the wall. The evidence is based on sublayer structure, as inferred from a comparison of two-phase flow data with expressions derived from mixing-length theory for velocity profile, friction factor, and void fraction. Different sublayer structures give rise to different forms of non-dimensional parameters appearing in these expressions. For nucleate boiling flows of the type considered by Mesler (1977), attached wall bubbles act as surface roughness elements of a magnitude determined by appropriate surface tension and shear forces. Consequently, such flows are characterized by a Weber number instead of a Reynolds number. Appropriate non-dimensional parameters for annular flows with attached wall bubbles are:

Weber number

$$We = G\langle j\rangle D/\sigma$$

Friction factor

$$f = 2\tau_w/(G\langle j\rangle)$$

Wall distance

$$y^+ = y\,We\,f/D$$

Local velocity

$$j^+ = \sqrt{2/f}(j/\langle j\rangle)$$

Void fraction relation

$$S^+ = (1 - \sqrt{\langle\alpha\rangle})We\,f/2$$

Liquid volume flow rate

$$Q^+ = We\sqrt{f/2}(1 - \beta)/(1 + \sqrt{\langle\alpha\rangle})$$

In the above, β is the ratio of the volume flow rate of gas to the total volume flow rate, and $\langle\text{---}\rangle$ denotes the average value over a cross-section. Other symbols follow usual notation.

Experimental data are compared in Figures 1-3 with theoretical expressions for an annular flow with attached wall bubbles. It is clear that the data are compatible with a model which allows bubbles within the film region. Further examples have been reported (Beattie 1977).

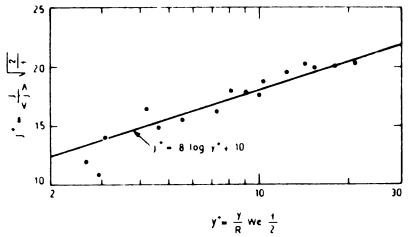

Fig. 1. Annular flow velocity profile (data from Kirilov et al (1973)).

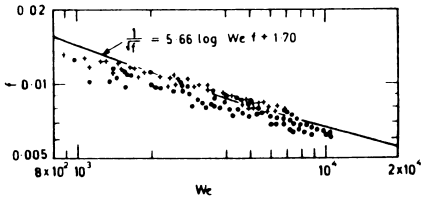

Fig. 2. Annular flow friction factor data from Alia et al (1968) (+) and Kirilov et al (1973) (●).

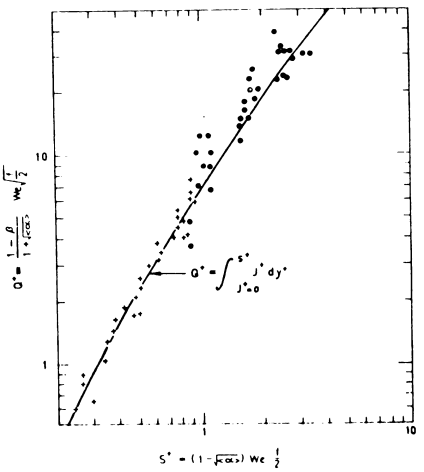

Fig. 3. Annular flow void relation [data from Alia et al (1968) (+) and Kirilov et al (1973) (●)].

Although the abovementioned AAEC work has concentrated on fluid mechanical aspects of two-phase annular flows, it has been found (Beattie and Lawther 1978) that, whenever the heat transfer characteristics in the approach to dryout show evidence of a marked local improvement in heat transfer through the film just before dryout is reached, then, in line with the heat transfer mechanism proposed by Mesler (1976), the corresponding friction factor data are consistent with the existence of attached wall bubbles in the film.

It is concluded that evidence from both fluid mechanical and heat transfer aspects is consistent with Mesler's hypothesis that the nucleate boiling mechanism can contribute to heat transfer in thin film annular flows.

D. R. H. Beattie
K. R. Lawther
Engineering Research Division
Australian Atomic Energy Commission
Research Establishment

LITERATURE CITED

Alia, P. et al., "Two-Phase (Gas & Liquid) Adiabatic Vertical Upflow: A Preliminary Study with a Rod Cluster Geometry," Report CISE-R-108 (1968).

Beattie, D. R. H., "Some Aspects of Two-Phase Flow Drag Reduction," 2nd Int. Conf. on Drag Reduction, BHRA Fluids Engng., Cranfield, UK (Sept. 1977).

Beattie, D. R. H., and K. R. Lawther, "Relationship Between Wall Shear Stress and the Heat Transfer Crisis Phenomenon with Vapour/Liquid Flows," Paper Accepted for 6th Int. Heat Transfer Conf., Toronto, Canada (August 1978).

Kirilov, P. L. et al., "Measurements of Some Characteristics of Steam-Water Flow in Round Tubes at a Pressure of 68.6 Bar," Report FEI-421 (1973).

Mesler, R. B., "A Mechanism Supported by Extensive Experimental Evidence to Explain High Heat Fluxes Observed during Nucleate Boiling," *AIChE J.*, **22**, 446 (March '76).

Mesler, R. B., "An Alternate to the Dengler and Addoms Convection Concept of Forced Convection Heat Transfer," *AIChE J.*, **23**, 448 (July 1977).

PREPRINT

This paper has been accepted for the XVIII IAHR Congress, Cagliari, Italy, 10-14 September 1979. It is made available on the understanding that, until it is published, it will not be abstracted, quoted, or referred to.

TWO-PHASE PRESSURE LOSS AND VOID FRACTION CHARACTERISTICS IN ROD BUNDLE GEOMETRIES

by D.R.H. Beattie

AAEC Research Establishment
Private Mail Bag, Sutherland, 2232, Australia

Many void fraction and pressure loss data have been examined in order to assess the validity of applying expressions from two-phase flow mixing length theory, as developed for flow through round tubes, to rod bundle geometries. The void fraction and pressure loss characteristics for rod bundles and round tubes are compared.

On a examiné plusieurs résultats des taux de vide et des pertes de pression pour vérifier les équations de la théorie du longueur de mélange pour les écoulements diphasiques, developpé pour les écoulements dans les tubes ronds, dans le cas des géométries de la barre. On a comparé les charactéristiques des taux de vide et des pertes de pression dans les cas des grappes et tubes ronds.

1 INTRODUCTION

Although the need for increased accuracy in the prediction of boiling coolant behaviour in rod bundle fuel elements of nuclear reactors has stimulated much of the recent two-phase flow research, most of the work, particularly that examining fluid mechanical aspects of the flow, has concentrated on adiabatic flow in simple geometries. With regard to pressure loss and void fraction characteristics, the current view is that these are influenced by neither heat transfer nor the form of the duct flow geometry, although there are some works in which heat transfer and/or geometry effects are either acknowledged[1,2,3] or specifically accounted for in calculational procedures[4-10].

One of these papers is based on mixing length theory applied to a round tube[10]. Heat transfer effects were considered to be caused by the effective roughening of the heated surface by attached wall bubbles, with the result that the Weber number replaced the Reynolds number as the determining parameter. Available round tube data confirmed this theory. Preliminary analysis of two-phase flow from rod cluster geometries led to tentative complex geometry recommendations in which the diameter term was replaced by the equivalent diameter, 4 x (flow area)/(flow perimeter), and in which empirical coefficients became dependent on duct shape.

This paper presents the results of a more complete analysis of two-phase flow data from complex geometries as examined in terms of the abovementioned mixing length theory[10].

2 TWO-PHASE FLOW MIXING-LENGTH THEORY EXPRESSIONS[10]

The conventional flow regime concept is replaced by a 'friction regime' concept in which the flow is characterized by a triad (m,n, z), where m and n are integers from which the non-dimensional velocity profile coefficients can be calculated, and z is a letter which specifies the sublayer structure (see Table 1). Non-dimensional groups for each type of sublayer are given in Table 1 and the relation between these groups can be obtained by substituting the appropriate m and n values into the generalized equations given in Table 2.

Friction factors are obtained from such equations as

$$\frac{D(dP/dz)_F}{2\bar{\rho}\langle j\rangle^2} = \max\{[\min f(0,-2,a);\ f(4,4,c)];\ f(2,0,a)\ ;\ \rho_g f(0,-2,d)/\bar{\rho}\} \qquad (1)$$

which is recommended for high pressure developed adiabatic steam-water flows in round tubes[10], and

$$\frac{D(dP/dz)_F}{2\bar{\rho}\langle j\rangle^2} = \max\{[\min f(0,-2,a);\ f(1,2,e)];\ \rho_g f(0,-2,d)/\bar{\rho}\} \qquad (2)$$

1 N. Zuber et al. GEAP report 5417 (1967).
2 C. Lombardi and I. Ceresa, Energ. Nucl. (Milan) 25, 181 (1978).
3 Z.I. Miropolski et al. Thermal Engineering No. 5, 80 (1965).
4 G.F. Hewitt, paper KS-13, 6th Int. Heat Transfer Conf., Toronto (1978).
5 G.P. Gaspari et al., CISE report R-83, (1964).
6 C.L. Lombardi and E. Pedrocchi, Energ. Nucl. (Milan), 19, 91 (1972).
7 P. Griffith, J. Heat Transfer, 86, 327 (1964).
8 N.V. Tarosova et al. 3rd Int. Heat Transfer Conf. (1966).
9 I. Michuyoshi and A. Serizawa, J. At. Energy Soc. Japan, 12, 311 (1970).
10 D.R.H. Beattie, Paper D1, 2nd Int. Conf. Drag Reduction, BHRA Fluids Eng., Cranfield, UK (1977).

which has been recommended for high pressure steam-water flows in annuli and clusters in which spacer influences are not expected to be strong[10].

It will be noted that friction regime maps for different systems can be constructed from equations such as equations (1) and (2).

In the case of void fraction calculations, it is also necessary to characterise the flow as being either distributed, i.e. one phase is continuous throughout the flow, or separated, i.e. the flow section can be divided into liquid-phase-continuous regions and gas-phase-continuous regions.

For liquid-phase-continuous flows the equation of Zuber et al.[1]

$$\langle j_g \rangle / \langle \alpha \rangle = C_o \langle j \rangle + V \qquad (3)$$

is suggested in conjunction with a friction-regime dependent distribution parameter C_o[10]

$$C_o = 1 + 2.60\sqrt{2}^{\,m} \sqrt{f(m,n,z)} \quad . \qquad (4)$$

These equations can be adapted for gas-phase continuous flows[11].

Evaluation of functional forms for the drift velocity V is outside the scope of mixing-length theory. The applicability of the round tube bubble flow drift velocity expression of Zuber et al.[1] to rod clusters is considered below, together with the complex geometry slug flow distribution parameter and drift velocity recommendations of Griffith[7].

For separated flows with a liquid-phase-continuous film and a gas-phase-continuous core, i.e. annular flow, it is necessary to introduce the core area fraction $A = (\alpha_f - \langle\alpha\rangle)/(\alpha_f - \alpha_c)$ and core volume flow fraction $B = (\beta_f - \beta)/(\beta_f - \beta_c)$ where entrainment is accounted for by the core and film volume flow fractions β_c, β_f and the core and film void fractions α_c, α_f, all of which are assumed constant over the appropriate regions of the flow. In the case of round tubes, entrainment is adequately accounted for[12] by $\alpha_f = 0.55$; β_f as obtained from the value of $\langle j_g \rangle / \langle j \rangle$ in equation (3) for the friction regime (0,-2,a) with $\langle\alpha\rangle = 0.55$; and, except for very high voidages, $\alpha_c = \beta_c = 1$.

The annular flow void fraction equation for a given friction regime can then be expressed as

$$Q^+ = \int_{j^+=0}^{S^+} j^+(m,n,z)\, dy^+ \qquad (5)$$

where Q^+, S^+ are the non-dimensional film volume flow rate and film thickness respectively. These are defined in Table 3. (Previous definitions of Q^+ and S^+ differed slightly[10], being based on a thick film approximation for annular flow. The present definitions are based on one version of the thin film approximation for annular flow. An examination has shown this approximation to be valid well beyond the limitations normally applied to such approximations and, in view of its simplicity, it is recommended instead of the thick film approximation given previously.)

---

11 D.R.H. Beattie, Proc. 2nd Austn. Conf. Heat and Mass Transfer (1977).
12 D.R.H. Beattie, Ph.D. thesis in preparation.

3 DATA ANALYSIS

Many voidage and pressure loss data from rod cluster and annular sections were examined to determine whether generalized theoretical expressions for round tubes, as summarised in Section 2, could be extended to complex geometries via the equivalent diameter concept and, if so, whether the friction regimes for simple and complex geometries were the same. The results, with the emphasis on high pressure steam-water flows, are now discussed.

As is the case with round tube data for low qualities, friction factors for low qualities tend to be compatible with the (0,-2,a) friction regime. However, there are more exceptions in the case of complex geometries. These exceptions tend to remain consistent with the generalized equation; tend to have sub-layer type a; and have friction factors which deviate significantly from those expected for the (0,-2,a) regime in the event of strong flow-disturbing effects associated with the entrance to the complex duct and/or the spacer arrangement separating the individual surfaces of the complex duct. Some examples are given in Figure 1.

Pressure loss data for higher quality flows in ducts of complex shape are generally consistent with the generalized surface tension dependent equation of Table 2. Some examples are given in Figure 2. Where data apply to both adiabatic and diabatic conditions, it is found that, unlike the case for round tube flows[10], the friction regime is not altered by heat transfer. Values for m and n required for calculating f(m,n,e) appear to depend on the entrance region, the distance between spacers, the type of spacers, the number of rods in the geometry, and the equivalent diameter of the system, in an as yet unresolved fashion. Despite this, most data examined are reasonably described by equation (2).

The above general picture for higher quality flows is not always correct; some data do not conform to the generalized equations of Tables 1 and 2 at all. These data tend to be for geometries with very narrow gaps between individual surfaces. Possibly, there are different sublayer structures on different surfaces. It is interesting that the low and very high quality ranges of such data are respectively compatible with f(0,-2,a) and f(0,-2,d), as was expected. In a few cases, data have characteristics expected for round tubes. The (4,4,e) data of Figure 1 give one such example, being the regime expected for under-developed adiabatic flow in round tubes[10]. A special case that is only partly an exception to the rule is that of incomplete dryout. The shear on dry surfaces is small compared with that on wet surfaces, and the system behaves as one with an equivalent shear diameter 4 area/(non-dried perimeter). The ∇ data of Figure 1 are for an annulus with the central rod heated beyond dryout and the shroud unheated. For round tube flows, f(4,2,a) is expected[10]; the data are consistent with this except at low Re values where sublayer bubbles behave as type b instead of type a.

In line with the trend observed for pressure losses, void characteristics for bubble flow in ducts of complex shape agree with those expected for round tubes only if spacer and/or entrance effects are small. Some data[13] suggest that the round tube drift velocity value is unaltered for flows only moderately disturbed by spacers, with the distribution parameter values for these flows being given by equation 4 if the appropriate friction regime can be determined from pressure gradient data. For strongly disturbed flows, the distribution parameter may become very large indeed (~3) and drift velocity values approximate $-\langle j_\ell \rangle_f$, suggesting a bubble retarding action by spacers and/or entrance regions[13].

Slug flow data, and indeed, many bubble flow data, tend to be very consistent with the recommendations of Griffith for slug flow in ducts of complex shape[7].

---

[13] D.R.H. Beattie and K.R. Lawther, paper accepted for ICHMT International Seminar on Interphase Phenomena in Two-phase Flow, Dubrovnik, 1978.

Given the experimental basis of his drift velocity correlations, the agreement here is not surprising, at least for slug flow data. In view of the speculative basis for his distribution parameter recommendations, the agreement here is rather surprising. However, a close examination of data indicates that, although the agreement with the Griffith[7] correlation is good, the data reveal a mass-flow dependent fine structure which is consistent with equation 4. An example is given in Figure 3.

In the case of voidage for annular flows in ducts of complex shape, most data are, as in the case for round tube data, for the (0,-2,a) friction regime. As can be seen from the representative data shown in Figure 4, the void fraction equations for flows in round tubes are in approximate agreement with these data also. In some cases, associated friction data indicate that the (0,-2,a) friction regime is inappropriate. The apparent contradiction is possibly because at least one pressure tapping in the pressure gradient measurements is likely to be in a region subject to entrance effects, whereas voidage measurements are generally made near the exit of test sections, where flows are more likely to be developed.

As described above, flow disturbing influences affect bubble flow voidage in such a way that the homogeneous model, which is inappropriate for developed flow, becomes even more inappropriate. On the other hand, the data suggest that flow disturbing influences tend to homogenise annular flow, at least as far as void fraction behaviour is concerned. Thus, annular flow data (i.e. $\langle\alpha\rangle > 0.55$) measured immediately downstream of a 36 rod cluster, marked • on Figure 4, are inconsistent with the theory given in Section 2 and instead are described by the homogeneous model.

The few annular flow void fraction data for rod clusters that exist for regimes other than (0,-2,a) and for which there are associated friction data, are also compatible with equation 5 of Section 2. An example is given in Figure 5 with entrainment being neglected.

4 CONCLUSIONS

In mixing-length theory, expressions for pressure loss and void friction as developed for round tubes can be extended to complex geometries via the use of the equivalent diameter concept. With the exception of low quality 'developed' flows (i.e. small entrance effects etc.),friction regimes for complex geometries differ from those for round tubes with the result that, generally, coefficients appearing in expressions based on mixing-length theory differ for round tubes and complex geometries. Unlike the case for flow in round tubes, complex geometry friction and voidage characteristics generally are not influenced by heat transfer. Hydrodynamic data from complex geometries are more likely to be for 'less developed' flows than is the case for round tubes; this appears to be due to the entrance region of complex geometries and/or the spacers separating independent surfaces in complex geometries.

---

14 P.A. Edwards, AEEW-R-371 (1964).
15 N. Adorni et al., CISE-R-30 (1961).
16 N. Adorni et al., CISE-R-31 (1961).
17 E. Schöneberg, EURAEC 2092 (1968).
18 P. Grillo and P. Marinelli, Nuc. Technol. 15, 25 (1972).
19 B. Matzner and J. Neill, DP-857 (1963).
20 Yu I. Dzarasov, Heat Tr. Sov. Res. 9, 261 (1978).
21 G.P. Gaspari et al., CISE-R-294 (1970).
22 N. Adorni et al., CISE-R-123 (1966).
23 G. Agostini et al., CISE-R-309 (1971).
24 Z.S. Rouhani, AE-238 (1966).

TABLE 1 DIMENSIONLESS-GROUP DEFINITIONS FOR VARIOUS TWO-PHASE FLOW SUB-LAYER TYPES

Sub-layer Type	Pressure Loss Characteristics	Local Structure
Viscosity dependent flows (a,b,c,d)	$f = \frac{D(dP/dz)_F}{2\rho\langle j\rangle^2} = f(Re = \frac{\rho\langle j\rangle D}{\mu})$	$j^+ = \frac{j}{\langle j\rangle}\sqrt{\frac{2}{f}} = j^+(y^+ = \frac{y}{R}\frac{Re}{2}\sqrt{\frac{f}{2}})$
Surface-tension dependent flows (e)	$f = \frac{D(dP/dz)_F}{2\rho\langle j\rangle^2} = f(We = \frac{\rho\langle j\rangle^2 D}{\sigma})$	$j^+ = \frac{j}{\langle j\rangle}\sqrt{\frac{2}{f}} = j^+(y^+ = \frac{y}{R}We\frac{f}{2})$

Sub-layer Type Notation	Density Definition	Viscosity Definition
a. Rigid surface bubbles	$\rho = \rho_\ell(1-\beta) + \rho_g\beta = \bar{\rho}$	$\mu = \mu_\ell(1+2.5\,\beta)$
b. Non-rigid surface bubbles	$\rho = \rho_\ell(1-\beta) + \rho_g\beta = \bar{\rho}$	$\mu = \mu_\ell(1 + \frac{2.5\,\mu_g + \mu_\ell}{\mu_g + \mu_\ell}\beta)$
c. Wavy-gas/ liquid interface	$\rho = \rho_\ell(1-\beta) + \rho_g\beta = \bar{\rho}$	$\mu = \mu_\ell(1-\beta) + \mu_g\beta$
d. Dry wall	$\rho = \rho_g$	$\mu = \mu_g$
e. Attached wall bubbles	$\rho = \rho_\ell(1-\beta) + \rho_g\beta = \bar{\rho}$	N.A.

TABLE 2 GENERALIZED PRESSURE LOSS AND VELOCITY PROFILE EQUATIONS

Sublayer Type	Pressure Loss Characteristics	Local Structure
Viscosity dependent flows (a,b,c,d)	$1/\sqrt{f} - (\sqrt{2})^{m+4}\{\log Re\sqrt{f} - (0.11m + 0.5n + 1.1)\}$	$j^+ = (\sqrt{2})^{m+5}\{\log y^+ - (0.11m + 0.5n)\}$
Surface tension dependent flows (e)	$1/\sqrt{f} = (\sqrt{2})^{m+4}\{\log Wef - (0.2m + 0.3n - 1.1)\}$	$j^+ = (\sqrt{2})^{m+5}\{\log y^+ - (0.2m + 0.3n - 2.05)\}$

TABLE 3 DEFINITIONS FOR NON-DIMENSIONAL FILM FLOW RATE AND FILM THICKNESS

Sublayer Type	Q^+	S^+
Viscosity dependent flows	$\frac{1-B}{4}Re(z)$	$\frac{1-A}{4}Re(z)\sqrt{\frac{f(m,n,z)}{2}}$
Surface tension dependent flows	$\frac{1-B}{2}We\sqrt{\frac{f(m,n,e)}{2}}$	$\frac{1-A}{4}We\,f(m,n,e)$

25 G. Agostini et al., CISE-R-295 (1970).
26 O. Nylund et al., FRIG-G-2 (1968).
27 P. Alia et al., CISE-R-108 (1968).

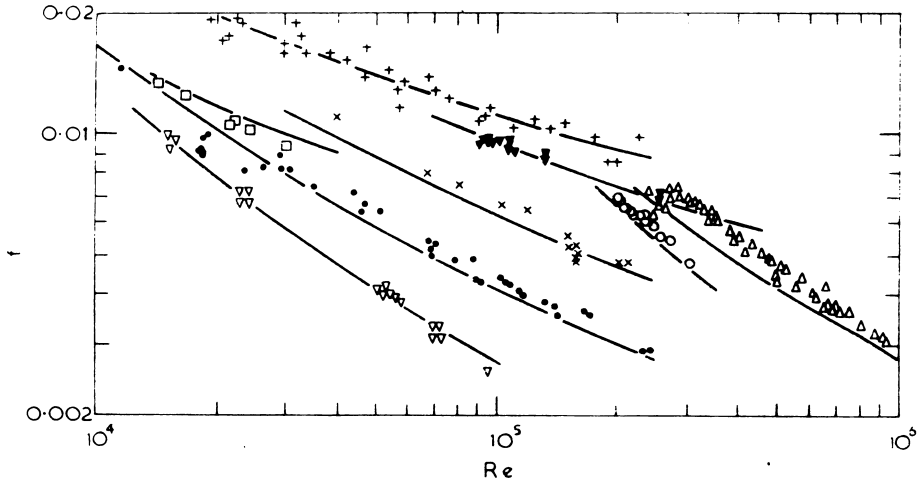

Fig.1 Typical viscosity-dependent complex geometry friction factors

Fig.1 Les coefficients de frottement typique, qui dépendent sur le viscosité, pour les écoulements dans les grappes

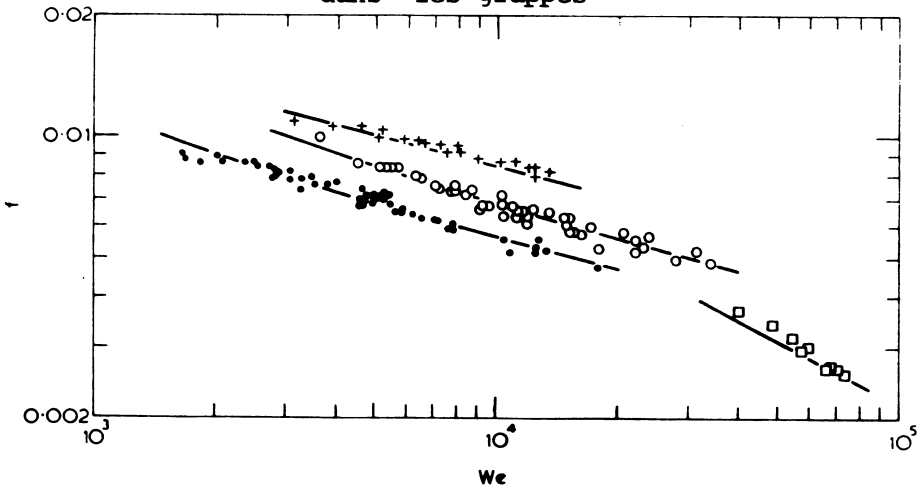

Fig.2 Typical surface-tension dependent complex geometry friction factors

Fig.2 Les coefficients de frottement typique, qui dépendent sur la tension superficielle, pour les écoulements dans les grappes

	Symbol	No. of rods (Test section name)	Friction regime	Ref.
Fig.1	●	19 (No. 1)	(3,2,a)	14
	+	19 (No. 2)	(0,1,a)	14
	Δ	1 (03)	(4,4,c)	15
	▽	1 (85)	(4,2,a/b)	16
	▼	1	(1,2,a)	17
	o	4	(5,4,b)	17
	x	36	(2,2,a)	18
	□	7 (A)	(1,1,a)	19
Fig.2	□	1	(5,5,e)	20
	●	19 (IT34)	(1,1,e)	21
	+	3 (333)	(0,1,e)	22
	o	7 (G8a,b)	(1,2,e)	22

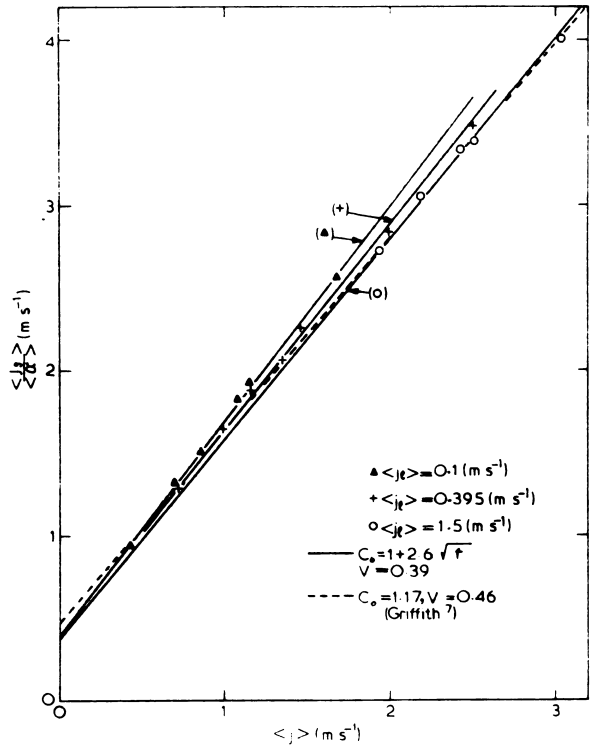

Fig.3 (0,-2,a) slug flow void fraction data for a 7 rod cluster[13]

Fig.3 Les taux de vide pour les écoulements bouchons (0,-2,a) dans une géometrie de 7 barre[13]

Symbol	No. of rods (Test section name)	G kg $m^{-2}s^{-1}$	D mm	P MPa	Ref.
▲	4	750	21.1	7.1	17
o	19 (IT25)	2164	7.5	2.9	23
+	1	132	13	3.9	24
x	1 (IT45)	3489	9.0	5.0	25
▽	1 (IT37)	412	3.0	5.0	25
•	Downstream of 37 rods	various	27	5.0	26

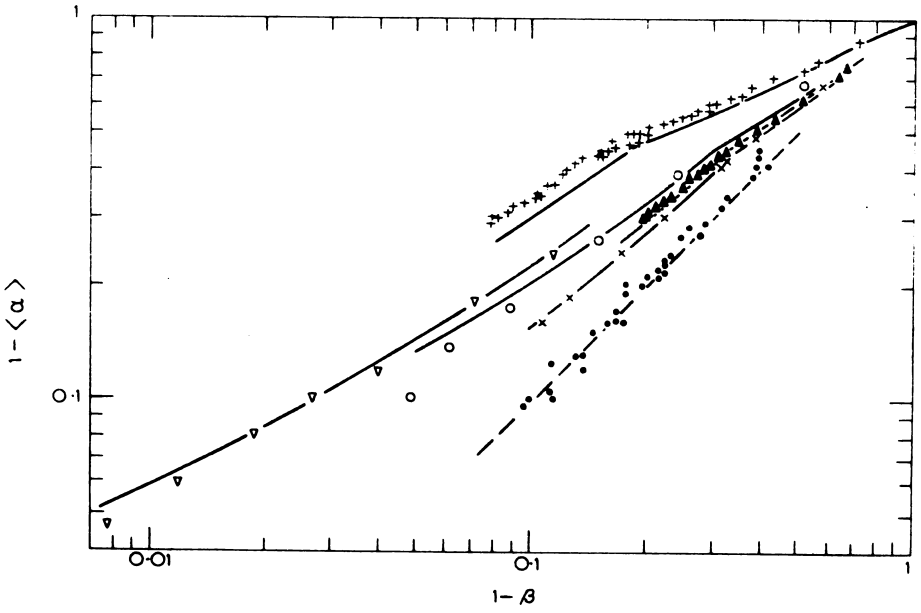

Fig.4 Comparison of typical (0,-2,a) complex geometry void fraction data with theory

Fig.4 Une comparaison des résultats typique (0,-2,a) pour les taux de vide dans les grappes avec la théorie

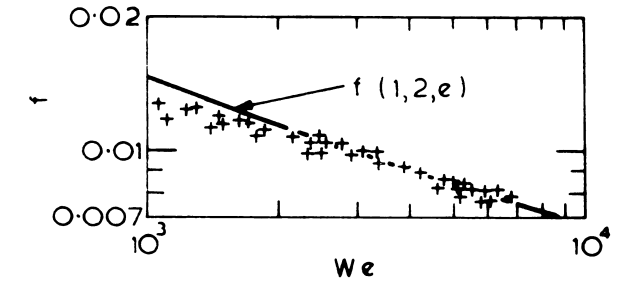

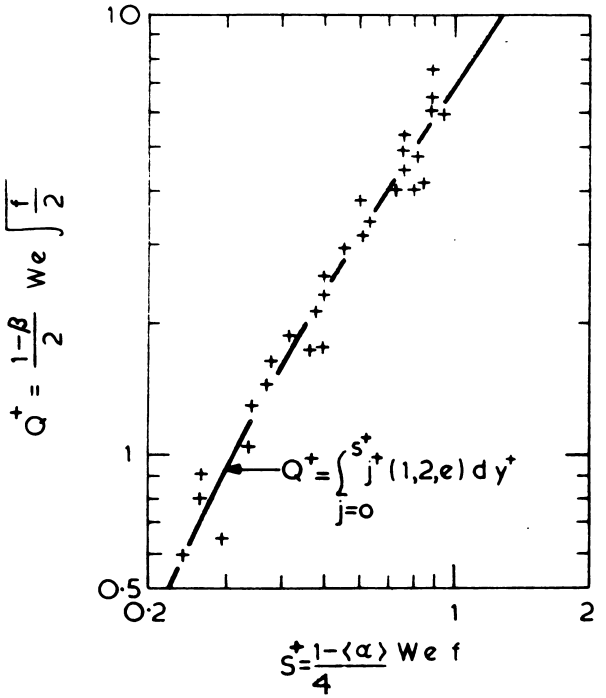

Fig.5 Comparison of (1,2,e) 7 rod cluster annular flow void fraction data[27] with theory

Fig.5 Une comparaison des taux de vide (1,2,e) pour les écoulements annulaires dans une grappe de 7 barre[27] avec la théorie

FLUID MECHANICS–Soviet Research, Vol. 8, No. 2, March-April 1979

LETTER TO THE EDITORS

Void Fraction and Pressure Drop in Two-Phase Upflow at Atmospheric Pressure

V. M. Borishanskiy et al. [1] have presented some void fraction and pressure drop data for air-water upflow at atmospheric pressure in a 2-m long 11-mm diameter round tube, and have compared their data with various published equations recommended for both void fraction and pressure drop. Of the 23 void fraction equations considered, two compared favorably with the void fraction data; and none of the 10 pressure loss equations agreed adequately with the pressure drop data.

Three of the 10 pressure loss equations are from some AAEC work [2], which has since been generalized [3] and extended to include the prediction of void fraction. A comparison of the author's data [1] with the generalized equations* of [2] disagree with the authors' data, the implications concerning the validity of the AAEC equations must be reconsidered.

The relevant equations of [3], using, where appropriate, the authors' notation, are summarized below:

$$\frac{dP}{d\ell} = \left.\frac{dP}{d\ell}\right|_{fr} + \left.\frac{dP}{d\ell}\right|_{gr}, \quad (1)$$

$$\left.\frac{dP}{d\ell}\right|_{fr} = \frac{2f}{D}\,(\omega_o'\,\rho' + \omega_o''\,\rho'')(\omega_o' + \omega_o''). \quad (2)$$

The friction factor f is a function of Reynolds number $Re = \frac{D(\omega_o'\,\rho' + \omega_o''\,\rho'')}{\mu}$ where viscosity μ depends on sublayer structure:

$\mu = \mu'\,(1+2.5\beta)$ (rigid-surface-bubble sublayer); (a)

$\mu = \mu'\left(1 + \frac{2.5\mu'' + \mu'}{\mu'' + \mu'}\beta\right)$ (nonrigid-surface bubble sublayer); (b)

$\mu = \mu'\,(1-\beta) + \mu''\beta$ (wavy core/film interface). (c)

Empirically, f as a function of Re can be obtained from a generalized equation

$$1/\sqrt{f} = (\sqrt{2})^{m+4}\,\{\log Re\sqrt{f} - (0.11\,m + 0.50\,n + 1.1)\} \quad (3)$$

ISSN0096-0764/79/0020-0169$07.50/0

© 1979 Scripta Publishing Co.

*insert 'of [3] indicates that, although the AAEC equations'

by suitable integer choices for m and n. A friction regime is characterized by appropriate m and n values and the appropriate sublayer. The notation (m, n, z) is used, where m and n are the relevant integers from which the f:Re equation can be obtained from equation (3), and where z, for the present purposes, indicates the appropriate viscosity definition (equation (a), (b) or (c)). The relationship (m,n) = (0,-2) generates the single-phase flow equation, also applicable to developed low-quality two-phase flows. The equations corresponding to (0,-2,a) (0,-2,b), and (0,-2,c) are, in effect, the three AAEC equations considered by Borishanskiy et al. [1].

With regard to gravitational head and void fraction prediction,

$$\left.\frac{dP}{d\ell}\right|_{gr} = [\rho'(1-\phi) + \rho''\phi]g \qquad (4)$$

where ϕ is obtained from the Zuber and Findlay [4] equation

$$\omega_o''/\phi = C_o(\omega_o'' + \omega_o') + V \qquad (5)$$

where V is the drift velocity and C_0 is a distribution parameter which depends on the friction regime [3]:

$$C_o = 1 + 2.60\,(\sqrt{2})^m\sqrt{f} \qquad (6)$$

The drift velocity V depends on the flow structure. For bubble flows

$$V = V_{bubble} = 1.4\left[\frac{\sigma g(\rho'-\rho'')}{(\rho')^2}\right]^{0.25} = 0.22 \text{ m s}^{-1} \text{ for the data of [1];} \qquad (7)$$

for slug and bubble/slug flows

$$V = V_{slug} = 0.35\sqrt{g D} = 0.115 \text{ m s}^{-1} \text{ for the data of [1]; and} \qquad (8)$$

for flows with a froth core,

$$V = V_{froth} = 0. \qquad (9)$$

Sublayers (a) and (b) must have V given by equations (7) or (8), and sublayer (c) must have V given by equations (8) or (9).

AAEC work indicates that developed bubble flow data are consistent with the (0,-2,a) friction regime. As noted, f(0,-2,a) was evaluated by Borishanskiy et al. [1] and found to be incompatible with their data.

However, extension of the AAEC prediction to the evaluation of void fraction leads to the contradictory result that the AAEC friction factor calculations, as used in the estimate of void fractions, are correct, at least for the high mass flux data of [1]. This is demonstrated in Table 1, which compares experimental values of ϕ and $\frac{dP}{d\ell}$ with those based on $\phi(0,-2,a, V_{bubble})$ and $f(0,-2,a)$. The agreement between experimental and predicted ϕ values is remarkable: the discrepancy is less than experimental round-off in more than half the cases, and the maximum discrepancy is less than 2%. Summarizing the predictions for the other data of [1]: those based on $\phi(0,-2,a,V_{slug})$ and $f(0,-2,a)$ reasonably describe the $\omega_o' = 1.4$ m s^{-1} data for both void fraction and pressure drop; and neither the void nor pressure drop data for $\omega_o' = 0.5$ m s^{-1} are compatible with the (0,-2,a) friction regime.

The agreement between the experimental and predicted void fractions in Table 1 supports both the experimental data and the predictive method used. In particular, the agreement suggests that f(0,-2,a) is valid. Contradicting this, the pressure gradient data indicate that f(0,-2,a) is invalid. The apparent contradiction suggests that void fractions were measured near the exit of the test section, where flows might be expected to have been more developed, i.e., where the friction regime was that for (0,-2,a); and that pressure gradients were measured over a less-developed part of the test section where (0,-2,a) is invalid. The details of the experimental arrangement, which apparently are described in Ref. 4 of [1], would confirm, or disprove, this hypothesis. However, a copy of this work was not readily obtainable.

The above hypothesis suggests that estimates of frictional pressure gradients, obtained by subtracting gravitational heads based on experimental values of void fraction from measured values of total pressure drops, could be in error for data where the frictional head was not dominant. Thus, in considering the experimental data, comparison between experimental data for the total pressure gradient and predictions for this quantity, where both gravitational and frictional gradients are calculated for the same friction regime, appeared more sensible than comparison between the "experimental" frictional gradient (this being the measured total minus the possibly inappropriate inferred "experimental" value of gravitational gradient) and calculated frictional gradients.

For those data of [1] where the pressure gradient is predominantly frictional, the "experimental" frictional gradient is compatible with f(-1,-3,b) for low voidages, and f(0,0,c) for high voidages. On the basis of low voidage friction factors for steam-water flows, given by $f = \min [f(0,-2,a); f(4,4,c)]$ (i.e., the smaller of the two friction factors) [3], it was supposed that $f = \min [f(-1,-3,b); f(0,0,c)]$ would describe all the frictional pressure gradient data of [1]. For $f(-1,-3,b) < f(0,0,c)$, the gravitational head was based on $\phi(-1,-3,b,V_{bubble})$. For $f(0,0,c) < f(-1,-3,b)$, the gravitation head was based on $\phi(0,0,c,V_{slug})$ except for the low gas flow rate conditions with $\omega_o' = 0.5$ m s^{-1}, in which case $\phi(0,0,c,V_{froth})$ was used, simply because calculations based on the above

Table 1

Comparison of Higher Mass Flux Void Fractions and Pressure Gradients with Those Calculated for the (0, -2, a) Friction Regime

ω'_o m s^{-1}	ω''_o m s^{-1}	ϕ, %		$\frac{dP}{d\ell}$, kg m^{-3}	
		Expt.	Pred.	Expt.	Pred.
2.91	0.11	2.86	2.86	2168	1936
2.91	0.094	2.46	2.46	2188	2034
2.91	0.122	3.16	3.16	2198	1940
2.88	0.22	5.6	5.57	2208	1947
2.87	0.302	7.4	7.48	2228	1961
2.87	0.407	9.8	9.76	2268	1987
2.87	0.42	10	10.0	2268	1992
2.87	0.69	15.2	15.3	2418	2063
2.87	0.755	16.3	16.4	-	-
2.78	1.16	23.1	23.2	-	-
2.51	1.25	26.1	26.1	2238	1933
2.51	1.84	33.4	33.4	-	-
2.51	0.950	21.6	21.5	2148	1890
2.51	0.735	17.7	17.7	2078	1841
2.51	0.54	13.8	13.8	2033	1799
2.51	0.394	10.7	10.6	1973	1769
2.51	0.318	8.8	8.75	1948	1754
2.51	0.228	6.6	6.47	1923	1737
2.51	0.181	5.29	5.22	1921	1730
2.51	0.122	3.64	3.60	1903	1721

Table 2

Comparison of Measured Void Fractions and Pressure Gradients with Those Calculated for the (-1, -3, b) and (0, 0, c) Friction Regimes, the Regime Boundary Being Given by f(-1, -3, b) = f(0, 0, c)

ω'_o m s^{-1}	ω''_o m s^{-1}	ϕ, %		$\frac{dP}{d\ell}$, kg m^{-3}	
		Exp.	Calc.	Expt.	Calc.
0.517	5.12	71	71.5	724	793
0.517	6.83	73	73.5	1636	925
0.503	4.03	72	70.7	650	712
0.49	3.12	68	68.4	591	657
0.509	7.3	73	73.7	1973	907
0.521	0.6	40	40.8	658	747
0.521	0.92	49	49.5	608	691
0.518	1.11	53	52.6	576	678
0.518	0.77	45.5	45.7	623	717
0.518	1.62	59.5	59.0	556	657
0.518	2.16	63.5	63.2	592	660
1.41	3.68	57	57.8	1570	1663
1.42	4.68	60.5	60.8	1830	1812
1.42	2.56	50.5	50.0	1518	1540
1.42	1.98	46	46.1	1400	1463
1.41	1.58	41.5	41.8	1338	1387
1.42	1.21	36	36.2	1308	1343
1.42	0.88	30	29.8	1210	1311
1.42	0.65	24.6	24.3	1273	1298
1.40	0.48	20	19.6	1269	1285
1.42	0.374	16	15.9	1281	1301
1.42	0.268	12.00	12.1	1288	1308
1.43	0.115	5.76	5.61	1312	1331
1.43	0.165	7.6	7.82	1306	1324
1.43	0.084	4.3	4.17	1319	1336
2.91	0.11	2.86	2.94	2168	2270
2.91	0.094	2.46	2.52	2188	2265
2.91	0.122	3.16	3.25	2198	2273
2.88	0.22	5.6	5.73	2208	2276
2.87	0.302	7.4	7.69	2228	2291
2.87	0.407	9.8	10.1	2268	2321
2.87	0.42	10	10.3	2268	2325
2.87	0.69	15.2	15.7	2418	2409
2.87	0.755	16.3	16.9	-	-
2.78	1.16	23.1	24.0	-	-
2.51	1.25	26.1	27.0	2238	2261
2.51	1.84	33.4	34.6	-	-
2.51	0.950	21.6	22.2	2148	2172
2.51	0.735	17.7	18.3	2078	2113
2.51	0.54	13.8	14.2	2033	2064
2.51	0.394	10.7	10.9	1973	2030
2.51	0.318	8.8	9.00	1948	2013

Table 2 (Continued)

ω'_o, m s^{-1}	ω''_o, m s^{-1}	ϕ, %		$\frac{dP}{d\ell}$, kg m^{-3}	
		Exp.	Calc.	Expt.	Calc.
2.51	0.228	6.6	6.65	1923	1995
2.51	0.181	5.29	5.37	1921	1986
2.51	0.122	3.64	3.70	1903	1975
2.51	0.091	1.98	2.79	1893	1970

gave slightly better agreement with the reported data. Experimental observations, not reported in [1], would be relevant to the validity of the above approach.

Calculations based on the above are compared with the data of [1] in Table 2. Considering pressure gradient data first, it is clear that, in all but two cases, the calculated values are close to, and almost consistently slightly larger than, the experimental values, by about 60 kg m^{-3}. It is possible that this systematic difference could have been caused by a zero error in the pressure drop measuring apparatus. If there was such a zero error, the "experimental" frictional pressure gradients (i.e., total minus gravitational gradient based on measured voidage) would be significantly in error for those data dominated by gravity.

The agreement between the calculated and measured pressure gradients in Table 2 implies that the calculational procedure used, including that for the gravitational component, is applicable to the flow system between the test section pressure taps. As noted, the experimental void fraction values, presumed measured near the exit of the test section, are not necessarily applicable between the pressure taps. However, the agreement between experimental and calculated void fractions in Table 2 suggests that any friction regime change arising from flow development, such as appears to be the case for the high mass flux data, did not significantly alter void fraction values.

In summary, the discrepancy observed by Borishanskiy et al. [1] between early AAEC friction factor equations [2] and their pressure gradient data appears to be because their data are for nondeveloped flow and the early AAEC equations are for developed flow. Void fraction data in conjunction with the pressure gradient data suggest a developing flow situation, the equations of [2] being applicable for developed regions. The pressure gradient data of [1] are consistent with nondeveloped flows described by equations given in [3].

REFERENCES

1. Borishanskiy, V. M., et al., Void Fraction and Pressure Drop in Two-Phase Upflow at Atmospheric Pressure. Fluid Mechanics Soviet Research 6, 6, 51, 1977. Originally published in Trudy TsKTI, 139, 72, 1976.

2. Beattie, D. R. H., A Note on the Calculation of Two-phase Pressure Losses, Nuc. Eng. Des., 25, 335, 1973.
3. Beattie, D. R. H. Some Aspects of Two-phase Flow Drag Reduction. Paper D1, 2nd Int. Conf. Drag Reduction, Cambridge, UK, Proceedings published by BHRA Fluid Engng. Cranfield, UK.
4. Zuber, N. and Findlay, J. A. Average Volumetric Concentration in Two-phase Flow systems. J. Heat Transfer, 87, 453, 1965.

D. R. H. Beattie,
AAEC Research Establishment,
Private Mail Bag,
Sutherland, 2232, Australia

□◆◆◆□

Int. J. Multiphase Flow Vol. 6, pp. 273–274
Pergamon/Elsevier, 1980. Printed in Great Britain

LETTER TO THE EDITOR

Choked Foam Flows in a Convergent–divergent Nozzle

Sandhu & Jameson (1979) have presented interesting experimental data for choked foam flows in a convergent–divergent nozzle, and have compared these data with a theory which they based partially on the assumption of a flat voidage profile in the flow. They conclude that their data are compatible with isothermal gas behaviour and no relative motion between the phases at low gas concentrations, and with relative motion between the phases (a velocity ratio up to 1.5) together with isentropic gas expansion at higher gas concentrations.

A simpler interpretation of the data can be made if it is assumed that the gas concentration profile is not flat. "Slip" between the phases may then be due solely to the concentration of gas in higher velocity regions of the flow, not to relative motion between the phases.

The theory of choked flows in such systems differs from that of Sandhu and Jameson. The key feature is the use of a distribution parameter, C_0, developed by Zuber & Findlay (1965), which is a coefficient dependent on the shape of the concentration and velocity profiles. A flat concentration or velocity profile results in a distribution parameter value of unity; peaked profiles give values greater than unity. Typically, $C_0 \simeq 1.2$ for low voidage flows.

Critical flow expressions for flow where "slip" is due to concentration and velocity profile effects are given in Beattie (1976) and Beattie & Thompson (1976). For isothermal gas behaviour,

$$U_m \sqrt{(\rho_L / P_t)} \simeq \left(1 + \frac{1}{\delta_t}\right)\left(\frac{\delta_t}{1 - (C_0 - 1)(1 + 2\delta_t)}\right)^{1/2} , \qquad [1]$$

where U_m is the mixture velocity, and P_t and δ_t are the throat pressure and gas/liquid volume flow ratio, respectively.

Figure 1 indicates that the data are consistent with a non-flat concentration profile such that $C_0 \simeq 1.06$ for all gas concentrations. This value, which is rather low, is consistent with the view

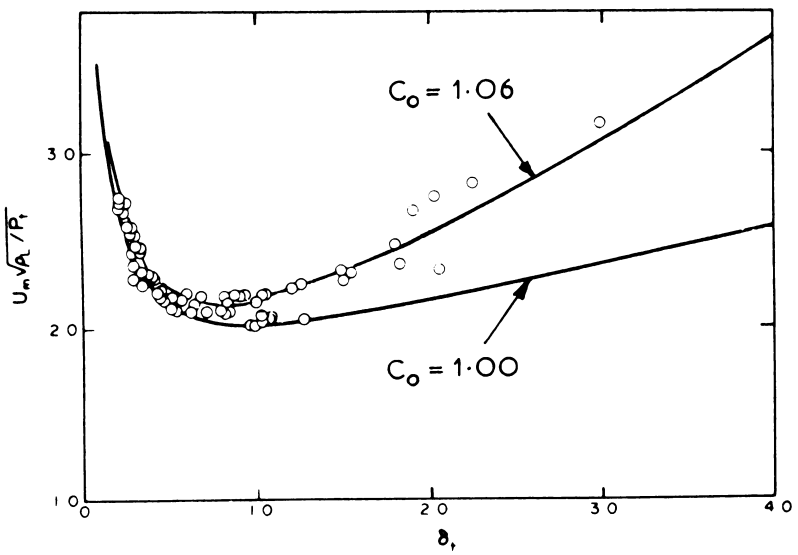

Figure 1. Experimental and theoretical dimensionless choking velocity as a function of throat volume ratio (adapted from Sandhu & Jameson 1979: figure 9); ——, [1].

of Sandhu and Jameson that their flows were comparatively homogeneous. This can be further seen by considering velocity ratio values. For flows in which Sandhu and Jameson require a velocity ratio k of 1.5 for agreement with their theory, the present model gives $k = 1 + (C_0 - 1)(1 + \delta_t) \simeq 1.1$.

AAEC Research Establishment
Lucas Heights, Australia, 2232

D. R. H. BEATTIE

REFERENCES

BEATTIE, D. R. H. 1976 Pressure pulse and critical flow behaviour in distributed gas–liquid systems. *Proc. 2nd Int. Conf. Pressure Surges, BHRA Fluids Engineering*, Cranfield, England.

BEATTIE, D. R. H. & THOMPSON, J. J. 1976 The effect of flow velocity on two-phase propagation phenomena. *Proc. 2nd Int. Conf. Pressure Surges, BHRA Fluids Engineering*, Cranfield, England.

SANDHU, N. & JAMESON, G. J. 1979 An experimental study of choked foam flows in a convergent–divergent nozzle. *Int. J. Multiphase Flow* **5**, 39–58.

ZUBER, N. & FINDLAY, J. A. 1965 Average volumetric concentration in two-phase flow systems. *J. Heat Transfer* **87**, 453–468.

European Two-Phase Flow Group Meeting, Strathclyde University
3-6 June, 1980

A POINT OF INFLECTION CRITERION FOR ANNULAR TWO-PHASE FLOW

D.R.H. BEATTIE

Australian Atomic Energy Commission, on attachment to
AERE, Harwell, from June 1980

ABSTRACT

The film and core regions of annular flow are considered here as regions in which turbulence is confined to the liquid phase and to the gas phase respectively. The film boundary of equilibrium annular flow coincides with an inflection in the voidage profile. This inflection is predicted by mixing-length theory. Non-equilibrium entrainment levels are associated with non-coincidence of the film boundary and the inflection point.

INTRODUCTION

Although there are two physically distinct regions in annular two-phase flows - a liquid-phase-continuous film region and a gas-phase-continuous core - the statistical nature of the film/core interface, in addition to the entrainment of both core and film, gives rise to a rather gradual transition between the two regions. Consequently, the concept of a characteristic film thickness for a given flow becomes, like the interface itself, somewhat ill-defined. Reflecting this, experimental 'film thickness' values are usually based on arbitrary criteria to enable conversion of fluctuating film thickness probe signals to unique values, and/or may be based on unrealistic assumptions (such as the absence of entrainment). Comparison of film thickness data usually becomes meaningless unless the same measurement technique has been used and the same interpretation process applied to all data. More importantly, incompatibility of measurement and analysis using a model of annular flow may make some film thickness data inappropriate for development of the model.

A model of two-phase flow, based on Prandtl's mixing-length theory, is being developed at the Australian Atomic Energy Commission's Research Establishment. In line with the above discussion, the extent of the film region in annular flow is chosen to be compatible with this model. Application of the mixing-length theory has involved the assumption that turbulence is confined to one phase only [1], an assumption originally introduced to allow flow regime effects to be incorporated into the model. The film and core regions of annular flow are, quite simply, viewed as regions where turbulence is confined to the liquid and gas phases respectively.

Although this model of annular flow was originally thought to represent the conventional view of a liquid-phase-continuous film and a gas-phase-continuous core, extensive analysis of data has indicated that the two-region

turbulence model of two-phase flow may differ from the conventional view. In particular, the core region may be liquid-phase-continuous (such as a froth condition) but still compatible with the gas-phase-turbulence equations of the model. (See, for example, the data of Fohrman [2]. Fohrman's regimes, defined on a visual basis, cover bubble, plug, stratified, wavy, slug, and stratified-annular froth flow; and his average voidage data, when considered in terms of the AAEC mixing-length view of two-phase flow, are all compatible with liquid-phase continuous flows throughout the cross-section; but his voidage profile and pressure loss data are all compatible with a liquid-phase-turbulent region near the wall and a gas-phase-turbulent core.) Also relevant to the alternative views of annular flows is the 'roll wave', which is conventionally regarded as a component of the film region. Again, however, analysis of extensive data has shown that regions which contain roll waves are generally compatible with the gas-phase-turbulence equations developed from mixing-length theory.

Film thickness values, based on voidage profile data [3] which have been examined in terms of the two-region turbulence view of annular flow, have been compared [1] with estimates of film thickness [3] obtained under the same flow conditions using wall conductivity probes. As expected, the two sets of film thickness values did not agree since the conductivity-based set does not account for entrained bubble contributions to the film thickness. In line with this, integrations of the voidage profiles over the film thicknesses corresponding to the mixing-length theory concept led to values of liquid contents in the film which, with one exception, are compatible with the conductivity-based values of film thickness. In the exception, the conductivity-based value of film thickness is more than twice the calculated liquid thickness. This was possibly caused by the contribution of a froth region in the core to the conductivity-based value of film thickness.

Although the mixing-length approach to annular flow, as outlined above, is compatible with flow structure data [1] and also with some global characteristics, such as pressure losses (see e.g. [4]), detailed examination of voidage profile data shows that the two-region turbulence model of annular flow is only an approximation; a narrow transition region exists between the film and the core where the voidage profile is incompatible with both the equations developed for gas-phase turbulence and for liquid-phase turbulence. Furthermore, the model is not at a stage where entrainment, film thickness and boundary conditions for annular flow can be predicted.

In this paper, the film/core interface of annular flow is examined in terms of the flow structure equations for the film region which are considered in isolation from the core region equations. This examination provides some possible answers to questions as yet unanswered by mixing-length theory as applied to annular flow.

VOIDAGE AND VELOCITY PROFILES

Voidage (α) and velocity (j) profiles for the liquid-phase turbulent regions of round tube flows are described by

$$(1-\alpha)^{3/2} = (1-\alpha_c)^{3/2} - \frac{3a\sqrt{\tau_w/\rho_\ell}}{2\,k} \ell n \frac{y}{R} \qquad (1)$$

and

$$\alpha = a\,j + b \ . \qquad (2)$$

For gas-phase turbulent regions, the corresponding equations are

$$\alpha^{3/2} = \alpha_c^{3/2} + \frac{3}{2} \frac{c\sqrt{\tau_w/\rho_g}}{k} \ln \frac{y}{R} \qquad (3)$$

and

$$\alpha = c\,j + d \quad . \qquad (4)$$

The development of these equations and their compatibility with available data have been discussed elsewhere [1]. Note, however, that the analytic work is not yet at a stage where the coefficients a, b, c, d can be predicted.

As implied in the introduction, equations (1) and (2) are considered appropriate for the film region of annular flow, and equations (3) and (4) for the core region; the intersect of equations (1) and (3) defines the boundary between the film and core regions, and detailed examination of voidage profiles indicates that this view of annular flow is reasonable, except for a small transition region where neither equation (1) nor (3) is valid.

Although the form of the voidage profile differs in the film and core regions, the same is not true for the velocity profile, at least to a first approximation. This can be demonstrated by linearising the 3/2 power terms of equations (1) and (3) about a mean voidage value and substituting equations (2) and (4),which produces the familiar velocity defect equation for both regions. Velocity profile data (e.g. data from [3] analysed in [4]) indicate that coefficients in the velocity defect equation do not change across the film/core interface of annular flow.

It has been noted elsewhere [3,5] that qualitative examinations of voidage and/or velocity profiles do not suggest any criteria from which film/core interface positions may be determined. From the above, quantitative examination of voidage profiles in terms of equations (1) and (3) allows the interface positions to be estimated, but velocity profiles do not appear to indicate the position of the film/core interface. Note, however, that equations (1)-(4) imply that the velocity profile equations are not identical for the film and core regions. Even though differences may be second order, the following analysis suggests that they are crucial in determining the position of the core-film interface.

A POINT OF INFLECTION CRITERION

Examination of equations (1) and (3) indicates that the curves for $\alpha(y)$ generated by these equations contain inflection points at

$$y_{inf} = e^{-1/3}\, y_1 \qquad (5)$$

where y_1 represents an extreme position on the curve of equations (1) or (3) defined by

$$\alpha\,(y_1) = 1 \quad \text{(liquid-phase turbulence)} \qquad (6a)$$

and

$$\alpha\,(y_1) = 0 \quad \text{(gas-phase turbulence)}. \qquad (6b)$$

The points of inflection will occur outside the physically meaningful range $0 < \alpha < 1$ for the core region of a two-region flow, but will occur within this range for the turbulent region near the wall. Furthermore, the co-

efficients in equations (1)-(4) may be such that the point of inflection occurs in the physically meaningful range $y_{inf} < R$.

DATA ANALYSIS

Annular flow voidage profile data in the literature were analysed in terms of equations (1)-(4) to ascertain whether the point of inflection represented by equation (5) is physically significant. Only data where the voidage profiles extended to within the film region, as defined by the applicability of equation (1), were considered. The data were obtained using isokinetic sampling techniques, needle conductivity probes, or wall-mounted conductivity probes. The conductivity probe data were usually presented as 'relative film contact time' curves or, equivalently, as 'film thickness probability distribution' curves. Since these curves indicate the probability that a given point is in the liquid phase, and local voidage $\alpha(y)$ can be regarded as the probability that gas exists at position y, they may be interpreted as curves of $(1-\alpha(y))$.

RESULTS

The annular flow voidage profiles found were consistent with a previous analysis [1]: the near-wall region is compatible with equation (1) and the core region with equation (3). The intersect of the two equations provides a suitable basis for defining a film/core interface and, as discussed, a narrow region of the profile - a film/core transition region - is incompatible with both equations (1) and (3) near the intersect position.

The point of inflection defined by equation (5) generally coincides with the upper validity limit of equation (1), i.e. the film region equation remains valid up to the inflection point. Examples are given in figures 1 and 2. Although the coincidence of the inflection point and the start of the transition region was not observed in all data examined, the frequency of the coincidence (~75% of all voidage profiles examined) indicates that the point of inflection is of significance. On the other hand, a statistically significant minority of voidage profile data (~25%) did not display this coincidence, indicating that although the film boundary can be regarded in terms of the inflection point for some flows, this does not have general validity.

DISCUSSION

In view of equations (2) and (4), an inflection point in the voidage profile implies that an inflection point also exists in the velocity profile. Because velocity profile inflection points have a destabilising influence, at least for single phase laminar flows [6], an inflection point in the film region of annular flow also could have a destabilising influence.

If this is so, it would explain the comparative scarcity of voidage profile data in cases where the film (defined by the applicability of equation (1)) extends beyond the inflection point y_{inf} (defined by equation (5)), since stable annular flows should be limited to flows in which the film does not extend beyond the inflection point.

This suggests that the film region (defined by the applicability of equation (1)) of stable annular flow must be limited to a distance less than y_{inf}. However, a comparative scarcity of voidage profile data in which the film does not extend to y_{inf} suggests that a mechanism exists whereby flow development produces film boundary and inflection point coincidence. In this regard, limited evidence, based on conductivity probe data, suggests that at least some flows in which the film thickness is less than y_{inf} have a froth in the region

of the core near the film. It is conceivable that such flows are in hydro-mechanical dis-equilibrium, with the froth becoming integrated into the film region.

Similarly, a point of inflection which occurs within a film can be viewed as indicating hydro-mechanical dis-equilibrium. In view of the postulated instability inherent in such a situation, the instability could produce interface activity which removes excess film liquid to the core. It is known that roll waves on the film are the major source of core entrainment [7]. Presumably this process should continue until the film boundary coincides with the inflection point.

A picture thus emerges in which equilibrium between core entrainment and deposition occurs when the inflection point coincides with the film boundary. An imbalance between entrainment and deposition occurs when the inflection point falls outside the film (a deficiency of liquid in the film) or within the film (a deficiency of entrained core liquid).

As a secondary consideration, it may be that the position of an inflection point at a duct centre represents an upper voidage limit of stable bubble flow. As part of the present work, a number of developed bubble flow voidage profiles were examined and were all such that the inflection point y_{inf} occurred in the physically meaningless range $y_{inf} > R$. A change of bubble flow conditions so as to bring the inflection point to a position $y_{inf} < R$ should, in view of stability considerations, represent the onset of slugging or semi-annular flows. A number of voidage profiles from such flows were also examined: these were similar to the annular flow voidage profiles except that the validity limit of equation (1) extended over a much larger section of the flow, rather than being confined to only a narrow region near the wall.

As a final comment, one can reasonably suppose that the inflection point criterion is as relevant to inverse annular flows, i.e. film boiling flows, as it is to annular flows, but lack of relevant voidage profile data for inverse annular flows precludes confirmation of this supposition.

CONCLUSIONS

A mixing-length theory approach to two-phase flow analysis has resulted in voidage and velocity profile equations which provide inflection points. Such points may occur within physically meaningful regions of the flow, and data analysis indicates that there is a strong connection between the position of such an inflection and the film boundary for annular flow. The location of this inflection is a determining factor in relation to the onset of annular flow and in producing a balance between entrainment and deposition processes in annular flow.

ACKNOWLEDGEMENT

Helpful discussions with Dr. K.R. Lawther, Head, Heat Transfer Section, AAEC, are gratefully acknowledged.

NOTATION

a,b,c,d	coefficients in equations (1)-(4)
j	local mixture velocity
k	mixing-length coefficient
R	duct radius
y	distance from wall
y_1	wall distance defined by equation (6)
y_{inf}	position of inflection point
α	local void fraction
α_c	centre-line void fraction
ρ_g	gas density
ρ_ℓ	liquid density
τ_w	wall shear stress

REFERENCES

1. Beattie, D.R.H., 'Two-phase flow structure and mixing length theory', Nuc. Eng. Des. 21, 46-64 (1972).

2. Fohrman, M.J, 'The effect of the liquid viscosity in two-phase, two-component flow', ANL Report ANL-6256 (1960).

3. Alia, P., Cravarolo, L., Hassid, A. and Pedrocchi, E., 'Phase and velocity distribution in two-phase adiabatic annular dispersed flow', CISE report R-109 (1966).

4. Beattie, D.R.H., 'Some aspects of two-phase flow drag reduction', Paper D1, Proc. 2nd Int. Conf. Drag Reduction, BHRA Fluid Engng, Cranfield, UK, (1977).

5. Webb, D., 'Studies of the characteristics of downward annular two-phase flow', AERE report R6426 (1970).

6. Schlichting, H., 'Boundary-layer Theory', McGraw-Hill (1968).

7. Hewitt, G.F. and Hall Taylor N.S., 'Annular Two-phase Flow', Pergamon, (1970).

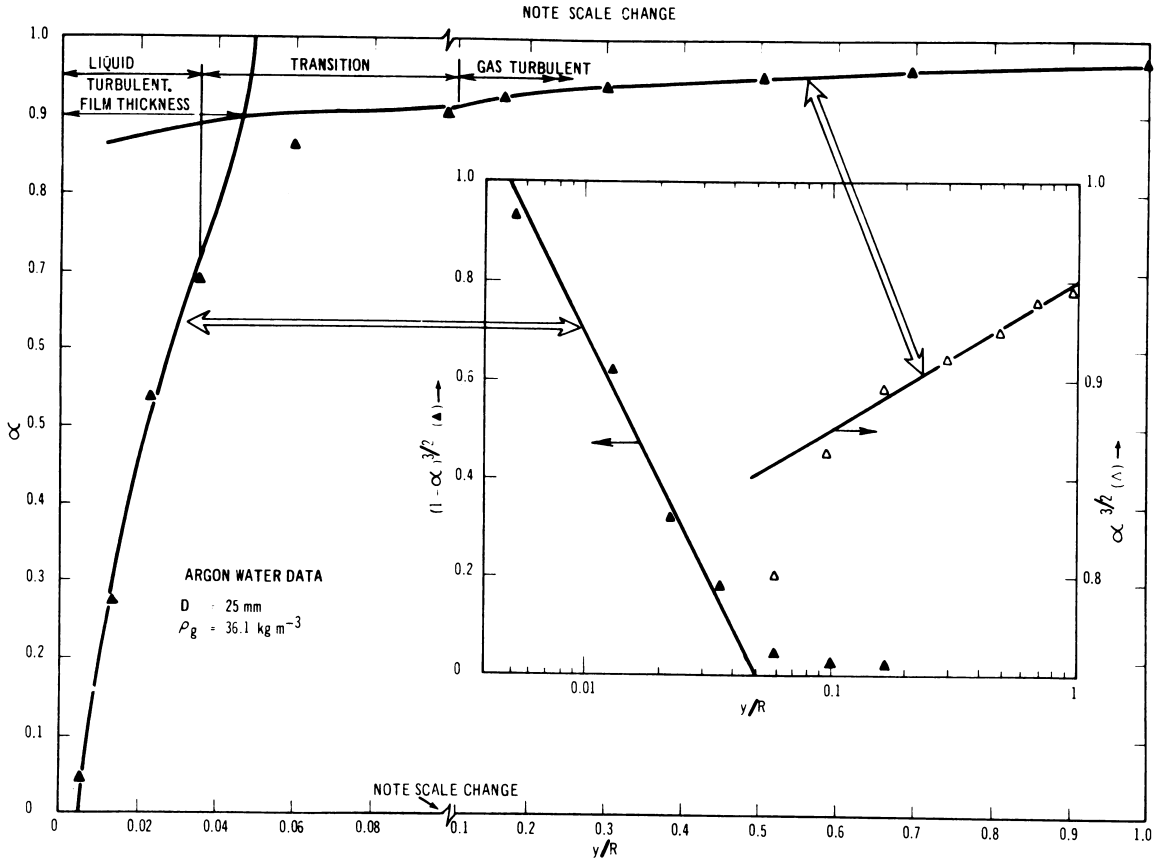

Fig. 1 Film region analyses for ref. [3], table xii data

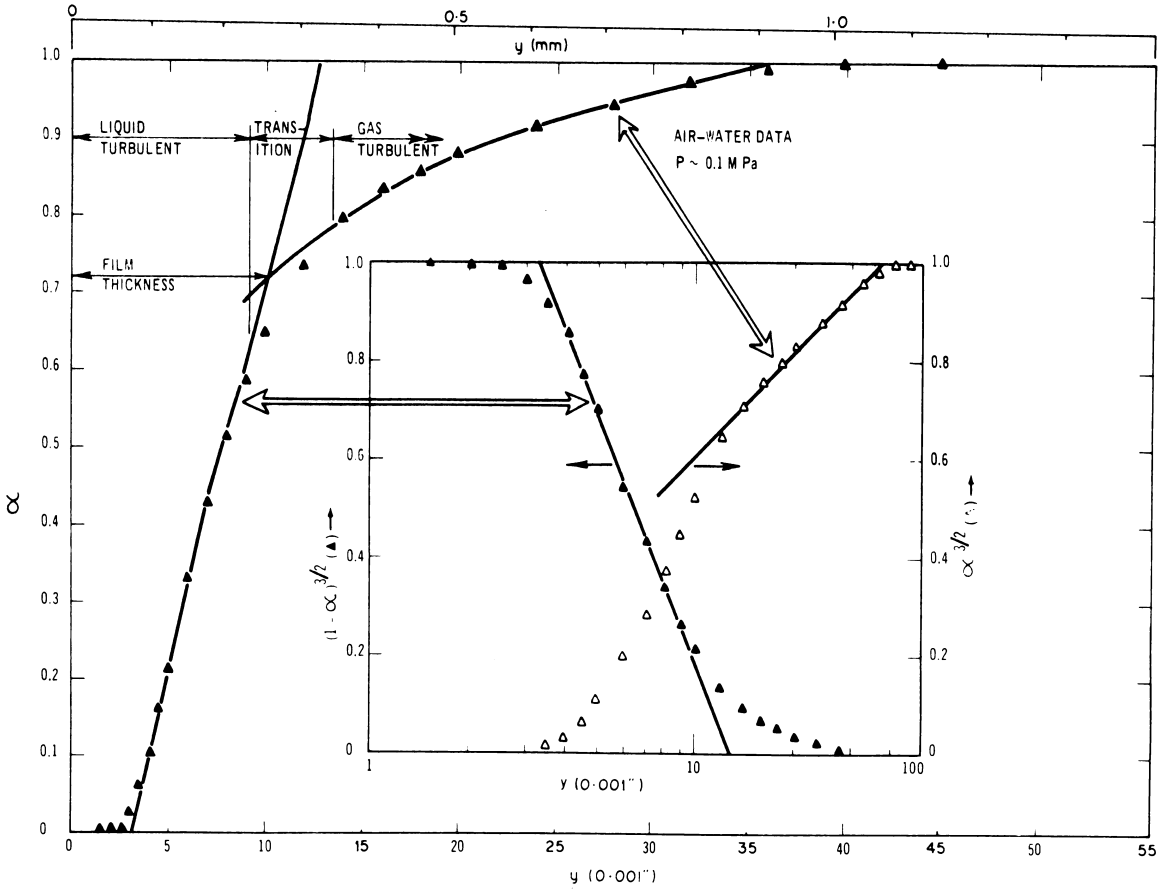

Fig. 2 Film region analyses for ref. [5], run 61 data

Pressure Pulse Propagation in Two-Component Slug Flow[1]

D. R. H. BEATTIE.[2] The work of Professors Martin and Padmanabhan should help dispel the widely held but erroneous belief, stemming from the work of Henry, et al., [2, 3], that pressure pulse behavior in two-phase slug flow is fundamentally different from that in bubble flow. The theory of Henry, et al., assumes no mechanical coupling between the phases, a condition which was simulated in their somewhat artificial "slug flow" experiments performed to confirm their theory. The theory of Martin and Padmanabhan takes account of this mechanical coupling between the phases, which in reality is almost complete, as is the case for bubble flow. Thus slug flow pressure pulse characteristics should be similar to those expected from bubble flow. This is verified by the experimental data of Martin and Padmanabhan.

If thermal coupling between the phases is considered, a minor flow regime effect might be expected. The low thermal coupling expected for slug flow is such that the isentropic temperature change occurring during the pulse passage might reasonably be expected to be confined to the gas phase, with the result that, as supposed by Martin and Padmanabhan, the specific heat ratio γ in the theory is that for the gas, C_{gp}/C_{gv}. On the other hand, the more uniform dispersion of the phases in bubble flow is such that an assumption of thermal equilibrium is more reasonable. In this case, as shown by Miyazahi et al., [7], the value of γ then becomes

$$\frac{x\ C_{gp}+(1-x)\ C_l}{x\ C_{gv}+(1-x)\ C_l}$$

where x is the mass fraction of gas, and C_l the liquid specific heat. For the small gas mass fractions occurring in the described air-water slug flow experiments, γ might be expected to be closer to unity if bubble flow had occurred. However, this dependence of pressure pulse velocity on flow regime, which is not taken into account in the theory of Martin and Padmanabhan, is small and of the order of normal data scatter. As expected, then, the experiments of Miyazahi, et al., [6], which covered both bubble and slug flow, did not indicate any discernible influence of flow regime on pressure pulse velocity characteristics.

Martin and Padmanabhan's treatment of the drift flux model is such that the distribution parameter, C_0, is assumed to be unity. Their conclusion that the pressure pulse velocity is that given by the homogeneous model with respect to the mixture center of mass velocity applies only if the "slip" between the phases is caused only by a drift velocity v_{gj} and is not general. Distribution parameter effects are considered in [19] and its supplement [22] which give the result

$$a=\sqrt{\frac{\gamma p}{\alpha(1-C_0\alpha)\rho_l}}$$

(which reduces to equation (15) for $C_0 = 1$) with respect not to the center of mass velocity but, if $j >> v_{gj}$, to $j(C_0 + (1 - C_0\rho_l/\bar{\rho})$ where $\bar{\rho}$ is the homogeneous mixture density, and C_0 is as calculated in [19].

The theory of [19] applies for developed flows and, as such, is not strictly applicable to the experiments of Martin and Padmanabhan where the experimental distribution parameters, which are less than unity because of the skewed voidage profiles, indicate non-developed conditions. Nevertheless, the theory of [19], as indicated in the accompanying table, predicts the pressure pulse velocity data of Martin and Padmanabhan better than the homogeneous model does, even though the developed flow void fractions predicted by the method of [19] are clearly inappropriate. This suggests that, for pressure pulse velocity prediction, the theory of [19] can be extended to nondeveloped conditions, at least when the nondevelopment is characterized by skewed voidage profiles.

Table 1 Error statistics for pressure pulse velocity data of Martin and Padmanabhan. Errors are (calculated velocity - measurement velocity)/(measured velocity)

	Mean error	R.M.S. error
Homogeneous model	− 17.4%	18.1%
Method of [19]	− 3.2%	6.7%

Additional Reference

22 Beattie, D. R. H., and Thompson, J. J., "The Effect of Flow Velocity on Two-Phase Propagation Phenomena," *Proceedings, Second International Conference on Pressure Surges*, London, Sept. 1976, supplement to paper D3.

[1] By C. Samuel Martin and M. Padmanabhan, published in the March, 1979, issue of the ASME JOURNAL OF FLUIDS ENGINEERING, Vol. 101, No. 1, pp. 44-52.

[2] Senior Research Scientist, Australian Atomic Energy Commission, N.S.W. Australia

7th Australasian Hydraulics and Fluid Mechanics Conference, Brisbane, 18-22 August, 1980

Experiments on Air-Water Flows in an Eccentric Annular Channel

D.R.H. BEATTIE
Senior Research Scientist, Australian Atomic Energy Commission, Sydney
and
K.R. LAWTHER
Principal Research Scientist, Australian Atomic Energy Commission, Sydney

SUMMARY The structure of two-phase flow has been investigated for air-water flows in a vertical eccentric annular channel. The results, which include axial pressure gradients and velocity profiles near the wall, were obtained for a wide range of flow conditions. The region near the wall was investigated by means of a variable height scoop assembly, which was used both as an isokinetic flow sampling device and as a Preston probe. Azimuthal variations were also investigated for each flow condition. Experimental results are, on the whole, consistent with a mixing length approach to two-phase flow characteristics. The results indicate that the flow is much less developed than that in a corresponding concentric annular channel, and that intrusions into the flow, such as spacer elements or probes, have much more significant effects on the local flow structure in the eccentric annular channel.

NOTATION

i	scoop gap
D	equivalent diameter
D_s	shroud diameter
f	friction factor, $2\tau_w/(G \langle j \rangle)$
G	mass flux
j	mixture velocity
$\langle j \rangle$	cross-sectional average mixture velocity
j^+	$\sqrt{2}\ j/(\langle j \rangle \sqrt{f})$
K	loss coefficient, $\Delta P/(G \langle j \rangle)$
u_g	local gas velocity
Q	extracted volume flow rate
Q^+	$\dfrac{Q\ Re}{\langle j \rangle D \times (\text{scoop width})}$
Re	Reynolds number, DG/μ
V_p	'Preston velocity' (see section 3.4)
y	distance from shroud
y^+	$y\ Re\sqrt{f}\ /\ (D\sqrt{2})$
α	void fraction
β	volumetric flow ratio
ρ	density
μ	viscosity of sub-layer
μ_ℓ	viscosity of liquid
μ_g	viscosity of gas
θ	angle defined in fig.1.

1 INTRODUCTION

A program of research into the fluid mechanics of two-phase flows in rod cluster geometries has been conducted at the AAEC Research Establishment over the last seven years. The program was initiated to improve understanding of two-phase fluid mechanics in water-cooled nuclear reactor systems in relation to predicting coolant flow behaviour for abnormal operating conditions as in a loss-of-coolant accident. It has incorporated the use of analytic and experimental methods and included experiments with air-water flows in round tube and concentric annular flow channels.

This paper describes air-water flow experiments with an eccentric annular channel. This was considered a suitable next phase of the program since it would result in a simple three-dimensional flow, not unlike that expected for a rod-centred sub-channel of a multi-rod reactor fuel element assembly.

2 TEST SECTION

The annular channel consisted of a 90 cm long, 25.4 mm i.d. shroud, with a 12.7 mm dia. rod offset by 3.1 mm from the centre. This geometry was chosen to be similar to the channel used by Schraub et al. (1969). The present results, covering the gas volume flow ratio range $0.16 < \beta < 0.87$, were obtained with the idea of complementing the high gas content ($\beta > 0.94$) air-water data of Schraub et al. (1969).

The rod was positioned by spacers at points upstream and downstream of the main test section, and, in the earlier part of the experiment, also in the middle of the test section. The central spacer was simply 6 small screws inserted through the shroud at equal azimuthal spacings, and was removed in an attempt to encourage developed flow at the test section exit after preliminary tests indicated that flow development was considerably less than for the earlier concentric annular channel and round tube experiments on the same rig.

3 INSTRUMENTATION

3.1 Needle Conductivity Probes

Traversing needle conductivity probes (see Herringe and Davis, 1974) were used to detect the presence or absence of air at any point in the flow. The local voidage, α, is the probability that gas exists at the point considered. Ideally, for a flow with stationary characteristics, the needle signal will be a simple on-off response, the time average of which can be interpreted as the local voidage. However, real systems are not ideal, and, for a number of reasons, the 'on' signal may not reach the level anticipated, and may even be of a

comparable size to noise encountered in the 'off' level. Often, arbitrary discriminator levels are applied to decide whether the signal is 'on' or 'off' (Herringe and Davis, 1974). Each signal in the present experiments was analysed in terms of probability distribution curves. The shapes of these curves were used to determine a non-arbitrary discriminator level for each signal, from which the void fraction was obtained.

As discussed by Herringe and Davis (1974), cross-correlation of the signals from two such probes, separated axially by a small distance, can be used to determine the interface velocity. For low voidage flows, this velocity can be interpreted as the gas velocity.

A traversing double needle probe of 4 mm separation was used at distances 22.5 cm (18 diameters) and 67.5 cm (53 dia.) from the test section inlet for local voidage and interface velocity measurements. The probe could be positioned within 0.5 mm of the shroud and 1.5 mm of the rod. It was intended to use this probe at different azimuthal positions to obtain void fraction and velocity maps for different flow conditions.

3.2 Manometers

The test section contained four pressure tappings, positioned to measure pressure gradients in upstream and downstream parts of the test section, and the pressure drop across the middle spacer. Lines from the tappings were filled with water and connected to dye-coloured Freon-113 manometers. Line purging was not necessary with this arrangement; furthermore, liquid in the lines damped pressure fluctuations, resulting in steady manometer readings. An additional benefit is the low effective density of the manometer fluid (570 kg m^{-3}) which results in high sensitivity.

3.3 Wall-region Isokinetic Sampling Scoop

In the present experiments, the region near the shroud was examined with a variable gap isokinetic sampling scoop. The design was adapted from that of Adorni et al. (1963) and the device is shown schematically in fig.1. In principle, the flow is extracted through the scoop at a rate such that pressures at points A and B (fig.1) are equal. Under these conditions, it is assumed that the probe does not disturb the flow and that the measured rate of extracted flow is the same as that which would have passed through the scoop flow area in the absence of the scoop.

To obtain a high sensitivity, pressure tappings A and B were connected by a horizontal water-filled glass tube and a device for injecting single air bubbles was provided at the centre of this tube. The extracted flow was adjusted by means of needle valve C (fig.1) till an injected bubble remained stationary. Then the sampled flow rate was measured.

Measurement consisted of determining (a) the volume of water extracted during a given time, and (b) the air content by using quick-closing valves to collect a given volume of extracted flow in a glass tube.

The scoop-shroud gap was adjusted between 0.25 mm (the minimum) and approximately 0.9 mm (the maximum at which isokinetic extraction could be achieved), with a traverse consisting of extractions at 5 or 6 positions, including the two extreme locations. It was found necessary to connect a vacuum pump to the extraction circuit for gaps greater than ~ 0.5 mm.

To determine azimuthal variation due to rod eccentricity, traverses were made for θ equal to 0°, 45°, 90°, 135°, and 180° (fig.1).

Before the present experiments, the device was tested with single phase (air) flow in a round tube, using a differential pressure gauge between pressure tappings A and B. Extracted flows were consistent with those expected on the basis of the universal velocity profile.

3.4 Preston Probe

A Preston tube is a pitot tube placed in contact with a sheared surface. When calibrated, the tube impact pressure is a direct measure of the local wall shear stress (Preston, 1954).

Under zero extraction conditions, the scoop on the isokinetic sampling probe can serve as a Preston probe. In the present experiments, the velocity head was determined from the velocity of the water in the sight-tube between pressure tappings A and B (fig.1), hereafter called 'Preston velocity', as determined by timing the transport of a bubble injected into this tube.

The theory behind the application of the Preston tube to two-phase flow is uncertain. Nevertheless, Preston velocity values were readily measured and were obtained following each isokinetic extraction.

4 BACKGROUND THEORY

Aspects of the two-phase mixing-length theory (Beattie, 1972) which are relevant to the present experiments are as follows:

(i) A linear relation is expected between $(1-\alpha)^{3/2}$ and log y and also between local voidage and local liquid velocity.

(ii) Friction factors and pressure loss coefficients depend on Reynolds number D G/μ where:

(a) $\mu = \mu_\ell (1+2.5\ \beta)$ for bubbly flows with no movement on the individual bubble surfaces,

(b) $\mu = \mu_\ell \left\{ 1 + \dfrac{2.5\mu_g + \mu_\ell}{\mu_g + \mu_\ell} \beta \right\}$ for bubbly flows where there is movement on bubble surfaces,

(c) $\mu = \mu_\ell (1-\beta) + \mu_g \beta$ for wavy gas/liquid interface in the sublayer.

(iii) Obstruction pressure loss coefficient dependence on Reynolds number should be the same as for single-phase flow with the appropriate viscosity in the Reynolds number.

(iv) Coefficients appearing in the two-phase friction factor Reynolds number (with appropriate viscosity) relation, and the corresponding non-dimensional velocity profile, may differ from those in the single-phase relations. However, there are distinct constraints on these values. The coefficients in the friction factor relation, together with the appropriate viscosity definition, identify a particular two-phase flow regime.

Further aspects of the above concepts have been given by Beattie (1972, 1973, 1977).

5 RESULTS

5.1 Conductivity Probe Data

Voidage and velocity profile data were found (a) to be incompatible with theoretical expectation, (b) to have shapes suggesting a strong degree of non-development, and (c) to exhibit non-reproducibility. Since meaningful voidage and velocity maps could not be obtained, these measurements were abandoned early in the experiments.

Typical results, from measurements in the narrow part of the annulus, are shown in fig.2. Results from similar experiments with a concentric annular channel indicated a higher degree of flow development than was found with the present experiments.

5.2 Spacer Pressure Loss Coefficient

Spacer pressure loss coefficient data correlated with Reynolds number using viscosity (c) (see section 4) for all flow conditions. This viscosity suggests that the flow had become separated when passing over the central spacer. Because of this, and the high degree of non-development exhibited by the conductivity probe data, the spacer was removed early in the experiments.

Data are shown in fig.3. The correlating curve was obtained from earlier tests with single-phase flow over the spacer used in the concentric annular channel. The agreement between the single-phase curve and the two-phase data is consistent with the theoretical expectations outlined in section 4.

5.3 Friction Factors

Friction factors were obtained from pressure drop data with the gravitational head being accounted for by using the Zuber and Findlay (1965) correlation for void fraction. This correlation is unlikely to be valid for the non-developed flows described here, but as the gravitational component of the total head was generally small, the effects of such errors on the friction factor data are expected to be small.

Flow data at low voidage values were correlated using viscosity (b), compatible with bubbly flow; and flow data at high voidage values, with viscosity (c), compatible with annular flow. The data are shown in figs.4 and 5. The coefficients in the correlating curves are consistent with constraints described by Beattie (1977). The data scatter is consistent with the non-reproducible voidage profile data (section 5.1), which implies a non-reproducible gravitational component of the total head.

These results differ from those found earlier with the concentric annular channel. In that case, friction factor data for both high and low voidage flow conditions were correlated using the Nikuradse equation with bubble viscosity 'a) in the Reynolds number.

5.4 Isokinetic Sampling Data

Data for extracted volumetric flow Q and scoop gap d were plotted in non-dimensional form as Q^+ against $d^+ = (d/D)\ Re\ \sqrt{f/2}$. Data did not correlate when plotted using viscosity (c) in Re, but did, when plotted using viscosity (a) or (b). This applied to both high and low voidage conditions. When compared with the results described in section 5.3, the implication is that the probe induced a regime change, a situation that appears to have occurred with other isokinetic sampling data (Beattie 1977).

When plotted in terms of viscosity (a), and friction factor, f, calculated according to the Nikuradse equation incorporating this viscosity, the correlating curve is the integral of the 'universal' velocity profile (fig.6). This is the result expected for developed flows. The scatter in fig.6 is largely due to difficulty found in determining isokinetic sampling flow conditions for low momentum flows. As can be seen from fig.6, no azimuthal variation was found in the results.

5.5 Preston Probe Data

Preston velocity data - this term is described in section 3.4 - were plotted as a function of scoop gap for each flow condition. Typical data are shown in fig.7. Again, there is no apparent azimuthal variation.

An attempt was made to convert such data to local shear stress data by calibrating the Preston probe using single-phase flow in a round tube. However, the dependence on the scoop gap was considerably less in the single-phase calibration runs, indicating that the single-phase results did not apply to the two-phase case. This may be due to the Preston tube concept being inappropriate to two-phase flows, or, more likely, in line with the non-development suggested by earlier results, be due to the two-phase non-dimensional velocity profile being steeper in the wall region than would be the case for more developed flows.

6 CONCLUSIONS

A wide range of experiments has been performed for air-water two-phase flow through an eccentric annular channel. With the exception of core region voidage and velocity profile data, the results are consistent with expressions obtained previously using a two-phase mixing length concept. The results indicate that the flow is less developed than indicated by corresponding results obtained with the rod positioned concentrically. Intrusions into the flow, such as spacers or probes, affect the flow locally so that results obtained with these intrusions are not necessarily representative of behaviour in their absence.

REFERENCES

ADORNI, N. et al. (1963). An isokinetic sampling probe for phase and velocity distribution measurements in two-phase flow near the wall of the conduit. CISE report R89.

BEATTIE, D.R.H. (1972). Two-phase flow structure and mixing length theory. Nuc. Eng. & Des. Vol.21, pp 46-64.

BEATTIE, D.R.H. (1973). A note on the calculation of two-phase pressure losses. Nuc. Eng. & Des. Vol. 25, pp 395-402.

BEATTIE, D.R.H. (1977). Some aspects of two-phase flow drag reduction. Proc. 2nd Int. Conf. on Drag Reduction, Cambridge, U.K., paper D1.

HERRINGE, R.A. and DAVIS, M.R. (1974). Detection of instantaneous phase changes in gas-liquid mixtures. J. Phys. E, Scientific Instruments, Vol. 7, pp 807-812.

PRESTON, J.H. (1954). The determination of turbulent skin friction by means of Pitot tubes. J. Roy. Aero. Soc., Vol. 58, p 109.

SCHRAUB, F.A. et al. (1969). Two-phase flow and heat transfer in multirod geometries. GEAP report 5739.

ZUBER, N. and FINDLAY, J.A. (1965). Average volumetric concentrations in two-phase flow systems. J. Ht. Transfer, Vol. 87, pp 453-468.

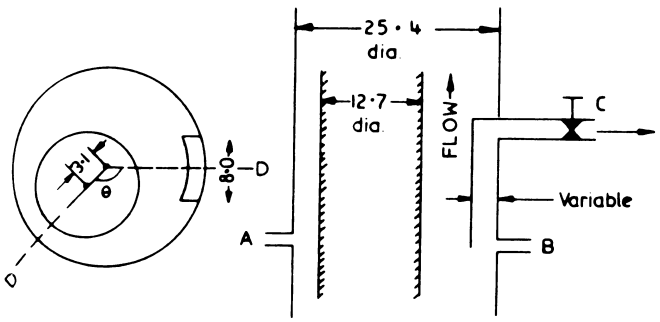

Figure 1 Test Section with isokinetic sampling device located at exit

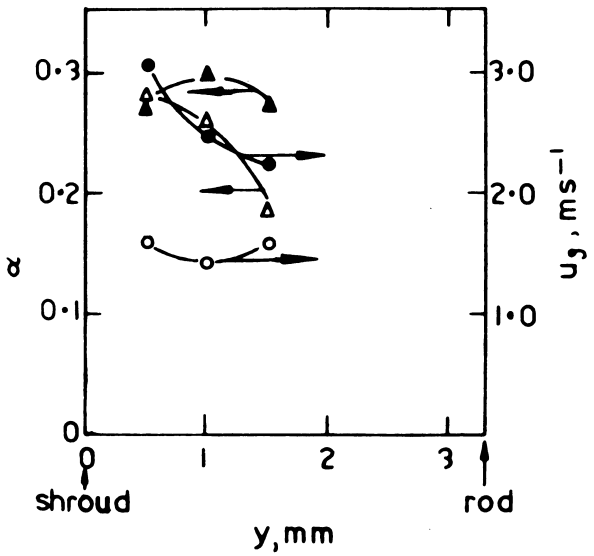

Figure 2 Typical voidage and velocity profiles; θ = 180°; $\langle j_g \rangle$ = 0.66 m s^{-1}; $\langle j_l \rangle$ = 2.00 m s^{-1}; ▲,● = profiles 22 cm from inlet; Δ,o = profiles 67 cm from inlet.

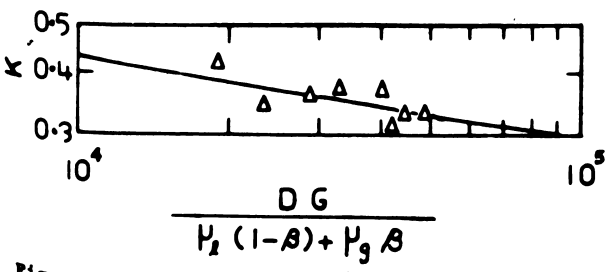

Figure 3 Space loss coefficient

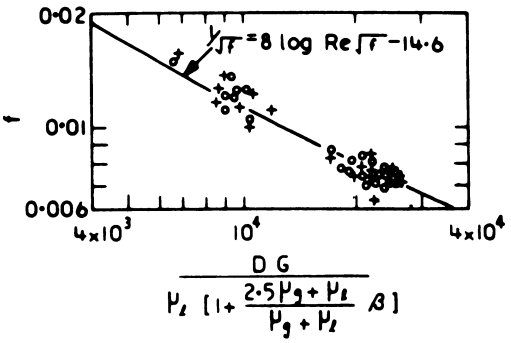

Figure 4 Low voidage friction factors.+, data from pressure tappings 5 and 40 cm from inlet, o, data from pressure tappings 50 and 85 cm from inlet.

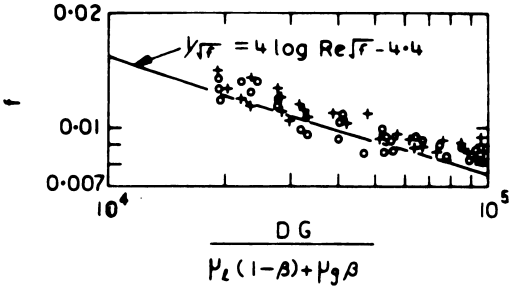

Figure 5 High voidage friction factors. Notation as in fig.4.

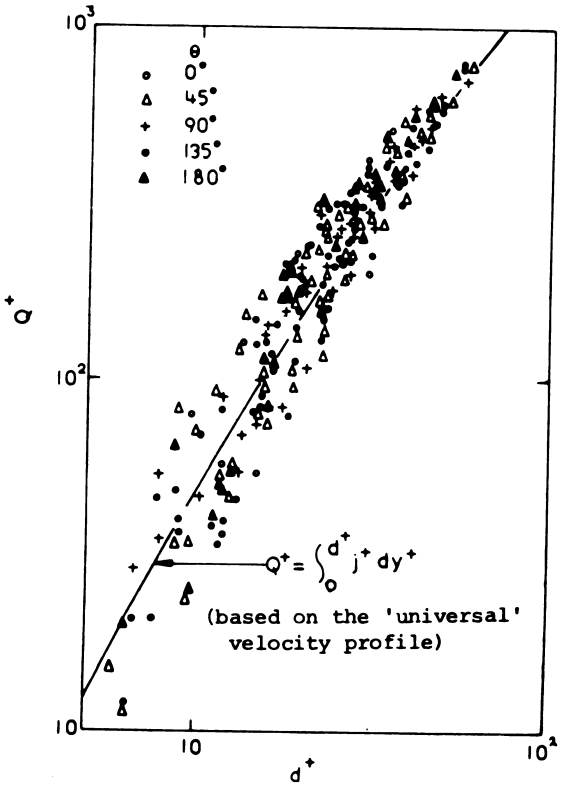

Figure 6 Isokinetically sampled volume flow, $\langle j_l \rangle$ = 1, 2 m s^{-1}; 0.4 m s^{-1} < $\langle j_g \rangle$ < 6.5 m s^{-1}.

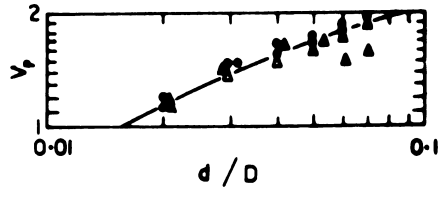

Figure 7 'Preston velocity' data, $\langle j_l \rangle$ = 1 m s^{-1}, $\langle j_g \rangle$ = 0.7 m s^{-1}. Notation as in fig.6.

EIGHTH NATIONAL CHEMICAL ENGINEERING CONFERENCE

at

MELBOURNE, AUSTRALIA

AUGUST 24-27, 1980

THE ACCURATE MEASUREMENT OF FLOW RATES IN GAS AND GAS-LIQUID SYSTEMS USING A RADIO-TRACER TECHNIQUE

by

Beattie, D.R.H. and Hanna, G.L.

SUMMARY

The utilisation of fluid resources relies heavily on the measurement of flow during processing, transport and custody transfer. To improve and maintain accuracy in industry, periodic calibration against a standard is required. The AAEC's adaptation of the radio-isotope dilution method of measuring mass flow in gas systems offers a calibration technique with potentially low cost, accuracy and precision which equal or approach the best available with established techniques. The method is absolute, independent of pipe diameter and surface condition, and can be applied either in situ or to meters mounted in a calibration facility. The AAEC is constructing a test facility for thorough investigation of the technique over the mass flow range 0.16 - 1.5 kg s^{-1} using compressed air. A description of the facility is given.

The technique could also be applied to two-phase systems such as steam circuits and natural and petroleum gas pipelines. The application to wet steam flows is discussed. The existence of two phases presents problems with respect to inter-phase mixing of the radio-tracer but these are expected to be small compared with those encountered with conventional flow metering methods. A steam-water loop, involving special monitoring techniques, has been constructed in order to evaluate the method's potential for wet-steam flow measurements. Flow rates of 0.2 to 0.8 kg s^{-1} (at 1.4 MPa and 300°C) are being studied.

1. INTRODUCTION

In the use of a fluid resource or commodity, great reliance is placed on the measurement of flow during processing, transport and custody transfer. Industrial flow meters are manufactured either to conform to an engineering code, which guarantees a certain level of accuracy, or to be calibrated against a primary or transfer standard. Where codes are followed accuracies for gases are generally about 1 to 1.5 per cent. Where meters are calibrated, accuracies are better (0.25 to 0.5 per cent) but costs of calibration comparable to the costs of the meters themselves are a recurring expense if the level of accuracy is to be maintained.

Improvement of metering accuracy from say, 1.5 to 0.5 per cent could represent a significant improvement in process control which could lead ultimately to substantial savings in the commodity being processed and/or in fuel required for the processing. If such an improvement could be made via a calibration process that is cheap and involves little or no downtime of plant, the idea of regular calibration might be more attractive to industry than it is at present.

Radioisotopes have been used to measure flow rates for many years, probably more frequently for liquids than for gases, but the advantages of this application to industry have not been fully exploited, particularly in Australia. Radio-tracer techniques can involve measurement of one of the following: the time of flight of the tracer pulse along a pipe of known cross-section; of the total count as the pulse passes a radiation counter operating under calibrated detection geometry; the dilution of the pulse in the process fluid as it flows down the pipe [1]. The dilution technique is inherently suitable for calibration purposes because it is independent of both the pipeline characteristics and the properties of the fluid, and generally can be used on-stream without interference to plant operation.

Beattie and Hanna, Australian Atomic Energy Commission, Research Establishment, Private Mail Bag, Sutherland, 2232, NSW, Australia.

In 1975, a significant advance in the application of the tracer dilution method to the measurement of gas flow was made by the Australian Atomic Energy Commission [2]. In Section 2 a major experimental program is described which includes a large test facility now being constructed by the AAEC for fully proving this method.

As well as gas and liquid flows, flows of gas-liquid mixtures are commonly encountered in industrial processes. Because of the complex nature of such flows, conventional single-phase flow monitoring techniques cannot be used; a meter response, which can be expressed unambiguously in terms of mass flow rate for single phase flow, becomes a function of mass flow rate, gas content, and also of the nature of the flow structure (bubble, stratified, etc.) for a two-phase system.

With this background, the AAEC considered that industry might benefit if the basically straight forward radio-tracer pulse dilution method outlined above could be adapted to gas-liquid flow systems. A research and development program, designed to test the feasibility of monitoring the mass flow rate of wet steam flows via the dilution of an injected pulse of water labelled with tritium (a radioactive isotope of hydrogen), is described in Section 3.

2. GAS FLOW MEASUREMENT

The AAEC's adaptation of the gas flow measurement technique is described in detail by Spragg and Seatonberry [2]. An aliquot of radioactive tracer gas (usually ^{85}Kr) of activity A is injected into the pipeline and, at a point downstream where the tracer and the flowing gas have mixed uniformly across the pipe, a sample is withdrawn over a time interval t (which includes the time of transit of the tracer pulse past the sampling point). The activity of the sampled gas is measured in a radiation counter (giving a count rate C) which is calibrated by injecting a second aliquot A_o into a large air-filled vessel whose volume V and in which the air density ρ_o are accurately known. After mixing, the radioactivity in this air is measured in the same radiation counter (giving count rate C_o) and the mass flow is calculated from the expression

$$\text{Mass Flow} = W = \frac{V C_o A}{t C A_o} \rho_o \qquad (1)$$

This procedure has the advantages that it does not require the absolute activity of the injected tracer aliquot A to be determined, and it measures the activity of the sampled gas by comparing it to that of another sample diluted to a comparable level. Earlier methods compared the activity of the sampled gas with that of the injected aliquot and the ratio of the activities was large (e.g. 3×10^5 [3]). In the AAEC method, the ratio is much lower (close to unity) and the error in measuring the activity ratio (here it is C_o/C) is much lower. The ratio A/A_o is determined accurately (0.2 per cent), not in terms of the activity but of the temperature and pressure at which each aliquot is loaded into the injection cartridge. In addition the volume of the dilution vessel has been calibrated to 0.02 per cent by the National Measurement Laboratory of CSIRO.

An error analysis [2] suggested that the method is capable of an overall error in flow measurement of about 0.3 per cent r.m.s.; that is, comparable with the best calibration methods currently available.

Field trials in Victoria and South Australia [2] supported the error estimate given above and the AAEC is now constructing a gas flow test facility in which a thorough and systematic evaluation of the method will be made. The project is being developed under the guidance of a steering committee comprising senior representatives from the AAEC Research Establishment and the National Measurement Laboratory. Construction of the facility should be completed during 1981.

An artist's sketch of the facility is shown in Fig.1. The test fluid will be compressed air from the Research Establishment's air supply system which has been upgraded to meet the rig requirements. Design parameters for the test facility are:

Maximum flow rate:	1.45 kg s^{-1} (0.83 m^3 s^{-1} at s.t.p.)
Operating pressure:	250-650 kPa absolute
Maximum design pressure:	1 MPa
Operating temperature:	Ambient
Test section diameters:	50, 100 and 150 mm
Test section length:	42 metre, maximum

The air supply system comprises five compressors with a total capacity of 1 m^3 s^{-1}, three receivers of 3.4 m^3 total capacity, filters and a cooling tower. However, not all of this capacity will be available to the rig, and the supply will have to be boosted with hired diesel compressors to achieve the maximum design flow rate. The air will be partially dried to keep it above saturation point. The oil content is expected to be less than 15 ppm.

The facility will consist of three horizontal test sections (arranged parallel in the

vertical plane) incorporating mechanical flow meters of three different types to provide bases against which the radiotracer measurements can be assessed. Financial constraints require that the number of flow meters required to cover the range of flow and pipe diameters be minimised. Thus, cross-over pieces will be installed, as required, so that flow meters designed for and installed in one leg can be used when tracer measurements are required in another leg. Where cross-over pieces are used, the straight length of test sections available for tracer injection and sampling will be reduced, but will exceed the calculated minimum mixing distance (ca. 100 diameters) in all legs [4].

Each test section will be made up from flanged sections to facilitate the exchange or rearrangement of flow meters, insertion of cross-overs, and, if required, the insertion of special sections or flow meters for calibration. Tapping points will be provided at pre-determined intervals for tracer injection, sample withdrawal, and pressure and temperature measurement. The number and disposition of tapping points should permit a thorough study of the mixing behaviour as the tracer pulse flows down a test section.

Conventional flow monitoring will be done using a turbine meter, critical flow meters, and orifice plate meters.

A calibrated turbine meter, which will be at the downstream end of the facility, has been chosen as the basic reference flow meter because of its wide flow range (10:1 volume flow ratio and 27:1 mass flow ratio over the linear range, and wider still if calibrated into the non-linear range) and excellent short-term repeatability (±0.1 per cent).

Critical nozzles, which are insensitive to downstream pressures and can be machined to give a design flow rate at given upstream pressures to high tolerance [5] will be used at the upstream end of the test section as flow generators/meters. A set of interchangeable nozzles will permit coverage of the design flow range in about three steps for each test leg.

Flange tap orifice plate meters will be installed just upstream of the turbine meter to provide a comparison with a meter type which is widely used and accepted in industry. The orifice meters will be designed primarily to British Standard BS-1042 and will incorporate the requirement of International Standard ISO-5167 as far as possible. The overall uncertainty should be ±1 per cent.

Pressure and temperature will be measured to an accuracy and precision consistent with the expected performance of the mechanical flow meters. The radio-tracer method measures mass flow independent of the pipeline pressure and temperature but it does require an accurate measurement (0.25 per cent or better) of pressures and temperature during tracer dispensing and calibration operations.

Initial operation of the facility will be devoted to an intercomparison of the mechanical flow meters over as much of the design flow range as can be achieved with the on-site compressors. Repeat intercomparisons, and ultimately comparison against the radioisotope method, will allow the long-term repeatability of the meters to be monitored.

The gas flow facility will be used to meet two broad objectives: (a) a thorough statistical evaluation of the precision of the tracer dilution technique; and (b) a study of the mixing behaviour of the tracer in the flowing gas. These will be pursued simultaneously but additional runs might be needed to complete the understanding of mixing behaviour, particularly if the effects of bends, constrictions, etc. are to be included.

The initial series of experiments will be designed to give at least four replicate measurements at each set of conditions: pipe diameters of 50, 100 and 150 mm; high, medium and low flow rates; high and low pipeline pressures; central and side tracer injection; high and low injection pressures, and sampling at various radial and six axial positions. This will require nearly 3500 samples to be taken and measured in some 600 to 1800 runs, depending on the number of samples that can be taken simultaneously.

The only estimate of accuracy obtainable up to this stage will be from comparison with the mechanical flow meters, particularly the turbine meter which should perform as a suitable transfer standard. A less ambiguous determination of accuracy could require a series of experiments in another facility which incorporates a primary (e.g. gravimetric) standard of flow.

3. MEASUREMENT OF WET STEAM FLOWS

The measured dilution of an injected pulse of tritiated water into a steam-water flow system can provide a measurement of the total steam-water flow rate, provided two conditions are satisfied: (a) the isotope mixes appropriately over the flow section; and (b) the isotope mixes appropriately between the steam and water phases of the flow.

As with single phase flow, the validity of condition (a) can be tested by repeated testing in which the flow is sampled at different radial positions. If the measurement is independent of sampling position, this condition is satisfied. Although this result is not likely to be obtained for two-phase systems, unless condition (b) is also satisfied, the present R & D program incorporates a technique by which condition (b) can be evaluated independently. This technique involves a special sampling probe described below which was designed for a thorough examination of the feasibility of the method. Once demonstrated, the wet steam flow measurement method is expected to be valid with any sampling tube.

The steam content of a sampled flow of wet steam is unlikely to represent the local steam content at the sampling position unless special precautions are taken. This is because the tip of the sampling tube interacts differently with the flow of droplets compared with that of the steam. The flow of droplets is barely influenced by the tube, while the steam flow may be greatly influenced by it. If pressures at points A and B (Fig.2) are equal, the sampling tube can be assumed to have no effect on the flow at the tube inlet, and the extracted flow should represent the flow at the sampling position. Using valve C to vary the pressure at point B alters the extracted steam flow more than it does the droplet flow. As a result, the steam content of the extracted flow is altered.

In view of the above, interphase mixing of the injected radioisotope pulse can be examined by repeated tests in which the steam content of the extracted flow is varied at each sampling position. Adequate interphase mixing exists if the calculated value of mass flow rate is independent of the rate of extraction.

To examine the feasibility of measuring wet steam flow rates by means of the dilution of a pulse of tritiated water, a 50 mm bore, 20 m long, horizontal steel test section, with a 300 mm radius U bend at the middle, has been connected to an existing steam-raising facility.

The tracer, a measured volume of about 0.01 mL, is injected into the test section from between two ball valves on a side arm near the steam inlet. Rapid injection can be effected by opening the two valves simultaneously thus allowing a jet of steam from a pressure vessel (3.1 MPa, 450°C) to flush the tracer into the test section.

A special traversing sampling probe, of the type shown in Fig.2, has been constructed. This has been positioned at 7.4 m from the tracer injection point. The test section has been constructed so that the sampling assembly can alternatively be placed at a further 8 m from the injection point. Although not necessary for field tests, where simple condensation of the sampled flow is sufficient, a calorimetric condenser is to be connected to the sampling line to enable measurement of the actual steam content of each sample.

Preliminary commissioning tests have been performed with wet steam at 1.5 MPa for a 65% steam content, 0.19 kg s^{-1} flow, representing 90 kg m^{-2} s^{-1}, and for a 26% steam content, 0.61 kg s^{-1} flow, representing 280 kg m^{-2} s^{-1}. These tests indicate that the traversing sampling probe performs as expected. Tests with tritiated water will commence in the near future.

4. CONCLUDING DISCUSSION

We are confident that the outcome of the gas flow development project will be a well proven measurement technique suitable for calibrating industrial flow meters in situ, and a versatile facility capable of providing a wide range of closely characterised flow conditions suitable for calibrating meters off-line or for development purposes where characterised flows are needed. In this respect, the National Measurement Laboratory has expressed interest in using the facility for extending its work on critical flow nozzles to sizes larger than can be accommodated on equipment currently available.

An ultimate objective is for both the technique and the gas flow facility to become accepted for flow calibration by the National Association of Testing Authorities of Australia (NATAA), thus providing a gas flow calibration service not presently available to Australian industry.

We also expect that, as discussed in Section 3, the isotope dilution technique can be extended to the measurement of wet steam mass flow rates, for which there is currently no convenient reliable method. This development should prove useful for industrial processes which use wet steam flows.

5. REFERENCES

[1] Lafferty, R.N. Flow Measurements with Radioisotopes. Isotop. Radiat. Technol. 8, (3), 287 (1971)

[2] Spragg, W.T. and Seatonberry, B.W. A Radioisotope Dilution Method for the Precise Absolute Determination of the Flow Rate of Gases under Industrial Conditions. Int. Conf. on Fluid Flow Measurements, National Energy Laboratory, Glasgow (1975).

[3] Fries, B.A. Fluid Flow Measurement Method. U.S. Pat. 3, 161, 767 (1964).
[4] ISO/DIS 4053/1 Draft International Standard. Measurement of Gas Flow in Conduits, Tracer Method, Part I : General. International Organisation for Standardisation.
[5] Smith, R.E. and Matz, R.J. A Theoretical Method of Determining Discharge Coefficients for Venturis Operating at Critical Flow Conditions. Trans. A.S.M.E. 84, 434 (1962).

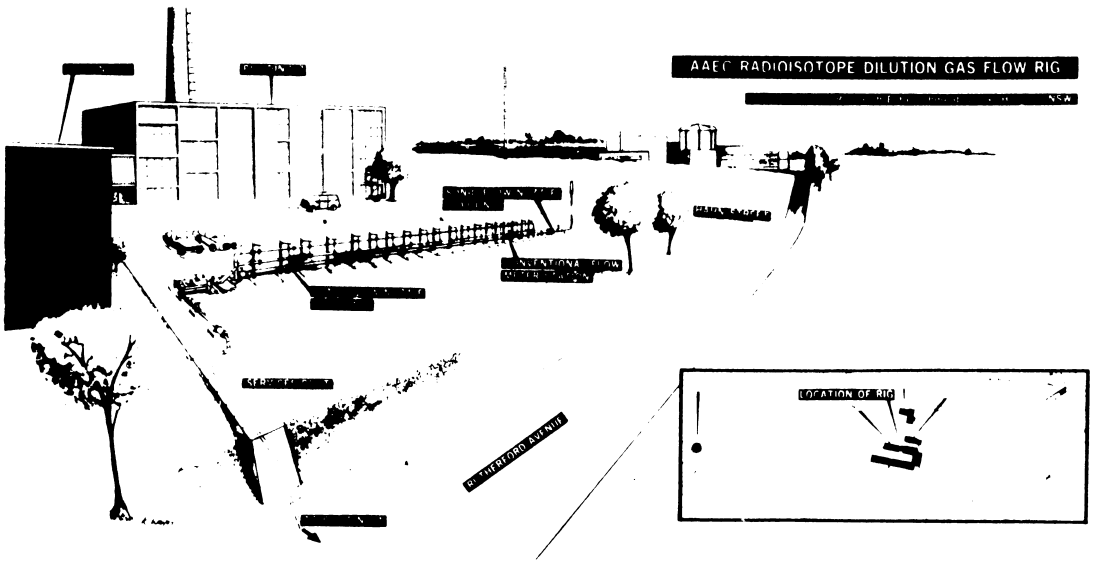

Fig.1 Sketch of gas flow test facility

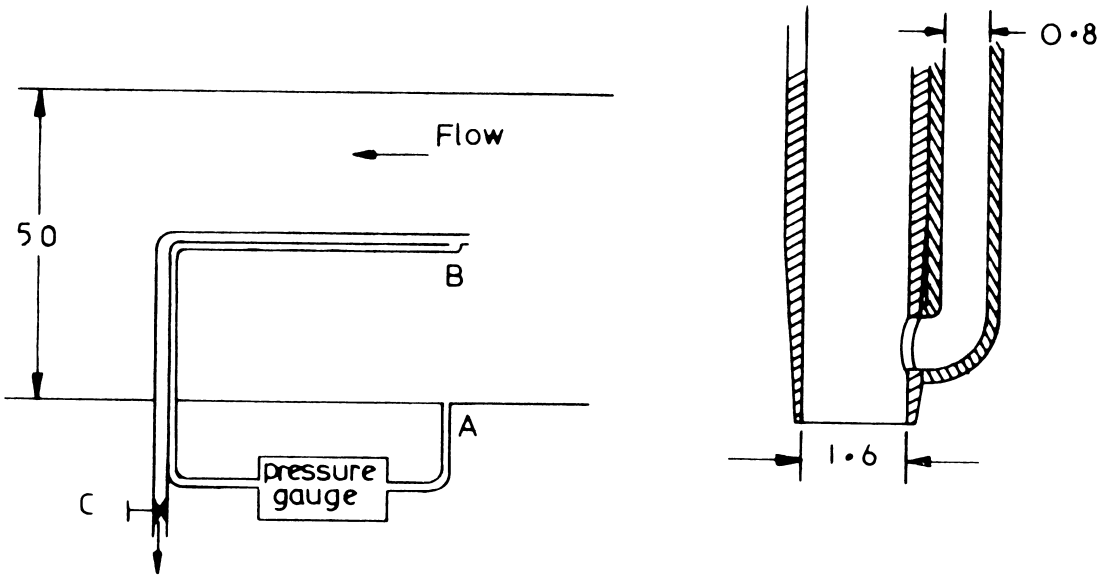

Fig.2 Sampling probe for assessment of the radio-tracer dilution method of measuring wet steam mass flow rates

PREPRINT

This paper has been submitted for the ANS-ASME Topical Meeting on Nuclear Reactor Thermohydraulics to be held at Saratoga, New York in October 1980. It is made available on the understanding that, until it is published, it will not be abstracted, quoted, or referred to.

AN EVALUATION OF TWO BUBBLE-DETACHMENT MODELS FOR TWO-PHASE FLOW

D.R.H. Beattie

AAEC Research Establishment
Private Mail Bag
Sutherland, NSW, 2232
Australia

AN EVALUATION OF TWO BUBBLE-DETACHMENT MODELS FOR TWO-PHASE FLOW

D.R.H. Beattie

ABSTRACT

Two-phase flows with attached wall bubbles are considered as flows in roughened ducts with roughness elements equal in magnitude to the bubble detachment diameters determined by a force balance analysis. Two methods for determining the drag component of the forces acting on a bubble give distinctly different mixing-length theory expressions for velocity profile, friction factor, and void fraction. Available data are shown to be compatible with that set of expressions in which drag is due primarily to skin friction rather than form drag.

1. INTRODUCTION

As is the case with single-phase flows, the thermohydraulic characteristics of turbulent two-phase flows are largely determined by the flow boundary conditions. Since much research is concerned with characteristics of heated or flashing two-phase flows, a boundary condition of special interest is that associated with the ebullition process. Despite this interest, comparatively little effort has been spent examining the influence of attached wall bubbles on two-phase flow characteristics.

Representative studies of the influence of boiling on flow characteristics include experiments in which boiling is simulated by injecting gas through porous walls [1]; analyses of critical heat flux by considering the effect of the gas flux from the wall [2] and the bubble mechanics at dryout [3]; subcooled boiling analyses in which bubble detachment defines the onset of a particular subcooled boiling regime [4,5]; and a mixing-length treatment of net quality flows in which attached wall bubbles are treated as roughness elements of duct walls [6].

The critical bubble size at which detachment from the wall occurs is estimated from a balance of the forces acting on the bubble [3,4,5,6]. Of special interest to this work is the shear stress component of this force balance, F_F.

Staub [5] considers a bubble layer and regards the shear acting on this to be the same as that on the duct wall, τ_w, so the corresponding force on a bubble can be considered as

$$F_F \sim \tau_w d^2 \quad . \tag{1}$$

AAEC Research Establishment,
Private Mail Bag,
Sutherland, NSW, 2232,
Australia.

Staub observes that the same functional form also applies if isolated bubbles are considered, although the magnitude of F_F will depend on the degree of interaction of bubbles. Most other bubble force balances, such as those of Chang [3] and Beattie [6], evaluate the shear stress component in a way which is either identical to, or which can be considered as a variation of, the method of Staub.

An alternative approach is given by Levy [4]. His frictional force component of the bubble force balance is in fact the pressure gradient component of the form drag on an isolated wall bubble where the pressure gradient is dominated by the frictional component. This leads to an expression

$$F_F \sim \tau_w d^3/D \quad . \tag{2}$$

It is reasonable to suppose that allowance for bubble interaction leads to the same functional form. It is relevant that Levy [4] also considered relation (1) but found that the subcooled boiling data analysed by him are more compatible with relation (2).

In reality, relation (2) is not an alternative to (1); the form drag and the shear stress components can both be included in a bubble force balance, although estimates of the coefficients required to complete relations (1) and (2) suggest that the shear stress acting on a wall bubble is likely to be considerably larger than the form drag.

However, the right-hand expressions of relations (1) and (2) are usually treated not as different components of a force balance but as alternative models of the one component [4,5,9]. In view of this practice, the present work presupposes this to be valid, and analyses data in a manner which assesses the relative merits of relations (1) and (2). This is achieved by considering net quality flows in which attached wall bubbles protrude beyond the laminar sublayer. These bubbles act as effective surface roughness elements, and relations (1) and (2) are used to calculate the effective surface roughness height for flows where surface tension and drag forces dominate the wall bubble force balance. The two surface roughness expressions are then applied as boundary conditions to two-phase mixing length theory to derive expressions for velocity profile, friction factor, and void fraction for 'completely rough wall' flows, i.e. for flows where attached wall bubbles protrude into the turbulent core, rendering the flow characteristics independent of Reynolds number. The theoretical expressions arising from each drag model are then compared with available data to assess the validity of each model.

Assessment of the two bubble drag models could also be achieved, in principle, by considering roughness effects on flow characteristics other than those mentioned above (e.g. on critical heat flux), or on 'partially roughened wall' data, i.e. data with flow characteristics dependent on both Reynolds number and bubble detachment size. Although data exist for both possibilities, the current level of theory is such that useful comparisons with data cannot yet be made on these bases.

2. ANALYTICAL DEVELOPMENT

The two models for drag on wall bubbles mentioned in the introduction will be referred to as model 1 and model 2. The hydrodynamic relations corresponding to these models are summarised in Table 1 in terms of parameters defined in the nomenclature. The steps involved in developing the expressions of Table 1 are space-consuming but straightforward. Hence, rather than present a full analysis, the principles involved in the development of the expressions are summarised below.

For the present purposes, the drag force F_F is opposed by a surface tension force $F_s \sim d\,\sigma$. The critical departure diameter, d_d, at which the drag force is sufficient to overcome the surface tension force, is given when $F_s = F_F$, yielding the Table 1 expressions for the effective surface roughness.

The other expressions in Table 1 are based on the non-dimensional velocity profile expression. In two-phase rough wall flows, this expression is of the same form as that for single-phase flow [7].

Following single-phase practice, the non-dimensional wall distance, y^+, should be based on wall distance y normalised by roughness height - in this case, d_d. This is not practical because the complete functional form of d_d is not known for either model. Instead, y is normalised with respect to the right-hand expressions for d_d in Table 1. This is reasonable if the right-hand expressions are assumed proportional to d_d. The single-phase practice is then effectively followed, except that the proportionality constant can be regarded as being incorporated in the velocity profile coefficient 'b' instead of in y^+.

The non-dimensional velocity profiles, when integrated over the flow cross-section, can be used to yield the friction factor expressions, and when integrated over the film region of annular flow, to yield the annular flow void fraction relations.

With regard to the annular flow void fraction relations, a particular version of the 'thin film' approximation has been utilised. Analysis has shown that, despite the assumptions involved, this version of the approximation is surprisingly good, even for very thick films. Also, the annular flow voidage relations are expressed in terms of the core volume fraction and core volume flow fraction, A and B respectively, which are related to the gas volume fraction $\langle\alpha\rangle$ and volume flow fraction $\langle\beta\rangle$ by the core region and film region void fractions and volume flow fractions, α_c, β_c, α_f, β_f, these being assumed constant over each region. It can be seen that annular flow average voidages depend on these values*. Analysis of Reynolds number-dependent data suggests that the assumption $\alpha_c = \beta_c = 1$ is reasonable except at very high voidages, and that, for a given mass flux, values of $\langle\alpha\rangle$ and $\langle\beta\rangle$ at the onset of annular flow (i.e. at the validity limit of the distributed flow voidage equations of Table 1) can reasonably be used as estimates of α_f and β_f.

The distributed flow voidage equation is in fact the Zuber and Findlay [8] equation, with the distribution parameter (C_o) equation being derived from the relation $C_o = j_{max}/\langle j\rangle$ [7].

* $A = (\langle\alpha\rangle-\alpha_f)/(\alpha_c-\alpha_f)$, $B = (\langle\beta\rangle-\beta_f)/(\beta_c-\beta_f)$.

Table 1

Theoretical Characteristics of Flows with Attached Wall Bubbles

Parameter	Model 1	Model 2
Wall bubble drag force	$F_F \sim \tau_w d^3/D$	$F_F \sim \tau_w d^2$
Effective surface roughness	$d_d \sim (\sigma D/\tau_w)^{\frac{1}{2}}$	$d_d \sim \sigma/\tau_w$
Non-dimensional wall distance	$y^+ = \frac{y}{R} (We \frac{f}{2})^{\frac{1}{2}}$	$y^+ = \frac{y}{R} We \frac{f}{2}$
Non-dimensional velocity profile	$j^+ = a \ln y^+ + b$	$j^+ = a \ln y^+ + b$
Friction factor	$\frac{1}{\sqrt{f}} = \frac{a}{\sqrt{2}} \ln (We f)^{\frac{1}{2}} + + \frac{b - 3a/2 - (a \ln 2)/2}{\sqrt{2}}$	$\frac{1}{\sqrt{f}} = \frac{a}{\sqrt{2}} \ln (We f) + + \frac{b - 3a/2 - a \ln 2}{\sqrt{2}}$
Distributed flow voidage	$\langle u_g \alpha \rangle / \langle \alpha \rangle = C_o \langle j \rangle + v$	$\langle u_g \alpha \rangle / \langle \alpha \rangle = C_o \langle j \rangle + v$
Distribution parameter	$C_o = 1 + \frac{3}{2} a \sqrt{\frac{f}{2}}$	$C_o = 1 + \frac{3}{2} a \sqrt{\frac{f}{2}}$
Film flow rate for annular flow	$Q^+ = \int_o^{S^+} j^+ dy^+,$ $Q^+ = \frac{1-B}{2} \sqrt{We},$ $S^+ = \frac{1-A}{2} \sqrt{We\ f/2}$	$Q^+ = \int_o^{S^+} j^+ dy^+,$ $Q^+ = \frac{1-B}{2} We \sqrt{\frac{f}{2}},$ $S^+ = \frac{1-A}{4} We\ f$

The validity of the two models considered in this paper can be assessed by comparing relevant data with the expressions summarised in Table 1. Preliminary work [6] has indicated that, unlike the case for single-phase flows, the coefficients a, b in Table 1 are not unique, but remain constant for a given 'friction regime' and change values at the boundaries of such regimes. Thus, Weber number-dependent friction data are not in themselves sufficient to assess the relative validity of the two models, since data conforming to the friction factor expression for one model will also conform to that of the other by changing the coefficients a, b. Other characteristics summarised in Table 1 depend on the friction factor:Weber number relation, and the dependence of a flow on the Weber number instead of the Reynolds number cannot readily be ascertained from data other than friction factor data.

Table 2

Generalised Characteristics for Flows with Attached Wall Bubble. Correct integer choices of m, n, yield characteristics for any particular regime.

Parameter	Model 1	Model 2
Friction factor	$\frac{1}{\sqrt{f}} = (\sqrt{2})^{m+6} \{\log \sqrt{We\ f}$ $- 0.225\ m - 0.075\ n + 0.48\}$	$\frac{1}{\sqrt{f}} = (\sqrt{2})^{m+4} \{\log (We\ f)$ $- 0.45\ m - 0.15\ n + 0.96\}$
Non-dimensional velocity profile	$j^+ = (\sqrt{2})^{m+7} \{\log y^+$ $- 0.225\ m - 0.075\ n + 1.21\}$	$j^+ = (\sqrt{2})^{m+5} \{\log y^+$ $- 0.45\ m - 0.15\ n + 1.91\}$
Distribution parameter	$C_o = 1 + 5.22\ (\sqrt{2})^m \sqrt{f}$	$C_o = 1 + 2.61\ (\sqrt{2})^m \sqrt{f}$

Hence, an assessment of the relative validity of the two models can best be achieved by an analysis of Weber number dependent friction factor data in conjunction with associated data for velocity profiles and/or void fraction. The friction factor data can be used to evaluate appropriate 'a' and 'b' values for each model. The values can then be used to generate void fraction and/or velocity profile expressions which can be compared with data for these characteristics.

3. DATA ANALYSIS

A search was made for available pressure gradient data with Weber number-dependent friction factors. Approximately 100 such sets of data were found, covering approximately 40 friction regimes; i.e. 40 different sets of a, b in the f:We relation of Table 1 were required to describe all the Weber number-dependent friction factor data. Empirically obtained values of a and b proved to be subsets of simple series, and it was observed that the various friction factor curves could usually be generated from a single generalised equation

$$1/\sqrt{f} = \sqrt{2}^{\,m+4} \{\log (We\ f) - 0.45\ m - 0.15\ n + 0.96\}$$

by integer number choices for m and n. Table 2 restates relations from Table 1 in terms of m and n. The different Weber number-dependent friction regimes can thus be characterised by the values of m and n required to convert the generalised friction factor equation to one appropriate to the relevant regime. The notation (m,n) will be used here to specify a given friction regime. Figure 1 shows some typical (4,n) data.

Symbol	Friction Regime	Test Section Name(s)	D mm	P MPa	Heat Flux	Ref.
Δ	(5,-4)	-	8	14.7	zero	10
●	(5,-2)	54	5	7	Near or at CHF*	13
+	(5,-1)	648, 640, 632,624,616	6	7	At CHF	12
▲	(5, 0)	914	9	5	At CHF	11
o	(5, 1)	-	8	5	zero	10

* Critical Heat Flux

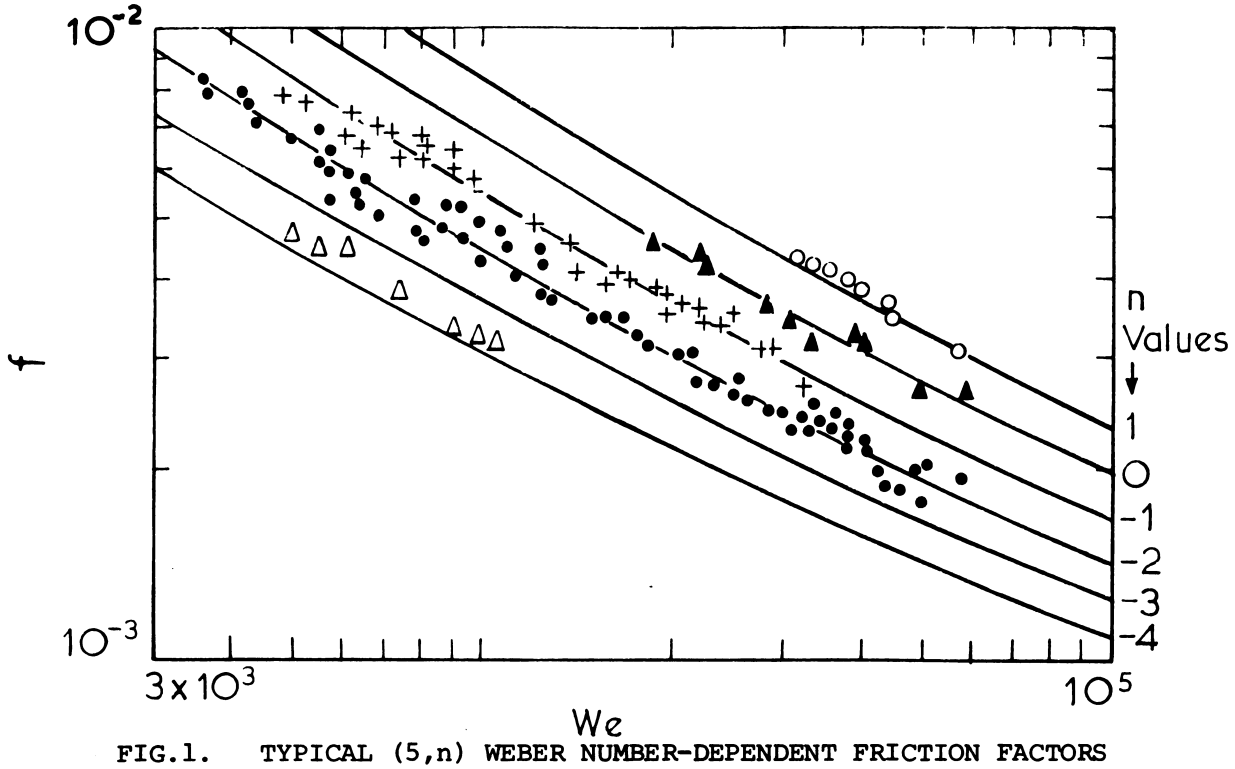

FIG.1. TYPICAL (5,n) WEBER NUMBER-DEPENDENT FRICTION FACTORS

As stated in the previous section, assessment of the validity of models 1 and 2 requires analysis of voidage and/or velocity profile data in conjunction with friction factor data. Of the various Weber number-dependent friction factor data sets, ten had associated average voidage and/or velocity profile data; these covered 8 friction regimes. The data are compared with the expressions based on models 1 and 2 in Figs. 2-9.

With regard to the annular flow average voidage plots in these figures, knowledge of film and core entrainment is required. In the present work, core entrainment has been neglected and the film voidage and gas volume flow fraction, α_f and β_f, have been identified with $\langle\alpha\rangle$ and $\langle\beta\rangle$ at the onset of annular flow. Three methods were used for estimating this regime boundary. Firstly, voidage data were plotted on the $\langle u_g\alpha\rangle/\langle\alpha\rangle$:$\langle j\rangle$ plane. Usually, an abrupt change of slope occurs at the distributed flow:annular flow boundary, with the slope being near unity for the annular flow data. Secondly, voidage data were plotted on the log $(1-\langle\alpha\rangle)$:log $(1-\langle\beta\rangle)$ plane. Again, an abrupt change of slope usually occurs at the distributed flow:annular flow boundary,

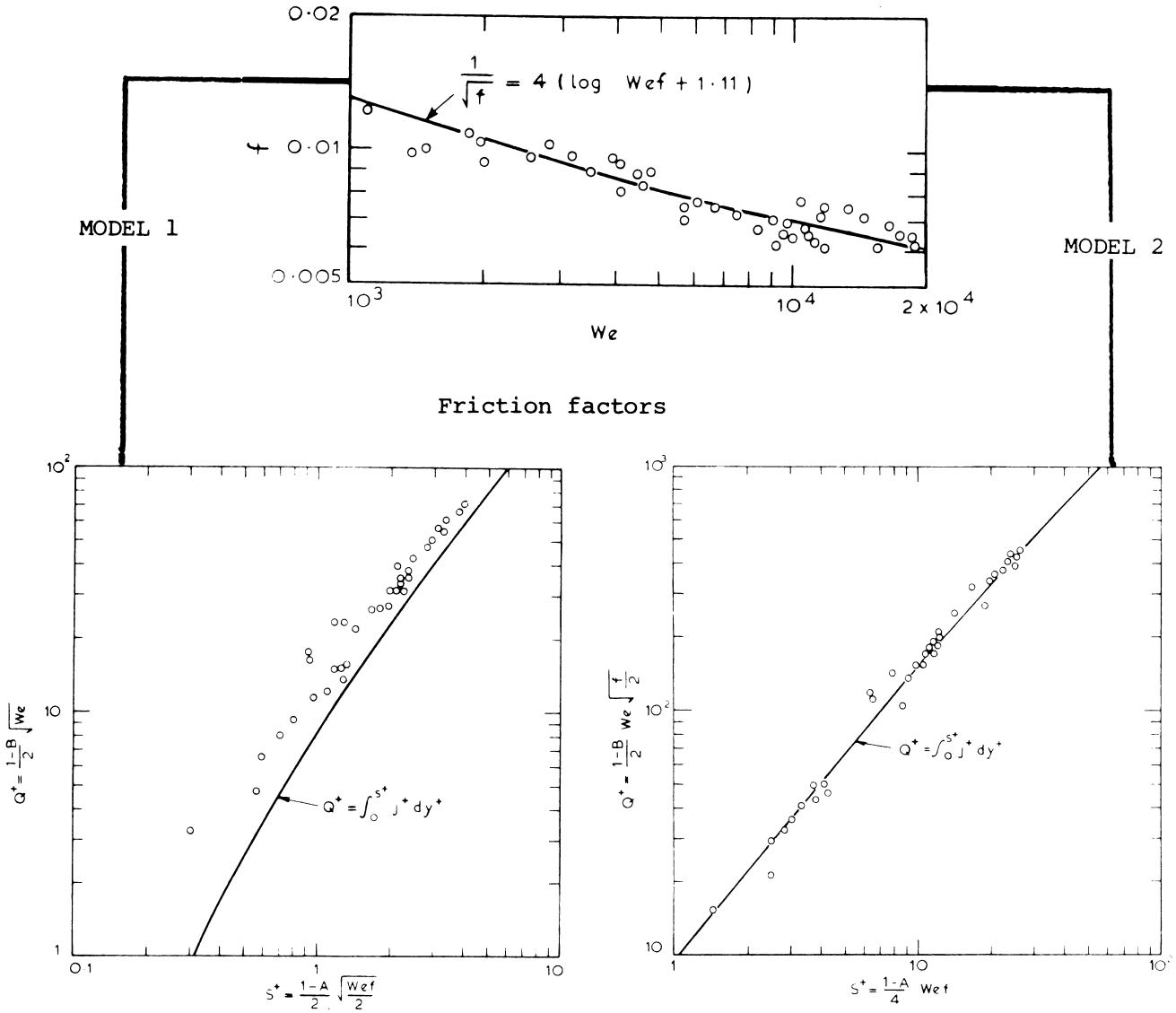

FIG.2. COMPARISON OF (0,-1) ANNULAR FLOW DATA WITH THEORY: FREON 113 ADIABATIC UPFLOW IN A 10 mm TUBE; ρ_ℓ/ρ_g = 21,58, DATA FROM REF. [14]

with the slope being near unity for the annular flow data. Thirdly, friction factors were plotted as a function of quality. A change of flow regime from distributed to annular may coincide with a change of friction regime, as is evident from the friction factor plots. The influence of entrainment on annular flow voidage will be considered further in the next section.

The velocity data in Figs. 3, 5, 8 and 9 are based on a no-slip treatment of isokinetic sampling data [15,21]. The no-slip assumption is questionable in the vicinity of the gas/liquid interface. In order to eliminate suspect data obtained near the wall, the figures include only those data where corresponding experimental voidage values are compatible with the voidage defect equation [24] based on mixing-length theory for the core region of annular flow.

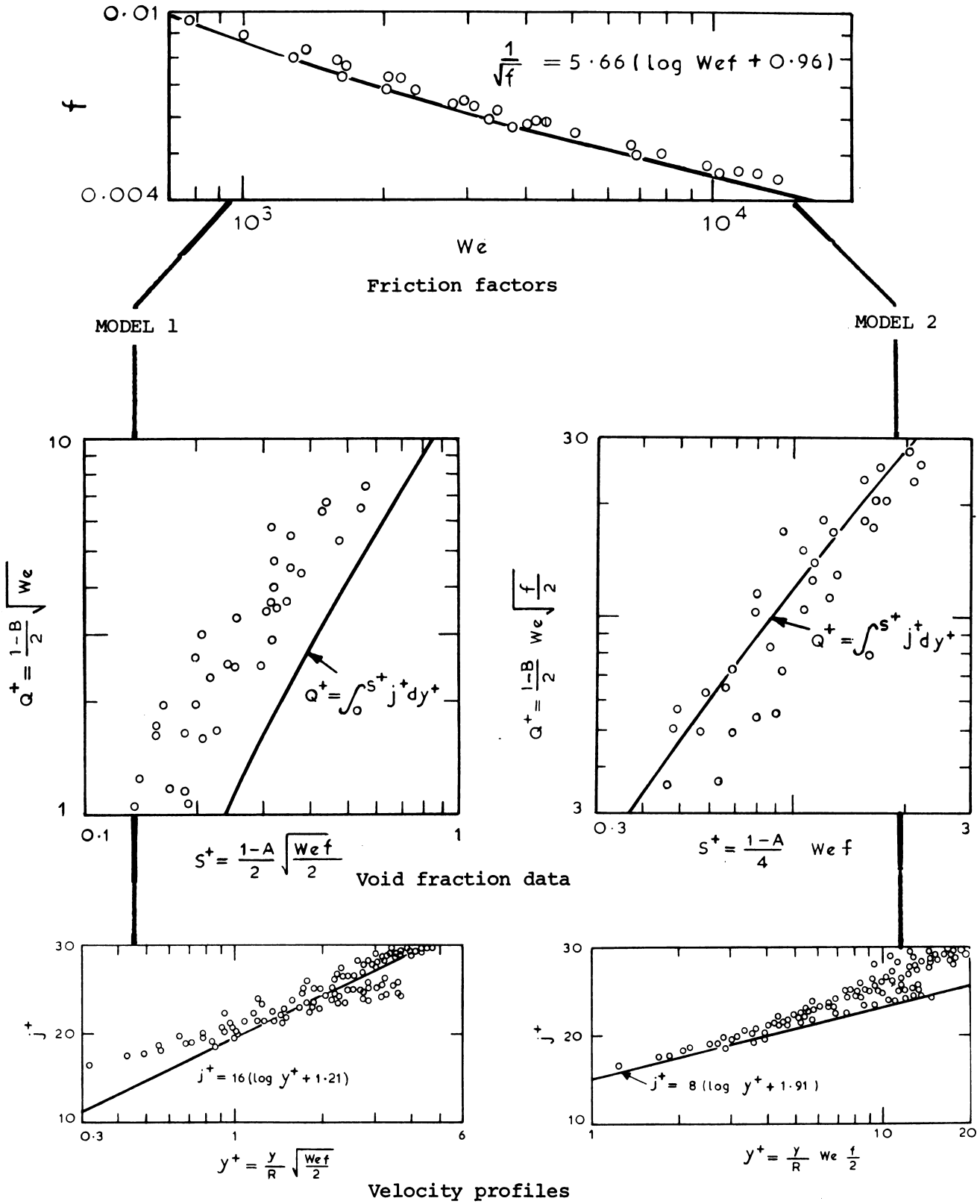

FIG.3. COMPARISON OF (1,-3) ANNULAR FLOW DATA WITH THEORY: WATER ADIABATIC UPFLOW IN A 17.1 mm TUBE, ρ_ℓ/ρ_g = 21, DATA FROM REFS. [15, 21, 22]

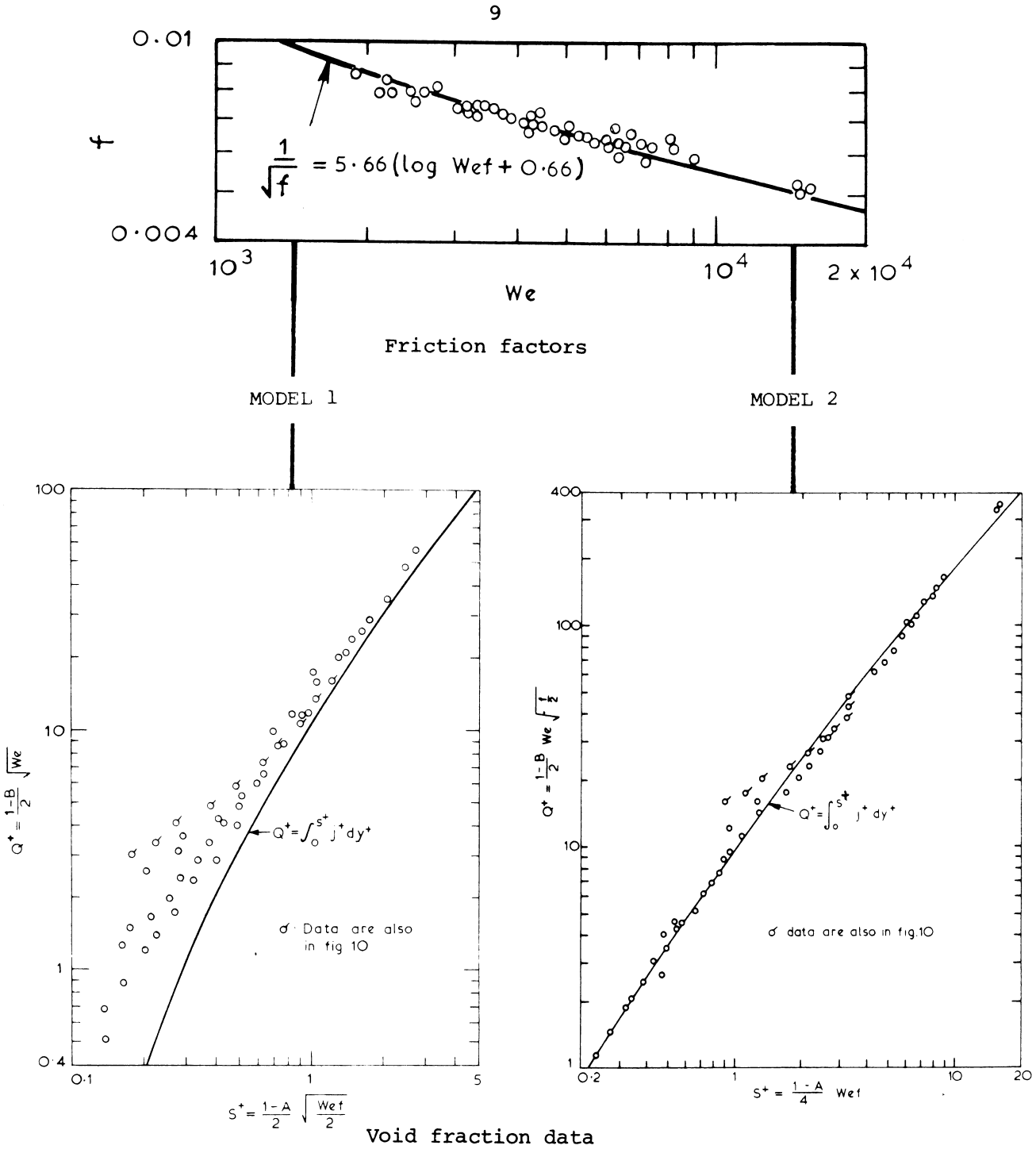

FIG.4. COMPARISON OF (1,-1) ANNULAR FLOW DATA WITH THEORY: WATER ADIABATIC AND DIABATIC UPFLOW IN A 7.5 mm EQUIVALENT DIAMETER 19 ROD CLUSTER (IT25), ρ_ℓ/ρ_g = 31, 42, DATA FROM REFS. [16, 17]

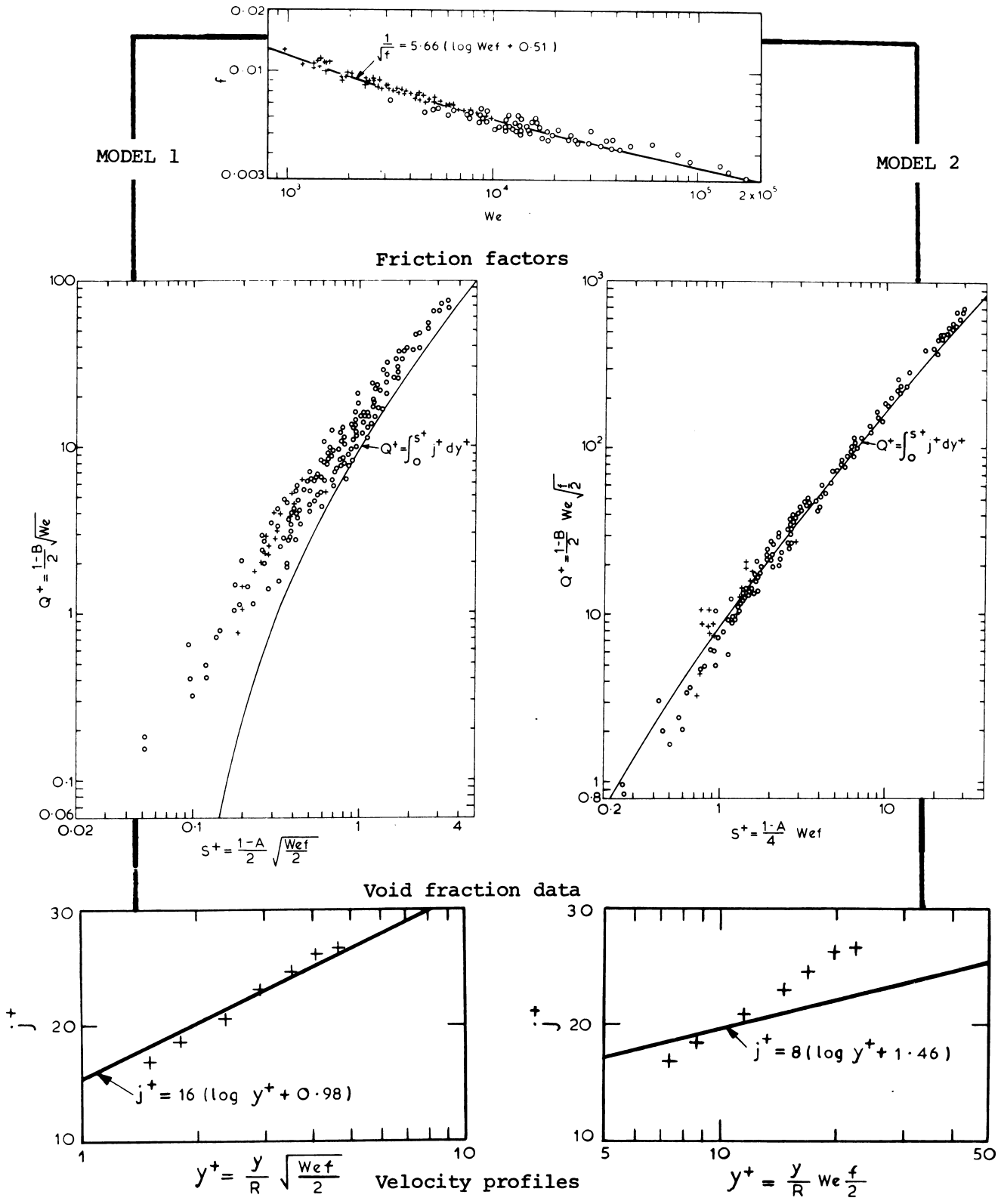

FIG.5. COMPARISON OF (1,0) ANNULAR FLOW DATA WITH THEORY: FREON 12 UPFLOW IN 10.1 mm AND 12.95 mm TUBES, $7 < \rho_\ell/\rho_g < 40$, DATA FROM REFS. [18, 19], NOTATION 0, ALSO WATER DIABATIC (0.23 MW m^{-2}) UPFLOW IN A 17.1 mm TUBE, $\rho_\ell/\rho_g = 21$, DATA FROM REF. [15], NOTATION +.

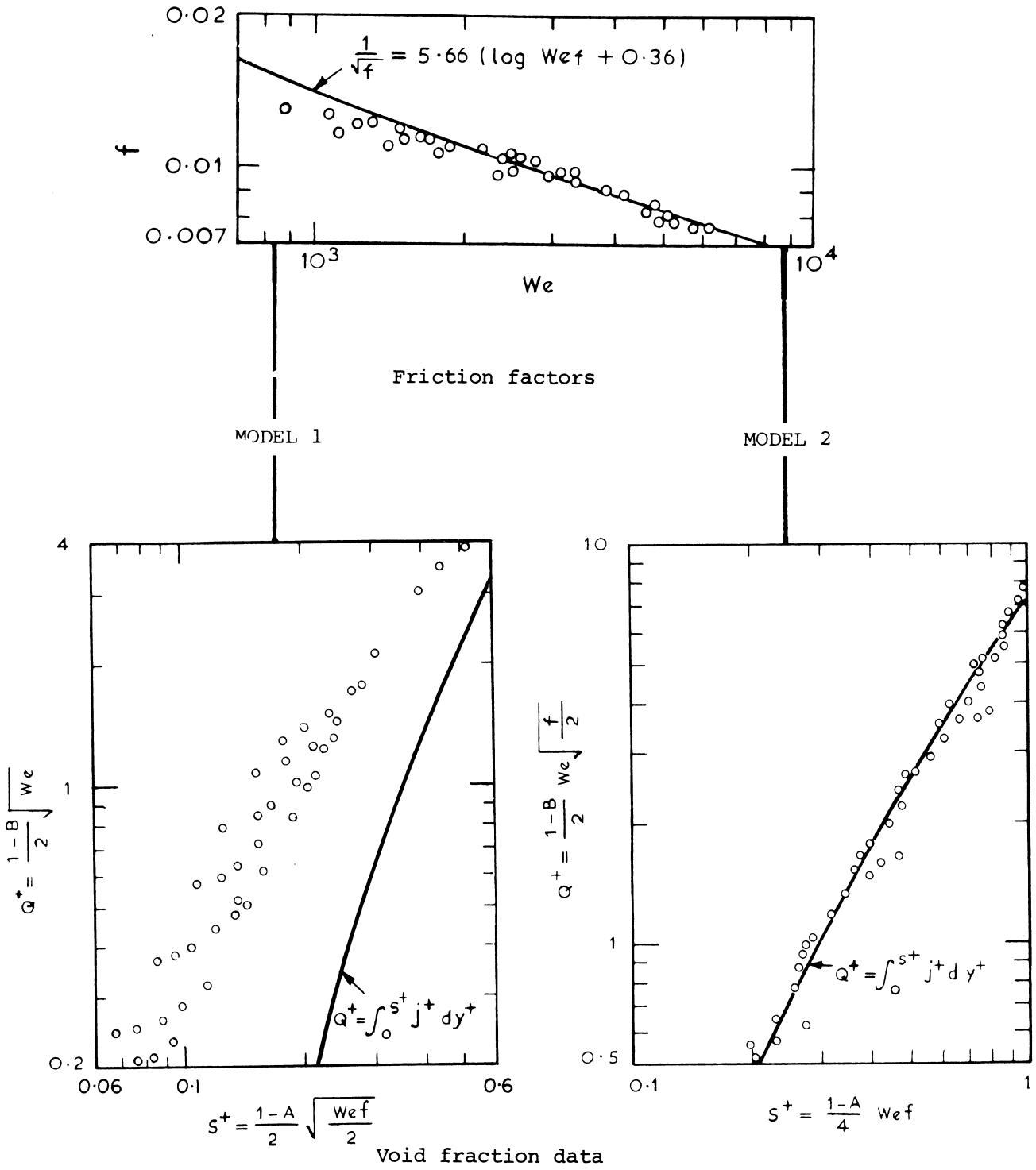

FIG.6. COMPARISON OF (1,1) ANNULAR FLOW DATA WITH THEORY: ARGON/WATER UP-FLOW IN A 12.2 mm EQUIVALENT DIAMETER 7 ROD CLUSTER, ρ_ℓ/ρ_g = 28, 53, DATA FROM REF. [20]

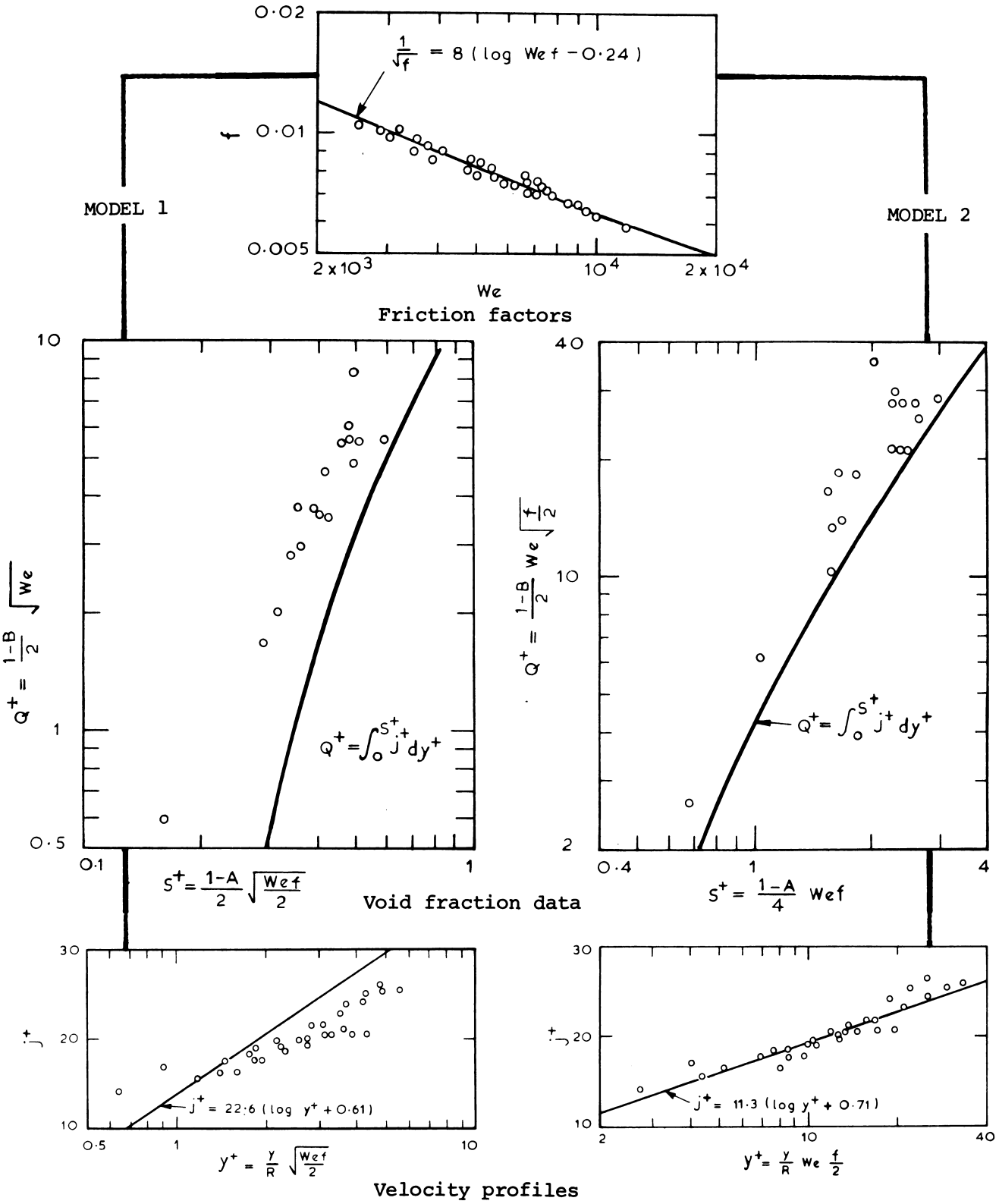

FIG. 7. COMPARISON OF (2,2) ANNULAR FLOW DATA WITH THEORY: WATER DIABATIC (0.46 MW m^{-2}) UPFLOW IN A 17.1 mm TUBE, ρ_ℓ/ρ_g = 21, DATA FROM [15].

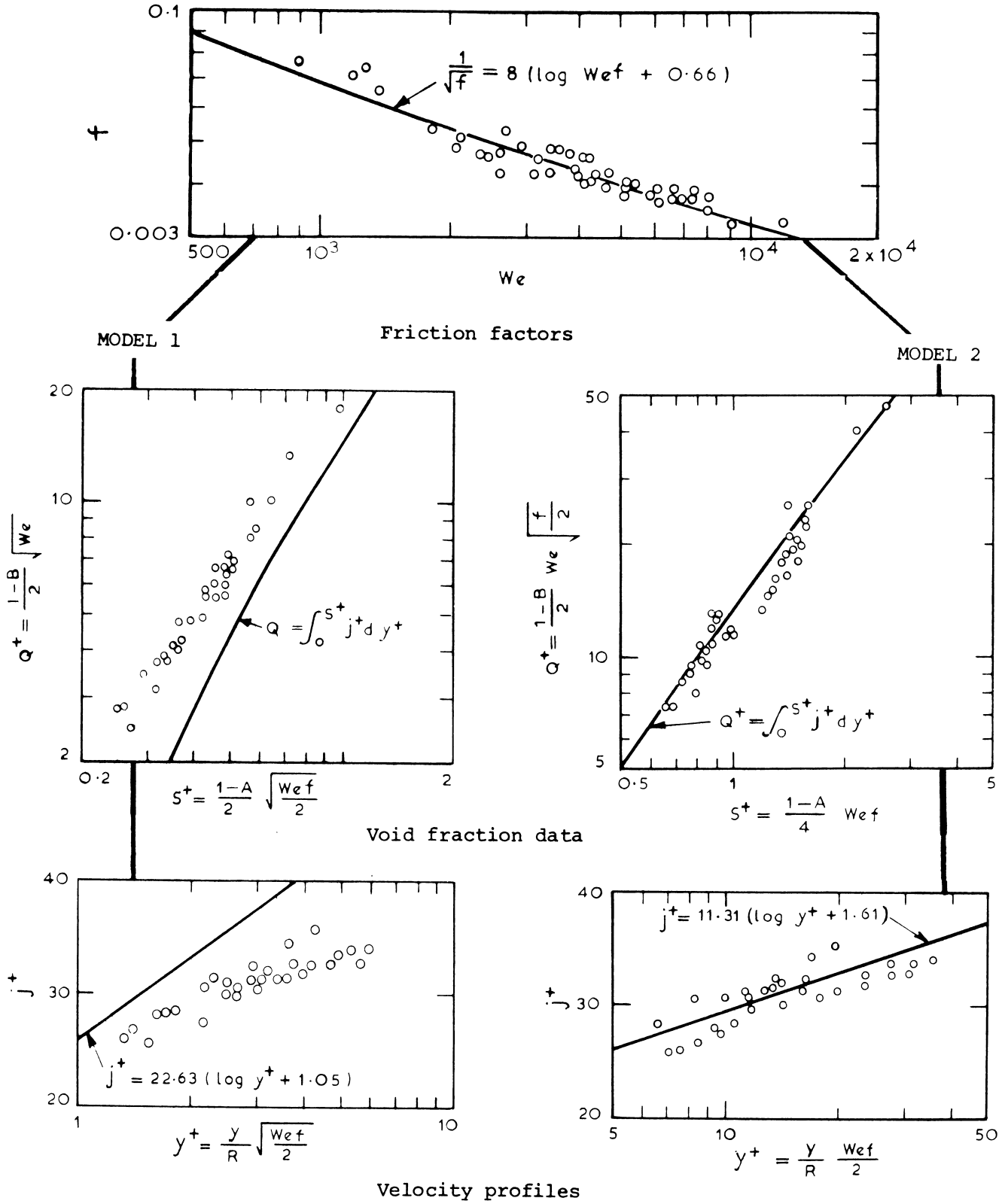

FIG. 8. COMPARISON OF (2,-4) ANNULAR FLOW DATA WITH THEORY: WATER ADIABATIC UPFLOW IN A 17.1 mm TUBE, ρ_ℓ/ρ_g = 13, DATA FROM [21, 22].

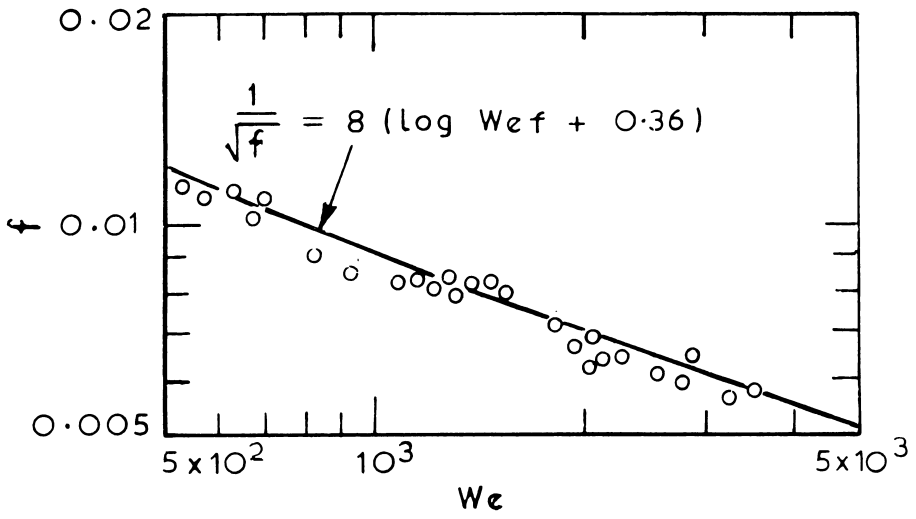

Friction factors

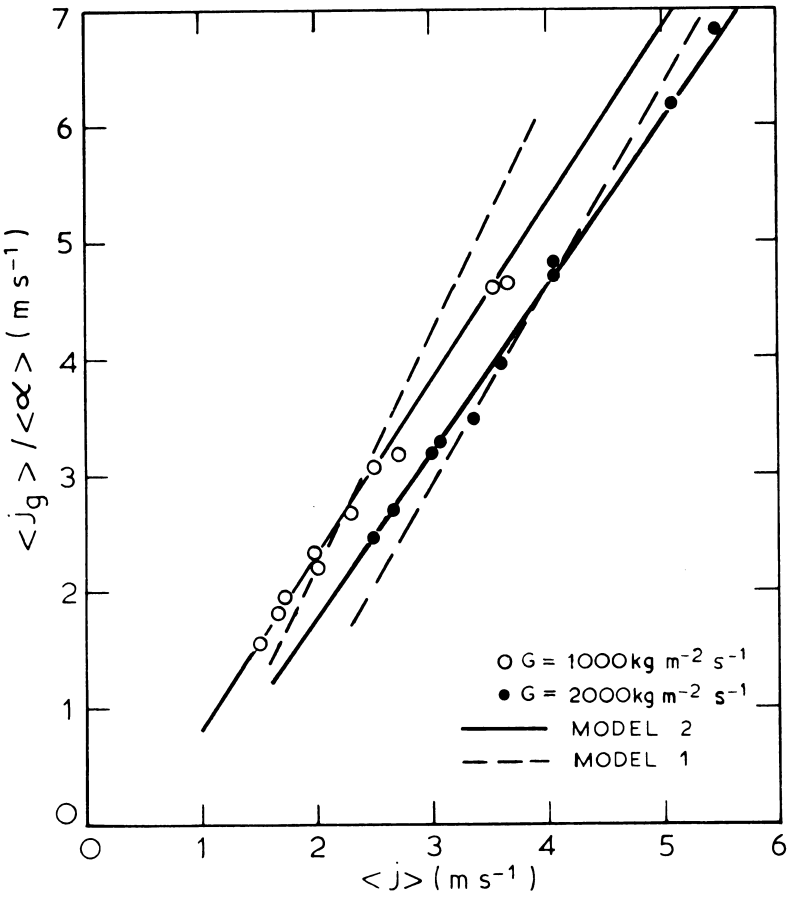

Void fraction data

FIG.9. COMPARISON OF (2,-2) DISTRIBUTED FLOW DATA WITH THEORY: ARGON/WATER UPFLOW IN A 25 mm TUBE, ρ_ℓ/ρ_g = 28,36,53, DATA FROM REF. [23]

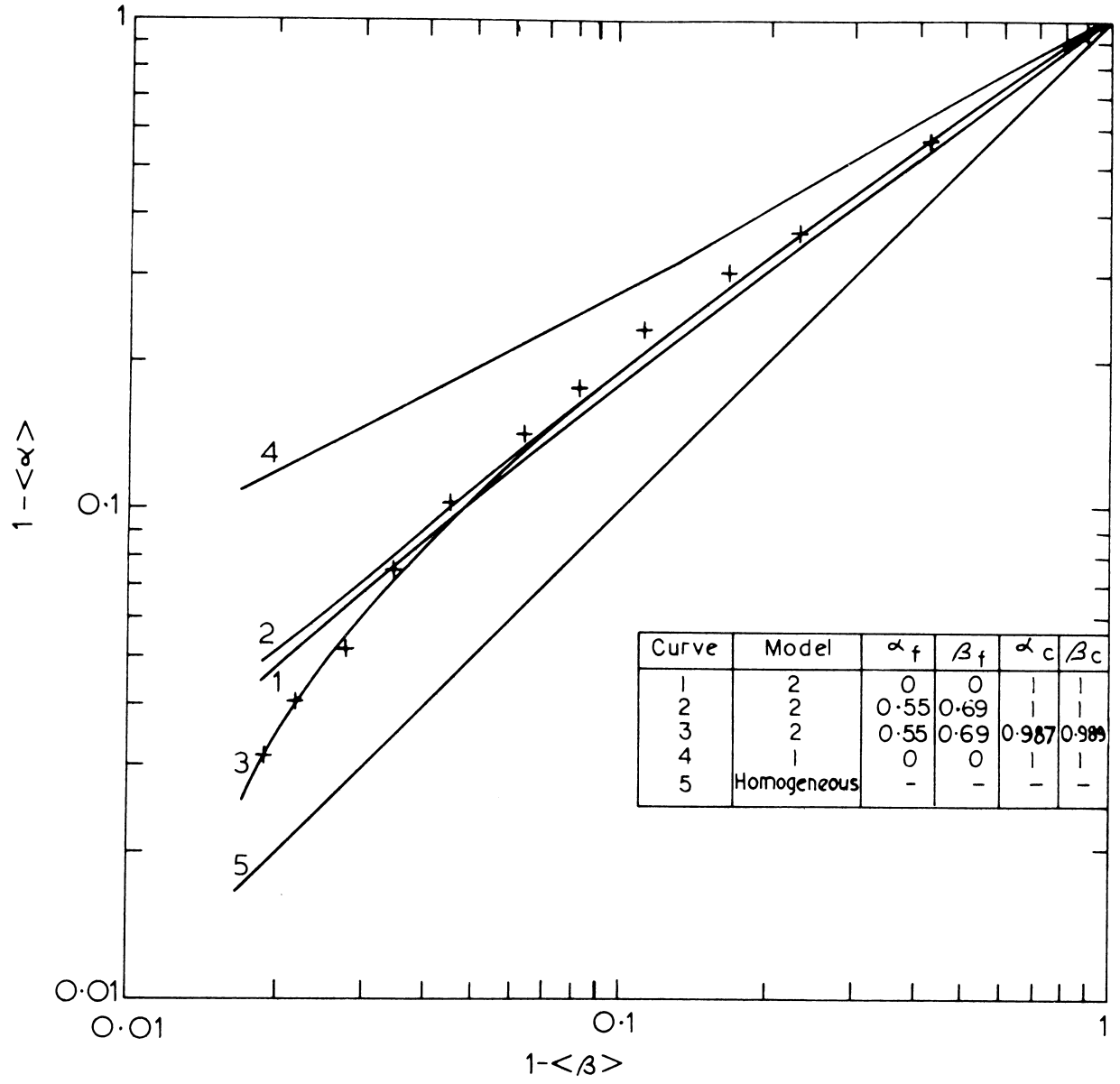

FIG.10. COMPARISON OF (1,-1) ANNULAR FLOW VOID DATA WITH THEORY: WATER ADIABATIC UPFLOW IN A 7.5 mm EQUIVALENT DIAMETER 19 ROD CLUSTER (IT25), ρ_ℓ/ρ_g = 42, G = 1076 kg m^{-2} s^{-1}, DATA FROM REF. [16]

4. DISCUSSION

With the exception of a few velocity data, the data in Figs. 2 to 9 agree with model 2 and not model 1. In view of the general agreement with model 2, the exceptions, which are in Figs. 3 and 5, are not sufficient to validate model 1. The behaviour of the velocity data is consistent with an earlier observation [6] that isokinetic sampling probes may induce a change of friction regime. The anomalous velocity data of Figs. 3 and 5 agree with model 2 if the friction regimes are assumed to be characterised by (m,n) = (2,-2) and (4,1) respectively, instead of by (1,-3) and (1,0). Thus, allowing for possible probe-induced flow regime changes, all relevant data agree with model 2.

The analysis of the friction factor data indicated that Reynolds number-dependent, and also Weber number-dependent, flows covered both adiabatic and diabatic flow conditions. This was somewhat surprising in view of the fact that the two Weber number-based models considered here were conceived specifically for heated flow situations. With regard to one-component flows the following observations can be made:

(a) Low quality flows generally depend on Reynolds number. Friction factors are slightly higher with heat transfer, suggesting that attached wall bubbles act as surface roughness elements of a magnitude that confines them to the laminar sublayer.

(b) High quality flows in round tubes generally behave as expected, i.e. adiabatic and low heat flux data are Reynolds number-dependent, and high heat flux data are Weber number-dependent.

(c) Some low pressure adiabatic data are Weber number-dependent, suggesting that situations in which the pressure drop is comparable to the system pressure allow flashing, thus simulating diabatic conditions. This is exemplified by the Freon data of Figs. 2 and 5.

(d) Adiabatic flows within about 100 diameters of an abrupt pressure loss, even if this loss is small, are Weber number-dependent, suggesting a delayed flashing mechanism. Flows from systems with abrupt contractions at the inlet of the test section; or where high pressure fluid is flashed down to the system pressure (many Eastern European test rigs operate on this principle; such data are given in Figs. 1, 3 and 8); or in rod cluster geometries where the rods are separated by local spacers (e.g. the data in Fig. 4) are flows of this type.

(e) Swirl flow data from tests with swirlers, wire-wrapped spacers in rod clusters, etc., usually depend on Reynolds number, even under diabatic conditions, suggesting that swirl suppresses the nucleation process.

Available two-component data were not usually dependent on Weber number, even for those data relating to the passage of gas through a porous wall to simulate boiling. Two exceptions are shown in Figs. 6 and 9; both data sets are from comparatively high pressure rigs. The data in Fig. 9 were obtained in a system in which a floating sleeve device was used to measure wall shear. The shear force on the sleeve was balanced by a differential gas pressure.

Some of this gas leaking into the test section could have caused bubbles to attach to the perimeter of the floating sleeve.

As noted earlier, three methods were used to estimate film entrainment for the analysis of the annular flow voidage data in Figs. 2-8. This was because Reynolds number-dependent flow data had indicated that film entrainment significantly influenced annular flow voidage. The present analysis indicates that this is generally not the case for Weber number-dependent flows. An exception occurs for the data of Fig. 2. There was, however, very little evidence of the onset of annular flow for most of the other data, and in Figs. 3, 5, 6, 7 and 8, it was assumed to occur whenever gas was present, i.e. gas entrainment was neglected for these figures. Inclusion of entrainment by having non-zero α_f and β_f in these figures adjusts both abscissa and ordinate values for the annular flow voidage data such that they are shifted parallel to the predicted curves, indicating little dependence of average voidage on entrainment. Some small dependence occurs with the data of Fig. 4. On the basis of Reynolds number-dependent data from the same experimental rig, 55% voidage was chosen as the onset of annular flow (i.e. $\alpha_f = 0.55$) for the data of Fig. 4.

The Fig. 4 data for one flow condition, this condition being chosen because the data show some dependence on both film and core entrainment, are plotted directly as voidage values in Fig. 10. Also shown are predictions based on no entrainment, no core entrainment but film entrainment, and entrainment in both core and film. It is seen that film entrainment produces an effect only at high voidages.

Finally, in view of the earlier comment that models 1 and 2 are not alternative shear stress treatments, as is often supposed, but are models for wall bubble shear stress (model 2) and form drag (model 1), the present work can be viewed as indicating not that model 1 is invalid for the data analysed, but rather that, as expected for the data analysed, the dominant wall bubble force opposing surface tension is due to shear and not to form drag.

5. CONCLUSIONS

Heat transfer rates of sufficient magnitude, and flashing caused by comparatively large pressure gradients or by localised obstructions, give rise to attached wall bubbles in two-phase one-component flows. If these protrude beyond the laminar sublayer, the flows are characterised by a Weber number, effectively reflecting a completely roughened wall system with roughness height (bubble size) given by a balance of shear and surface tension forces. Two theoretical models in the literature relevant to this situation were applied to the prediction of non-dimensional velocity profiles, friction factors, average void fraction for annular flow, and average void fraction for distributed flow. Available data were found to be consistent with one of these models. Various apparently different Weber number-dependent flow characteristics are found to be special cases, corresponding to different friction regimes, of a generalised flow equation.

6. ACKNOWLEDGEMENT

Helpful discussions with Professor J.J. Thompson, UNSW, are gratefully acknowledged.

NOMENCLATURE

A	area fraction of core in annular flow, $(\langle\alpha\rangle-\alpha_f)/(\alpha_c-\alpha_f)$
B	volume flow fraction of core in annular flow $(\langle\beta\rangle-\beta_f)/(\beta_c-\beta_f)$
C_o	distribution parameter (Table 1)
d	wall bubble diameter
D	diameter
f	friction factor, $2\tau_w/(G\langle j\rangle)$
F	force on wall-bubble
G	mass flux
j	mixture velocity
j^+	$\sqrt{2/f}\ .\ j/\langle j\rangle$
m,n	integers characterising friction regime
Q^+	non-dimensional film flow rate of annular flow (Table 1)
R	equivalent radius - 2 x flow area/sheared perimeter
S^+	non-dimensional film thickness of annular flow (Table 1)
u	local phase velocity
v	drift velocity
We	Weber number, $2G\langle j\rangle R/\sigma$
y	wall distance
y^+	non-dimensional wall distance (Table 1)
α	void fraction
β	gas volume flow fraction
σ	surface tension
τ	shear stress

Subscripts

c	core value (annular flow)
d	value at departure from wall
f	film value (annular flow)
F	frictional component
s	surface tension component
w	wall value

Other

<--->	quantity is averaged over flow cross-section
~	'varies as'

REFERENCES

1. Wallis G.B. "Some Hydrodynamic Aspects of Two-phase Flow and Boiling", pp.319-340 in International Developments in Heat Transfer, Pt.II, ASME (1961).
2. Tong L.S. "Boiling Crisis and Critical Heat Flux", TID-25887 (1972).
3. Chang Y.P. "An Analysis of the Critical Conditions and Burnout in Boiling Heat Transfer", TID-14004 (1961).

4. Levy S. "Forced Convection Subcooled Boiling-Prediction of Vapor Volumetric Fraction", International Journal of Heat and Mass Transfer, Vol.10, (1967) 951-965.

5. Staub F.W. "The Void Fraction in Subcooled Boiling - Prediction of the Initial Point of Net Vapor Generation", Journal of Heat Transfer, Vol.906, (1968), 151-157.

6. Beattie D.R.H. "Some Aspects of Two-phase Flow Drag Reduction", Paper D1, Proc. Second International Conference on Drag Reduction, BHRA Fluid Engineering, (1977).

7. Beattie D.R.H. "Pressure Pulse and Critical Flow Behaviour in Distributed Gas-liquid Systems", Paper D3, Proc. Second International Conference on Pressure Surges, BHRA Fluid Engineering, (1976).

8. Zuber N. and Findlay J.A. "Average Volumetric Concentration in Two-phase Flow Systems", Journal of Heat Transfer, Vol.87, (1965), 453-468.

9. Collier J.G. "Convective Boiling and Condensation", McGraw-Hill, (1972).

10. Tarasova N.V. et al. "Pressure Drop of Boiling Subcooled Water and Steam-Water Mixture Flowing in Heated Channels", Proc. Third International Heat Transfer Conference, Vol.4, Paper 113 (1966).

11. Gaspari G.P., Lombardi C., Peterlongo G. "Pressure Drops in Steam-Water Mixtures", CISE-R-83 (1964).

12. Era A. et al. "Heat Transfer Data in the Liquid Deficient Region for Steam-Water Mixtures at 70 kg/cm^2 Flowing in Tubular and Annular Conduits", CISE-R-184, (1966).

13. Berkowitz L. et al. "Pressure Drop, Heat Transfer and Burnout Measurements with Round Tubes", CISE-R-27 (1960).

14. Nabizadeh H. "Uebertragungsgesetze zwischen Wasser und Freon 113 für mittleren volumetrischen Dampf gehalt, Druchabfall und kritische Heizflaechenbelastung", European Two-phase Flow Group Meeting, Grenoble, Paper E6 (1977).

15. Kirillov P.L. et al. "Measurement of Some Characteristics of Steam-Water Flow in Round Tubes at a Pressure of 68.6 Bar" (in Russian) FEI-421, (1973).

16. Agostini G. et al. "Density of Steam-Water Mixtures Flowing in 19-rod Clusters under Adiabatic and Heated Conditions", CISE-R-309 (1971).

17. Gaspari G.P. et al. "Heat Transfer Crisis and Pressure Drop Measurements with Steam-Water Mixture in CIRENE 19-rod Clusters (4 m long)", CISE-R-339 (1973).

18. Friedel L. "Modellgesetz für den Reibungsdruckverlust in der Zweiphasenströmung", VDI-Forschungsheft 572, (1975).

19. Friedel L., Mayinger F. "Scaling of Two-phase Pressure Drop", European Two-phase Flow Group Meeting, Harwell, Paper B2 (1974).

20. Alia P. et al. "Two-phase (Gas + Liquid) Adiabatic Vertical Upflow: A Preliminary Study with a Rod Cluster Geometry", CISE-R-108 (1968).

21. Kirillov P.L. et al. "Calculating the Hydraulic Losses in an Adiabatic High-Pressure Steam-Water Flow", Thermal Engineering, Vol.24, No. 10, (1977), 41-44.

22. Subbotin V.I. et al. "Measurement of Some Characteristics of a Steam-Water Flow in a Round Tube at Pressures of 70 and 100 atm", ASME Paper WA-75/HT21 (1975).

23. Cravarolo L. et al. "A Device for the Measurement of Shear Stress on the Wall of a Conduit. Its Application in the Mean Density Determination in Two-phase Flow:Shear-Stress Data in Two-phase Adiabatic Vertical Flow", CISE-R-82 (1964).

24. Beattie D.R.H. "Two-phase Flow Structure and Mixing Length Theory", Nuclear Engineering & Design, Vol.21 (1972), 46-64.

Int. J. Multiphase Flow Vol. 7, pp. 423–437, 1981
Printed in Great Britain

0301-9322/81/040423-15$02.00/0
Pergamon Elsevier

TWO-PHASE HYDRODYNAMIC EXPERIMENTS WITH AXIAL FLOW THROUGH SEVEN-ROD CLUSTERS

D. R. H. BEATTIE and K. R. LAWTHER

AAEC Research Establishment, Lucas Heights, NSW 2232, Australia

(*Received* 16 *March* 1979; *in revised form* 2 *December* 1980)

Abstract—Hydrodynamic experiments have been carried out with upflow of air–water mixtures through vertical seven-rod clusters at atmospheric pressure. Results obtained from measurements of flow characteristics, including pressure drops, local velocity and voidage distribution, are discussed in terms of relations developed for two-phase flow in round tubes. Effects on the flow characteristics of spacer elements and bowing of a cluster are also discussed.

INTRODUCTION

An understanding of two-phase fluid mechanics in complex channel geometries is required because of the importance of flow boiling in water-cooled nuclear reactor systems, particularly in relation to predicting the consequences of accident or other abnormal conditions. At the Australian Atomic Energy Commission Research Establishment, single phase turbulent flow theory is being adapted to two-phase flows (Beattie 1972). Turbulence theory is not readily adaptable to flow in channels of complex geometry, even for single phase flow (Hooper 1975). However, it is known (e.g. Tong & Weisman 1970) that with single phase flow, pressure loss equations for flow in round tubes can be extended, with little loss in accuracy, to complex geometries by replacing the diameter term in relevant dimensionless groups with the equivalent hydraulic diameter, $D_e = 4\ A/p$, where A is the flow area and p is the sheared surface perimeter.

Although the use of D_e is based on empiricism rather than theory, it has led to reasonably accurate predictive methods for single phase flows in complex geometries. As a result, the AAEC program examined the validity of applying expressions obtained from mixing-length theory (as developed for two-phase flow through round tubes) to rod bundle geometries, by using the equivalent diameter concept (Beattie 1979). In that work, a large number of data from various sources were considered, with emphasis on high pressure steam–water systems, and the equivalent diameter concept was concluded to be valid for pressure loss and void fraction expressions. However, it was noted that the flow disturbance effects of the entrance region and of spacers in complex geometries may cause coefficients in the equations to be different from those for round tubes.

An investigation into the validity of the mixing-length concept for two-phase flows requires experimental data on such local flow structure as voidage and velocity profiles, as well as more global characteristics such as friction factors and average void fractions. Although in the literature there are several sources of data on such global and local characteristics of two-phase flow in round tubes, this is not the case for two-phase flow in complex geometries. Therefore, experiments have been conducted on seven-rod clusters for air–water flows in which local voidage and velocity data were obtained, as well as data on friction factors, average void fractions and rod-spacer pressure loss coefficients. The results of this investigation are reported here.

Air–water at atmospheric pressure is a convenient fluid system for two-phase flow experiments. Although the liquid/gas density ratio is much higher than the water/steam density ratio in a water-cooled nuclear power reactor under normal operating conditions, information obtained on flow characteristics from such experiments at low quality conditions would probably have general relevance to vapour/liquid systems and be particularly relevant to a water-cooled reactor system under the depressurisation conditions of a loss-of-coolant accident.

BACKGROUND THEORY

Relevant equations developed from the Prandtl mixing-length concept, as applied to two-phase flows in round tubes, are presented below Detailed discussion of these equations has been presented elsewhere (Beattie 1972, 1976, 1977).

Pressure drop components

The acceleration component of the axial gradient in static pressure is negligible in air–water upflow experiments of the type described here. Effectively the pressure gradient, dP/dz, is made up of two components, i.e.

$$dP/dz = [dP/dz]_f + [dP/dz]_g \quad [1]$$

where $[dP/dz]_f$ is the frictional component given by

$$[dP/dz]_f = 2f G\langle j\rangle/D_e, \quad [2]$$

and $[dP/dz]_g$ is the gravitational component, given by

$$[dP/dz]_g = \{\rho_L(1-\langle\alpha\rangle) + \rho_G\langle\alpha\rangle\}g. \quad [3]$$

In the above, f is the friction factor, G is mass flux of fluid mixture, $\langle---\rangle$ denotes a cross-section average value, j is mixture velocity, α is void fraction, ρ_L and ρ_G are the densities of the liquid and gas phases, and g is the acceleration due to gravity.

The calculation of dP/dz for a given flow thus depends on the values of friction factor, f, and void fraction, $\langle\alpha\rangle$. The methods adopted for evaluating these are described below.

Friction factor

The friction factor f, is dependent on the "friction regime" of the sublayer. Regimes are characterised by a triad (m, n, z) where m and n are integers which depend on the turbulent core flow structure and z is a letter (a, b or c here) indicating the nature of the sublayer (table 1). Relations between the friction factor and Reynolds number, $\mathrm{Re} = D_eG/\mu$, where the definition of the viscosity, μ, is sublayer-dependent (see table 1), are established through values of m and n by the equation (Beattie 1977):

$$1/\sqrt{f} = (\sqrt{2})^{m+4}\{\log \mathrm{Re}\sqrt{f} - (0.11m + 0.50n + 1.1)\}. \quad [4]$$

An extensive analysis of data, some of which have been reported by Beattie (1977), indicated that, in the absence of strong flow-disturbing influences, the two lowest quality regimes are usually characterised by $(m, n, z) = (0, -2, a)$ (low-voidage bubble-sublayer flows) and (m, n, c) (semi-annular flows), where m and n for the semi-annular regime appear to depend on pressure and characteristic channel dimension. The boundary between these two regimes is given by:

$$f(0, -2, a) = f(m, n, c), \quad [5]$$

Table 1. Two-phase flow sublayer viscosity relations

Sublayer type	*Viscosity relation*
(a) Rigid surface bubbles	$\mu = \mu_L(1 + 2.5\beta)$
(b) Non-rigid surface bubbles	$\mu = \mu_L\left\{1 + \left(\frac{\mu_L + 2.5\mu_G}{\mu_L + \mu_G}\right)\beta\right\}$
(c) Wavy gas–liquid interface	$\mu = \mu_L(1-\beta) + \mu_G\beta$

and the relation

$$f = \min\{f(0, -2, a), f(m, n, c)\} \quad [6]$$

selects the appropriate friction factor value.

In the case of obstructions, the relation between the two-phase pressure loss coefficient and Reynolds number coincides with the single phase relation if the Reynolds number, based on the relevant viscosity as given in table 1, is defined according to the nature of the flow over the obstruction (Beattie 1973).

Average voidage

Local voidage, α, and local velocity, j, vary with distance from the wall, y, such that

$$(1 - \alpha)^{3/2} = a + b \ln y \quad [7]$$

and

$$j = a' + b' \ln y \quad [8]$$

where a, b, a', b' are coefficients which are independent of radial position (Beattie 1972).

For low-voidage distributed flows, the void fraction averaged over the cross-section, $\langle\alpha\rangle$, is given by the Zuber & Findlay (1965) equation:

$$\frac{\langle j_G\rangle}{\langle\alpha\rangle} = C_0\langle j\rangle + V \quad [9]$$

where $\langle j_G\rangle$ is the superficial gas velocity; $\langle j\rangle$ is the average mixture velocity; V is a regime-dependent drift velocity, values of which can be obtained from semi-empirical equations given by Zuber & Findlay (1965) and by Griffith (1964); and C_0 is a "distribution parameter" which accounts for the fact that the gas phase concentrates in the faster moving regions of the flow. The distribution parameter is regime-dependent and its value is given by Beattie (1977) as

$$C_0 = 1 + 2.60\,(\sqrt{2})^m\,\sqrt{(f(m, n, z))}. \quad [10]$$

For annular flow within no entrainment the liquid volume fraction, $1 - \langle\alpha\rangle$, is related to the liquid volume flow fraction, $1 - \beta$, by

$$Q^+ = \int_0^{S^+} j^+ \, dy^+ \quad [11]$$

where

$$Q^+ = \frac{1 - \beta}{4}\,\mathrm{Re}\,(z), \quad [12]$$

$$S^+ = \frac{1 - \langle\alpha\rangle}{4}\,\mathrm{Re}(z)\,\sqrt{\left(\frac{f(m, n, z)}{2}\right)}, \quad [13]$$

Re(z) is the Reynolds number for the relevant sublayer as given in table 1, and j^+ is the non-dimensional local velocity appropriate to the relevant (m, n, z) regime (Beattie 1977), expressed as a function of non-dimensional distance from the wall, y^+.

Interpretation of pressure drop data

Pressure gradients in experiments of the type described here may be dominated by the frictional component or by the gravitational component, or may have contributions of a similar magnitude from both these components. In the first two cases the pressure drop data may be used directly to estimate values of the friction factor or voidage respectively.

In cases where neither the frictional component nor the gravitational component dominates, conventional wisdom dictates that some additional measurement be made before the axial gradient of static pressure can be resolved into its two components. This is really unnecessary since the interrelation between void fraction and friction factor, as described above, provides a relation equivalent to that which would be obtained by the additional measurement.

Therefore, in principle, pressure gradient data covering a wide range of flow conditions for a particular flow regime can be used to determine the appropriate values of the triad (m, n, z) for that regime, and hence the values of both the frictional and gravitational components for a given flow condition, irrespective of the relative contribution of each to the total pressure gradient. In practice, however, the relatively weak dependence of distribution parameter on friction factor in [10] means that, for distributed flows, voidage data (or equivalently, gravity-dominated pressure gradient data) analysed in terms of [9] cannot provide accurate estimates of friction factors; so evaluation of (m, n, z) for the regime becomes uncertain. Examination of [11]–[13] reveals that the same problem arises with gravity-dominated pressure gradient data for annular flows. The uncertainty should disappear for pressure gradient data where the friction contribution becomes substantial.

EXPERIMENTAL PROGRAM

Experimental assemblies

Three different rod-cluster arrangements were used with upflow of air–water mixtures through vertical seven-rod clusters in a transparent shroud, 95 mm dia., 3.66 m length. Pressure tappings were located 1.97 and 2.69 m from the inlet end of the shroud.

The *first* cluster arrangement (42 mm equivalent dia. × 3.66 m) comprised a central rod, 15.9 mm dia., surrounded by six equidistant rods, 12.7 mm dia. on a pitch circle, 50.8 mm dia. The rods were held in position relative to each other by seven sets of spacers, made from 13 × 0.9 mm metal strip, which were placed at equal intervals along the cluster as shown in Figure 1. The cluster was held centrally in the shroud by connections screwed axially into the central rod at each end. A probe housing 2.07 m from the inlet end enabled local voidage and gas bubble velocity to be measured by a double-needle conductivity probe of the type commonly used in two-phase flow experiments (e.g. Herringe & Davis 1974). The probe could be moved in both radial and circumferential directions relative to the cluster.

The *second* cluster arrangement was the same as the first except that the rod bundle was bowed into near contact with the shroud, 2.44 m from the inlet end, by means of screwed rods through the shroud. The rod cluster was thus in an extremely eccentric position in the region of the pressure tappings and the double-needle probe.

The *third* cluster arrangement (17 mm equivalent dia. × 3.66 m) comprised seven 25.4 mm dia. rods in the same shroud, six rods being equispaced on a 60 mm pitch circle diameter around the seventh. Sets of spacers, each consisting of eighteen 4.7 mm lengths of 4.7 mm dia. threaded rod, separated the rods from each other and from the shroud, as shown in figure 1; one of these was located 1 m below the upstream pressure tapping and another 77 mm above the downstream tapping. Results from the first and second cluster arrangements indicated that spacers significantly influenced the flow, so for this assembly, in order to examine pressure recovery after the spacer, four additional pressure tappings were located downstream of the second spacer set as shown in figure 1. Voidage and velocity contour maps were not obtained with this cluster because of practical limitations associated with the small flow section.

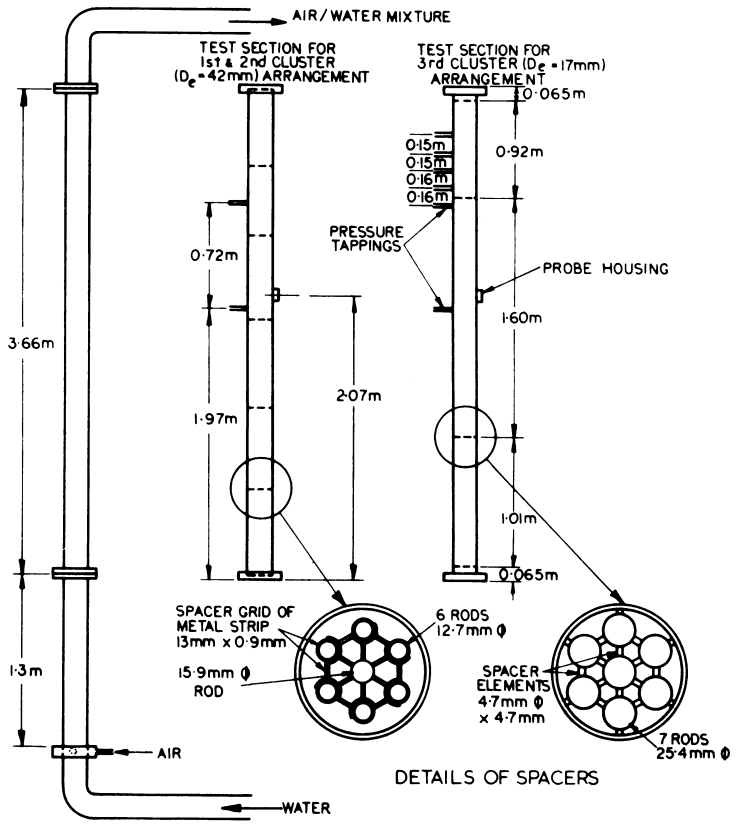

Figure 1. Test arrangements.

Experiment conditions

Experimental data were obtained for flows of air–water mixtures with atmospheric pressure at the test section exit. The flowrates for experiments with the first two cluster arrangements correspond to gas and liquid superficial velocities ranging from 0 to 3.0 m s^{-1} for $\langle j_G \rangle$, and 0 to 2.0 m s^{-1} for $\langle i_L \rangle$. Flowrates in the third cluster arrangement correspond to gas and liquid superficial velocities ranging from 0 to 16 m s^{-1} for $\langle j_G \rangle$, and 0.08 to 2.0 m s^{-1} for $\langle j_L \rangle$.

Gas and liquid flowrates were measured separately upstream of the mixer section. For the first two cluster arrangements, local phase content and gas bubble velocity data were obtained from radial traverses at the probe housing for a number of azimuthal positions of the probe housing, relative to the cluster.

RESULTS

(a) *42 mm equivalent diameter, cluster arrangements*

(i) *Pressure gradient data.* Single phase pressure drop measurements resulted in friction factors for the first and second cluster arrangements which are respectively ~30 and ~20 per cent above those corresponding to the Nikuradse equation:

$$1/\sqrt{f} = 4 \log \mathrm{Re}\sqrt{f} - 0.4. \qquad [14]$$

These are somewhat higher than expected, and apparently reflect an influence of the spacers and the probe assembly. Further evidence of this influence comes from an analysis of the two-phase voidage data discussed below. The reduction of friction factors on bowing was expected and can be explained by a decrease in effective shear surface under bowed conditions.

The two-phase flows were observed to be bubble flows, either with or without slugs. Axial pressure gradients in these flows had significant contributions from both gravity and friction for the bubble-slug flows, whereas those in the bubble flows were due predominantly to gravity.

Pressure gradient data were analysed by subtracting estimates of the frictional component and, from the resulting gravitational components, average voidage values were obtained by means of [3], which were then plotted on the $(\langle j_G\rangle/\langle\alpha\rangle):\langle j\rangle$ plane.

The friction regime which, on the basis of round tube data for similar flow conditions, was expected to apply here, is that characterised by $(0, -2, a)$ (Beattie 1977). However, $(m, n) = (0, -2)$ in [4] corresponds to the Nikuradse equation which, although valid for flow through round tubes, underpredicts the single phase friction losses for these assemblies; so values of two-phase friction factor used for estimating the frictional components were obtained for sublayer *a* (table 1) but based on the friction factor/Reynolds number relation corresponding to the experimental single phase values instead of the Nikuradse equation.

The resulting void fraction data are shown in figure 2. This figure shows that two distinct characteristics occurred, and that bowing did not have any detectable influence on the voidage characteristics. This latter finding is as expected since, as already noted, bowing has a small effect on the friction factor, and [9] and [10] indicate that, for a given regime, a change in friction factor has only a second-order effect on void fraction.

The boundary between the two characteristics on figure 2 occurs at a voidage of ~23 per cent. At lower voidage values the flow was visually observed to be bubble flow, and at higher voidages, bubble-slug flow.

The bubble flow data have drift velocity values which are negative and approximated by $V = -\langle j_L\rangle$, and distribution parameters C_0 which are large (~ 2.0) and, in view of [10], are incompatible with the *a* type sublayer regime, for which $C_0 \sim 1.2$. This indicates that the estimated frictional components for these data are incorrect. However, as noted, the frictional components for these data are negligible; hence the void fraction values for these data would not be invalidated.

The negative drift velocities and the incompatibility of the distribution parameter values with the *a* type sublayer regime, indicate that the flow was strongly underdeveloped. As air

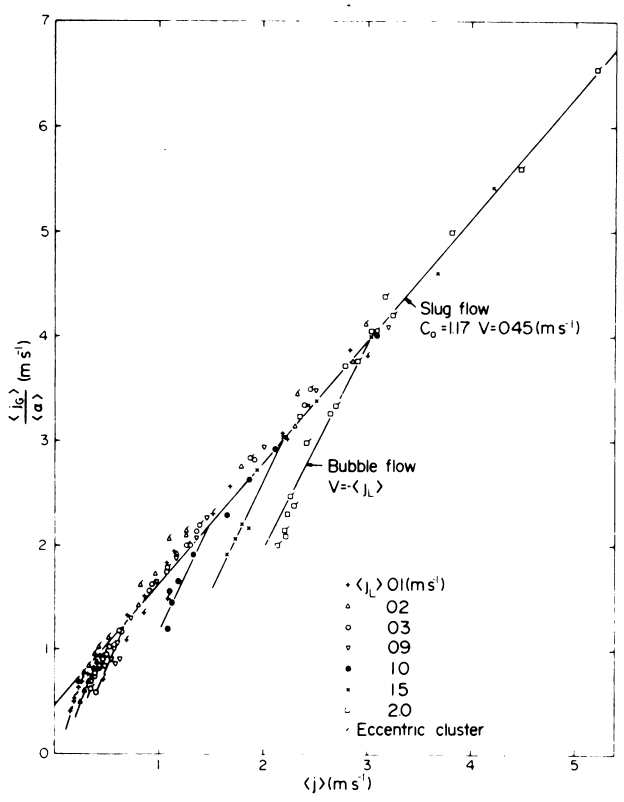

Figure 2. Average voidage data for bowed and non-bowed 42 mm equivalent dia., rod cluster.

"wakes" were observed at the spacers, the flows could have been disturbed by a bubble-retarding action of the spacers which would have produced a drift velocity of $-\langle j_L \rangle$ and also prevented establishment of the $(0, -2, a)$ regime.

The slug flow data of figure 2 are very close to a slug flow version of [9], in which values of $C_0 = 1.17$ and $V = 0.45\ \mathrm{m\,s^{-1}}$ were obtained from curves given by Griffith (1964).

The agreement with the Griffith equation appears encouraging but, given his computational procedure (zero net flow experiments to obtain V, and speculative arguments to derive C_0 values), it seems rather surprising. Close examination of the slug flow data, however, reveals a small but significant mass flux effect. Figure 3 indicates that although the Griffith equation is in fair agreement with the data, the actual drift velocity, V, is somewhat lower than that proposed by Griffith, and C_0 values are really mass-flux dependent and larger than that recommended by Griffith.

Figure 3 also indicates that distribution parameter values are compatible with [10] for the $(0, -2, a)$ friction regime, thus confirming the method of obtaining the frictional component of the pressure drop, which was not negligible for the bubble-slug flow.

(ii) *Flow structure.* The double-needle conductivity probe was used to obtain local voidage and bubble velocity contour maps for selected flow conditions in both cluster arrangements. The conductivity probe measurements were confined to bubble flows because preliminary tests indicated that meaningful velocities could not be obtained if slugs were present.

Figures 4 and 5 show typical flow structure results in which the velocity and voidage contours follow the broadly expected trends, but two points are noteworthy. The first is that the rods are not necessarily at the centre of the subchannel boundaries obtained from the contours; this is relevant for rod-centred subchannel analysis studies. The second point is that secondary flows, as evidenced by irregularities in the velocity contours in the rod-free region of the bowed cluster data, play a stronger role than is the case in single phase flows. A similar situation occurs in two-phase flows around bends (Hoang & Davis 1977).

The two-phase mixing-length theory expressions for bubble flow, [7] and [8], appear to be locally valid (figures 6 and 7), although, as is the case in single phase flow through rod-cluster assemblies (Hooper 1975), for any given flow, values of the coefficients vary with azimuthal

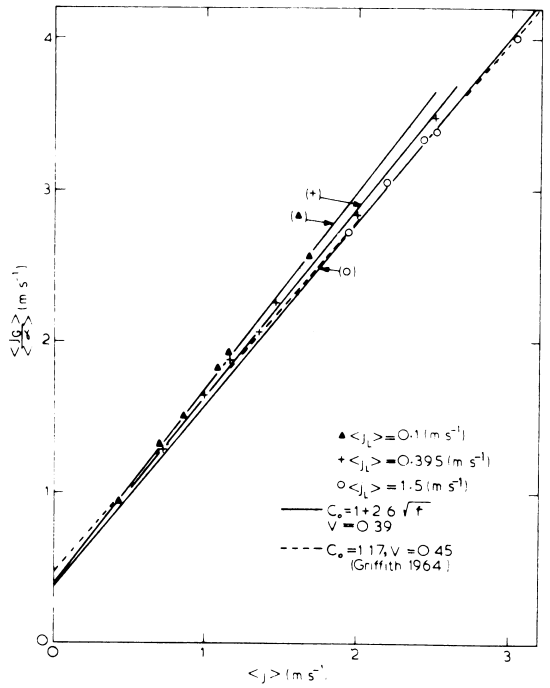

Figure 3. The effect of mass flux on slug flow void fraction (42 mm equivalent dia., non-bowed rod cluster).

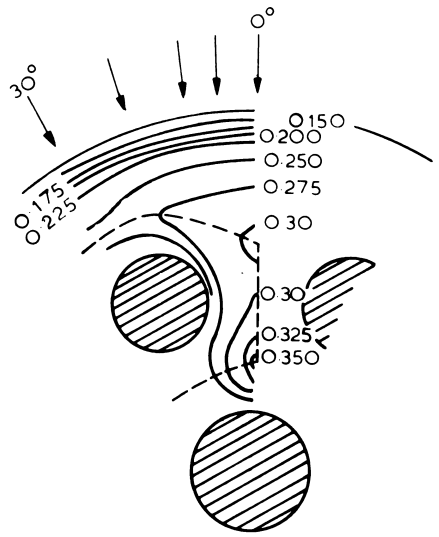

Figure 4. Voidage contour map for non-bowed 42 mm equivalent dia., rod cluster with $\langle j_L \rangle = 0.390\ \mathrm{m\,s^{-1}}$ and $\langle j_G \rangle = 0.175\ \mathrm{m\,s^{-1}}$. Probe traverse positions are arrowed.

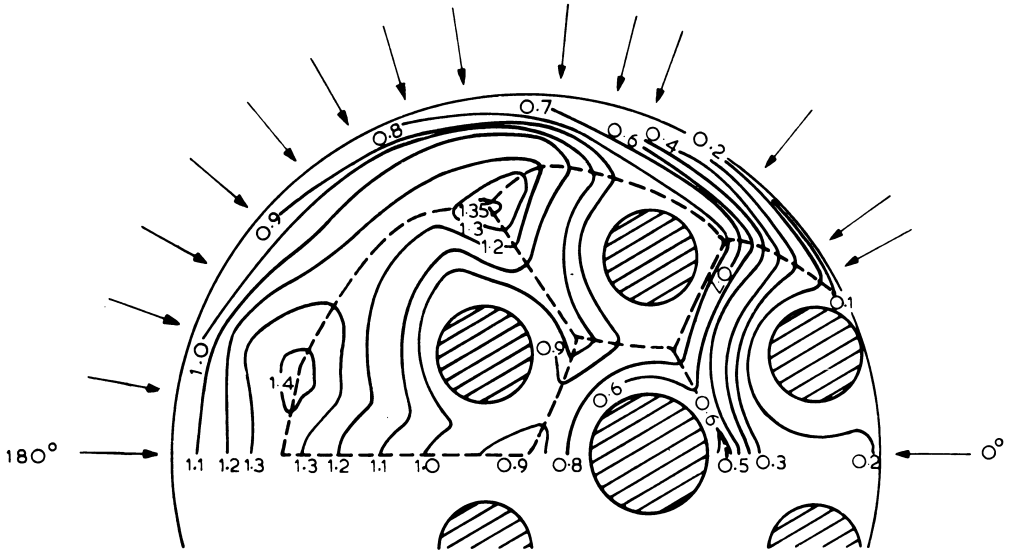

Figure 5. Bubble velocity contour map in $\mathrm{m\,s^{-1}}$ for bowed 42 mm equivalent dia., rod cluster with $\langle j_L \rangle = 0.320\ \mathrm{m\,s^{-1}}$ and $\langle j_G \rangle = 0.175\ \mathrm{m\,s^{-1}}$. Probe traverse positions are arrowed.

position. The steep velocity profiles are consistent with the large distribution parameter values found in the average voidage analysis, although no quantifiable crosscheck between the two quantities can be made at present.

(b) 17 *mm equivalent diameter, cluster arrangement*

(i) *Pressure losses.* Pressure gradients were examined upstream and downstream of one of the spacers. For superficial liquid velocities greater than $1\ \mathrm{m\,s^{-1}}$, the pressure gradient was predominantly frictional, and the gravitational component was allowed for, using [9] with the bubble flow expression for drift velocity (Zuber & Findlay 1965)

$$V = 1.4\,(\sigma g/\rho_L)^{0.25} \qquad [15]$$

where σ is the surface tension; and distribution parameter, C_0, equal to 1.2, this being an

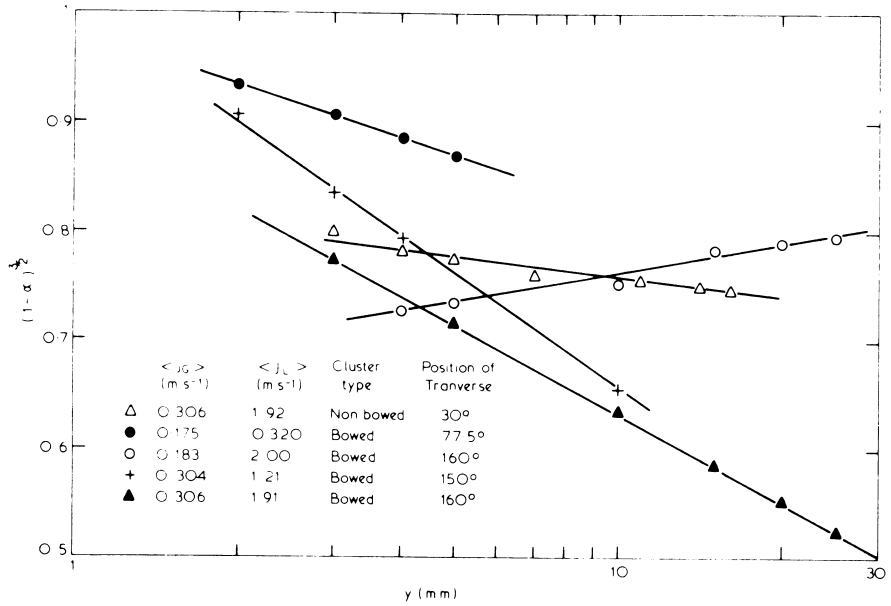

Figure 6. Voidage distribution data near shroud of 42 mm equivalent dia., rod cluster.

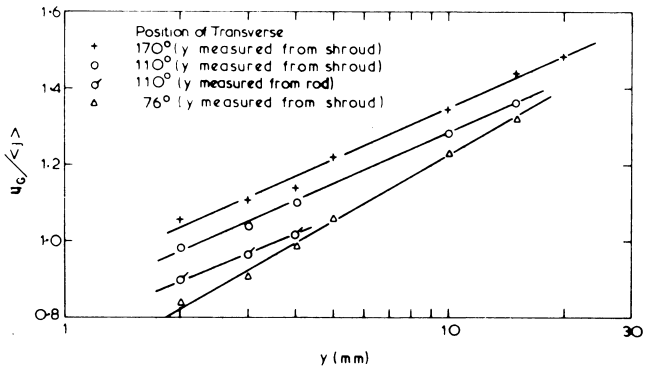

Figure 7. Velocity distribution data near the wall for 42 mm equivalent dia., rod cluster with $\langle j_L \rangle = 2.00\ \mathrm{m\,s^{-1}}$ and $\langle j_G \rangle = 0.18\ \mathrm{m\,s^{-1}}$.

approximation to values calculated from [10] for the $(0, -2, a)$ friction regime anticipated for these flow conditions (Beattie 1977). Errors in this voidage calculation procedure have a negligible effect on the estimate of the frictional component for superficial liquid velocities greater than $1\ \mathrm{m\,s^{-1}}$.

The pressure gradients downstream of the spacer, determined from measurements at the four downstream pressure tappings, indicated that the effect of the spacer had largely disappeared after five hydraulic diameters and rarely extended to 15 diameters. Friction factors beyond 15 diameters downstream of the spacer were the same as those upstream of the spacer. The upstream and the recovered downstream axial static pressure profiles were extrapolated to determine the pressure losses associated with the spacer, and hence the spacer loss coefficients.

Low voidage, pressure loss data were consistent with sublayer type *a* (table 1), and pressure losses at higher voidages, with sublayer type *c*. The lower voidage friction factors are shown in figure 8 and generally correspond to $f(0, -2, a)$ as obtained from [4] (which gives the Nikuradse equation). As shown in figure 8, single phase data also are consistent with the same curve. The applicability of $f(0, -2, a)$ verifies the method used to estimate the gravitational components in the pressure gradient data, and indicates that spacer effects are smaller for this

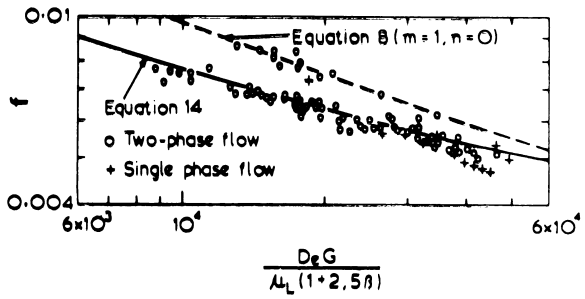

Figure 8. Bubble flow friction factors upstream of spacer of 17 mm equivalent dia., rod cluster.

cluster than the previous one. This is consistent with the rapid pressure recovery following the spacer as noted above. A few of the data in figure 8 deviate from $f(0, -2, a)$ and instead, were correlated by $f(1, 0, a)$.

The friction data for higher voidages could not be correlated with [4] if m and n are integers. However, the data do agree with the equation if a half-integer value of m is used. It has been noted elsewhere (Beattie 1977) that, although [4] is compatible with most data sets by appropriate integer choice for m and n, some data require half-integer values. As shown in figure 9, the higher voidage friction data for cluster arrangement No. 3 are consistent with $f(-2, -6.5, c)$.

In line with the general case described by [6], all friction factor values for $\langle j_L \rangle$ above 1 m s^{-1} in this cluster agree with

$$f = \min \{f(0, -2, a); f(-2, -6.5, c)\}. \quad [16]$$

It has been suggested (Beattie 1973) that single phase pressure loss coefficient/Reynolds number curves should apply to the two-phase case, provided that the two-phase Reynolds number is appropriately defined. This is the case with the present spacer loss coefficient data (figure 10). The applicability of Reynolds number, based on sublayer c for all the data, indicates that flow over the spacers was separated flow for both low and high voidage conditions. The scatter in the data is caused by the relatively small pressure drop across the spacer, combined with the extrapolation procedure necessary to estimate this pressure drop.

For superficial liquid velocities less than 1 m s^{-1}, the pressure drop was predominantly gravitational. However, the frictional component was not negligible, particularly at high voidages. Being predominantly gravitational, these data more appropriately belong in the next section. The analysis discussed there indicates that the friction factors at low voidage do not agree with $f(0, -2, a)$ and instead agree with $f(4, -1, a)$ which indicates an undeveloped flow condition at low superficial velocities.

(ii) *Void fraction.* As already stated, the pressure gradient data were gravity-dominated at superficial velocities less than 1 m s^{-1}. For larger liquid velocities, friction factors were calculated by assuming that voidage could be evaluated from [9] using the estimate based on $f(0, -2, a)$, for distribution parameter in [10] and the drift velocity for bubble flow in [15]. This led to friction factor values compatible with $f(0, -2, a)$, at least for low voidages, suggesting that, for these data, the procedure for calculating voidage was correct. On the other hand, friction factors for flows with higher voidage, $f(-2, -6.5, c)$, indicate that the procedure used for calculating voidage is not correct at higher voidages. Since, for these conditions, the gravity component in the pressure gradient was negligible, voidage data cannot be extracted from these data. However, voidage values calculated for the $(-2, -6.5, c)$ regime, using relationships given in the section on background theory, should apply to these data.

Although pressure gradient data were gravity-dominated at low superficial liquid velocities (<1 m s^{-1}), the frictional components were not negligible and needed fairly accurate estimation. Lower voidage values for these liquid flowrates were initially assessed by assuming that

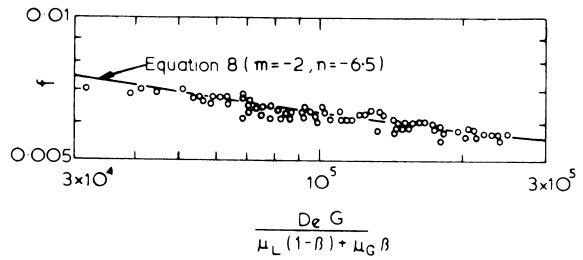

Figure 9. Annular flow friction factors upstream of spacer of 17 mm equivalent dia., rod cluster.

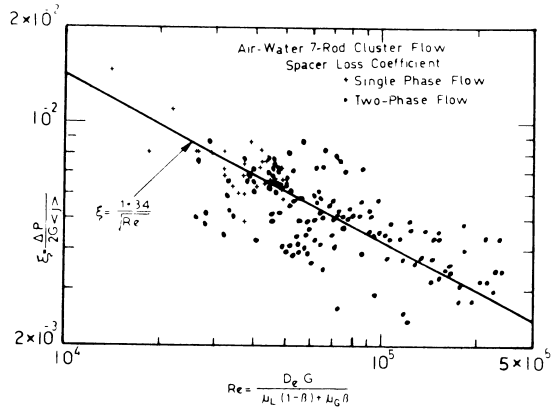

Figure 10. Spacer loss coefficients for 17 mm equivalent dia., rod cluster.

$f(0, -2, a)$ applies for the frictional component. However, this assumption led to estimated values of voidage which were incompatible with the $(0, -2, a)$ regime. Trial and error indicated that, if friction was calculated according to $f(4, -1, a)$, the resulting estimates of voidage, when plotted on the $\langle j_G \rangle / \langle \alpha \rangle$: $\langle j \rangle$ plane, produced distribution parameters from [10] consistent with $f(4, -1, a)$, indicating that $(4, -1, a)$ is the appropriate regime for these conditions. The void fraction data so estimated are shown in figure 11. Note that the two empirical drift velocity values from figure 11 agree with the bubble flow drift velocity, 23 $cm\,s^{-1}$ given by [15], and the drift velocity for developed slugflow in rod clusters, calculated from the graphs of Griffith (1964).

It would appear from the above that, for the 17 mm rod cluster, spacers did not influence the flow at high mass-flux bubble flows, but at low mass-flux bubble flows the regime was altered from $(0, -2, a)$ to $(4, -1, a)$. However, unlike the case with the 42 mm cluster, drift velocity values were not noticeably affected.

In the case of annular flows at low mass flux (i.e. $\langle j_L \rangle < 1\ m\,s^{-1}$), various frictional relations were tried for the frictional component of the pressure drop, but none corresponded to voidage values compatible with the original friction factor assumptions. However, an assumed friction factor of 0.006, which is reasonable in view of the annular flow friction factor data of figure 9, resulted in voidage values which, when analysed in the annular flow plane

$$\left\{\frac{1-\beta}{4}\,\mathrm{Re}\right\} : \left\{\frac{1-\langle\alpha\rangle}{4}\,\mathrm{Re}\,\sqrt{\left(\frac{f}{2}\right)}\right\},$$

were well correlated, provided that Re was defined using viscosity a (figure 12). No spacer effect is discernible. Furthermore, the correlating equation is the integral of the "universal" velocity profile. Thus, although the flow cannot be specified completely, the conclusion can be drawn that the data of figure 12 are for annular flow with entrained bubbles in the film, with the

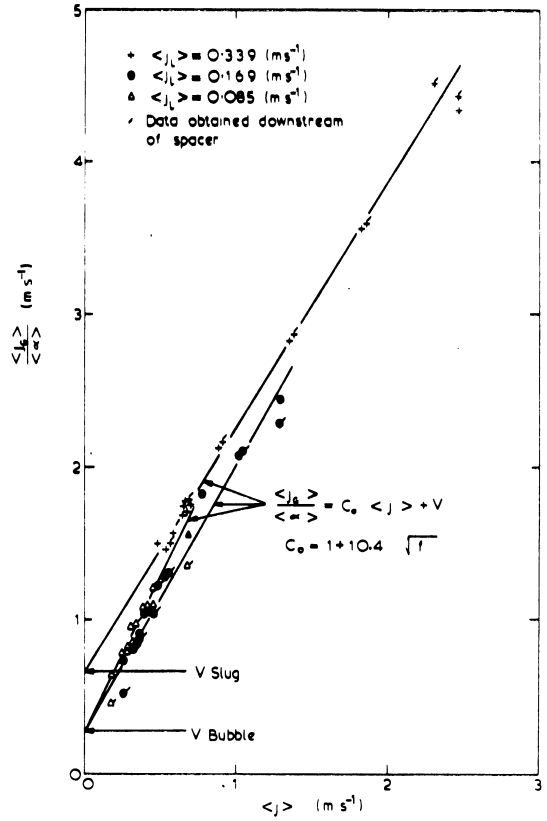

Figure 11. Bubble flow voidage data for 17 mm equivalent dia., rod cluster.

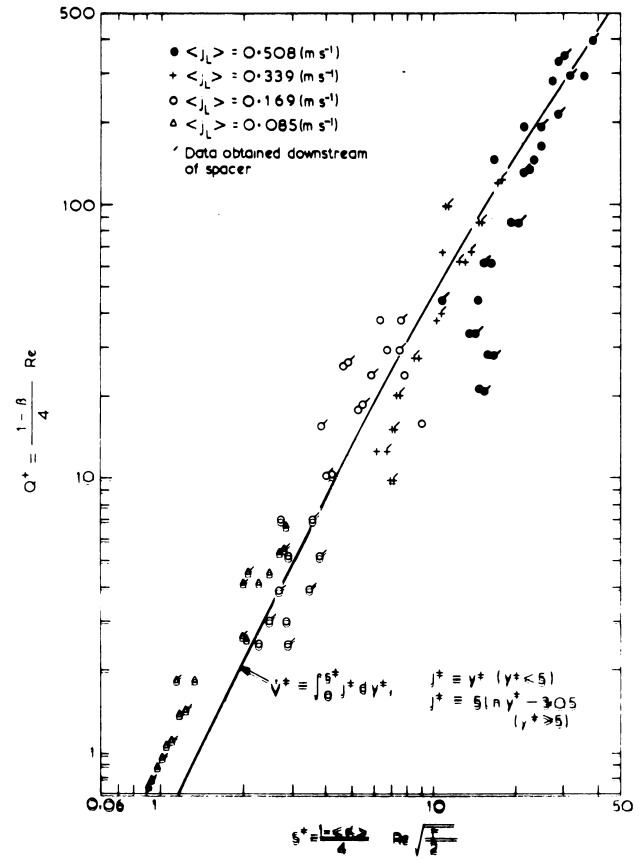

Figure 12. Annular flow voidage data for 17 mm equivalent dia., rod cluster, with $f = 0.006$ and $Re = D_e G/\mu_L(1 + 2.5\beta)$.

"universal" velocity profile being valid within the film, but that deviations from the "universal" profile occur in the core region, such that $f \sim 0.006$ for the flow conditions of figure 12.

COMPARISONS WITH OTHER TWO-PHASE FLOW ROD CLUSTER DATA

Data on average void fraction from relatively low pressure systems (Condon & Sher 1962, Muchiyoshi & Serizawa 1970, Moussez *et al.* 1965) have characteristics similar to those obtained here, with strong mass-flux effects and negative drift-velocities at low voidages, and at high voidages have constant drift-velocities and distribution parameters consistent with [10] ($m = 0$). The results from Moussez *et al.* (1965) are particularly interesting: as in the case here, a test section modification (the introduction of swirlers rather than the bowing used in this work) produced changes in friction characteristics but no discernible changes in average voidage characteristics. However, with at least one exception (Sher *et al.* 1965), which behaves as above, high pressure steam–water distributed flow data for average void fraction (Agostini *et al.* 1971, Schoneberg 1968, Nylund *et al.* 1967–70) behave differently, corresponding to developed bubble-flow behaviour, with C_0 given by [10] ($m = 0$) and drift velocity by [15]. High pressure, low voidage, two-component flows (Alia *et al.* 1968*a*, *b*, Colombo *et al.* 1967) have values of the distribution parameter which also are consistent with [10] ($m = 0$).

Only limited data are available in the literature on two-phase flow structure in rod bundles. Low voidage, local void fraction and velocity data for diabatic steam–water flow in a seven-rod cluster (Bosio & Imset 1973) have similar trends to the data presented here. Detailed data have been reported by Schraub *et al.* (1969) for annular air–water flow in a nine-rod cluster. As with the present experiments, the shroud surface appears to influence the flow more strongly than the rod surfaces. Rod-cluster voidage profiles obtained from radiation attenuation methods (Condon & Sher 1962, Sher *et al.* 1965, Nylund *et al.* 1967–70) are necessarily only semi-local, and cannot be readily compared with the present data. Nevertheless, it is of interest that such local voidage data (Sher *et al.* 1965), both near rods and near the shroud, are consistent with [7].

Friction factor data for low voidage flows through rod clusters generally correspond to the $(0, -2, a)$ friction regime (Beattie 1979) as found here. However, several exceptions have been noted (Beattie 1979), and it is interesting that some data from the 17 mm equivalent dia., cluster arrangement are consistent with $f(1, 0, a)$ since low quality steam–water data which deviate from $f(0, -2, a)$ often agree with $f(1, 0, a)$: for example, data from the 3.64 mm annulus used by Tarasova *et al.* (1966) and Klyushnev & Tarasova (1966) appear to have a substantial amount of scatter, but this is because some are consistent with $f(1, 0, a)$ and the rest with $f(0, -2, a)$; also, all the data for annulus 140 A of Adorni *et al.* (1965) provide another example. With regard to the $f(1, 0, a)$ data of figure 8, there were no obvious differences in operating conditions for these data. In fact, some points represent non-repeatability for nominally identical conditions.

In general, friction data for high voidage flows through rod clusters have been found to depend on surface tension rather than viscosity, in a friction factor/Weber number relation which depends on a number of duct geometry factors, including details of the rod spacers (Beattie 1979). However, this is not the case here where $f(0, -2, a)$ applies for the 42 mm cluster and $f(-2, -6.5, c)$ for the 17 mm cluster.

CONCLUSIONS

Experiments with air–water flows through seven-rod clusters have provided data on local velocity and voidage distribution, friction factors and average voidage. These data are consistent with a mixing-length concept developed for two-phase flow in round tubes and applied to rod cluster assemblies by using the equivalent diameter concept.

Bowing of a rod cluster resulted in a decrease of ~ 10 per cent in two-phase friction loss, even though secondary flows appear to play a stronger role in two-phase flows than in single phase flow. There was no discernible effect on average voidage.

The presence of rod spacer grids can result in flow characteristics consistent with non-developed flow conditions. Single phase pressure loss coefficients of rod spacer elements are applicable to two-phase flow conditions for the appropriate Reynolds numbers.

Acknowledgments—The assistance of Mr. C. Evans with the experimental work and preliminary analysis is gratefully acknowledged.

REFERENCES

ADORNI, N., GASPARI, P. G., GERMANI, G., PETERLONGO, G., RAVETTA, R. & ZAVATTARELLI, R. 1965 Heat transfer crisis with steam-water mixtures in complex geometries: experimental data in annuli and clusters. CISE-R-123.

AGOSTINI, G., PREMOLI, A., PRINCE, A., RAVETTA, R. & RUBIERA, L. 1971. Density of steam-water mixtures flowing in 19-rod clusters under adiabatic and heated conditions. CISE-R-309.

ALIA, P., CRAVAROLO, L., HASSID, A. & PEDROCCHI, E. 1968a Two-phase (gas + liquid) adiabatic vertical upflow: a preliminary study with a rod cluster geometry. CISE-R-108.

ALIA, P., COLOMBO, A., HASSID, A., PREMOLI, A. & SPADONI, B. 1968b Measurements of liquid volume fraction for adiabatic two-phase two-component mixtures flowing in annular and rod cluster channels. CISE-R-186.

BEATTIE, D. R. H. 1972 Two-phase flow structure and mixing-length theory. *Nucl. Engng Des.* **21**, 46–64.

BEATTIE, D. R. H. 1973 A note on the calculation of two-phase pressure losses. *Nucl. Engng Des.* **25**, 395–402.

BEATTIE, D. R. H. 1976 Pressure pulse and critical flow behaviour in distributed gas–liquid systems. Paper D3, *Proc. 2nd Int. Conf. Pressure Surges*, BHRA Fluid Engng, Cranfield, U.K.

BEATTIE, D. R. H. 1977 Some aspects of two-phase flow drag reduction. Paper D1, *Proc. 2nd Int. Conf. Drag Reduction*, BHRA Fluid Engng, Cranfield, U.K.

BEATTIE, D. R. H. 1979 Two-phase pressure loss and void fraction characteristics in rod bundle geometries. Paper in *18th Cong. Int. Assoc. Hydraulic Research*, Cagliari, Italy.

BOSIO, J. & IMSET, O. R. 1973 Two-phase flow investigations in a seven-rod bundle. Paper 31, *Int. Meeting on Reactor Heat Transfer*, Karlsruhe.

COLOMBO, A., ERA, A., HASSID, A., PREMOLI, A., SPADONI, B. & ZAVATTARELLI, R. 1967. Density measurements with two-phase mixtures in adiabatic and heated channels at high pressure by means of a quick closing valve method. CISE-R-225.

CONDON, R. A. & SHER, N. C. 1962 Measurement of void fraction in parallel rod arrays. *Nucl. Sci. Engng* **14**, 327–338.

GRIFFITH, P. 1964 The prediction of low quality boiling voids. *J. Heat Transfer* **86**, 327–333.

HERRINGE, R. A. & DAVIS, M. R. 1974 Detection of instantaneous phase changes in gas–liquid mixtures. *J. Phys. E.* **7**, 807–812.

HOANG, K. & DAVIS, M. R. 1977 Void, velocity and bubble size distributions for two-phase flow in 180° pipe bends. Univ. NSW Rep. 1977/FMT/4.

HOOPER, J. D. 1975 The calculation of fully developed turbulent and laminar single phase flow in four-rod subchannels. AAEC/E351.

KLYUSHNEV, V. E. & TARASOVA, N. V. 1966 Hydraulic resistance to steam-water flow in annular channels. *Thermal Engng* **13**, 118.

MOUSSEZ, C., ROSUEL, A., SOURIOUS, G., DU BOUCHERON, G. & EIDELMAN, D. 1965 Ecoulements giratoires dans l'eau bouillante. EUR 1785.

MUCHIYOSHI, I. & SERIZAWA, A. 1970 Steam volume fraction in two-phase flow (111), rod bundle geometry. *J. Nucl. Energy Soc. Japan* **12**(6), 311–316.

NYLUND, 0., BECKER, K. M., EKLUND, R., GELIUS, O., HAGA, I., HANSSON, P. T., HERNBORG, G. & AKERHIELM, F. 1967 Measurements of hydrodynamic characteristics, instability thresholds,

and burnout limits for six-rod clusters in natural and forced circulation. ASEA–AB Atomenergi Rep. FRIGG–1.

NYLUND, O., BECKER, K. M., EKLUND, R., GELIUS, O., HAGA, I., HERNBORG, G., ROUHANI, Z. & AKERHIELM, F. 1968 Hydrodynamic and heat transfer measurements on a full scale simulated 36–rod Marviken fuel element with uniform heat flux distribution. ASEA–AB Atomenergi Rep. FRIGG–2.

NYLUND, O., BECKER, K. M., EKLUND, R., GELIUS, O., HAGA, I., JENSEN, A., MALNES, D., OLSEN, A., ROUHANI, Z., SKAUG, J. & AKERHIELM, F. 1969 Hydrodynamic and heat transfer measurement on a full-scale simulated 36-rod Marviken fuel element with non-uniform radial heat flux distribution. ASEA–ATOM Rep. FRIGG–3.

NYLUND, O., BECKER, K. M., EKLUND, R., GELIUS, O., HAGA, I., JENSEN, A., MALNES, D., OLSEN, A., ROUHANI, Z., & AKERHIELM, F. 1970 Hydrodynamic and heat transfer measurements on a full-scale simulated 36-rod BHWR fuel element with non-uniform axial and radial heat flux distribution. ASEA–ATOM Rep. FRIGG–4.

SCHONEBERG, E. 1968 Stability studies for boiling water reactors. EURAEC 2092.

SCHRAUB, F. A., SIMPSON, R. L. & JANSEN, E. 1969 Air–water flow structure data for a round tube, concentric and eccentric annulus, and nine-rod bundle. General Electric Rep. GEAP 5739.

SHER, N. C., KANGAS, G. J. & NEUSEN, K. F. 1965 On the phenomenon of boiling flow in a parallel rod array. *Chem. Engng Prog. Symp. Ser.* **61**, 127–156.

TARASOVA, N. V., LEONTIEV, A. I., HLOPUSHIN, V. I. & ORLOV, V. M. 1966 Pressure drop of boiling subcooled water and steam–water mixture flowing in heated channels. Paper 133, *Proc. 3rd Int. Heat Transfer Conf.*, Vol. 4, pp. 178–183.

TONG, L. S. & WEISMAN, J. 1970 *Thermal Analysis of Pressurised Water Reactors.* American Nuclear Society, Hinsdale, Il.

ZUBER, N. & FINDLAY, J. A. 1965 Average volumetric concentration in two-phase flow systems. *J. Heat Transfer* **87**, 453–468.

EUROPEAN TWO-PHASE FLOW GROUP MEETING
EINDHOVEN UNIVERSITY OF TECHNOLOGY
2ND to 5TH JUNE 1981

HYDRODYNAMIC REGIME CHANGE EFFECTS ON CRITICAL HEAT FLUX CHARACTERISTICS

by

D. R. H. Beattie
Australian Atomic Energy Commission
Private Mail Bag, Sutherland 2232,
Australia*

ABSTRACT

Critical heat flux characteristics depend on flow regime. Limiting quality crises, minima in crisis characteristics, and upstream dryout are caused by discontinuities in critical heat flux characteristics due to a pre-crisis regime change. The regime change quality, and hence the quality at the above crisis effects, may be predicted from pre-crisis shear stress characteristics.

* Work performed while attached to Engineering Sciences Division, AERE Harwell, UK.

CONTENTS

		Page No.
1.	INTRODUCTION	1
	1.1 The Limiting Quality Phenomenon	2
	1.2 Minima in Exit Crisis Characteristics	3
	1.3 Upstream Dryout	3
2.	PRE-CRISIS REGIME CHANGE EFFECTS ON CRITICAL HEAT FLUX	4
	2.1 The Limiting Quality Phenomenon	4
	2.2 Minima in Exit Crisis Characteristics	5
	2.3 Upstream Crisis	5
3.	PRE-CRISIS REGIME CHANGE MECHANISM	6
4.	SHEAR STRESS CHARACTERISTICS	7
	4.1 General	7
	4.2 CISE Diabatic Friction Factor Data	9
5.	DATA ANALYSIS	11
	5.1 Limiting Quality Data	11
	5.1.1 CISE limiting quality data	11
	5.1.2 East European limiting quality data	12
	5.2 Minima in Exit Crisis Characteristics	13
	5.3 Upstream Dryout	14
6.	DISCUSSION	14
7.	CONCLUSIONS	21
	NOTATION	23
	REFERENCES	24

CONTENTS (continued)

Page No.

TABLES

Table 1	CISE Limiting Quality Crisis Data, Viscosity According to Equation (6)	28
Table 2	CISE Limiting Quality Crisis Data, Viscosity According to Equation (5)	30
Table 3	CISE Steady Flow Heat Transfer Crisis Data with Minima	31
Table 4	Ispra [43-45] Limiting Quality Crisis Data	32

1. INTRODUCTION

The view that thermohydraulic characteristics of two-phase flow are flow-regime dependent is becoming more prevalent [1]. With regard to critical heat flux, this viewpoint is implicit in current calculation methods and models of the phenomenon. Low quality crises are considered as examples of departure from nucleate boiling caused by bubble coalescence inducing vapour blanketing of the heated surface, and tend to be regarded as being limited to bubbly and similar flows. Higher quality crises are associated with the drying out of the liquid film of annular flow. Applicability limits of different calculation methods can be loosely associated with regime boundaries.

Examination of any regime-dependent aspects of critical heat flux characteristics requires detailed consideration of the nature of two-phase flow regimes. Since regime boundaries are studied because of the supposed regime-dependency of flow characteristics, the most appropriate approach to regime boundary determination is to associate boundaries with changes in the nature of flow characteristics of practical interest.

Although this approach differs from the current main stream of two-phase flow regime boundary research, it has been followed for some years at the Australian Atomic Energy Commission [2,3], where shear stress characteristics have been used as a basis for regime definition. Regime boundaries so determined do not necessarily coincide with conventionally defined boundaries. They are, however, more appropriate to shear stress evaluation. Moreover, detailed study [4] has indicated that they are also appropriate for the evaluation of void fraction and other two-phase characteristics.

The above concept of flow regime has also been applied to the interpretation of critical heat flux characteristics [5]. In that work, it was demonstrated that different regions of critical heat flux: quality curves could be associated with different friction regimes, with a crisis occurring at the boundary between a particular friction regime and the dry wall flow friction regime.

Further analysis of critical heat flux data has since indicated that, although separate regions of critical heat flux curves can often be associated with a transition between a particular friction regime and dry

wall flows, this is not always so. In this paper, the exceptions are considered not in terms of a transition between a particular pre-crisis friction regime and the dry wall regime, but, instead, in terms of a transition between two pre-crisis regimes.

As with the earlier work [5], the present analysis associates each pre-crisis regime with particular heat transfer crisis characteristics, effectively defining the boundary between the pre-crisis regime and the dry wall regime.

The present work also considers effects of pre-crisis hydrodynamically induced regime changes on critical heat flux characteristics. As with the concepts described in [5], such a regime change requires a change in the form of critical heat flux characteristic, and the underlying concept of the present work is that any regime-change induced transition from one type of critical heat flux curve to another may be discontinuous. It is proposed here that discontinuities of this type give rise to three types of crisis characteristic described below. The exact mechanism giving rise to the characteristics is discussed following this description of crisis characteristics examined in this work.

1.1 The Limiting Quality Phenomenon

There are several sets of critical heat flux data which conform to the general trend shown in Figure 1, which shows critical heat flux ϕ_{CHF} plotted against exit, or crisis, quality x_{cr}. The critical quality x_{cr} is, within data scatter, independent of critical heat flux (or approximately so) in the region BC, and crises occurring at this quality are referred to as 'crises of the second kind' in Eastern European literature [6-13], where the phenomenon was first investigated in the mid-1960's, in order to differentiate between higher heat flux, more frequently encountered 'crises of the first kind' represented by the line AB in Figure 1. The more descriptive 'limiting quality phenomenon' tends to be preferred in Western work [14-16]. In the present work, the limiting quality will be denoted by x_{lim}.

More detailed descriptions of the phenomenon, postulated mechanisms, etc., are given in the review of [14]. The discussion of that work need not be repeated here. It is, however, pertinent to note that the phenomenon is

disputed by some researchers, e.g. [16], and that, even if accepted, there appears to be some controversy concerning its role [17]. Also, it is often claimed, e.g. [16], that data consistent with the phenomenon tend to be primarily associated with two-phase inlet conditions to heated sections. Data examination performed as part of the present study indicated that this is not the case for data from either Western, e.g. [18], or East European, e.g. [19], sources. The phenomenon is, in fact, unaltered by a transition from positive to negative inlet quality conditions, e.g. Table 1/37 of [20].

1.2 Minima in Exit Crisis Characteristics

Although critical heat flux generally decreases monotonically with increasing enthalpy, it may increase under conditions of high mass flux, e.g. [21-25], or swirl, e.g. [25-28], giving rise to minima in the exit crisis characteristics. An idealised representation of such behaviour is presented in Figure 2. The quality at the minimum position, point B, will be denoted here as x_{min}.

The minima considered here are not those which may occur near zero inlet quality when data are presented in terms of inlet, not exit, enthalpy. Such minima occur at low mass fluxes and are widely recognised as being associated with pulsations in the flow, e.g. [29]. The minima considered here are for steady conditions, and, as stated, tend to occur at high, not low, mass fluxes.

1.3 Upstream Dryout

Regions of exit crisis characteristics where exit critical heat flux increases with exit crisis quality, as described above, allow the possibility of a crisis first occurring at some position upstream of the exit, even for uniform heat flux being applied to the test section under consideration. Such upstream crises, associated with minima in exit characteristics, have been observed [21-26]. The local crisis quality at the upstream crisis position will be referred to here as x_{ud}.

Related to upstream crises are distributed crises, where a crisis does not occur at a particular position in a heat section but instead occurs simultaneously over a region. High mass flux distributed crises are

reported in [21,22].

2. PRE-CRISIS REGIME CHANGE EFFECTS ON CRITICAL HEAT FLUX

We consider here a regime change which, for a given test section, pressure, and mass flux, occurs at a quality denoted by x_{Tr}. This regime-change quality is considered at this stage as being independent of heat-flux. The validity of this assumption, and the exact mechanism by which the regime change is induced, is discussed later.

The relation between the supposed regime change and the three types of crisis characteristic outlined in the previous section is discussed below.

2.1 The Limiting Quality Phenomenon

Reconsidering Figure 1, it can be seen that, in terms of the present concepts, region AB of the crisis curve is that component of the curve corresponding to the lower quality regime and, on regime change, the characteristics change to those represented by CD.

The relation between the regime change quality x_{Tr} and the limiting quality x_{lim} is, quite simply, that they are the same. That this is so and that the region BC appears as part of the crisis curve can be seen as follows: consider an operating characteristic

$$x_{out} = x_{in} + \frac{4 \phi L}{G D \lambda} \qquad (1)$$

which intersects BC. At a quality $x_{Tr} - \delta$ near x_{Tr} on the characteristic, conditions are pre-crises since the regime is such that the crisis is determined by region AB of the curve. A slight increase in power raising the exit quality beyond x_{Tr}, i.e. inducing a regime change, will place the exit at a condition which, under equilibrium conditions, is post-crisis, since the crisis limit for the new regime has been changed to section CD of the curve. A crisis will thus be induced. The assumed independence of x_{Tr} on heat flux thus gives rise to heat flux-independent crises at x_{Tr}, i.e. $x_{lim} \equiv x_{Tr}$.

2.2 Minima in Exit Crisis Characteristics

The previous section considered a regime transition such that the higher quality regime had lower heat flux crisis characteristics. Flow conditions where the high quality regime has higher heat flux crisis characteristics give rise to minima in the exit characteristics:- exit qualities near but less than x_{Tr} will be limited by lower critical heat fluxes than qualities near but greater than x_{Tr}. The transition from one critical heat flux curve to the other does not occur at a heat flux independent curve at x_{Tr}, as was the case with the limiting crisis, since the form of operating characteristic prevents this.

Reconsidering Figure 2, AB represents the lower quality regime crisis limit, and CD represents the higher qualities regime limit. Operating characteristics with exit quality less than the regime change quality x_{Tr} will be limited by the curve AB, and those with higher exit qualities will be limited by CD. The transition thus occurs at an exit quality equal to x_{Tr} but with heat flux slightly less than the limit at B on curve AB.

The curve of Figure 2 is thus made up as follows: AB represents the lower quality regime critical heat flux limit, the minimum at B is such that x_{min} coincides with the regime transition x_{Tr}, BC is a section of that operating characteristic which meets AB at B, and CD is part of the higher quality regime heat transfer crisis curve.

In terms of the idealised model presented here, critical heat flux data plotted as inlet enthalpy will have a step increase when the exit conditions coincide with the minimum in the heat flux: exit quality curve. Additional variables, such as heated length, are thus necessary to specify the enthalpy at the step change in the critical heat flux:. inlet enthalpy curve.

2.3 Upstream Crises

Concepts described above for minimum exit crisis characteristics were confined to the exit only. Applying the same concepts to any point in a heated test section, it can be seen that, for exit qualities greater than x_{Tr}, the local position in a heated section at qualities near to but less than x_{Tr} are more likely to reach critical conditions than

positions near this but with local qualities slightly greater than x_{Tr} if the lower quality regime has a lower heat flux limit.

Thus, conditions where minima in exit characteristics may occur also allow the possibility of crises first being initiated at an upstream position. Local upstream crises qualities x_{ud} should be identical to the quality at which exit characteristics are minimum, x_{min}, since both can be identified with the regime change quality x_{Tr}.

3. PRE-CRISIS REGIME CHANGE MECHANISM

The regime transition criterion considered here is that postulated in [3]: a transition occurs such that there is no discontinuity in entropy production rate. Entropy production is due primarily to flow redistribution on regime change; shear stress and viscous dissipation; and heat transfer effects. In the special case of a direct change from pre-crisis to dry wall conditions, entropy production considerations suggest that there is some trade-off between the reduced shear stress on reaching dry wall conditions and the increased wall temperature. Higher wall temperatures obtained by increasing heat flux thus cause a transition at lower qualities to induce larger step-decrease in wall shear, thus explaining the negative critical heat flux: critical quality slope usually encountered [5].

The present work, however, considers an indirect transition to crisis conditions via a pre-crisis transition for the limiting quality phenomenon, and also considers pre-crisis transitions in relation to upstream crises and minima in exit characteristics.

Since wall temperature changes and flow redistribution occurring at pre-crisis regime transitions can be expected to be small, it follows that changes in shear stress at these transitions will also be small. Knowledge of shear characteristics for regimes on both sides of the transition can thus be used to predict the transition, since, for reasons given, the transition will occur when the shear stress for both regimes is the same.

The quality at transition, x_{Tr}, which has been identified above with the limiting quality x_{lim} for the limiting quality phenomenon; with the quality where minima may occur in exit characteristics x_{min}; and with local upstream dryout qualities x_{ud}, can thus be predicted from

knowledge of shear characteristics for relevant pre-crisis regimes. Shear stress characteristics related to this are discussed below.

4. SHEAR STRESS CHARACTERISTICS

4.1 General

In this section, shear stress characteristics for two pre-crisis regimes are discussed. The transition between these regimes is that transition which gives rise to the particular crisis characteristics discussed above. For simplicity, discussion, and later data analysis, is confined to round tube geometries.

As with single phase flow, friction characteristics are largely determined by the nature of the flow in the boundary region near the tube wall. The regimes of interest are associated with a boiling (i.e. wall nucleation) sublayer and a diabatic non-boiling flow.

The non-boiling flow is necessarily of annular structure, with phase change occurring by evaporation at the film/core interface. Heat transfer crises are due to film dryout. As with single phase flow, the friction factor $f = 2\,\tau_w/(\rho_h\, v^2)$ is determined by the viscous sublayer, and a dependence on Reynolds number results [4]:

$$f = f\,(Re) \qquad (2)$$

$$\text{with } Re = D\,G/\mu \quad . \qquad (3)$$

The viscosity definition depends on the structure of the sublayer. For annular flow with no entrained bubbles,

$$\mu = \mu_l\,(1 - \beta) + \mu_g \beta \quad ; \qquad (4)$$

for a bubbly film with no bubble surface movement,

$$\mu = \mu_l\,(1 + 2.5\,\beta) \quad ; \qquad (5)$$

and for a bubbly film where bubble surface movement can occur

$$\mu = \mu_l \left[1 + \frac{2.5\,\mu_g + \mu_l}{\mu_g + \mu_l}\,\beta \right] . \qquad (6)$$

Equation (5) is based on the work of Einstein [30], who considered the viscosity of a liquid containing solid spheres. Equation (6) is based on the work of Taylor [31], who adapted Einstein's model to allow for viscous dissipation within bubbles. Ideally, equation (6) should apply to a bubbly system, but, as has been pointed out elsewhere [4], the polar molecules of liquids usually encountered in two-phase systems encourages impurities to concentrate on bubble interfaces, thus preventing surface movement, with the consequence that the viscosity is usually best described by equation (5).

Whereas the above considerations generally apply to adiabatic systems, an additional factor comes into play with diabatic flow. This factor arises because bubbles formed in the lower quality boiling region of a heated section require some time before liquid contaminants migrate to the bubble interfaces. If this time is long compared with the transport time through the heated section, the viscosity of a bubbly film in any non-boiling region may be consistent with equation (6) instead of equation (5). Thus, non-boiling diabatic annular flows with bubbly films may have friction characteristics of the same form as for adiabatic flows but in which the viscosity is given by equation (6) instead of equation (5), particularly at higher velocity conditions.

In the case of boiling flows, the flows may be either of annular, semi-annular, or bubbly structure, although the transition to non-boiling diabatic annular flows is envisaged to occur at conditions when the boiling sublayer is within the film region of an annular flow. Heat transfer crises are due to departure from nucleate boiling, and the friction factor is related to the Weber number

$$We = G^2 D/(\rho_h \sigma) , \qquad (7)$$

$$f = f(We) . \qquad (8)$$

This is because boiling bubbles act as wall roughness elements which detach when they are sufficiently large for shearing forces to overcome surface tension holding them to the wall [32]. The effective roughness height - and this determines the friction factor for rough wall flows - is thus determined by a Weber number criterion.

Applying the above to previous concepts, regions AB of Figures 1 and 2 correspond to departure from nucleate boiling, and have friction factors of the form f = f (We); regions CD of the figures correspond to dryout and have friction factors of the form f = f (Re); the transition between the boiling and non-boiling regions is given by

$$f = f(We) = f(Re) ; \qquad (9)$$

and the quality at which this occurs, x_{Tr}, can be identified with the x_{lim}, x_{min} and x_{ud} components of heat transfer crisis characteristics.

It follows from the above that local conditions corresponding to limit quality crises; minima in crisis characteristics; and upstream crises should correlate on the Re : We plane with the correlating curve being obtained from friction factor characteristics as per equation (9).

4.2 CISE Diabatic Friction Factor Data

The preceding discussion indicates that adequate testing of the present model of limiting quality crises, minima in crises characteristics, and upstream dryout can best be achieved by considering critical heat flux data showing these characteristics and which also have pressure drop data from which friction factor characteristics can be also obtained. The only critical heat flux data found showing trends relevant to this present work and which have associated pressure gradient data were obtained at CISE laboratories [20,28,32-38].

Much of the pressure gradient data have already been analysed in terms of the present friction factor: Weber number or friction factor: Reynolds number concepts [4,32]. In the case of diabatic flows, which are of special interest here, it has been shown elsewhere [2] that for symmetric heat flux profiles, the average pressure gradient between pressure taps is approximately identical to the mid-point gradient if the flow regime does not change between pressure taps and the friction factor does not increase strongly with quality (the assumption is less severe for friction factors which decrease with increasing quality) and/or the quality increment between pressure taps is small. Diabatic data can thus often be used to obtain mid-point gradients at mid-point qualities, i.e. local instead of integrated

friction factors.

With regard to Weber number dependent friction factors, a tentative correlation of CISE data has been presented previously [4]. This equation is not consistent with constraints suggested later [32]. Adjusting coefficients to produce consistency with the constraints results in

$$1/\sqrt{f} = 16 \log We\ f - 13.4 , \qquad (10)$$

which is close to the form originally proposed [4] over the range of Weber numbers encountered in the data analysed.

Equation (10) is compared with some CISE diabatic friction factor data in Figure 3.

Friction factor data analysed as part of the present work indicated that much of the higher quality diabatic data depended not on Weber number but, instead, on Reynolds number. Non-recognition of this fact produced scatter on the earlier friction factor: Weber number correlation [4], and was in fact the prime cause of coefficients in the earlier correlation differing from those in equation (10).

Earlier work [4] indicated that higher quality adiabatic friction factor data were consistent with

$$1/\sqrt{f} = 16 \log Re\ \sqrt{f} - 40.1 \qquad (11)$$

with Re involving viscosity as given by equation (5). It might be expected that this equation would also apply to non-boiling diabatic flows at similar conditions. This was found to be so, except that the viscosity generally needed to be replaced by the definition given by equation (6), a situation not unexpected in view of the discussion following equation (6). The applicability of this viscosity, instead of that given by equation (5), is equivalent to a reduction of pressure gradient by about 25%. Some typical diabatic Reynolds number dependent data are compared with equation (11) in Figure 4.

A very small fraction of diabatic Reynolds number dependent data were found to agree with the adiabatic correlation, i.e. equation (11), with

viscosity defined by equation (5). Some such data are shown in Figure 5.

From previous discussion, the regime change between the boiling and non-boiling diabatic flow regimes should occur when

$$1/\sqrt{f} = 16 \log We\ f - 13.4 = 16 \log Re\ \sqrt{f} - 40.1 . \qquad (12)$$

This can be considered as a relation between We and Re at the regime boundary.

5. DATA ANALYSIS

5.1 Limiting Quality Data

5.1.1 CISE limiting quality data

As stated, CISE data were considered in depth because of the availability of pressure gradient data associated with heat transfer crisis data, the two being necessary for a full test of the present model.

Critical heat flux data connected with low mass flux, pulsating conditions, i.e. with minima in heat flux: inlet enthalpy plots, were removed. Of the remaining data, those consistent with the limiting quality phenomenon were analysed and conditions where limiting quality crises occurred were tabulated. Some examples could very clearly be regarded as limiting crises; other examples were less clear because of the combination of data scatter and the comparatively narrow heat flux range of the (possible) limiting quality region. Nevertheless, all such data were tabulated, and then were plotted in the Re (viscosity given by equation (6)): We plane.

Most of the data correlated on two separate curves. One of these correlations was close to equation (12), which is the correlation predicted by the model. These data are shown in Figure 6. Although a better correlating curve can be postulated, equation (12) is not in serious disagreement with the data. Limiting quality conditions for the data shown in Figure 6 are listed in Table 1.

The second set of data which correlated on the Re : We plane were replotted but with Reynolds number based on viscosity as defined by equation (5). With this definition, these data also agreed with equation (12). These data are compared with equation (12) in Figure 7. Limiting quality conditions for the data of Figure 7 are listed in Table 2.

The separation of CISE limiting quality data into two groups, each consistent with the model prediction (equation (12)) but requiring different viscosity definitions is consistent with the previous observation that CISE non-boiling diabatic pressure gradient data could be separated into two groups, each consistent with equation (11) but requiring the same two different viscosity definitions.

The above analysis indicates that the suggested relation between pressure loss data and the limiting crisis phenomenon is supported by CISE data. The confirmation is, however, incomplete: although the CISE data as a whole contains a considerable number of limiting quality crises; considerable Weber number dependent friction factor data; and considerable Reynolds number dependent friction factor data, all of which are necessary to adequately confirm the model, very few individual sets of data contain sufficiently extensive examples of all three types of data. According to the present model, this is because the nature of the limiting crisis phenomenon is such that its onset prevents the region of Reynolds number dependent shear coming into existence.

Some data sets do, however, contain such shear data in the low heat flux range; and also higher heat flux Weber number dependent shear data and limiting crises data. These data sets allow direct confirmation of the model. CISE data obtained with test section 58C [34,36] are shown in Figure 7. The data are consistent with all aspects of the model.

5.1.2 East European limiting quality data

As noted, the limiting quality phenomenon was first examined during East European research. Several sets of tables of limiting quality conditions for 8 mm tubes have been produced [7-13] and these have been used in the present analysis instead of the actual data. As the tables involve some interpolation, some spot checks were performed on typical East European limiting quality data to confirm that the tables do in fact reflect the

data. Some disagreement exists between some tables. This presumably reflects both data scatter and disagreement between data from different sources. The most recent table [13] in fact presents limiting quality ranges rather than values for different conditions, thus acknowledging the inability of specific values to accurately represent all data. (The ranges given are consistent with the data scatter in Figures 6 and 7.)

In order to minimise data scatter, emphasis in this work was placed on tables presented by Doroschuk and his co-workers [7-10]. These cover a wide range of conditions and presumably are weighted towards data from one source (the All-Union Heat Energy Institute, VTI, of Doroschuk and his co-workers) and hence presumably contain a large degree of internal consistency.

These data were plotted in the Re : We plane. At low pressures, data correlated if the Reynolds number was based on viscosity as defined by equation (4). These data are shown in Figure 9.

Higher pressure data correlated using viscosity defined by equation (5) or equation (6). Ispra data, discussed later, suggest that equation (6) is probably more appropriate to the data. The correlation based on this definition is shown in Figure 10.

Although internally self consistent, and also generally compatible with the present model, neither the low or high pressure correlation agrees with the trends shown in the CISE data (Figures 6, 7 and 8). In the absence of pressure loss data associated with the data of Figures 10 and 11, which could be used to predict a correlating equation (as was done with the CISE data), the correlating equations of Figures 9 and 10 are simply lines of best fit.

5.2 Minima in Exit Crisis Characteristics

As stated in the introduction, various data of this type have appeared in the open literature [21-28]. Data from different sources appear to be incompatible when examined in terms of the present model, a fact which may reflect different shear characteristics (these usually not being available) for data from different sources. Furthermore, only one set of data, discussed below, was sufficiently extensive for meaningful data analysis in terms of presentation of data in the Re : We plane.

CISE data with minima in exit crisis characteristics were collected as part of the exercise in which limiting quality crisis data were collected. Most of the CISE showing minima were obtained from swirl flow tests. Data correlated with equation (12) when plotted on the Re (viscosity given by equation (5)): We plane (Figure 11). The swirl involved with the tests meant that pressure gradient data presented with the crises data could not be readily reduced. However, non-swirl diabatic pressure drop data from the same test section indicate that equation (11), which gives rise to equation (12), describes the data if viscosity is given by equation (5), thus indirectly confirming the viscosity form of Figure 11. These pressure gradient data have already been presented as Figure 5.

Conditions for the data shown in Figure 11 are listed in Table 3.

5.3 Upstream Dryout

As with data containing minima in exit crisis characteristics, insufficient data were found for meaningful data analysis in terms of concepts of the present model.

Upstream crisis data [20-26] were, however, consistent with one aspect of the model: there is a tendency for upstream crises to occur at a quality close to that where exit characteristics reach a minimum. Some examples, from [23], are shown in Figure 12.

6. DISCUSSION

A hydrodynamically based pre-crisis regime change mechanism has been postulated as being responsible for three types of crisis characteristics. Relevant data are qualitatively, and, when data are such that a full test of the model can be made, quantitatively consistent with the model. There are, however, several features of the model and the data analysis that deserve detailed discussion.

The present work suggests that the limiting quality phenomenon, and the phenomenon of minima in exit crisis characteristics together with possible upstream dryout, although different in nature, can be regarded as different manifestations of the one phenomenon - a simple pre-crisis regime change. The two different ways which the regime change can influence crisis

characteristics depend on the relative magnitude of departure from nucleate boiling and dryout heat fluxes at the regime transition: a lower (higher) dryout heat flux results in limiting quality crises (a minimum in the exit characteristics) at the regime boundary.

Even without a full understanding of departure from nucleate boiling and dryout, the fact that the first can be assumed to be dominated by the local heat flux and the latter by the total section power required to remove the liquid film allows a simple qualitative picture to be developed for conditions when limiting crises or exit crises minima may or may not occur.

For a given flow and inlet quality, the power to reach the regime boundary quality remains constant, so a long (and hence low heat flux) section will be less likely to reach the departure from nucleate boiling limit than a short tube. Thus, long tubes are more likely to have limiting quality crises, and short tubes minima in exit crisis characteristics. In a similar manner it can be seen that limiting quality crises will occur at lower mass fluxes and minima in exit crisis characteristics at higher mass fluxes. Swirl flow is not likely to have a strong effect on departure from nucleate boiling heat flux, but, because of droplet deposition induced by swirl, will cause a higher power to be required for film dryout. Minima in exit characteristics are therefore more likely under swirl conditions. These qualitative considerations are consistent with empirical observations. Support for this type of reasoning comes from the fact that similar arguments provide a picture which is consistent with experimental data from sections with heat flux spikes.

With regard to limiting quality crises, it is sometimes (e.g. [16]) considered that limiting qualities will have a length-to-diameter dependence, and that it is primarily a positive inlet quality phenomenon. The present model and data analysis indicates that this is not so. (A possible indirect length-to-diameter effect may arise through the dependence on viscosity. This will be discussed in more detail below.) Also, the present model contradicts the widely held view [16] that annular flow crises occur only as a consequence of a smooth local reduction of the film flow rate to zero. This is probably so for crises denoted by the term 'dryout' in the present work, but, according to the present model, should not be true for annular flow departure from nucleate boiling or limiting quality crises. It is relevant that several researchers have measured residual film flows or

film thicknesses at annular flow crises conditions [39-41], and these are often of a magnitude that cannot be explained as being caused by residual rivulets in the crisis region.

The phenomena examined here are viewed as a consequence of a pre-crisis friction regime change. Analysis of friction factor data indicates that a second, lower quality friction regime change, also exists. This suggests that a complete heat transfer crisis curve may contain not only one region with one of the phenomena discussed, but also a second similar region.

Additional support for the present model is obtained from qualitative analysis of observed heat transfer characteristics in the vicinity of the heat transfer crisis. Several laboratories have reported local wall temperature decreases in the vicinity of some heat transfer crises. CISE tabulated data indicate if such a decrease did or did not occur with each heat transfer crises, and it has been noted elsewhere [5] that the absence (presence) of a pre-crisis wall temperature decrease appears to be associated with Reynolds number dependent (Weber number dependent) friction factors. It was suggested that the temperature drop could thus be associated with the boiling process. The absence of wall nucleation would thus prevent the phenomenon being observed with Reynolds number dependent flows.

An at least partial explanation of the pre-crisis wall temperature drop phenomenon in the case of limiting quality crises is readily provided by the present model:- the pre-crisis regime transition which precipitates limiting quality crises will cause a change in pre-crisis heat transfer coefficient because of an expected dependence of heat transfer on flow regime. Because of the nature of the model of the crises, such a change in heat transfer coefficient will necessarily occur in the vicinity of the crisis. Thus, observed heat transfer behaviour as well as pressure gradient data supports the present model of limiting quality crises.

Similar arguments applied to crisis data for which minima exit in exit characteristics suggest that any wall temperature drop will be larger and will occur somewhat before the crisis, because the regime change resulting in a changed heat transfer coefficient does not induce a crisis and, further, occurs at a lower quality (corresponding to the minima in the crisis characteristics) than dryout. CISE wall temperature decrease data, as reported for swirl flow experiments [28] (for which minima in crisis

characteristics exist - see Section 5.2) are consistent with this expectation.

Whereas, as described above, heat transfer characteristics qualitatively support the present model for some types of crisis, it should be emphasised that the CISE pressure gradient data provide not only qualitative but quantitative support for the model, as indicated in Figures 6, 7, 8 and 11. It is particularly relevant that the friction factor equations (10) and (11), from which the predictions in Figures 6, 7, 8 and 11 have been derived, have been obtained from previous publications [4,32]. No empirical adjustments of coefficients in the friction factor equations was introduced in order to produce the compatibility of the equations with heat transfer crisis characteristics as suggested by the present model.

It may be noted, however, that the model does not provide the best possible prediction of those heat transfer crises relevant to the model. It can be seen from Figure 6, for example, that although limiting quality crises correlate within data scatter on the Re : We plane, as anticipated by the model, a better correlating curve than that provided by the model can be fitted to the data. A contributing factor to the error may be that the idealised nature of the model could lead to a too approximate quantitative description of phenomena, even if basic concepts behind the model are plausible. The regime transition quality, x_{Tr}, which has been identified here with some crisis characteristics, has been assumed to be given by the intersect of two friction factor equations on the basis that flow redistribution and wall temperature changes can be neglected for pre-crisis friction regime changes in the annular flow pattern, yet, as discussed above, wall temperature changes do occur, even if small. Similarly, flow redistribution can be expected if for no other reason than the regime change postulated implies a cessation of wall boiling. Thus, from the above, a slight heat flux dependence of critical quality for limiting quality crises, for example, can be expected, and a fit of higher heat flux limiting quality data by a constant quality may well coincide with the regime change quality but this will differ slightly from that based on the intersection of the relevant friction factor equations. This could explain the discrepancy between data and prediction in Figure 6. Discrepancies in Figures 7 and 11, which are postulated to be associated with a different form of viscosity for non-boiling diabatic conditions, are smaller. The changed form of viscosity suggests a different level of change

in flow redistribution and wall temperature on regime change (as compared with Figure 6) so a different degree of prediction error can be expected for the idealised regime change model suggested here.

In a similar manner, actual characteristics relating to minima in exit crisis curves and upstream dryout can be expected to differ (but not significantly) from the model outlined in Section 3 if idealised regime change mechanisms are supposed. Relevant data, e.g. Figure 12, support this.

Some comment on the two forms of viscosity required to correlate the CISE data (Figures 6, 7 and 11) is necessary. In Section 4.2 it was indicated that the polar nature of water molecules together with impurities, which are difficult to eliminate, usually lead to a viscosity compatible with equation (5) due to the tendency of impurities to then concentrate on vapour/liquid interfaces. It was also suggested that viscosity as given by equation (6), where viscous dissipation within bubbles can occur, may be appropriate for recently generated bubbles if the time since generation is less than that required for impurities to migrate to the bubble surfaces and so prevent surface movement. If this is correct, equation (5) would be more likely to apply to longer test sections under otherwise nominally similar conditions since bubbles generated in the heated section would then exist for a longer time prior to any exit heat transfer crisis. Examination of flow conditions for CISE data discussed in this work (Tables 1, 2 and 3) indicate that this is correct: equation (6) does tend to apply more for shorter sections and also higher velocity flows. There also appears to be a diameter effect:- viscosity as given by equation (5) appears to apply more for larger diameter sections for similar mass flow, length and pressure conditions. This is possibly because higher turbulent mixing for higher Weber number (i.e. larger diameter) conditions reduces the time required for impurities to migrate to bubble surfaces.

The East European limiting quality crisis data (Figures 9 and 10) differs from that obtained at CISE laboratories (Figures 7 and 8). It has been noted elsewhere [17] that East European limiting quality crisis data does not always agree with critical heat flux data obtained elsewhere. The present model indicates that the East European data were obtained under conditions where friction factor characteristics differ from those obtained in the CISE tests. Although no pressure gradient data were available for

the crises data examined in Figures 9 and 10, previous work [4,32] indicates that at least some East European pressure loss characteristics, both for Reynolds number dependent and Weber number dependent flows, differ from those obtained at CISE. The preferred East European method of providing fluid for test sections (flashing down from super-critical pressure boilers) [17] differs from methods generally used elsewhere. This may be a contributing factor to differences in East European characteristics, although some West European limiting quality crisis data, discussed later, agrees with the East European data trend, perhaps because the West European data applies to very high pressure conditions.

The data in Figures 9 and 10 indicate a change in the nature of non-boiling flows at a pressure of around 10 MPa. The correlation forms suggest entrained bubbles in the annular film at higher pressures, but no entrained film bubbles at lower pressure. (The differently behaved CISE data imply entrained film bubbles at pressures lower than 10 MPa.) The above result is physically reasonable: entrainment is partly a result of gas-liquid interactions at the film interface, and the lower gas density at lower pressures implies lower gas momentum fluxes for similar mass fluxes and quality conditions. The entraining process may thus be smaller at lower pressures.

It has been noted elsewhere [42] that crisis characteristics often change at about 10 MPa. This may be related to the above mentioned change from a non-bubbly viscosity to a bubbly viscosity at higher pressures.

It is worth noting that mechanisms postulated in East European literature (e.g. [6]) for the limiting quality phenomenon bears a superficial similarity to the model presented here, particularly since both involve a regime change precipitating the crisis and both involve a corresponding change in pressure loss characteristics. However, the two concepts of flow regime differ and hence so does the concept of a regime change, and the pressure loss characteristic referred to in Eastern European models of the heat transfer crisis phenomenon emphasise a 'pressure loss crisis' which is not the same as the friction regime change discussed here. It may, however, be synonymous with the lower quality friction regime change metnioned earlier, and hence may be related to a lower quality limiting quality condition.

The correlating curve for the 8 mm diameter data in Figure 10, $Re = 113\ We^{2/3}$, can be rearranged to yield, as an approximation,

$$x_{lim} \sim \frac{\rho_g \sigma}{\mu^{1.5}} \sqrt{\frac{D}{G}} \qquad (13)$$

This approximation is possible because viscosity as given by equation (6) does not vary significantly with quality except at low qualities. (This is also true of equation (5).) The mass flow and pressure dependence in this equation is close to those suggested in Eastern European correlations [9,10], but the diameter dependence, here a power of 0.5, differs from values suggested by East European researchers. An early recommendation of a - 0.15 power [9] has recently [10] been altered to a power of - 0.25, reflecting some uncertainty in the value. However, neither of these values is close to the power suggested here, 0.5. Since this raises doubts on the present modelling, the dependence on diameter needs examination.

A clue comes from the analysis of the CISE data of Figures 6 and 7. As discussed, equation (12) applies to both figures, but different forms of viscosity (equations (5) or (6)) are required. Moreover, it was found that the higher valued viscosity was found to be more appropriate with larger diameters. Thus, while equation (13) may be valid, a possible additional diameter effect may appear through the viscosity term. Although the viscosity does not change smoothly with diameter, a higher value encountered with larger diameters will distort (and reduce) the 0.5 power dependence on diameter if not included in the vicosity term. The non-smooth dependence of viscosity on diameter arising from the limitation of two unique possible values for given conditions (equations (5) or (6)), could explain the apparent confusion in resolving the diameter dependence (an apparent power of - 0.25 or - 0.15).

In order to test the hypothesis of a diameter dependence appearing via the viscosity term, limiting quality crisis data from Ispra [43-45], which covered 10 mm and 20 mm tubes, was examined. The data were obtained from graphs presenting wall temperature as a function of quality produced as part of an examination of post-crisis heat transfer. A non-dependence of critical quality on heat transfer appeared with some crises and these were tabulated (Table 4) and also plotted in the Re : We plane. The 10 mm data agreed with the correlation of Figure 10, equation (13), if the same form of viscosity as used in Figure 10, equation (6), was used in the Reynolds

number. Conversely, the 20 mm data agreed with equation (13) if the larger valued viscosity, given by equation (5), was used, except at the highest pressure (20.5 MPa) considered, when equation (6) appears more appropriate. The data are shown in Figure 13.

This indicates that the correlation of the East European limiting crisis data, equation (13), extends to other diameters provided the influence of diameter on viscosity is allowed for. The apparent contradition between equation (13) and East European recommendations on diameter dependence is a consequence of an indirect diameter dependence appearing in equation (13) via the viscosity term.

A final point worth mentioning in view of the current interest in scaling high pressure steam-water systems with low pressure refrigerants is that the present work indicates that both Reynolds number and Weber number scaling is necessary for a full scaling of heat transfer and hydrodynamic aspects of the flow.

7. CONCLUSIONS

Boiling diabatic two-phase flows have Weber number dependent flow characteristics, and heat transfer crises for boiling flows are induced by heat flux controlled departure from nucleate boiling. Non-boiling diabatic two-phase flows have Reynolds number dependent flow characteristics, and heat transfer crises for non-boiling flows are due to a system power controlled dryout of the liquid film of annular flow. Pre-crisis transition from boiling to non-boiling evaporative flow is hydrodynamically controlled rather than heat flux controlled. The discontinuity that appears in the heat transfer crisis characteristics on transition appear as a limiting quality crisis region of the characteristics if the dryout characteristics are lower than departure from nucleate boiling characteristics at the transition quality, and cause minima in crisis characteristics together with possible upstream crises if the dryout characteristics are above those for departure from nucleate boiling at the transition. The regime transition quality occurs so that there is little change in wall shear on transition. This allows the transition quality to be obtained from a knowledge of shear characteristics for boiling and non-boiling flows. Because these respectively depend on Weber number and Reynolds number, the transition can be represented by a curve on the Reynolds number : Weber number plane. The

definition of viscosity appearing in the Reynolds number is determined by the nature of the sublayer flow. The transition quality coincides with the limiting quality for limiting quality crisis data; and with the quality at the minimum in crisis characteristics and the quality at upstream crisis if these occur. The transition characteristics are not universal, and, because of upstream and other effects, may even differ for nominally identical conditions.

NOTATION

D	Diameter
f	Friction factor, $\tau_w/(\frac{1}{2}\ \rho_h\ v^2)$
G	Mass flux
L	Test section length
P	Pressure
Re	Reynolds number, $D\ G/\mu$
v	Mixture velocity G/ρ_h
We	Weber number $G^2\ D/(\rho_h \sigma)$
x_{in}	Inlet quality
x_{lim}	Quality for limiting quality crises
x_{min}	Quality at minimum in critical heat flux: exit quality plots
x_{out}	Outlet quality
x_{Tr}	Quality at pre-crisis boiling flow/non-boiling flow transition
x_{ud}	Quality at upstream dryout
β	Volumetric flow fraction, $x\ \rho_l/(x\ \rho_l + (1 - x)\ \rho_g)$
ϕ	Heat flux
ϕ_{CHF}	Critical heat flux
μ	Viscosity
μ_g	Gas viscosity
μ_l	Liquid viscosity
ρ_g	Gas density
ρ_h	$\rho_l\ (1 - \beta) + \rho_g \beta$
ρ_l	Liquid density
σ	Surface tension
τ_w	Wall shear

REFERENCES

[1] DUKLER, A. E. (1978) Modelling two phase flow and heat transfer. Proc. 6th Int. Heat Transfer Conf., Toronto, Canada, Hemisphere.

[2] BEATTIE, D. R. H. (1971) Two-phase pressure losses - Flow regime effects and associated phenomena. AAEC/TM 589.

[3] BEATTIE, D. R. H. (1975) Friction factors and regime transitions in high pressure steam-water flows. ASME paper 75-WA/HT-4.

[4] BEATTIE, D. R. H. (1977) Some aspects of two-phase flow drag reduction. Paper D1. Proc. 2nd Int. Conf. Drag Reduction, Cambridge, U.K., DHRA Fluid Engineering.

[5] BEATTIE, D. R. H. and LAWTHER, K. R. (1978) Relationship between wall shear stress and the heat transfer crisis phenomenon with vapour/liquid flows. Paper FB23. Proc. 6th Int. Heat Transer Conf., Toronto, Canada, Hemisphere.

[6] DOROSCHUK, V. E. (1966) Heat transfer crisis in an evaporating pipe. High Temp., 4, 522.

[7] DOROSCHUK, V. E., LEVITAN, L. L. and LANTZMAN, F. P. (1975) Investigation into burnout in uniformly heated tubes. ASME paper 75-WA/HT-22.

[8] DOROSCHUK, V. E., LEVITAN, L. L. and LANTZMAN, F. P. (1975) Recommendations for calculating burnout in a round tube with uniform heat release. Thermal Engng., 22, (12), 77.

[9] LEVITAN, L. L. and LANTZMAN, F. P. (1975) Investigating burnout with flow of a steam-water mixture in a round tube. Thermal Engng., 22, (1), 80.

[10] LEVITAN, L. L. and LANTZMAN, F. P. (1980) Effect of diameter on tube dryout. Heat Transfer - Soviet Research, 12, (3), 100.

[11] HEAT AND MASS TRANSFER SECTION, Scientific Council of the Academy of Sciences of the USSR (1975) Recommendations for calculating the critical heat flux for water boiling in uniformly heated round tubes. BTD OKB INTAN, Moscow, pre-print 3-004.

[12] HEAT AND MASS TRANSFER SECTION, Scientific Council of the Academy of Sciences of the USSR (1976) Tabular data for calculating burnout when boiling water in uniformly heated round tubes. Thermal Engng., 23, (9), 77.

[13] HEAT AND MASS TRANSFER SECTION, Scientific Council of the Academy of Sciences (1980) Recommendations for calculating the critical heat flux for water boiling in round tubes. Institute of High Temperature, pre-print 1-57.

[14] KITTO, J. B. (1980) Critical heat flux and the limiting quality phenomenon. AIChE Symp. Series, 76, 199, 57.

[15] CUMO, M., PALAZZI, G. and URBANI, G. C. (1979) On the limiting critical quality and the 'deposition controlled' burnout. CNEN-RT/ING (79) 4.

[16] HEWITT, G. F. (1978) Critical heat flux in flow boiling. Proc. 6th Int. Heat Transfer Conference, Toronto, Canada, Hemisphere.

[17] SMOLIN, V. N., SHPANSKII, S. V., EIKOV, V. I. and SEDOVA, T. K. Comments on VTI recommendations for calculation of critical heat flux in a round tube.

[18] ILIC, V. (1974) The effect of pressure on burnout in a round tube cooled by freon 12. AAEC/E 325.

[19] ZENKEVICH, B. A., PESKOV, O. L., PETRISHCHEVA, G. A., SERGEEV, N. D. and SUBBOTIN, V. I. (1969) Analysis and correlation of experimental critical heat flux data for forced flow of boiling water in tubes. Physico-Energetics Institute Report.

[20] PETERLONGO, G., RAVETTA, R., RIVA, B., RUBIERA, L. and TACCONI, F. A. (1964) Further critical power and pressure drop measurements in round vertical tubes with and without internal obstacles. CISE-R-122.

[21] MERILO, M. (1977) Critical heat flux experiments in a vertical and horizontal tube with both freon 12 and water as a coolant. Nuc. Eng. and Des., 44, (1), 1.

[22] MERILO, M. and AHMAD, S. Y. (1979) The effect of diameter on vertical and horizontal flow boiling in a tube cooled by freon 12. AECL 6485.

[23] GROENEVELD, D. C. (1974) The occurrence of upstream dryout in uniformly heated channels. Paper B6.6. Proc. 5th Int. Heat Transfer Conf., Japan.

[24] WATERS, E. D., ANDERSON, J. K., THORNE, W. L. and BATCH, J. M. (1965) Experimental observations of upstream boiling burnout. Chem. Eng. Prog. Symp. Series, 61, (57), 230.

[25] MATZNER, B., MOECK, E. O., CASTERLINE, J. E. and WIKHAMMER, G. A. (1965) Critical heat flux in long tubes at 1000 psi with and without swirl promoters. ASME paper 65-WA/HT-30.

[26] JENSEN, M. K. and BERGLES, A. E. (1980) Boiling heat transfer and critical heat flux in helical coils. ASME paper 80-HT-49.

[27] MAYINGER, F., SCHAD, O. and WEISS, E. (1967) Investigations into the critical heat flux in boiling water. EUR 3347 e.

[28] HASSID, A., MANZONI, G. C., RAVETTA, R. and RUBIERA, L. (1966) Heat transfer crisis with steam-water mixtures: an experimental study on the increase of critical power with local swirl promoters in round tubes. CISE-R 169.

[29] BERTOLETTI, S., GASPARI, G. P., LOMBARDI, C., PETERLONGO, G., SILVESTRI, M. and TACCONI, F. A. (1965) Heat transfer crisis with steam-water mixtures. Energia Nucleare, 12, (3), 121.

[30] EINSTEIN, A. (1906) A new determination of molecular dimensions. Ann. Phys., 19, 289.

[31] TAYLOR, G. I. (1932) The viscosity of a fluid containing small drops of another fluid. Proc. Royal Soc., 138, 41.

[32] BEATTIE, D. R. H. (1980) An evaluation of two bubble detachment models for two-phase flow. ANS-ASME Topical Meeting on Nuclear Reactor Thermodynamics, New York. NUREG/CP-0014, p.1343.

[33] BERKOWITZ, L., BERTOLETTI, S., LESAGE, J., PETERLONGO, G., SOLDAINI, G. and ZAVATTARELLI, R. (1960) Pressure drop, heat transfer and burnout measurements with round tubes. CISE-R 27.

[34] GASPARI, G. P., LOMBARDI, C. and PETERLONGO, G. (1964) Pressure drops in steam-water mixtures. CISE-R 83.

[35] ALLEZANDRINI, A., PETERLONGO, G. and RAVETTA, R. (1963) Critical heat flux and pressure drop measurements in round vertical tubes at the pressure of 51 kg/cm^2 abs. CISE-R 86.

[36] BERTOLETTI, S., GASPARI, G. P., LOMBARDI, C., SOLDAINI, G. and ZAVATTARELLI, R. (1964) Heat transfer crisis in steam-water mixtures. Experimental data in round tubes and vertical upflow obtained during the CAN-2 program. CISE-R 90.

[37] ERA, A., GASPARI, G. P., HASSID, A. and ZAVATTARELLI, R. (1967) Heat transfer crisis and pressure drop for steam-water mixtures at 70 kg/cm^2 flowing upwards and downwards in circular conduits. CISE-R 185.

[38] CERESA, I., ERA, A., GRECO, G. and LUCCHINI, F. (1974) Dryout with steam-water mixture at 50 bars in uniformly heated round ducts. CISE-R 359.

[39] KAZNOVZKII, S. P., POMET'KO, R. S. and RASHICHEV, V. V. (1978) Critical heat transfer and distribution of the liquid in disperse annular flow. High Temp., 16, (1), 75.

[40] BERGLES, A. E. and ROOS, J. P. (1968) Film thickness and critical heat flux observations for high pressure water in spray annular flow. Paper E6. Proc. Int. Symp. Res. Cocurrent Gas-Liquid Flow. U. Waterloo.

[41] STANISFORTH, R., STEVENS, G. E. and WOOD, R. W. (1965) An experimental investigation into the relationship between burnout and film flowrate in a uniformly heated round tube. AEEW-R 430.

[42] CAMPOLUNGHI, F., CUMO, M., FERRARI, F. and VACCARO, G. (1974) Burnout power in once through tubular steam generators. Vol. IV, 5th Int. Heat Transfer Conf., Tokyo.

[43] HERKENRATH, H., MORK-MORKENSTEIN, P., JUNG, U. and WECKERMAN, F. J. (1967) Heat transfer in water with forced convective flow in the pressure range 140 to 250 bar. EUR 3658 d.

[44] BAHR, A., HERKENRATH, H. and MORK-MORKENSTEIN, P. (1971) Development of the heat transfer crisis as a function of the entrance conditions. Paper B1. European Two-Phase Flow Group Meeting, Risø, Denmark.

[45] BAHR, A., HERKENRATH, H. and MORK-MORKENSTEIN, P. The development of the heat transfer crisis in once through boilers affected by pressure, entrance conditions and geometry. Paper L5. European Two-Phase Flow Group Meeting.

TABLE 1

CISE Limiting Quality Crisis Data, Viscosity According to Equation (6)

Reference	P MPa	Test Section	D cm	L cm	G kg m^{-2} s^{-1}	x_{lim}
36	5	58C	0.499	80	1108	0.61
36	5	86A	0.807	64.5	1095	0.56
36	5	86A	0.807	64.5	2210	0.32
38	5		0.790	183	800	0.81
38	5		0.790	183	2000	0.40
38	5		0.790	400	800	0.82
38	5		0.790	400	1500	0.57
38	5		0.790	600	1500	0.62
28	5	G11	1.51	32*	1100	0.69
28	5	G11	1.51	33*	2200	0.39
28	5	G11	1.51	36*	2200	0.40
28	5	G11	1.51	37*	2200	0.40
28	5	G11	1.51	38*	2200	0.43
28	5	G11	1.51	39*	2200	0.50
28	5	G11	1.51	40*	2200	0.39
28	5	G11	1.51	42*	2200	0.43
28	5	G11	1.51	44*	2200	0.43
28	5	G13	1.51	45*	2200	0.53
28	5	G13	1.51	45*	3800	0.41
28	5	G13	1.51	46*	1100	0.64
20	5	G5	1.51	411	1500	0.50
20	5	G5	1.51	411	2200	0.38
20	5	G5	1.51	411	3020	0.32
20	5	G5	1.51	329	2240	0.37
35	5	G2	1.51	246	1120	0.60
35	5	G2	1.51	246	2200	0.50
35	5	G2	1.51	246	3800	0.38
33	7	38	0.317	80	3450	0.31
36	7	54B (I)	0.500	40	1100	0.62
36	7	54C	0.490	39	1100	0.60
36	7	54C	0.490	39	3920	0.20
36	7	570	0.500	70	1300	0.62
36	7	570	0.500	70	2200	0.37
34	7	570	0.500	70	3000	0.33
36	7	570	0.500	70	3920	0.25
36	7	575	0.500	75	2250	0.39
34	7	575	0.500	75	3000	0.33
36	7	575	0.500	75	3920	0.24
33	7	58	0.52	80	1110	0.72
33	7	58	0.52	80	1490	0.60
33	7	58	0.52	80	2300	0.40
33	7	58	0.52	80	3930	0.31
36	7	58C	0.499	80	1100	0.71
36	7	58C	0.499	80	1300	0.63
36	7	58C	0.499	80	1520	0.56
36	7	58C	0.499	80	2280	0.41
36	7	58C	0.499	80	2700	0.35
36	7	58C	0.499	80	3800	0.27

Table 1 (continued)

Reference	P MPa	Test Section	D cm	L cm	G kg m^{-2} s^{-1}	x_{lim}
36	7	58B	0.500	80	1100	0.67
36	7	58B	0.500	80	1360	0.59
36	7	58B	0.500	80	1490	0.53
36	7	58B	0.500	80	1520	0.51
36	7	58B	0.500	80	2280	0.36
36	7	58B	0.500	80	2880	0.30
36	7	58B	0.500	80	3900	0.26
36	7	58B (F)	0.500	80	1100	0.69
36	7	58B (F)	0.500	80	1300	0.64
36	7	58B (F)	0.500	80	1530	0.56
36	7	510	0.509	110	1100	0.71
36	7	510	0.509	110	2170	0.41
36	7	510	0.509	110	3800	0.25
36	7	511	0.506	110	1040	0.72
36	7	511	0.506	110	1073	0.74
36	7	511	0.506	110	1260	0.65
36	7	511	0.506	110	1450	0.58
36	7	511	0.506	110	2150	0.42
36	7	511	0.506	110	2950	0.35
36	7	511	0.506	110	3800	0.30
33	7	68	0.626	80	1050	0.67
33	7	68	0.626	80	1470	0.57
33	7	68	0.626	80	2190	0.43
33	7	68	0.626	80	2990	0.36
33	7	68	0.626	80	3460	0.32
28	7	G13	1.51	64	2200	0.57
36	8.9	511	0.506	110	2960	0.30
36	8.9	511	0.506	110	3830	0.26
36	8.9	527	0.490	267	1100	0.66
36	8.9	527	0.490	267	1500	0.52
36	8.9	527	0.490	267	2200	0.38
36	8.9	527	0.490	267	2950	0.33
36	8.9	527	0.490	267	3800	0.30

* With special inlet arrangements for refs. [20,28] data, L is replaced by test series [28] or table number [20] so that inlet arrangement can be identified.

TABLE 2

CISE Limiting Quality Crisis Data, Viscosity According to Equation (5)

Reference	P MPa	Test Section	D cm	L cm	G kg m^{-2} s^{-1}	x_{lim}
28	5	G11	1.51	8*	1100	0.50
28	5	G11	1.51	8*	2200	0.31
28	5	G13	1.51	9*	1100	0.54
28	5	G13	1.51	9*	2200	0.33
28	5	G13	1.51	10*	1100	0.53
28	5	G13	1.51	10*	2200	0.33
28	5	G13	1.51	11*	1100	0.53
28	5	G13	1.51	11*	2200	0.32
28	5	G11	1.51	40*	1100	0.53
20	5	G4	1.51	329	1100	0.56
20	5	G4	1.51	1/27*	1100	0.56
20	5	G4	1.51	1/37*	1100	0.58
20	5	G4	1.51	1/37*	2200	0.56
20	5	G4	1.51	1/37*	3800	0.24
28	6.5	G5	1.51	412	1100	0.50
28	6.5	G5	1.51	412	1490	0.40
28	6.5	G5	1.51	412	2200	0.34
28	6.5	G2	1.51	245	1100	0.48
28	6.5	G4	1.51	1/26*	1100	0.50
28	6.5	G4	1.51	1/38*	1100	0.53
28	6.5	G4	1.51	1/38*	2200	0.32
36	7	914	0.918	140	1080	0.59
36	7	914	0.918	140	1300	0.52
36	7	914	0.918	140	1500	0.46
36	7	914	0.918	140	1800	0.41
36	7	914	0.918	140	2190	0.34
37	7	914	0.918	140	1100	0.61
37	7	914	0.918	140	2200	0.35
28	7	G13	1.51	397	1100	0.52
28	7	G13	1.51	397	2200	0.33
28	7	G13	1.51	237	1100	0.50
28	7	G13	1.51	157	2200	0.40
28	7	G13	1.51	13*	1100	0.50
28	7	G13	1.51	13*	2200	0.31
28	7	G13	1.51	14*	1100	0.50
28	7	G13	1.51	51*	1100	0.61
28	7	G13	1.51	55*	1100	0.62
28	7	G13	1.51	63*	1100	0.62
28	7	G13	1.51	63*	3800	0.31
36	9	58C	0.499	80	1100	0.40
36	9	58C	0.499	80	1500	0.36
36	9	58C	0.499	80	2280	0.29
36	9	511	0.506	110	2180	0.30
36	9	914	0.918	140	1080	0.50
36	9	914	0.918	140	2200	0.31

* With special inlet arrangements for refs. [20,28] data, L is replaced by test series [28] or table number [20] so that inlet arrangement can be identified.

TABLE 3

CISE Steady Flow Heat Transfer Crisis Data with Minima

Reference	P MPa	Test Section	D cm	L cm	G kg m^{-2} s^{-1}	x_{min}
36	5	86A	0.807	65	3905	0.13
28	5	G11	1.51	32*	2160	0.26
28	5	G11	1.51	33*	2200	0.28
28	5	G11	1.51	34*	2200	0.29
28	5	G11	1.51	34*	3800	0.23
28	5	G11	1.51	35*	1100	0.60
28	5	G11	1.51	35*	2200	0.31
28	5	G11	1.51	35*	3800	0.18
28	5	G11	1.51	36*	3800	0.18
28	5	G11	1.51	37*	2200	0.30
28	5	G11	1.51	37*	3800	0.20
28	5	G11	1.51	38*	2200	0.33
28	5	G11	1.51	38*	3800	0.17
28	5	G11	1.51	39*	3800	0.17
28	5	G11	1.51	41*	3800	0.19
28	5	G11	1.51	42*	3800	0.20
28	5	G13	1.51	50*	3800	0.19
28	5	G13	1.51	53*	3800	0.21

* With special inlet arrangements for refs. [20,28] data, L is replaced by test series [28] or table number [20] so that inlet arrangement can be identified.

TABLE 4

Ispra [43-45] Limiting Quality Crisis Data

P MPa	D cm	G kg m^{-2} s^{-1}	x_{lim}	Viscosity Equation
14	10	1000	0.45	6
14	20	700	0.44	5
14	20	1000	0.38	5
14	20	1500	0.30	5
14	20	2250	0.26	5
14	20	3500	0.27	5
17	10	700	0.48	6
17	10	2250	0.31	6
17	20	1000	0.38	5
18.5	20	1000	0.32	5
20.5	20	700	0.29	6
20.5	20	1000	0.31	6
20.5	20	1500	0.28	6

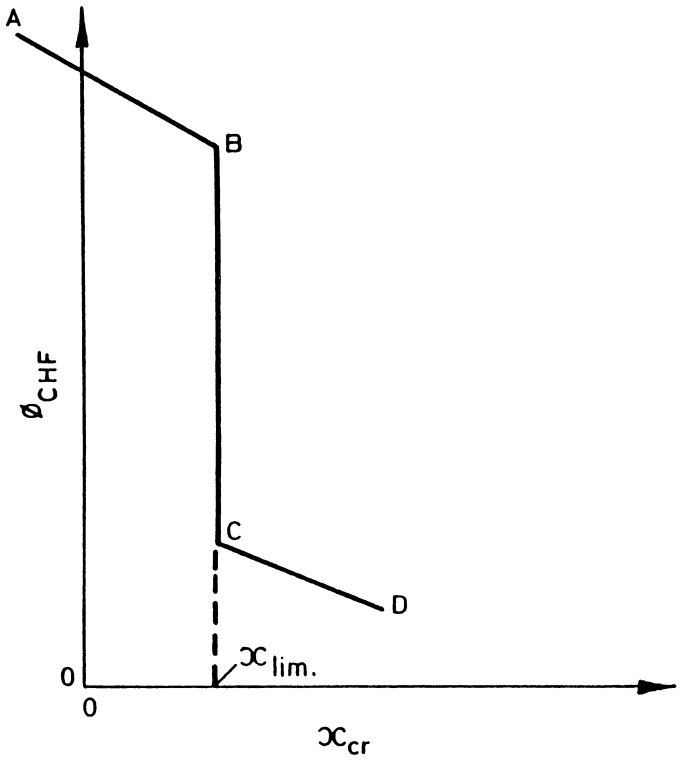

FIG.1. CRITICAL HEAT FLUX CHARACTERISTIC SHOWING THE LIMITING QUALITY CRISIS PHENOMENON.

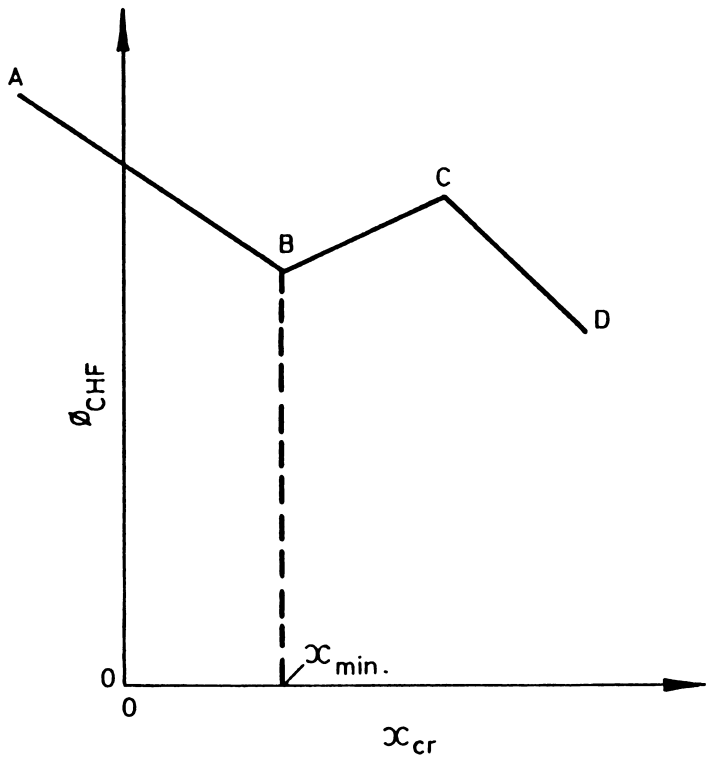

FIG.2. CRITICAL HEAT FLUX CHARACTERISTIC WITH MINIMUM.

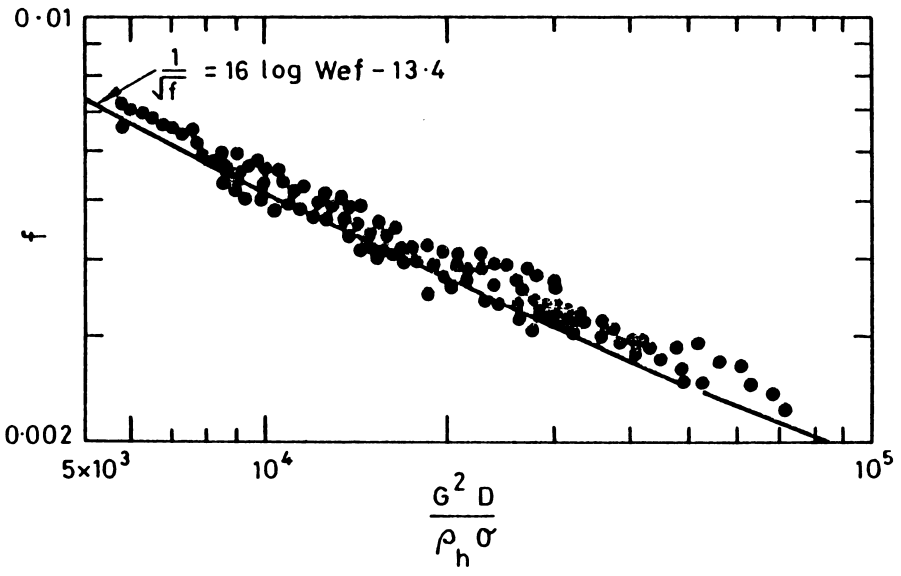

FIG. 3. CISE DIABATIC BOILING WEBER-NUMBER DEPENDENT FRICTION FACTOR DATA. DATA FOR TEST SECTION 914 AT 7 MPa [36].

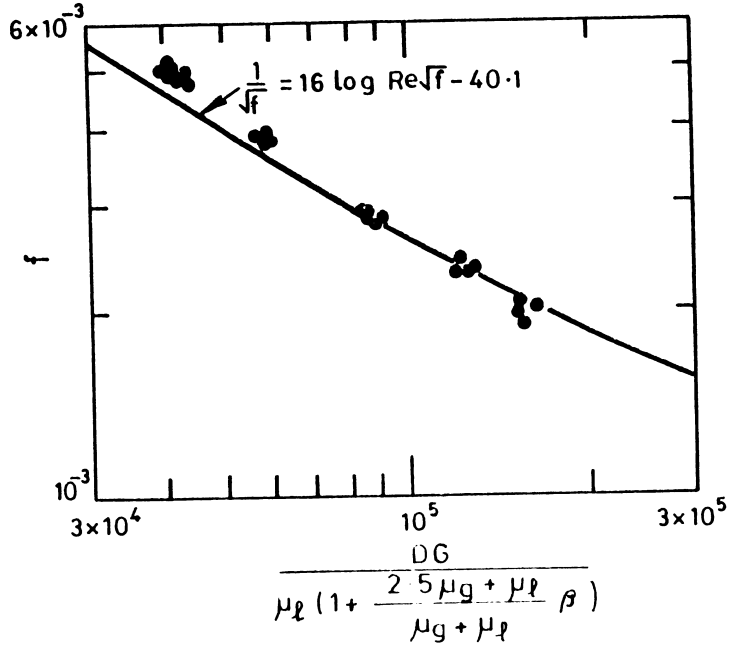

FIG. 4. CISE DIABATIC NON-BOILING REYNOLDS NUMBER DEPENDENT FRICTION FACTOR DATA, VISCOSITY FROM EQUATION 6, DATA FOR TEST SECTION 88 AT 7 MPa AND ABOUT HALF CHF [33].

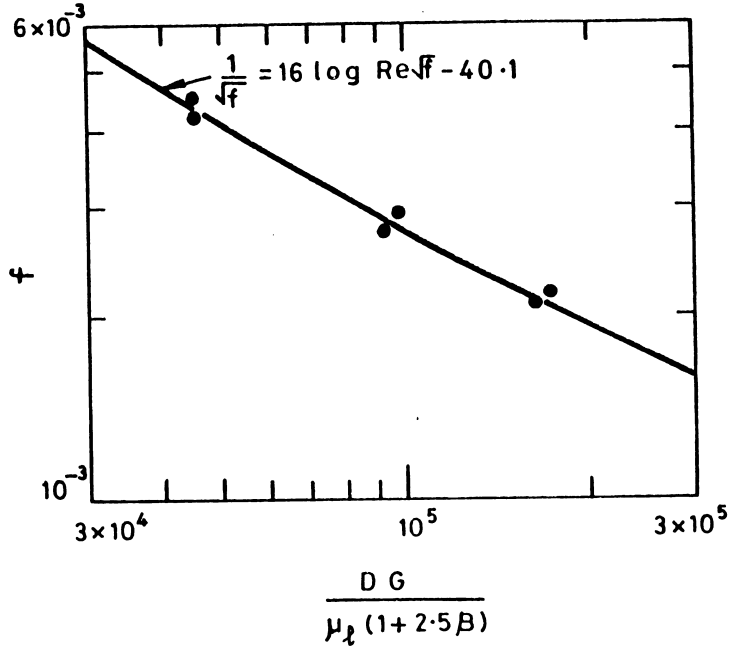

FIG. 5. CISE DIABATIC NON-BOILING REYNOLDS NUMBER DEPENDENT FRICTION FACTOR DATA, VISCOSITY FROM EQUATION 5, DATA FOR SERIES 1, REF. [28].

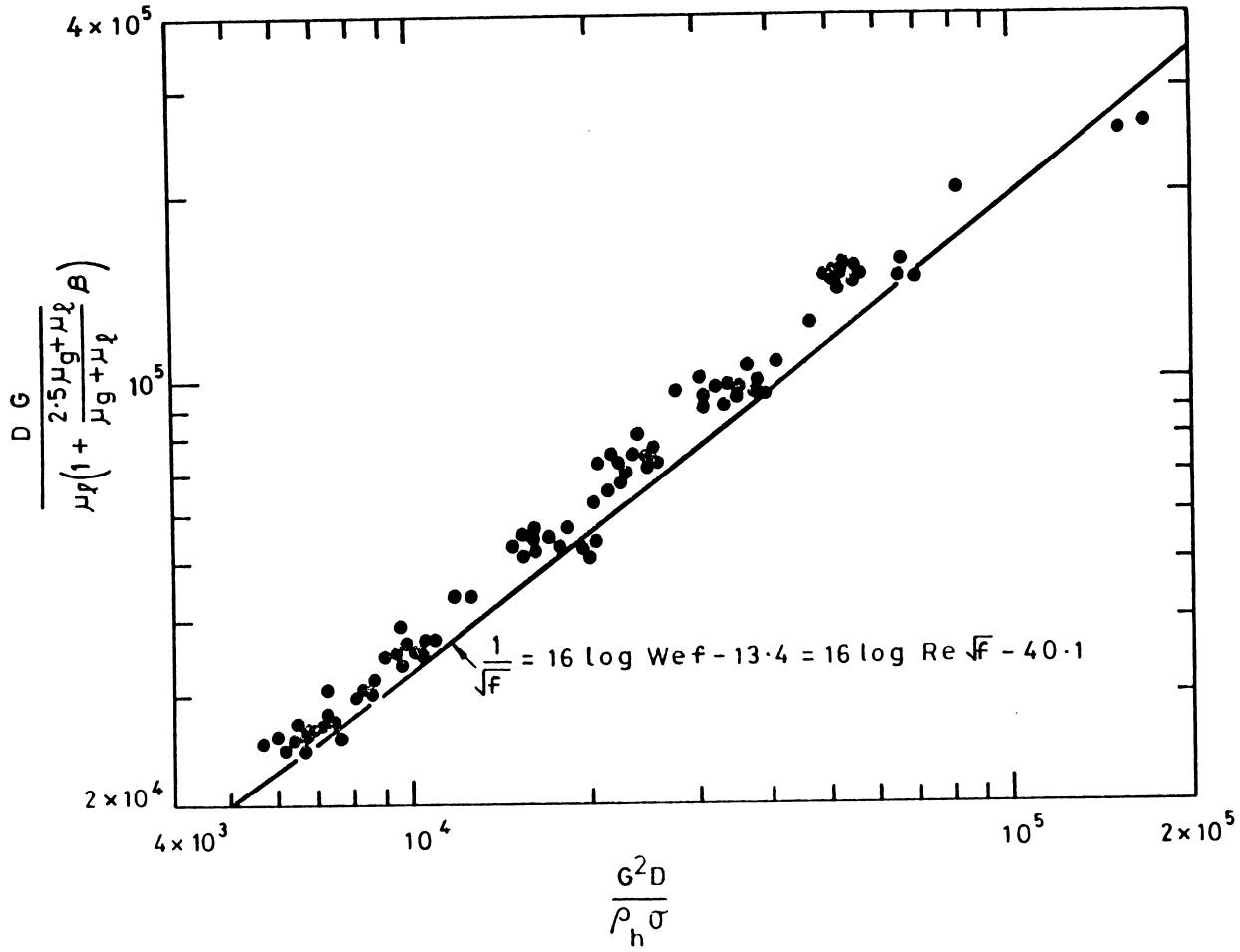

FIG. 6. CISE LIMITING QUALITY DATA, SHOWING DATA OF TABLE 1.

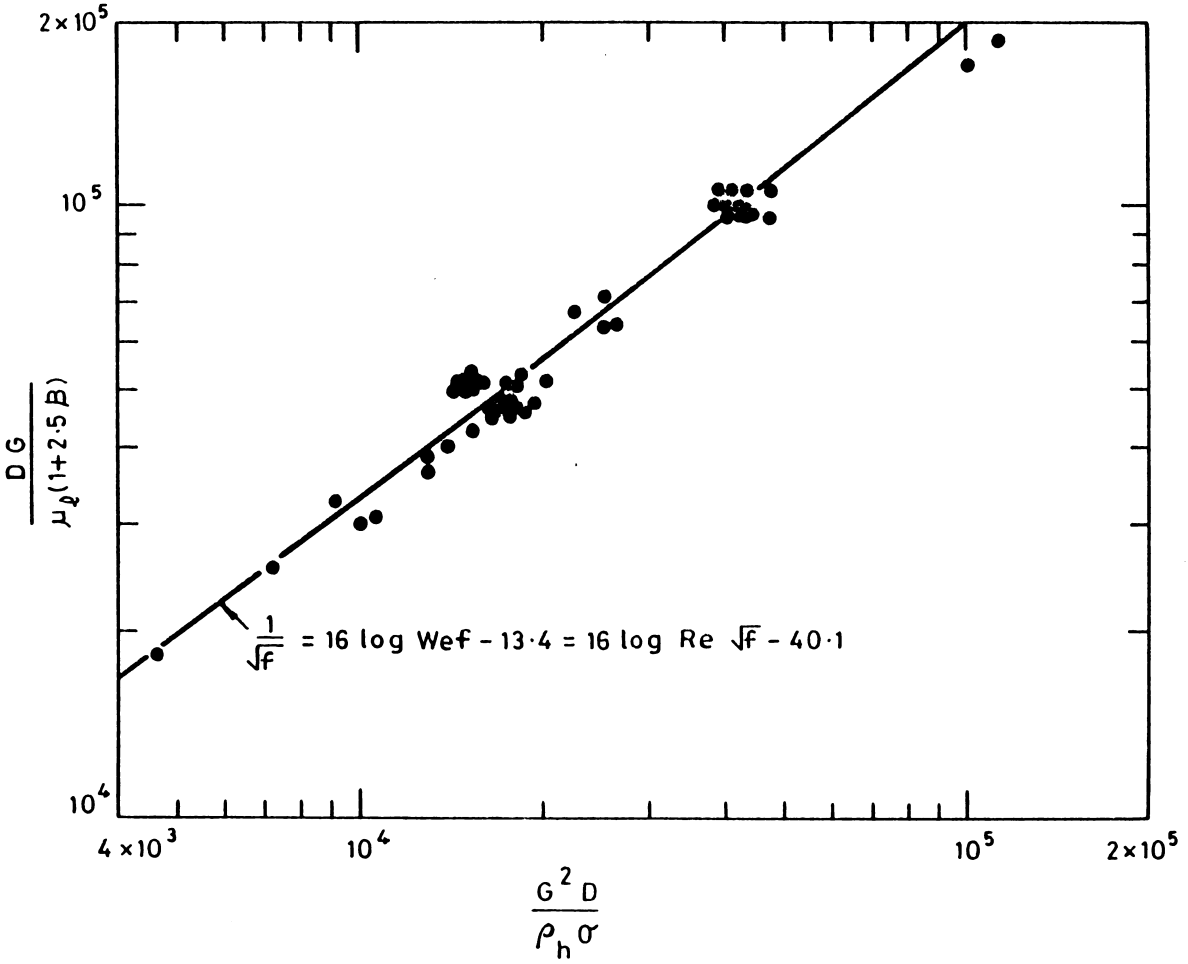

FIG. 7. CISE LIMITING QUALITY DATA, SHOWING DATA OF TABLE 2.

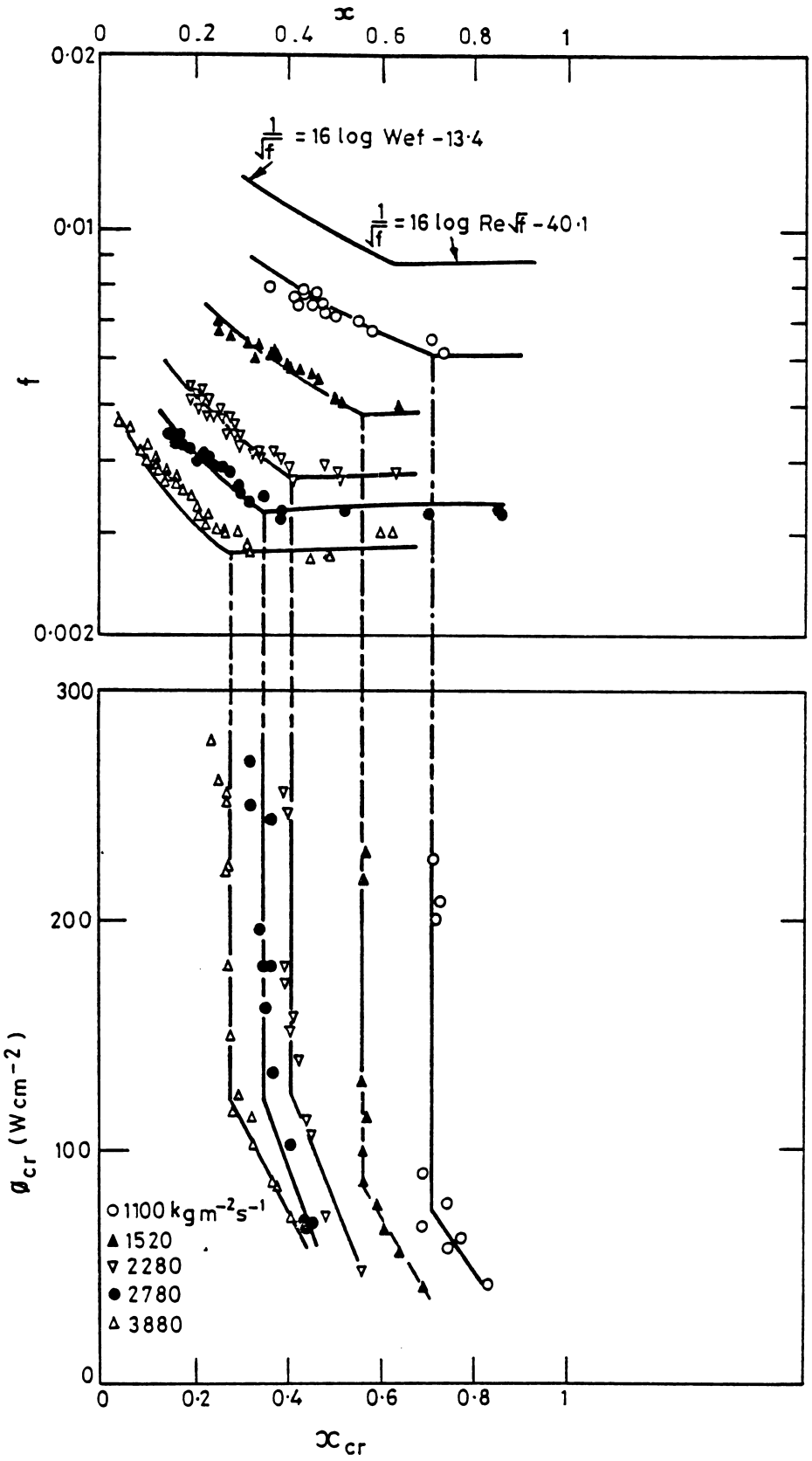

FIG.8. CISE TEST SECTION 58C CRITICAL HEAT FLUX [36] AND PRESSURE LOSS [34] DATA AT 7MPa. VISCOSITY FROM EQUATION 6

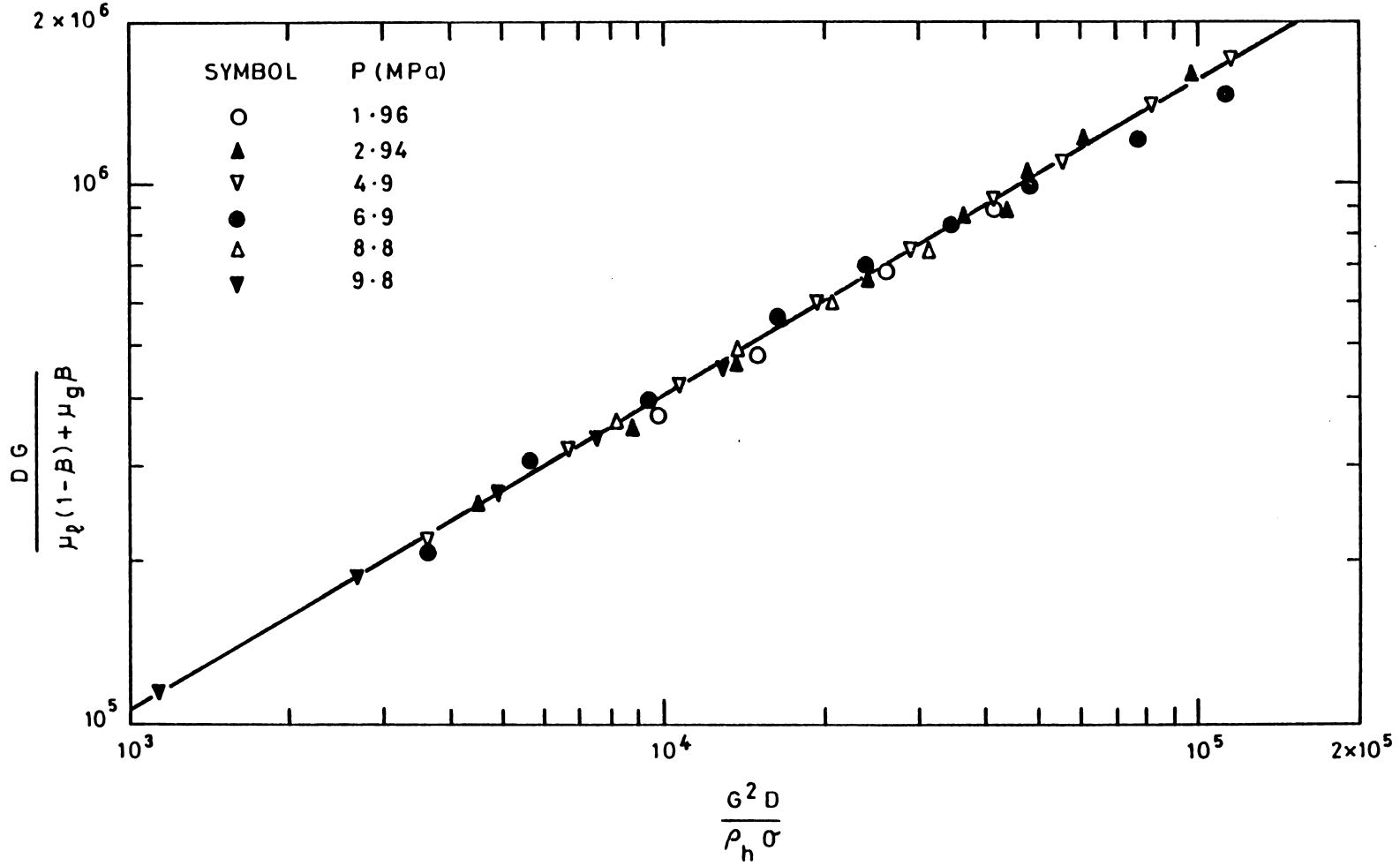

FIG. 9. CORRELATION OF VTI LOWER PRESSURE TABULATED LIMITING QUALITY CRITICAL HEAT FLUX DATA FOR 8mm TUBES [7-11], 300-5000kg m^{-2}s^{-1}.

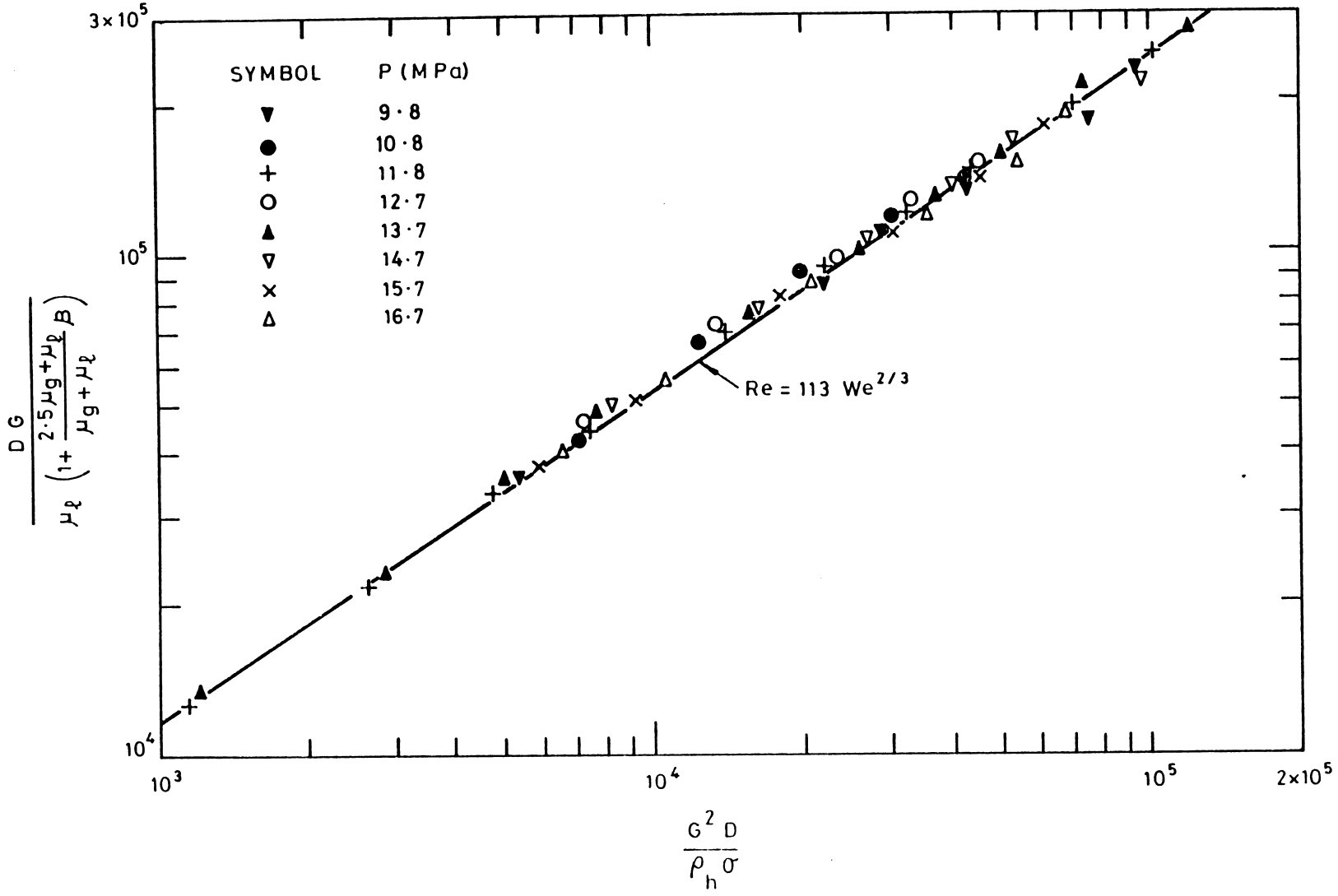

FIG. 10. CORRELATION OF VTI HIGHER PRESSURE TABULATED LIMITING QUALITY CRITICAL HEAT FLUX DATA FOR 8mm TUBES [7-11], 300-5000kg m^{-2}s^{-1}.

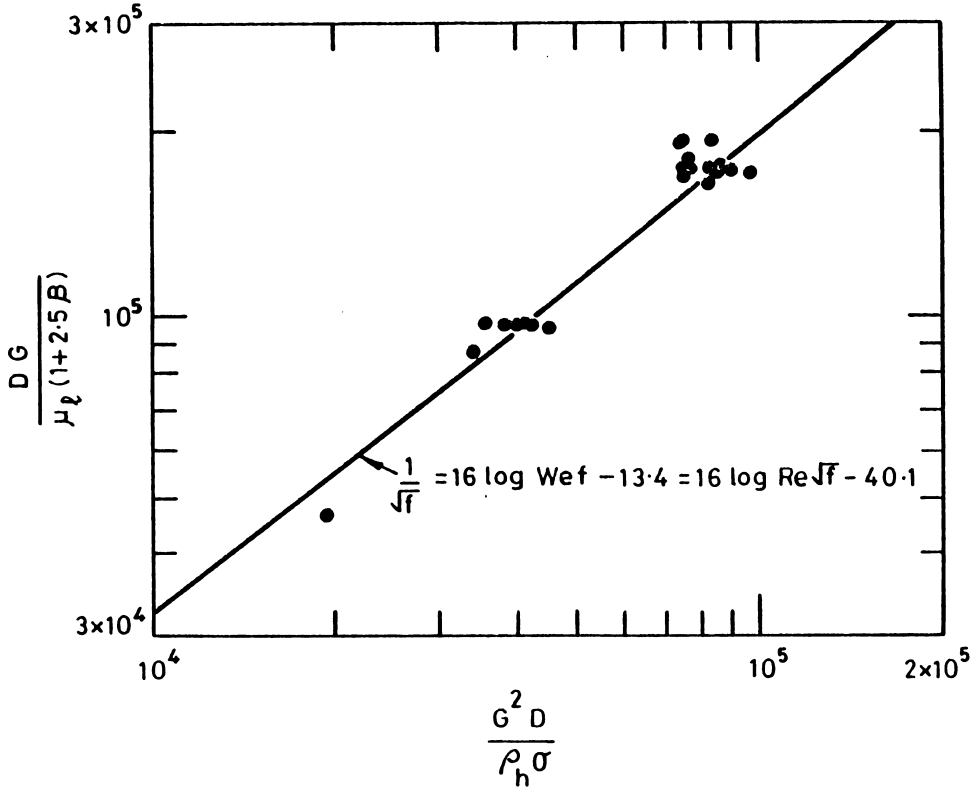

FIG. 11. CISE MINIMUM QUALITY CHF DATA, SHOWING DATA OF TABLE 3.

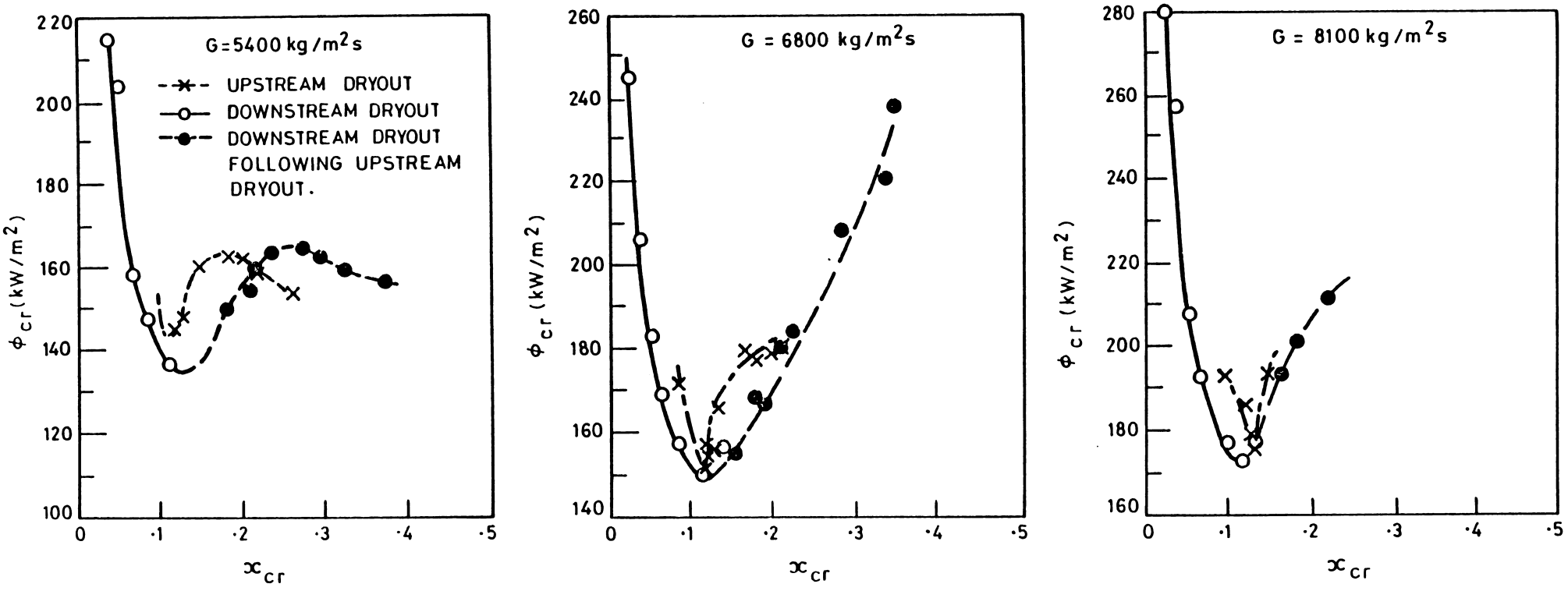

FIG. 12. AECL CRITICAL HEAT FLUX DATA WITH MINIMA AND UPSTREAM HEAT TRANSFER CRISES [23].

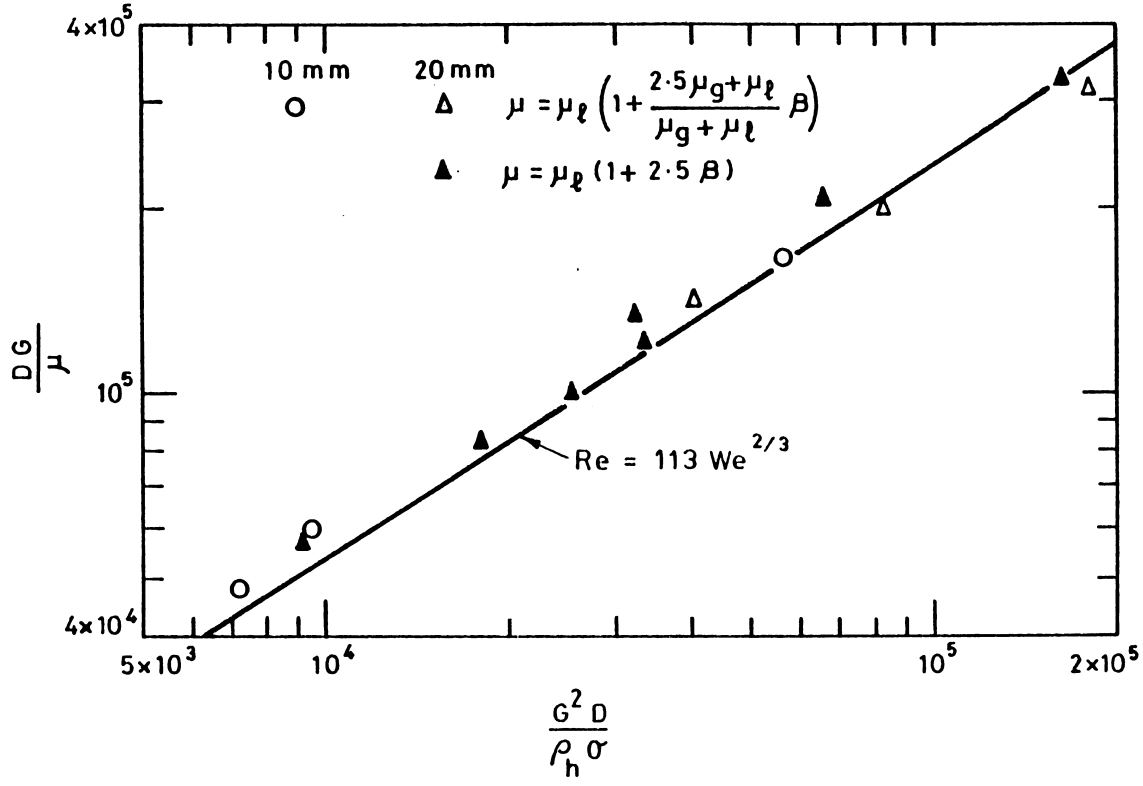

FIG. 13. EURATOM LIMITING QUALITY DATA SHOWING DATA OF TABLE 4.

Comparison of the contributions.

The approaches of the participants are described on the following pages by the authors theirselves:
The pages marked A1 to A11 are from mr. Azzopardi and mr. Beattie, CH1 to CH3 are from mr. B. Chojnowski and mr. B. Scruton, and the other pages are from mr. Köhler. Their predictions are compared in the figures $1^{a)}$ to $1^{e)}$ and $2^{a)}$ to $2^{e)}$. The experimental results from Nijhawan e.a. concern a test-section with an inner diameter of 14,1 mm, a mass flux of 18 to 80 kg/m^2 sec, a heat flux of 11 kW/m^2 and pressures up to 3 bars.
Mr. Chojnowski and mr. Scruton merely evaluated the Groeneveld-Delorme and the Chen correlations for the special test-conditions proposed in the exercise. Mr. Köhler and mr. Arropardi give a careful account of the way their codes handle the problem of superheating. Mr. Beattie is the first one who investigates the effect of radial distribution of several physically relevant quantities. He uses a distribution parameter to bring a two-dimensional character into a one-dimensional model. A totally different approach is offered by mr. van Koppen, who introduces the concept of a developping thermal boundary layer and assumes logarithmic profiles for all relevant parameters in order to be able to calculate as much as possible without the help of the computer.

1. General

The calculations presented here are based on concepts presented by Bennett et al (Heat transfer to steam-water mixtures flowing in uniformly heated tubes in which the critical heat flux has been exceeded, AERE R5373, 1967), and by Beattie (Two-phase fluid mechanics and heat transfer in the dry wall region, Proc 2nd Australian Conf Heat and Mass Transfer, University of Sydney, 1977). These two works examine different aspects of post dry-out heat transfer mechanisms and together cover most of the items considered important in the calculation exercise notes.

The notes suggest using the Groeveveld-Delorme and Chen correlations. Both these methods in effect present a correlation of 'experimental' flow quality in terms of thermodynamic equilibrium quality. The 'experimental' qualities are chosen so as to produce consistency of data with an assumed heat transfer equation. Because of assumptions involved, these 'experimental' qualities may differ significantly from actual flow qualities.

In keeping with the exercise philosophy of examining mechanisms involved in post-crisis heat transfer, we have discarded the empirically based correlations of Groeneveld and Delorme and of Chen in fvour of a more fundamentally based attempt to evaluate thermal non-equilibrium.

The exercise notes also suggest the use of physical property data as supplied with the notes. Our calculations require more physical properties than those supplied, and, for consistency, we have used the 1967 IFC equations for all properties. The supplied table for specific volume, enthalpy and entrophy are based on these equations. However, the supplied table for Prandtl number disagrees significantly with tables available to us. Since the supplied Prandtl number table suggests a critical pressure of between 350 and 375 bar, we suspect that we have been supplied with a Prandtl number table for a fluid other than water.

2. The Baseline Case

2.1 The basic model

The basic model follows from earlier work of Bennett et al and assumes that the main mechanisms of heat transfer are:

(i) Convective heat transfer from the wall to the vapour

(ii) Convective/conductive heat transfer from the vapour to the drops

These two concepts are incorporated in a system of equations which are integrated along the tube.

For transfer from the wall to the vapour the following equation is used

$$\phi = H (T_w - T_v)$$

where the heat transfer coefficient H is determined from the Heineman equation, see section 2.2 below.

In the transfer from the vapour to the drops it is assumed that evporation is controlled by the transfer of heat to the drop. The rate of change of vapour temperature is then determined from the following equations.

The change of drop size is given by

$$\frac{dd}{dz} = - \frac{2}{\rho_L \lambda U_D} (T_v - T_L) \frac{N_u \, d}{k} \quad ,$$

the change of drop velocity

$$\frac{du_D}{dz} = 0.75 \frac{C_D (U_v - U_D)^2}{d \, U_D \, \rho_L} \rho_v - \frac{g}{U_D} \left(\frac{\rho_L - \rho_v}{\rho_L}\right) ,$$

the change in mass quality

$$\frac{dx}{dz} = - 3 \, d^2 \frac{dd}{dz} \left(\frac{1 - X_{BO}}{d_{BO}^3}\right) \quad ,$$

and the change in vapour temperature by

$$\frac{dT_v}{dz} = \left(4\phi - DG \, (h_v - h_{Ls}) \frac{dx}{dz}\right) \frac{1}{DG \, U_D \, C_{pv}}$$

2.2 Heat transfer to vapour

The single phase Heineman equation for steam has been used in the present analysis:-

$$\frac{\phi \, D}{k_{vf} \, (T_w - \langle T_v \rangle)} = 0.0157 \left(\frac{\rho_v \langle U_v \rangle D}{\mu_{vf}}\right)^{0.84} Pr_{vf}^{\frac{1}{3}} (L/D)^{-0.04} \quad , \; 6 < L/D < 60,$$

$$= 0.1033 \left(\frac{\rho_v \langle U_v \rangle D}{\mu_{vf}}\right)^{0.84} Pr_{vf} \quad , \; L/D > 60$$

2.3 Drop/vapour heat transfer coefficient

The equation of Ranz and Marshall is used for the heat transfer coefficient to the drops. This is a single sphere equation and has been chosen after an examination of several equations against a bank of experimental data.

The equation is

$$Nu = 2 + 0.6\, Re^{0.5}\, Pr^{0.33}$$

A correction factor has been applied to this equation, taken from the work of Hoffman and Ross, which accounts for the slowing down of heat reaching the drop by the outward movement of cooler vapour emanating from the surface of the drop. Therefore

$$Nu = Nu_o \left(\frac{1}{1 + B}\right)^{0.6}$$

where B is the dimensionless Spaulding number $\left(= \frac{h_v - h_{vs}}{h_v - h_L}\right)$

2.4 Drag coefficient

The equation of Schiller and Nauman has been used for calculation of drag coefficient

$$C_D = \frac{24}{Re_D} \left(1 + 0.15\, Re_D^{0.687}\right)$$

where

$$Re_D = \frac{\rho_v \, (U_v - U_D) d}{\mu_v}$$

2.5 Initial drop size

The initial drop size is specified by means of the correlation of Azzopardi et al (1980)

$$d = d_t \left(1.9 \frac{Re_t^{0.1}}{We_t^{0.6}} \left(\frac{\rho_G}{\rho_L}\right)^{0.6} + 0.4 \frac{G_{LE}}{G_G}\right)$$

where $Re_t = \dfrac{\rho_v U_v d_t}{\mu_v}$

$$We_t = \frac{\rho_v U^2_v d_t}{\sigma}$$

In the calculations no allowance has been made for the distribution of drop sizes. Earlier unpublished computations show that the use of a distribution of drop sizes produces only a small difference in the results, predicting slightly higher wall temperatures than when a mean size is used. This effect requires a little further investigation.

3. Droplet Concentration Distribution

The exercise notes present the topic as one of the main subjects for the calculation exervise. It is part of a broader problem of allowing for phase, velocity and temperature profile effects so that terms such as $<\rho h>$, which appear in the conservation equations, can be resolved into a product of terms $<\rho>$ $<h>$. (The notation $<--->$ indicates the cross-section averaging operator $\frac{1}{A}\int_A --- \, dA$).

It is shown here how the analysis of section 2 may be altered to allow for the radial droplet concentration distribution. Only those features of the model of section 2 which are directly influenced by droplet distribution effects are discussed.

3.1 The distribution parameter

The droplet concetration is unknown in detail but droplets can be assumed to be confined to the central region where velocity profiles, and hence, by Reynolds Analogy, also temperature profile, are fairly flat. A distribution parameter c_o, which quantitatively allows averages of products to be reduced to products of averages, can then be introduced:

$$c_o \equiv \frac{<(1-\alpha)j>}{<1-\alpha><j>} = \frac{j_c}{<j>} = \frac{T_w - T_{vc}}{T_w - <T_v>} = 1 + 2.6\sqrt{f}$$

where f is the frication factor given by

$$1/\sqrt{f} = 4 \log Re\sqrt{f} - 0.4, \quad Re = \frac{D \rho_v <j>}{\mu_v}$$

The second and fourth component of the above distribution parameter equation set are based on the concept of droplets being confined to the flatter part of the velocity profile, and the third component is based on Reynolds analogy.

3.2 Wall temperature equation

The analysis of section 2 allowed the wall temperature to be obtained from an analysis of the heat transferred to the gas after thermal non-equilibrium was allowed for:-

$$(T_w - T_s) = (T_w - \langle T_v \rangle) + \Delta T_{vL}$$

The first right-hand side term was obtained from the Heineman equation, and the second right-hand side term, which allows for thermal non-equilibrium, was obtained by considering the heat transferred from the superheated vapour to the droplets.

An additional effect exists if droplet concetration effects are allowed for:- droplets are cooler than the mean vapour temperature not only bacause of local thermal non-equilibrium, but also because droplets are confined to the cooler region of the vapour temperature profile. When the second effect is allowed for using concepts outlined in section 3.1, the above equation becomes

$$(T_w - T_s) = c_o (T_w - \langle T_v \rangle) + \Delta T_{vL}$$

This can be regarded as the Reynolds analogy heat transfer version of the Zuber-Findlay drift flux slip equation. The form of equation indicates that plots of $T_w - T_s$ against $T_w - \langle T_v \rangle$ may be more readily interpreted than plots of $\langle T_v \rangle - T_s$ against $T_w - T_s$ as suggested in the notes.

3.3 Flow quality

The flow quality $x \equiv \langle \rho_g U_g \alpha \rangle / \langle \rho_g U_g \alpha + \rho_L U_L (1-\alpha) \rangle$ is obtained from the system enthalpy as obtained from the energy equation:-

$$Gh \equiv \langle \rho_L h_L U_L (1-\alpha) + \rho_v h_v U_v \alpha \rangle$$

For liquid at saturation temperature and vapour at a uniform superheated temperature, it is readily shown that this reduces to a relation between flow quality and thermodynamic equilibrium quality x_{eq}.

$$h_{Ls}\ (1 - x_{eq}) + h_{vs}\ x_{eq} = h_{Ls}\ (1 - x) + \langle h_g \rangle\ x,$$

an equation which is implicit in the analysis of section 2 and indeed in most current thermal non-equilibrium models of post-dryout heat transfer. Phase and temperature distribution effects, for which the present assumptions are that, locally, $h_v = h_{vc}$ for $\alpha < 1$, lead to an additional term on the right-hand side of the quality equation, which now becomes (as a first approximation)

$$h_{Ls}\ (1 - x) + \langle h_g \rangle x + (c_o - 1)\ (\rho_v/\rho_L)\ (1 - x)\ c_{pv}\ (T_w - \langle T_v \rangle)$$

Neglect of the additional term leads to an underestimate of the difference between the true quality and the thermodyanamic equilibrium quality.

4. Results

Correct programming of the equations of section 3 to allow for droplet distribution effects was not achieved in the time available, so predictions for the flow conditions suggested in the exercise notes were made using the baseline model described in section 2.

Predictions were made for the post-crisis region of a 10 m tube. The crisis position was predicted using the HANA code with zero inlet sub-cooling. Notes pertinent to the present exercise are given in table 1.

Predicted post-crisis conditions are shown in the attached figures together with relevant data of Scrutton and Chojnowski and of Barzoni et al. In comparing the predictions with the data it should be kept in mind that neither these data nor any other post-dryout data were used in the formulation of the predictive method.

5. Notation

A	Area
B	Spalding number
C_D	drag coefficient
C_p	specific heat
c_o	distribution parameter
d	droplet diameter
D	tube diameter
f	friction factor
G	mass flux

h specific enthalpy

H heat transfer coefficient

k thermal conductivity

L distance from dryout location

Nu Nusselt number

Pr Prandtl number

Re Reynolds number

T Temperature

ΔT_{vL} Local vapour liquid temperature difference

U local velocity

x quality

z axial position

α local voidage

ϕ heat flux

λ latent heat

ρ density

Subscripts

BO burnout

c centre line value

D droplet value

eq thermal equilibrium

e entrained value

f film temperature value

L liquid value

s saturation value

v vapour value

w wall value

<--> quantity is averaged over flow cross-section

References

Azzopardi B J et al (1980), Drop size and deposition in annular two-phase flow. AERE R9634

Barzoni G et al (1980), Post dryout heat transfer tests in a two-section heat tube. Paper C2, ETPFGM

Beattie D R H (1977), Two-phase fluid mechanics and heat transfer in the dry wall region. Proc 2nd Australian Conf Heat and Mass Transfer, Univ Sydney

Bennett A W et al (1967), Heat transfer to steam-water mixture flowing in uniformly heated tubes in which the critical heat flux has been exceeded. AERE R5373

Chen J C et al (1979), A phenomenological model of post dryout heat transfer. Nucl Eng Ses 51, 143-155

Groeneveld D C and Delorme G G J (1976), Prediction of thermal non-equilibrium in the post-dryout regime. Nucl Eng Des 36, 17-26

Heineman J B (1960), An experimental investigation of heat transfer to superheated steam in round and rectangular tubes. ANL - 6213

Ranz W E and Marshall W R (1952), Evaporation from drops. Chem Engng Progr, 48, Pt 1, No 3, 141-146, No 4 Pt2, 173-180

Schiller L and Nauman A Z (1933), Ver Deut Ing, 77, 318-320.

Scrutton B and Chojnouwski B (1980), Post dryout heat transfer for steam/water flowing in vertical tubes at high pressure. Paper C1, ETPFGM

May 1981

TABLE 1

Conditions Studied for 1981 ETPFG Meeting Exercise

D mm	P bar	G kg $m^{-2}s^{-1}$	ϕ k W m^{-2}	Notes
19	165	400	200	
19	165	700	200	x_{eq} = 1 not reached in 10 m
19	165	1000	200	Dryout not predicted in 10 m
19	165	1250	200	Dryout not predicted in 10 m
19	165	400	400	
19	165	700	400	
19	165	1000	400	x_{eq} = 1 not reached in 10 m
19	165	1250	400	x_{eq} = 1 not reached in 10 m
19	165	400	600	Run terminated due to predicted negative slip
19	165	700	600	
19	165	1000	600	
19	165	1250	600	
12	50	500	200	Dryout not predicted in 10 m
12	50	1000	200	Dryout not predicted in 10 m
12	50	500	600	
12	50	1000	600	
12	50	500	1000	Program failed - faulty 1/P data?
12	50	1000	1000	Program failed - faulty 1/P data?

Figure 1

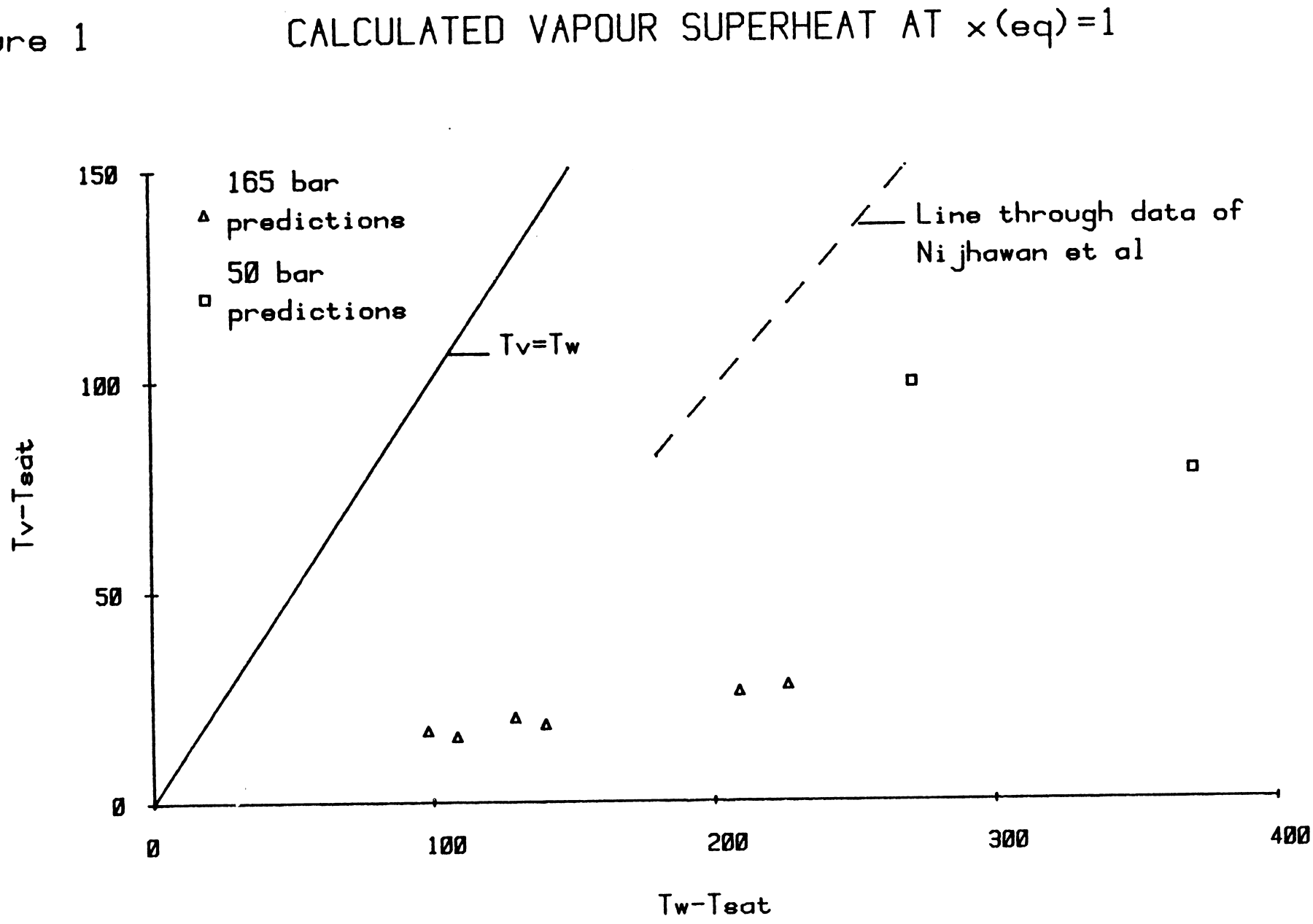
CALCULATED VAPOUR SUPERHEAT AT x(eq)=1
165 bar predictions
50 bar predictions
Tv=Tw
Line through data of Nijhawan et al
Tv-Tsat
Tw-Tsat
150
100
50
0
0
100
200
300
400

Figure 2

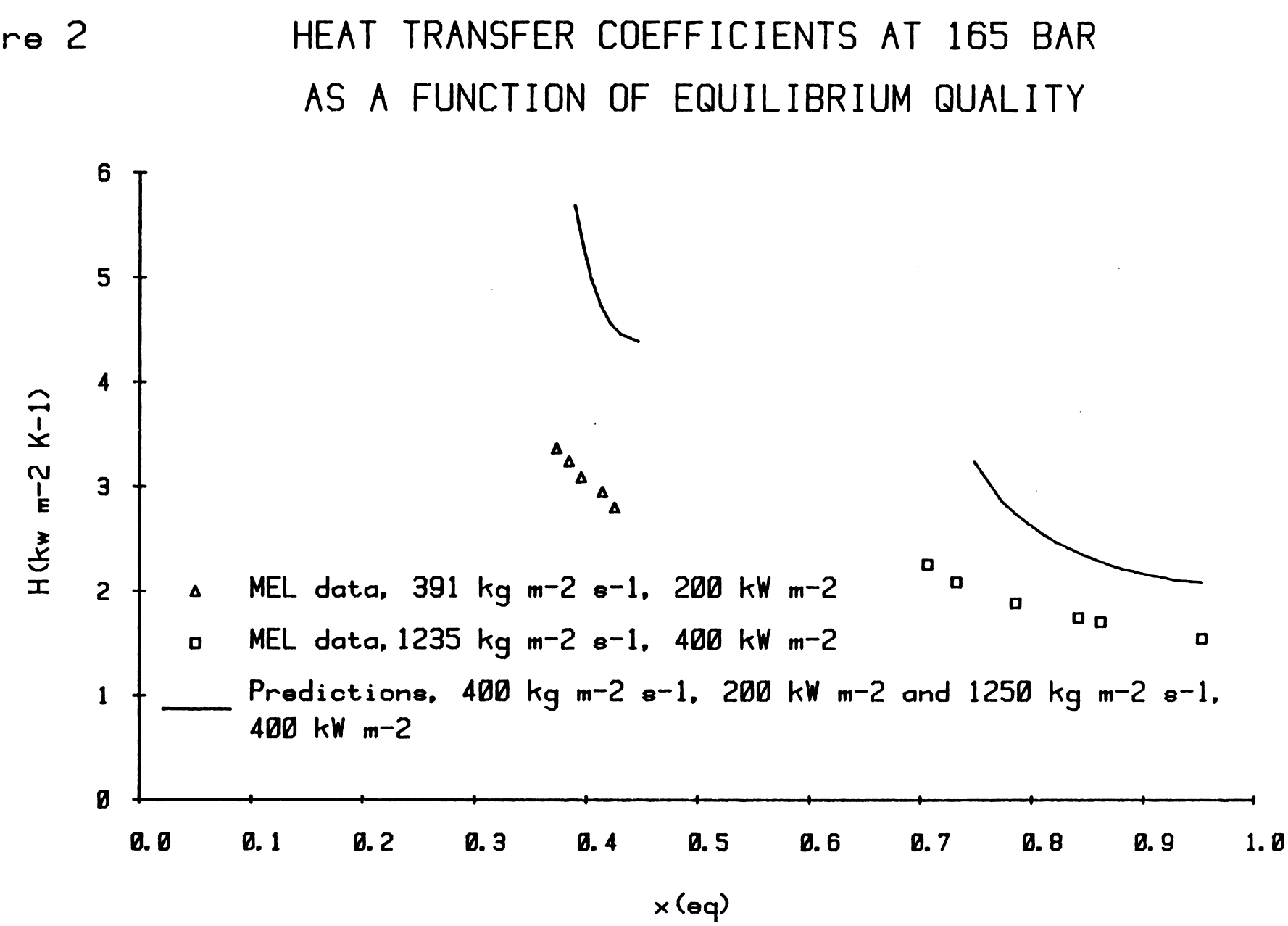
HEAT TRANSFER COEFFICIENTS AT 165 BAR
AS A FUNCTION OF EQUILIBRIUM QUALITY
H(kw m-2 K-1)
6
5
4
3
2
1
0
0.0
0.1
0.2
0.3
0.4
0.5
0.6
0.7
0.8
0.9
1.0
x(eq)
MEL data, 391 kg m-2 s-1, 200 kW m-2
MEL data, 1235 kg m-2 s-1, 400 kW m-2
Predictions, 400 kg m-2 s-1, 200 kW m-2 and 1250 kg m-2 s-1, 400 kW m-2

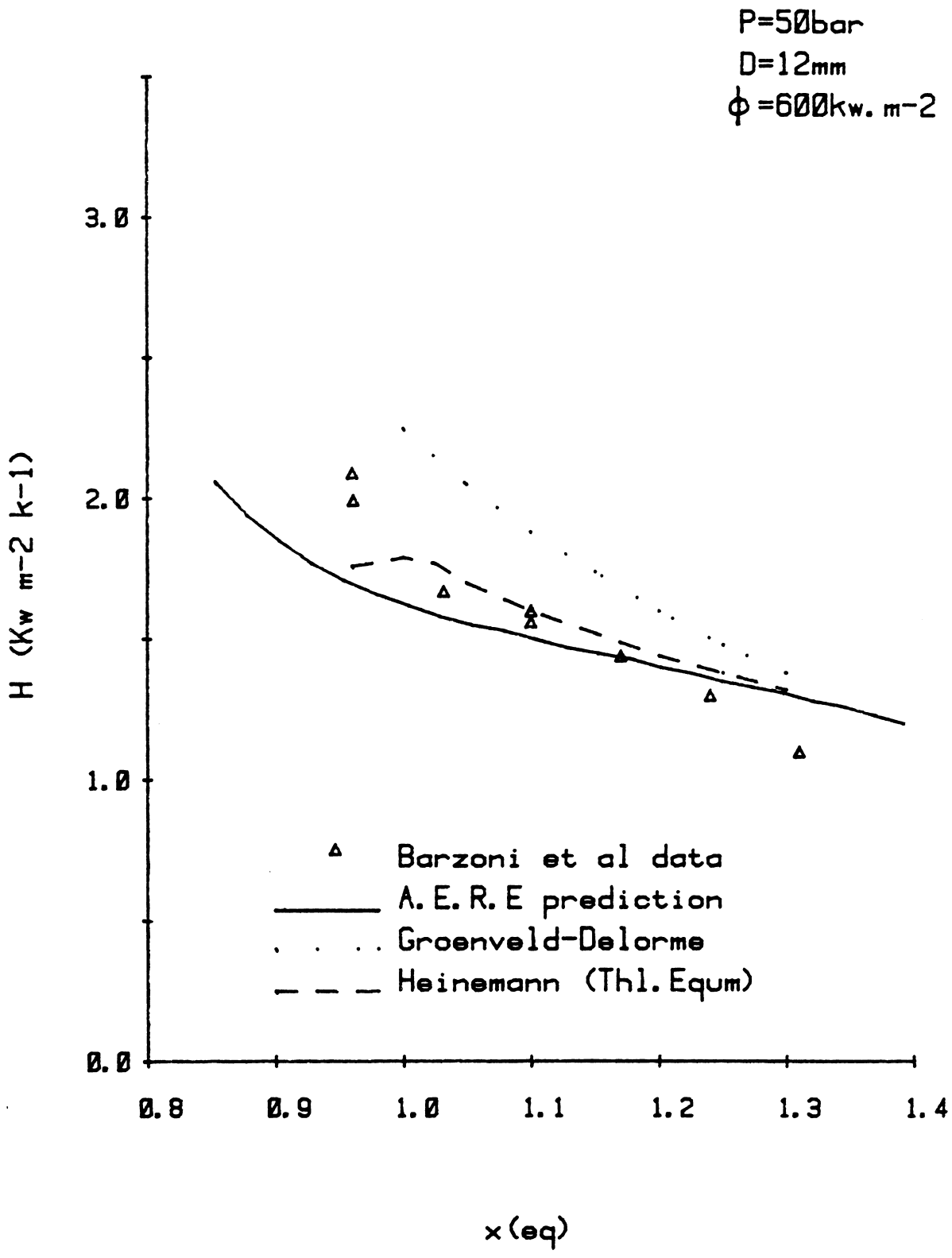

Figure 3

POST-CRISIS HEAT TRANSFER COEFFICENT AS A FUNCTION OF EQUILIBRIUM QUALITY

Figure 4 WALL TEMPERATURE PROFILE, 12 mm TUBE, 50BAR, 500 kg m-2 s-1 AND 600 kW m-2

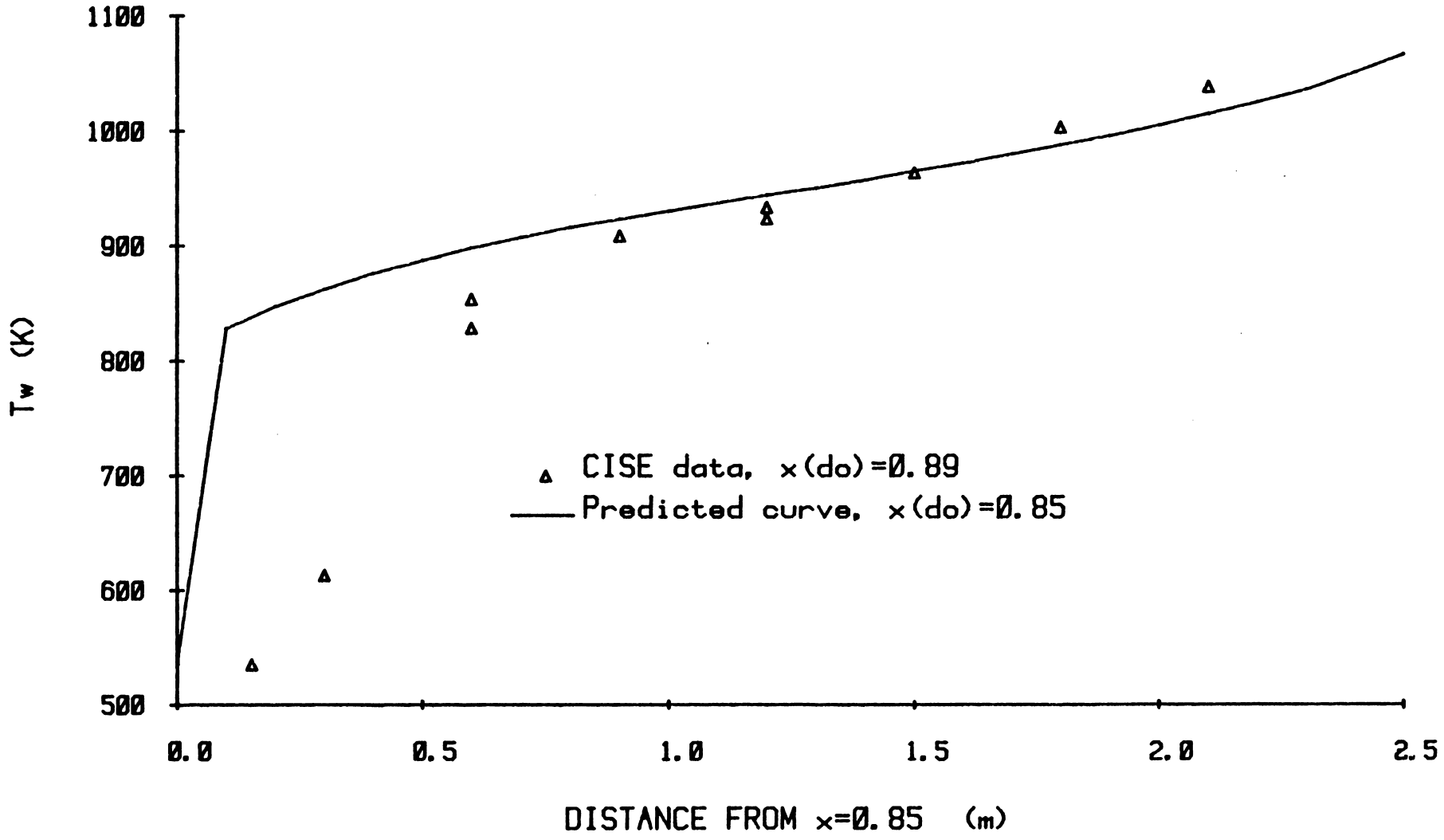

A SMOOTH TUBE ANALOGUE OF ROUGHENED WALL THERMOHYDRAULICS

by

D. R. H. Beattie

Australian Atomic Energy Commission
Private Mail Bag, Sutherland, 2232, Australia

Work performed while attached to Engineering Sciences Division, AERE Harwell, U.K.

ABSTRACT

Viscous sublayer velocity and temperature-profiles in the near-wall region of rough wall flows are modelled by a smooth-tube flow with suitably-chosen altered viscosity and thermal conductivity values over a region corresponding to the range of influence of the roughness elements. This modifes the form of classical smooth tube turbulence theory boundary conditions and leads to expressions in which the single roughness parameter equations of classical theory are replaced by multi-parameter roughness expressions, thus allowing thermohydraulics for different roughness types to be adequately described by the model.

NOMENCLATURE

B	Constant
C	Constant
c_p	Specific heat
D	Constant
f	Fanning friction factor
K	von Karmon constant
M	Factor
Nu	Nusselt number
Pr	Prandtl number
$\dot{q}$	Heat flux
Re	Reynolds number
u	Local velocity
u^+	Non-dimensional velocity
u*	Shear velocity
v	Cross-section averaged velocity
v^+	Non-dimensional wall distance
y	Wall distance

Greek

α	Heat transfer coefficient
β	Surface roughness function
γ	Volume fraction of spheres
ΔT	Temperature difference
δ	Reference position
ε	Roughness height
ε^+	Non-dimensional roughness height
ε_s	Nikuradse's sand roughness
η	Viscosity
κ	Smooth tube flow values
λ	Thermal conductivity
ρ	Density
τ_w	Wall shear
$\langle\ \rangle$	Cross sectional averaged value

1. INTRODUCTION

Classical turbulence theory has provided a reasonably firm basis for equations describing mean velocity distribution and wall shear for turbulent flow in smooth ducts. These equations are Reynolds number dependent and are regarded as having a "universal" character.

The theory has also provided a basis for similar equations in the case of flows in "completely roughened" ducts. These equations are independent of Reynolds number - this is the basis for the description "completely rough" - and instead depend on a dimensionless roughness height. Although the equations are well established, it is recognised that the basis for them is not as sound as it is for smooth ducts. This is largely because the roughness influence is characterised by a single parameter, whereas in reality, roughness, and hence its influence, is not a one-parameter property.

Classical theory is also conceptually applicable to flows in partially roughened ducts, this description being applied to flow conditions when the wall shear depends on both Reynolds number and roughness characteristics. However, whereas a single roughness characteristic leads to adequate equations for completely rough wall flows, this is not so in the transition region between smooth wall flows and completely rough wall flows: the characteristics depend on roughness type as well as magnitude. As a result, existing design characteristics depend more on empiricism than classical theory. Standard texts usually consider two such characteristics, those for commercial tubes, which, fortunately, are described by an empirical but nevertheless very neat synthesis, due to Colebrook (1939), of rough wall and smooth wall equations and, secondly the empirical curves of Nikuradse (1933), applicable to uniform sand grains from a particular source. (As noted by various authors; e.g. Robertson et al (1965), different curves are obtained for sand collected from different sources.) Examples of other transition region characteristics can also be found in work of Robertson et al (1965), Ruffel (1977) and Gudmundsson et al (1977), among others.

As with fluid mechanics smooth duct heat transfer is comparatively well understood. This has been achieved through the application of Reynolds analogy concepts, relating eddy diffusion of heat and momentum, to fluid mechanical equations developed from classical turbulence theory.

On the other hand, application of Reynolds analogy concepts to rough ducts is complicated by the fact that the augmentation of shear stress by transmission of turbulent stresses to the wall through pressure forces acting on protruberances has no analogy for heat transfer. Furthermore, roughness effects on heat transfer are, for the same reason, less than on wall shear, so there has been less incentive to understand rough wall heat transfer. The current situation is that a specific form of heat transfer equation, containing an unknown function of dimensionless roughness height, has been derived on the hypothesis that the influence of roughness on heat transfer is confined to the region near the wall (Dipprey and Sabersky, 1963). The form of the unknown function has been determined empirically by various authors. The lack of agreement between various proposals indicates that a general form is still evolving. A fuller description of the current state-of-the-art for rough wall heat transfer is given in the review by Bergles (1979) and Dalle Donne (1979).

In this paper, the effect of roughness on thermohydraulics is examined by considering the alteration to the velocity and temperature profiles in the region of the roughness elements. This allows rough duct flows to be analytically modelled by smooth duct flow of fluid with changes in physical properties near the wall, the changes in physical properties being chosen to produce profiles simulating those in the rough duct. By this method, the comparatively well established equations for smooth duct flow can be extended to provide rough duct equations which are more general than those existing at present.

The analysis neglects form drag on roughness elements, and, as such, does not extend to artifically rib-roughened and similar surfaces.

Equations describing the thermohydraulics of such surfaces can be found in the analysis by Lewis (1975).

For simplicity, the model is presented for round tube flows. Extension to other geometries can be achieved through the application of one of the various transformations summarised by Dalle Donne (1979).

Since the model is based on the results of classical turbulence theory for smooth ducts, and since it is desirable that equations developed from the model be matched with existing equations for rough wall flows, it is necessary to summarise relevant aspects of classical turbulence theory before presenting the model.

2. CLASSICAL THEORY OF TURBULENT PIPE FLOW

Local velocity u is considered as a function of wall distance y, viscosity η, density ρ, wall shear τ_w, and a characteristic surface roughness height ε:

$$u = u(y, \eta, \rho, \tau_w, \varepsilon) \qquad (1)$$

from which dimensional analysis gives

$$u^+ = u^+(y^+, \varepsilon^+) \qquad (2)$$

where $u^+ = u/u^*$ is a non-dimensional velocity, $y^+ = y \rho u^*/\eta$ is a non-dimensional wall distance, and $\varepsilon^+ = \varepsilon \rho u^*/\eta$ is a non-dimensional roughness height. In these definitions, $u^* = \sqrt{\tau_w/\rho}$ is the "shear velocity".

For a full description of roughness, the roughness height ε in equation (1) should be replaced by a set of length parameters A, each term describing one aspect of the roughness. In considering a single parameter of the set, classical theory can only be applied to ducts with geometrically similar roughness: a single parameter can completely specify the roughness of a set of different roughnesses with geometric similarity. In principle, classical theory must be re-applied to each different roughness type, producing different roughness-type expressions for u^+.

A feature of classical turbulence theory is the "velocity defect equation", applicable to the turbulent core of the flow:

$$u^+ = u^+_\delta + \frac{1}{K} \ln (y/\delta) \qquad (3)$$

where δ is a suitably chosen reference position. If the buffer region between the viscous-dominated near-wall region and the turbulence dominated core is neglected, it is convenient to choose δ as the assumed turbulent core boundary.

For smooth tubes, equations (1) and (2) reduce to

$$u = u(y, \eta, \rho, \tau_w) \qquad (4)$$

and $$u^+ = u^+(y^+) \qquad (5)$$

The velocity profile in the near wall region for smooth tubes is determined by Newton's law of viscosity:

$$\tau \simeq \tau_w = du/dy \simeq \eta\, u/y \qquad (6)$$

which can be re-expressed in terms of previously-defined dimensionless quantities as

$$u^+ = y^+ \qquad (7)$$

This is assumed to apply to a limiting u^+ value given by

$$u^+_\delta = C \qquad (8)$$

a "universal" constant.

Substitution of (8) and appropriate empirically-based numerical values for C and K into (3) leads to the smooth tube core region velocity profile

$$u^+ = 5.66 \log y^+ + 5.66 \qquad (9)$$

which, when averaged over the flow section, results in the Nikuradse friction factor: Reynolds number relation

$$1/\sqrt{f} = 4 \log Re \sqrt{f} - 0.4 , \qquad (10)$$

where $f = 2 \tau_w/(\rho v^2)$ is the Fanning friction

factor, Re = ρ v D/η is the Reynolds number, and v is the cross-section averaged velocity.

(The coefficients in equation (9) differ from those usually presented in standard texts. The equivalent equations usually presented are, however, incompatable with the Nikuradse equation. Equation (9) is not. For the remainder of this paper, when generally-quoted local velocity equations are inconsistent with generally-quoted friction factor equations, which are in effect the cross-section averaged local equations, coefficients in the local equations are altered to produce consistency with their friction-factor equivalent equations.)

For "completely rough" tubes, parameters relating to wall shear are independent of fluid viscosity, and, in classical theory, equations (1) and (2) are re-expressed as

$$u = u\,(y, \tau_w, \rho, \varepsilon) \qquad (11)$$

and

$$u^+ = u^+\,(y/\varepsilon) \qquad (12)$$

The boundary for equation (3), for a given roughness type, is of the form

$$u^+_\varepsilon = B \qquad (13)$$

In the special case of roughness due to sand grains from a particular source, Nikuradse found B to be 8.5, which, together with the appropriate value for von Karmon constant K reduces equation (3) to

$$u^+ = 5.66 \log \frac{y}{\varepsilon_s} + 8.5 \qquad (14)$$

where the ε_s indicates the value for the special case of Nikuradse's sand roughness. For the remainder of this paper, 8.5 is replaced by 8.62 to produce consistency with shear stress data.

The friction factor expression obtained by integrating equation (14) with 8.62 is

$$1/\sqrt{f} = 4 \log (D/\varepsilon_s) + 2.28 \qquad (15a)$$

In order to show the similarities between this, the friction factor equation for smooth tubes (equation 10), and later equations, it is convenient to express equation (15a) as

$$1/\sqrt{f} = -0.4 - 4 \log (0.214\ \varepsilon_s/D) \qquad (15b)$$

In accordance with expectations based on geometric similarity arguments given above, the constant "B" of equation (13) differs from that appropriate to Nikuradse's sand roughnesses when different types of roughness are used. A survey of relevant studies on this is contained in the work of Robertson et al (1965). Since equations (14) and (15) are well established, it has become convenient from an engineering viewpoint to consider roughness height for a particular type of "completely rough" tube not as some mean actual roughness height, but instead as an "equivalent sand roughness" whose value, when substituted in equations (14) and (15), produces consistency of those equations with the rough tube.

Equation (15a) indicates that resistance is proportional to the square of the velocity in the "completely rough" region of pressure loss characteristics. Since form drag also obeys a velocity-squared law, classical turbulence theory considers that friction for "completely rough" pipes is due to form drag acting on roughness elements projecting into the turbulent core of the flow.

Although the equivalent sand roughness concept is able to overcome some of the shortcomings due to characterising roughness by a single parameter, at least in the completely rough region of friction characteristics, the benefits do not extend to the "partially rough" region of the characteristics since the roughness type which influences the characteristics here cannot be adequately incorporated into a single roughness parameter.

Because characteristics for two types of roughness - that found in commercial pipes, and the sand-grained roughness studied by Nikuradse - are well established, emphasis will be placed on these roughness types later in this work.

For commercial pipes, friction factors agree with the smooth tube equation, equation (10), at low Reynolds numbers; decrease monotonically with Reynolds number but with a steady deviation from equation (10); and asymptotically approach the Reynolds number independent curve, equation (15a), for the appropriate equivalent sand roughness. Although classical theory has not been able to model these characteristics, Colebrook (1939) produced an elegant empirical synthesis of equations (10) and (15b):

$$1/\sqrt{f} = -0.4 - 4 \log \left(0.214\ \epsilon_s/D + 1/Re\ \sqrt{f}\right) \quad (16)$$

which has been found to be a very good description of commercial pipe friction characteristics. In view of the importance of commercial pipes in industry, the existence of the above simple friction factor equation is very fortunate.

The uniform sand grained roughness studied by Nikuradse has different friction characteristics. At lower Reynolds numbers, friction factors, although above those for smooth tubes, are much closer to the smooth tube equation (equation 10), (and indeed may be approximated by this equation) than friction factors for commercial papers of equivalent sand roughnesses. With increasing Reynolds number, the sand roughness friction factors reach a minimum, then increase and asymptotically approach the completely rough region of the curve described by equation (15a).

The difference between the above two types of roughness friction factor curve is conventionally explained as being due to the difference in the uniform sand roughness height and the more random roughness height distribution of commercial tubes. It is argued that the roughness influence is due to roughness elements extending into the turbulent core, i.e. being larger than $y^+ = 5$. With commercial tubes, a gradually increasing number of roughness elements will protrude into the turbulent core with decreasing sublayer thickness defined by $y^+ = 5$ and hence with increasing Reynolds numbers, hence the gradual deviation from the smooth tube equation. On the other hand, so the argument goes, all roughness elements of uniform sand roughness will remain within the sublayer for $\epsilon^+ < 5$, hence the closeness to the smooth tube equation. With decreasing sublayer thickness (i.e. increasing Reynolds number), a critical value is reached when all roughness elements then protrude into the turbulent core. The existence of a buffer region between the sublayer and turbulent core is regarded as preventing the transition from smooth-tube type characteristics to completely rough tube characteristics from being too abrupt.

Although the transition region for sand roughness is usually presented as empirical curves, usually in terms of "B" of equation (13) as a function of ϵ_s^+, Nedderman and Shearer (1964) used the above explanation to provide a two-region semi-empirical description for Nikuradse's data as the smooth tube equation (equation 10) for $\epsilon_s^+ < 11.8$, and

$$\frac{1}{\sqrt{f}} = -0.4 - 4 \log \left\{ 0.214 - \left(\frac{\epsilon_s}{D} - \frac{5\sqrt{2}}{Re\sqrt{f}} \right) \right\} \quad (17)$$

for $\epsilon_s > 11.8$. It should be noted that, if the buffer region is neglected, the transition between the sublayer and turbulent core occurs at $y^+ = 11.8$.

In the case of heat transfer to turbulent flow in a pipe, Reynolds analogy between eddy transport of heat and momentum leads to

$$\frac{\dot{q}}{\tau_w c_p} = \frac{\langle \Delta T \rangle - \Delta T_\delta}{\langle u \rangle - u_\delta} \quad (18)$$

where $\dot{q}$ is the heat flux, c_p is the specific heat, ΔT the temperature difference between the heated wall and the point of interest in the flow, $\langle -- \rangle$ denotes the cross-section averaged value, and other symbols are as defined earlier.

For smooth walls, the heat transfer in the molecular-transport dominated near wall region given by

$$\dot{q} = \lambda \frac{d\Delta T}{dy} \simeq \lambda \frac{\Delta T}{y} \qquad (19)$$

where λ is the thermal conductivity. Equation (19) is analogous to equation (6). From equations (6) and (19),

$$\frac{\dot{q}}{\tau_w c_p} = \frac{\Delta T_\delta}{u_\delta} \frac{\lambda}{\eta c_p} \qquad (20)$$

Eliminating ΔT_δ from equations (18) and (20),

$$\frac{\dot{q}}{\tau_w c_p} = \frac{<\Delta T_\delta>}{<u> \left\{ 1 + \frac{u_\delta}{<u>} \left(\frac{\eta c_p}{\lambda} - 1 \right) \right\}} \qquad (21)$$

which re-arranges to

$$Nu = \frac{\frac{f}{2} Re\ Pr}{1 + 5 \sqrt{\frac{f}{2}} (Pr - 1)} \qquad (22)$$

where $Nu = \alpha D/\lambda$ is the Nusselt number, α is the heat transfer coefficient and $Pr = \eta c_p/\lambda$ is the Prandtl number. The coefficient 5 in the denominator is based on the limit $y^+ = 5$ for the sublayer, rather than the intersect of the sublayer and turbulent core velocity profiles at $y^+ = 11.5$.

As stated previously, the situation for rough pipe heat transfer is less resolved. However, the general analyse of Dipprey and Sabersky (1963), which leads to

$$Nu = \frac{\frac{f}{2} Re\ Pr}{1 + 5 \sqrt{\frac{f}{2}}\ \beta\ (\varepsilon^+, Pr)} \qquad (23)$$

where $\beta\ (\varepsilon^+, Pr)$ is a function which allows for surface roughness effects, is generally regarded as appropriate. Various empirical versions of the functional form of β are summarised by Bergles (1974).

3. A SMOOTH TUBE ANALOGUE OF ROUGH TUBE THERMOHYDRAULICS

This smooth tube analogue of rough tube thermohydraulics is summarised in Figure 1. The main features are:

(1) The region of influence of roughness on velocity profile extends beyond the position of an appropriately defined mean roughness height ε by a factor M. This must be the case for non-uniform roughness, and is also expected for uniform roughness. In order to avoid the problem of form drag on roughness elements protruding into the turbulent core, the present model is confined to the case where $M\varepsilon$ lies within the viscous-dominated sublayer region.

(2) The velocity profile in the region $y < M\varepsilon$ for a rough wall flow with fluid viscosity η is similar to that for a smooth tube flow of fluid with viscosity $\eta_\varepsilon > \eta$. Although a suitably chosen varying viscosity would more exactly model the roughness region velocity profile, our present knowledge of the velocity behaviour in the roughness region is such that there is little to be gained by such an approach, so the simpler treatment involving a constant η_ε in the region $y < M\varepsilon$ is followed here.

The near-wall velocity profile then obeys

$$\tau = \eta_\varepsilon\ du/dy \simeq \tau_w,\ y < M\varepsilon \qquad (24)$$

(3) The velocity profile is continuous at $y = M\varepsilon$ and in the outer viscous dominated region is controlled by

$$\tau = \eta\ du/dy \simeq \tau_w,\ M\varepsilon \leq y < \delta \qquad (25)$$

The upper validity limit of this equation is given by $u^+ = 11.8$. As with the summary of classical theory presented earlier, this upper limit neglects the exitence of a buffer region. A buffer region can be readily allowed for, but is omitted from this analysis because its inclusion produces algebraic complexity and has little effect on the main consequences of the model.

(4) As in the general case of classical turbulence theory, the turbulent core is described by a logarithmic equation. However, whereas there is a unique well-defined reference position ($y = 0$) for this logarithmic layer in the case of smooth tube flows, it does not follow that the position $y\ (u = 0) = 0$ is by definition the appropriate reference for the logarithmic layer in rough tubes. Indeed, many experimenters studying artificial roughness, e.g. Perry and Joubert (1963), have reported

that the logarithmic velocity profile does not necessarily have its origin at the base level of the roughness elements. This is allowed for in the present model by having an origin at y_o, which may be regarded as one of the parameters required for a full description of roughness. As a result, the velocity defect equation (equation 3) is replaced by

$$\frac{u}{u^*} = \frac{u_\delta}{u^*} + \frac{1}{\kappa} \ln \frac{y - y_o}{\delta - y_o} \qquad (26)$$

Equations (24) - (26) are similar to their smooth tube equivalents, equations (6) and (3). The classical turbulence theory development of equations (6) and (3) can thus be adapted to equations (24) - (26).

From equation (24)

$$\tau_w = \eta_\varepsilon \frac{u}{y} \quad , \quad y < M\varepsilon \qquad (27)$$

$$\therefore \quad \frac{u}{\sqrt{\tau_w/\rho}} = \frac{y \sqrt{\tau_w \rho}}{\eta} \quad , \quad y < M\varepsilon \qquad (28)$$

and at $y = M$

$$\frac{u_{M\varepsilon}}{\sqrt{\tau_w/\rho}} = \frac{M\varepsilon \sqrt{\tau_w \rho}}{\eta_\varepsilon} \, . \qquad (29)$$

From equation (25)

$$\tau_w = \eta \frac{(u - u_{M\varepsilon})}{y - M\varepsilon} \quad , \quad M\varepsilon \leq y < \delta \qquad (30)$$

which, with the aid of equation (29), rearranges to

$$\frac{u}{\sqrt{\tau_w/\rho}} = \sqrt{\tau_w \rho} \left\{ \frac{y}{\eta} - \frac{M\varepsilon}{\eta} \left(1 - \frac{\eta}{\eta_\varepsilon} \right) \right\} ,$$

$$M\varepsilon \leq y < \delta. \qquad (31)$$

Together, equations (25) and (31) can be regarded as components of the sublayer equation

$$u^+ = y^+ \quad , \quad y < \delta \qquad (7)$$

This interpretation incorporates a change in the definition of y^+ at $y = M$ due to the change in effective viscosity at this position.

The classical theory upper limit to equation (7),

$$u_\delta^+ = \delta^+ = C \qquad (8)$$

is assumed to apply also in the present case of a two-level sublayer, producing

$$\frac{u_\delta}{\sqrt{\tau_w/\rho}} = C \qquad (32a)$$

and $$\frac{\delta \sqrt{\tau_w \rho}}{\eta} = C + \frac{M\varepsilon}{\eta} \frac{\sqrt{\tau_w \rho}}{\eta} \left(1 - \frac{\eta}{\eta_\varepsilon} \right) \qquad (32b)$$

Equation (32b) implies that the sublayer thickness in the case of a rough tube is thicker than for a smooth tube with the same flow conditions, even though the same boundary conditions apply to the two systems.

Applying the limits expressed by equations (32) to the velocity defect equation (equation 26), leads to the core region velocity profile equation:

$$\frac{u}{\sqrt{\tau_w/\rho}} = (C - \frac{1}{\kappa} \ln C) + \frac{1}{\kappa} \ln \left\{ \frac{\frac{y - y_o}{\eta} \sqrt{\tau_w \rho}}{1 + \frac{M}{C} \varepsilon \left(1 - \frac{\eta}{\eta_\varepsilon} \right) \frac{\sqrt{\tau_w \rho}}{\eta} - \frac{y_o}{C} \frac{\sqrt{\tau_w \rho}}{\eta}} \right\} ,$$

$$y > \delta \qquad (33)$$

Considered in conjunction with equation (7), equation (33) indicates that the "universal" profile for smooth tubes also applies to rough tubes if the definition of y^+ changes not only at $y = M\varepsilon$ but also at $y = \delta$. (This feature of the model is not altered by the inclusion of a buffer region between the viscous sublayer and the turbulent core, if an additional definition of y^+ is also allowed for in this region.)

Although y_o is an as yet unquantified parameter of the model, the reasons for its inclusion suggest $y_o < M\varepsilon$. Since the present model is confined to the case where $M\varepsilon$ lies within the viscous region, we can then make the assumption $y - y_o \simeq y$ over the range of validity of equation (33). This approximation, together with appropriate smooth tube flow values for C and κ, reduce equation (33) to

$$\frac{u}{\sqrt{\tau_w/\rho}} = 5.66 - 2.46 \ln\left\{\left(\frac{y\sqrt{\tau_w\rho}}{\eta}\right)^{-1} + 0.08\frac{M\varepsilon}{y}\left(1 - \frac{\eta}{\eta_\varepsilon}\right) - 0.08\frac{y_o}{y}\right\}$$

$$u^+ > 11.8 \qquad (34)$$

The above development has omitted the buffer layer region of the velocity profile. When this is included in the analysis, equation (34) is replaced by

$$\frac{u}{\sqrt{\tau_w/\rho}} = 5.66 - 2.46 \ln\left\{\left(\frac{y\sqrt{\tau_w\rho}}{\eta}\right)^{-1} + 0.2\frac{M\varepsilon}{y}\left(1 - \frac{\eta}{\eta_\varepsilon}\right) - 0.2\frac{y_o}{y}\right\}$$

$$u^+ > 30 . \qquad (35)$$

Averaging this equation over the flow section leads to the friction factor equation

$$\frac{1}{\sqrt{f}} = -0.4 - 4 \log\left\{(Re\sqrt{f})^{-1} + 0.142\frac{M\varepsilon}{D}\left(1 - \frac{\eta}{\eta_\varepsilon}\right) - 0.142\frac{y_o}{D}\right\} \qquad (36)$$

Heat transfer for rough wall flows is modelled in a similar way to the above treatment for fluid mechanics. The fluid temperature profile in the sublayer region will be flatter in the region of roughness elements, and this effect is simulated by a smooth tube model with a larger fluid thermal conductivity λ_ε, over the region of influence of the roughness elements. For simplicity, that region is assumed to be the same as for the roughness region of influence for fluid mechanics, i.e. $y < M\varepsilon$.

Adapting the classical theory summarised earlier, the core region heat transfer is, as before,

$$\frac{\dot{q}}{\tau_w c_p} = \frac{\langle\Delta T\rangle - \Delta T_\delta}{u - u_\delta} \qquad (18)$$

From equations (27) and (30)

$$\tau_w = \frac{u_{M\varepsilon}}{M\varepsilon/\eta_\varepsilon} = \frac{u_\delta - u_{M\varepsilon}}{(\delta - M\varepsilon)/\eta}$$

$$\therefore \tau_w = \frac{u_\delta}{\frac{M\varepsilon}{\eta_\varepsilon} + \frac{\delta - M\varepsilon}{\eta}} \qquad (37)$$

A similar treatment for heat transfer leads to

$$\dot{q} = \frac{\Delta T_\delta}{\frac{M\varepsilon}{\lambda_\varepsilon} + \frac{\delta - M\varepsilon}{\lambda}} \qquad (38)$$

Eliminating δ from (37) and (38)

$$\frac{\dot{q}}{\tau_w c_p} = \frac{\Delta T_\delta}{u_\delta}\frac{\lambda}{\eta c_p} + \frac{M\varepsilon}{\lambda}\frac{\dot{q}}{u_\delta}\frac{\lambda}{\eta c_p}\left(\frac{\eta}{\eta_\varepsilon} - \frac{\lambda}{\lambda_\varepsilon}\right) \qquad (39)$$

which is an extension of equation (20). As in the development of equation (22) from equations (18) and (20), the heat transfer coefficients for the smooth tube simulation of rough tubes is obtained by eliminating ΔT_δ from equations (18) and (39), and replacing $u_\delta/\langle u\rangle$ by $5\sqrt{f/2}$. The final equation is

$$Nu = \frac{\alpha D}{\lambda} = \frac{\frac{f}{2} Re\, Pr}{1+5\sqrt{\frac{f}{2}}(Pr-1) + \frac{M\varepsilon}{D}\frac{f}{2} Re\, Pr\left(\frac{\eta}{\eta_\varepsilon} - \frac{\lambda}{\lambda_\varepsilon}\right)} \qquad (40)$$

4. DISCUSSION

Considering fluid mechanical aspects first, it can be seen from equations (35) and (36) that the model has led to a four parameter ε, M, $(1 - \eta/\eta_\varepsilon)$ and y_o description of roughness effects on turbulent pipe flow instead of the one ε_s, of classical theory. Moreover it is reasonable to suppose that the parameters M, $(1 - \eta/\eta_\varepsilon)$ and y_o are all related to roughness element density and shape. This aspect will be examined in more detail later.

The increased number of roughness parameters incorporated in equations (35) and (36) places these equations in a better position to be adapted to the various empirically obtained characteristics for different roughness types than the one-parameter roughness modelling of classical theory. Since roughness data tend to be presented as $B(\varepsilon_s^+)$, where B is defined by equation (13), a comparison of the present

equations with data is best achieved by expressing the present equations in terms of B.

Considering the large ϵ asymptote of equation (35),

$$u^+ = 5.66 - 5.66 \log \left\{ 0.2 \frac{M\epsilon}{y} \left(1 - \frac{\eta}{\eta_\epsilon} \right) \right\},$$

it is clear that this can be equated to the "completely rough" sand roughness equation, equation (14), by the substitution

$$\epsilon_s = \frac{2}{3} M \epsilon \left(1 - \frac{\eta}{\eta_\epsilon} \right) \qquad (41)$$

From the definition of B as

$$B = u^+ - 5.66 \log y/\epsilon_s ,$$

equation (35) can now be expressed as

$$B = 5.66 \left[1 - \log \left\{ (\epsilon_s^+)^{-1} + 0.3 \left\{ 1 - 2\, y_o/(3\epsilon_s) \right\} \right\} \right] \qquad (42)$$

The choice of the product of the roughness parameters M and $(1 - \eta/\eta_\epsilon)$ in the relation of the actual mean roughness height ϵ and the equivalent sand roughness ϵ_s, as given in equation (41), ensures that equation (42) goes to the correct asymptote at large ϵ_s^+. At smaller ϵ_s^+, the value of B depends on the value y_o which defines the origin for the logarithmic region of the velocity profile.

In the case of a random distribution of roughness element size, there appears to be only one position in the roughness region which would form a well-defined origin for the logarithmic layer - that at y = 0. This choice reduces B to

$$B = 5.66 \left[1 - \log \left\{ (\epsilon_s^+)^{-1} + 0.3 \right\} \right] \qquad (43)$$

which, in fact, is the form appropriate to commercial tube of random roughness size. This can be more readily seen by substituting equation (41), and y = 0, (which reduced equation (35) to (43)), into the friction-factor equation for the present model, equation (36). These substitutions convert that equation to the empirically-based Colebrook equation, (equation 16), which has been found appropriate for commercial tubes.

In the case of uniform roughness distribution such as was examined by Nikuradse with his artificial sand roughened tubes, the position of the tops of the roughness element also presents a well defined position with respect to the roughened region. Moreover, it is conceivable that at this position might be a more suitable origin for the logarithmic region than y = 0: the rather abrupt transition at the outer edge of the roughness layer could inhibit the turbulence generation mechanism within the roughness layer. Now, although ϵ_s represents the size of sand grains used by Nikuradse, the coatings on the grains necessary to cause adhesion to the surfaces studied means that the actual roughness protrusions were slightly larger than ϵ_s. Allowing a factor 1.25 for the ratio of coated to uncoated grain size (Robertson et al (1965) quote figures which suggest that this is reasonable), a choice

$$y_o = 1.25\, \epsilon_s$$

then places the origin of the logarithmic region at the surface of the roughness elements. This choice of y_o reduces equation (42) to

$$B = 5.66 \left\{ 1 - \log \left(\frac{1}{\epsilon_s^+} + 0.005 \right) \right\} \qquad (44)$$

This equation is compared with Nikuradse's data in Figure 2. The agreement with the low ϵ_s^+ data indicates that concepts behind equation (44) are reasonable up to $\epsilon_s^+ \simeq 7$. Also shown is the "smooth tube" relation

$$B = 5.66 \,(1 + \log \epsilon_s^+) \qquad (45)$$

which is usually regarded as being appropriate for low values of artificial ϵ_s^+. It is seen that equation (44) is more appropriate; a situation which reflects the fact that, although low Reynolds number sand-roughness friction factors are close to the smooth tube friction factor - Reynolds number relation, they are slightly above. It follows from equation (44) that the appropriate equation for sand-roughness friction factors in the low Reynolds number region is

$$\frac{1}{\sqrt{f}} = -0.4-4\log\left\{(Re\sqrt{f})^{-1} - 0.036\frac{\epsilon_s}{D}\right\} \quad (46)$$

The deviation of Nikuradse's data from equation (44) at higher ϵ_s^+ values require a form of equation (42) which intersects equation (44) in the region $\epsilon_s^+ = 10$. Trial and error indicates that a choice of y_o given by $y_o^+ = 11.8$, which is the position of the intersection of the laminar sublayer equation (equation 7) and the turbulent core equation (equation 9) for turbulent smooth tube flow of constant viscosity, provides

$$B = 5.66\left\{1 - \log(0.3 - 1.36/\epsilon_s^+)\right\} \quad (47)$$

which adequately describes Nikuradse's high ϵ_s^+ data (Figure 2). (The discrepancy at very high ϵ_s^+ values is associated with the previously mentioned slight discrepancy between velocity profile coefficients as obtained from velocity profile data and as obtained from shear stress data. The coefficients of the present equations are chosen to ensure agreement with accepted shear stress equations.)

The friction factor equation corresponding to equation (47) is

$$\frac{1}{\sqrt{f}} = -0.4-4\log\left\{0.214\left(\frac{\epsilon_s}{D} - \frac{4.56\sqrt{2}}{Re\sqrt{f}}\right)\right\} \quad (48)$$

which is close to equation (17) proposed by Nedderman and Shearer (1964).

The similarity between equations (17) and (48) and between equations (44) and (45), camouflages the fundamentally different bases for the different pairs of equations. Recalling the classical arguments presented earlier, the classical concept is that roughness only manifests itself if roughness elements protrude into the turbulent core. Consequently, uniform roughness elements within the viscous sublayer have no influence (hence the "smooth tube" relation, equation (45)) and if the roughness elements protrude into the core region, the effective significant roughness is the true roughness height minus the sublayer thickness (hence equation (17)).

On the other hand, the present model considers the effect of roughness confined to the viscous dominated region to be generally significant. In fact, it has been demonstrated that the classical arguments supporting the "smooth tube" relation, equation (45), provide instead a basis for the semi-empirical commercial rough tube equation proposed by Colebrook. In the present work, the shape of uniform roughness characteristics is explained by the logarithmic region origin being the minimum of the outer layer of the roughness region and the position where the turbulent region would have started in the absence of the roughness. (Since, the the present model, the roughness is considered as being entirely in the viscous sublayer, the second option for the log-layer origin indirectly supports the current view that the viscous dominated sublayer is not entirely devoid of turbulence.)

Further study of friction characteristics of roughnesses types other than those analysed above requires knowledge of the relation between the actual roughness height and the equivalent sand roughness. Although other characteristics can probably be curve-fitted through simple choices of y_o in equation (42), as has been done above, adequate interpretations of y_o values so obtained might not be achieved without knowledge of the relation between ϵ and ϵ_s. In the case of the above analyses of Nikuradse's sand-roughness data, for example, the interpretation of lower values of y_o as the actual height of the uniform roughness depended on an estimate of the height (which represent coated sand grains) in terms of the stated uncoated sand grain dimensions.

With regard to the relation between ϵ_s and actual roughness parameters, work at Babcock Ltd. (Ruffel, 1977) has examined (and is examining) the inter-relation between friction factor - Reynolds number characteristics and actual roughness characteristics for different roughness types as obtained from a Talysurf machine. An inter-relation between the two has not been successfully achieved, possibly because the single parameter 'equivalent sand roughness' of classical theory cannot readily incorporate different roughness types. It is

conceivable that the present model, with several parameters included in the description of roughness, could assist in the coupling of Babcock's friction and roughness characteristics.

Although a full analysis which relates actual roughness ε and equivalent sand roughness ε_s is beyond the scope of this work, some general aspects of the influence of roughness element shape and density of packing can be obtained by considering the role of the equivalent smooth tube viscosity η_ε used to model the velocity in the roughness region.

It has been shown by Einstein (1906) that the viscosity of a liquid containing non-interacting solid spheres can be approximated by

$$\eta_\varepsilon = \eta\ (1 + 2.5\gamma)$$

where γ is the volume fraction of the spheres, for low values of γ. The approximations used in the final stages of Einstein's analyses can be adapted to yield instead

$$\eta_\varepsilon = \eta\ (1 - 2.5\gamma)^{-1}$$

which in fact agrees with available data (see for example Sather and Lee, 1974) to higher γ values.

The coefficient 2.5 in Einstein's analysis is a consequence of the spherical shape assumed for the solid objects within the fluid. Different shaped objects could be expected to yield different coefficients.

Thus, Einstein's analysis suggests that the effective smooth tube viscosity η_ε of this work can be described by

$$1 - \frac{\eta}{\eta_\varepsilon} \propto \gamma \qquad (49)$$

where the proportionality factor is a function of the shape of roughness elements, and γ is the volume fraction of roughness elements in the roughness region.

If the roughness influence range multiplier M is assumed to be a constant for a given roughness element shape, it follows from equations (40) and (49) that

$$\varepsilon_s/\varepsilon = K\gamma \qquad (50)$$

where K is a function of roughness shape only. Figure 3 shows that this is a reasonable description for artificial roughness elements made from rods, slats, spheres, spherical segements and cones, at least in the lower voidage region where the assumed linear voidage - effective viscosity relation is more plausible.

Turning now to heat transfer characteristics, we note that the present heat transfer model contains an extra degree of complexity due to the introduction of an extra variable, the effective sublayer conductivity in the roughness region. For this reason, the heat transfer equation derived from the model, equation (40), has not been further developed by comparison with data as was done with the purely fluid mechanical aspects of the model. Nevertheless, there are several aspects of equation (40) which can be noted:

(1) The form of equation (40) is consistent with the general form proposed by Dipprey and Sabersky (1963), equation (23). However equation (40) suggests that the function $\beta\ (\varepsilon^+, Pr)$ of equation (23) cannot be separated into the form $\beta_1\ (\varepsilon^+)\ \beta_2\ (Pr)$ as was supposed by Dipprey and Sapersky (1963) and Webb et al (1971).

(2) Just as η_ε can be modelled as depending on roughness element shape and volume fraction, as described above, so can λ_ε. However, the modelling for λ_ε must be different, leading to a different dependence on shape and volume fraction. Knowledge of equivalent sand roughness (cf. equation 41) is thus not sufficient to quantify the term $M\varepsilon\ (\eta/\eta_\varepsilon - \lambda/\lambda_\varepsilon)$ appearing in the heat transfer equation (equation 40).

(3) Since heat transfer through the roughness region involves heat transfer through both roughness elements and liquid, the effective thermal conductivity λ_ε required for smooth tube modelling of the roughness region

temperature profile will involve both the fluid thermal conductivity and the wall conductivity λ_w. For example, for uniform height roughness elements of parallel sides it is clear that $\lambda_e = (1 - \alpha)\lambda_w + \gamma\lambda$. According to equation (40), the overall Nusselt number will therefore depend slightly on the tube thermal conductivity, a feature not included in equation (23), but nevertheless consistent with empirical observations (Kimpton and Lyall, 1972; Mantle et al, 1971).

A particular point of discussion concerns the nature of the smooth tube, double viscosity model of rough wall lows. Although the model may appear somewhat artificial, there are, in fact, some experimental data which support the concept behind it.

The most directly relevant data is that obtained by Fleming et al (1972), who measured shear stresses due to turbulent mercury flow in copper tubes. Two tubes were used, each initially clean. Initial f:Re plots agreed with the smooth tube relation, but later friction factors behaved as if in rough tubes: the friction factors became independent of Reynolds number, at least, up to a limit to be discussed below. Moreover, the effective apparent roughnesses increased with time, and was more apparent in the smaller tube.

Although detailed explanation of the phenomena could not be given by the authors, it was recognised by them that the effects were due to the growth of a viscous layer of amalgam of mercury and copper at the tube wall. Although actual thicknesses of the amalgam were not measured, the friction factor behaviour is in qualitative agreement with the two-viscosity model proposed here. Water flowing through the amalgamated tubes had smooth tube characteristics, suggesting an amalgam-surface origin for the logarithmic layer during the water experiments.

In addition to the above experiments, there are a substantial number of data from a particular type of system involving the simultaneous flow of gas and liquid. At high velocities with very small fractions of liquid, the liquid flows predominantly along the walls of the duct, with the gas flowing in the core region of the flow (annular flow). Although these flows are not fully understood, the best current models for very thin films at not too high values of Reynolds number are based on the idea of gas flowing in an effectively roughened tube, with roughness elements consisting of waves on the liquid film (Hewitt and Hall-Taylor, 1970). It could be argued that the characteristics are due instead to differences in the gas and liquid viscosities. The characteristics therefore qualitatively support the present model, suggesting it is not that the film acts as a roughened surface, but rather a rough surface acts like the film region of annular flow. In principle the present model can be developed to qualitatively test this interpretation of two-phase annular flow. In practice, the additional variable due to non-constant radial density has not yet been satisfactorily incorporated into the model.

As already pointed out, the present model of roughness is based on the concept of an influence in the viscous dominated region of the flow, a view which contradicts currently accepted concepts of roughness effects in turbulent flow. Having quoted data pertaining to mercury flow in copper tubes and annular two-phase flow, it is relevant to point out that these same data are also relevant to the present modelling of roughness for roughness elements that may protrude into the turbulent core.

As pointed out, the mercury flow Reynolds number independent friction factor which increased with time can be explained in terms of the present model by the growth of a high-viscosity region near the wall. However, this behaviour was observed only at lower (but nevertheless turbulent) Reynolds numbers. At high Reynolds numbers, the friction factor data reverted back to a dependence on Reynolds number, and an independence of time (i.e. of the region of higher viscosity). However, the f:Re relation differs significantly from that usually encountered, reflecting an alteration of the coefficients of the velocity defect equation from those usually encountered. (The

usually encountered form is an integral part of the present model.)

Similarly, unlike the lower Reynolds number annular flow situation described above, higher Reynolds number two-phase annular flow friction factors appear to be independent of film thickness, and, instead, depend on Reynolds number, with the dependence being different from the usually-encountered smooth tube equation (Beattie, 1977).

A possible explanation of the above is that higher Reynolds number place the turbulent core boundary within the higher viscosity region of the amalgamated mercury and the two-phase flow systems. The influence of the increased viscosity is then not confined to the effect within the viscous dominated sublayer, and the effect in the turbulent core is to change the turbulence characteristics, not just the turbulent core boundary conditions, as is the case in the present analysis.

The higher Reynolds number flow characteristics described above, in conjunction with the present model, suggest that friction characteristics for roughness elements which would protrude into the turbulent core, actually become independent of the roughness, and instead revert to a dependence on Reynolds number, with characteristics above those for smooth tube flows. There are at least some roughened wall friction characteristics (Gudmundsson et al, 1977; Ruffel, 1977) consistent with this decription.

5. SUMMARY AND CONCLUSIONS

Roughness elements in duct walls alter the fluid velocity and temperature profiles in the roughness region. These effects may be analysed in terms of a smooth tube flow with altered viscosity and thermal conductivity in the near-wall region. The effective viscosity required to produce the same effect as roughness elements is a function of roughness element shape and density as well as the fluid viscosity. The effective thermal conductivity is a function of roughness element shape, density, fluid thermal conductivity, and also duct wall conductivity. The equivalent sand roughness for fluid mechanical calculation is a function of the mean roughness height, roughness element shape, and roughness element density. Due to different dependences of the effective wall region conductivity and viscosity on roughness parameters, the hydraulically-based equivalent sand roughness is not appropriate to heat transfer calculations except insofar as the heat transfer depends on friction factor.

The origin of the logarithmic layer of the turbulent flow may be altered by roughness elements. The position of the origin may be regarded as a length parameter relevant to a full description of roughness, and differences in its value for different types of roughness are the prime cause of different types of roughness effect on turbulent flow. Random sizes roughness elements have the origin at the base of the roughness elements; roughness elements of uniform size present an alternative well-defined suitable origin for the log-layer at the outer edge of the roughness layer.

The model has been used to develop general equations relevant to rough wall thermo-hydraulics. The equations relevant to fluid mechanics were further developed by examining the nature of "equivalent sand roughness" and the origin of the turbulent core log-layer. Colebrook's empirically based equation evolved naturally from the model by considering a base-level for the log-layer origin; Nikuradse's sand-roughness data were described by the same equations, but with the origin of the log-layer being given by the minimum of the sand roughness height and the position where the turbulent core boundary would be in the absence of the roughness elements.

Roughness elements need not protrude into the turbulent core to influence thermohydraulic characteristics. Roughness elements cause an increase inthe extent of the viscous dominated region, so are more likely to remain within this region than is considered by earlier roughness models. The influence on the flow characteristics is due to the widening of the viscous-dominated region. Roughness elements

protruding into the turbulent core may alter the turbulent structure of the core as well as the boundary conditions to the turbulent core.

Available smooth-tube variable viscosity shear-stress data are in qualitative agreement with the model presented here and thus support the concept of a smooth-tube two-viscosity flow simulation of rough wall pipe flow.

REFERENCES

BEATTIE, D.R.H. (1977) "Some Aspects of Two-Phase Flow Drag Reduction", Proc. 2nd Int. Conf. Drag Reduction, BHRA Fluid Engng., Paper D1.

BERGLES, A.E. (1979) "Augmentation of Forced-Convection Heat Transfer: Article in Turbulence Forced Convection in Channels and Bundles", Ed. KAKAC and SPALDING, McGraw-Hill, New York.

COLEBROOK, C.F. (1939) "Turbulent Flow in Pipes, with Particular Reference to the Transition Between the Smooth and Rough Pipe Laws", J. Inst. Civil Engrs., Vol. 11, pp.133-156.

DALLE-DONNE, M. (1979) "Convective Heat Transfer from Rough Surfaces: Article in Turbulence Forced Convection in Channels and Bundles", Ed. KAKAC and SPALDING, McGraw-Hill, New York.

DIPPREY, D.F. and SABERSKY, R.H. (1963) "Heat and Momentum Transfer in Smooth and Rough Tubes at Various Prandtl Numbers", Int. J. Heat Mass Transfer, Vol. 6, pp.329-353.

EINSTEIN, A. (1906) "A New Determination of Molecular Dimensions", Ann. Phys. (Leipzig), Vol. 19, No. 4, pp.289-306.

FLEMING, I.K., MOLLOY, N.A. and McCARTHY, M.J. (1972) "Mercury Flow in Metallic Conduits Under Non-Wetting and Amalgamating Conditions", Nature Phys. Sci., Vol. 240, No. 99, pp.69-71.

GUDMUNDSSON, J.S., NEWSON, I.H. and BOTT, T.R. (1977) "Rippled Deposits: Formation and Pressure Drop Effects. HTFS RS179, AERE-R 8703.

HEWITT, G.F. and HALL-TAYLOR, N. (1970) "Annular Two-Phase Flow", Pergamon Press, Oxford.

JONASSEN, F. (1942) "Artificial Roughness", U. California, Fluid Mech. Lab., (Data quoted by Robertson et al, 1965).

KIMPTON, A.D. and LYALL, H.G. (1972) "The Heat Transfer and Pressure Drop Performance of a Surface Roughened by Small Square Ribs", J. Britt. Nucl. Energy. Soc., Vol. 11, pp.271-277.

MANTEL, P.L., FREEMAN, A.R. and WATTS, J. (1971) "Conductivity Effects on Ribbed Surface Heat Transfer", Int. J. Heat Mass Transfer, Vol. 14, pp.1825-1834.

NEDDERMAN, R.M. and SHEARER, C.J. (1964) "Correlations for the Friction Factor and Velocity Profile in the Transition Region for Flow in Sand-Roughened Pipes", Chem. Engng. Sci., Vol. 19, pp.423-428.

LEWIS, M.J. (1975) "An Elementary Analysis for Predicting the Momentum- and Heat-Transfer Characteristics of a Hydraulically Rough Surface", J. Heat Transfer, Vol. 97, pp.249-254.

NIKURADSE, J. (1933) "Laws for Flow in Rough Pipes", VDI-Forschungscheft 361, Series B, No. 4 (NACA TM 1291 (1950)).

PERRY, A.E. and JOUBERT, P.N. (1963) "Rough-Wall Boundary Layers in Adverse Pressure Gradients", J. Fluid Mech., Vol. 17, pp.193-211.

POWELL, R.W. (1944) Proc. Am. Soc. Civil Engrs., No. 410, pp.531-554 (also Trans. Am. Soc. Civil Engrs., Vol. 111 (1946)) (Data quoted by Robertson et al, 1965).

ROBERTSON, J.M., MARTIN, J.D. and BUCKHART, T.H. (1965) "Turbulent Flow in Rough Pipes", I&EC Fundam., Vol. 7, No. 2, pp.253-265.

RUFFEL, A.E. (1977) "The Relation Between Tube Bore Roughness and Friction Pressure Loss Characteristics", Private Communication.

SATHER, N.F. and LEE, K.J. (1974) "Viscosity of Concentrated Suspensions of Spheres", Progress in Heat and Mass Transfer, Vol. 6, pp.575-589, Pergamon Press.

SCHLICHTING, H. (1936) "Experimentelle Untersuchung zum Rauhigkeitsproblem", Ingenieur Archiv. No. 7, pp.1-34 (Data obtained from SCHLICHTING, H. (1965) "Boundary Layer Theory", 6th Ed., McGraw-Hill, New York.)

STEVENSON, M. (1960) "Roughness Effect and Wake Influence for Two- Dimensional Wire Roughness", Inst. for Fluid Dynamics and Appl. Math., U. Maryland, Tech. Note BN-219 (Data quoted by Robertson et al, 1965).

WEBB, R.L., ECKERT, E.R. and GOLDSTEIN, R.J. (1971) "Heat Transfer and Friction in Tubes with Repeated-Rib Roughness", Int. J. Heat Mass Transfer, Vol. 14, pp.601-617.

ILLUSTRATIONS

Figure 1 Turbulent Flow Thermohydraulics.

Figure 2 Roughness Function B in Terms of ϵ_s^+ for Nikuradse's Sand Roughness and Commercial Tubes.

Figure 3 Relation Between Equivalent Sand Roughness, Roughness Height, Roughness Shape, and Roughness Concentration at Low Roughness Concentrations.

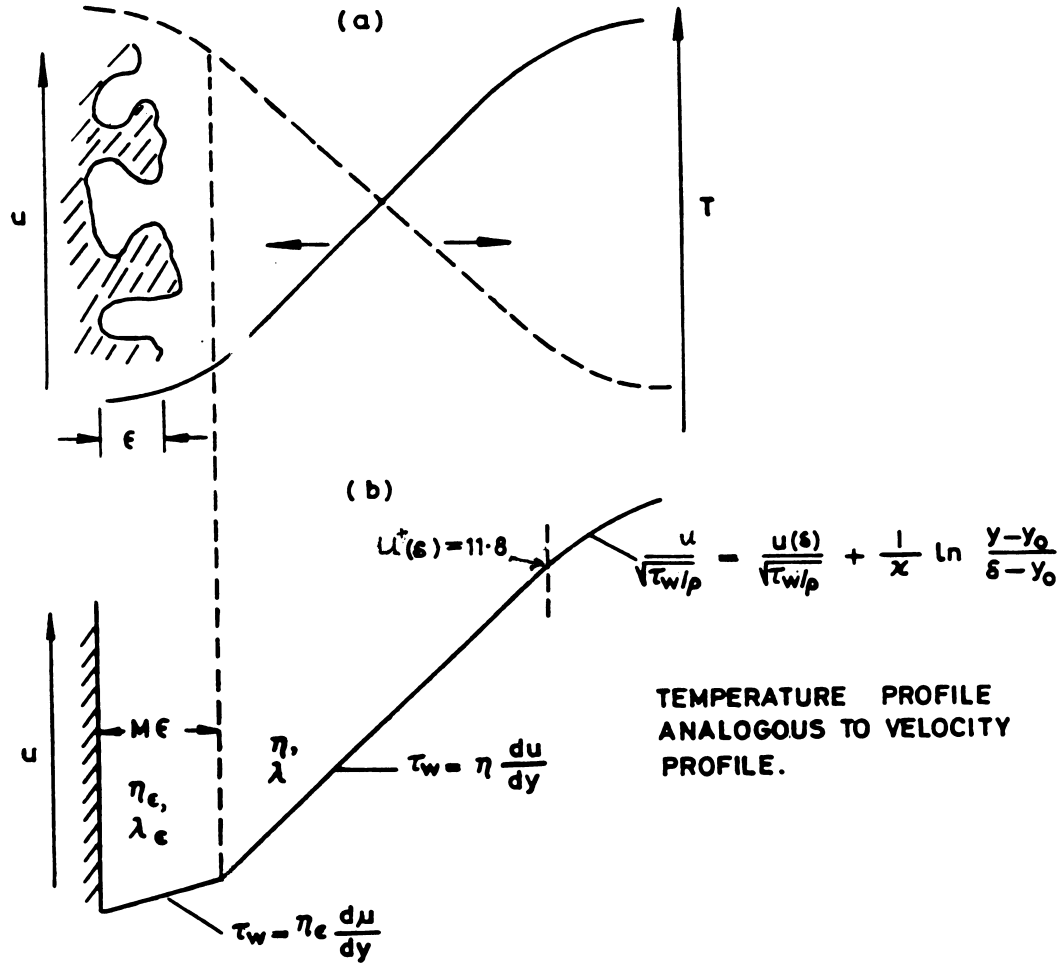

FIG.1. TURBULANT FLOW THERMOHYDRAULICS, (a) ROUGH PIPE FLOW. (b) SMOOTH TUBE ANALOGUE OF CASE a.

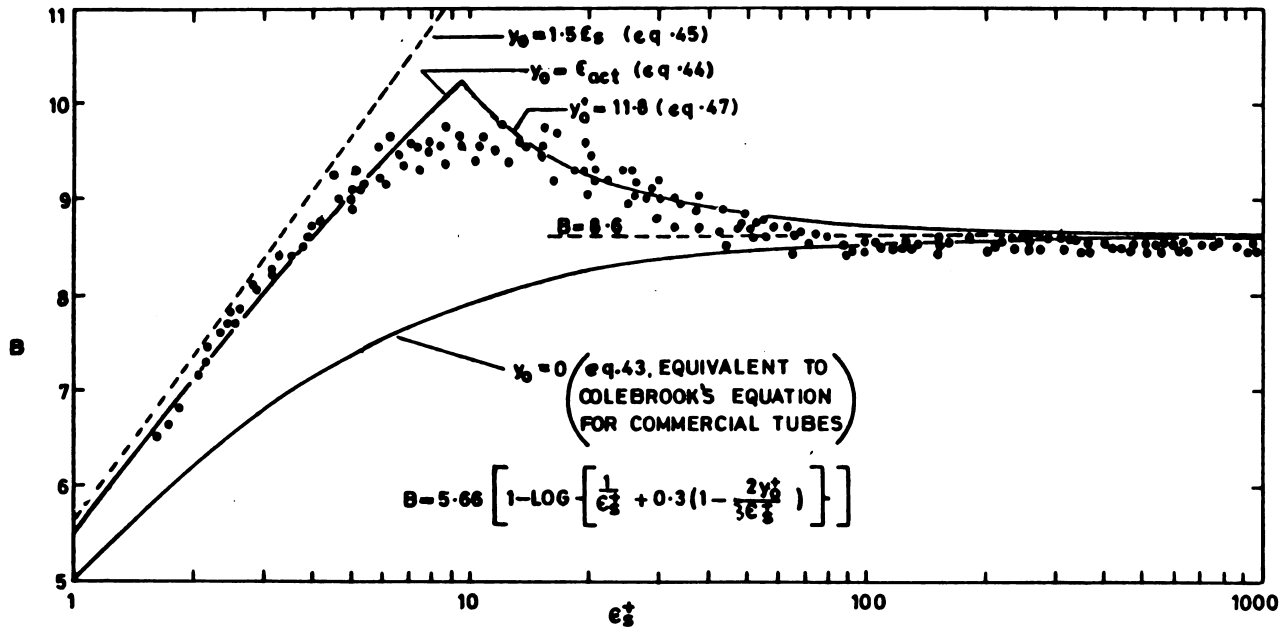

FIG 2 ROUGHNESS FUNCTION B IN TERMS OF ϵ_s^+ FOR NIKURADSE'S SAND ROUGHNESS AND FOR COMMERCIAL TUBES.

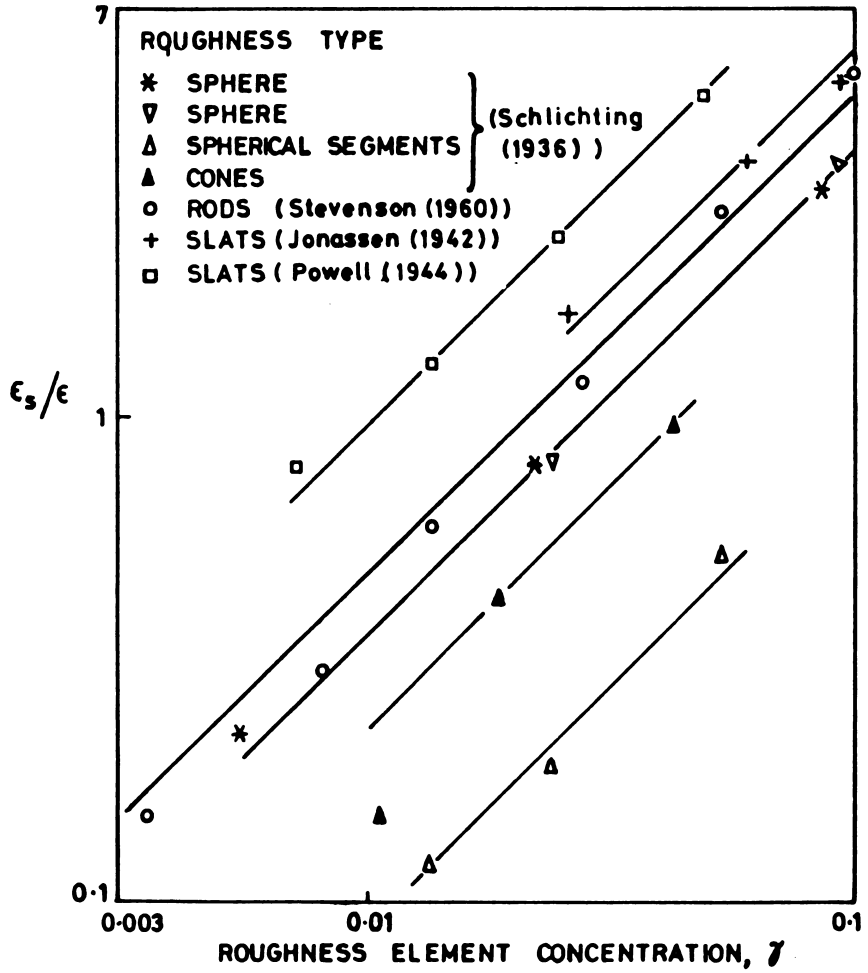

FIG. 3. RELATION BETWEEN EQUIVALENT SAND ROUGHNESS, ROUGHNESS HEIGHT, ROUGHNESS SHAPE, AND ROUGHNESS CONCENTRATION AT LOW ROUGHNESS CONCENTRATIONS.

Int. J. Multiphase Flow Vol. 8, No. 1, pp. 83–87, 1982
Printed in Great Britain.

APPENDIX A29

0301-9322/82/010083-05$03.00/0
Pergamon/Elsevier

BRIEF COMMUNICATION

A SIMPLE TWO-PHASE FRICTIONAL PRESSURE DROP CALCULATION METHOD

D. R. H. BEATTIE† and P. B. WHALLEY‡
Engineering Sciences Division, AERE Harwell, Didcot, Oxon OX11 ORA, England

(*Received* 4 *February* 1981; *in revised form* 18 *May* 1981)

1. INTRODUCTION

Despite the importance of pressure drop in two-phase flow processes, and the consequent extensive research into the topic, there is still no satisfactory method for calculating two-phase pressure drop. The best current methods are cumbersome in structure, heavily dependent on empirically determined coefficients, and have considerable uncertainty. Simpler forms or firmer theoretical bases for predictive methods can only be achieved with a narrowing of the ranges of applicability.

In this note, a theoretically based, flow pattern dependent calculation method is adapted to yield a simple predictive method in which flow pattern influences are partially allowed for in an implicit manner and therefore need not be explicitly taken into account when using the method.

2. METHOD

It has been shown that pressure drop equations derived from mixing length theory are applicable to two-phase conditions provided flow pattern effects are taken into account (Beattie 1977). However, the correct allowance for flow pattern effects is not understood. If it is assumed that coefficients appearing in mixing-length theory are the same as those in the single-phase application of the theory, loss of generality occurs. However the familiar Colebrook–White equation relating Fanning friction factor f, Reynolds number Re, and surface roughness/diameter ratio ϵ/D, is found:

$$\frac{1}{\sqrt{f}} = 3.48 - 4\log_{10}[2\epsilon/D + 9.35/(\mathrm{Re}\sqrt{f})]. \qquad [1]$$

Despite the loss of generality, [1] remains valid for many two-phase flow situations provided flow pattern effects are considered in the definition of the friction factor and Reynolds number (Beattie 1973). Especially relevant to this note are definitions applicable to bubble and annular flows. For these flows, Re and f are the same as in the homogeneous model:

$$f = \frac{\bar{\rho} D\left[\frac{dp}{dz}\right]_F}{2G^2} \qquad [2]$$

$$\mathrm{Re} = \frac{DG}{\mu} \qquad [3]$$

†Attached from AAEC Research Establishment, Private Mail Bag, Sutherland, 2232, Australia.
‡Present address: Department of Engineering Science, University of Oxford, Parks Road, Oxford OX11 3PJ, England.

where $[dp/dz]_F$ is the frictional pressure gradient, G is the mass flux, μ is the two-phase viscosity, and $\bar{\rho}$ is the homogeneous density given by

$$\frac{1}{\bar{\rho}} = \frac{x}{\rho_g} + \frac{1-x}{\rho_l}$$

where x is the gas mass flow fraction (quality), ρ_g is the gas density and ρ_l is the liquid density.

Flow pattern effects are allowed for in the viscosity definition. For many bubble and annular flows, the appropriate definitions are

$$\mu = \mu_l(1 + 2.5\beta) \quad \text{(bubble flow)} \qquad [4]$$

and

$$\mu = \mu_l(1-\beta) + \mu_g\beta \quad \text{(annular flow)} \qquad [5]$$

where β is the homogeneous void fraction

$$\beta = \frac{\rho_l x}{\rho_l x + \rho_g(1-x)},$$

μ_l is the liquid viscosity and μ_g is the gas viscosity. [4] and [5] approach μ_l as the void fraction tends to zero.

The bubble flow definition [4], is based on the theoretical work of Einstein (1906). Direct measurements of bubble viscosity (Huige & Ohki 1972) have confirmed the validity of a variation of [4] up to a voidage of about 20%. The equation found valid by Huige & Ohki (1972) reflects the surface chemistry of liquids studied by them, and their results indicate that [4] is applicable for fluids usually encountered in gas–liquid systems. The applicability of [4] to friction factor calculations at very much higher voidage (Beattie 1973 and 1977) appears to be due to an overestimate of the viscous sublayer void fraction, taken as β, being compensated for by the coefficient 2.5, which data suggest is too low at high void fractions.

The annular flow definition, [5], is based on the concept that, due to interfacial waves, the viscosity at the outer region of the viscous sublayer intermittently changes between μ_l and μ_g, with the intermittency fraction (i.e. local voidage) being assumed to be β.

We propose that [4] and [5] be replaced by a hybrid definition

$$\mu = \mu_l(1-\beta)(1+2.5\beta) + \mu_g\beta. \qquad [6]$$

The structure of [6] is consistent with the form that might be expected for some gravity dominated flows such as horizontal stratified bubbly flow or vertical bubbly/slug flow. For such flows, it might be expected that the viscosity for annular flows, [5], applies provided μ_l is replaced by [4] to allow for entrained bubbles in the liquid region of the flow.

The assumption that mixing-length theory results apply to horizontal flows is based on the observation (Beattie 1972) that opposite sides of asymetric flow profiles often coincide when normalised with respect to the distance between the wall and the position of zero shear stress.

The proposed method thus involves [1–3, 6]. A special feature of the model is the use of [1] for all values of Re, even for those values where single-phase behaviour would suggest its replacement by a laminar flow relation. This is because turbulent-like characteristics extend to very low Reynolds numbers in two-phase flows. This is perhaps not surprising because even in the absence of turbulence, Reynolds stresses can be expected in two-phase flow due to the interaction of gas–liquid interfaces with the flow field.

3. COMPARISON WITH DATA

Since the proposed method aims to allow approximately for flow pattern effect without specific knowledge of flow pattern boundaries, a proper test of the method should involve a comparison with data covering various flow patterns. Clearly, the method would not, for example, compare as favourably with bubble flow data as well as the bubble flow model which involves [4] instead of [6]. In order to achieve an adequate test of the method, use was made of a proprietary adiabatic, round tube pressure drop data bank covering both horizontal flow and vertical upflow (HTFS 1981). This data bank covers a wide range of fluids and flow conditions.

The results of the comparison are summarised in table 1. Calculation methods commonly used in two-phase flow are also included in table 1. The correction factor of table 1 is the average value of

$$\frac{\text{actual total pressure drop}}{\text{calculated total pressure drop}}$$

and the range factor is the factor by which the corrected calculated value must be multiplied and divided to give the range for 99% probability and 95% confidence. Thus, the accuracy of a particular predictive method is best improved by multiplying the prediction by the correction factor. Multiplying and dividing a prediction thus corrected by the range factor produces a range which has a 95% probability of including 99% of relevant data. The range factor is thus a measure of the spread of errors.

The method proposed here predicts only the frictional component of the pressure drop, whereas the test of the method involves also the estimation of the accelerational pressure drop, and, in the case of upflow, the gravitational pressure drop. The accelerational pressure drop was calculated using the homogeneous model. The number of data points in the bank with significant contributions from the accelerational head are small enough for error statistics of table 1 not to be influenced by errors in the estimate of the accelerational head.

On the other hand, sufficient of the vertical flow data of the data bank had significant gravitational pressure drop contributions for the error statistics of table 1 to be influenced by

Table 1. Comparison of pressure loss correlations with HTFS (1981) data bank

Frictional Pressure Drop Correlation	Non Steam/Water				Steam/Water			
	Horizontal		Vertical		Horizontal		Vertical	
	Correction Factor	Range Factor	Correction Factor	Range Factor	Correction Factor	Range Factor	Correction Factor	Range Factor
HTFS (1981)	1.00	2.6	1.13	2.0	0.82	2.4	0.97	1.5
Baroczy (1966)	0.92(1)	2.4	1.17(1)	2.2	0.77(1)	2.8	0.97(1)	1.5
Friedel (1979)	0.77(1)	4.0	1.01(1)	2.0	0.85	2.4	0.97	1.6
Lockhart-Martinelli (1949)	0.99	2.8	0.96	1.9	0.43	3.9	0.59	3.3
Martinelli-Nelson (1948)					0.58	2.6	0.76	2.2
Thom (1964)					0.87(1)	2.4	0.93(1)	1.7
Chisholm (1978)	0.74	4.8	0.94	2.1	0.68	2.9	0.92	1.6
Isbin et al (1954)	1.07	3.8	2.00	3.8	0.94	2.6	1.16	2.2
Owens (1961)	0.53	9.1	1.39	4.6	0.85	2.6	1.10	2.2
Cicchitti et al (1960)	0.61	6.2	1.53	4.1	0.89	2.6	1.12	2.2
Dukler et al (case 2) (1964)	1.18	3.1	2.08	3.9	0.97	2.6	1.20	2.2
Equations 1,2,3,6	1.05	3.1	1.16	2.1	0.94	2.5	1.01	1.7
Number of data points	7168		2011		1236		3095	

Note: (1) indicates that, due to limitation on the correlation applicability range, comparison has been made with a reduced number of data.

the gravitational pressure drop calculation method. Since the Isbin *et al.* (1954), Owens (1961), Cicchitti *et al.* (1960) and Dukler *et al.* (1964) methods can be regarded as variations of the homogeneous model, the gravitational head for these models was calculated using the homogeneous void fraction model. The gravitational head for the other pressure loss models was calculated using an unpublished void fraction correlation (HTFS 1981), an independent examination having shown this to be the most reliable for the range of conditions covered by the data bank.

Although the error statistics for the vertical flow cases of table 1 depend on the gravitational pressure drop calculation method, the use of an apparently reliable gravitational method or, in some cases, a gravitational method consistent with the frictional method, means that the error statistics for vertical uplow can be primarily associated with errors in the frictional methods.

4. DISCUSSION

Table 1 indicates that, despite its simplicity, the proposed frictional pressure drop calculation method generally gives more accurate results than alternatives tested apart from the HTFS correlation. At first sight this is unexpected: the proposed method gives a two-phase multiplier approximately independent of mass flux, whereas this multiplier is known to be strongly influenced by mass flux. Indeed, the HTFS, Baroczy (1966), Friedel (1979) and Chisholm (1978) correlations specifically allow for this effect. However from an examination of the data it seems probable that a large contribution to the range factors occurs because of the inability to allow for effects such as entrance conditions which are known to effect two-phase pressure drop. The comparatively good performance of the present method suggests that errors due to the neglect of mass flux effects are not as significant as those due to the neglect of other effects.

The present method has been tested only against adiabatic, round tube, data. It has not been compared with diabatic or complex geometry data, which are known to have different pressure drop characteristics (Beattie 1977). However, the characteristics for these systems are similar to those for round tube adiabatic flows, particularly at low void fraction, and it is expected that application of the present model to diabatic and complex geometry systems should give reasonable results though with a larger error than for adiabatic round tube flows. The larger error will arise, for example, from additional flow disturbance effects, such as from spacers in rod bundles. The present model underpredicts condensation pressure drop by a considerable margin. A preliminary comparison with condensation data indicates that [1–4] give reasonable estimates of pressure drop during condensation.

5. SUMMARY AND CONCLUSIONS

A mixing-length theory model of two-phase pressure drop has been adapted to give a simple calculation method, of the same form as that used for single phase flow, in which flow pattern effects are partially accounted for implicitly. Comparison of the method with an extensive adiabatic round tube data bank shows it to be as good as most alternative, more complex, methods. Errors in the present method are due primarily to the neglect of effects such as entrance effects rather than the neglect of mass flux effects, so methods which more correctly allow for mass flow effects do not necessarily result in more reliable predictions. Except for condensing flows, the method should also yield reasonable pressure loss estimates for diabatic and/or complex geometry flows.

REFERENCES

BAROCZY, C. J. 1966 A systematic correlation for two-phase pressure drop. *Chem. Engng Prog. Symp. Ser.* **62**, 232–249.

BEATTIE, D. R. H. 1972 Two-phase flow structure and mixing length theory. *Nuc. Engng Des.* **21**, 46–64.

BEATTIE, D. R. H. 1973 A note on the calculation of two-phase pressure losses. *Nuc. Engng Des.* **25**, 395–402.

BEATTIE, D. R. H. 1977 Some aspects of two-phase flow drag reduction. *Proc. Second Int. Conf. Drag Reduction*, Paper D1. BHRA Fluids Engineering.

CHISHOLM, D. 1978 Influence of pipe surface roughness on friction pressure gradient during two-phase flow. *Mech. Engng Sci.* **20**, 353–354.

CICCHITTI, A., LOMBARDI, C., SILVESTRI, M., SOLDAINI, G. & ZAVATTAREUI, R. 1960 Two-phase cooling experiments—pressure drop, heat transfer and burnout measurements. *Energia. Nucl.* **7**, 407–425.

DUKLER, A. E., WICKS, M. & CLEAVELAND, R. G. 1964 Pressure drop and hold up in two-phase flow. *AIChE J.* **10**, 44–51.

EINSTEIN, A. 1906 A new determination of molecular dimensions. *Ann. Phys.* **19**, 289.

FRIEDEL, L. 1979 Improved friction pressure drop correlations for horizontal and vertical two-phase pipe flow. *European Two-Phase Flow Group Meeting.* Paper E2, Ispra.

HTFS 1981 (Heat Transfer and Fluid Flow Service), AERE Harwell and NEL East Kibride, Unpublished information.

HUIGE, J. & OHKI, M. 1971 The relationship between the apparent coefficient of viscosity and the void fraction in two-phase flow of mixtures of gas and liquid. *Trans. Jap. Soc. Mech. Engng* **37**, 97.

ISBIN, H. S., MOEN, R. H. & WICKEY, R. C. 1954 Two-phase pressure drops. *USAEC Report AECU-2994.*

LOCHART, R. W. & MARTINELLI, R. C. 1949 Proposed correlation of data for isothermal two-phase two-compartment flow in pipes. *Chem. Engng Prog.* **45**, 39–48.

MARTINELLI, R. C. & NELSON, D. B. 1948 Prediction of pressure drops during forced circulation boiling of water. *Trans. ASME* **70**, 695–702.

OWENS, W. S. 1961 Two-phase pressure gradient. *International Developments in Heat Transfer*, Pt. II. ASME.

THOM, J. R. S. 1964 Prediction of pressure drop during forced circulation of water. *Int. J. Heat Mass Transfer* **7**, 709–724.

C102/83

Thermohydraulics aspects of nuclear safety research in Australia

D R H BEATTIE, BSc, BE, MEngSci, A G CHAPMAN, BSc, G W K FORD, MBE, MA, CEng, MIMechE, W J GREEN, BSc, MEngSci, K R LAWTHER, BSc, BE, PhD, J MARSHALL, BSc, ME and W J TURNER, BSc
Australian Atomic Energy Commission Research Establishment, Lucas Heights, Australia

SYNOPSIS This review outlines a program of investigations on the prediction of thermohydraulics aspects of a loss-of-coolant accident in a water-cooled nuclear reactor. It includes mathematical modelling of the transient coolant conditions, modelling of fluid conditions in a containment structure, and information on relevant two-phase flow and heat transfer characteristics.

1 INTRODUCTION

A number of important aspects of nuclear reactor safety have been investigated in a thermohydraulics program at the AAEC's Research Establishment at Lucas Heights, New South Wales. Most of the work is relevant to both research and power reactor systems. Projects directed at specific problems in the AAEC's HIFAR research reactor, such as evaluation of the emergency core cooling system, have been excluded since they are specific to that reactor type.

Of particular concern is the behaviour of water-cooled nuclear reactor systems under loss-of-coolant accident (LOCA) conditions, such as a fracture of the primary circuit pipework, which could lead to severe overheating of fuel in the reactor core. A number of computer codes have been developed to model overall thermohydraulic characteristics of the primary circuit of such a system, including the effects of a LOCA. Some of these codes are quite complex. The AAEC code NAIAD is relatively simple but has certain advantages in modelling the transient conditions.

The reactor containment structure is of key importance to reactor safety. To develop suitable methods for predicting the conditions which such a structure must withstand following a LOCA, a number of relatively small-scale experiments on blowdown from a small vessel, containing heated water under pressure, into a much larger vessel representing the reactor containment have been made. In an international program under the auspices of the Organisation for Economic Co-operation and Development (OECD) Nuclear Energy Agency Committee on the Safety of Nuclear Installations (CSNI), the results are being compared with predictions from computer programs developed to calculate conditions encountered in the containment during such transients.

Calculations of transient conditions are dependent on the development of suitable models of thermohydraulic behaviour for liquid/vapour coolant flows and, in particular, on relationships developed from data on two-phase flow and heat transfer characteristics. This has led to investigations of flow structure, pressure drop and choked flow for two-phase flow conditions, and aspects of heat transfer including the onset of boiling 'burnout' (critical heat flux) and heat transfer coefficients under burnout conditions.

2 MODELLING OVERALL THERMOHYDRAULICS IN THE PRIMARY CIRCUIT OF A WATER-COOLED REACTOR SYSTEM

The computer program NAIAD [1] was developed as a means of testing numerical methods used in thermohydraulics calculations for water-cooled nuclear reactors. The finite difference method used in this code is rather different from that used in earlier programs. All quantities are evaluated at one set of finite difference nodes rather than at nodes and 'half-nodes' in the usual staggered mesh approach. Thus a direct solution method is used and large time steps are made when slow changes are occurring. This results in reduced computational times. The formulation of the finite difference equations is carefully chosen to ensure that the steady-state solution is as accurate as possible for the specified number of nodes. The choke flow boundary condition is arranged so that the flow model specified is automatically used to determine the choke flow [2]. A new approach to the 'water packing' problem has been included. This is a numerical problem which occurs in calculations involving transitions from a two-phase fluid to a liquid phase and arises because of the associated large step change in compressibility. The new method allows completely smooth phase transitions [3].

The method used to solve the complete set of equations describing the network is highly efficient, solving all the linear equations by a direct method, making use of the network structure to identify tridiagonal sections of the overall matrix, and only using an iterative method for non-linear relationships in the network (pumps and choke flow points). Unusual hydraulic components can be included in the network by means of user routines.

Most of the simulations with NAIAD have been made in conjunction with the CSNI working group on emergency core cooling (ECC). Solutions were submitted for five standard problems on emergency core cooling. Further calculations

C102/83 © IMechE 1983

of one of these have since been completed [4] in an attempt to resolve differences between calculated and measured coolant temperatures. The Italian IETI-1 test rig simulated in this standard problem is shown in Figure 1. Figure 2 shows the excellent agreement between calculated and measured masses of coolant during the experiment. Quite good agreement was also obtained between calculated and measured pressures and wall temperatures.

Recently the ECC working group began a new series of international comparison problems. The Australian solution to the first problem in the series was the only one both numerically stable and able to resolve all the phenomena. Details of the problem and the NAIAD solution are contained in reference [3].

3 MODELLING BLOWDOWN INTO A CONTAINMENT

Investigations into the conditions likely to arise within a containment during a LOCA were started at Lucas Heights in 1974. A small blowdown and containment rig was built with a pressure vessel of about 14 dm^3 capacity to contain fluid at up to ~14 MPa and 345°C, connected to a vessel of 1.8 m^3 capacity which represents a reactor containment structure. The current arrangement is sketched in Figure 3.

During an experiment, the pressure vessel is first evacuated of air, then a measured amount of water is added and an electric immersion heater in the base of the pressure vessel is used to boil the water and attain the required pressurisation. To start the blowdown, a copper disc in the bursting disc assembly, which blocks the passage between pressure vessel and containment, is ruptured. Measurements of the transient conditions of pressure, temperature, or flow rate are made at various points in the system and transmitted to a computer. These data may subsequently be accessed, analysed and plotted locally or transferred to a large central computer. Until 1981, the containment was a single compartment and runs were made for a range of initial conditions in the pressure vessel, i.e. water content and pressure, and different outlet flow restrictors, initial air pressure in the containment vessel ranging from near vacuum to one atmosphere [5].

A small computer program was written to calculate conditions in the rig and to investigate methods of calculating heat transfer coefficients. A measurement system was developed to monitor heat transfer from the bulk fluid to the containment walls during the transient [6]. This system measures the temperature transient at a point within a thin metal rod which is insulated except at an end surface exposed to the containment atmosphere (see Figure 4). The temperature and heat flux at this surface are calculated by a Fourier transform method and used, together with a measurement of bulk fluid temperature, to calculate the heat transfer coefficient (h.t.c.) transient. From a survey of methods used in computer codes for calculating such heat transfer coefficients, it was found that these are generally inadequate because they are usually based on data from steady state experiments and do not take into account the highly turbulent conditions during a blowdown. Also they sometimes fail to account satisfactorily for the presence of air and its effect on condensation [5,7]. An alternative was devised, which depends on the instantaneous energy of the fluid inflow [6,8]. This gave h.t.c. transients similar to the measured transients and resulted in calculated pressures closer to the measured values.

The containment was divided into two compartments to allow investigations into multi-compartments. The OECD/CSNI working group on reactor containment requested that experimental results be provided as a Containment Analysis Standard Problem (CASP) so that the computer codes used by member countries could be tested against a different scale and arrangement of model to that used in previous CASPs. The results of the experiment have been made available for this purpose. The pressure transients from this experiment are shown in Figure 5 and the heat transfer coefficient transient obtained from measurements in the top compartment is shown in Figure 4. Also included in these figures are the AAEC calculated transients using the ZOCO V computer code [9] with modifications to the heat transfer correlations and inter-compartment flow computations in this code [10].

4 TWO-PHASE FLOW CHARACTERISTICS

Mixing-length theory has been used to formulate voidage [11] and velocity [12,13] defect equations for two-phase (gas/liquid) flows. Different sublayer structures (bubbly, vapour only, attached wall bubbles, etc.) mean different boundary conditions and lead to non-dimensional logarithmic velocity profiles with dimensionless group definitions which depend on the sublayer structure [14]. Coefficients in the logarithmic profile may differ from those of the single phase equation, but remain constant for flows in a given 'friction regime' [14,15].

As with single phase flow, friction factor expressions [14,15] have been obtained by averaging the non-dimensional velocity profile. The Reynolds analogues of these expressions then provide heat transfer coefficient equations; however, this has only been verified for the important case of post-dryout flows [13]. Average voidage for annular flow has been derived from the relation between film thickness and film flow rate obtained by integrating the velocity profile over the film region with allowance being made for core and film entrainment [14,15]. Average voidage for distributed flow has been derived using the Zuber 'drift-flux' equation, the distribution parameter values being obtained from the friction factor (Table 2) [12-13]. When coupled with the heat transfer coefficient equation, the Reynolds analogue of the drift flux equation enabled thermal non-equilibrium to be evaluated [13].

A general form of the two-phase flow distribution parameter in terms of higher order correlation coefficients has been utilised to deduce momentum and kinetic energy fluxes. These enable the prediction [12,13] of propagation phenomena such as sonic velocity and choked flow which are important in safety analyses. Although developed for flow through round tubes, the various theoretical expressions are also applicable to flow through ducts of complex cross-section; however, values of the coefficients

© IMechE 1983 C102/83

may be different under these conditions [16,17].

Specification of friction regime in terms of sublayer type and non-dimensional velocity profile coefficients is necessary for prediction of the various parameters mentioned above. On the basis of approximately 10 000 world pressure drop data, recommendations have been given for high pressure steam water flows [14]. With some qualifications, the regime boundaries are consistent with a requirement for continuity of wall shear stress at the boundaries. This continuity does not extend to some of the other characteristics, and the discontinuity in critical heat flux at a friction regime boundary provides an explanation for the heat-flux-independent 'limiting quality' boiling crisis and also upstream dryout [18]. Similarly, the dry wall friction regime boundary provides a zero heat flux limit of the boiling crisis quality [19]. The interrelation between friction and critical heat flux characteristics is shown in Figure 6. This figure also demonstrates the good friction factor predictions achieved using the friction regime concept.

The theory described here has been based on an analysis of world data supplemented by data obtained from experiments on air-water (Table 1) and adiabatic and diabatic Freon-12 at 1 MPa in a 1 cm dia. x 80 cm long tube. A summary of some equations developed in the AAEC's research program on two-phase flow characteristics is given in Table 2. These equations are for developed flows in round tubes; values of the coefficients may be different for non-developed flows and/or other duct geometries.

5 CRITICAL HEAT FLUX AND POST-DRYOUT EXPERIMENTS

5.1 Critical Heat Flux Experiments

On the basis of preliminary investigations at the UKAEA's Atomic Energy Establishment at Winfrith, Dorset, into the use of Freon-12 as a model fluid for high pressure water in critical heat flux (CHF) experiments, a CHF experimental program was carried out at Lucas Heights on the AAEC Freon-12 heat transfer rig [21]. These experiments used uniformly heated vertical round tubes, annuli and a rod cluster [22-25] (see Table 3) to obtain information on the effects of coolant conditions (mass flux, pressure, enthalpy) on CHF, and some effects of flow channel geometry, including in particular, effects of spacer elements in the case of annuli [26,27].

5.2 Correlation of CHF Data for Round Tubes

When the CHF data obtained in the AAEC Freon-12 rig for uniformly heated round tubes were compared with published CHF correlations [28,29], there were substantial discrepancies, particularly at low mass fluxes (less than 500 kg s^{-1} m^{-2}) [30]. To achieve a more satisfactory correlation, a dimensional analysis approach was used in which dimensionless groups were interrelated with other dimensionless groups not only in the usual simple product relationship but also as power functions of each other [31]. This led to the formulation of a CHF correlation for Freon-12 which was so general in form that only minor modification was needed for it to be applicable to water data [32,33]. Subsequently, this correlation was compared favourably with nitrogen data [34]. The correlation is as follows:

$$\frac{qD}{\mu_v \lambda} = 9 \times 10^{-5} \, Re_v^{\,n} \left(\frac{\rho_\ell}{\rho_v}\right)^m \sigma_N^{\,p} \, Pr_v^{\,w} \cdot f(L_s/D)(1+\delta)(1-\delta_1),$$

where

$$Re_v = \frac{DG}{\mu_v}\left[x + (1-x)\,\rho_v/\rho_\ell\right]$$

$$\sigma_N = \sigma/(D\lambda\rho_v)$$

L_s/D = saturation or boiling length ratio

$$f(L_s/D) = \exp\{3.83\, e^{-0.00396\, L_s/D} - 0.00055\, L_s/D\}$$

$$n = 1 - e^{-0.0067\, L_s/D},$$

$$m = 0.1 + e^{-0.007\, L_s/D},$$

$$p = -0.5\,(0.15 + e^{-0.007\, L_s/D}),$$

$$w = -\,(0.21 + 0.55\, e^{-0.007\, L_s/D}),$$

$$\delta = \exp\{-0.14 \times 10^8 \sigma_N - 0.02\,(L/D)\,Pr_v\},$$

$$\delta_1 = 0.75 \exp\left\{-B \cdot \frac{L}{D} \cdot \frac{G\sigma}{\rho_\ell \mu_\ell \lambda}\right\},$$

and $B = 130.5 \exp\{5.0 \exp(-0.02\, L/D)\}$.

This correlation applies over a wide range of coolant conditions and tube dimensions provided that dryout qualities are greater than 0.1 and coolant mass fluxes are greater than 300 kg s^{-1} m^{-2}. For mass fluxes less than 300 kg s^{-1} m^{-2}, a second correlation has been developed which is also of a general form [35], and has been verified against the limited experimental data available at these low flow rates. This correlation is:

$$\frac{qD}{\mu_v \lambda} = 0.25\, Re_v \left(\frac{D}{L_s}\right)\left(\frac{1}{1+\delta_2}\right)$$

where

$$\delta_2 = 0.046\,(L/D)^{1.12}\,(D/L_s)^{1.65} \exp\{25 \times 10^3\, LFN - 0.038\, \rho_\ell/\rho_v\}$$

$$LFN = G\sigma/(\rho_\ell \mu_\ell \lambda).$$

5.3 Correlation of CHF Data for Rod Bundles

In a nuclear power reactor core, the fuel is usually in rod bundle assemblies. A significant difference between these assemblies and round tubes is that the local conditions at the onset of burnout cannot be as well represented in terms of radially-averaged flow and simple geometric parameters alone. The development of rod bundle CHF conditions is therefore likely to be much less successful. Nevertheless, more than a score of rod bundle CHF correlations are available; these are generally based on intuitive adaptations of round tube or annulus CHF correlations, the empirical coefficients being optimised on rod bundle CHF data.

Used with discretion, these rod bundle CHF correlations provide a simple means of predicting the onset of burnout in reactor fuel elements. Whereas they have been replaced by a

subchannel analysis approach which can be more accurate in reactor design applications, they are still useful where speed of solution to cover a wide range of conditions is important, as in reactor safety analysis. However, very little guidance has been given on their use. Accuracies have been quoted for somewhat small sets of data in which the parameters, although seemingly wide in their ranges are not simultaneously represented at their limits. Other data falling within the same parameter ranges are often not correlated with the same accuracy. To examine the limitations of these correlations an extensive bank of experimental data on burnout in water-cooled rod bundles has been compiled [36], and a computer program developed to analyse the performance of these burnout correlations over selected parameter ranges. An example of contour plots of correlation accuracy with simultaneous variation of two parameters is given in Figure 7. Empirical coefficients can be re-optimised to improve performance in certain areas, and the performances of different correlations compared to indicate the best for selected conditions. Such analyses will provide the knowledge required for discerning use of these rod bundle burnout correlations.

5.4 Post-dryout Heat Transfer

A sensitivity analysis [37] of the blowdown phase of a hypothetical LOCA in a pressurised water reactor showed that maximum surface temperatures for the cladding of a nuclear fuel element at relatively low coolant mass fluxes are highly dependent on the heat transfer relationships assumed to apply for the onset of dryout and during the subsequent post-dryout conditions (see Figure 8). An experimental investigation into post-dryout heat transfer was undertaken with Freon-12 as the coolant, and electrical power transients were applied to a tube serving as the heat dissipating surface. Initially, tests were conducted in which the uniform heat input to the whole tube was increased in steps until dryout was induced over the exit region of the tube [38]. Later a short downstream section of this tube was heated independently while the heat input to the upstream section was maintained constant; the power of the short exit section was increased in steps until this section reached dryout [39]. Experiments are now being performed in which the short exit test section has a high thermal capacity. This enables heat transfer to be studied under slow dryout and rewetting conditions.

The experimental data obtained from each of these test programs are in the form of wall temperature transients. Such data are analysed by matching recorded responses with those calculated with the transient thermal hydraulic code THETRAN [40]. This code contains models for the onset of dryout, the post-dryout transition region, the minimum heat flux film boiling region, an intermediate film boiling region, and a high temperature film boiling region (Figure 8). It has been found [41] that the relative extent of these regions can vary substantially, in particular, the minimum heat flux film boiling region may cover a very wide or a very narrow range of surface temperatures. So far, it has been found that for Freon-12 (a) experimental data for the minimum heat flux region may be correlated by $q_{min} = A\ (DG/\mu_v)^{0.54}$ (Figure 9), where A is a function of the properties of the coolant [42] - this correlation applies provided the minimum heat flux is less than 70% of the CHF; (b) the data for the intermediate film boiling region are represented by the equation

$$q/q_{fb} = 1 + 3.65 \exp\{11.0\ [(T_w-T_s)/T_s]\ L_s/L\}$$

where q_{fb} is the surface heat flux corresponding to the high temperature film boiling region; and (c) the data for the high temperature film boiling region are correlated by

$$q_{fb} = 0.85 \exp\{1.33\ (D/L_{Do}) - 0.15\ L/L_s\} q_{DR}$$

where L_{Do} is the length in dryout and q_{DR} is the surface heat flux given by the Dougall-Rohsenow film boiling correlation [43], i.e.

$$q_{DR} = 0.023 \frac{k_v}{D} Pr_v^{0.4} \left(\frac{DG}{\mu_v}\right)^{0.8} [x+(1-x)\rho_v/\rho_\ell]^{0.8} (T_w-T_s).$$

6 CONCLUSIONS

The AAEC program on thermohydraulics aspects of nuclear safety research has contributed significantly to an understanding of the processes involved in predicting the consequences of a loss-of-coolant accident in a water-cooled nuclear reactor system. This contribution has enhanced our knowledge of (i) modelling relatively simple thermohydraulic transients, (ii) fluid conditions associated with depressurisation into a containment vessel, (iii) two-phase flow relationships, and (iv) heat transfer under dryout conditions.

(1) Trimble, G.D. and Turner, W.J. AAEC/E318, 1974.
(2) Turner, W.J. and Trimble, G.D. OECD-NEA-CSNI Specialist Meeting on Transient Two-phase Flow, Toronto, Canada, 1976.
(3) Turner, W.J. Nucl. Eng. Design, 1980, 60, 431.
(4) Turner, W.J. and Trimble, G.D. Proc. SIMSIG-78: Simulation Conf., Canberra, Australia, 1978.
(5) Marshall, J. and Holland, P.G. Proc. Second Australasian Conf. Heat and Mass Transfer, p.339, Sydney, NSW, 1977.
(6) Marshall, J. Nucl. Eng. Design, 1979, 51, 409-415.
(7) Marshall, J. and Holland, P.G. Proc. Conf. Heat & Fluid Flow in Water Reactor Safety, Inst. Mech. Eng., Manchester, UK, 1977.
(8) Marshall, J. M.E. Thesis, Univ. NSW, Sydney 1979.
(9) Broche, D. Nucl. Eng. Design, 1972, 23, 239-272.
(10) Marshall, J. OECD-CSNI SINDOC(82) , 1982 (unpublished report).
(11) Beattie, D.R.H. Nucl. Eng. Design, 1972, 21, 46-64.
(12) Beattie, D.R.H. Paper D3, Proc. 2nd Int. Conf. Press. Surges, Cambridge, British Hydromechanics Research Association Fluid Engineering, 1976.
(13) Beattie, D.R.H. Proc. Second Australasian Conf. Heat and Mass Transfer, Sydney, NSW, 1977, 329-337.
(14) Beattie, D.R.H. Paper D1, Proc. Second Int.

© IMechE 1983 C102/83

Conf. Drag Reduction, Cambridge, British Hydromechanics Research Association Fluid Engineering, 1977.
(15) Beattie, D.R.H. NUREG/CP-0014, 1980, 1343-1362.
(16) Beattie, D.R.H. Proc. 18th International Association for Hydraulics Research (IAHR) Congress, Cagliari, Italy, 1979.
(17) Beattie, D.R.H. and Lawther, K.R. Int. J. Multiphase Flow, 1981, 7, 423-437.
(18) Beattie, D.R.H. Paper C9, European Two-phase Flow Group Meeting, Eindhoven, The Netherlands, 1981.
(19) Beattie, D.R.H. and Lawther, K.R. Paper FB23, Proc. 6th Int. Heat Transfer Conf., Toronto, Canada, 1978.
(20) Beattie, D.R.H. and Lawther, K.R. Proc. 7th Australasian Conf. Hydraulics and Fluid Mechanics, Brisbane, Queensland, 1980, 412-415.
(21) Ilic, V. AAEC/TM632, 1972.
(22) Ilic, V. AAEC/E325, 1974.
(23) Stevens, J.R. and Miles, D.N. AAEC/E506, 1980.
(24) Ilic, V. AAEC/E323, 1974.
(25) Ilic, V. AAEC/E324, 1974.
(26) Ilic, V. and Lawther, K.R. 1st Australasian Conf. on Heat and Mass Transfer, Melbourne, 1973.
(27) Ilic, V. AAEC/E349, 1975.
(28) Bertoletti, S., Gaspari, G.P., Lombardi C., Peterlongo, G. and Tacconi, F.A. CISE-99, 1964.
(29) Groeneveld, D.C. AECL-3418, 1969.
(30) Green, W.J. and Stevens, J.R. AAEC/E517, 1981.
(31) Green, W.J. AAEC/E528, 1981.
(32) Green, W.J. AAEC/E532, 1981.
(33) Green, W.J. AAEC/E536, 1982.
(34) Green, W.J. and Lawther, K.R. Paper FB-18, Proc. 7th Int. Heat Transfer Conference, Münich, Federal Republic of Germany, 1982.
(35) Green, W.J. Nucl. Eng. & Design, 1982, 72.
(36) Chapman, A.G. and Carrard, G. AAEC/E500, 1981.
(37) Green, W.J. and Lawther, K.R. Nucl. Eng. & Design, 1978, 47, 87.
(38) Green, W.J. AAEC/E452, 1978.
(39) Green, W.J. and Lawther, K.R. Third CSNI Specialist Meeting on Transient Two-phase Flow, Pasadena, California, 1981.
(40) Green, W.J. and Jacobs, W. AAEC/E507, 1981.
(41) Green, W.J. and Lawther, K.R. Nucl. Eng. & Design, 1979, 55, 131-144.
(42) Green, W.J. and Lawther, K.R. NUREG/CP-0014, 1092, 1980.
(43) Dougall, R.S. and Rohsenow, W.M. MIT-TR-9079-26, 1963.

Table 1 Air-water experiments

	Test Section: Type	tube	tube	tube	tube & grid obstruction	concentric annulus	concentric annulus & spacer obstruction	eccentric annulus	concentric annulus expanding into tube	7-rod cluster	bowed 7-rod cluster	7-rod cluster + grid obstruction
	Test Section: Dia. (mm)	25.4	12.7	6.3	25.4	25.4 x 12.7	25.4 x 12.7	25.4 x 12.7	25.4 x 7.5 25.4	95 (7x12.7)	95 (7x12.7)	95 (7x25.4)
	Measured quantity: Ref.							20		17	17	17
Bubble flow	Pressure gradient	✓	✓	✓	✓	✓	✓	✓	✓	✓	✓	✓
Bubble flow	Voidage profile map	✓			✓	✓	✓	✓	✓	✓	✓	
Bubble flow	Velocity profile map	✓			✓	✓	✓	✓	✓	✓	✓	
Bubble flow	Flow structure near wall	✓			✓	✓	✓	✓				
Bubble flow	Average voidage	✓			✓					✓	✓	
Bubble flow	Bubble size distribution and/or slug shape	✓										
Climbing film flow	Film thickness					✓						
Climbing film flow	Film flow rate					✓						
Climbing film flow	Flow structure near wall	✓				✓						
Climbing film flow	Pressure gradient	✓				✓						✓

Table 2 Some equations developed in the AAEC program for two-phase flow characteristics

	Bubble Flow	Boiling Annular Flow	Post-dryout Flow
Relevant dimensionless groups (β = volumetric flow fraction of vapour; j = local flow velocity; y = distance from wall)	$f = 2\tau_w/\{[\rho_\ell(1-\beta) + \rho_v\beta]\langle j\rangle^2\}$ $Re = DG/[\mu_\ell(1+2.5\beta)]$ $j^+ = j\sqrt{2/f}/\langle j\rangle$ $y^+ = y\,Re\sqrt{f/2}/D$	$f = 2\tau_w/\{[\rho_\ell(1-\beta]+\rho_v\beta]\langle j\rangle^2\}$ $We = G\langle j\rangle D/\sigma$ $j^+ = j\sqrt{2/f}/\langle j\rangle$ $y^+ = y\,We\,f/D$	$f = 2\tau_w/(\rho_v\langle j\rangle^2)$ $Re = \rho_v\langle j\rangle D/\mu_v$ $j^+ = j\sqrt{2/f}/\langle j\rangle$ $y^+ = y\,Re\sqrt{f/2}\ /\ D$
Voidage defect equation (subscript 'o' denotes value at a reference position)	$(1-\alpha)^{3/2}-(1-\alpha_o)^{3/2} \propto \ln(y/y_o)$	$(1-\alpha)^{3/2}-(1-\alpha_o)^{3/2} \propto \ln(y/y_o)$ in film $\alpha^{3/2} - \alpha_o^{3/2} \propto \ln(y/y_o)$ in core	$\alpha^{3/2} - \alpha_o^{3/2} \propto \ln(y/y_o)$
Velocity profile	$j^+ = 5.66 \log y^+ + 5.66$	$j^+ = 22.63 \log y^+ + 2.49$	$j^+ = 5.66 \log y^+ + 5.66$
Friction factor (smooth tube)	$1/\sqrt{f} = 4 \log (Re\sqrt{f}) - 0.4$	$1/\sqrt{f} = 16 \log(We\ f) - 13.4$	$1/\sqrt{f} = 4 \log(Re\sqrt{f}) - 0.4$
Distribution parameter	$C_o = 1 + 2.6\sqrt{f}$	Not applicable	$C_o = 1 + 2.6\sqrt{f}$
Average voidage (upflow) (S = liquid film thickness)	$\langle j_v\rangle/\langle\alpha\rangle = C_o\langle j\rangle + 1.4(\sigma g\Delta\rho/\rho_\ell^2)^{\frac{1}{4}}$ $\Delta\rho = \rho_\ell - \rho_v$	$\frac{1-\beta}{2}\,We\sqrt{\frac{f}{2}} = \int_{j=0}^{s^+} j^+\,dy^+$ $s^+ = \frac{1}{2}(1-\langle\alpha\rangle)We\,f$	$(1-\langle\alpha\rangle) = (1-\beta)/C_o$
Heat transfer coefficient (T_s = saturation temperature)	To be determined	To be determined	$\frac{qD}{k_v(T_w-\langle T_v\rangle)} = 0.023\,Re^{0.8}\,(Pr_v)^{0.4}$ $(T_w - T_s) = C_o(T_w-\langle T_v\rangle)+(T_v-T_\ell)$
Thermal non-equilibrium (x = flow quality; x_{eq} = equilibrium value of x)	To be determined	To be determined	$x = \frac{[x_{eq}\lambda - c_{pv}(T_w-\langle T_v\rangle)(C_o-1)\rho_v/\rho_\ell]}{\left[\lambda + c_{pv}(T_v-T_\ell) + c_{pv}(1-\rho_v/\rho_\ell)(C_o-1)(T_w-\langle T_v\rangle)\right]}$
Sonic velocity	$V_s = \sqrt{\gamma P/\rho_\ell}\,[\langle\alpha\rangle(1-C_o\langle\alpha\rangle)]^{-\frac{1}{2}}$	To be determined	See ref. [13]
Choked flow	$G_c = \sqrt{\gamma P\rho_v/x}\{1-(C_o-1)[1+2x(\rho_\ell/\rho_v-1)]\}^{-\frac{1}{2}}$	To be determined	See ref. [13]

Table 3 CHF experiments with vertical upflow of Freon-12

Geometry Tested	Shroud Tube Bore mm	Inner Tube Outside Diameter mm	Heated Length mm	Coolant Pressure MPa	Exit Quality	Mass Flux kg $s^{-1}m^{-2}$	Heating Distribution	Reference
Round tube	16.1	N/A	2860	0.89 → 1.60	0.035 → 1	200 → 4100	Uniform	[22]
Round tubes	15.3 16.1 21.5	N/A	2850 → 3940	0.96 → 1.05	0.007 → 0.78	450 → 3850	Uniform	[23]
Round tubes	8.5 16.8 21.3	N/A	2870 → 3700	0.90 → 1.32	0.19 → 0.86	380 → 2800	Uniform and axially non-uniform	[30]
Annuli	9.5 → 26.6	8.0 → 18.6	457 → 4280	1.04	0.04 → 1	660 → 4160	(1) Shroud only, (2) Inner tube only, or (3) Both shroud and inner tube; Uniform in each case, also chopped cosine axially for case (2)	[24]
Annuli	21.0 22.1 22.7	14.4 15.9	1830 2740	0.83 → 1.65	0.002 → 0.76	670 → 4200	Heated shroud or inner tube - axially uniform	[25]
19-rod cluster	114	15.9	1250	1.05 → 1.69	0.49 → 1	47 → 260	Axially uniform - shroud not heated	[25]

© IMechE 1983 C102/83

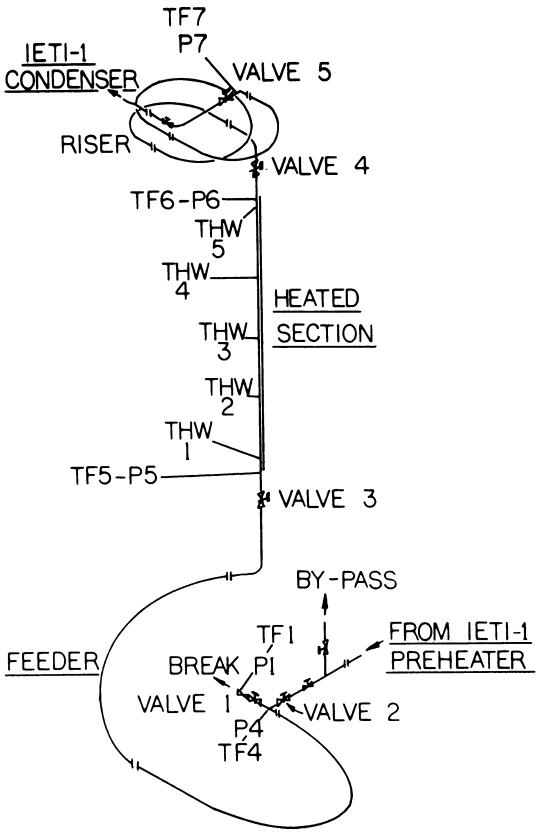

Fig 1 IETI-1 test rig

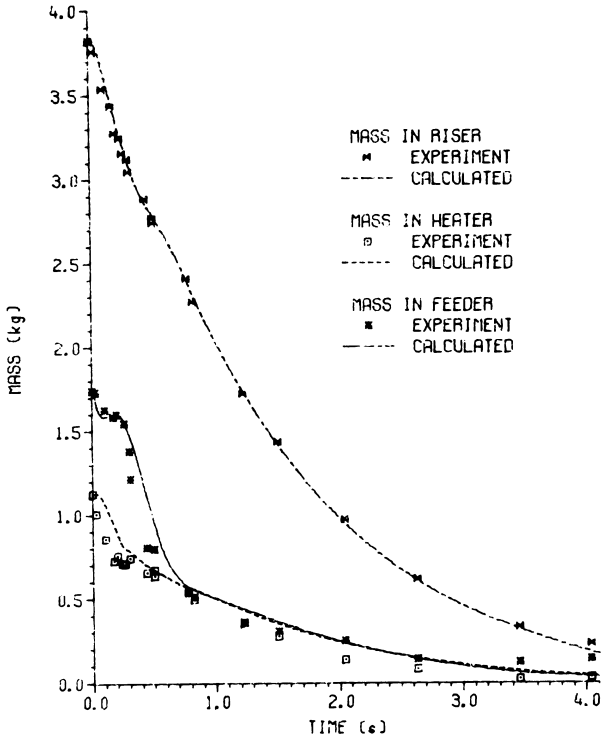

Fig 2 Mass contents in CSNI benchmark experiment

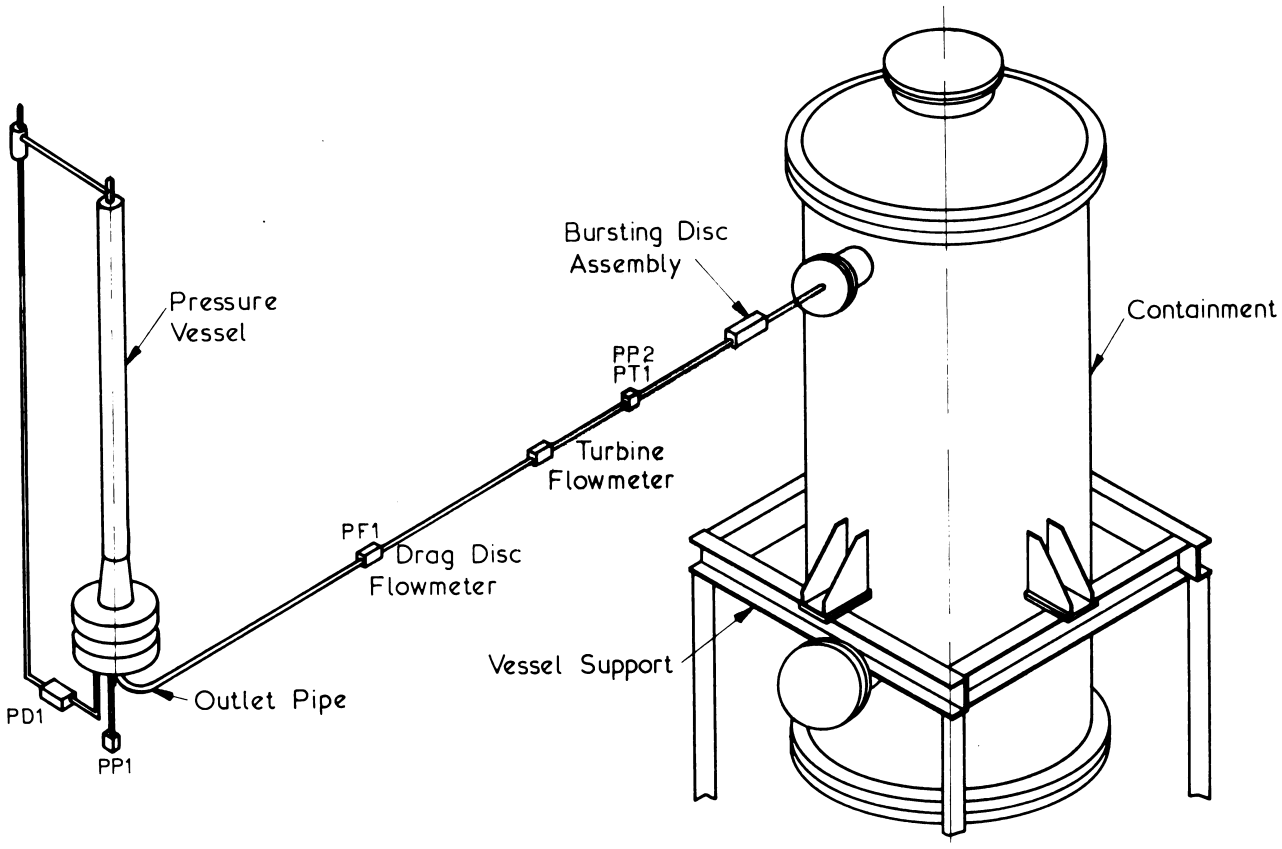

Fig 3 Blowdown containment rig general arrangement

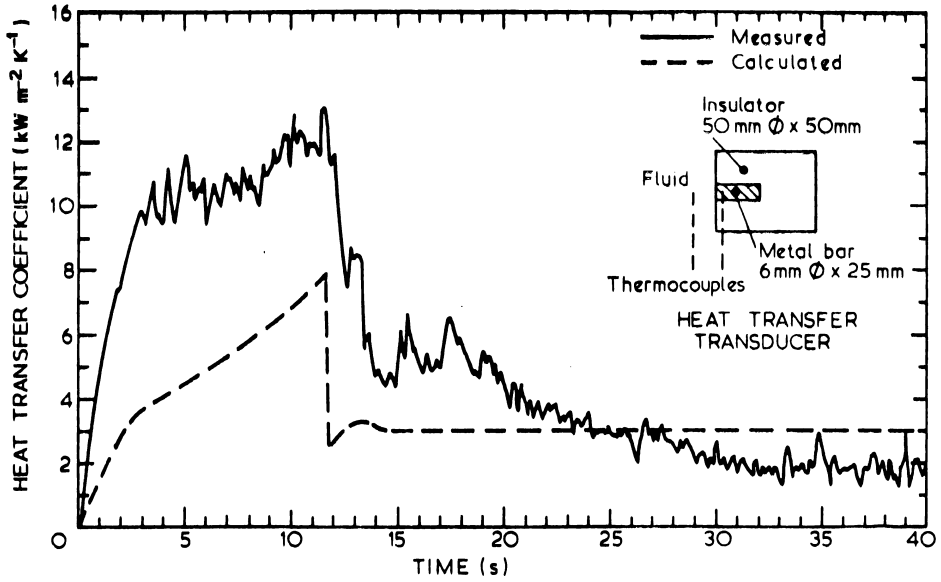

Fig 4 CASP3: heat transfer, top compartment

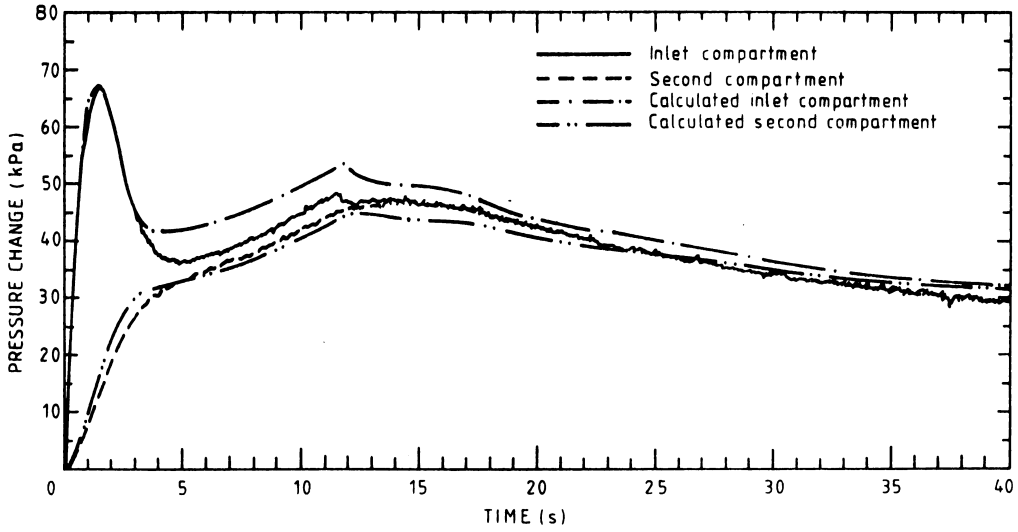

Fig 5 CASP3: containment pressures

© IMechE 1983 C102/83

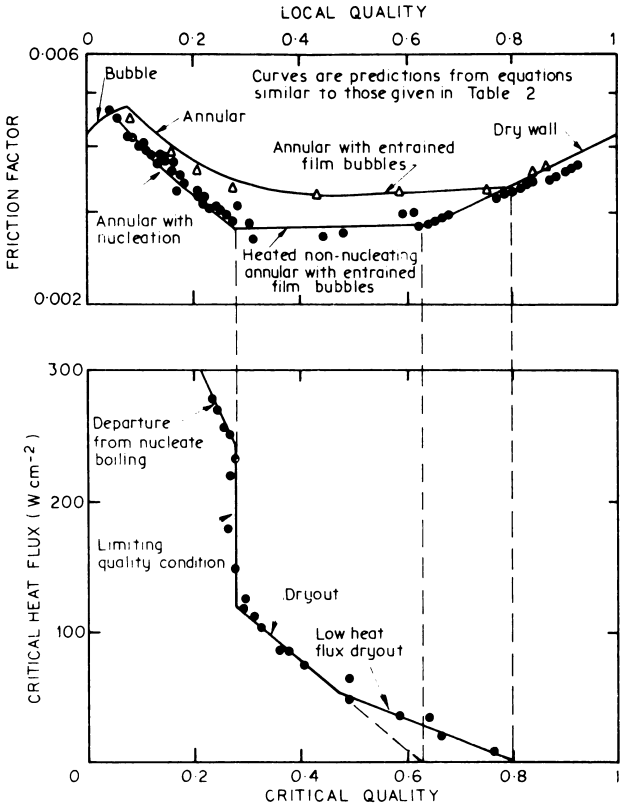

Fig 6 Comparison of predicted and experimental friction factor characteristics and the interrelation with critical heat flux characteristic; CISE test section 58C, 5 mm diameter 80 cm long, 7 MPa, 3800 kg m^{-2} s^{-1}, · diabatic, △ adiabatic. Data from CISE-R-83 and CISE-R-90

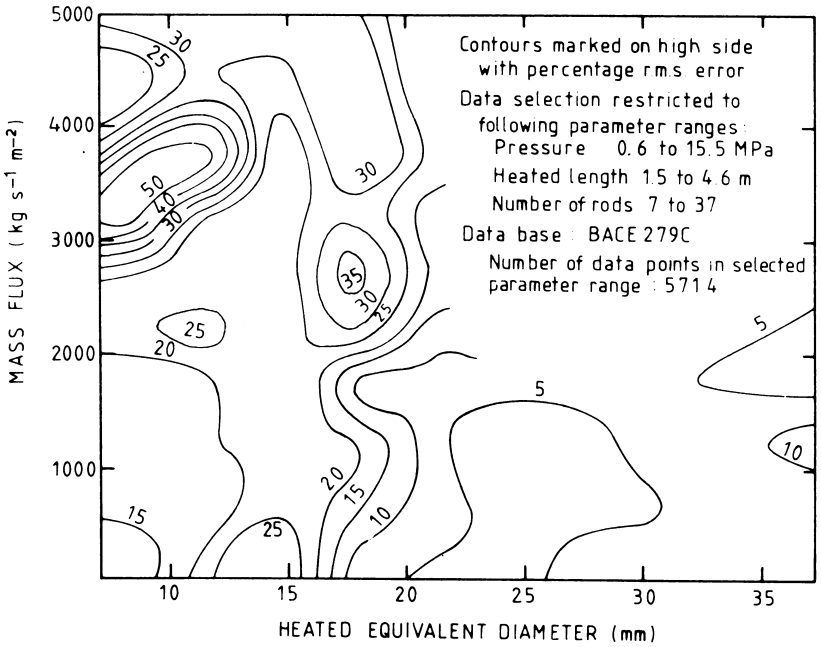

Fig 7 Contour plot of r.m.s. error of Bowring rod cluster CHF correlation when compared with experimental results

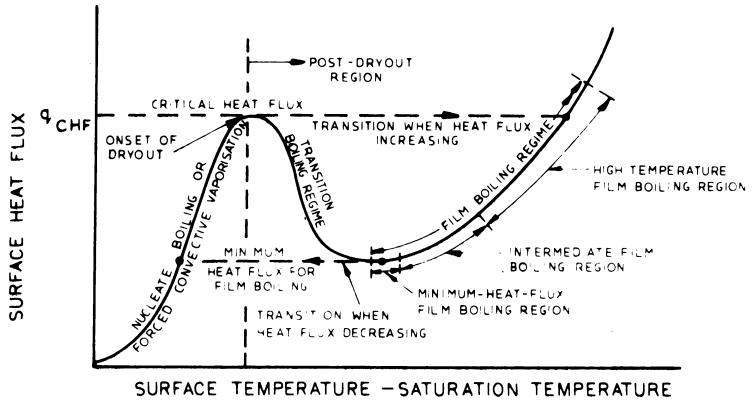

Fig 8 Simplified representation of boiling curve

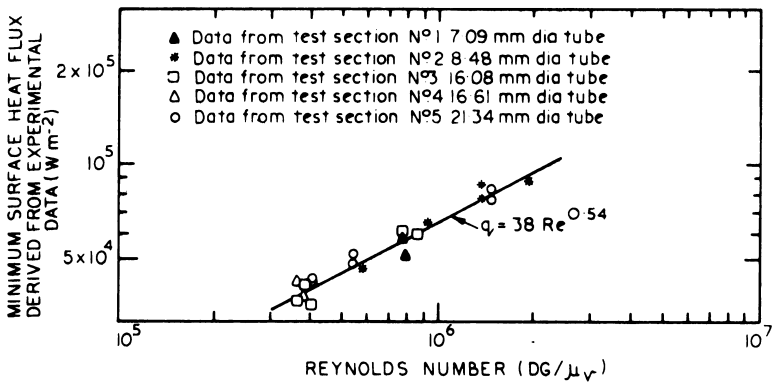

Fig 9 Relationship between minimum heat flux of film boiling and Reynolds number

© IMechE 1983 C102/83